Quasi-instantaneous and Long-term Deformations of High-Performance Concrete with Some Related Properties

Persson, Bertil

1998

LUND UNIVERSITY, LUND
Lund Institute of Technology
Division of Building Materials

QUASI-INSTANTANEOUS AND LONG-TERM DEFORMATIONS OF HIGH-PERFORMANCE CONCRETE

with Some Related Properties

Bertil Persson

Report TVBM-1016
Lund 1998

Keywords:

Cement
Concrete
Creep
Deformations
Elastic modulus
High-Performance Concrete
Hydration
Long-term
Relative humidity
Shrinkage
Strength
Quasi-instantaneous

ISRN LUTVDG/TVBM--98/1016--SE(1-250)
ISSN 0348-7911 TVBM
ISBN 91-630-6969-5

Lund Institute of Technology
Division of Building Materials
P.O. Box 118, SE-221 00 Lund
Sweden
Telephone: +46 46 222 74 15
Telefax: +46 46 222 44 27
E-mail: postmaster@byggtek.lth.se
Internet: ldc.lu.se/lthbml/index.htm

For Eva, Ulrika and Madeleine

ABSTRACT

This report outlines an experimental and numerical study on quasi-instantaneous and long-term deformations of High-Performance Concrete, HPC, with some related properties. For this purpose about two hundred small cylinders and about one thousand cubes of eight types of HPC were cast. The age at loading varied between 18h and 28 days. Other principal properties of HPC were studied up to 4 years' age. Creep deformations of the HPC were studied from 0.01 s of loading time until 5 years' age. The work also includes observations of recovery at unloading and transversal deformations (Poisson's ratio). Elastic modulus and dynamic modulus of elasticity were studied on both young and mature concrete. Parallel studies were performed on shrinkage, strength, hydration, carbonation and on internal relative humidity of HPC. Supplementary dimensional studies were performed on twenty larger cylinders. Field studies were carried out on almost thirty prestressed beams. The results show good correlation between maturity and the quantity of creep of HPC. The results also show good correlation between, on one hand, the stress level and the mix design of the HPC and, on the other hand, the creep properties of HPC given a constant loading time. The phenomenon named autogenous shrinkage was observed during the study. The autogenous shrinkage was related to the self-desiccation and chemical shrinkage in HPC. Also the elastic properties of HPC were dependent on the moisture state at testing. The field studies on beams confirmed the findings in the laboratory. The short-term studies indicated that the creep rate (related to unit stress) of mature HPC was fairly independent of the compressive strength. The short-term basic creep rate (related to unit stress) of HPC after heat curing was observed to be twice as large at -1°C as at other temperatures. Besides loading time, the long-term compliance of HPC was mainly dependent on the maturity and the compressive strength both when loading the HPC and at 28 days' age. The creep was slightly reduced by use of 10% silica fume instead of 5%. The calculated long-term total compliance of the present study coincided reasonably well with previous research, taking into account that the exact HPC mix was unknown. However, the observed creep compliance was slightly larger than previously seen. The initial compliance calculated according to the previous studies was more affected by the strength than were the results of the present study. The following principal results were obtained:

- Elastic modulus was related to compressive strength and porosity as demonstrated in normal strength concrete, NSC.
- The creep rate (related to unit stress) was dependent on both the duration of loading and the maturity of the HPC.
- Creep properties of the HPCs obtained by the quasi-instantaneous loading were applicable to the long-term studies performed with a much lower loading rate.
- Specific creep was shown to be reduced with increase in silica fume content.
- Autogenous shrinkage was reduced by the use of granulated silica fume instead of silica fume slurry, likely due to the greater fineness of the silica fume slurry.

PREFACE

This study has been carried out at the Division of Building Materials, Lund Institute of Technology, Lund University, Lund from 1991 to 1998 under the supervision of Professor Göran Fagerlund. Besides this principal paper the report is based on the following papers:

I B Persson (1996). Self-desiccation and Its Importance in Concrete Technology. Materials and Structures. Vol. 30. RILEM. 1996. Pp. 293-305.

II B Persson (1997). Long-term Effect of Silica Fume on the Principal Properties of Low-temperature-cured Ceramics. Cement and Concrete Research. Vol. 27. 1997. Pp. 1667-1680.

III B Persson (1997). Basic Deformations of High-Performance Concrete. Nordic Concrete Research. Vol. 20. 1997. Pp. 59-74.

IV B Persson (1998). Quasi-instantaneous and Long-term Deformations of High-Performance Concrete with Sealed Curing. Advanced Cement Based Materials. *(Accepted for publication, 1998.)*

The study was also presented in the following papers:

V B Persson (1996). Hydration and Strength of High-Performance Concrete. Advanced Cement Based Material. Vol. 3. 1996. Pp. 107-123.

VI B Persson (1996). Moisture in Concrete Subjected to Different Kinds of Curing. Materials and Structures. Vol. 30. RILEM 1996. Pp. 533-544.

VII B Persson (1998). Self-desiccation and Its Importance in Concrete Technology. Nordic Concrete Research. 10 pp. *(Accepted for publication, 1998.)*

VIII B Persson (1998). Effect of Cement Type, Silica Fume, Water-cement Ratio, Age and Moderate Shift in Temperature on Self-desiccation in Concrete. Nordic Concrete Research. 22 pp. *(Accepted for publication, 1998.)*

IX B Persson (1998). Pozzolanic Interaction Between Portland Cement and Silica Fume in Concrete. Proceedings of the Sixth CANMET/ACI/JCI International Conference on Fly Ash, Silica Fume, Slag and Natural Pozzolans in Concrete. Bangkok. Ed. by V M Malhotra. 1998. Pp. 631-660.

X B Persson (1998). Seven-year Study on the Effect of Silica Fume in Concrete. Advanced Cement Based Materials. 22 pp. *(Accepted for publication, 1998.)*

XI B Persson (1997). Long-term Shrinkage of High-Performance Concrete. Proceedings of the 10th International Congress on the Chemistry of Cement. Contribution 2ii073. Gothenburg. 1997. Ed. by H Justnes. 9 pp.

XII B Persson (1998). Experimental Studies on Shrinkage of High-Performance Concrete. Cement and Concrete Research. 13 pp. *(Accepted for publication, 1998.)*

XIII B Persson (1998). Shrinkage of High-Performance Concrete. Proceedings of the International Workshop on Autogenous Shrinkage of Concrete. Hiroshima. 1998. Ed. by E Tazawa. E & FN Spon. London. 1998. Pp. 101-118.

XIV B Persson (1998). Creep of Heat-cured High-Performance Concrete Subjected to Freezing or Elevated Temperatures. Proceedings of the Second International Conference on Concrete under Severe Conditions. Tromsø. 1998. Ed. by O Gjørv, K Sakai and N Banthia. E & FN Spon. London. 1998. Pp. 1616-1626.

XV B Persson (1998). Conditions for Carbonation of Silica Fume Concretes. Proceedings of the Fifth International Weimar Workshop. Weirnar. 1998. Ed. by F H Wittmann and P Schwesinger. Freiburg and Unterengstringen. *(Accepted for publication, 1998.)*

ACKNOWLEDGEMENTS

I am most indebted to Professor Göran Fagerlund, who initiated the projects on High-Performance Concrete at our department in 1989, made the general outlines from the start of the present study in 1991 and reviewed this report three times. His great experience was of the utmost importance for the project.

I am likewise most grateful to Stefan Backe, responsible for the measurements of the internal temperature, to Alan Crozier, who revised the English, to Ingemar Larsson, who assembled the cast-in items and performed the moisture insulation of the specimens. Thord Lundgren developed the new method of data collection. Bengt Nilsson was responsible for measurements of air content and density, mixed the heated concrete, poured it and did the demoulding for the tests performed at different temperatures. Per-Olof Rosenquist was responsible for the MTS testing machine and Sture Sahlén calibrated the dew-point meters. I am most grateful to all the persons mentioned.

Anders Johansson and Peter Johansson mixed the concrete at the tests of specimens with different dimensions, poured it and did the demoulding. They also performed all loadings, unloading, strength tests and measurements connected to these tests. Rune Egardsson, Fredrik Holst, Lennart Norberg, Gunnar Rise and Bo Wiberg were responsible for the mix design, the mixing, pouring and loading of the specimens used in the field tests. I am most thankful to all the persons mentioned.

The major part of the research was financed by THE CONSORTIUM FOR RESEARCH ON HIGH-PERFORMANCE CONCRETE, that consisted of BFR (the Swedish Council of Building Research), NUTEK (the Swedish Board of Technical Development), Cementa, Elkem, Euroc Beton, NCC Bygg, SKANSKA and Strängbetong, which I hereby gratefully acknowledge.

Finally, I am most thankful to my family, Eva, Ulrika and Madeleine, for their great patience during several late hours of work within the study, during preparation, loading and early measurements of the specimens, during seventy week-ends of work at the short-term studies and furthermore during many hours of work at home during the preparation of this report.

Lund, 22 July 1998

Bertil Persson

CONTENTS PAGE

SYMBOLS

a	centre distance of LVDT or creep rate {mm, [millionths/(MPa·age)]}
a_B	the compliance rate with sealed curing [millionths/(MPa·age)]
a_D	the compliance rate with air curing [millionths/(MPa·age)]
$a_{0.3}$	the creep rate with stresslstrength = 0.3 [millionths/(MPa·age)]
$a_{0.6}$	the creep rate with stresslstrength = 0.6 [millionths/(MPa·age)]
b	initial compliance at loading (millionths/MPa)
c	amount of cement or cylinder (kg/m^3, -)
d	time or diameter of cylinder specimen (days, mm)
d_c	the depth of carbonation (mm)
e	eccentricity (mm)
e_x	estimated eccentricity to the "x" axis (mm)
e_y	estimated eccentricity to the "y" axis (mm)
f_c	compressive strength (MPa)
$f_{c,cyl}$	strength of cylinders (diameter 55 mm, length 200 mm, MPa)
$f_{c,cube}$	compressive strength of cubes (100 mm, MPa)
f_{cun}	compressive cube strength at unloading (MPa)
f_{cB}	strength with sealed curing (basic creep, MPa)
f_{cBsl}	strength of sealed HPC with 10% silica fume slurry (basic creep, MPa)
f_{cD}	strength of HPC with air curing (drying creep, MPa)
f_{cDsl}	strength of drying HPC with 10% silica fume slurry (drying creep, MPa)
f_{c28}	28-day compressive strength (MPa)
f_c/f_{c28}	28-day relative strength
Δf_c	strength growth between loading and unloading (MPa)
f_{sp}	split tensile strength (MPa)
k_i	efficiency factor of silica fume
k_s	efficiency factor of silica fume as regards compressive strength
k_{sc}	efficiency factor of silica fume related to compressive strength of sealed cylinders
l	air volume in the concrete (l/m^3)
$\ln(t)$	natural logarithm of age, t
Δl_i	LVDT deformation
n	number of measured values or an exponent for elastic modulus or the fundamental transverse frequency (-, -, Hz)
s	content of silica fume (kg/m^3)
t	age (s, h, days, months)
t'	age at loading (s, h, days)
$t-t'$	loading time (s, h, days)
w	amount of mixing water (kg/m^3)
$(w/c)_{eff}$	$= w/(c+k_i \cdot s)$
$(w/c)_{eff2}$	$= w/(c+2 \cdot s)$
w_a	weight of aggregate (kg/m^3)
w_e	evaporable water (kg/m^3)
w_e/w	relative evaporable water (evaporable water to mixing water, kg/kg)

w_n	non-evaporable water (kg/m^3)
$w_{n,pre}$	hydrated water of HPC after pre-drying in exsiccator
w_n/w	relative hydration (non-evaporable water to mixing water, kg/kg)
w^{105}	weight after drying at 105 °C (kg)
w^{1050}	weight after ignition at 1050 °C (kg)
B	basic creep (sealed curing)
dC(t,28)/dt	creep rate for HPC mature when loading [millionths/(MPa·day)]
D	drying creep (air curing)
D_c	modulus of deformation of the concrete (GPa)
D_p	deformation modulus of the cement-paste (GPa)
D_{p28}	28-day deformation modulus of cement paste after 0.01 s of loading (GPa)
$D_{p,0.01}$	deformation modulus of cement paste at 0.01 s loading time (GPa)
$D_{t\text{-}t'}$	modulus of deformation (GPa)
D_B	deformation modulus with sealed curing (basic creep, GPa)
D_D	deformation modulus of HPC with air curing (GPa)
E_a	modulus of elasticity of the aggregate (GPa)
E_{dyn}	dynamic modulus for a cylinder (GPa)
E_l	long-term modulus of elasticity (GPa)
E_{mat}	elastic modulus of mature concrete at unloading (GPa)
E_{stat}	static modulus of elasticity at unloading (GPa)
E_B	elastic modulus of sealed concrete (GPa)
E_{Bma}	elastic modulus of sealed mature HPC (GPa)
E_D	elastic modulus of drying concrete (GPa)
E_{Dma}	elastic modulus of drying mature HPC (GPa)
E_{Dyo}	elastic modulus of drying concrete, young when loading (GPa)
EC	concrete with expanded clay
G	weight (kg)
HPC	High-Performance Concrete
J(t,t′)	compliance at loading time t and age t' (millionths/MPa)
J_{el}	long-term elastic compliance (millionths/MPa)
J_{pl}	long-term plastic compliance (millionths/MPa)
J_{vi}	long-term viscous compliance (millionths/MPa)
$\Delta J_l(t, t')$	difference in compliance at unloading (millionths/MPa)
J_{pl}/J_{el}	ratio of viscous-plastic to elastic compliance at unloading
J_{vi}/J_{el}	ratio of viscous-elastic to elastic compliance at unloading
L	length of specimen (in. = inch)
M_e	additional moment due to eccentricity (Nm)
MC 90	Model Code 90
NSC	normal strength concrete
P	testing force (N)
$(P_{cap})_p$	capillary porosity of the cement paste
P_p	porosity of the cement paste
RH	relative humidity (%, -)

$$R^2 = 1 - \frac{\sum (Y_i - Y_m)^2}{(\sum Y_i^2) - \frac{(\sum Y_i)^2}{n}}$$

SRG	concrete with river gravel aggregate
W	weight of specimen (lb.)
Y_i	measured value
Y_m	average measured value
α	degree of hydration (-)
ε	deformation or total shrinkage (-, per mil)
ε_{el}	elastic strain of mature HPC at unloading (per mil)
ε_{pl}	plastic strain of mature HPC after unloading and recovery (per mil)
ε_{vi}	viscous strain of mature HPC at recovery (per mil)
ε_B	autogenous shrinkage (per mil)
ε_{Bel}	elastic strain of sealed HPC at unloading (per mil)
ε_{Bpl}	plastic strain of sealed HPC after unloading (per mil)
ε_{Bvi}	viscous strain of sealed HPC at recovery (per mil)
ε_{Bn}	shrinkage in HPC with no loss of weight (per mil)
ε_C	carbonation shrinkage (per mil)
ε_D	drying shrinkage (per mil)
γ	ratio of aggregate to cement (kg/kg)
μ_a	ignition losses for aggregate (kgkg)
μ_{ai}	volume share of air-entrainment
μ_c	ignition losses for cement (kgkg)
ρ_a	density of the cement (kglm^3)
ρ_w	density of the water (kglm^3)
σ	stress (MPa)
σ/f_c	stresslcube strength ratio at loading
$\Delta\sigma$	additional compressive stress in the specimen (MPa)
σ_x	longitudinal stress
σ_y	lateral stress
υ	Poisson's ratio
υ_B	Poisson's ratio at loading or unloading of sealed HPC
υ_D	Poisson's ratio at loading or unloading of drying HPC
Ø	internal relative humidity (-)
$Ø_i$	internal relative humidity of the inner part of the cylinder
$Ø_s$	relative humidity of the surface of the cylinder
$\Delta Ø$	difference between relative humidity of inner part and surface of cylinder
6..	HPC mix
...01	= loading at 0.8 days' age with stresslcylinder strength = 0.84
...02	= loading at 2 days' age with stress/cylinder strength = 0.84
...03	= loading at 2 days' age with stresslcylinder strength = 0.42
...28	= loading at 28 days' age with stresslcylinder strength = 0.42

SUMMARY

Quasi-instantaneous loading and short term deformations

Several mixes of High-Performance Concrete, HPC, were studied, both in the laboratory and in the field. The results in the field studies generally confirmed the laboratory findings. By use of an optimised mix, an ideal grading curve and a correct order of mixing, the HPC obtained good workability and high strength. A new method of rapid loading and simultaneous registration of measurements was developed. The age of the HPC was 1, 2 or 28 days at the start of testing. The loading, as much as 100 kN, was applied very rapidly within 0.01 s. The quasi-instantaneous loading gave the possibility of estimating the initial strain (true modulus of elasticity) and very early creep. The rapid loading method separated the elastic strain of HPC from the viscous elastic and the plastic part. Studies on several drying and sealed specimens were carried out for 66 h each. The rate of creep was dependent on the relative strength at loading and on the stress level.

The deformation modulus, i.e. the inverse of the compliance, was studied on several drying HPC cylinders with a loading time of 0.01 s. The results were compared with studies on several sealed cylinders. The size of the deformation modulus of HPC was dependent on the loading time, especially for young HPC. Correlations between the deformation modulus and the compressive strength of HPC were obtained within loading times varying between 0.01 s and 1 s. The deformation modulus of HPC was also dependent on the stress to strength ratio at loading. The moisture condition of the HPC specimen had a substantial effect on the measured deformation modulus. The largest values of the deformation modulus were recorded on sealed HPC specimens. Parallel studies on the hydration of HPCs made calculations of the porosity conceivable. Correlations were obtained between the deformation modulus of HPC and the porosity of cement paste. Results were also obtained concerning the development of the deformation modulus of young HPC.

Unloading deformations and Poisson's ratio

One hundred tests on the unloading deformations of HPC after short-term creep were performed, half of them on sealed HPC. The experimentally determined modulus of elasticity at unloading of air-cured mature HPC was about 10% smaller than that of sealed HPC, perhaps due to the larger mobility of the water in a drying HPC structure. The experimentally obtained modulus of elasticity at unloading of HPC coincided well with the deformation modulus at loading of HPC given a loading time of 0.01 s. An HPC that was loaded young obtained a larger elastic modulus when unloaded than HPC that was mature when loading, owing to the ongoing hydration. The measured modulus of elasticity was also related to the

internal relative humidity in parallel tests on fragments of HPC. Two hundred tests of Poisson's ratio were carried out, of which 50 were on young HPC. The tests on young HPC were supplemented by further loading and unloading tests on mature HPC. This study showed that Poisson's ratio was found to be around 0.13- 0.14 in HPC with quartzite sandstone and granulated silica fume, which is smaller than for normal strength concrete, NSC (0.18). Poisson's ratio of sealed mature HPC with granite and silica fume slurry was found to be around 0.16.

Moduli of elasticity and recovery deformation

Several tests of the dynamic modulus of elasticity of drying (young or mature) HPC detected by the fundamental transverse frequency were performed. The results were compared with several tests of young HPC (both drying and sealed). The results of the dynamic modulus of elasticity were also compared with several tests of mature HPC with an age varying between 28 and 720 days. The different moduli of drying, mature HPC coincided well with the dynamic modulus of elasticity. The dynamic modulus of elasticity of young HPC overestimated the static modulus of elasticity by as much as 20%, probably because of the higher internal relative humidity in young HPC than in mature HPC. The time-dependent ageing effect of the modulus of elasticity between 1 and 24 months' age was estimated by an exponent of time up to 0.02.

The elastic strain studies of several HPC cylinders during 66 h were followed by observations of viscous elastic strain and plastic (irreversible) strain during 100 h. The viscous strain of air-cured mature HPC was equal to the viscous strain of sealed curing. The plastic strain of air-cured mature HPC was much larger than the viscous strain. The plastic strain of sealed mature HPC was about equal to the viscous strain. The viscous strain of young HPC was dependent on the strength growth during the loading. The plastic strain of young HPC was dependent both on the stresslstrength level and on the strength growth from loading till unloading.

.ong term deformations

The autogenous shrinkage (with sealed HPC) was dependent on age, w/c and type and content of silica fume. The autogenous shrinkage of HPC was related to the decline of internal relative humidity. Slow drying shrinkage of mature HPC was correlated to the amount of evaporated water. The conditions for gradual carbonation shrinkage of HPC were settled related to w/c and content of silica fume. Age at the start of the carbonation shrinkage of HPC was related to the water-cement ratio, w/c. The drying shrinkage of young HPC was related to age and to the loss of weight. The carbonation rate of HPC was related to age and w/c by a logarithmic equation. The total shrinkage after 5 years was related to age, w/c and

type and content of silica fume. The carbonation shrinkage was also related to the carbonation depth.

Several air-cured or sealed specimens were studied up to 5 years. Spring-loading devices were used. The studies took place in a climate chamber. The loading was applied by hydraulic equipment with the control of a precision load-cell. The loading was controlled at each occasion of measurement. The deformation of the HPC in the spring-loading devices coincided well with the deformations of specimens that were studied in parallel short-term tests measured by LVDTs. The measurements were taken mechanically on three sides of the specimen, which made it possible to obtain the eccentricity of the loading given elastic conditions. The eccentricity did not significantly influence the amount of deformation. After the long-term measurement period the specimens were unloaded and the elastic deformation recorded. The plastic and the viscous elastic deformations after long-term loading were also studied. Compressive strength, hydration, weight losses and internal relative humidity were studied parallel to the creep study.

The long-term creep of HPC with air curing was influenced mainly by time, w/c, air-entrainment, type of silica fume, stresslstrength level, strength at loading and 28-day strength. The long-term creep of HPC with sealed curing was influenced mainly by time, w/c, amount of silica fume, type of silica fume, stresslstrength level, strength at loading and 28-day strength. The rate of creep was related to the strength growth rate of HPC. The rate of creep of drying HPC was dependent on air-entrainment, amount and type of silica fume. The rate of creep of drying HPC was dependent on air-entrainment, amount and type of silica fume. The creep rate (related to unit stress) of sealed HPC was dependent on air-entrainment and amount of silica fume. The rate of creep in HPC was also related to the internal relative humidity.

The elastic modulus of HPC with air curing that was obtained in the present study was smaller than the elastic modulus estimated according to the proposed extension of Model Code 90 given constant strength. The elastic modulus of HPC with sealed curing that was obtained in the present study was larger than the elastic modulus estimated according to the proposed extension of Model Code 90 given constant strength. These results were explained by the increased immobility of water in sealed specimens compared with drying HPC. The viscous elastic partition of creep was small and hardly detectable at $w/c < 0.35$. The long-term plastic compliance to elastic compliance ratio of air-cured HPC was influenced mainly by time, w/c, air-entrainment, type of silica fume, stresslstrength level, strength at loading and 28-day strength. The long-term plastic compliance to elastic compliance ratio of sealed HPC was influenced mainly by time, w/c, type of silica fume, stresslstrength level, strength at loading and 28-day strength.

Creep after heat curing, short-term basic creep (after heat curing) at elevated temperatures or at temperatures under the freezing point, dimensional effect on creep and field studies

Short-term creep of one heat-cured HPC was studied at six temperatures varying between -16 and 58 "C. The rate of creep was correlated to the temperature except for -1 "C at which temperature rapid failures were repeatedly observed during the creep tests, perhaps due to formation of salts, which were only stable at this temperature. Long-term creep of HPC after heat curing was studied for 3 years.

Parallel studies were carried out related to strength, hydration, internal relative humidity, weight losses and shrinkage. The creep rate (related to unit stress) of HPC during short-term creep increased mainly with the stress to strength ratio and but also (slightly) with the temperature. The long-term creep rate (related to unit stress) with sealed curing also increased with the increase of curing temperature, which coincided well with the findings of short-term creep tests.

The results and analysis of the creep and shrinkage investigation presented above performed on more than one hundred small cylinders were compared with tests on several larger cylinders. The drying shrinkage rate was correlated to half the inverted hydraulic radius (exponent: 2/3) and also to age (exponent: –1). The drying creep rate (related to unit stress) was correlated to half the hydraulic radius of the specimen. The creep compliance studied on the larger cylinders coincided well with the results of creep studies performed on small cylinders taking into account half the hydraulic radius of the specimens.

Seven prestressed "hat" beams and 20 square beams were studied in the field up to 200 days. The measured strain in the field was compared with estimated strain according to the prediction formulas (equations) obtained from the data of the studies in the laboratory. The estimated deformation modulus was slightly smaller than the measured deformation modulus given constant strength. The estimated creep compliance was slightly larger than the measured compliance. In both cases the predicted elastic and creep properties of HPC were slightly larger. The estimated shrinkage was slightly smaller than the measured shrinkage.

Calculations with suggested prediction formulas: comparison with other research

After the comparison between the results of the field tests and the laboratory studies was performed, further calculations with the suggested prediction formulas were done. The results after use of all the suggested prediction formulas seemed to coincide reasonably well with laboratory data. The accuracy parameter (R^2) of the suggested prediction formulas is given. Comparison was also performed with results obtained by other researchers. The comparison showed that the results in this study coincided reasonably well with the results of other researchers.

1. DEFINITION OF CONCEPTS

1.1 High-Performance Concrete

High-Performance Concrete, HPC, is concrete with 28-day 100-mm cube compressive strength exceeding 80 MPa. HPC has good rheological properties. In fresh state it is possible to mix, transport and cast HPC with existing methods. The maximum compressive strength will be about 180 MPa in these conditions. Because such concrete possesses - besides high strength - several other favourable qualities such as low permeability and self-desiccation, the new definition was originated.

The ratio of the amount of water to the amount of cement in the concrete, w/c, is larger than 0.38 for a normal strength concrete, NSC, while it varies between 0.18 and.0.38 for HPC. Low wlc requires a special additive in the concrete, silica fume, and above all superplasticiser to obtain a good workability. Most often special cements are also required. The type of aggregate is important for obtaining high strength. The grading of the aggregate influences the workability, especially the fine part. The order of mixing the material involved is also important for the workability.

Several properties of the concrete are firmly related to w/c, such as compressive strength, internal relative humidity, hydration and compliance, ε/σ. Other properties such as the elastic modulus, Poisson's ratio and the creep coefficient do not vary more than in normal strength concrete, NSC, since they are mainly dependent on the quality of the aggregate.

1.2 Basic creep

Generally, basic creep deformations include the effect of loading on the concrete at constant climate. The ambient temperature must be held constant. The moisture exchange from the concrete to the surroundings must be zero, i.e. the weight of the concrete is also constant. The basic creep of HPC excludes a phenomenon unknown in NSC, called autogenous shrinkage. The autogenous strain is withdrawn from the measured basic creep.

The autogenous shrinkage of HPC is an effect of its self-desiccation. Self-desiccation in turn depends on the decrease of the volume of the water, which takes place when attached to the cement during hydration. The self-desiccation of HPC is beneficial for solving problems related to moisture from the concrete during construction. However, autogenous shrinkage perhaps causes cracking even when the concrete is exposed to water, also an effect of the low permeability of the concrete. Autogenous shrinkage perhaps is beneficial as it acts in the opposite direction as the temperature expansion during the very early hydration. However, later on, during cooling of HPC, autogenous shrinkage increases the tensile strain and thus the risk of thermal cracking. In **Figure 1.1** the concept definition for basic creep is shown versus time for the different types of deformations.

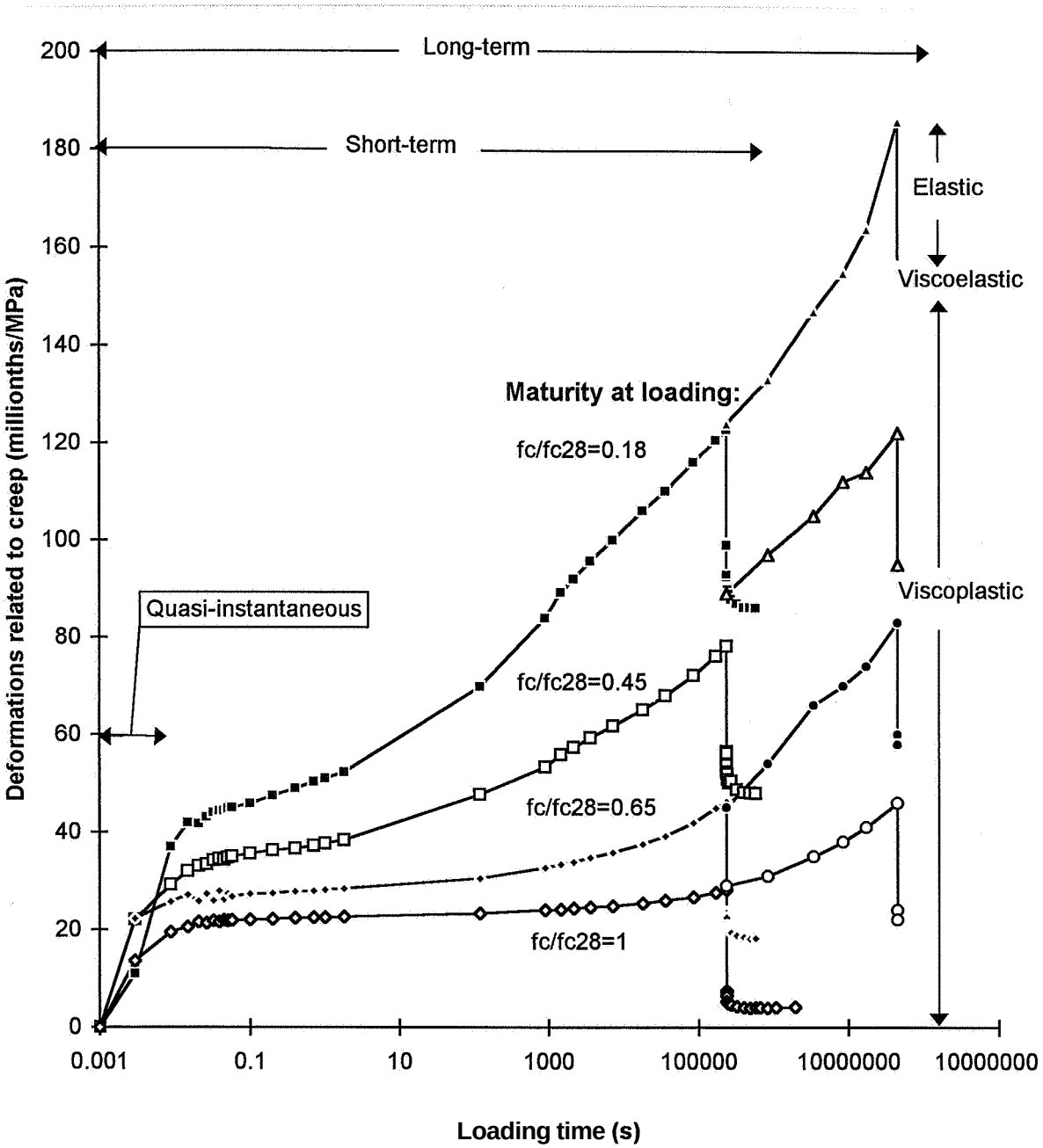

Figure 1.1 - Deformations related to creep versus time. fc/fc28 denotes the strength to the 28-day strength ratio at loading.

1.3 Drying creep

Drying creep deformations include the effect of loading on the concrete at constant climate. The ambient temperature must be held constant. Moisture exchange exists from the concrete to the surroundings, i.e. the weight of the concrete is not constant. Shrinkage is not includes in the drying creep. The shrinkage strain is deducted from the total strain to obtain the drying creep strain. **Figure 1.2** shows the Pickett's paradox: creep of dry concrete (a), basic creep (b), and drying creep (c), **Acker (1993).** The drying creep changes gradually from state (b) to state (a).

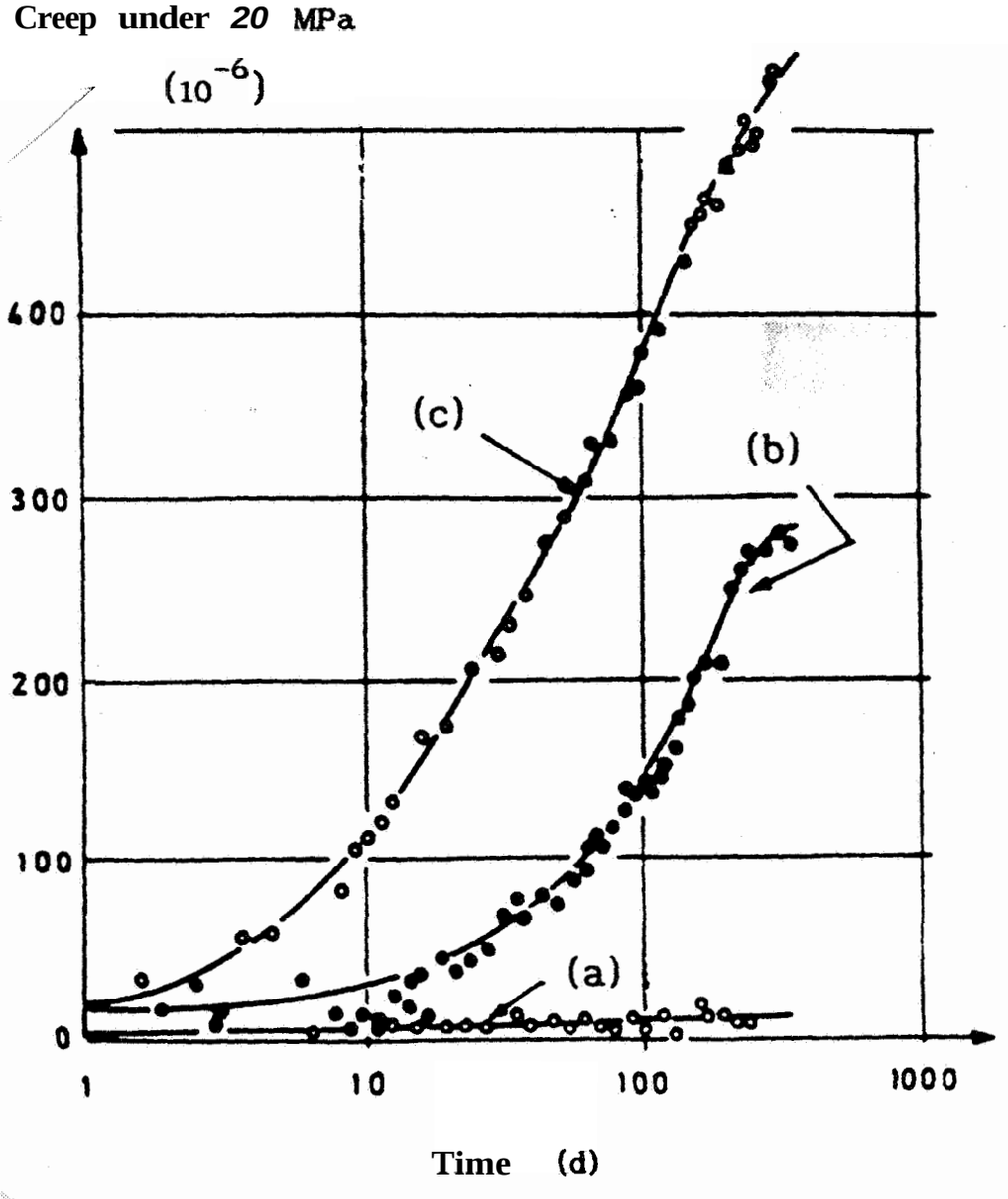

Figure 1.2 - Pickett's paradox: (a) previously dried concrete exhibits practically no creep; (b) basic creep; (c) drying creep, Acker (1993). d = days of loading.

1.4 Deformation modulus and elastic modulus

In this report the deformations modulus is defmed by the inverted compliance (specific deformation, ε/σ) of the concrete within a loading time varying between 0.01 and 1 s (laboratory tests) or within a loading time of 100 s (field tests). The loading time is specified at each occasion.

The results of the elastic modulus reported in this study is defmed by the inverted compliance at unloading of the concrete within 1 s (laboratory tests). The unloading time is specified at each occasion. The results of the dynamic modulus of elasticity presinted in this report is detected by the fundamental transversal frequency.

2. PROBLEMS RELATED TO CREEP OF HIGH-PERFORMANCE CONCRETE

2.1 General

Creep and shrinkage are two major problems to be considered when using concrete. These problems are especially pronounced when the concrete is used in prestressed structures. When prestressing is done at one side of the structure, the result is often a bent element caused by creep due to the prestressing. The creep and shrinkage influence the properties of the young concrete as well as the long-term behaviour of the concrete, as regards deformations, stability and durability. One of the great advantages of HPC seems to be low creep and shrinkage compared with NSC, **Penttala and Hayrinen** (1992). **Nielsen** (1972) gives an interesting review of the factors affecting the long-term deformations of concrete.

2.2 Causal relationship

The fundamental cause of creep is still unknown. The dominant opinion is that creep is related to moisture movements in the concrete due to the imposed loading on the concrete. Moisture movement in the gel of HPC is another probable cause of creep. At low imposed loading the HPC shrinks as long as the self-desiccation continues. When the cement is hydrated by the mixing water in the HPC, the hydration causes a 25% chemical shrinkage of the volume of the water, **Powers and Brownyard** (1946-1948). With sealed curing the chemical shrinkage creates an air-filled volume ratio in the gel of about 1.5%, **Persson (1993A)**, fairly independent of the water-cement ratio of the concrete. As the hydration ceases at a low internal relative humidity in a sealed-cured HPC, the autogenous shrinkage also ceases. With drying creep the surface of the concrete dries out while the interior of the concrete still contains an excess of moisture compared to the ambient conditions. Most probably micro-cracking occurs in the surface and causes the cracking due to shrinkage, **Sicard** (1993). When the stress is applied to the concrete, the distribution will be uneven throughout the concrete. The interior will obtain larger compressive stress than the surface, perhaps a reason why drying creep is larger than basic creep.

2.3 Early creep

Acker (1993) pointed out the importance of new experimental approaches. Nitrogen accumulators and electronic servo controls make it possible to apply the loading instantaneously to allow for fine separation of the instantaneous and the delayed strains. A quasi-instantaneously applied creep loading would probably be a way to separate the viscous and the plastic creep from the elastic deformation. **Evans**

(1958) carried out tests in an testing machine working with compressed air. He managed to apply the loading within 0.005 s. However, according to **Evans (1958)** the full loading seems to be applied within 0.02 s. **Bazant (1995)** stated that the static modulus of deformation normally was obtained at a loading time of about 0.01 days, i.e. about 860 s. However the dynamic modulus is possible to obtain after about 10^{-9} day (0.001 s) of loading. **Bazant (1995)** also observed that the short-term creep curves for various ages at loading all meet at the same point as the time of loading approaches zero, independent of the age of the concrete. **Schwesinger (1996)** used extremely accurate equipment with nitrogen accumulators and electronic servo controls in order to study the long-term and short-term mechanical, thermal and hygral properties of concrete.

2.4 Creep during hydration

Emborg (1989) studied creep of concrete during hydration in order to separate the viscoelastic and viscoplastic deformations. **Lokhorst and van Breugel (1993)** presented an interesting model to describe the creep during hydration by inserting bars. As the hydration proceeds, more and more bars appear in the rheological model. The later bars applied will then be free of stress. It would be of interest to study and further develop models for creep during hydration. Hydration occurs, for example, after a prestressed loading is applied in many prefabricated structures, such as beams and slabs. Creep during hydration also occurs when the moulds are removed from self-desiccating slabs at early ages, perhaps causing deformation problems. **Sellevold (1958)** measured the flexural recovery of small beams of cement paste and also (parallel) the dynamic modulus of elasticity on the beams.

2.5 High stress/strength ratio (load level)

At high load level ($\sigma/f_c \approx 0.6$) the creep increases compared with normal stress/strength level ($\sigma/f_c \approx 0.3$). With drying creep the load level increases in the interior of the concrete compared with the surface since shrinkage occurs especially at the surface. High stress/strength levels occur, for example, after a prestressed loading is transformed to the concrete structures, such as beams and slabs.

2.6 Elastic modulus, Poisson's ratio and dynamic modulus

The elastic modulus follows the square root of the compressive strength well for NSC. If this applies to HPC as well, the deformations of HPC structures will perhaps be problematic, as the elastic modulus does not follow the compressive strength. Owing to the more or less constant elastic modulus related to the compressive strength, perhaps it will be difficult to use HPC, for example, for beams. The deformations perhaps will be too large. One way to diminish the deformations due to the disadvantage of the elastic modulus is perhaps to optimise

the section of a beam, i.e. to diminish the width but to maintain the height of such structures. The dead weight will also decrease in this way. Different types of aggregate may improve the elastic modulus for HPC. This has to be investigated further to fully exploit HPC. Another question of structural importance is the relationship between longitudinal and transversal deformation at loading: Poisson's ratio. Is Poisson's ratio like that for NSC or does it differ in a beneficial or harmful way? What is the influence of current strength on Poisson's ratio? Does it vary between loading and unloading, affecting for example the dynamic durability of HPC? These questions will be investigated before HPC can be used in structures.

2.7 Autogenous shrinkage and carbonation shrinkage

Autogenous shrinkage is deducted from the measured strain in order to obtain the basic creep. The autogenous shrinkage is due to the chemical shrinkage of the water when it is bound to the cement. In normal strength concrete, besides drying shrinkage, another type of shrinkage occurs, called carbonation shrinkage. During carbonation shrinkage the weight of the concrete specimen increases but the specimen is still decreasing in length. These three types of shrinkage will be investigated. HPC has a very low permeability. Does it show carbonation at all at a very low water-cement ratio? Do pozzolanic interaction limits exist in HPC, i.e. is the amount carbon hydroxide decreased at such low level due to the reaction with silica fume, that carbonation stops in HPC? Such effects will perhaps diminish the cover layer for the reinforcement.

2.8 Strength after long term loading

During hydration of HPC there is too little water for the process to proceed to a fully hydrated gel. Large quantities of unhydrated cement appear in the gel. These unhydrated volumes of cement in the gel perhaps will affect the long-term strength of the material. Long-term high loading perhaps also will affect the strength of HPC, i.e. lower the strength of HPC subjected to sustained loading compared with the strength of an unloaded specimen. This may be studied on unloaded cylinders used in the studies of shrinkage and on cylinders used in the long-term creep tests.

2.9 Creep at different temperatures

It is generally known that the creep rate for NSC increases with the temperature. The reason for this is perhaps that the internal relative humidity also increases with the temperature in the concrete, **Nilsson (1987), Persson (1995A)**. Does this also apply to HPC? It also is of great interest to study the creep of concrete at lower temperatures than the normal temperature in the laboratory, which is about 20 "C. In the Nordic countries prestressed structures are often stored outside at low ambient temperature at very early ages. How does the early cold storing of the concrete

affect its creep? Is it possible to use a high stress/strength level at for example -20 "C? The sensitivity of ambient temperature was an interesting problem to investigate.

10 Dimensional effect on creep and shrinkage

The dimension of the specimen does not affect basic creep, i.e. creep in HPC with sealed curing. Autogenous shrinkage is also independent of size. However, under drying conditions, there exists a substantial effect of the size of the structure on the development of creep and shrinkage, since those properties in turn are dependent on moisture movements in the structure. In HPC a great part of creep and shrinkage probably takes place owing to self-desiccation when the specimen is sealed.

2.11 Field studies

It is important for the study to confirm the laboratory results by field studies of concrete, to see if the observations in the field coincide with the results that are obtained in the laboratory. Prestressed concrete is a suitable type of construction to study since the creep rate is expected to be high, especially at early ages.

2.12 Prediction of creep and shrinkage

Sakata (1993), Figure 2.1, compared the calculated creep coefficient according to ACI-209 on the basis of the measured creep coefficient for 104 beams. In most cases the measured creep coefficient is larger than the predicted creep coefficient. In California, USA, **Scordelis** (1991, **1993)**, the Parrot's Ferry Bridge (394 m) obtained ≈ 0.8 m larger centre span (195m) sag after 25 years compared with the design based on modern codes. In Sweden the Tjorn bridges after 25 years had about 0.5 m larger deflection than foreseen, which required extraordinary measures to stabilise the structures. Structures are often subjected to environmental effects that do not exist in laboratory tests. Examples of such effects are temperature cycling, **Shkoukani and Walraven (1993)**, external moisture, **Miiller and Pristl (1993)**, cycling loading and creep after heat curing (or early freezing of the concrete). The question is whether or not HPC exhibits the same sensitivity to these effects as NSC. This question is to be investigated. **Bazant** (1995) presented a new model B_3 to estimate creep and shrinkage of concrete. In **Figure** 2.2 typical creep and shrinkage curves are shown versus logarithmic time. After justification and refinements, **Bazant and Baweja (1995)**, the new model fitted experimental data better than ACI and CEB models. The following symbols are used in Figure 2.2:

t	time, representing the age of the concrete (days)
t'	time, representing the age of the concrete (days), at loading
t_0	time, representing the age of the concrete (days), at start of drying
J(t,t′)	strain at time t caused by an uniaxial stress applied at age t' (millionths/psi)

2. PROBLEMS RELATED TO CREEP OF CONCRETE

2.1 General

Creep and shrinkage are two major problems to be considered when using concrete. These problems are especially pronounced when the concrete is used in prestressed structures. When prestressing is done at one side of the structure, the result is often a bent element caused by creep due to the prestressing. The creep and shrinkage influence the properties of the young concrete as well as the long-term behaviour of the concrete, as regards deformations, stability and durability. One of the great advantages of HPC seems to be low creep and shrinkage compared with NSC, **Penttala and Hayrinen** (1992). **Nielsen** (1972) gives an interesting review of the factors affecting the long-term deformations of concrete.

2.2 Causal relationship

The fundamental cause of creep is still unknown. The dominant opinion is that creep is related to moisture movements in the concrete due to the imposed loading on the concrete. Moisture movement in the gel of HPC is another probable cause of creep. At low imposed loading the HPC shrinks as long as the self-desiccation continues. When the cement is hydrated by the mixing water in the HPC, the hydration causes a 25% chemical shrinkage of the volume of the water, **Powers and Brownyard (1946-1948).** With sealed curing the chemical shrinkage creates an air-filled volume ratio in the gel of about 1.5%, **Persson (1993A)**, fairly independent of the water-cement ratio of the concrete. As the hydration ceases at a low internal relative humidity in a sealed-cured HPC, the autogenous shrinkage also ceases. With drying creep the surface of the concrete dries out while the interior of the concrete still contains an excess of moisture compared to the ambient conditions. Most probably micro-cracking occurs in the surface and causes the cracking due to shrinkage, **Sicard** (1993). When the stress is applied to the concrete, the distribution will be uneven throughout the concrete. The interior will obtain larger compressive stress than the surface, perhaps a reason why drying creep is larger than basic creep.

2.3 Early creep

Acker (1993) pointed out the importance of new experimental approaches. Nitrogen accumulators and electronic servo controls make it possible to apply the loading instantaneously to allow for fine separation of the instantaneous and the delayed strains. A quasi-instantaneously applied creep loading would probably be a way to separate the viscous and the plastic creep from the elastic deformation. **Evans** (1958) carried out tests in an testing machine working with compressed air. He

managed to apply the loading within 0.005 s. However, according to **Evans (1958)** the full loading seems to be applied within 0.02 s. **Bazant (1995)** stated that the static modulus of deformation normally was obtained at a loading time of about 0.01 days, i.e. about 860 s. However the dynamic modulus is possible to obtain after about 10^{-9} day (0.001 s) of loading. **Bazant (1995)** also observed that the short-term creep curves for various ages at loading all meet at the same point as the time of loading approaches zero, independent of the age of the concrete. **Schwesinger (1996)** used extremely accurate equipment with nitrogen accumulators and electronic servo controls in order to study the long-term and short-term mechanical, thermal and hygral properties of concrete.

2.4 Creep during hydration

Emborg (1989) studied creep of concrete during hydration in order to separate the viscous elastic and viscous plastic deformations. **Lokhorst and van Breugel (1993)** presented an interesting model to describe the creep during hydration by inserting bars. As the hydration proceeds, more and more bars appear in the rheological model. The later bars applied will then be fiee of stress. It would be of interest to study and further develop models for creep during hydration. Hydration occurs, for example, after a prestressed loading is applied in many prefabricated structures, such as beams and slabs. Creep during hydration also occurs when the moulds are removed from self-desiccating slabs at early ages, perhaps causing deformation problems. **Sellevold (1958)** measured the flexural recovery of small beams of cement paste and also (parallel) the dynamic modulus of elasticity on the beams.

2.5 High stress/strength ratio (load level)

At high load level ($\sigma/f_c \approx 0.6$) the creep increases compared with normal stresslstrength level ($\sigma/f_c \approx 0.3$). With drying creep the load level increases in the interior of the concrete compared with the surface since shrinkage occurs especially at the surface. High stresslstrength levels occur, for example, after a prestressed loading is transformed to the concrete structures, such as beams and slabs.

2.6 Elastic modulus, Poisson s ratio and dynamic modulus

The elastic modulus follows the square root of the compressive strength well for NSC. If this applies to HPC as well, the deformations of HPC structures will perhaps be problematic, as the elastic modulus does not follow the compressive strength. Owing to the more or less constant elastic modulus related to the compressive strength, perhaps it will be difficult to use HPC, for example, for beams. The deformations perhaps will be too large. One way to diminish the deformations due to the disadvantage of the elastic modulus is perhaps to optimise the section of a beam, i.e. to diminish the width but to maintain the height of such

structures. The dead weight will also decrease in this way. Different types of aggregate may improve the elastic modulus for HPC. This has to be investigated further to fully exploit HPC. Another question of structural importance is the relationship between longitudinal and transversal deformation at loading: Poisson's ratio. Is Poisson's ratio like that for NSC or does it differ in a beneficial or harmful way? What is the influence of current strength on Poisson's ratio? Does it vary between loading and unloading, affecting for example the dynamic durability of HPC? These questions will be investigated before HPC can be used in structures.

2.7 Autogenous shrinkage and carbonation shrinkage

Autogenous shrinkage is deducted from the measured strain in order to obtain the basic creep. The autogenous shrinkage is due to the chemical shrinkage of the water when it is bound to the cement. In normal strength concrete, besides drying shrinkage, another type of shrinkage occurs, called carbonation shrinkage. During carbonation shrinkage the weight of the concrete specimen increases but the specimen is still decreasing in length. These three types of shrinkage will be investigated. HPC has a very low permeability. Does it show carbonation at all at a very low water-cement ratio? Do pozzolanic interaction limits exist in HPC, i.e. is the amount carbon hydroxide decreased at such low level due to the reaction with silica fume, that carbonation stops in HPC? Such effects will perhaps diminish the cover layer for the reinforcement.

2.8 Strength after long-term loading

During hydration of HPC there is too little water for the process to proceed to a fully hydrated gel. Large quantities of unhydrated cement appear in the gel. These unhydrated volumes of cement in the gel perhaps will affect the long-term strength of the material. Long-term high loading perhaps also will affect the strength of HPC, i.e. lower the strength of HPC subjected to sustained loading compared with the strength of an unloaded specimen. This may be studied on unloaded cylinders used in the studies of shrinkage and on cylinders used in the long-term creep tests.

2.9 Creep at different temperatures

It is generally known that the creep rate for NSC increases with the temperature. The reason for this is perhaps that the internal relative humidity also increases with the temperature in the concrete, **Nilsson (1987)**, **Persson (1995A)**. Does this also apply to HPC? It also is of great interest to study the creep of concrete at lower temperatures than the normal temperature in the laboratory, which is about 20 "C. In the Nordic countries prestressed structures are often stored outside at low ambient temperature at very early ages. How does the early cold storing of the concrete affect its creep? Is it possible to use a high stress/strength level at for example -20

°C? The sensitivity of ambient temperature was an interesting problem to investigate.

2.10 Dimensional effect on creep and shrinkage

The dimension of the specimen does not affect basic creep, i.e. creep in HPC with sealed curing. Autogenous shrinkage is also independent of size. However, under drying conditions, there exists a substantial effect of the size of the structure on the development of creep and shrinkage, since those properties in turn are dependent on moisture movements in the structure. In HPC a great part of creep and shrinkage probably takes place owing to self-desiccation when the specimen is sealed.

2.11 Field studies

It is important for the study to confirm the laboratory results by field studies of concrete, to see if the observations in the field coincide with the results that are obtained in the laboratory. Prestressed concrete is a suitable type of construction to study since the creep rate is expected to be high, especially at early ages.

2.12 Prediction of creep and shrinkage

Sakata (1993), Figure 2.1, compared the calculated creep coefficient according to ACI-209 on the basis of the measured creep coefficient for 104 beams made of NSC. In most cases the measured creep coefficient is larger than the predicted creep coefficient. In California, USA, **Scordelis (1991, 1993)**, the Parrot's Ferry Bridge (394 m) obtained ≈ 0.8 m larger centre span (195m) sag after 25 years compared with the design based on modem codes. In Sweden the Tjörn bridges after 25 years had about 0.5 m larger deflection than foreseen, which required extraordinary measures to stabilise the structures. Structures are often subjected to environmental effects that do not exist in laboratory tests. Examples of such effects are temperature cycling, **Shkoukani and Walraven (1993)**, external moisture, **Miiller and Pristl (1993)**, cycling loading and creep after heat curing (or early freezing of the concrete). The question is whether or not HPC exhibits the same sensitivity to these effects as NSC. This question is to be investigated. **Bazant** (1995) presented a new model B_3 to estimate creep and shrinkage of concrete. In **Figure 2.2** typical creep and shrinkage curves are shown versus logarithmic time. After justification and refmements, **Bazant and Baweja (1995)**, the new model fitted experimental data better than ACI and CEB models. The following symbols are used in Figure 2.2:

h	ambient relative humidity (%)
t	time, representing the age of the concrete (days)
t'	time, representing the age of the concrete (days), at loading
t_0	time, representing the age of the concrete (days), at start of drying
J(t,t′)	strain at time t caused by an uniaxial stress applied at age t' (millionths/psi)

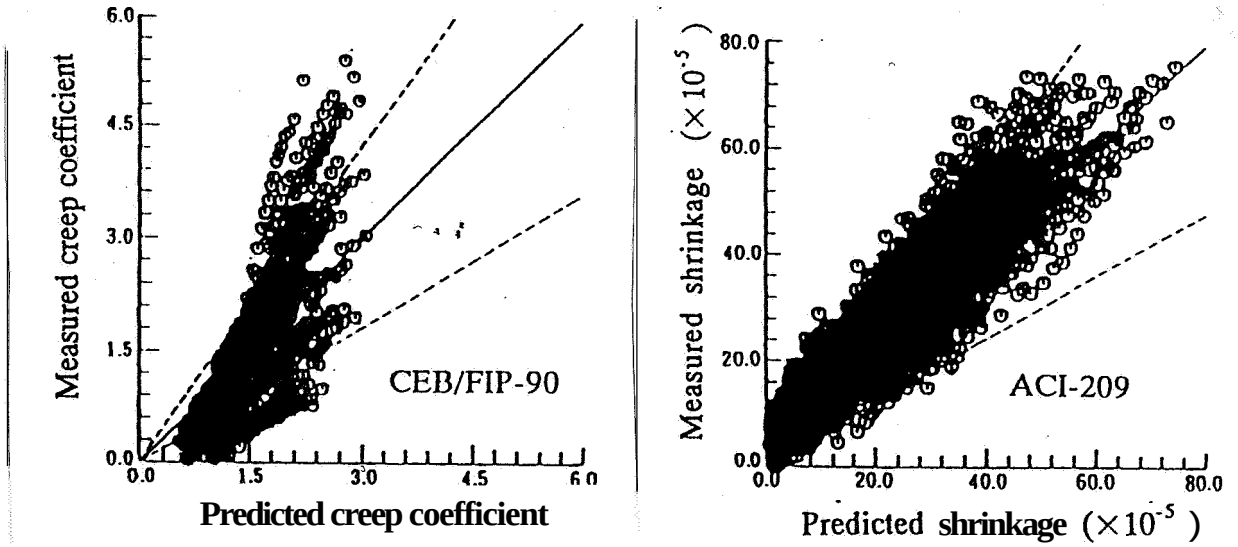

Figure 2.1 – Measured and predicted creep and shrinkage, Sakata (1993).

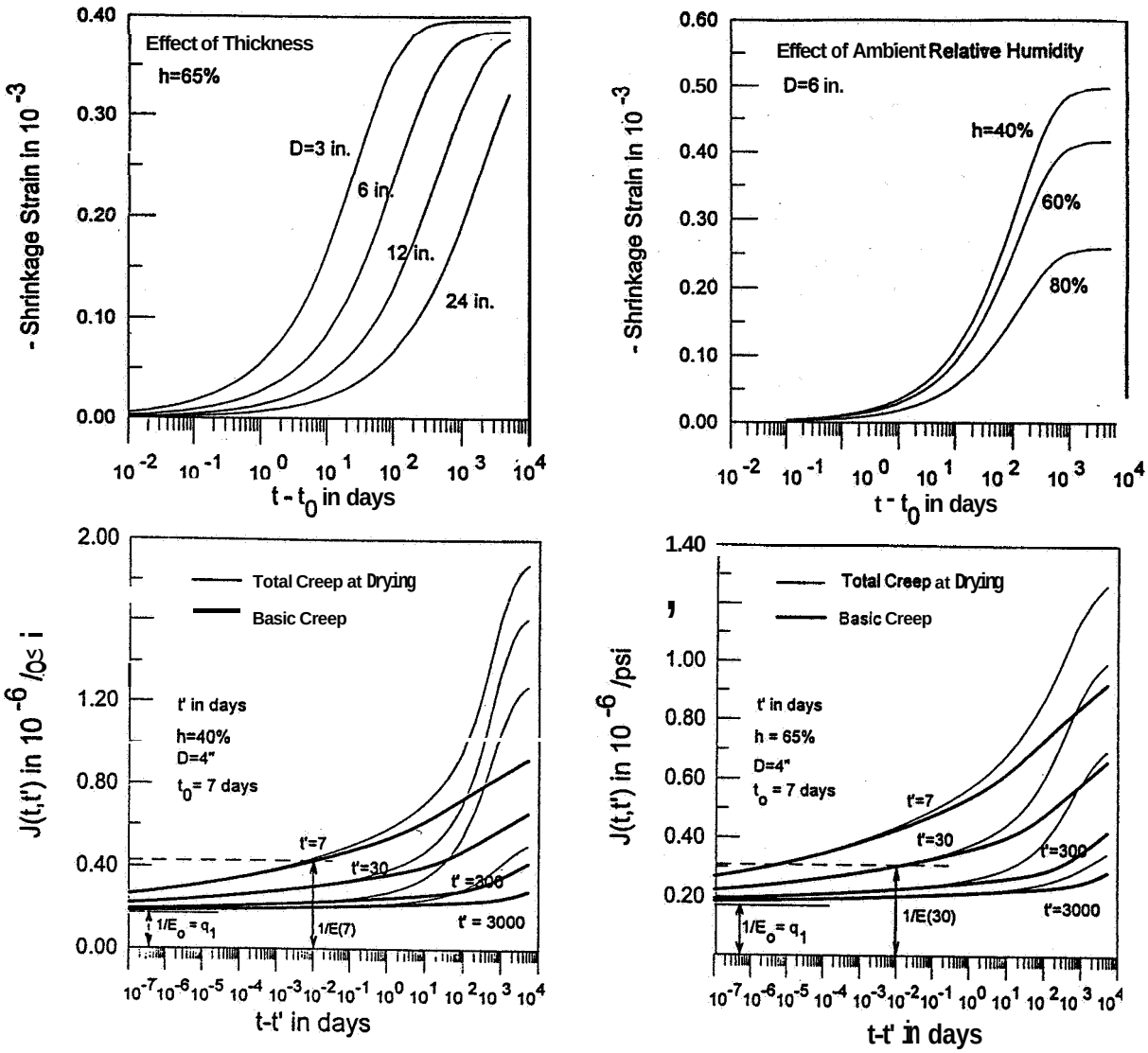

Figure 2.2 - Typical creep and shrinkage curves, model B,, Bazant (1995).

3. OBJECTIVES, CONDITIONS AND GENERAL LAYOUT OF THE STUDY

3.1 Objectives

The present study considers some of the range of problems described in Section 2:

- To ascertain creep and shrinkage of HPC with w/c varying between 0.25 and 0.38. The effect of air-entrainment and of amount and type of silica fume additive was to be ascertained at one water-cement ratio only.
- To ascertain the amount of elastic deformation, plastic and viscous sealed or drying creep of HPC by studying both well-hardened concrete and concrete during hydration. At 28 days HPC is well-cured and the compliance, J(t,28), is linear elastic. At 2 days the specific deformations of HPC are partly plastic, J(t,2). The specific plastic and viscous deformation at 2 days could be read:

$$J_{pl}(2,2) \approx J(2,2) - J(2,28) \qquad (3.1)$$

The viscous elastic part of the compliance could (depending on the age of the concrete) be separated after unloading of HPC, cp. **Figure 1.1:**

$$J_v(t,t') \approx J(t+\Delta t,t') - J(t,t') \qquad (3.2)$$

- To ascertain the effect of maturity on creep of HPC by studying both well hardened concrete and concrete during hydration. To obtain a relationship between deformation, ε, and strength, f_c, according to:

$$d\varepsilon/dt \approx f(w/c, \text{ and so on}) \cdot df_c/dt \qquad (3.3)$$

$d\varepsilon/dt$	denotes the creep rate
df_c/dt	denotes the strength growth rate.
f(w/c, and so on)	denotes a function dependent on the mix design (on w/c, on air-entrainment and type and amount of silica fume)

- To verify the effect of high stresslstrength ratio (load level) on the creep of HPC during hydration by studying HPC at high load. At two days' age and at a load level of 60% of the ultimate load (calculated on the basis of cube strength) the concrete compliance by certain is non-linear. The non-linear part of the compliance at 60% load level could be estimated over a period of about 3 days:

$$\Delta J_{60}(5,2) \approx J_{60}(5,2) - J_{30}(5,2) \qquad (3.4)$$

$\Delta J_{60}(5,2)$ denotes the additional compliance at 60% stress/cube strength level of HPC loaded at 2 days' age and unloaded at 5 days' age compared with creep at 30% load level calculated on the basis of cube strength

$J_{60}(5,2)$ denotes the 5-day compliance of HPC loaded at 2 days' age at 60% stress/strength ratio

$J_{30}(5,2)$ denotes the 5-day compliance of HPC loaded at 2 days' age at 30% stresslstrength ratio

- To ascertain a separation of autogenous, carbonation or drying shrinkage by studying HPC with w/c varying between 0.25 and 0.38 parallel with the weight losses and the internal relative humidity of the concrete. The shrinkage was to be studied for 5 years. The effect of air-entrainment and of amount and type of silica fume additive was to be ascertained at one w/c only. National concrete mix proportions were to be included in the study. To ascertain separation of different kinds of shrinkage by parallel studies of HPC made from the same batch.
- To ascertain the long-term compressive strength of HPC with w/c varying between 0.25 and 0.38 by studying both well-hardened concrete and concrete during hydration. Before the comparison the specimens should be subjected to basic creep or drying creep for at least 2 years. The strength of HPC subjected to load-term loading was to be compared with the strength of HPC without loading.
- To ascertain the effect of moisture on the deformation modulus (at loading), Poisson's ratio and the elastic modulus (at unloading, Figure 1.1) of HPC with wlc varying between 0.25 and 0.38, by studying both well-hardened concrete and concrete during hydration. Parallel studies to be performed on the internal relative humidity of the HPC. Studies of the moduli and the internal relative humidity to be performed on sealed and air-cured specimens.
- To ascertain the effect of hydration on the relationship between the deformation and elastic moduli and the elastic dynamic modulus. The dynamic modulus of elasticity to be obtained for drying creep only.
- To ascertain in particular the basic creep rate at the temperatures -16 "C, -1 "C, +20 "C, +32 "C, +38 "C and + 58 "C for HPC initially cured at 48 "C for 16 h (heat-cured in similar conditions to those existing in a pre-fabrication concrete element plant). The results to be compared with results of creep of HPC cured at 20 "C. One type of HPC was to be studied at temperatures different from 20 "C.
- To ascertain the dimensional effect on both basic and drying creep by parallel studies with larger specimens. The studies were to be performed at different ages of HPC at the start of the loading. To ascertain the laboratory results in the field by studies of basic and drying creep, autogenous and drying shrinkage at pre-fabrication concrete plants on HPC similar to the types that were used in the laboratory studies. The creep studies were to be performed for at least 1 month up to 7 months. The studies of shrinkage were performed for more than 1 year.
- To propose general relationships between maturity and creep and shrinkage of HPC. Basic and drying creep was to be included in the relationships. Short-term and long-term creep was to be included in the relationships. Young and mature

concrete was to be included in the relationships. Autogenous, carbonation and drying shrinkage of HPC was to be predicted. The effect of temperature on the short-term basic creep was to be formulated. Finally, prediction was to be done of the dimensional effect on creep and shrinkage based on laboratory studies on larger specimens and on field studies on beams.

3.2 Conditions

Elastic deformation, plastic and viscous creep:

The HPC was either 1, 2 or 28 day old at the start of the studies (20 °C ambient temperature). The unloading was performed 66 hours after the loading or at more than 3 years' age. The viscous creep was studied for another 400 hours. Both basic and drying creep were studied.

Strength, creep during hydration and stress/strength ratio at loading:

The studies were limited to an age varying between 16 h and 2 years. Strength and degree of hydration were measured at 1, 2, 3, 4, 6, 28, 360 and at 720 days' age. Concretes of 1 and 2 days' age at loading were studied at 60% stresslcube strength ratio. At 2 or 28 days' age the loading level was limited to 30% stress/cube strength ratio. However, during the hydration the stresslstrength declined substantially.

Strength after long-term loading and shrinkage:

The long-term creep was limited to studies of basic creep and drying creep over at least 3 years. After the creep studies the strength of previous loaded HPC was compared with the strength of unloaded HPC specimens from studies of shrinkage. The studies started at 16 h age and were limited to 5 years. The weight of the specimen and the internal relative humidity were studied at 1, 2, 3, 4, 6, 28 days', 1, 2 and 4 years' age. Autogenous, carbonation, and drying shrinkage were all studied.

Size of specimen, materials, ambient climate, and so on:

The specimen size was limited to 55.5 mm in diameter and 300 mm in length or cylinders 100 mm in diameter and 500 mm in length. Other dimensions of the specimens applied in the field tests. Most of the studies of compressive strength were performed for 100-mm cubes. The measurement points for deformation measurements were cast in the cylinders. The depth of the cast-in items was 20 mm. The sealed cured specimens were insulated with 2 mm vulcanised butyl rubber clothing. Aggregates of crushed quartzite and natural sand of gneiss apply for the mix proportions. Low-alkali Portland cement was used. With the exception of the national mix proportions, granulated silica fume was used. The air-entrainment varied between 1 and 5% calculated on the basis of the total volume of the HPC.

Superplasticiser based on melamine formaldehyde was used for all the mix proportions. The national mix proportions recommend silica fume slurry, crushed granite and natural sand based on granite. Short-term studies were performed at 20 °C and sealed conditions or at RH = 55%. The long-term studies were performed in moisture-insulated conditions (basic creep) or at RH 55% ambient relative humidity. Basic creep for one HPC was studied at five other temperatures.

3.3 General layout of the work

Short-term studies performed in the MTS machine:

Short-term creep studies were performed in an MTS-machine with high accuracy. From these studies separation of elastic deformation fiom plastic and viscous creep was possible. The deformation and the elastic moduli and the early creep rate were obtained fiom these studies, Figures **1.1, 3.1** and **3.2.** Separate LVDT displacement and gauging transducers collecting data measured the deformations by a separate computer. The full level of loading was applied within ≈ 0.01 s. At loading and unloading the measurements were performed about 1000 times per second including 3 longitudinal LVDTs and one LVDT placed transversally to the HPC cylinder.

Long-term studies performed in spring loading devices:

Long-term strength tests, plastic and viscous creep tests at 3 years' age were performed on **HPC** cylinders in traditional mechanical spring loading devices. These studies also provided results on the long-term creep rate and on the elastic modulus. The specified loading of the springs was applied at all times of measurement. The loading of the spring device was applied simultaneously to the loading in the MTS machine on a **HPC** specimen fabricated from the same batch of HPC. Thus the studies of creep performed by quasi-instantaneous loading in the MTS-machine were prolonged by studies of creep in the traditional spring devices, Figures **1.1, 3.1** and **3.2.** The cylinders were weighed before and after the studies.

Long-term studies of shrinkage and strength on 55-mm cylinders:

Studies of shrinkage were performed on horizontal (lying) cylinders. The cylinders were turned a third of a full turn at each measurement to avoid bending effects. The cylinder was continuously weighed. All the short-term and long-term creep studies were performed on cylinders (diameter: 55.5 mm, length: 300 mm). Autogenous shrinkage, carbonation shrinkage and drying shrinkage were studied for the same type of cylinders. More than 30 tests of compressive strength and hydration for the drying creep studies were performed on cylinders (diameter: 55.5 mm, length: 200 mm). Finally, the studies of long-term strength were performed on cylinders previously used in the tests of long-term creep and shrinkage.

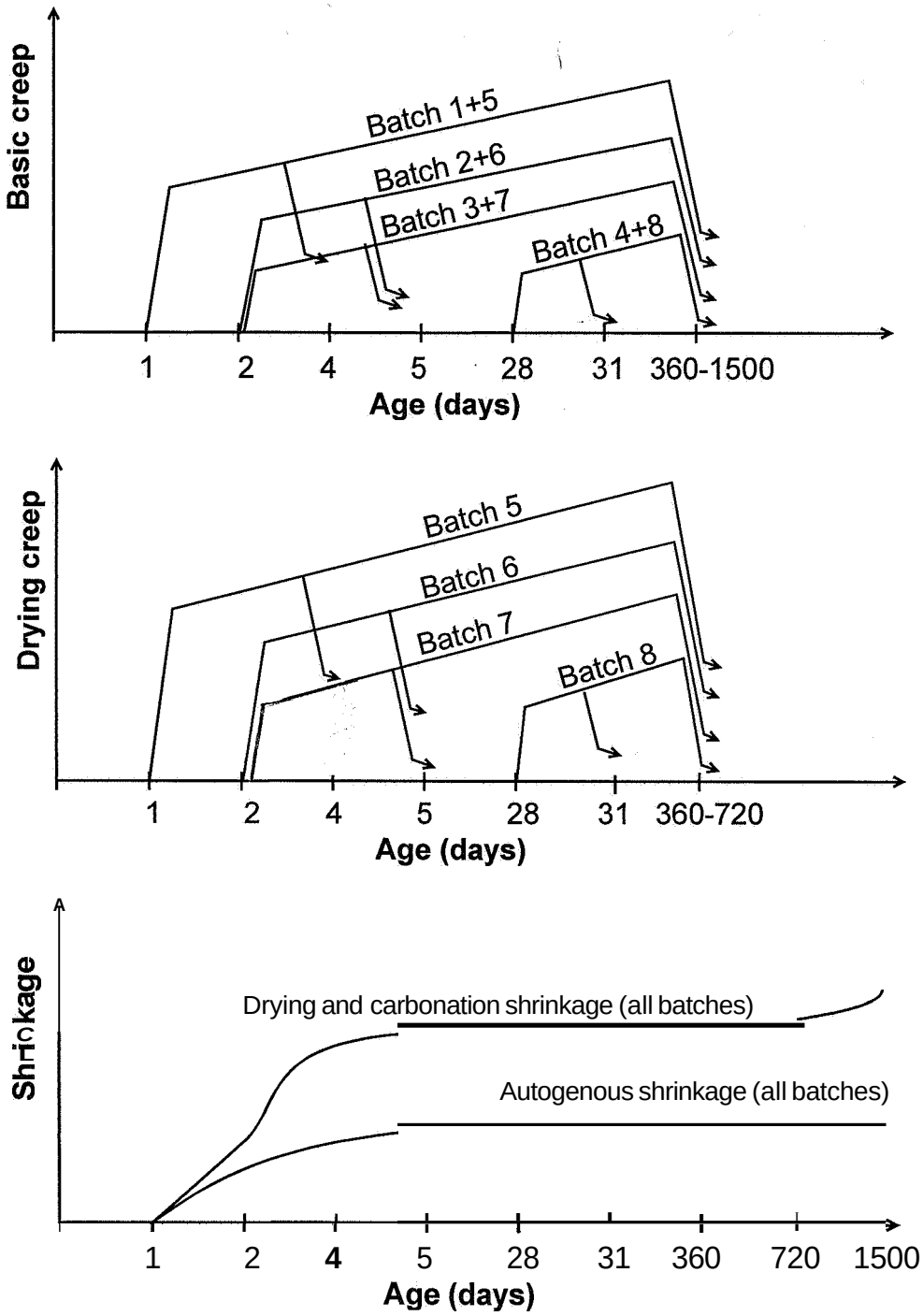

Figure 3.1 - Summary of deformations that were measured for each mix of HPC.

Strength, hydration, internal relative humidity on cubes and ambient climate:

Strength, hydration and internal relative humidity were studied on 100-mm cubes. The fragments from the strength-tested cubes were used to measure the internal relative humidity and the degree of hydration of the concretes. The specified climate was supplied by an external air-conditioning. The ambient climate for the short-term test of drying creep was supplied by a separate climate aggregate connected to the MTS machine by insulated pipes and by a high-speed air fan.

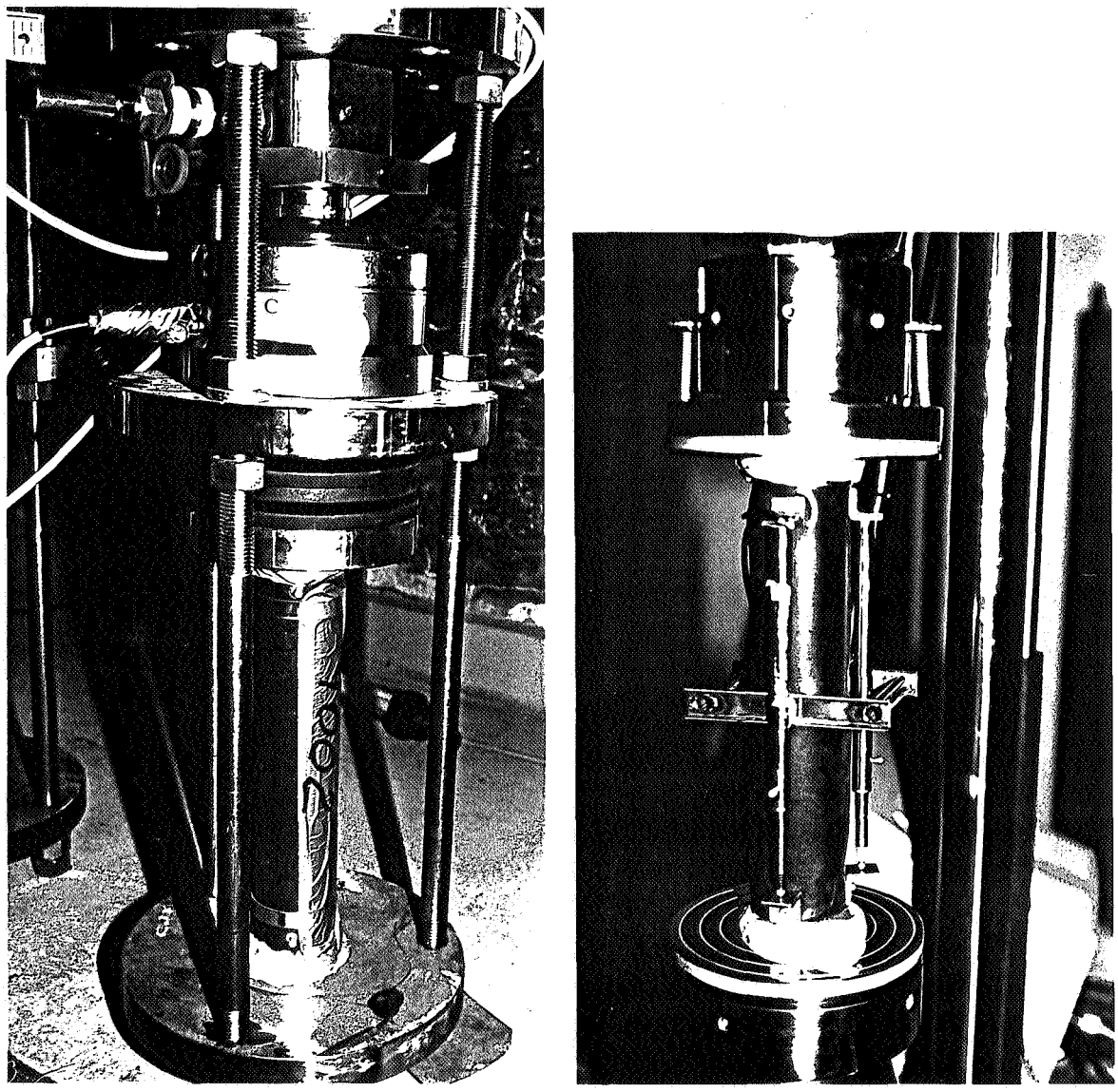

Figure 3.2 - Specimens in a spring-loading device (to the left) and in the MTS machine (to the right), **Persson (1995A)**. Measurement points (to the left) and LVDTs (to the right). (Hinges existed between the plate springs and between the load cell and the hydraulic jack in the spring-loading device and furthermore above the upper plate in the MTS machine.)

Dimensional effect on creep and shrinkage; field studies:

Parallel studies on larger cylinders than these used in the main laboratory tests (100 mm in diameter and 500 mm in length compared with 55.5 mm in diameter and 300 mm in length used in the laboratory tests). Two types of concrete were studied with the larger cylinders for about 1 year. The HPCs in the dimensional studies were sealed cured or drying. Twenty-seven prestressed beams, which were produced in a normal fabrication of concrete elements in two field plants, were studied. The force from the strands was transferred to the concrete after curing periods varying between 18 hours and 4 days. The creep of the beams was studied for 7 months.

4. MATERIALS, PREPARATION OF SPECIMENS, CHRONOLOGY AND NUMBER OF SPECIMENS

4.1 Materials

HPCs of 6 standard mix proportions and 2 national mix proportions were used for the full programme in the laboratory tests. Together with the modified national mix proportions, 90 concrete batches of HPC were cast in the laboratory to make the specimens. The field tests were performed on HPC fabricated in 20 different batches.

Aggregates:

The main characteristics of the aggregates used in the laboratory are given in **Table** 4.1, **Hassanzadeh** (1994). **Appendix** 1 gives the sieve curves for the aggregates. Some modifications of the aggregates were made during the field studies. The maximum size of the aggregate (16 mm) was larger than 1/5 of the minimum size of the specimen as required according to guidelines, **Bazant and Carol** (1993). However, at the time of batching the specimen size was required to be at least 3 times the maximum aggregate, i.e. 48 mm, to avoid effects of the surface layer of the specimen on the properties of the concrete. In small specimens with relatively large aggregate size, a concentration of aggregate perhaps appears in the centre of the specimen. More cement paste perhaps occurs at the surface of the specimen. On the other hand, problems with too large temperature rise, due to heat of hydration may occur when too a large diameter of specimen is chosen. A large specimen diameter also increases the required force in creep testing devices.

Cement:

Only a low-alkali Portland cement, Degerhamn Standard, was used. To obtain a High-Performance Concrete, it was necessary to use a low-alkali cement, **Persson (1992A)**. In the field studies a modified (further ground) Portland cement, Degerhamn P400, was used. The chemical composition and the main characteristics of cements are given in **Table** 4.2. The granulometry of the cements is given in **Appendix 1.** Some additional modifications of the cement was performed during the field studies.

Silica fume:

For the standard mix proportions a granulated silica fume was used (fmeness: 17.5 m^2/g, ignition losses 2.3% by weight). For the national mix proportions and the field studies a micro silica fume slurry was used (fmeness: *22.5* m^2/g, ignition losses: 1.9% by weight).

Table 4.1 - Characteristics of the aggregates.

Material/characteristics	Modulus of elasticity	Compressive strength	Split tensile strength	Ignition losses
Quartzite sandstone, Hardeberga	60 GPa	330 MPa	15 MPa	0.3%
Natural sand, Åstorp				0.8%
Granite, Norrköping	61 GPa	150 MPa	10 MPa	1.7%
Pea gravel, Toresta				1.6%
Crushed sand, Bålsta	59 GPa	230 MPa	14 MPa	2%

Table 4.2 - Chemical composition and the main characteristics of the cements.

Low-alkali cement Degerhamn	Standard	P 400
X-ray fluorescence analysis (%):		
CaO	64.9	64.0
SiO_2	22.2	22.0
Al_2O_3	3.36	3.71
Fe_2O_3	4.78	4.80
MgO	0.91	0.91
ICP-analysis (Oh):		
K_2O	0.56	0.55
Na_2O	0.04	0.04
LECO apparatus (%):		
Ignition losses at 950 °C	0.63	0.63
so3	2.00	2.22
Physical properties:		
Specific surface according to Blaine (m^2/kg)	302	404
Density (kg/m^3)	3220	3210
Setting time:		
Vicat (minutes)	135	95
Water (%)	26.0	26.8
Standard test (prisms 40x40x160 mm, MPa):		
1 day	11.0	16.2
2 days	20.2	25.4
7 days	35.8	41.3
28 days	52.6	59.5

Superplasticiser and air-entrainment agent:

For all mix proportions superplasticiser based on melamine formaldehyde applies. Some modification of the superplasticiser was made during the field studies.
For the mix proportions that contained air-entrainment an air-entrainment agent was added, based on vinsole resin.

4.2 Preparation of specimen

Materials and mixing:

The fabrication of the specimens was performed in the following way:

- All the material (even the water) had a temperature of 22 "C.
- The aggregates were stored in rubber barrels to maintain moisture content of about 4% by weight. The mixing of HPC is performed more efficiently when aggregate with moisture is used, **Persson (1992A)**.
- The moisture content was measured before each mixing. compensation for the moisture content was made when adding the remaining mixing water (some mixing water also appears together with the material and the superplasticiser).
- The mixing of the HPC took placed in a 40-1 compulsive mixer.
- At first all material except for the silica slurry, if *any*, and the superplasticiser was mixed for ½ minute.
- Then the silica fume slurry, if any, and the superplasticiser were added and the mixing continued for another 2% minutes.
- Finally the workability and the air-content of the HPC were obtained.

Moulds:

The circular moulds had an inner diameter of 55.5 mm and a length of 300 mm or 200 mm. Six cast-in items were placed 25 mm fiom the ends of the mould and 2 items on opposite sides the middle of the mould. 3-mm bolts through the steel mould fixed the items. The cast-in items had a diameter of 8 mm and a depth of 20 mm. They were provided with flanges and edged to avoid movement in the concrete. Thermo couples were cast in one cube and two cylinders of each batch.

Casting:

After measurement of air-entrainment and density, the moulds were filled up under vibration. The cylinders were levelled off at the upper end. A 10-mm steel plate was fixed and vibrated to the end of the cylinder horizontally (lying down). The ends of the cylinder were very smooth and no grinding was necessary. All specimens were placed in a rubber container to avoid losses of moisture. The cubes were placed together with the cylinders to avoid temperature differences in between.

Early curing and demoulding:

After casting and placing in the rubber container the specimens were stored in a 20 ±0.5 °C climate chamber. Typical internal temperature developments are shown in **Appendices 3-4.** The temperature drop was 1.5 "C initially. After 16 hours of curing the bolts were loosened fiom the cast-in items and the moulds removed.

Rubber insulation of basic creep specimen:

A 2-mm vulcanised butyl rubber cloth insulated the basic creep specimens (both cylinders and cubes). Butyl rubber cloths were placed at the ends of the cylinder and removed right before testing. Clamp hoses were placed at the end of the cylinders to avoid any moisture losses. The specimens were still stored in a 20 "C climate chamber. However, some temperature movements took place in the concrete due to hydration, **Appendix 3.** The maximum temperature was 24 "C about 15 hours after casting. After 30 hours the temperature varied between 21 and 20 "C.

Drying creep specimen:

After demoulding the specimen was first weighed and measured. The specimen was then stored in a climate room, at an ambient relative humidity, RH 55% and a temperature of 20 "C. Due to desiccation the temperature immediately dropped in the specimen, **Appendix 4.**

4.3 Chronology mber of imens d suppliers of mater :

Table 4.3 lists the suppliers of the laboratory material. **Table 4.4** shows the chronology of the study. **Table 4.5** shows the estimated number of specimens.

Table 4.3 - List of material suppliers

Material	Supplier
Quartzite sandstone 4-8, 8-12, 12-16 mm	Sydsten AB, Hardeberga
Natural sand, Åstorp 0-8 mm	Skånska Makadam AB, Åstorp
Granite, Norrköping 12-16 mm	NCC Ballast AB, Norrköping
Pea gravel, Toresta 8-16 mm	Skanska Betong AB, Stockholm
Natural sand, Bålsta 0-8 mm	Skanska Betong AB, Stockholm
Natural sand (filler) no 7	Baskarp AB, Baskarp
Veddige 0-8 mm	Bröderna Larssons AB
Veddige 11-18 mm	Bröderna Larssons AB
Cement, Degerhamn Anläggning Standard	Cementa AB
Cement, Degerhamn Anläggning P400	Cementa AB
Granulated Silica Fume, Micropoz	Cementa AB
Silica Fume Slurry, Elkem Micro Silica Fume	Elkem Materials A/S
Air-Entraining Agent, Cementa 88L (Vinsole Resin)	Cementa AB
Superplasticiser, Cementa Flyt 92 (Melamine Formaldehyde)	Cementa AB
Superplasticiser, Peramin F (Melamine Formaldehyde)	Perstorp AB

Table 4.4 - Chronology for the study

Year	1991	1992	1993	1994	1995	1996	1997	1998
Autogenous shrinkage	X	XXXX	XXXX	XXXX	XXXX	XXXX	XXXX	X
Basic creep (short-term)	X	XXXX	X					
Carbonation shrinkage			XXX	XXXX	XXXX	XXXX	XXXX	X
Compressive strength	X	XXXX	XXXX	XXXX	XXXX	XXXX	XXXX	X
Creep at varying temperature				X	X			
Dimensional effect						X	XXXX	
Drying creep (short-term)			XXX	XX				
Drying shrinkage			XXX	XXXX	XXXX	XXXX	XXXX	X
Dynamic elastic modulus			XXX	XX				
Field studies					XXXX	XX		
Hydration	X	XXXX	XXXX	XXXX	XXXX	XXXX		
Internal relative humidity	X	XXXX	XXXX	XXXX	XXXX	XXXX		
Long-term basic creep,	X	XXXX	XXXX	XXXX	XXXX	XXXX		
Long-term drying creep			XXX	XXXX	XXXX	XXXX		
Long-term stability							X	X
Plastic creep	X	XXXX	XXXX	XXXX	XXXX	XXXX		
Quasi-instantaneous loading	X	XXXX	XXXX					
Viscous creep	X	XXXX	XXXX	XXXX	XXXX	XXXX		

Table 4.5 – Estimated number of specimens.

Type of specimen	Cube 100 mm	Cylinder 0 5 5 mm	Cylinder 0 1 0 0 mm	Hat beam	Square beam
Autogenous shrinkage		70	4[6]		
Basic creep (short-term)		38			
Carbonation shrinkage		32			
Compressive strength	900	32			
Creep at varying temperature		6			
Dimensional effect			20		
Drying creep (short-term)		32			
Drying shrinkage		32[2]			
Dynamic elastic modulus		32			
Field studies				7	20
Hydration	900[1]	32[1]			
Internal relative humidity	900[1]	32[1]			
Long-term basic creep		58	8[6]		
Long-term drying creep		32	8[6]		
Long-term stability		90[3]			
Quasi-instantaneous loading		70[4]			
Plastic creep		160[5]			
Viscous creep		160[5]			

1) The same specimen was used for strength studies
2) The same specimen was used for studies of carbonation shrinkage
3) Specimens from studies of long-term creep and shrinkage
4) Specimens from short-term studies
5) Specimens from studies of long-term creep
6) Dimensional studies

5. PRINCIPAL PROPERTIES OF STUDIED CONCRETES

5.1 Concrete mix proportions

The mix proportions were based on previous experiences of the optimal proportions of HPC, **Persson (1992A)** and on pre-tests on the workability of HPC, **Persson (1992B, C, D), Persson (1993B)**. The mix proportions of the concretes were principally chosen in order to obtain a semi-logarithmic grading curve of all accumulated material passing through. This grading curve of the materials in the fresh concrete allows for a minimum requirement of cement, water and superplasticiser in the concrete, **Persson (1995B)**. **Table 5.1** gives concrete mix proportions and so on (kg/m^3 dry material, etcetera). **Appendix** 2 gives the grading curves in the mix proportions.

Table 5.1 - Mix proportions and so on (kg/m^3 dry material, and so on)

Material /Mix number	**1**	**1(3)**	**2**	**3**	**4**	**5**	**6**	**7**	**8**
Quartzite, 8-11 mm	460	440							
Quartzite, 11-16 mm	460	440	965	910		1010	985		1065
Sand, Åstorp 0-8 mm	800	1780	820	790		750	755		690
Granite, Norrköping 11-16								1030	
Gravel, Toresta 8-16 mm					1095				
Natural sand, Bålsta 0-8					780			780	
Cement, Degerhamn Std	430	410	440	445	455	495	530	490	545
Granulated silica fume	21	21	44	45		50	51		55
Silica fume slurry					23			49	
Air-entraining agent	0.02	0.04		0.02					
Superplasticiser	2.6	2.8	4.5	3.8	5.1	4.6	7.6	8.6	10.8
Water-cement ratio	0.38	0.38	0.37	0.37	0.33	0.31	0.30	0.30	0.25
Air-content (% by volume)	4.8	7.0	1.1	4.0	0.9	1.1	1.2	1.0	1.3
Aggregate content	0.74	0.74	0.73	0.72	0.75	0.71	0.70	0.72	0.70
Aggregate/cement ratio	4	4	4.1	3.8	4.1	3.6	3.3	3.7	3.2
Density (kg/m^3)	2335	2245	2440	2360	2510	2465	2480	2500	2490
Slump (mm)	140	140	160	170	45	200	130	45	45
28-d drying strength (MPa)	69	50	85	69	89	99	106	112	114
1-y drying strength (MPa)	70	54	89	76	97	109	112	121	125
3-y drying strength (MPa)	69		91		97		115	121	127
28-d sealed strength (MPa)	89	62	105	95	101	121	126	122	129
1-y sealed strength (MPa)	101	65	117	98	115	129	145	131	154
2-y sealed strength (MPa)	112				115			131	
3-y sealed strength (MPa)			123	102			141		145
4-y sealed strength (MPa)	102				113			129	

d= days' age, y= years' age (compressive strength observed for 100-mm cube)

5.2 Compressive strength

5.2.1 General

One of objectives of the study was to obtain a relationship between the creep rate and the rate of strength growth, cp. equation (3.3). It was essential to follow the compressive strength continuously for all concretes studied. Strength is defined as ultimate stress per unit of area. Among many other factors, the strength depends on the moisture conditions of the concrete. In Sweden the strength tests are often performed on drying specimens, while international tests are more often performed on wet specimens.

Many reports exist dealing with the drop of strength in concrete containing silica fume. Since silica fume is necessary to obtain an HPC with high strength, it is essential to define the curing conditions connected to these reports of strength drop. As pointed out by **Perraton** et al. **(1994)**, the major part of strength losses is due to differences of moisture within the specimens. When the specimens were pre-dried, no strength drop was observed **Perraton** et al. (1994).

To avoid these moisture effects it is necessary to cure the specimen under sealed conditions, Persson **(1992A)**. Such conditions exist when studying basic creep. However, with drying creep, the surface of the concrete will become prestressed. Initially the strength of drying concrete will then be measured larger than the property of the concrete, Atlassi (1993). However, a lower strength growth exists during drying conditions, especially for HPC, due to the low relative humidity, RH. The hydration was more or less inhibited at RH< 70%, **Norling Mjörnell (1994)**.

5.2.2 Previous studies of compressive strength

Persson **(1996A)** investigated compressive strength of more than 900 drilled cores from 8 concretes at 1, 3, 15 and 90 months' age. Half the number of concretes contained 10% silica fume. The diameter of the cores was 40 mm and the length 80 mm. Three ambient climates (20 "C) were studied: air curing, sealed curing and water curing. In moisture-sealed conditions (self-desiccation during sealed curing) relationship was found between the strength of the cores and the effective water-cement ratio, $(w/c)_{eff}$:

$$(w/c)_{eff} = w/(c+k_s \cdot s) \qquad (5.1)$$

w denotes the water content in the concrete (kglm^3)
c denotes the cement (kglm^3)
k, denotes the efficiency factor of silica fume related to compressive strength
s denotes the content of silica fume (kg/m^3)

The following equation expressed the strength efficiency factor of silica fume:

$$k_{sc} = 0.113 \cdot [4.44 - \ln(t)] \cdot (w/c)^{-0.056 \cdot [\ln(t)+35]} \quad \{1<t<90 \text{ months}; 0.24<w/c<0.48\} \qquad (5.2)$$

k_{sc} denotes the efficiency factor of silica fume related to compressive strength of sealed cylinders; 80 mm in length and 40 mm in diameter, equation (5.1)
t denotes age (months)

The efficiency factor was dependent on age and w/c. The efficiency factor of silica fume was astonishingly large at 28 days' age, especially in HPC with low w/c. However, the long-term effect of silica fume decreased to less than half at 450 days' age compared with the effect at 28 days' age. The strength increase of an HPC with silica fume was lower than the strength increase in concrete without silica fume, which explained the development of the efficiency factor.

5.2.3 Previous studies of split tensile strength

Split strength tests were performed, **Persson (1996A)**, on about 300 drilled cores of the concretes to obtain relationships between the compressive strength and the split tensile strength, f_{sp} at sealed curing (MPa):

$$f_{sp,s} = [0.281-0.0144\cdot\ln(t)]\cdot(f_c)^{0.744+0.0109\cdot\ln(t)} \{30< f_c <150 \text{ MPa}; 1<t<90 \text{ months}) \quad (5.3)$$

$$f_{sp} = [0.144+0.0084\cdot\ln(t)]\cdot(f_c)^{0.902-0.0165\cdot\ln(t)} \{30< f_c <150 \text{ MPa}; 1<t<90 \text{ months}) \quad (5.4)$$

f_c denotes the compressive strength (MPa)
f_{sp} denotes the split tensile strength (MPa)
In (t) denotes the natural logarithm of age, t (months)
s denotes 10% silica fume calculated on the basis of the cement content

The long-term split tensile strength decreased slightly compared with the compressive strength during sealed curing. With both air curing and water curing a significant decrease of the split tensile strength compared with the compressive strength was found after 450 days. No difference seemed to exist in the split tensile strength related to the compressive strength dependent on the content of silica fume in the concrete. The same type of materials were used in the concretes in equations (5.2) - (5.4) as reported in this study. No sign of decrease in strength was found during the sealed conditions that applied in equations (5.2) - (5.4).

5.2.4 Experimental procedure

After removing the butyl-rubber cloth, in the case of basic creep studies, the cube was measured and tested for compressive strength. The ultimate stress was applied at a rate of 1 MPa/s in a Seidner testing machine. Some tests of compressive strength with drying creep were performed on drying cylinders (55.5 mm in diameter and 200 mm in length). After the strength test the concrete fragments were used to obtain the internal relative humidity and the degree of hydration of the concrete.

5.2.5 Source of errors and accuracy

The testing machine was calibrated. The accurate strength perhaps would be 1 MPa higher, which is a small error. An eccentricity with placing the cube or the cylinder may have affected the test result. A special gauge was therefore used to centre the cube or the cylinder. The fault of eccentricity was less than 1 mm. The hourglass shape of fragments after testing the cube indicated a highly centric placing. At high strength a circular conical part of the cube remained after testing. The corners of the cube seemed to fail before the ultimate strength was reached. The cylinders obtained an inclined crack when they reached the ultimate strength.

Some tests of 1 and 2 year old concrete containing the national mix proportion exhibited an explosive failure when tested. The aggregate of the national mix proportions seemed more fragile than the aggregate of the resisting concretes. The testing machine was rigid enough since no explosion occurred when testing concretes from the standard mix proportions even at 160 MPa strength. The strength tests of cylinders gave an indication of the margin between the load in the creep tests and the ultimate load at failure of an identical cylinder.

5.2.6 Results

Figure 5.1 shows a typical development of strength versus time for HPC mix 6. Both air-curing and sealed curing is shown. **Figure 5.1** also shows the strength of cylinders. **Figure 5.2** provides the time-dependent development of strength with sealed curing. **Appendix 5** shows the strength development versus time of all HPCs tested. **Figure** 5.3 shows strength with air curing versus age for all HPCs studied. **Figure** 5.4 show the strength with air curing versus strength with sealed curing. **Figure 5.5** shows the strength of cylinders (55 mm in diameter, 200 mm in length) with air curing versus the strength of cubes (100x100 mm) in drying conditions.

5.2.7 Analysis

The effect of aggregate, silica fume, superplasticiser, air-entrainment etc., was estimated at constant w/c. As observed in the following equations, no effect of the type of aggregate, silica fume or superplasticiser was detected before 28 days' age:

$$f_{cB}=21.5\cdot k_a\cdot k_s\cdot[5.75+\ln(t)-11.5\cdot(w/c)] \quad \{0.8<t<28 \text{ days}\} \quad (5.5)$$

$$f_{cD}=30\cdot k_a\cdot k_s\cdot\{2.6+[1-1.2\cdot(w/c)]\cdot\ln(t)-3.9\cdot(w/c)\} \quad \{0.8<t<28 \text{ days}\} \quad (5.6)$$

f_{cB} denotes the strength with sealed curing (basic creep)
f_{cD} denotes the strength of HPC with air curing (drying creep)
k_a = 0.88 in concrete with 5% air-entrainment; k_a = 1 without air-entrainment
k_s = 0.77 in concretes 5% silica fume; k, = 1 in concrete with 10% silica fume
ln (t) denotes the natural logarithm of the age of the concrete {0.8<t<28 days)
w/c denotes the water-cement ratio

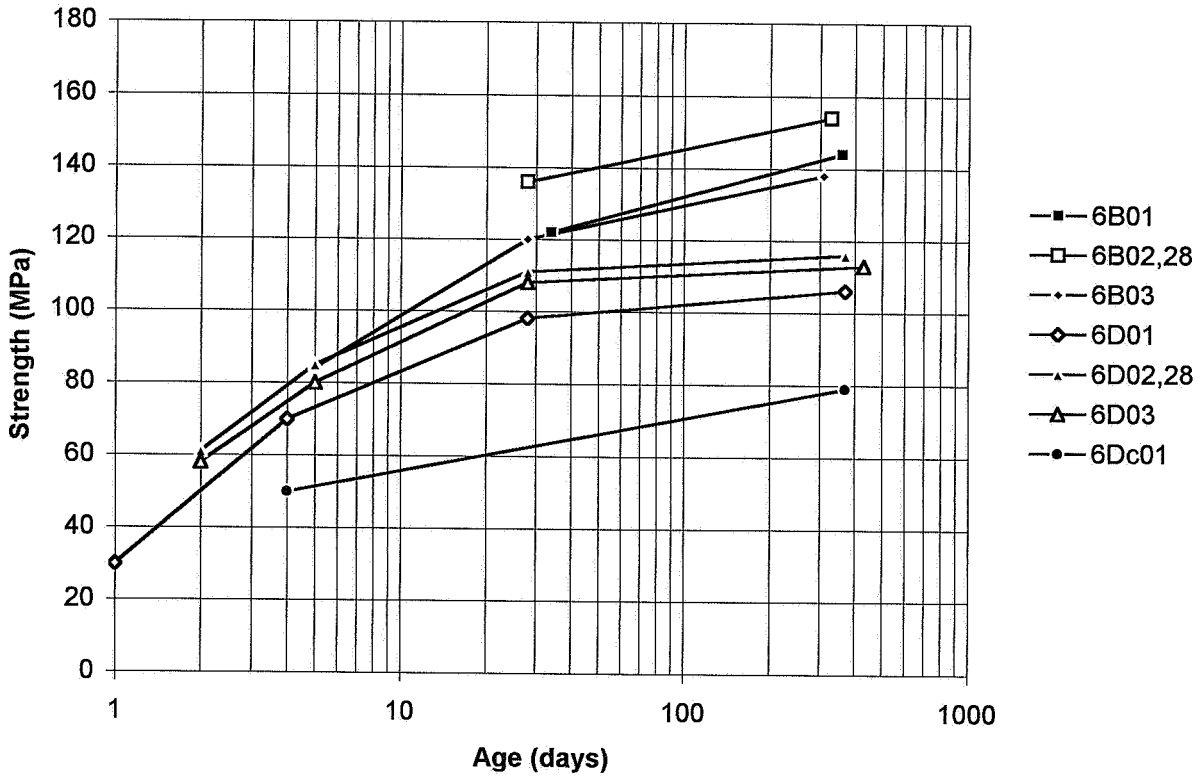

Figure 5.1 - Strength of mix *6* versus age. c= cylinder, B= sealed curing, D= air curing, 6= **HPC** mix, **Table 5.1,** 02= age at start of creep tests (days).

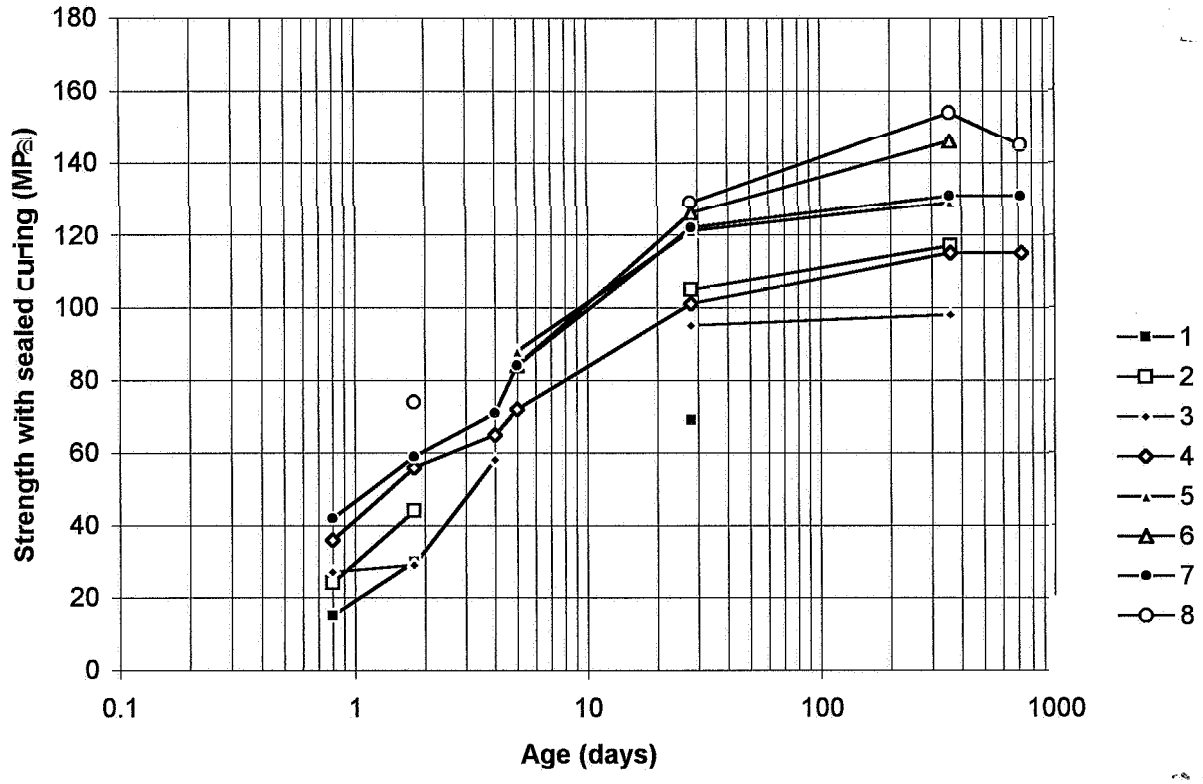

Figure 5.2 - Strength with sealed curing versus age. **HPC** mix is given.

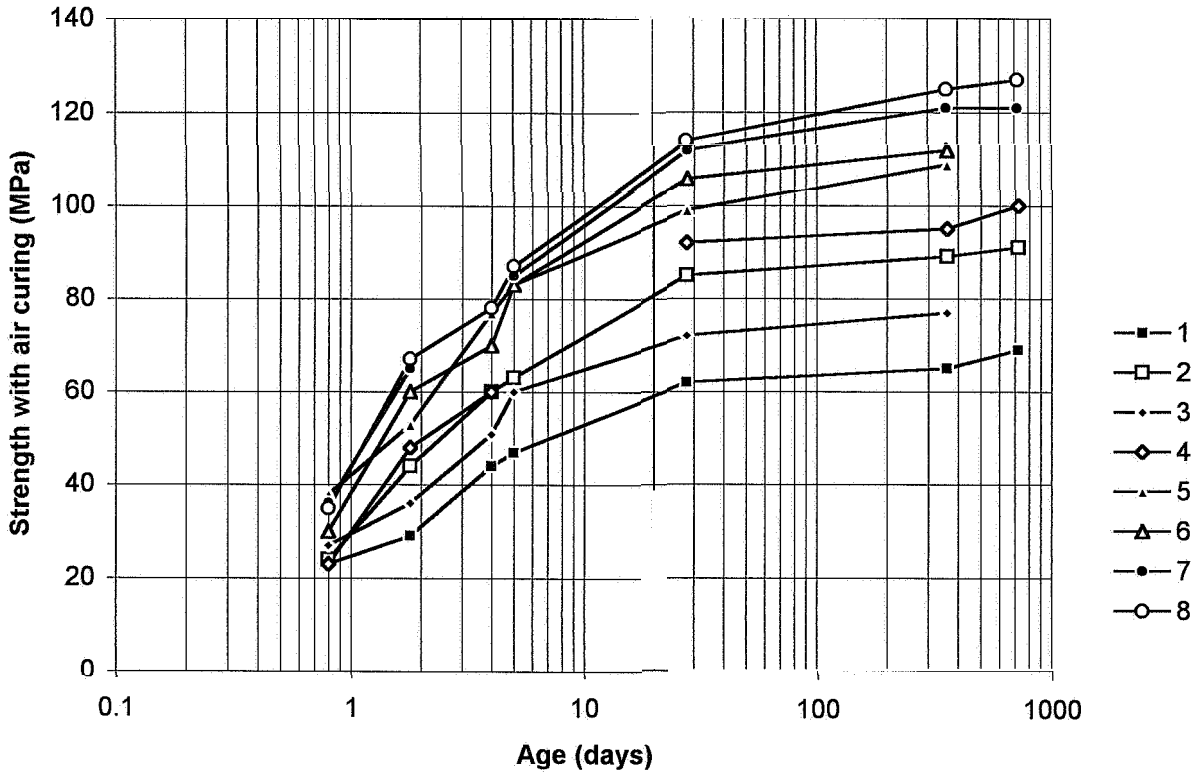

Figure 5.3 - Strength with air curing versus age. HPC mix is given.

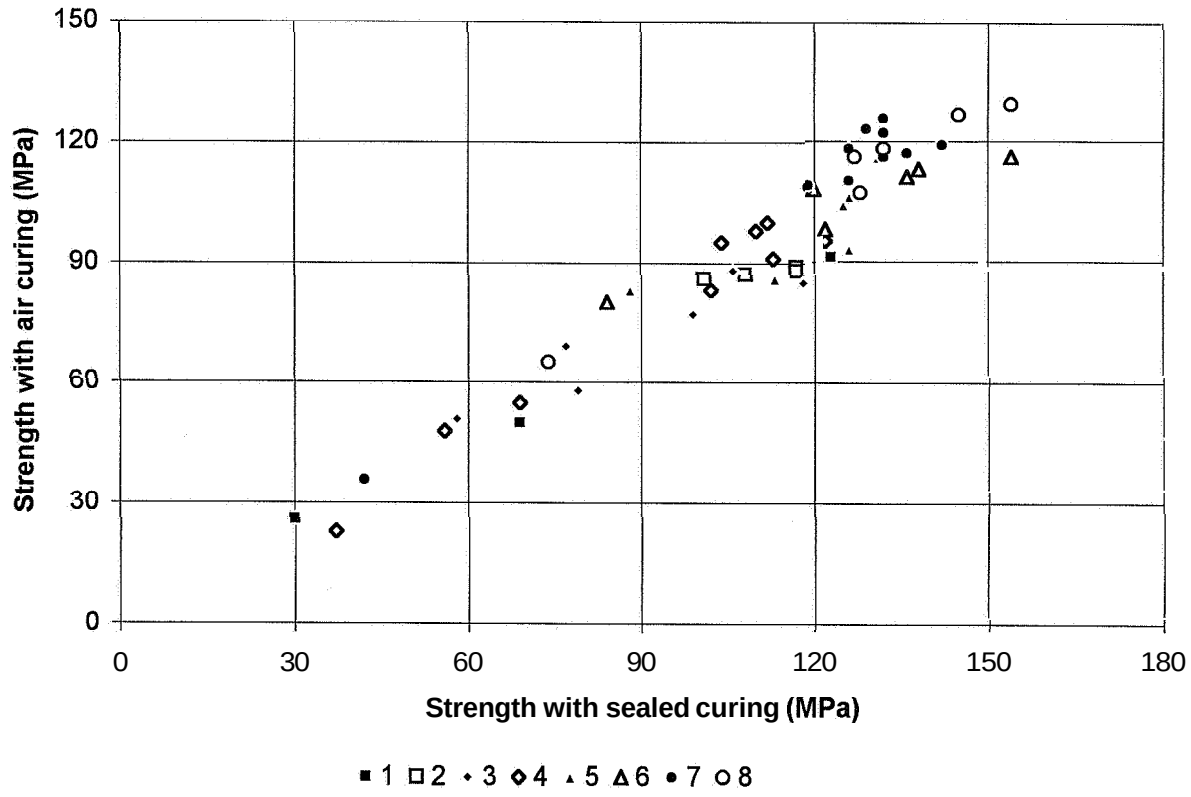

Figure 5.4 - Strength with air curing versus strength with sealed curing. HPC mixes.

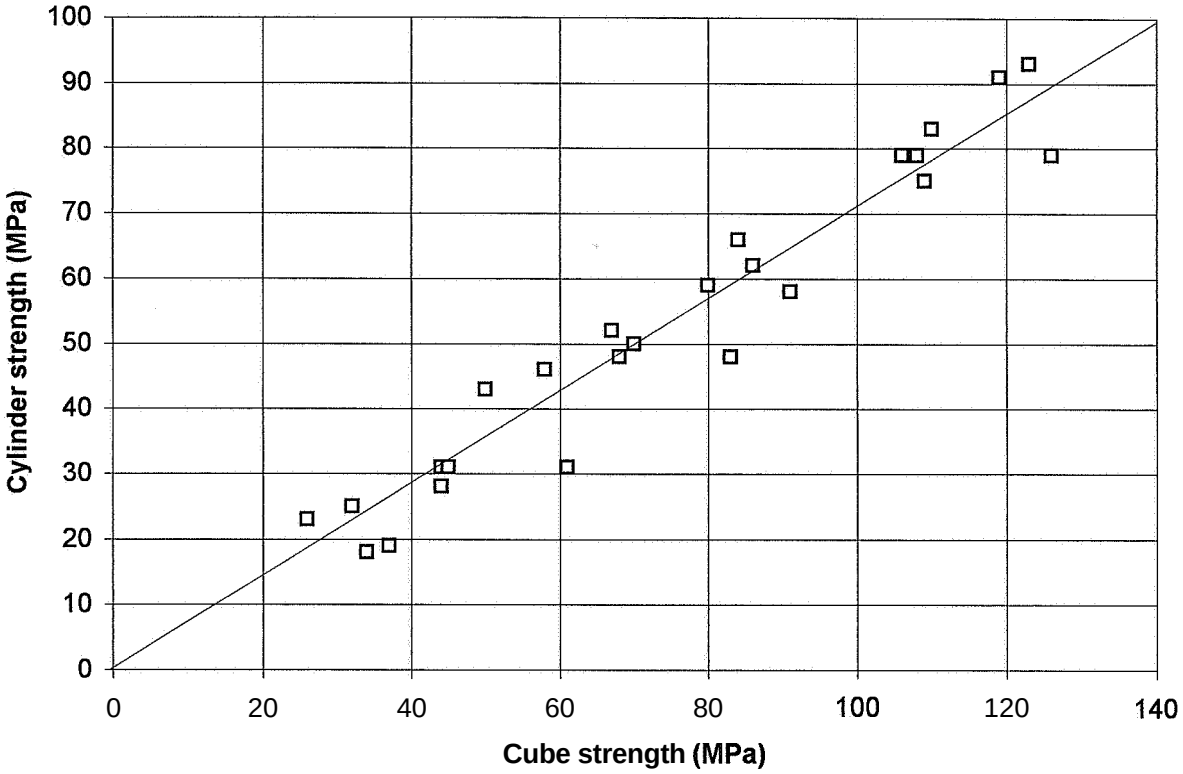

Figure 5.5 - Cylinder strength with air curing versus cube strength. All HPC mixes.

Figures 5.4 and 5.5 estimate the influence of air curing on the cube strength:

$$f_{cD}=a\cdot[0.93-0.36\cdot(w/c)]\cdot f_{cB} \qquad (5.7)$$

f_{cB} denotes the cylinder strength with sealed curing (basic creep)
f_{cD} denotes the cylinder strength with air curing (drying creep)
a = 1.1 in HPC with silica fume slurry; a= 0.94 with 5% silica fume; a= 1 in concrete with 10% granulated silica fume, **Figure 5.6.**

The effect of silica fume slurry on strength of HPC was probably explained by the more pronounced self-desiccation that took place compared with HPC with granulated silica fume, **Persson (1995A)**. Before 28 days' age HPC with silica fume slurry obtained about 4% lower internal relative humidity, RH, than HPC with granulated silica fume. The difference in RH of sealed HPC and air-cured HPC became less when HPC contained silica fume slurry than when it contained granulated silica fume. Dry HPC is known to obtain higher strength than moisturised HPC, **Persson (1992A)**. **Figure 5.5** gives the following equation:

$$f_{c,cyl} = 0.71\cdot f_{c,cube} \qquad \{15< f_{c,cyl} <100 \text{ MPa}\} \qquad (5.8)$$

$f_{c,cyl}$ denotes the strength of cylinders (diameter 55 mm, length 200 mm, MPa)
$f_{c,cube}$ denotes the compressive strength of cubes (100 mm, MPa)

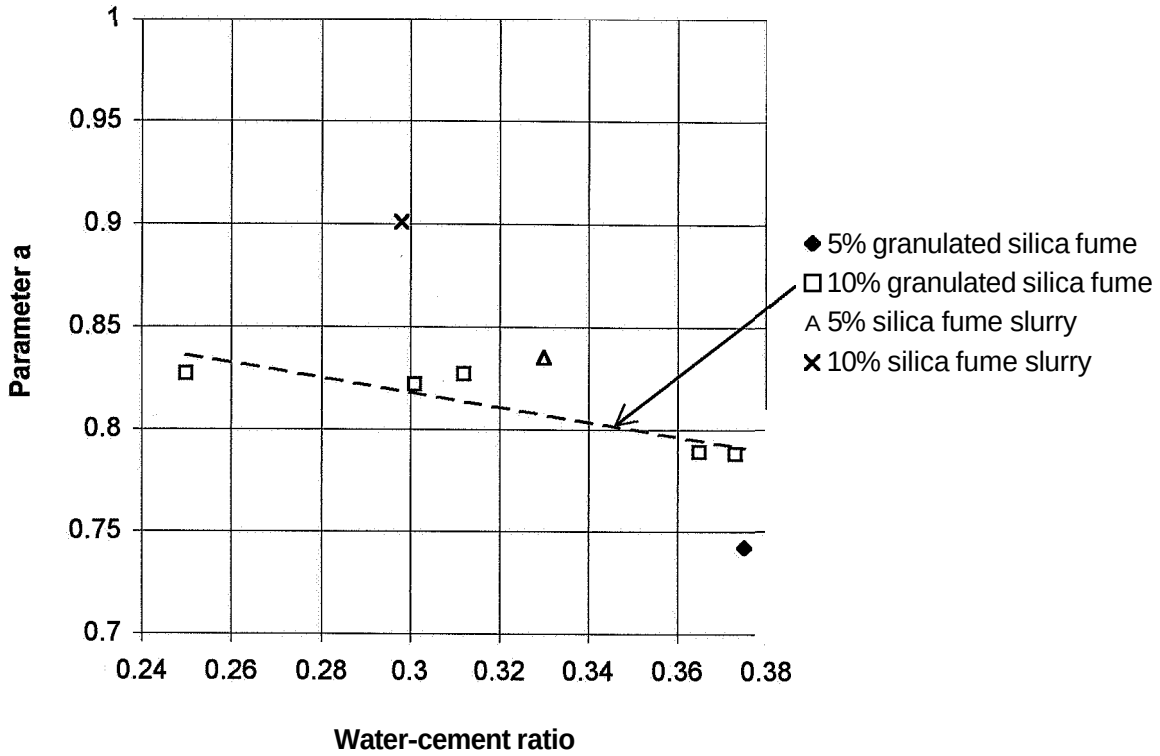

Figure 5.6 - Relationship between strength with air and sealed curing versus w/c.

In the limitations described above the stress/cube strength levels 0.30 and 0.60 were chosen. The actual stress/cylinder strength in use was 0.42 and 0.84 at start of the creep tests. It was also of interest to investigate the effect of the type of silica fume on the strength of the concrete. The silica fume slurry in the mixed proportions 4 and 7 was replaced by granulated silica fume, with the other component held constant. **Figure 5.7** and **5.8** show that the type of silica fumes did not affect the strength over a period of 3 years.

5.2.8 Analysis of compressive strength of HPC with sealed curing

Strength of the HPCs that were used in the basic short-term creep tests is shown in **Appendix 5, Persson (1995A).** The following equation estimates the 28-day compressive strength, f_{c28} of HPC mixes 2, 5, 6 and 8 (MPa):

$$f_{c28} = k \cdot 330 \cdot [0.645 - (w/c)_{eff2}] \qquad (5.9)$$

$$(w/c)_{eff2} = w/(c+2 \cdot s) \qquad (5.10)$$

s denotes the content of silica fume (kg/m^3)

The effect of type of aggregate and air-entrainment was estimated at a constant $(w/c)_{eff2}$. **Table 5.2** shows the correction factors for 28-day compressive strength

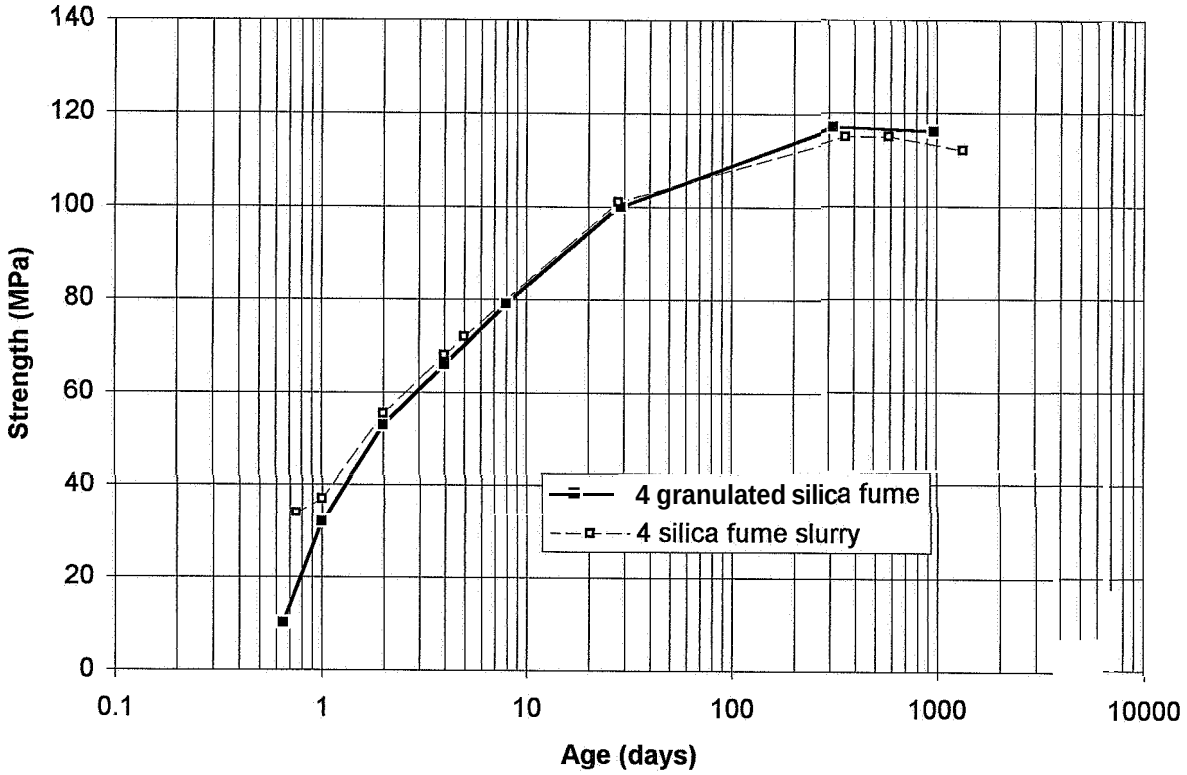

Figure 5.7 - Effect of type of silica fume on the strength of HPC mix 4, **Table 5.1.**

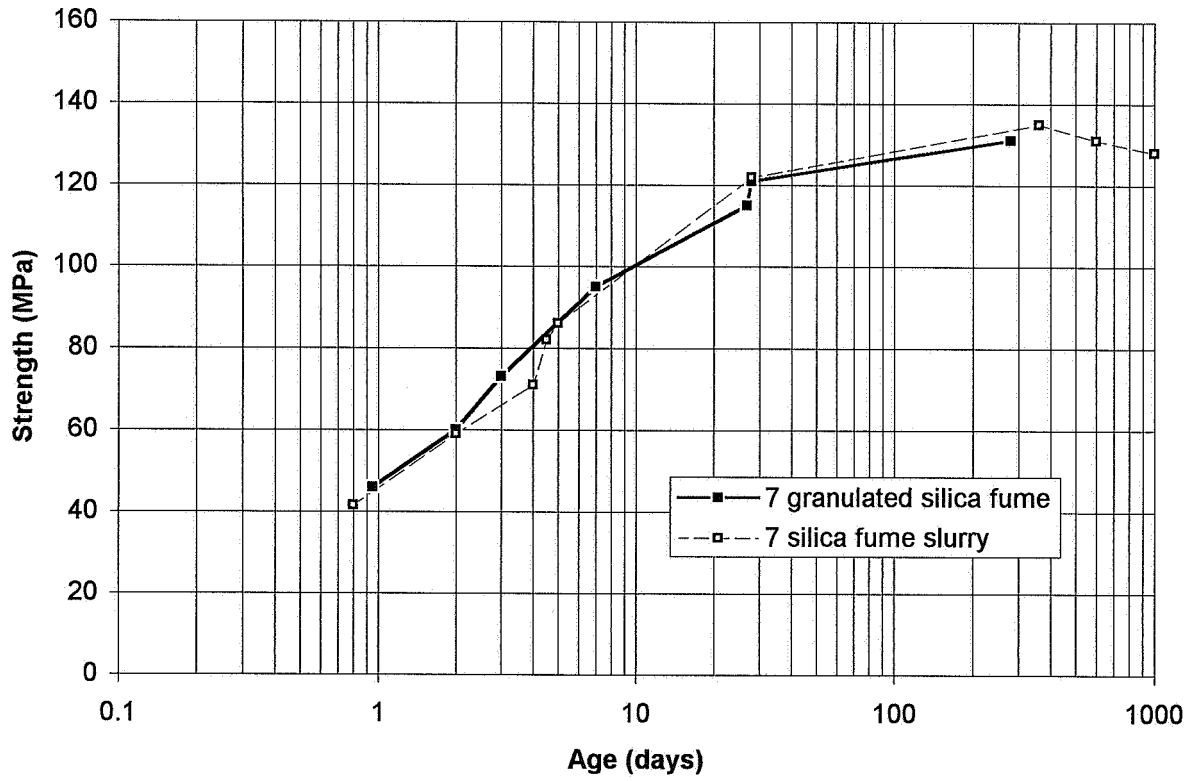

Figure 5.8 - Effect of type of silica fume on the strength of HPC type **7, Table 5.1**.

Table 5.2 - Correction of 28-day strength due to aggregate or air-entrainment.

Alteration	Mix	Correction factor k
National aggregate	4 (4 nos.), 7 (4 nos.)	0.91
Air-entrainment (≈ 4.4 %)	1, 3 (4 nos.)	0.85

The correction factor k for the compressive strength of the national recipes 4 and 7 was probably due to the lower compressive and split tensile strength of the aggregate, **Table 4.1.** The national aggregates all exhibit larger ignition losses than the quartzite sandstone. Norrkoping aggregate contained mica faults. When the concrete was tested, the split surfaces of the fragments were covered by mica. The Toresta pea gravel had a smooth surface compared with the Norrkoping granite, which was crushed. However, it has been shown that a very high compressive strength can be obtained by use of pea gravel in HPC, **Randall and Foot (1989), Persson (1992A)**. The workability is normally improved when pea gravel is used in HPC, which might compensate for any faults in the interfacial zone. Bålsta crushed sand has the highest ignition loss of all aggregates studied (7 times as much ignition loss compared with quartzite sandstone). Bålsta crushed sand was used in both the national recipes. The properties of Bålsta sand probably were the explanation for the decline in strength of the national recipes compared with the recipes that containing quartzite sandstone. The reducing correction factor of compressive strength due to air-entrainment is well known for NSC. It was possible to estimate the strength growth rate with a logarithmic equation. The following equation calculates the strength for a standard recipe (t=age of HPC in days, MPa):

$$f_c(t) = a \cdot {}^{10}\log(t) + b \qquad \{1<t<28 \text{ days}) \qquad (5.11)$$

$$a = k_a \cdot 34 \cdot [2.1-(w/c)_{eff2}] \qquad (5.12)$$

$$b = k_b \cdot 270 \cdot [0.40-(w/c)_{eff2})] \qquad (5.13)$$

Table 5.3 shows correction factors of equations (5.12) and (5.13), k_a and k_b, for HPC with national recipe or/and air-entrainment.

Table 5.3 - Correction for aggregate and air-entrainment in equations (5.12)-(5.13).

Alteration	Mix	Correction factor k_a	Correction factor k_b
National aggregate	4 (4 nos.), 7 (4 nos.)	0.79	1.24
Air-entrainment (≈ 4.4 %)	1, 3 (4 nos.)	0.73	1.32

The strength growth rate, df_c/dt, was obtained after derivation:

$$df_j dt = k_c \cdot 14.7 \cdot [2.1 - (w/c)_{eff2}]/t \qquad (5.14)$$

Table 5.4 shows the correction factor k_c in the strength growth equation (5.14).

Table 5.4 - Correction factor k_c in the strength growth equation (5.14)

Alteration	Recipe	Correction factor k_c
Standard aggregate	2, 5, 6, 8 (4 nos. of each mix)	1
National aggregate	4 (4 nos.), 7 (4 nos.)	0.79
Air-entrainment (≈ 4.4 %)	1, 3 (4 nos.)	0.73

5.3 Hydration of concrete

5.3.1 General

During the hydration process, when the water attaches to cement, a number of reaction products are created, which together with the aggregate are characterised as concrete. Calcium silicate hydrate, C-S-H, is the most essential product with regard to the strength of the concrete. Other products such as calcium hydrate, aluminate and sulphates contribute much less to the strength of the well-cured concrete. In the long-term, when silica fume is present, polymerisation creates longer chains of silicon and oxygen, which further increases the strength of the concrete. The larger the amount of originally added water (the mixing water) that is chemically bound (hydrated), the higher the strength of the concrete. From the strength point of view a high ratio, w_n/w, of the non-evaporable water, w_n, to the mixing water, w, is preferable. The ratio w_n/w is an inverted measurement of the porosity of concrete.

5.3.2 Previous studies of hydration of High-Performance Concrete

Fagerlund (1987) performed theoretical calculations of the relative compressive strength compared with the ratio, w_n/c, **Figure** 5.9. HPC contains less water than is necessary for the hydration to proceed to a final state of $w_n/c \approx 0.25$. The maximum degree of hydration, $\alpha = 1$, can only be obtained at a water-cement ratio, $w/c > 0.39$. The maximum degree of hydration, α, of HPC with $w/c < 0.39$ is linear-dependent on the wlc, **Powers and Brownyard (1946-1948):**

$$\alpha_{max} = w/(0.39 \cdot c) \qquad (5.15)$$

w denotes the mixing water of the concrete (kg/m^3)
c denotes the cement content of the concrete (kg/m^3)

The degree of hydration, a , can also be expressed as:

$$\alpha = w_n/(0.25 \cdot c) \qquad (5.16)$$

w_n denotes the non-evaporable water content of the concrete (kg/m^3)

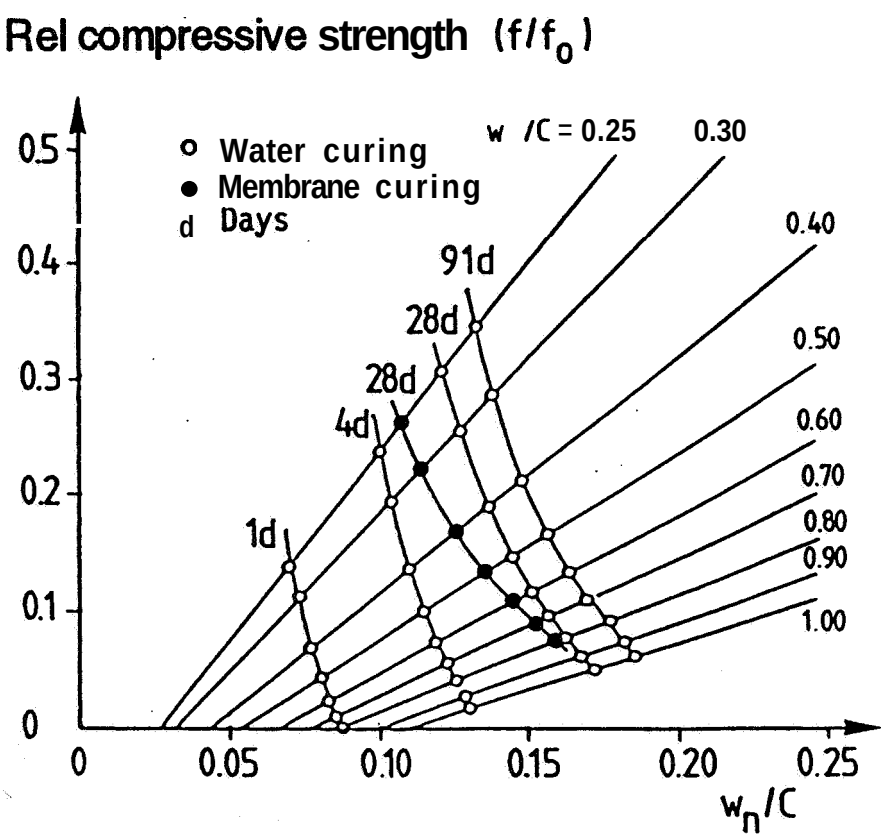

Figure 5.9 - Relative strength, f/f_0, of cement pastes versus non-evaporable water to the cement, w_n/c. Sealed curing. d = days' age; c = cement; Fagerlund (1987).

Dividing equation (5.16) by (5.15) gives the **maximum** value of relative hydration:

$$(w_n/w)_{max} = 0.64 \qquad \{0.20 < wlc < 0.39\} \qquad (5.17)$$

$$(w_n/w)_{max} = 0.25 \cdot c/w \qquad \{w/c > 0.39\} \qquad (5.18)$$

It is normally assumed that the hydration of the concrete (expressed as the ratio of non-evaporable water to the cement, w_n/c) increases with the strength of the concrete. This was not the case with concretes that contained silica fume. **Persson** (1996A) studied hydration and strength of more than 900 cores from 8 concretes at ages varying between 1 and 90 months. The silica fume in the concrete affected the hydration. **Figure 5.10** shows the strength of 40 mm cylinders versus the relative hydration, w_n/w. The strength of the concrete depended not only on the relative hydration, w_n/w, but also on the content of silica fume.

5.3.3 Experimental procedure

The specimen consisted of an eighth of a 100-mm cube. Right after the strength testing the bottom eighth of the cube (0.3 kg) was further crushed, divided into two

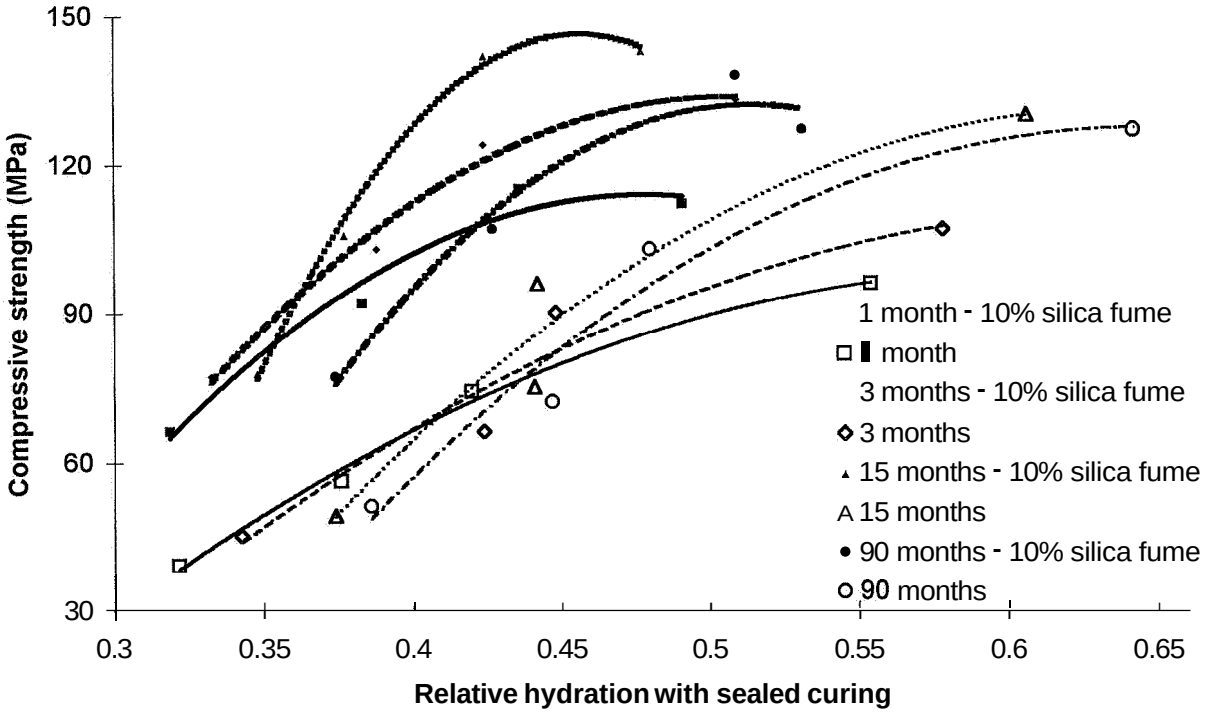

Figure 5.10 - Strength of concrete with sealed curing versus the relative hydration, w_n/w. Dense line = 10% silica fume, thin line = no silica fume) . Persson (1996A).

parts and placed in small containers. The concrete fragments were then immediately dried in a fan oven at 105 "C. The fragments were less than 5 mm in size.
After one week of intensive drying the fragments were weighed and ignited at 1050 "C for 16 h. Before weighing, the material was cooled in an exsiccator. In drying conditions one sample was taken from the surface of the eighth of the cube and another from the inner part of the cube. In drying conditions samples were also taken from fragments of the inner of 55-mm cylinders. By compensating for losses during the ignition of the different materials, Byfors (1980), the degree of hydration, w_n/c, was obtained (the losses of the separate materials are given above):

$$\frac{w_n}{c} = \frac{w^{105}(1-\eta) - w^{1050}}{w^{1050} - \frac{\psi \cdot \gamma}{1+\gamma} \cdot w^{105}} \qquad (5.19)$$

$$\psi = 1 - \mu_a \qquad (5.20)$$

$$\eta = \frac{\mu_c + \gamma \cdot \mu_a}{1+\gamma} \qquad (5.21)$$

$\frac{w_n}{w^{C_{105}}}$ denotes the ratio of non-evaporable water to amount of cement (kg/kg)

denotes the weight after drying at 105 °C (kg)

w^{1050} denotes the weight after ignition at 1050 "C (kg)
γ denotes the ratio of aggregate to cement
μ_a denotes the ignition losses for aggregate (kg/kg)
μ_c denotes the ignition losses for cement (kg/kg)

5.3.4 Sources of error

When testing hydration of concrete at early ages the main faults appear in the sampling and drying of the concrete, **Norling Mjörnell (1994)**. The distribution of aggregate in the concrete could cause problems if tendencies towards separation existed when the specimen was cast. None of the concretes in this work, however, had separation tendencies except for concrete type 7, **Table 5.1** (weak tendencies). The samples were furthermore taken at the bottom eighth of a cube used for compressive tests. At casting this part was placed sideways, which would further prevent any effect of possible separation. At the conical part of the fracture zone of the cube test, some aggregate could be lost and some additional aggregates from the fracture zone might affect the amount of aggregate in the samples compared to the original aggregate in the cast concrete. However, in HPC the surface of the fracture zone normally runs through the aggregate (not around the aggregate as in NSC). These fracture properties applied to all the concretes in the work except for concrete types 1 and 4. Both these concretes had only 5% silica fume content. The silica fume substantially improves the interfacial zone of the aggregate and cement paste in concrete, **Rosenberg and Gaidis (1989)**, **Persson (1992A)**. The concrete samples were rapidly dried in a 105 "C drying cabinet by a fan. The time taken to reach 105 °C was less than 10 minutes calculated from the start of the heating. The concrete was self-desiccated before the drying, which meant that no free water existed outside the concrete before the drying.

5.3.5 Results

Figure 5.11 shows the relative hydration (hydrated water to the mixing water, w_n/w) versus age for concrete with the mix proportion ***6***. A summary of the relative hydration, w_n/w, for the resisting concretes is given in **Appendix 5. Figures 5.12** and **5.13** show a summary of the development of the relative hydration with sealed and air curing respectively versus the water-cement ratio. **Figure 5.14** shows the influence of air curing on the relative hydration. In **Figure 5.15** the hydration of the surface layer of cubes with air curing is given versus the hydration of the interior of cubes with air curing. **Figure 5.16** shows the relative hydration of cylinders with air curing versus the relative hydration of cubes also with air curing. Symbols:

c denotes cylinder
d denotes days' age
i denotes inner part of the specimen
s denotes surface part of the specimen
B denotes basic creep (cubes with sealed curing)

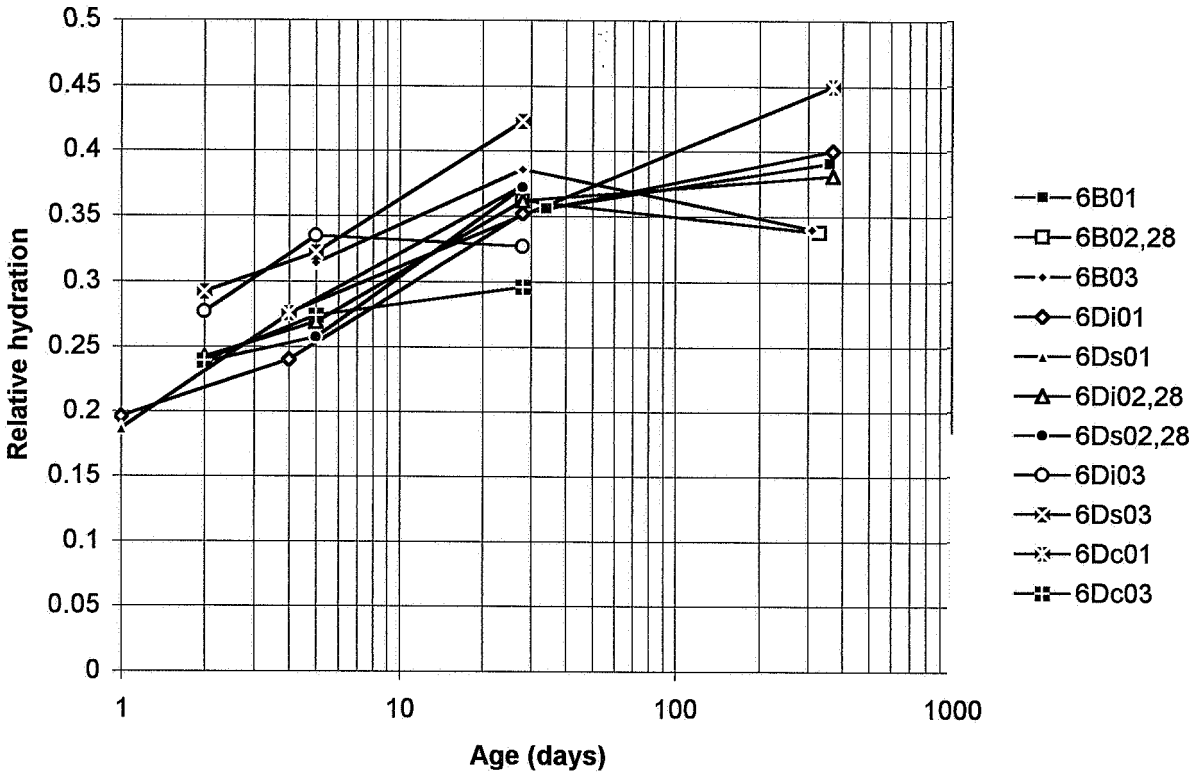

Figure 5.11 - Relative hydration, w_n/w, versus age for HPC mix ***6*, Table 5.1.**

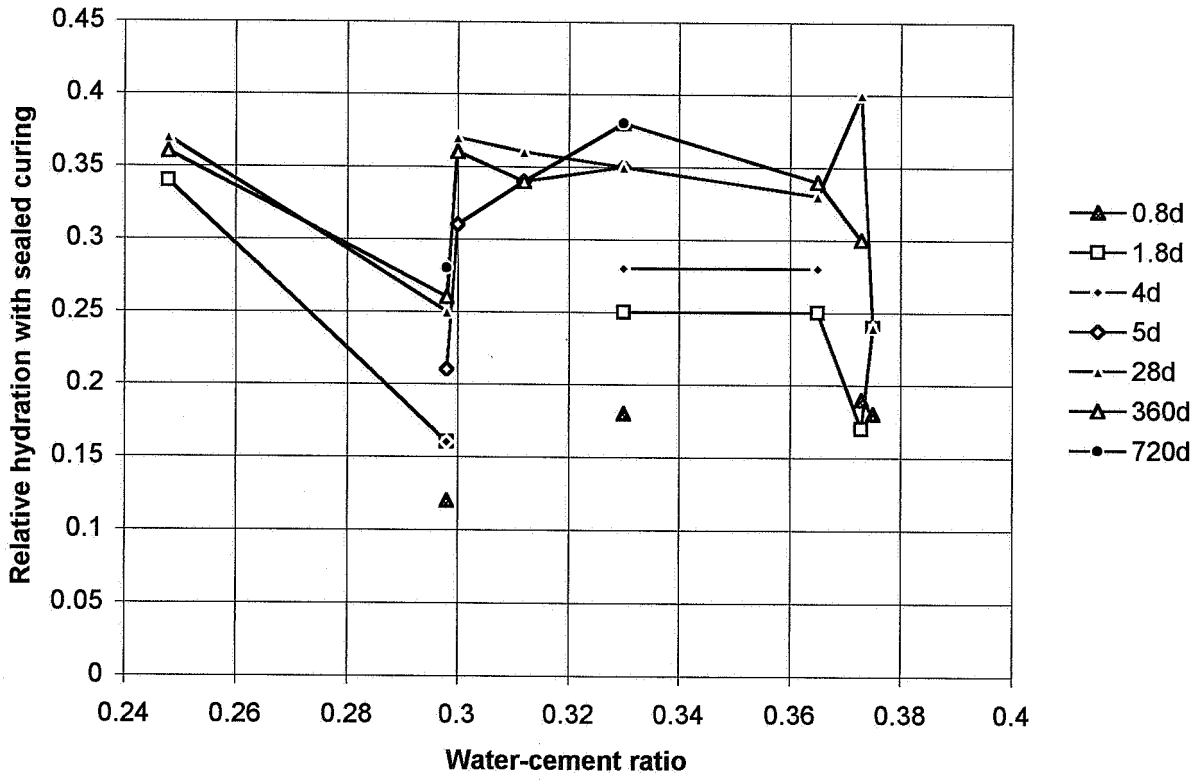

Figure 5.12 - Relative hydration, w_n/w, versus w/c for sealed-cured HPC. d= days.

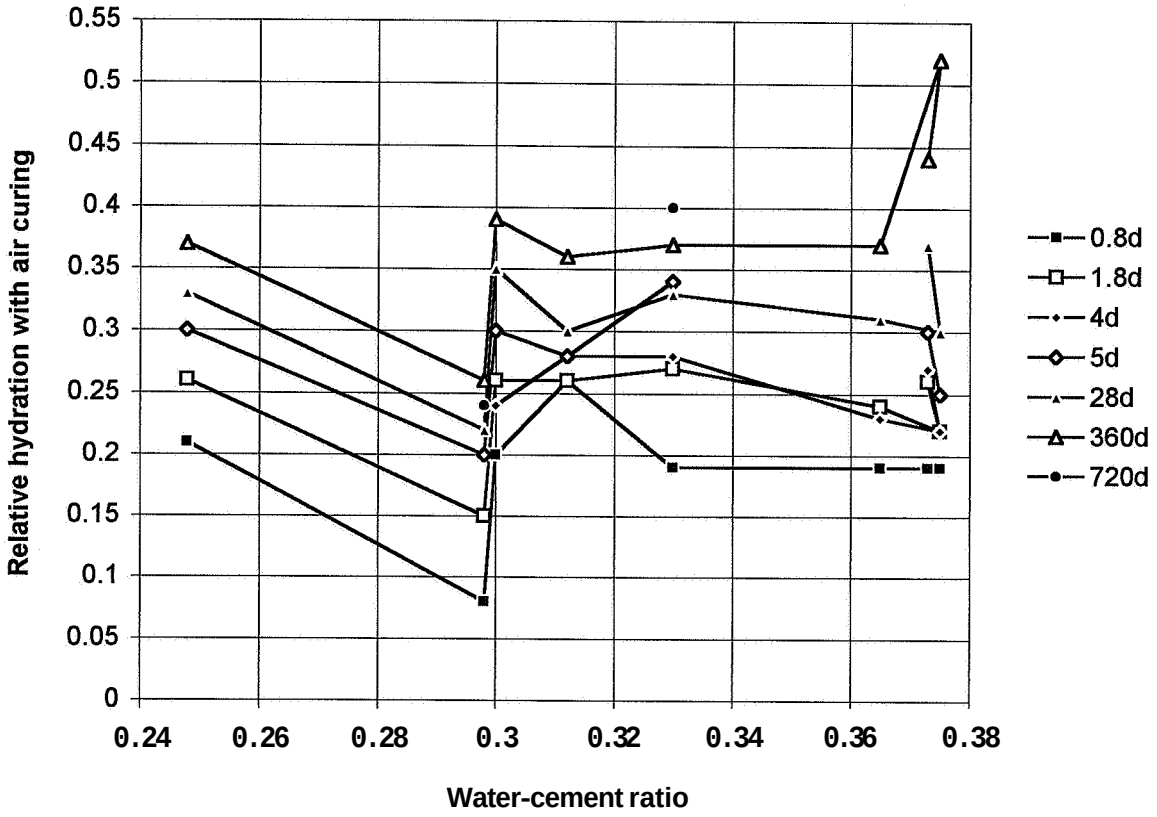

Figure 5.13 - Relative hydration versus the wlc for HPC with air curing. d= days.

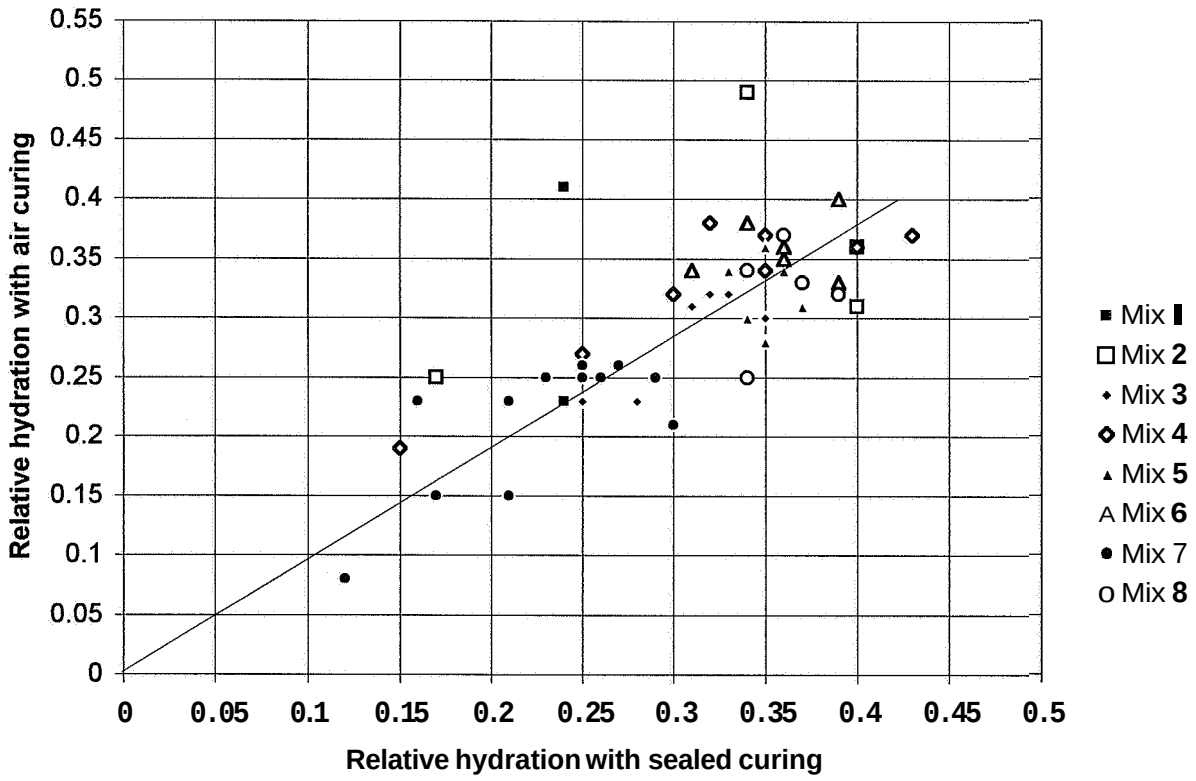

Figure 5.14 - Influence of air curing on relative hydration, w_n/w, of HPC cubes.

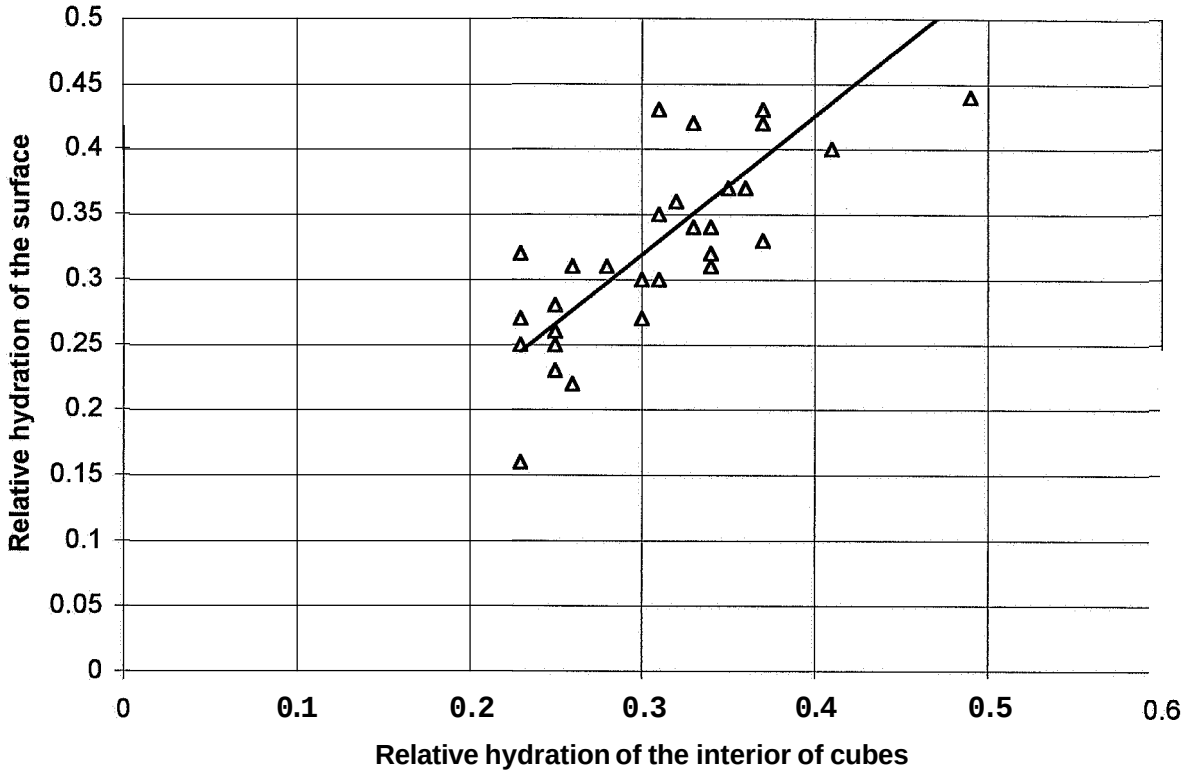

Figure 5.15 - Hydration of the surface layer versus the hydration of the interior

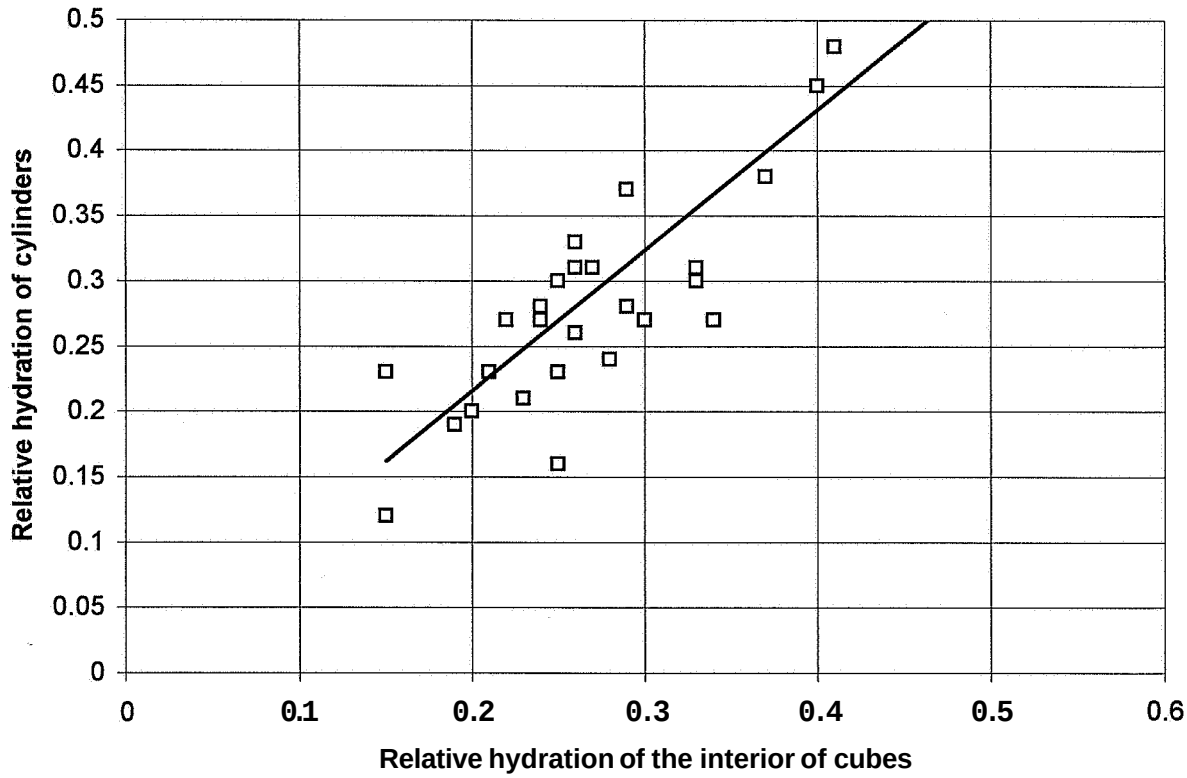

Figure 5.16 - Hydration of cylinders with air curing versus hydration of cubes.

D denotes drying creep (cubes with air curing)
6 denotes concrete type, **Table 5.1**.
...01 age at loading: 1 day; stresslcylinder strength ratio: 0.84
...02 age at loading: 2 days; stresslcylinder strength ratio: 0.84
...03 age at loading: 2 days; stresslcylinder strength ratio: 0.42
...28 age at loading: 28 days; stresslcylinder strength ratio: 0.42

5.3.6 Accuracy of hydration tests

Some sources of error were incorrect sampling and drying faults. The ambient moisture content in the laboratory was fairly low. Concrete that has been dried out requires an ambient relative humidity of 70% for the hydration to proceed, **Powers and Brownyard (1946-1948)**. The accuracy was tested with two methods.

Method 1 (standard procedure):

The sample was placed in a 105 "C drying cabinet directly after sampling. The heating was performed by fan within 10 minutes and continued for 1 week.

Method 2 (pre-drying procedure):

After 1 week of pre-drymg in an exsiccator (RH about 11%) the samples were placed in the 105 ° C drymg cabinet and further dried out for one week. The pre-drying of the concrete had a very small effect on the degree of hydration. The effect of pre-drymg on the degree of hydration, $4 \cdot w_{n,pre}/c$, was calculated by linear regression versus the standard procedure (Method 1):

$$w_{n,pre}/c = 1.03 \cdot w_n/c - 0.01 \qquad (5.22)$$

w_n denotes the measured hydrated water of HPC at immediate heating in 105°C.
$w_{n,pre}$ denotes the hydrated water of HPC after pre-drying in exsiccator, RH 11%

Pre-drying by Method 2 gave a slightly higher degree of hydration than Method 1 (standard procedure). This increase is probably due to the continued hydration inside the samples at 20 °C when placed in the exsiccator. Although the exsiccator contained lithium chloride with low relative humidity the concrete had a low permeability that did not affect the hydration of the fragments.

5.3.7 Analysis

Figure 5.14 gave a correlation between relative hydration for air and sealed curing:

$$(w_n/w)_{air} = 0.73 \cdot (w/c+1) \cdot (w_n/w)_{sealed} \qquad (5.23)$$

Or on average:

$$(w_n/w)_{air}=0.97\cdot(w_n/w)_{sealed} \quad (5.24)$$

Figure 5.15 gave a correlation between hydration of the surface and of the interior:

$$(w_n/w)_{surface}=1.06\cdot(w_n/w)_{interior} \quad (5.25)$$

Figure 5.16 gave a correlation between hydration of cylinders and cubes:

$$(w_n/w)_{cylinder} = 1.08\cdot(w_n/w)_{cubes} \quad (5.26)$$

Equations (5.25) and (5.26) both show that carbonation affected the measured hydration. Otherwise the hydration ought to be lower in the surface of cubes with air curing than interior, equation (5.25). The cylinder was more sensitive to carbonation due to the small size, equation (5.26). On average the hydration of cubes with air curing (interior) was less than the hydration of sealed cubes, equation (5.24). However, in concretes with higher water-cement ratio the carbonation affected the measured hydration more, which was indicated by equation (5.23). The hydration was often compared to the strength of the concrete, cp. **Figure 5.9 and 5.10.** The strength was known for identically the same specimens that were used for hydration tests. A relationship was thus obtained between the relative hydration, w_n/w, and the strength, f_c. From **Figures 5.2, 5.3, 5.12 and 5.13** it was possible to obtain the required correlation. **Figure 5.17** shows the strength of cubes with sealed curing versus the relative hydration. **Figure 5.18** shows the strength of cubes with air curing versus the relative hydration. **Figures 5.17** gave an expression for the strength with sealed curing, f_{cB}(MPa):

$$f_{cB} = 3.3\cdot k_a\cdot k_5(w/c)^{-4.63}\cdot[(w_n/w)-5.2\cdot k_a\cdot k_5\cdot e^{-11\cdot(w/c)}] \quad (5.27)$$

f_{cB} denotes the strength of sealed HPC (MPa)
e denotes the natural logarithm
k_a =2.2 for air-entrained HPC, k_a= 1 otherwise (except for HPC with 10% silica slurry)
k_5 =0.72 for HPC with 5% silica fume, k_5= 1 otherwise (except for HPC with 10% silica slurry)
w_n/w denotes the relative hydration (non-evaporable water to mixing water)

For concretes with 10% silica fume slurry the following equation was obtained:

$$f_{cBsl} = 600\cdot[(w_n/w)-0.052] \quad (5.28)$$

f_{cBsl} denotes the strength of sealed HPC with 10% silica fume slurry (MPa)
w_n/w denotes the relative hydration (non-evaporable water to mixing water)

After derivation an equation was obtained for the strength growth rate, df_{cB}/dw_n, versus the development of hydration (except for HPC with 10% silica slurry):

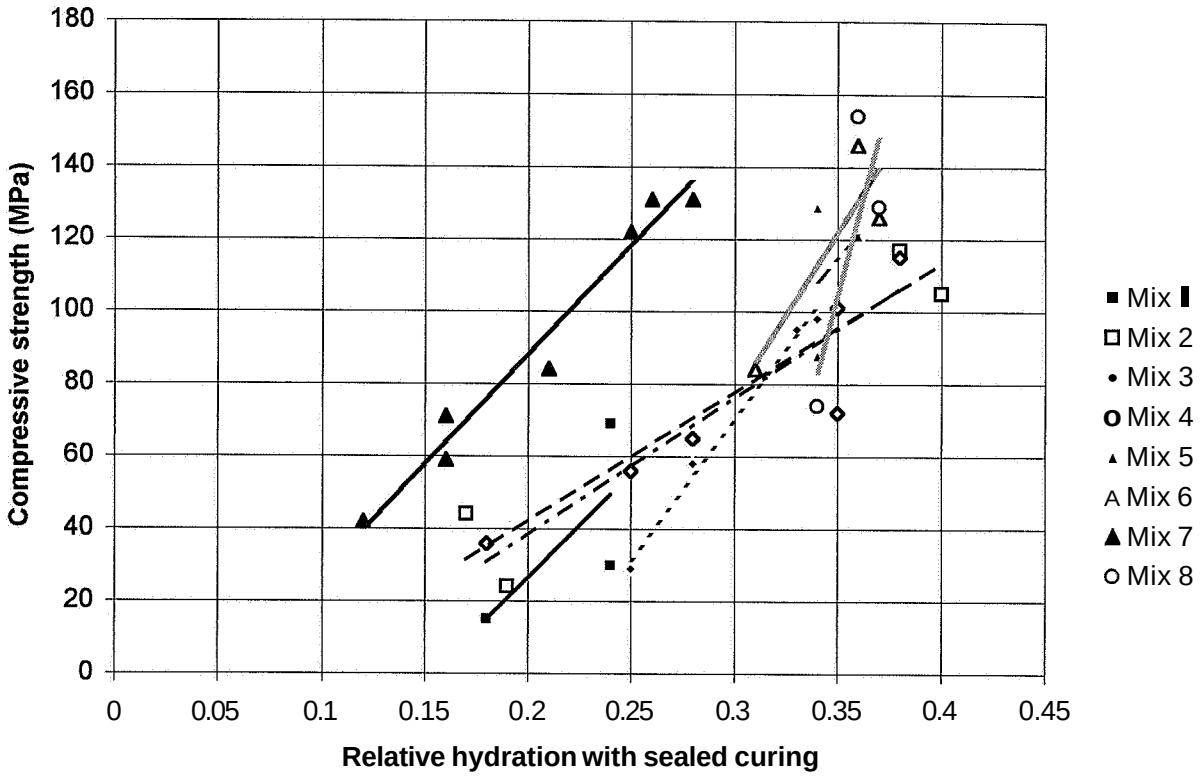

Figure 5.17 - Strength of cubes with sealed curing versus relative hydration.

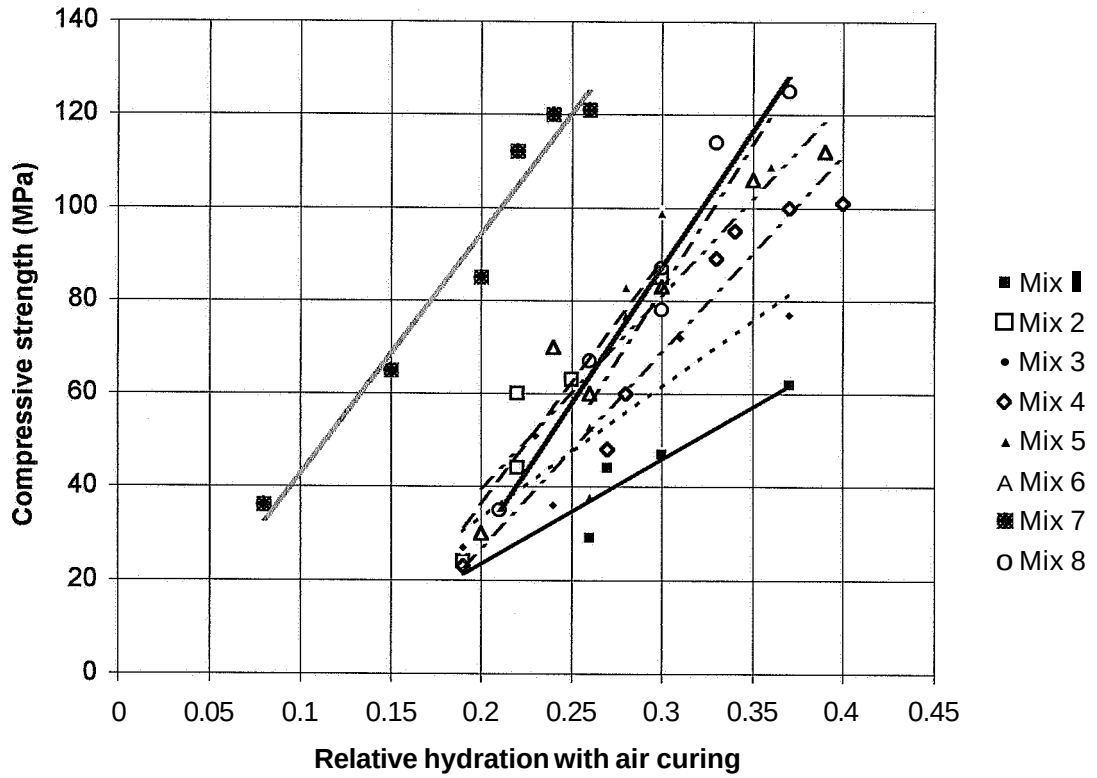

Figure 5.18 - Strength of cubes with air curing versus relative hydration.

$$df_{cB}/dw_n = (1/w)\cdot 3.3\cdot k_a\cdot k_5\cdot (w/c)^{-4.63} \quad (5.29)$$

k_a	=2.2 for air-entrained HPC, k_a= 1 otherwise (except for HPC with 10% silica slurry)
k_5	=0.72 for HPC with 5% silica fume, k_5= 1 otherwise (except for HPC with 10% silica slurry)
w	denotes the amount of mixing water (kg/m^3).
df_{cB}/dw_n	denotes the strength growth rate for sealed HPC (MPa/kg)

For HPC with 10% silica fume slurry the following equation was obtained for the strength growth rate:

$$df_{cBsl}/dw_n = (600/w) \quad (5.30)$$

w	denotes the mixing water (kg/m^3).
df_{cBsl}/dw_n	denotes the strength growth rate for sealed HPC with 10% silica fume slurry (MPa/kg)

Figures 5.18 gave a correlation between relative hydration and strength of HPC with air curing, f_{cD} (MPa):

$$f_{cD} = 530\cdot k_a\cdot k_5\cdot[(w_n/w)-k_a\cdot 0.14] \quad (5.31)$$

f_{cD}	denotes the strength of drying HPC
k_a	=0.6 for air-entrained HPC, k_a= 1 otherwise (except for 10% silica slurry)
k_5	=0.8 for HPC with 5% silica fume slurry, k_5= 1 otherwise (except for 10% silica slurry)
w_n/w	denotes the relative hydration (non-evaporable water to mixing water)

For concretes with 10% silica fume slurry the following equation was obtained:

$$f_{cDsl} = 510\cdot[(w_n/w)-0.015] \quad (5.32)$$

f_{cDsl}	denotes strength of drying HPC with 10% silica fume slurry (MPa)
w_n/w	denotes the relative hydration (non-evaporable water to mixing water)

The strength growth of HPC versus the development of hydration, df_{cD}/dw_n was expressed in the following equations (df_{cDsl}/dw_n for HPC with 10% silica fume slurry):

$$df_{cD}/dw_n = (1/w)\cdot 530\cdot k_a\cdot k_5 \quad (5.33)$$

$$df_{cDsl}/dw_n = (510/w) \quad (5.34)$$

5.4 Internal relative humidity

5.4.1 General

The decline of relative humidity, RH, was the most characteristic property, besides the high strength, of a sealed HPC. RH declined even when the weight of the specimen was constant due to the chemical shrinkage of the water when attached to cement, **Powers and Brownyard (1946-1948)**. The self-desiccation of HPC is very beneficial when it is utilised for solving building moisture problems for dwelling houses. However, the self-desiccation may be harmful. The self-desiccation perhaps causes HPC to shrink even when submerged. NSC shrinks only during sorption when exposed to air. In HPC a kind of internal sorption takes place due to the chemical shrinkage of the water when it is bound to the cement during the hydration process. Self-desiccation influences the elastic and long-term deformations of HPC. It was therefore essential to perform accurate experimental and numerical analysis of the development of RH, **Persson (1996B)**. It was also essential to estimate the difference in RH between the surface of the specimen and the interior since this difference perhaps affected the amount of drying shrinkage and drying creep. Finally, it was considered important to perform the measurement of RH on the same specimen as the measurements of strength, to avoid systematic faults.

5.4.2 Previous studies of self-desiccation

Persson (1996A) studied the internal relative humidity, RH, of 8 types of sealed HPC. Half of the concretes contained 10% silica fume calculated on the basis of the cement content. The age of measurement varied between 1 month and 90 months. A total of 234 measurements of RH were performed. The results indicated large differences in RH between concretes with 10% silica fume compared with Portland cement concretes. The following equations were obtained:

$$Ø(t,w/c)_s = 1.13\ [1-0.065\cdot\ln(t)]\cdot(w/c)^{0.24\cdot[1-0.1\cdot\ln(t)]} \qquad (5.35)$$

$$Ø(t,w/c) = 1.09\cdot(w/c)^{0.17\cdot(1+0.0451\cdot t)} \qquad (5.36)$$

t	denotes the age of the concrete {1<t <15 months)
w/c	denotes the water-cement ratio {0.22<w/c <0.58 }
s	denotes 10% silica fume
$Ø(t,w/c)$	denotes RH in Portland cement concrete with sealed curing
$Ø(t,w/c)_s$	denotes RH in sealed-cured concrete with 10% silica fume

Persson (1995A) studied the internal relative humidity, RH, in the 8 sealed concretes presented above, **Table 5.1. Appendix 5** provides the detailed measurements of RH denoted HPC with sealed curing after short-term creep studies. The following correlation was obtained from **Appendix 5, Persson (1995A)**:

$$\emptyset(wbr_{eff2},t) = 0.38\cdot(wbr_{eff2}+2.4-0.1\cdot\ln t)+\Delta\emptyset_{sl} \quad (5.37)$$

$$wbr_{eff2} = w/(c+2\cdot s) \quad (5.10)$$

c denotes the cement content in the concrete (kg/m^3)
s denotes the content of silica fume in the concrete (kg/m^3)
t denotes the age of the concrete {1<t<1000 days)
w denotes the water content in the concrete ($kglm^3$)
$\Delta\emptyset_{sl}$ = -0.035 for 5-10% silica fume slurry at age, t≤ 28 days

The rate of self-desiccation was estimated (day^{-1}):

$$d\emptyset/dt = -0.038/t \quad (5.38)$$

$d\emptyset/dt$ denotes the rate of self-desiccation (day^{-1})

5.4.3 Experimental methods

The specimen consisted of either 100-mm cubes or cylinders 55 mm in diameter. Directly after the strength tests were performed, fragments of HPC (minimum 5 mm in size) were collected in 100 ml glass test tubes (filled up to 2/3). From the drying specimens fragments were collected either from the surface of the specimen or from the internal part. The glass tubes were tightened with rubber plugs. The tubes with the fragments were kept at 20 °C for 1 day. A dew point meter then was used to measure RH. The sensor of the dew point meter was entered into the tube and rubber-tightened to the glass. Since HPC contained little moisture, the period of measurement of RH was set at 22 h to obtain a stable value (equilibrium between the moisture in air in the pores of HPC and the sensor of the dew point meter).

5.4.4 Sources of error and accuracy

Fragments collected from the inner part of the sealed cubes were used. From the drying cubes fragments both from the inner part and from the surface were studied. From the drying cylinders fragments were taken from the inner part. The cylinders were weighed before the strength test was performed. More than half of the test tube volume was filled with concrete fragments. Adopting a relative hydration of 50%, the moisture content in the HPC was about 75 $kglm^3$. The air in the pores of HPC and the air in the tube contained about 0.015 kg moisture/m^3 of air. There was about 5000 times as much moisture in HPC as required for moisture equilibrium between the air in the pores of HPC and the air in the tube. Possible lack of moisture was thus no source of error. Hydration heat appears at early ages. The temperature rise was 4 °C, **Appendix 3,** which caused an error in RH of about +1%, **Nilsson (1987).** The dew point meter was calibrated according to **ASTM** E **104-85.** The accuracy of the measurements was estimated to be about ± 1.5% RH, **Persson (1997C).**

5.4.5 Results

Figure 5.19 gives the relative humidity versus age for concrete 6, **Table** 5.1. **Appendix** 5 gives the relative humidity versus age for all the concretes. **Figure** 5.20 shows the relative humidity versus age for concrete 4 with sealed curing with the silica fume slurry or granulated silica fume. **Appendix** 5 provides the complete results of the RH-measurements. **Table** 5.2 shows a summary of the figures that in turn show the results of all RH-measurements. Symbols in **Figures 5.19-28**:

c denotes cylinder
d denotes days' age
i denotes inner part of the specimen
s denotes surface part of the specimen
B denotes basic creep (cubes with sealed curing)
D denotes drying creep (cubes with air curing)
6. denotes concrete type, **Table** 5.1.
...01 age at loading: 1 day; stresslcylinder strength ratio: 0.84
...02 age at loading: 2 days; stresslcylinder strength ratio: 0.84
...03 age at loading: 2 days; stresslcylinder strength ratio: 0.42
...28 age at loading: 28 days; stresslcylinder strength ratio: 0.42

Table 5.2 – Summary of figures showing results of the measurements of RH.

Type of specimen	Type of curing	Measurement	Figure
Cube, 100 mm and cylinders, 55 mm	Air or sealed curing	HPC mix 6, inner part or surface	5.19
Cube, 100 mm	Sealed curing	HPC mix 4, granulated silica fume or silica fume slurry	5.20
Cube, 100 mm	Sealed curing	Cube	5.21
Cube, 100 mm	Air curing	Inner part	5.22
Cube, 100 mm	Air curing	Surface	5.23
Cylinder 55 mm	Air curing	Inner part	5.24
Cube, 100 mm	Air and sealed	Inner part; difference	5.25
Cube, 100 mm	Air and sealed	Surface; difference	5.26
Cube and cylinder	Air (cylinder) and sealed (cube)	Inner part; difference	5.27
Cube 100 mm	Air curing	Inner part and surface (difference)	5.28

5.4.6 Analysis

As observed in **Figure** 5.20, the kind of silica fume had little influence on the measured relative humidity of the concretes. From **Figure** 5.21 it was observed that the amount of silica fume in the concrete (5% or 10%) had little influence on the measured relative humidity in the concretes.

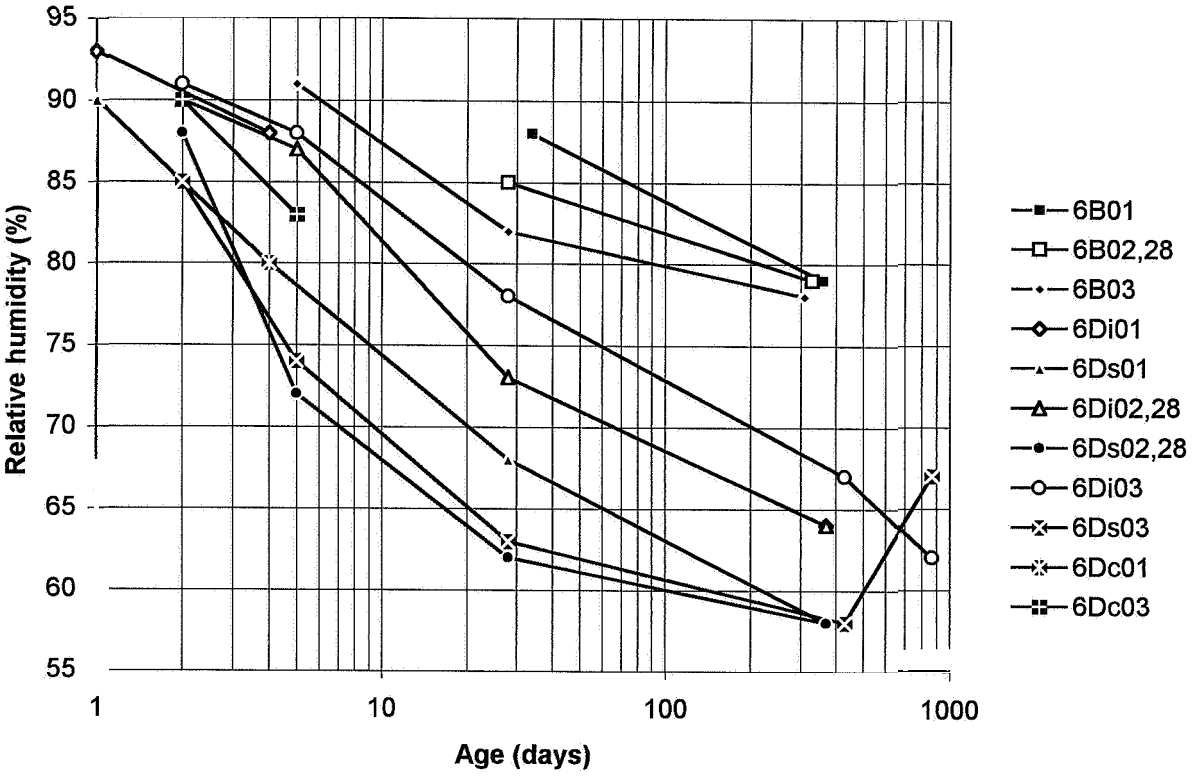

Figure 5.19 - Internal relative humidity in mix 6 versus age, symbols given above.

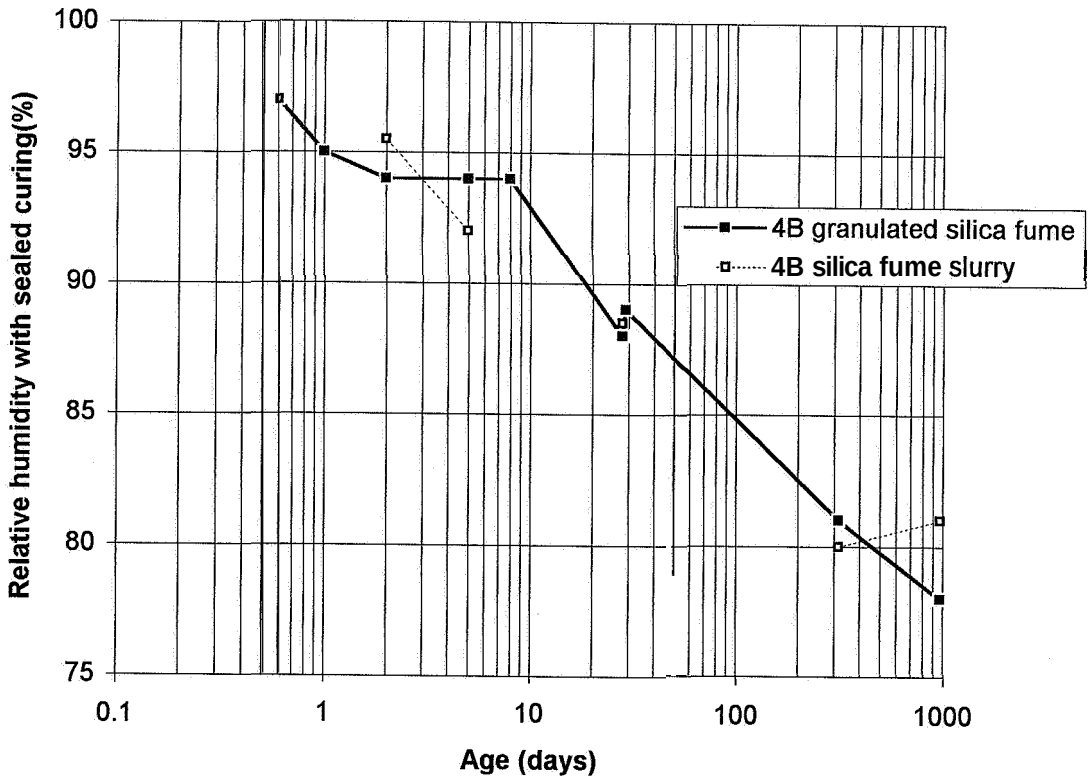

Figure 5.20 - Internal relative humidity in HPC mix 4 with sealed curing versus age.

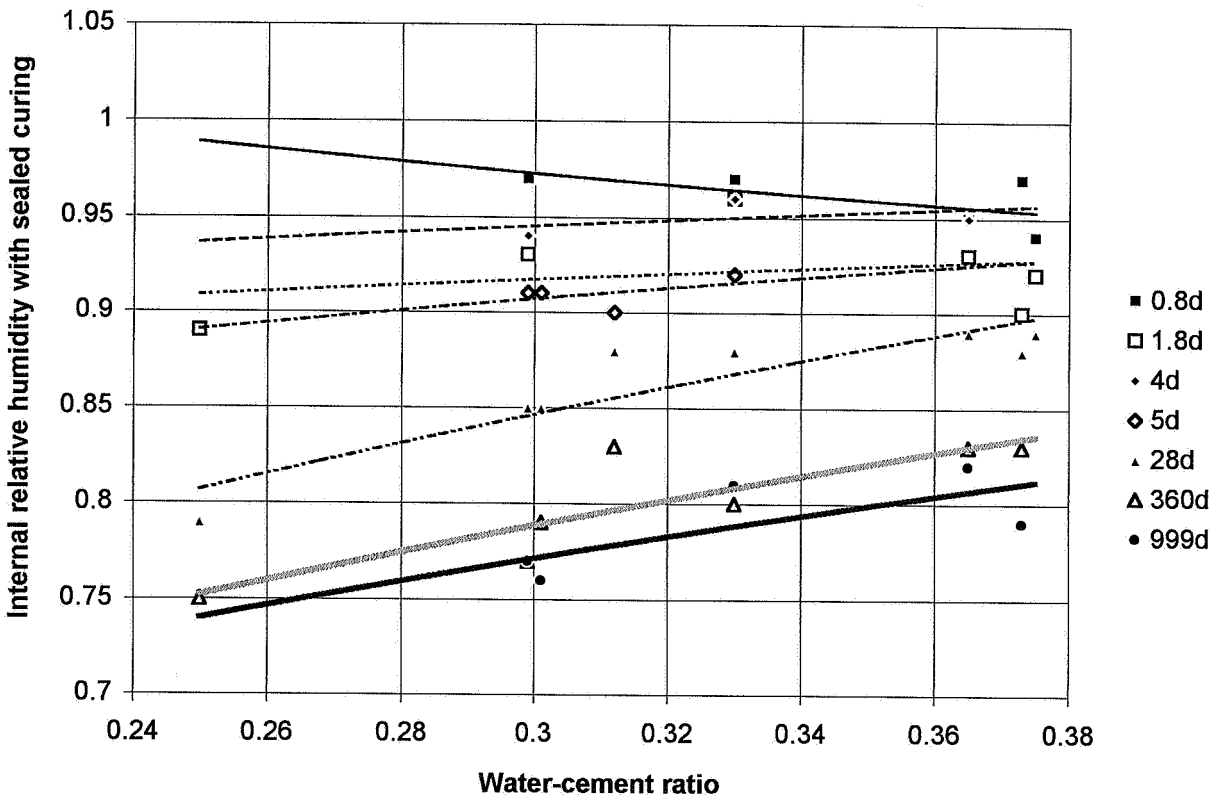

Figure 5.21 - Internal relative humidity in HPCs with sealed curing versus w/c.

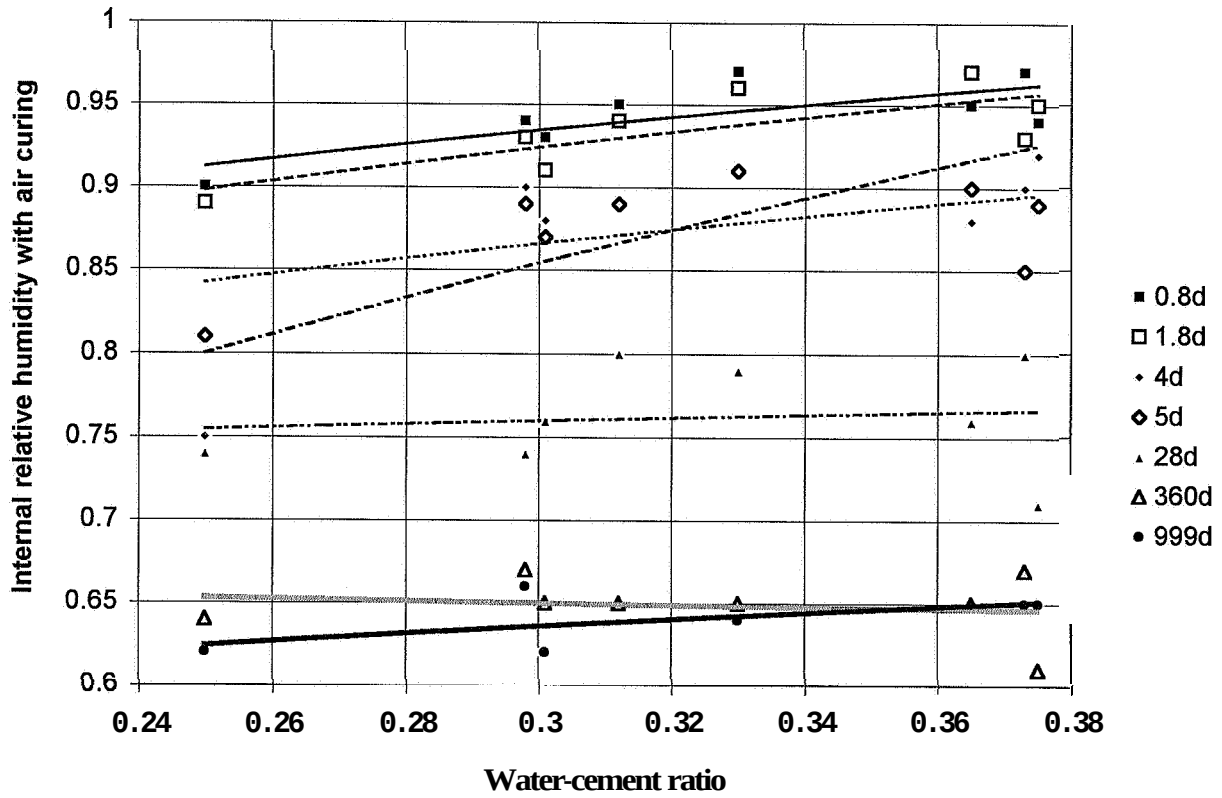

Figure 5.22 - RH of the inner part of HPC cubes with air curing versus w/c.

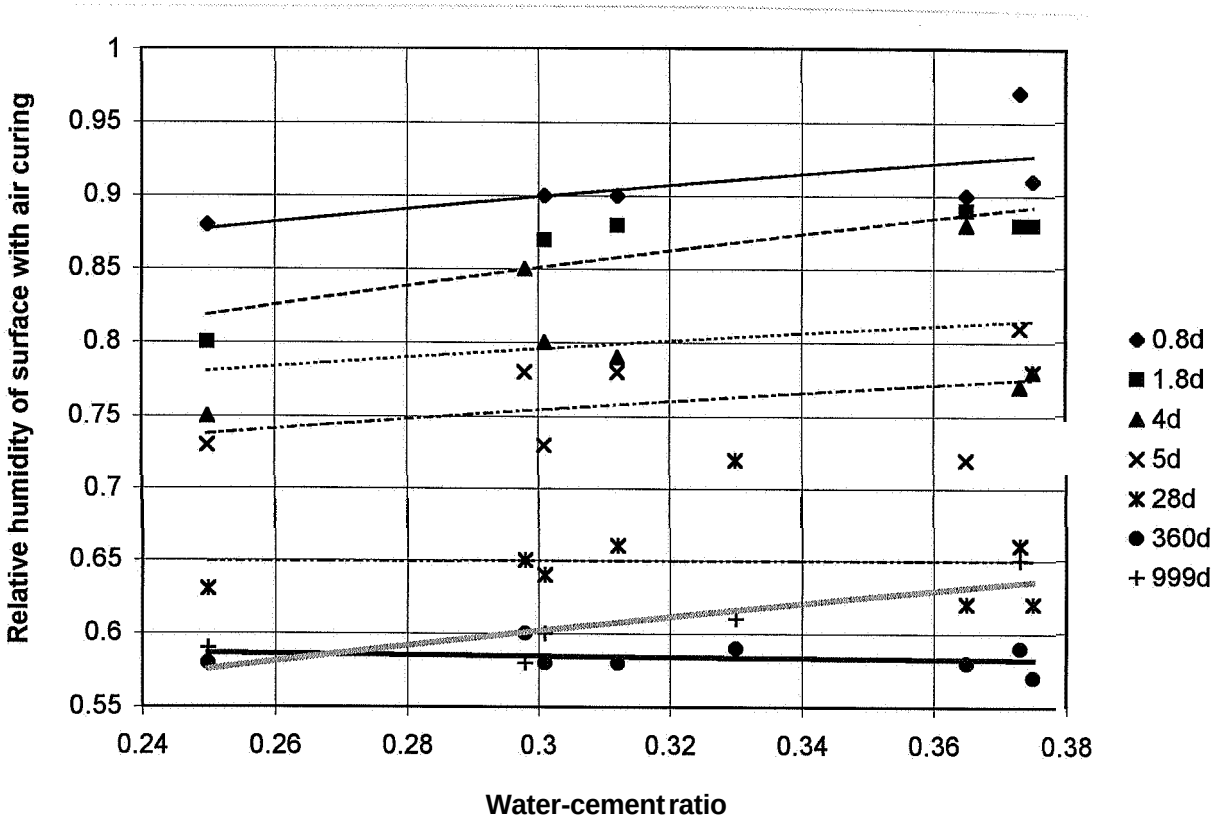

Figure 5.23 - RH of the surface of HPC cubes with air curing versus w/c.

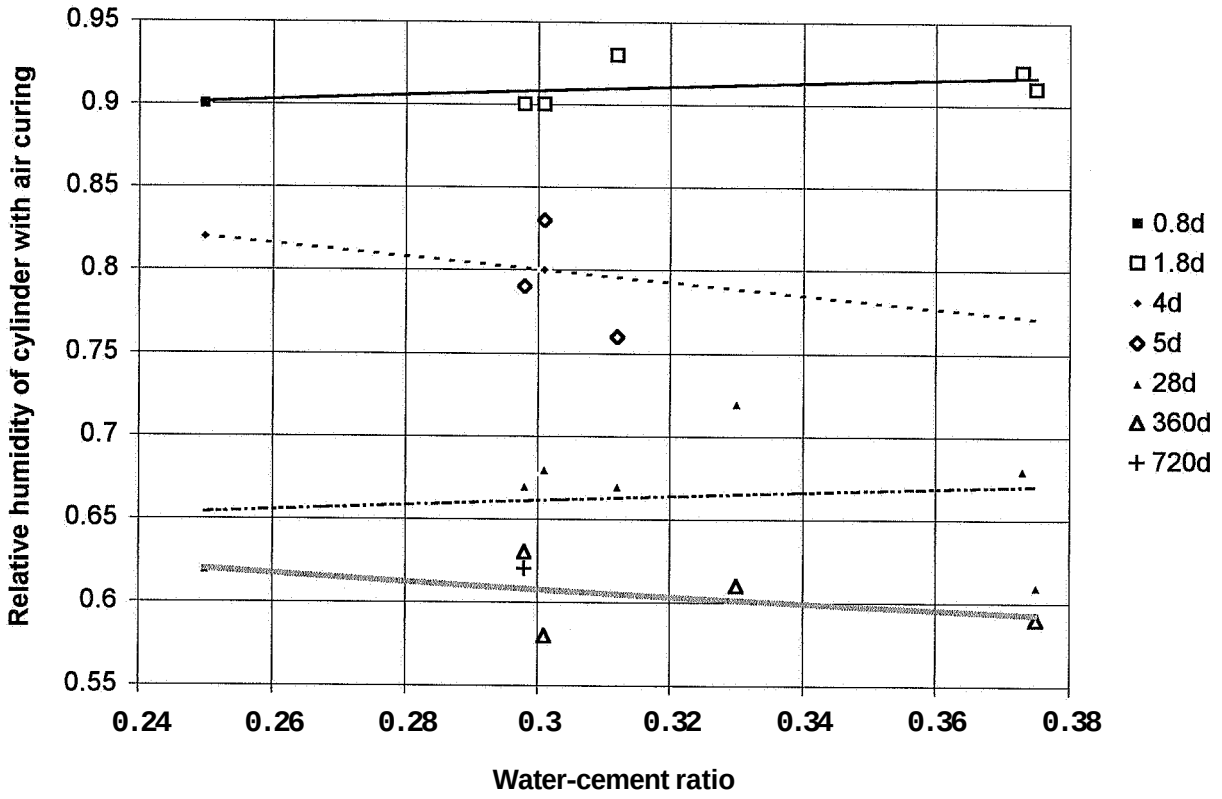

Figure 5.24 - RH of inner part of HPC cylinders with air curing versus w/c.

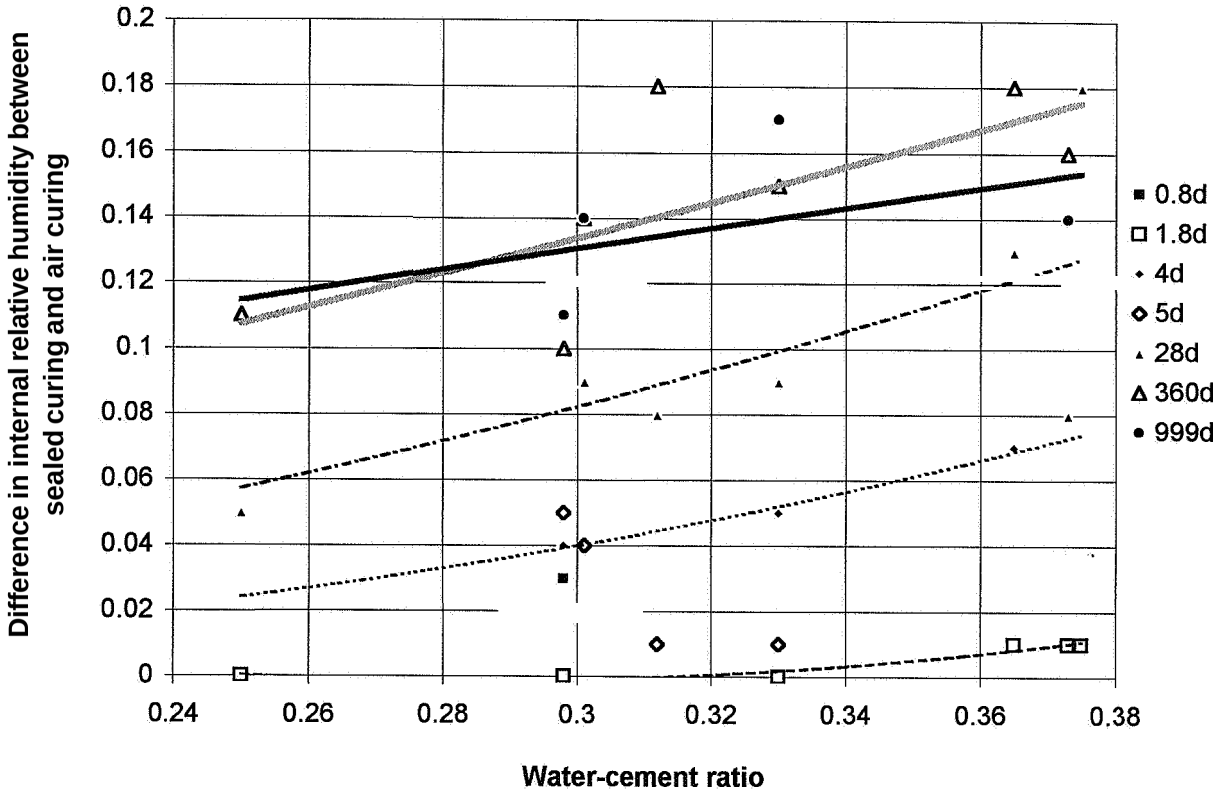

Figure 5.25 – RH-difference between inner part of sealed-cured and air-cured cubes.

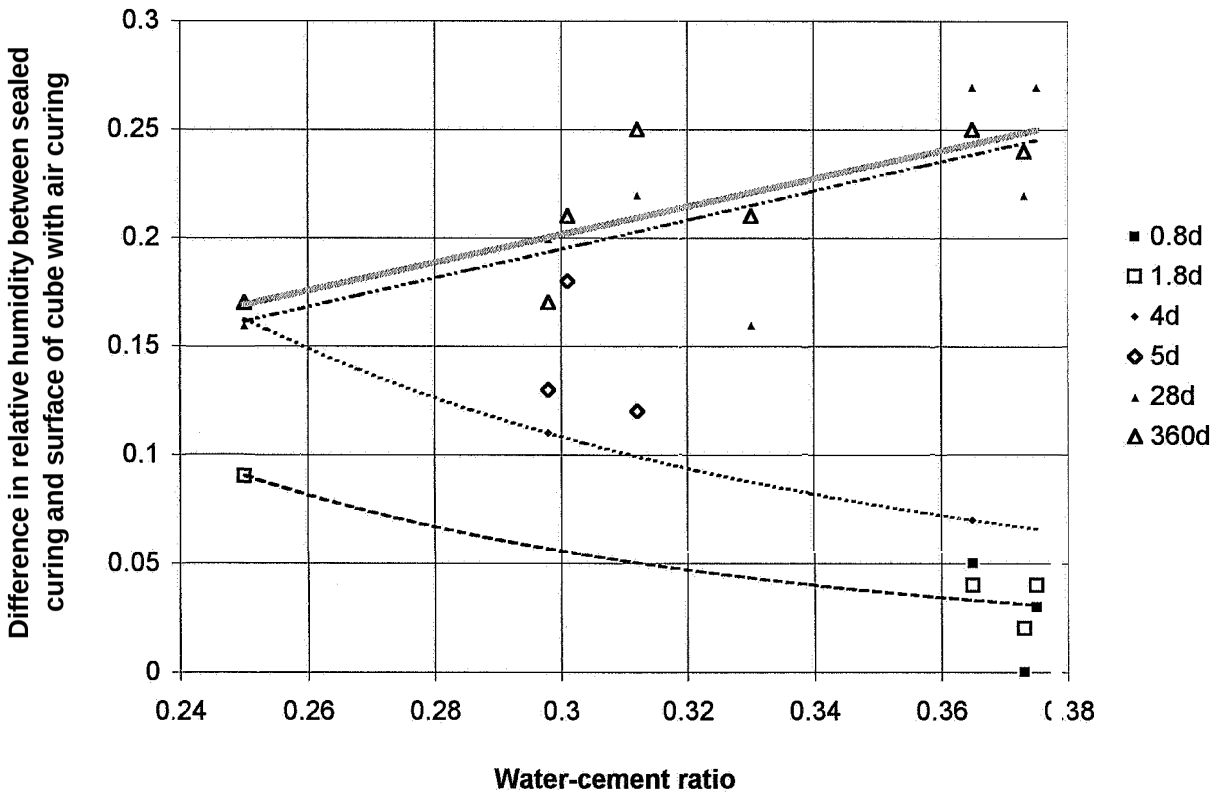

Figure 5.26 – RH-difference between surface of sealed-cured and air-cured cubes.

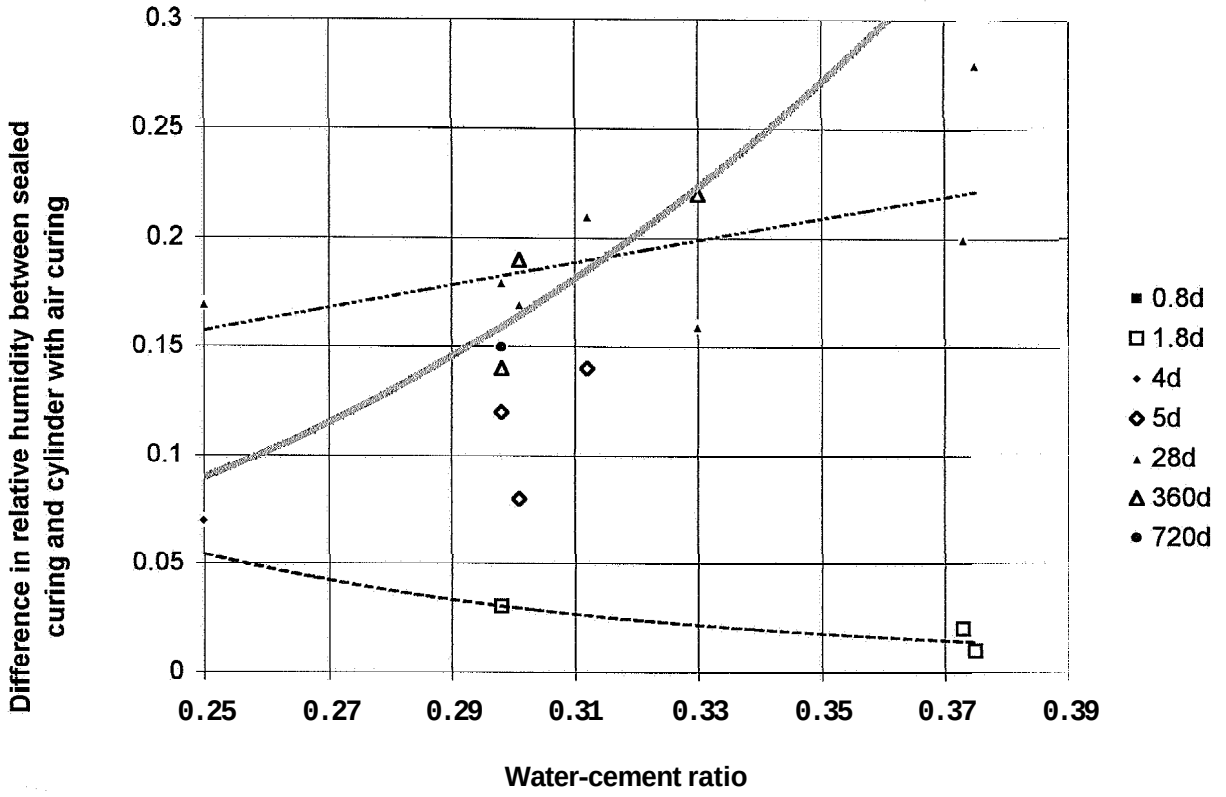

Figure 5.27 – RH-difference between sealed curing and air-cured cylinders.

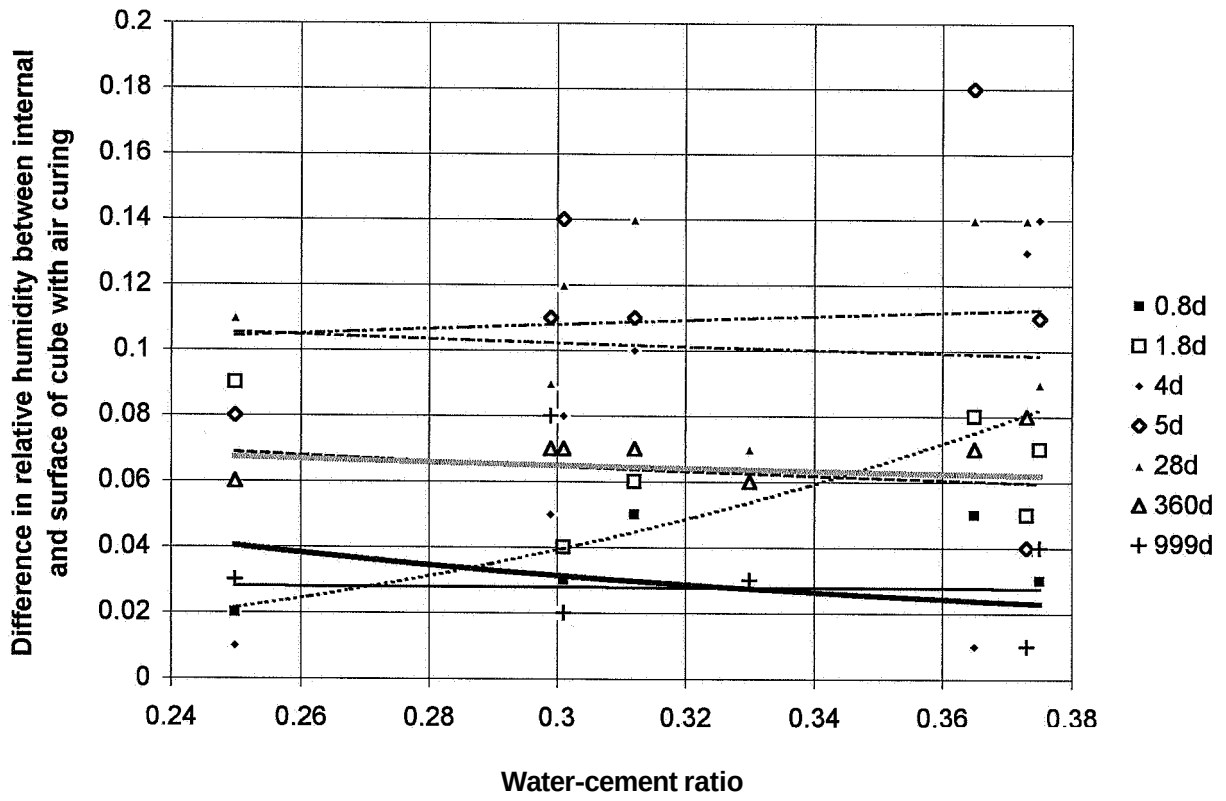

Figure *5.28* – RH-difference between inner **part** and surface of air-cured cubes.

As shown above, the main parameters affecting the internal relative humidity, RH (Ø), of HPC (when the temperature was held constant) were w/c, and age, t. The following general correlation was obtained:

$$O = a \cdot t^{b} \cdot (w/c)^{f \cdot \ln(t)+g} \qquad \{1<t<1000 \text{ days}; 0.25<w/c<0.38\} \qquad (5.39)$$

a, b, f, g denote constants given in **Table** 5.3.

Table 5.3- Constants in equation (5.31)

Curing type and type of measurement	**a**	**b**	f	**g**	**Fig.**
Sealed	0.965	0.0188	0.0331	0.0505	**5.21**
Air curing; inner part	1.193	-0.0883	-0.0155	0.1937	**5.22**
Air curing; surface	1	-0.0662	-0.0265	0.1564	**5.23**
Cylinder; inner part	1.0227	-0.1106	0.0128	0.0294	**5.24**
Difference between air and sealed curing; inner **part**	1.638	-0.2113	-0.3558	3.2275	**5.25**
Difference between air and sealed curing; surface	0.0022	1.1245	0.7537	-2.82	**5.26**
Difference between air and sealed curing; cylinder	0.0003	1.85	1.26	-3.86	**5.27**

It was also of interest to correlate the difference in relative humidity related to different kinds of curing versus age. **Figure *5.29*** shows the difference in relative humidity between sealed curing and air-cured cylinders (inner part) and **Figure *5.30*** the difference in relative humidity between inner and surface of cubes with *air* curing. The difference in relative humidity after 1000 days between sealed curing and *air* curing (inner part) was about 0.11 at a low water-cement ratio (w/c= 0.25), and about 0.18 at higher water-cement ratio (w/c= 0.37). The maximum difference in relative humidity between internal and surface with air curing was obtained at about 10 days' age (about 0.11 at a low water-cement ratio, w/c= 0.25 and about 0.18 at w/c= 0.37). The relative humidity, O, with sealed curing was correlated to the relative hydration, w_n/w:

$$Ø = 1.2 \cdot [(w/c)-0.467] \cdot \ln(w_n/w)+0.637 \cdot (w/c)+0.536$$
$$\{0.25<w/c<0.38;\ 0.10< w_n/w<0.60\} \qquad (5.40)$$

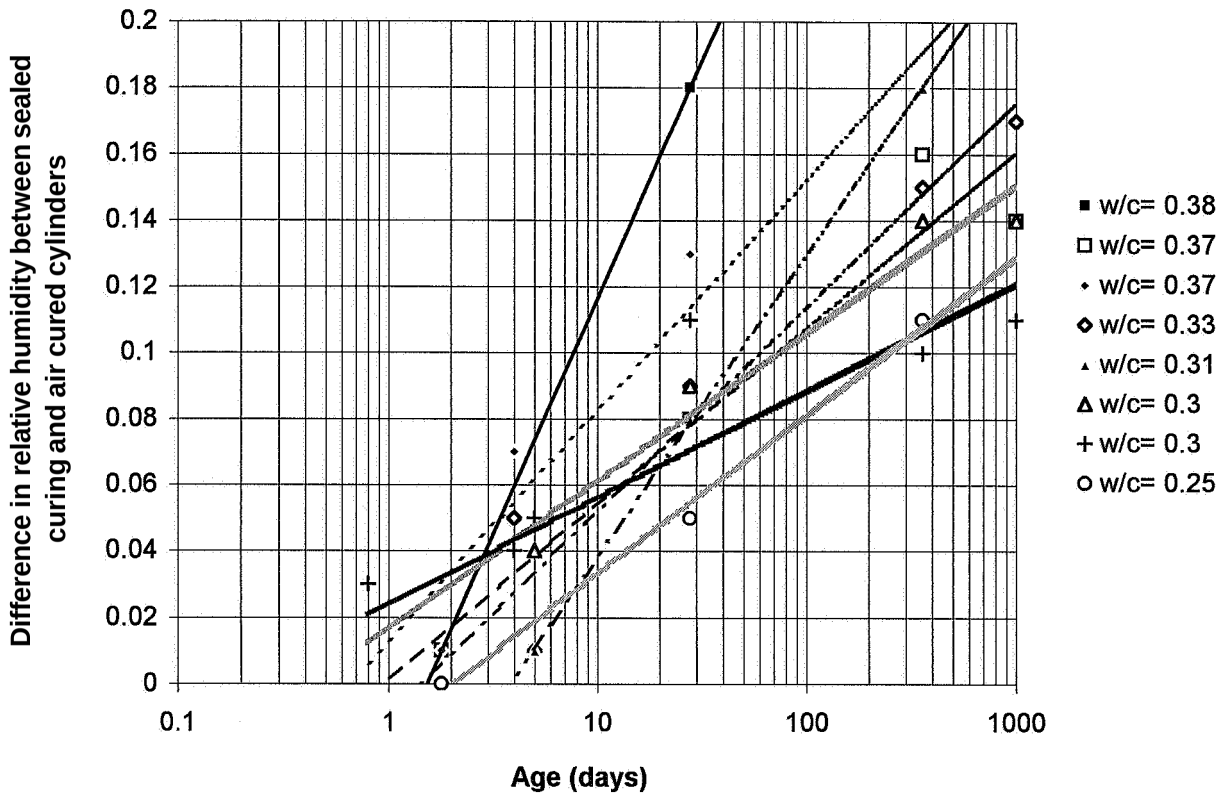

Figure 5.29 - RH-difference between inner part of sealed and air-cured cubes.

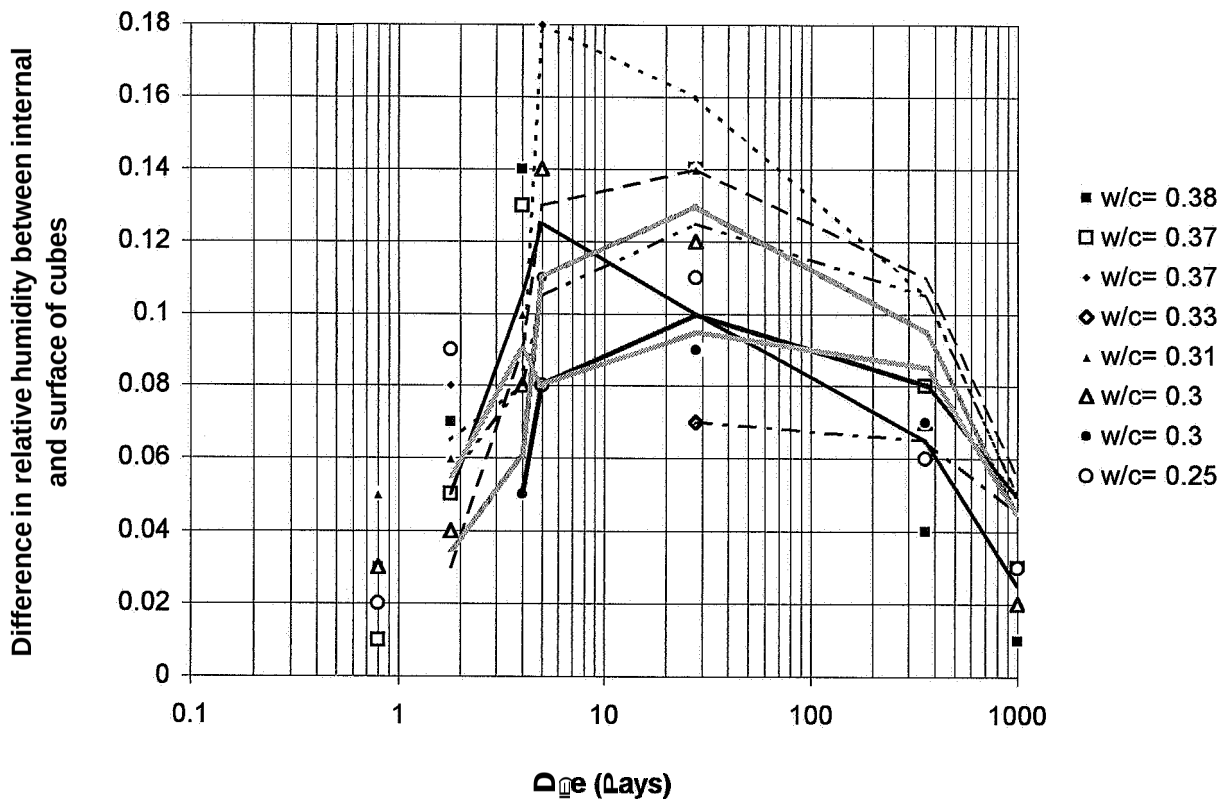

Figure 5.30 - RH-difference between internal and surface of cubes with air curing.

6. QUASI-INSTANTANEOUS DEFORMATIONS

6.1 General

Quasi-instantaneously performed creep loading is probably one way to separate the viscous and the plastic creep from the elastic deformation, **Acker (1993).** For mature concrete no differences seem to exist depending on whether the loading is rapidly applied or not, **Bazant (1995).** At early age and/or at a high stress/strength ratio the plastic deformations probably dominate the deformation. From the practical point of view, loading on concrete is often rapidly transferred when prestressing is done. The wires are cut with welding or grinding equipment, which imposes a sudden, more or less quasi-instantaneous loading on the concrete. One question of interest is whether this kind of loading causes larger creep deformation of the concrete than when the prestressing is slowly transferred to the concrete with hydraulic equipment. Finally, it was of interest to investigate early creep properties of HPC concerning its continued prolongation with long-term creep deformations.

6.2 xperimental procedure

6.2.1 Specimen and ambient climate

The general layout and the experimental approach are given in section 3.3 above. Materials, preparation of specimen and chronology are described in Section 4 above. The concrete mix proportions are presented in **Table 5.1**. The measurements were done in an extremely accurate MTS machine. Four measurement points were used outside the cylindrical specimen, 55 mm in diameter and 300 mm in length. Three measurements were taken parallel to the cylinder and one transversal. The length between the longitudinal measuring points was 250 mm and between the transversal points 55.5 mm. The measuring points were stiffly connected to the steel cast-in items in the specimen by pin bolts of 3 mm diameter. Schlumberger displacement and gauging transducers (LVDTs) fulfilled the measurements. The specimen was placed in a heat and moisture insulated box that was connected to a climate chamber. Thermo couples continuously registered the internal temperature of the specimen, **Figure 6.1.** Almost all the specimens obtained internal temperatures which varied between 19 and 21 "C. However, for one specimen (402) the temperature varied between 21 and 23 "C. Finally for two of the concretes (501 and 601) the temperature rose substantially after about 40 h of creep. **Figure 6.2** shows the ambient relative humidity recorded by a dew point meter, which was placed inside the insulated box close to the specimen. Symbols in Figures 6.1-6.2:

5...= HPC mix, **Table 5.1**
...01= loading at 0.8 day' age with stresslcylinder strength = 0.84
...02= loading at 2 days' age with stresslcylinder strength = 0.84
...03= loading at 2 days' age with stresslcylinder strength = 0.42
...28= loading at 28 days' age with stresslcylinder strength = 0.42

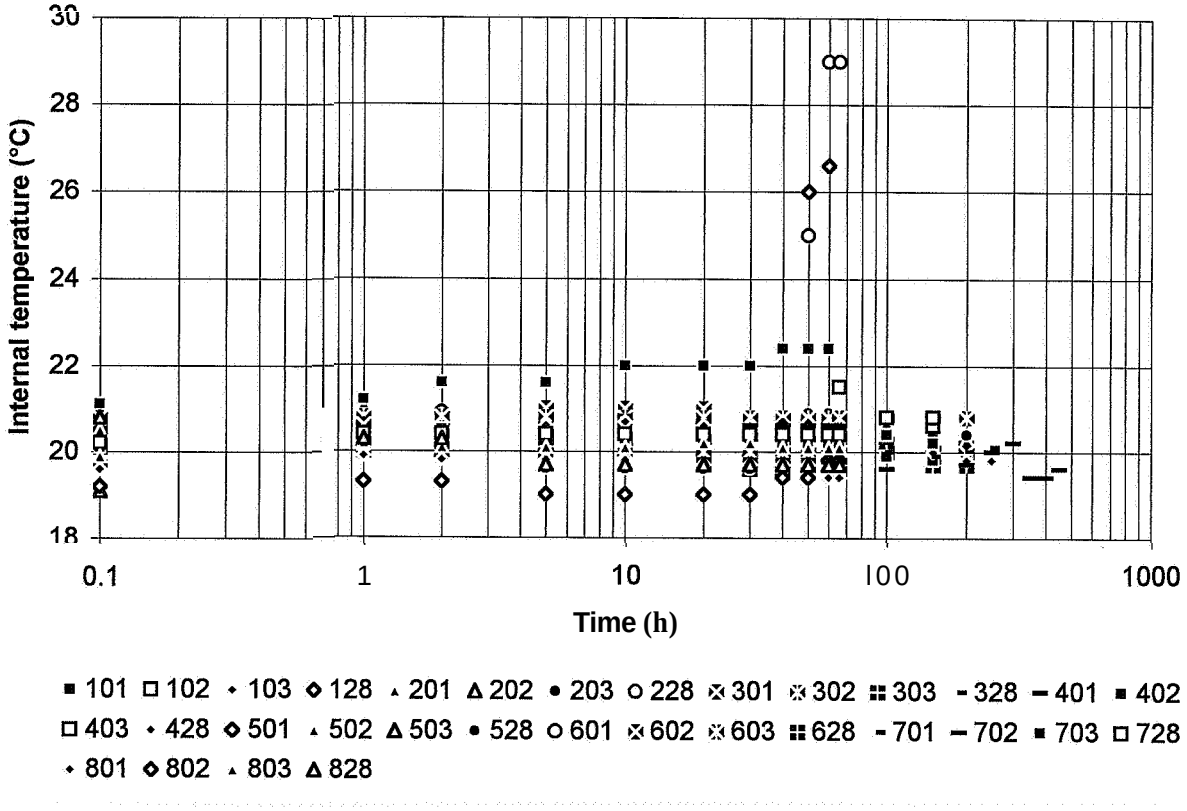

Figure 6.1 - Internal temperature of drying HPC. Symbols are given above.

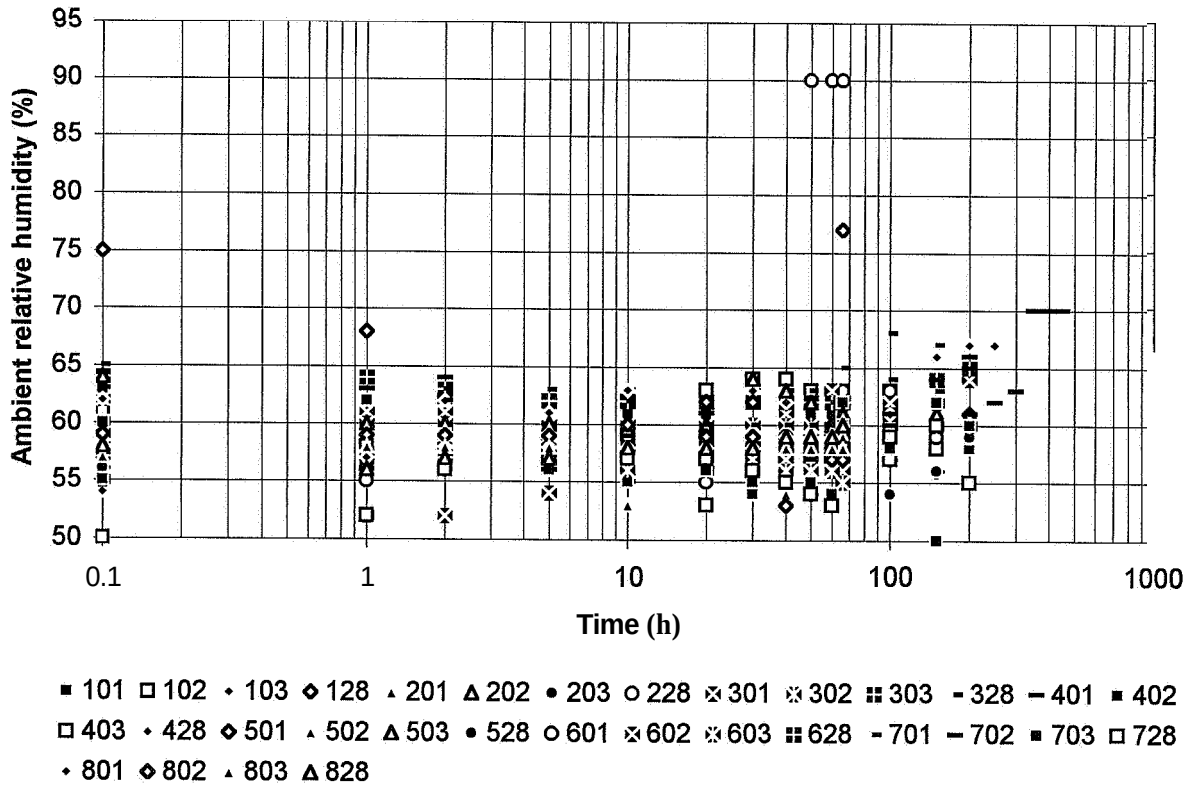

Figure 6.2 - Ambient relative humidity of drying HPC, symbols given above.

The temperature of the specimen and the ambient relative humidity were stabilised before the tests were commenced. The climate was controlled by the speed of the air-stream from a connecting climate chamber. When the internal temperature and the ambient relative humidity were stabilised, the revolution of the fan that controlled the air-stream was lowered to a minimum level. Within the period of short-term drying creep studies (66 hours' age) the ambient relative humidity of all specimens varied between 53% and 63%. After the short-term studies (during relaxation) the ambient relative humidity varied between 60% and 68% except for specimen 601 for which the relative humidity rose to 90% after 50 h of creep due to a failure in the equipment. The individual change for each specimen was normally within ± 3% RH. During the tests of basic creep in the MTS machine there was no insulated box around the specimen. The specimen was moisture insulated by 2-mm butyl rubber clothing as described above. The temperature was held constant at 20 ± 0.5 °C with air conditioning.

6.2.2 Loading and optimising the MTS machine

Before the creep tests were started the strength was obtained on cubes from the same batch of concrete as the cylinders, **Appendix** 5. The strength from the same batch of concrete was also recorded when the concrete was 28 days old. **Table 6.1** gives the strength/28-day strength ratio. The capacity of the MTS machine was enhanced to a sufficient level by the use of an extra nitrogen gas container. The pressure of the nitrogen gas was verified before the loading was applied.

As a preparation for the loading procedure an extra identically prepared specimen was placed in the MTS machine. The following routine was carried out before each test:

- The position of the specimen was measured in the MTS machine to ensure that it was centric.
- A loading of ≈ 0.1 kN was applied to the extra cylinder specimen in the MTS machine.
- **An** oscillation of ≈ 1 Hz was applied to the specimen.
- The gain, the loading speed and/or the braking rate of the loading in the MTS machine were preliminarily set dependent on the maturity of the concrete in the extra cylinder specimen.
- The rapid test loading was applied to the extra cylinder specimen.
- The loading in the MTS machine was recorded.
- LVDTs recorded the deformation of the cylinder specimen in an extra computer.
- Both the loading and the deformations were plotted to ensure that no load peak existed.
- If required, the gain, the loading speed and/or the braking rate of the loading in the MTS machine were adjusted to avoid any load summit.
- A short analysis was performed of the pre-test before the final loading was done.

6.2.3 Commencement of testing

After optimisation of the loading of the cylinder in the MTS machine, another specimen was placed in the machine for testing. The following routine was used:

- The LVDTs were firmly fixed to the cast-in items in the cylinder (3 LVDTs for longitudinal measurements and 1 LVDT to record the transversal deformation).
- The position of the cylinder in the MTS machine was adjusted to avoid eccentricities.
- A loading of 0.1 kN (0.04 MPa) was applied to the cylinder specimen to avoid dynamic effects at loading.
- The ambient climate box was placed and a constant climate provided by air conditioning for half an hour before the quasi-instantaneous loading.
- Thermo stability between the specimen and the ambient climate was established.
- The ambient relative humidity, RH, was set at RH= 55%.
- The computer recording of the LVDT deformations was started.
- The loading was applied in the MTS machine within 1 s fiom starting the computer recorder.
- About 6000 measurements were recorded during 3 s.
- The rapid recording of the deformations was interrupted.
- After about 1 minute the deformation measurement continued each minute.
- The loading was mainly applied within 0.015 s. There was no load-peak at the start of the testing. The loading was applied with a loading rate of about 1700 MPa/s. The loading was kept constant for 66 h.

6.3 Sources of error

Loading and eccentricity of loading:

The loading of the MTS machine was calibrated to the compressive testing machine by a precision load-cell. During the testing the loading was kept within 0.01 kN. The eccentricity was calculated for each loading experiment.

Deformations of the LVDTs:

The deformations given by the LVDTs were calibrated with a Mitutoyo micrometer.

Effects of lateral strain:

The specimen was fiee to move in the lateral direction. The lateral deformation was measured at the same time as the longitudinal. Deformation were recorded transversely to the specimen to obtain Poisson's ratio. Given a zero lateral displacement, a lateral stress around the specimen towards the centre line of it would have been required. The stress required was:

$$\sigma_y = \upsilon \cdot \sigma_x \qquad (6.1)$$

σ_x denotes the longitudinal stress
σ_y denotes the lateral stress
υ denotes Poisson's ratio

To compensate for the lateral stress and to achieve the same longitudinal deformation as measured without any lateral stress on the specimen, the longitudinal stress had to be increased. The total longitudinal stress including the increase due to the lateral stress was then:

$$\sigma_{x,tot} = \sigma_x \cdot (1+\upsilon^2) \qquad (6.2)$$

Effect of variation in ambient climate:

Another source of error was variation in the ambient climate. However, an air-conditioned box was placed in the MTS machine. These variations were small.

6.4 Results

Figure 6.3 gives the creep compliance [specific creep, J(t,t′)] of mix 6 versus time. **Figure** 6.4 shows the compliance of quasi-instantaneous loading for concretes at 28 days' age. **Appendix 6** gives all the quasi-instantaneous deformation of all the experiments. Symbols used in the figures:

t denotes age of the concrete
t' denotes age of the concrete when loading
J(t,t′) denotes creep compliance (millionths/MPa)
5... = HPC **mix, Table 5.1**
...01 = loading at 0.8 days' age with stresslcylinder strength = 0.84
...02 = loading at 2 days' age with stresslcylinder strength = 0.84
...03 = loading at 2 days' age with stresslcylinder strength = 0.42
...28 = loading at 28 days' age with stresslcylinder strength = 0.42

6.5 Accuracy

Loading:

The loading was kept within 0.01 kN, corresponding to a stress variation of ± 0.004 MPa.

Deformations of the LVDTs:

The accuracy of the calibrations was ± 0.002 mm. The compliance, J(t,t′), was evaluated:

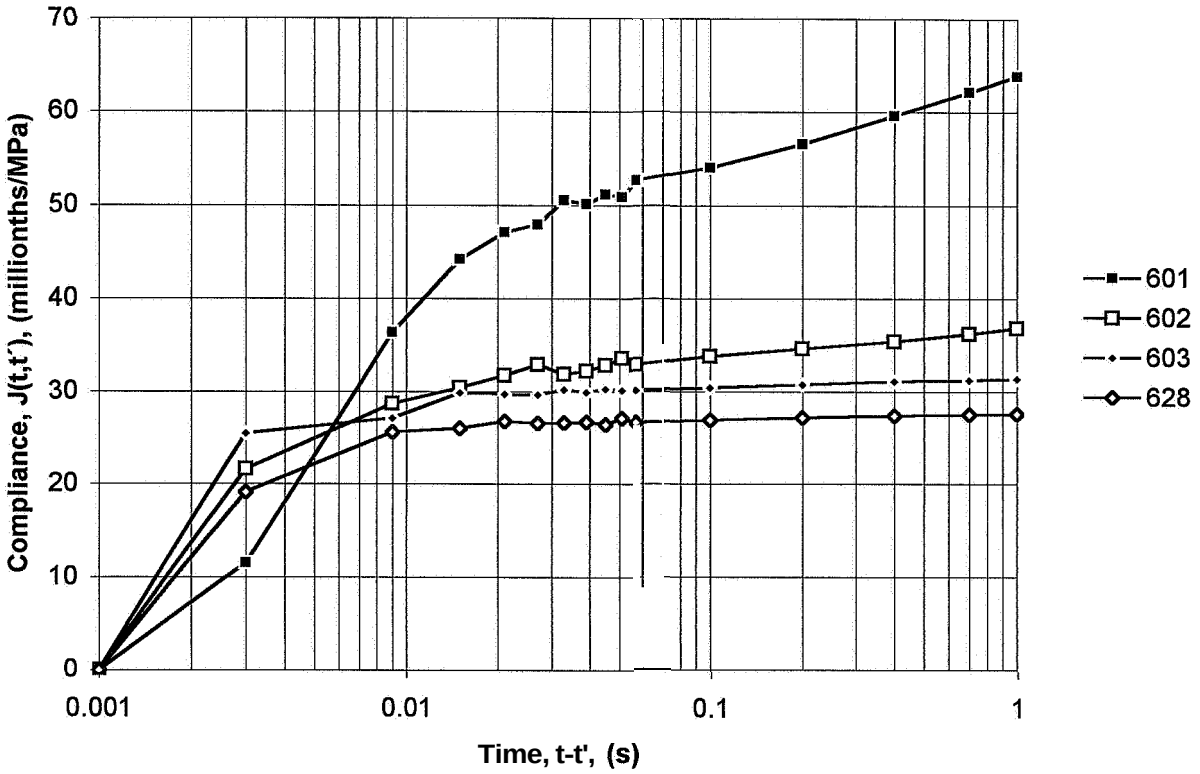

Figure 6.3 - Quasi-instantaneous compliance of mix 6. Symbols are given above.

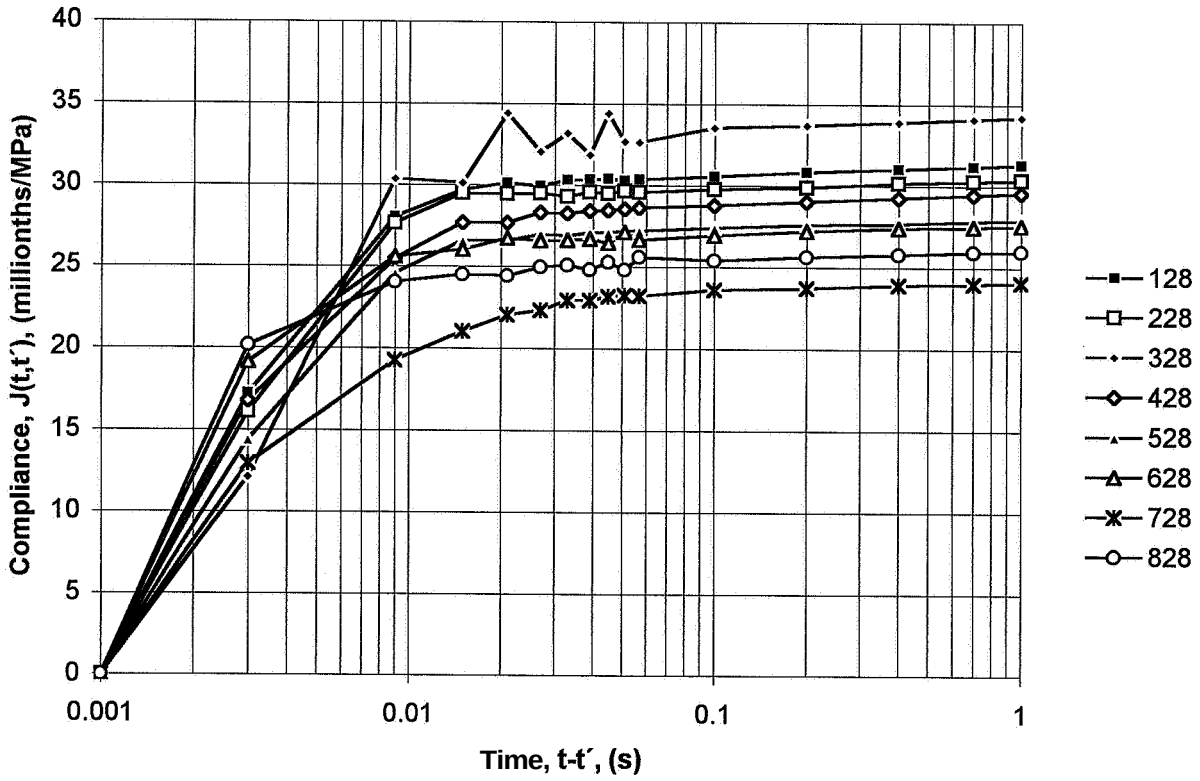

Figure 6.4- Quasi-instantaneous compliance of all mixes 28 days' age when loading.

$$J(t,t') = \varepsilon/\sigma \quad (6.3)$$

$J(t,t')$ denotes the compliance (specific creep, millionths/MPa)
E denotes the concrete deformation (millionths)
σ denotes the compressive stress (MPa)

The total accuracy of the compliance as regards the loading and deformation errors could then be expressed as $\delta J(t,t')/J(t,t')$. The logarithm of equation (6.3) was:

$$\ln J(t,t') = \ln \varepsilon - \ln \sigma \quad (6.4)$$

$\ln J(t,t')$ denotes the natural logarithm of compliance (specific creep)

After differentiation the relative fault, $\delta J(t,t')/J(t,t')$, was obtained [$\delta \ln J(t,t')/\delta J(t,t') = 1/J(t,t')$]:

$$\delta J(t,t')/J(t,t') = \delta\varepsilon/\varepsilon - \delta\sigma/\sigma \quad (6.5)$$

With 10 MPa stress the maximum fault was estimated according to equation (6.5): $\delta J(t,t')/J(t,t') = \delta\varepsilon/\varepsilon - \delta\sigma/\sigma = 0.004/0.25 - 0.008110 = 0.008 \approx 0.01$ thus very small.

Eccentricity:

Since the longitudinal measurements were collected at three sides of the specimen the eccentricity, e, of the loading could be calculated adopting elastic conditions:

$$e = \sqrt{e_x^2 + e_y^2} \quad (6.6)$$

$$e_x = \frac{a}{\Delta l} \cdot (\Delta l_1 - \frac{\Delta l_2}{2} - \frac{\Delta l_3}{2}) \quad (6.7)$$

$$e_y = \frac{a \cdot \sqrt{3}}{\Delta l \cdot 2} (\Delta l_2 - \Delta l_3) \quad (6.8)$$

$$\Delta l = \Delta l_1 + \Delta l_2 + \Delta l_3 \quad (6.9)$$

a denotes the centre distance of the LVDT (mm)
e eccentricity at loading provided elastic condition, which did not apply for young HPC (mm)
e_x denotes estimated eccentricity to the "x" axis (mm)
e_y denotes estimated eccentricity to the "y" axis (mm)
Δl denotes the total deformation of the LVDTs (mm)
Δl_i denotes deformation of the different LVDTs (mm)

However, as pointed out several times above, the conditions were not elastic during the tests of concrete at early ages. At early ages the concretes performed more plastically, which diminished the eccentricity. No estimation was performed to distribute the elastic/plastic behaviour of the concrete at early ages. Mature concrete was almost elastic. Still adopting elastic conditions, the maximum acceptable eccentricity to avoid compressive stress in the concrete that exceeded the ultimate strength of the concrete was easily estimated. The moment, M , due to the eccentricity was estimated by the following equation:

$$M_e = P \cdot e \qquad (6.10)$$

M_e denotes the moment due to the eccentricity (Nm)
P denotes the testing force (N)
e denotes the eccentricity (mm)

The stress, G, in the concrete due to a centric force P was (d= the diameter of the cylinder):

$$\sigma = \frac{P \cdot 4}{\pi \cdot d^2} \qquad (6.11)$$

d denotes the diameter of the specimen (mm)
P denotes the centric force loaded on the specimen (N)
G denotes the compressive stress in the specimen

The additional relative compressive stress, $\Delta\sigma$, due to the eccentricity was then:

$$\frac{\Delta\sigma}{\sigma} = \frac{P \cdot e \cdot 32}{\pi \cdot d^3} \cdot \frac{\pi \cdot d^2}{P \cdot 4} \qquad (6.12)$$

$\Delta\sigma$ denotes the additional compressive stress in the specimen

At stress/cube strength ratio = 0.3 (centric force), an eccentricity, e = 16 mm, gave the ultimate stress at the edge of the cylinder adopting elastic conditions. At stresslcube strength ratio = 0.6, an eccentricity, e = 4.5 mm, gave an ultimate stress at the edge of the cylinder adopting elastic conditions. The figures given applied to mature concrete. As mentioned above, a larger eccentricity applied to concrete at early ages, since the behaviour of the concrete then was more plastic. **Table 6.1** provides the strength/28-day strength ratio. **Table 6.2** shows the estimated eccentricities (mm) at the quasi-instantaneous loading given elastic conditions according to equation (6.6). Some of the eccentricities were quite large given elastic conditions. In reality the behaviour of the young concrete was more or less plastic, which diminished the eccentricity substantially. The effect of the eccentricity of the loading on the creep of the cylinders will be discussed below.

Table 6.1 - Strength/28-day strength ratio.

Concrete	01	02	03	28
1	0.338	0.464	0.520	1
2	0.279	0.506	0.530	1
3	0.350	0.517	0.524	1
4	0.277	0.390	0.505	1
5	0.359	0.523	0.442	1
6	0.306	0.550	0.537	1
7	0.330	0.573	0.568	1
8	0.327	0.585	0.560	1

Table 6.2 - Loading eccentricity (mm)

Concrete	01	02	03	28
1	19	6.5	3.2	4.8
2	11	7	9.7	4.9
3	9.8	16.2	5.8	4.1
4	5.6	2.9	14.9	3.4
5	2.3	9.1	12.4	3.2
6	8.3	19	14	2.2
7	9.5	2	5.5	2.8
8	11.8	4.3	8.8	9.6

Effect of lateral strain:

The effect of Poisson's ratio, υ, will be studied during unloading the specimen. The compliance is decreased by a multiplication factor of υ^2 due to the lateral strain.

6.6 Analyses

6.6.1 Stress and time dependence

The compliance during the first second was separated: one part expressed the deformation due to the initial loading; the other part the creep within 1 s of loading:

$$J(t,t') = a \cdot \int d(t-t')/(t-t') + b = a \cdot \int d(t-t')/(t-t') + 1000/D_{t'} \qquad (6.13)$$

a denotes the compliance rate, **Table 6.3** [millionths/(MPa·s)]
b denotes the initial compliance 1 s after loading, **Table 6.4** (millionths/MPa)
t denotes the age of the concrete (s)
t' denotes the age of the concrete at loading (s)
t-t' denotes loading time (s)
$D_{t'}$ denotes the deformation modulus after 1 s of loading (GPa)
$J(t,t')$ denotes the compliance (specific creep, millionths/MPa)

It was essential to define the initial compliance at loading, b, to make further evaluations of the deformation modulus (inverted compliance after loading) and the creep coefficient feasible. However some of the loadings were not made within 0.01 s. Then the initial compliance, b (millionths/MPa), at 0.01 s was calculated by logarithmic extrapolation from the time of stable loading. **Figure 6.5** shows the compliance rate of HPC specimen versus the maturity. The maturity is indicated as the relative 28-day strength, f_c / f_{c28}. The creep rate was dependent on the maturity and on the stress/strength level. **Appendix 6** shows an enlargement of **Figure 6.5.** **Figure 6.5** and **Appendix 6** show that the eccentricity had no influence on the creep rate even through the initial deformations mainly were plastic, **Figure 1.1. Figure 6.6** clearly shows that the compliance rate was fairly constant for mature concrete.

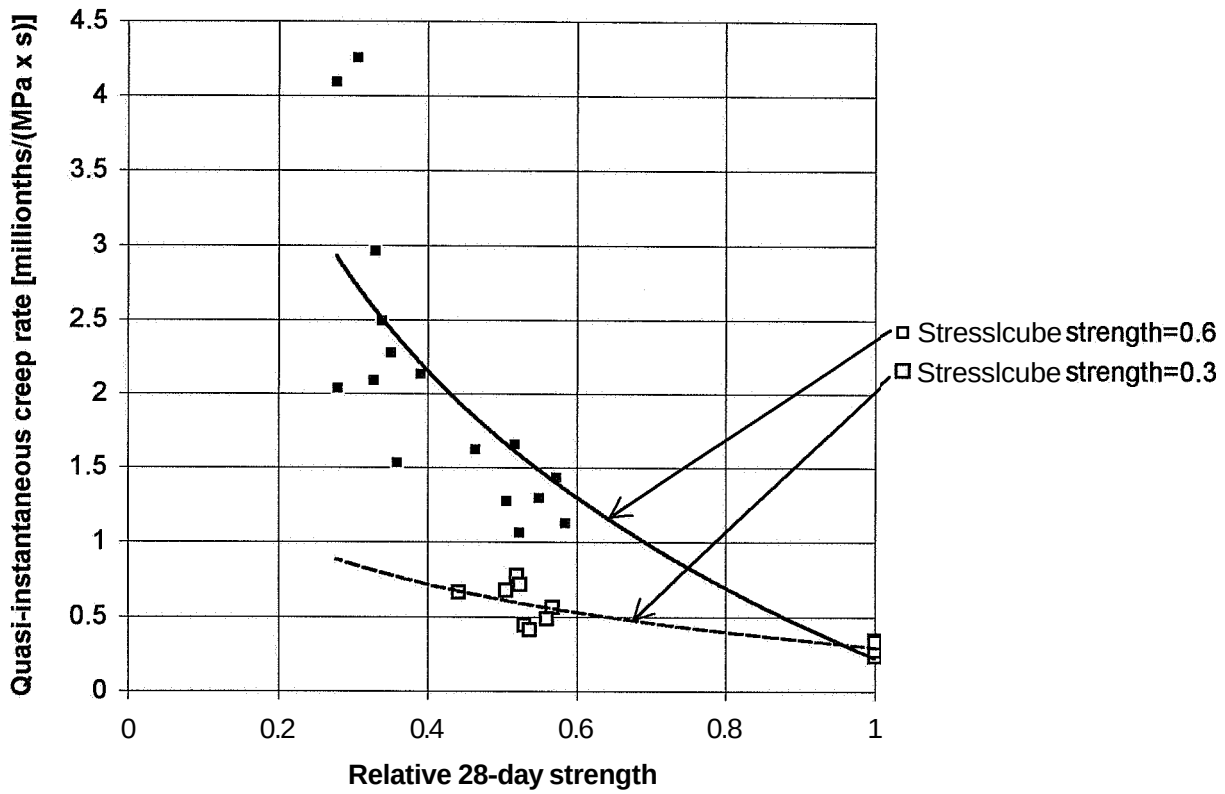

Figure 6.5 - Compliance rate versus maturity (28-day relative strength, f_c/f_{c28}).

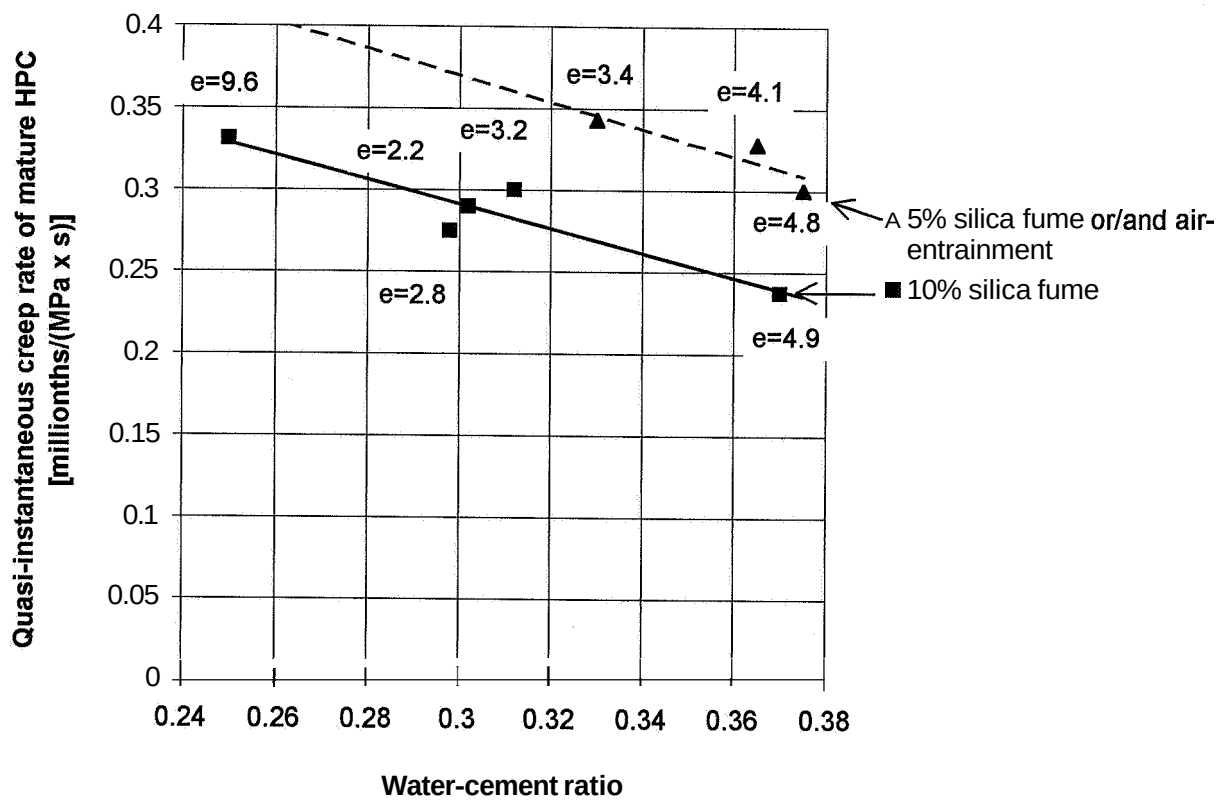

Figure 6.6 - Compliance rate of mature HPC versus w/c. Eccentricity, e (mm).

Table 6.3 - Compliance rate when loading (millionths/MPa·s)

Concrete	01	02	03	28
1	2.49	1.62	0.777	0.295
2	1.27	2.04	0.444	0.237
3	2.27	1.66	0.718	0.328
4	4.09	2.13	0.679	0.343
5	1.53	1.06	0.666	0.296
6	4.25	1.30	0.413	0.290
7	2.96	1.43	0.566	0.275
8	2.09	1.13	0.487	0.331

Table 6.4 - Compliance 1 s after loading (millionths/MPa)

Concrete	01	02	03	28
1	66.3	46.3	42.1	31.3
2	44.8	45.3	44.4	30.3
3	53.8	50.5	38.0	34.2
4	64.3	44.8	34.3	29.6
5	42.5	36.2	42.5	28.0
6	64.0	36.8	31.4	27.6
7	50.5	34.5	29.6	24.1
8	45.6	32.1	30.3	26.1

Figure 6.6 also shows that the eccentricity had no effect on the compliance rate when loading at 28 days' age with more or less elastic deformations during the first second of loading. However, the creep rate was about 10% larger in concretes that contained 5% silica fume or/and air-entrainment than in concretes with 10% silica fume. Addition of more silica fume seemed to decrease the creep rate when w/c was held constant. This is a secondary effect of strength growth, cp. Section 5 above. When silica fume was cast in HPC high strength growth was observed especially at early ages, **Persson (1996A)**. The following equation was obtained for the creep rate, a_D, of drying concrete [millionths/(MPa·s)]:

$$a_D = [0.37-0.23\cdot(\sigma/f_c)]\cdot s_{a5} + [1.2-5.5\cdot(\sigma/f_c)]\cdot \ln(f_c/f_{c28}) \qquad (6.14)$$

a_D denotes the compliance rate with air curing [millionths/(MPa·s)]
f_c/f_{c28} denotes the relative 28-day cube strength at loading $\{0.3< f_c/f_{c28}<1\}$
$\ln(f_c/f_{c28})$ denotes the natural logarithm of the relative 28-day cube strength
s_{a5} = 1.1 for HPC with 5% silica fume or/and air-entrainment; s_{a5} = 1 for HPC with 10% silica fume and no air-entrainment
σ/f_c denotes the stress/cube strength ratio at loading $\{0.3<\sigma/f_c<0.6\}$

6.6.2 Comparison with basic creep

As part of the project quasi-instantaneous loadings were performed on 32 sealed cylinders (constant moisture and temperature conditions), i.e. basic creep, **Persson (1995A), Appendix 6** (sealed specimen). **Figure 6.7** shows the relationship between compliance and the relative strength at loading during basic creep conditions. The stresslstrength levels 0.3 and 0.6 are indicated. However, the overlapping of relative strength, f_c/f_{c28}, where the creep was studied with a stresslstrength level at both 0.3 and 0.6, was very little (actually it varied only between 0.4 and 0.5). From a practical point of view, high stresslstrength ratio, $\sigma/f_c \approx 0.6$, is used for concrete at early ages, i.e. at low strength/28-day strength, f_c/f_{c28}. In the mature state lower $\sigma/f_c \approx 0.3$ is used. The results are thus of practical and theoretical interest. The following equation was obtained for the creep rate, a_B, of the concrete [millionths/(MPa·s)]:

$$a_B = [0.18+0.42\cdot(\sigma/f_c)]\cdot s_5 + [0.12-2\cdot(\sigma/f_c)]\cdot \ln(f_c/f_{c28}) \quad (6.15)$$

a_B	denotes the compliance rate with sealed curing [millionths/(MPa·s)]
f_c/f_{c28}	denotes strength/28-day strength $\{0.4< f_c/f_{c28}<1$ for $\sigma/f_c=0.3$; $0.15<f_c/f_{c28}<0.5$ for $\sigma/f_c=0.6\}$
$\ln(f_c/f_{c28})$	denotes the natural logarithm of the relative 28-day cube strength
s_5	= 1.5 for HPC with 5% silica fume; s_5= 1 for 10% silica fume
σ/f_c	denotes the stress/cube strength ratio at loading $\{0.3<\sigma/f_c<0.6\}$

6.6.3 Influence of moisture status

With the stresslstrength level = 0.3 the difference of creep rate between basic creep and drying creep was very little. However, with the stresslstrength level = 0.6 the creep rate under drying conditions (air curing) was about 50% larger than with sealed curing. During drying a certain amount of shrinkage occurred at the surface of the concrete, which caused an uneven distribution of stress in the cylinder. **Figure 6.8** shows the creep rate of HPC versus the relative strength with the difference in relative humidity indicated. From **Figure 6.8** the creep rate, $a_{\sigma/fc}$, versus the relative strength, f_c/f_{c28}, and the difference between the internal relative humidity of the inner part, $Ø_i$, and the surface, $Ø_s$, of the cylinder, $\Delta Ø = Ø_i - Ø_s$, was obtained, **Figure** 5.24 [millionths/(MPa·s)]:

$$a_{0.3} = 0.30-0.04\cdot\Delta Ø -(0.48+0.02\cdot\Delta Ø)\cdot\ln(f_c/f_{c28}) \quad \{\sigma/f_c=0.3;\ 0.4< f_c/f_{c28}<1\} \quad (6.16)$$

$$a_{0.6} = 0.43-2.7\cdot\Delta Ø-(1.07+5.14\cdot\Delta Ø)\cdot\ln(f_c/f_{c28}) \quad \{\sigma/f_c=0.6;\ 0.15< f_c/f_{c28}<0.5\} \quad (6.17)$$

$a_{0.3}$	denotes the creep rate with stresslstrength = 0.3 [millionths/(MPa·s)]
$a_{0.6}$	denotes the creep rate with stress/strength = 0.6 [millionths/(MPa·s)]
$\ln(f_c/f_{c28})$	denotes the natural logarithm of the relative strength/28-day strength $\{0.4< f_c/f_{c28}<1$ for $\sigma/f_c=0.3$; $0.15<f_c/f_{c28}<0.5$ for $\sigma/f_c=0.6\}$
$Ø_i$	denotes the internal relative humidity of the inner part of the cylinder
$Ø_s$	denotes the relative humidity of the surface of the cylinder
A 0	denotes the difference between the internal relative humidity of the inner part, $Ø_i$, and the surface, $Ø_s$, of the cylinder

The moisture gradient observed in drying specimens was the cause of the additional drying creep rate that was observed at drying compared with sealed curing.

6.7 Conclusions

- The early creep rate of HPC was obtained for both drying and sealed curing. The loading was performed within about 0.01 s.
- The effect of the maturity on the early deformations properties was detected. The effect of stress-level and eccentricity on the creep was also detected.

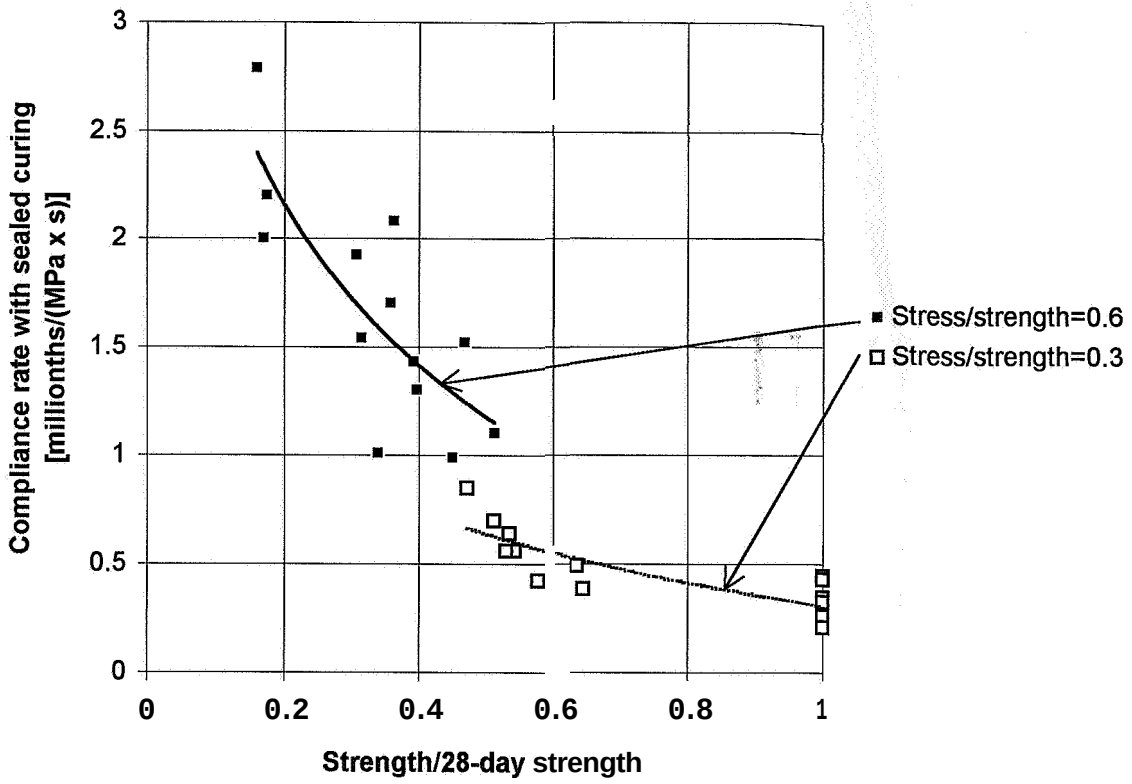

Figure 6.7 – Creep rate of HPC with sealed curing versus relative 28-day strength.

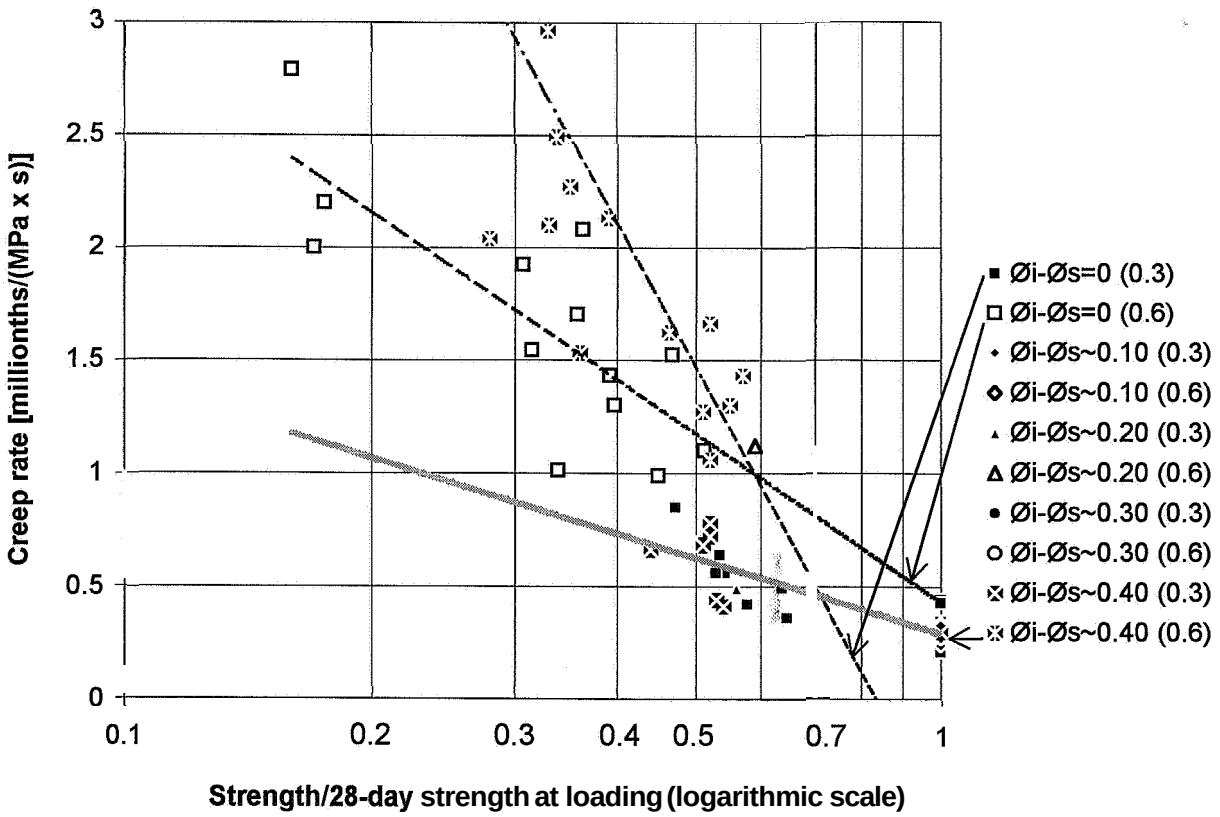

Figure 6.8 - Creep rate versus relative 28-day strength at loading, f_c/f_{c28}. Difference in relative humidity of cylinder surface, $Ø_s$, and the inside, $Ø_i$. **(0.3)** $= \sigma/f_c$.

7. DEFORMATION MODULUS AT QUASI-INSTANTANEOUS LOADING

7.1 General

The elastic modulus of HPC was defined in **Figure 1.1** as the immediate inverted difference of compliance when HPC was unloaded. Two kinds of elastic modulus were defined, short-term and long-term. These different kinds of elastic modulus were only experimental, i.e. only related to the present study. For convenience the short-term modulus was measured after one weekend of loading (66h). The long-term elastic modulus was measured after up to 5 years of loading in traditional spring-loading devices. Both measurements are important from a practical point of view. When young concrete is loaded, a large creep rate often occurs which leads to permanent deformations and possible damage to the structures. It was then considered essential to investigate parameters that affected the creep rate of HPC at early ages. After long all types of concrete become mature, i.e. all studies are perfomed on mature concrete even though it originally was loaded young. In mature concrete the deformation at rapid loading and unloading is more or less identical. Concrete behaves elastic in the mature state. The inverted compliance of concrete at loading is therefore often used as a substitute for the real elastic modulus that can only be measured when the concrete is unloaded, **Figure 1.1.** However, owing to the lifetime of concrete it is seldom possible to use the correct definition. For this study it was considered important to separate the two kinds of modulus. At loading a "modulus of deformation", $D_{t\text{-}t'}$, for concrete was defined according to the following equation (GPa):

$$D_{t\text{-}t'} = 1000/J(t,t') \qquad (7.1)$$

$D_{t\text{-}t'}$ denotes the deformation modulus (GPa)
$J(t,t')$ denotes the compliance at loading (millionths/MPa)
t denotes the age of the concrete
t' denotes the age at loading
t-t' denotes the loading time (s)

The experiments with quasi-instantaneous loading were the basis for these numerical evaluations of the deformation modulus. The MTS machine studies were performed with extremely high accuracy. In most cases the loading reached its correct level within 0.01 s. No overload was registered since the MTS machine was thoroughly optirnised for each mix and age of HPC, in all 70 optimisations in the study. In the case of delayed loading, i.e. when the loading was levelled after 0.01 s, it was possible to use all values of compliance after the full level was reached. By extrapolation backwards it was then possible to estimate the 0.01-s compliance. These extrapolations were performed provided that the full level of loading was reached within 0.03 s. (In most cases the full level of loading was reached within 0.015 s.) The loading was very rarely delayed after 0.02 s, **Appendix 6.**

7.2 Results of studies with air curing

Table 7.1 gives the strength at loading and **Table 7.2** the deformation modulus 1 s after loading. **Figures 7.1-7.3** show the deformation modulus versus strength 0.01 s, 0.1 s and 1 s after the loading was performed. **Appendix 7** shows the detailed deformation modulus versus the strength 0.01 s, 0.1 s and 1 s after the loading was performed. The deformation modulus 0.01 s after loading was larger than the deformation modulus 0.1 s and 1 s after loading. At 0.01 s of loading little creep occurred, which meant that the deformation and elastic modulus almost coincided.

Table 7.1. - Strength at loading (MPa)

Concrete	01	02	03	28
1	23	32	26	50
2	24	44	44	86
3	27	30	43	58
4	23	37	48	91
5	38	45	46	106
6	30	61	58	111
7	36	63	67	118
8	35	69	65	118

Table 7.2 - Deformation modulus 1 s after loading (GPa)

Concrete	01	02	03	28
1	15.1	21.6	23.8	31.9
2	22.3	22.1	22.5	33.0
3	18.6	19.8	26.3	29.2
4	15.6	22.3	29.2	33.8
5	23.5	27.6	23.5	35.7
6	15.6	27.2	31.9	36.2
7	19.8	29.0	33.8	41.5
8	21.9	31.2	33.0	38.3

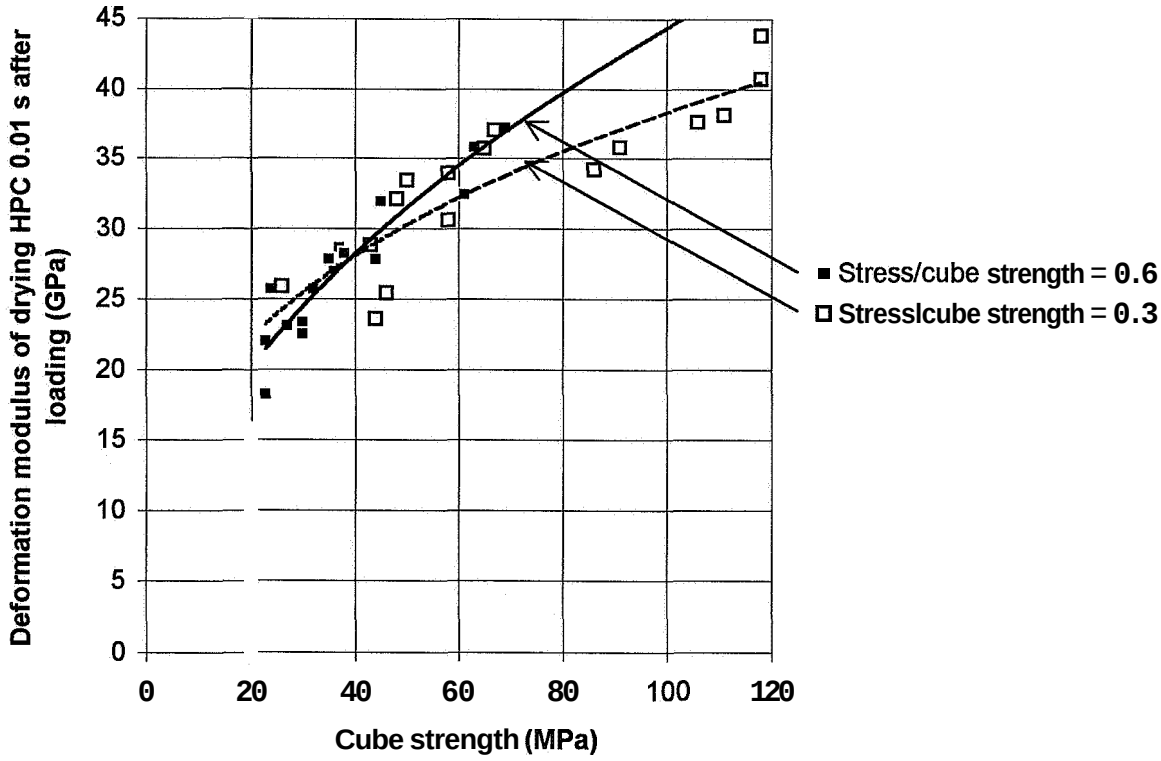

Figure 7.1 - Deformation modulus 0.01 s after loading, loading level indicated.

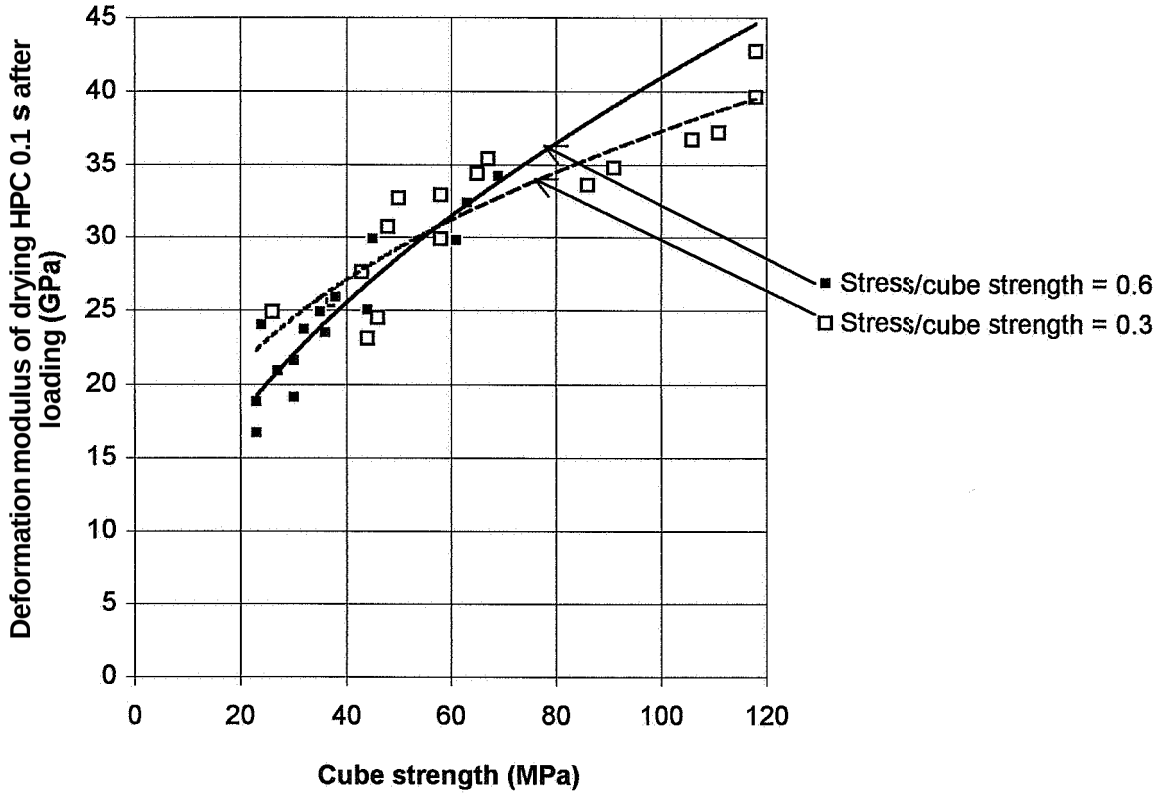

Figure 7.2 - Deformation modulus 0.1 s after loading. The loading level is indicated.

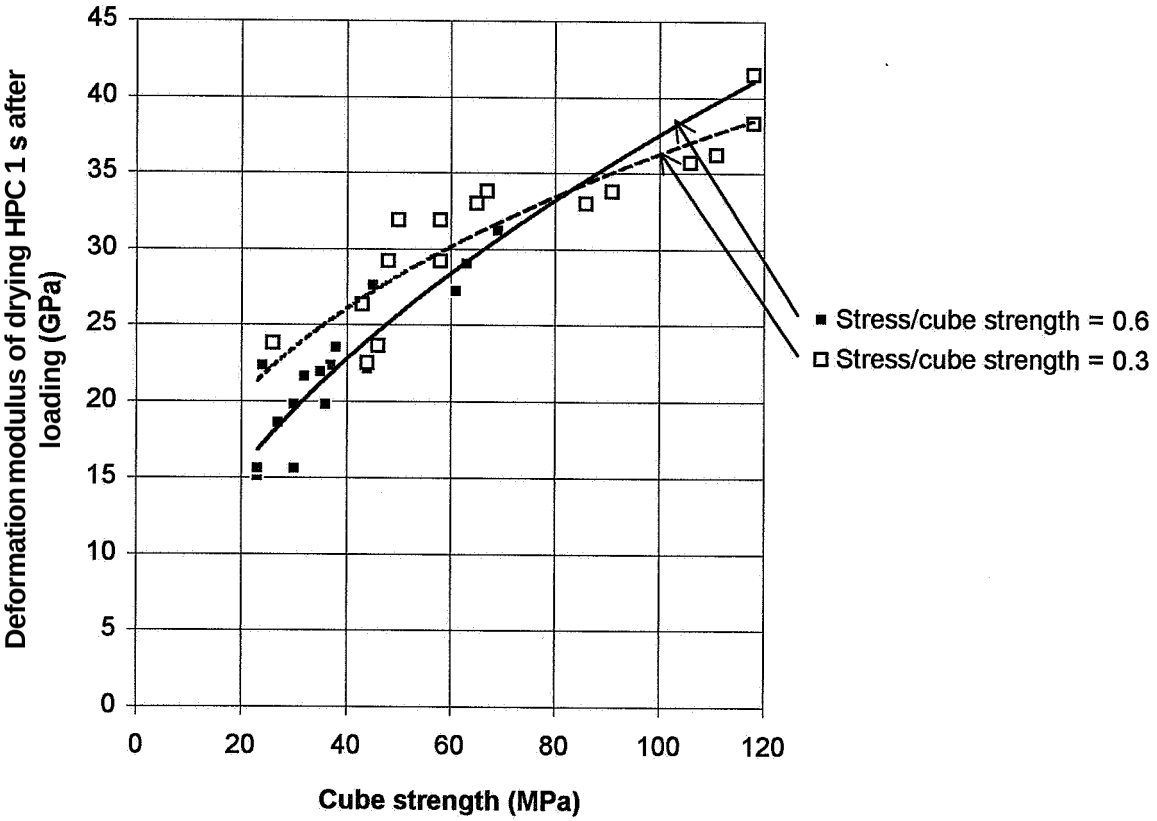

Figure 7.3 - Deformation modulus 1 s after loading versus strength.

7.3 Influence of eccentricities, strength, stress-level and time

At low strength the deformation modulus exhibits large variation, which is perhaps an effect of possible large eccentricities. In **Appendix 7** the deformation modulus at 1 **s** of loading is given versus the strength with the eccentricity indicated. From **Appendix 7** it was concluded that deformation modulus did not depend on the eccentricity of loading. However, the effect on the deformation modulus of the stress/strength level at loading was obvious, which also was shown in **Figures 7.1, 7.2 and 7.3.** The following equations were obtained for the deformation modulus of HPC with air curing, D_D (GPa):

$$D_D = a \cdot (f_c)^b \qquad (7.2)$$

$$D_D = [c \cdot \ln(t-t') + d] \cdot (f_c)^{e \cdot \ln(t-t') + f} \qquad \{0.01 < t-t' < 1s\} \qquad (7.3)$$

$$D_D(f_c; t-t'; \sigma/f_c) = \{10.7 - 12.8 \cdot (\sigma/f_c) - [0.15 + 0.29 \cdot (\sigma/f_c)] \cdot \ln(t-t')\} \cdot (f_c)^{0.18 + 0.61 \cdot (\sigma/fc) + 0.022 \cdot (\sigma/fc - 0.1) \cdot \ln(t-t')} \qquad (7.4)$$

a, b, c, d, e, f denotes constants given in **Table 7.3 and Table 7.4**

f_c	denotes the cube strength at loading (MPa) $\{20 < f_c < 120$ MPa$\}$
ln(t-t')	denotes the natural logarithm of the time elapsed from loading
t-t'	denotes loading time (s)
D_D	denotes the deformation modulus of HPC with air curing (GPa)
σ/f_c	denotes the stress to cube strength ratio at loading $\{0.3 < \sigma/f_c < 0.6\}$

Table 7.3 - Constants a and b of equation (7.2)

Loading time, t-t´(s)	**Stresslstrength level, $\sigma/f_c = 0.6$**		**Stresslstrength level, $\sigma/f_c = 0.3$**	
Constant	a	b	a	b
0.01	4.55	0.4947	8	0.3402
0.1	3.81	0.5155	7.45	0.35
1	3.04	0.5453	6.89	0.3606

Table 7.4 - Constants c, d, e and f

Stresslstrength level, $\sigma/f_c = 0.6$		**Stresslstrength level, $\sigma/f_c = 0.3$**	
c	-0.328	c	-0.241
d	3.05	d	6.89
e	0.011	e	0.0044
f	0.544	f	0.361

From the practical point of view estimations according to equation (7.2) exhibit quite sufficient accuracy and are also achievable. However, with a plain computer programme it also became feasible to use equations (7.3) and (7.4).

7.4 Comparison with basic creep

The deformation modulus was studied and calculated for 32 sealed cylinders under constant moisture and temperature conditions, i.e. basic creep **Persson (1995A), Appendices 6 and 7. Figure 7.4** shows the relationship between the deformation modulus of HPC with sealed curing and strength. The following equation was used:

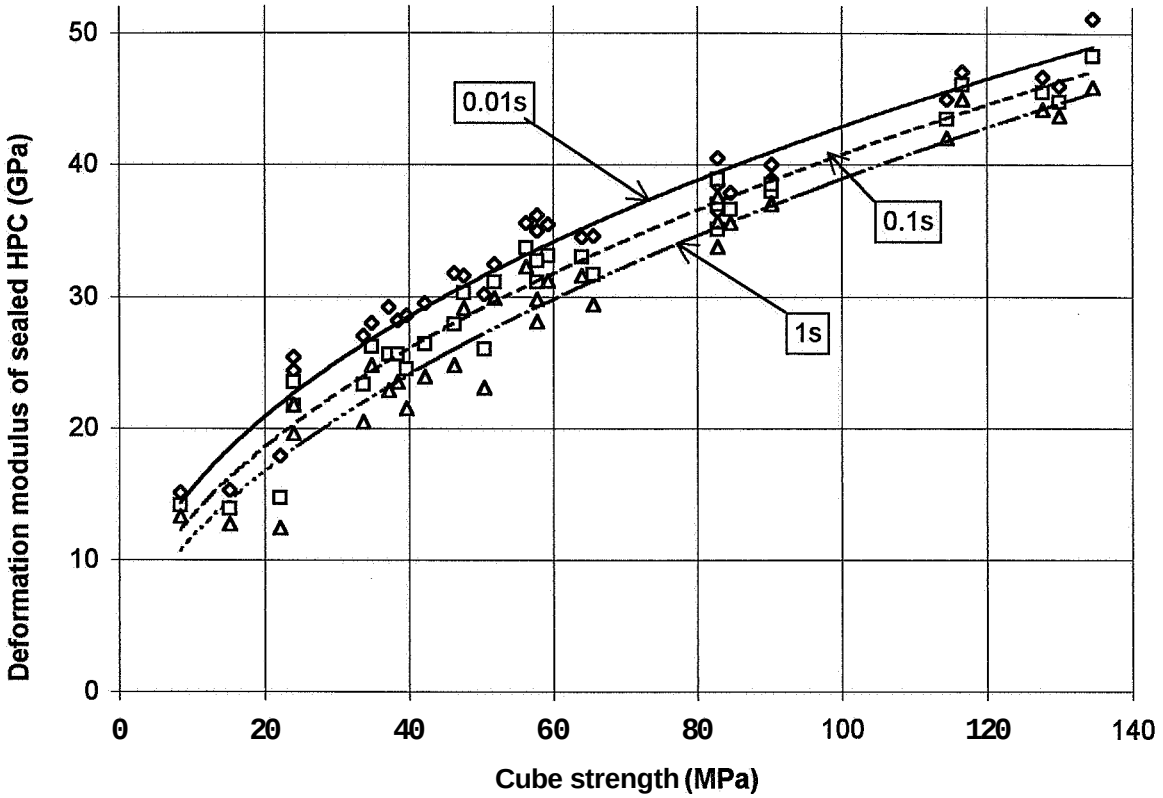

Figure 7.4 - Deformation modulus with sealed curing versus strength. Loading time.

$$D_B(f_c;t\text{-}t') = 0.43\cdot[7.9 - \ln(t\text{-}t')]\cdot(f_c)^{0.17\cdot[3.14+0.1\cdot\ln(t\text{-}t')]} \quad \{0.01<t\text{-}t'<1s\} \qquad (7.5)$$

f_c	denotes the compressive strength at loading (MPa) $\{10<f_c<140$ MPa$\}$
$\ln(t\text{-}t')$	denotes the natural logarithm of the time elapsed from loading
$t\text{-}t'$	denotes the loading time
D_B	denotes the deformation modulus with sealed curing (basic creep)

In **Appendix 7** comparisons were made between the deformation modulus with sealed and with air curing at 0.01 s, 0.1 s and 1 s after loading respectively. The stress/strength levels are indicated. The deformation modulus was larger with sealed than with air curing given a low stresslcube strength ratio, $\sigma/f_c = 0.3$. With high stresslcube strength ratio, $\sigma/f_c = 0.6$ and sealed curing the deformation modulus was initially larger than in specimen with air curing (at 0.01 s of loading). However, after 1 s of loading the deformation modulus became smaller with sealed than with air curing provided high stresslcube strength ratio, $\sigma/f_c = 0.6$. These observations were likewise explained by the early creep properties of concrete. The following general expressions were obtained for the deformation modulus of HPC with sealed curing, D_B (GPa):

$$D_B = a\cdot(f_c)^b \qquad \{10<f_c<140 \text{ MPa}\} \qquad (7.6)$$

$$D_B = [c\cdot\ln(t\text{-}t')+d]\cdot(f_c)^{e\cdot\ln(t\text{-}t')+f} \qquad \{0.01<t\text{-}t'<1s\} \qquad (7.7)$$

$$D_B(f_c;t\text{-}t';\sigma/f_c) = \{6.06\text{-}3.02\cdot(\sigma/f_c)\text{-}[0.44\text{-}0.51\cdot(\sigma/f_c)]\cdot\ln(t\text{-}t')\}\cdot(f_c)^{0.42+0.061\cdot(\sigma/fc)-\ 0.039\cdot(\sigma/fc\text{-}0.5)\cdot\ln(t\text{-}t')} \quad (7.8)$$

a, b, c, **d,** e, f denote constants given in **Table 7.5** and **Table 7.6**

f_c denotes the compressive strength at loading (MPa) $\{10<f_c<140$ MPa$\}$

$\ln(t\text{-}t')$ denotes the natural logarithm of the time elapsed fiom loading

$t\text{-}t'$ denotes the loading time

D_B denotes the deformation modulus **with** sealed curing (basic creep)

σ/f_c denotes the stress to cube strength ratio at loading $\{0.3<\sigma/f_c<0.6\}$

Table 7.5 - Constants a and b of equation (7.6)

Loading time, t-t′(s)	**Stresslstrength level, $\sigma/f_c = 0.6$**		**Stress/strength level, $\sigma/f_c = 0.3$**	
Constant	a	b	a	b
0.01	4.89	0.4813	6.59	0.4041
0.1	4.58	0.4682	5.64	0.4309
1	4.25	0.4595	5.25	0.4369

Table 7.6 - Constants c, d, e and f

Stresslstrength level, $\sigma/f_c = 0.6$		**Stress/strength level, $\sigma/f_c = 0.3$**	
c	-0.139	c	-0.291
d	4.25	d	5.16
e	-0.0047	e	0.0071
f	0.459	f	0.440

Equation (7.9) is the most **frequently** used formula to describe the deformation modulus.

$$D = a\cdot(f_c)^b \quad (7.9)$$

a, b denotes constants dependent on several conditions such as experimental procedure, loading time, **stress/strength** level, aggregate, age

f_c denotes compressive cube strength (MPa)

D denotes deformation modulus (GPa)

For **HPC** the multiplicand a in equation (7.10) is often set at 11 and the exponent at 0.3, **Jaccoud and Leclercq (1995). In** this case both the multiplicand a and the exponent b were corrected fiom cylinder to cube strength with equation **(5.8),** which concluded that the cylinder strength of this study was 71% of the cube strength. The most relevant comparison is performed at low **stress/cube** strength ratio, $\sigma/f_c = 0.3$ and rapid loading, **i.e.** 0.01 **s**. Again comparing **Tables 7.3 and 7.5,** the multiplicand a declined fiom 8 to 6.6 between **drying** creep and basic creep. The exponent b increased fiom 0.34 with air curing to 0.40 with sealed curing, imposing a larger deformation modulus at higher strength. Most probably these observations were related to moisture content **in** the concrete. Figures given by **Jaccoud and Leclercq (1995)** were in all likelihood obtained fiom a great number of experimental studies on different kinds of concrete, aggregate, etceteras. The most conservative combination of multiplicand a = 11 and exponent b = 0.30 was then chosen.

7.4 Deformation modulus and porosity with sealed curing

It is nothing new but well-known that the porosity of concrete affects most of its properties. Porosity is in turn related to strength, w/c, diffusivity and moisture state in NSC. In order to verify that the correlation between porosity and deformation properties also applies for HPC, a composite model, **Hansen (1966)**, for calculation of the modulus of elasticity was used:

$$D_c^{\,n} = A \cdot E_a^{\,n} + (1 - A - B) \cdot D_p^{\,n} \qquad (7.10)$$

$$A = w_a/\rho_a \qquad (7.11)$$

$$B = (w - k \cdot w_n)/\rho_w - \mu_{ai} = (w - 0.75 \cdot 0.25 \cdot \alpha \cdot c)/\rho_w - \mu_{ai} = (w - 0.19 \cdot \alpha \cdot c)/\rho_w - \mu_{ai} \qquad (7.12)$$

- c denotes the cement content (kglm^3)
- k denotes the specific volume of chemically bound water k= 0.75 according to **Powers and Brownyard (1946-1948)** and **Persson (1992A)**
- n denotes the exponent with n= +1 for the parallel model when $D_p >> E_a$; n= -1 for the serial model when $D_p << E_a$, **Hansen** (1966)
- w mixing water (kglm^3)
- w_a denotes the weight of aggregate (kglm^3)
- w_n denotes the chemically bound water (kg/m^3)
- A denotes the aggregate volume share = w_a/ρ_a
- B denotes the volume share owing to the chemical shrinkage and air-entrainment
- D_c denotes the modulus of deformation of the concrete (GPa)
- D_p denotes the deformation modulus of the cement paste (GPa)
- E_a denotes the modulus of elasticity of the aggregate (GPa)
- α denotes the degree of hydration of the cement
- ρ_a denotes the density of the aggregate (kg/m^3)
- ρ_w denotes the density of the water (kg/m^3)
- μ_{ai} denotes the volume share of air-entrainment

Equation (7.10) was used to calculate the deformation modulus of the cement paste at 28 days' age. The modulus of deformation of the concrete, D_c, was known according to equation (7.5) and **Figure** 7.4. The degree of hydration, *a,* is given in **Appendix** 5 (sealed curing), the modulus of elasticity of the aggregate is given in **Table** 4.1 (except for HPC mix 4) and the resisting figures required in equations (7.11) and (7.12) are given in **Table** 5.1. At early ages, when $D_p << E_a$, the exponent n in equation (7.10) became low, certainly < 0. In **Figure** 7.5 the deformation modulus of sealed cement paste (GPa) at 0.01 s loading time is given versus the porosity of the cement paste, P„ assuming the exponent, n, in equation (7.10) to be n= -0.67:

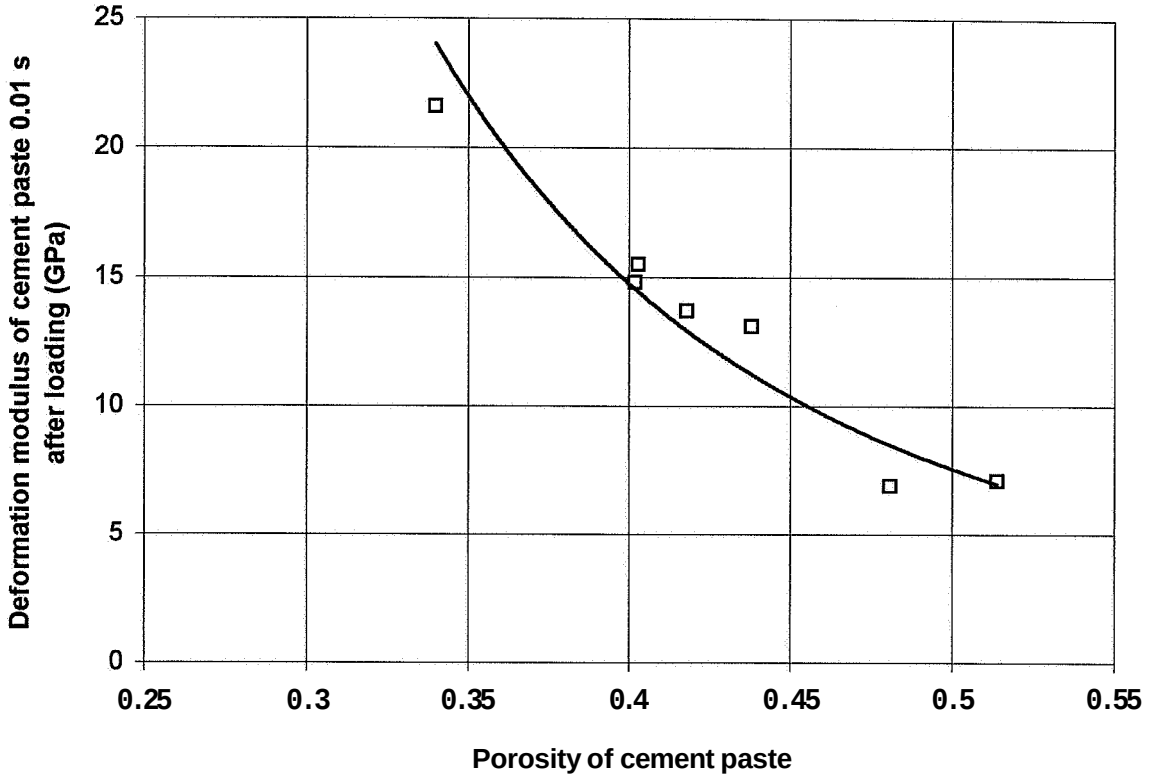

Figure 7.5 - Deformation modulus of the cement paste at 0.01 s versus the porosity.

$$P_{,,} = \frac{w - 0.19 \cdot \alpha \cdot c + 1}{\frac{c}{\rho_c} + w + 1} \qquad (7.13)$$

c	denotes the cement content	(kg/m^3)
w	denotes the mixing water	(kg/m^3)
l	denotes the air volume in the concrete	(l/m^3)
α	denotes the degree of hydration of the cement	
ρ_c	denotes the density of the cement	(kg/m^3)

The following equation for the deformation modulus of sealed cement paste was obtained from **Figure** 7.5:

$$D_{p,0.01} = 0.95 \cdot P_p^{-3} \qquad (7.14)$$

$D_{p,0.01}$ denotes the deformation modulus of sealed cement paste at 0.01 s loading time (GPa)

$P_,$ denotes the porosity of the cement paste according to equation (7.13).

The evaluated deformation modulus of the cement paste was also compared to the capillary porosity of the paste:

$$(P_{cap})_p = \frac{w - 0.39 \cdot \alpha \cdot c + 1}{\frac{c}{\rho_c} + w + 1} \qquad (7.15)$$

c	denotes the cement content	(kg/m^3)
1	denotes the air volume in the concrete	(l/m^3)
w	denotes the mixing water	(kg/m^3)
a	denotes the degree of hydration of the cement	
p,	denotes the density of the cement	(kg/m^3)

Figure 7.6 gives the deformation modulus of sealed mature cement paste versus the capillary porosity 0.01 s of loading. The full line in **Figure 7.6** indicates the deformation modulus according to equation (7.10) with n= -0.67:

$$D_{p,0.01} = 1.71 \cdot (P_{cap})_p^{-1.64} \qquad (7.16)$$

The dotted line in **Figure 7.6** indicates the expression for the deformation modulus of cement paste, D„ according to **Fagerlund (1972)** (GPa):

$$D_p = 32 \cdot [1 - (P_{cap})_p]^{2.5} \qquad (7.17)$$

$(P_{cap})_p$ denotes the capillary porosity of the cement paste

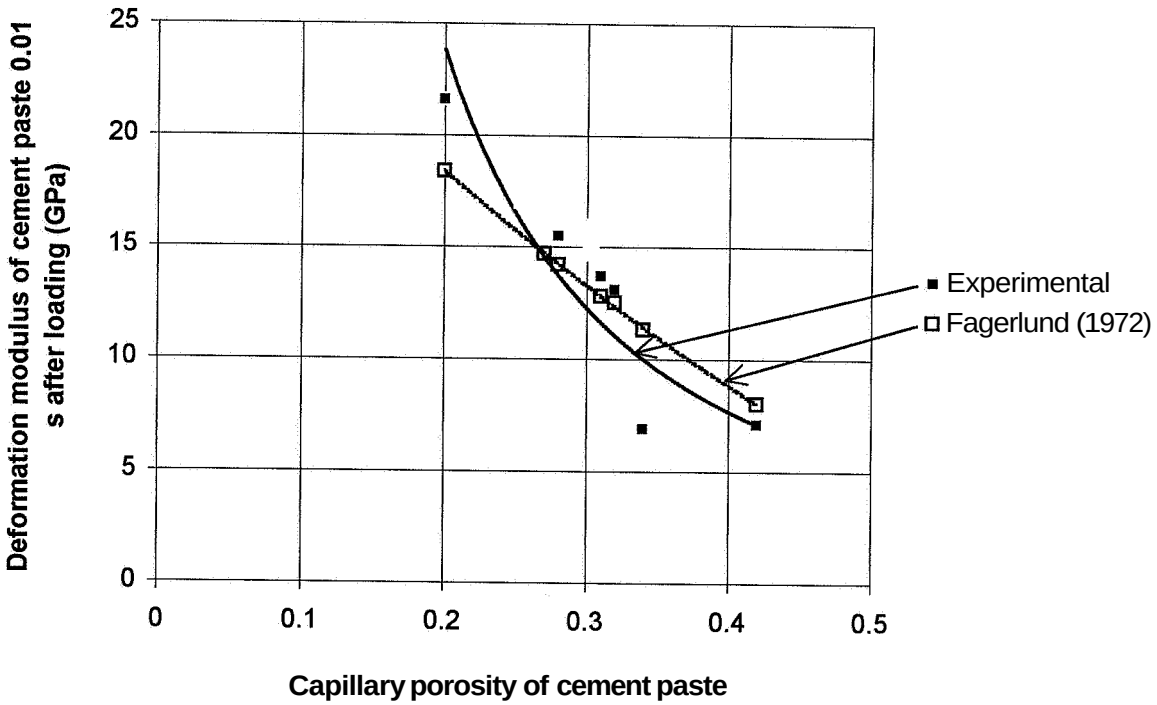

Figure 7.6 - Deformation modulus of the cement paste versus the capillary porosity.

On average the values of the deformation modulus of equations (7.16) and (7.17) agreed, but the influence of the porosity was larger in equation (7.16) than in equation (7.17). It was interesting to estimate the early development of the deformation modulus of the cement paste versus the maturity. **Figure 7.7** shows the 28-day relative deformation modulus of the cement paste at 0.01 s of loading versus the 28-day relative strength (the maturity of the concrete). The deformation modulus was calculated according to equation (7.16) with the exponent, n= -0.67.
The development of the cement paste deformation modulus was different between concrete with and without air-entrainment. The reason for this was probably moisture movement in the paste. When air-entrainment was used, the moisture probably moved rapidly into the air-filled space at loading, which caused a larger increase of the deformation modulus compared with the cement paste without air-entrainment. (However, it was noted that the total deformation of air-entrained concrete was larger than for concrete without air-entrainment, since the compressive strength was lower for air-entrained concrete.) It was interesting to calculate the early development of the deformation modulus of the concrete. The following expression applied for the early development of the deformation modulus:

$$(D_p/D_{p28}) = A\cdot(f_c/f_{c28})^2 + B\cdot(f_c/f_{c28}) \qquad (7.18)$$

f_c denotes the compressive strength of the concrete (MPa)
f_{c28} denotes the 28-day compressive strength of the concrete (MPa)
D_p/D_{p28} denotes the 28-day relative deformation modulus of cement paste

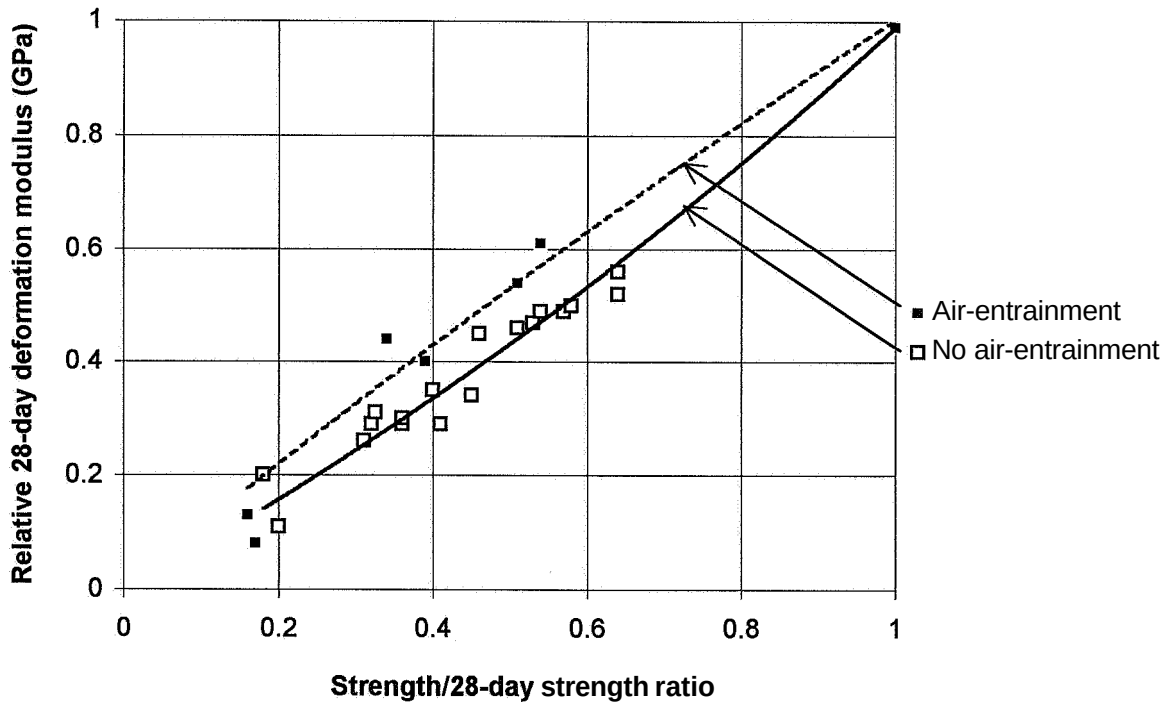

Figure 7.7 - The 28-day relative deformation modulus of the cement paste at 0.01 s of loading versus the 28-day relative strength.

A, B denote constants given in **Table** 7.7 below.
D_p denotes the deformation modulus of sealed cement paste after 0.01 s of loading (GPa)
D_{p28} denotes the 28-day deformation modulus of the cement paste after 0.01 s of loading (GPa)

Table 7.7 - Constants A and B in equation (7.18)

Constant	A	B
Air-entrainment	-0.12	1.12
No air-entrainment	0.25	0.75

'.5 Summar and conclusions

In all, **32 drying** HPC cylinders were studied related to the deformation modulus, i.e. the inverse of the compliance at loading at loading, ε/σ. Results **from** studies of quasi-instantaneous loading with a loading time varying between 0.01 s and 1 s were used in numerical estimations. The results were compared with the studies of the deformation modulus of at a total 32 HPC cylinders with sealed curing. The following conclusions were drawn:

- The size of the deformation modulus of HPC was dependent on the loading time, especially for young concrete. Correlations between the deformation modulus and the compressive strength of HPC were obtained within loading times varying between 0.01 s and 1 s.
- The deformation modulus of HPC was also dependent on the stress to strength ratio at loading. The effect of the stress to strength level was studied on HPCs with stress/strength levels that varied between 0.42 and 0.84 related to the cylinder strength. Formulas of the deformation modulus of HPC related to the strength were also presented in this case.
- The moisture condition of the HPC specimen had also an effect on the measured deformation modulus. The largest values of the deformation modulus were recorded on sealed HPC specimens with high moisture content and an internal relative humidity owing to self-desiccation. Also in this case correlations were obtained for both sealed and drying HPC.
- Parallel studies of the hydration of sealed HPCs made calculations of the porosity feasible. A composite formula was used to obtain the deformation modulus of sealed cement paste with low w/c. The size of the deformation modulus of the low-w/c cement paste coincided well with the deformation modulus of NSC given a constant porosity.
- Finally, results were obtained concerning the development of the deformation modulus of young concrete. Also in this case the moisture conditions effected the size of the deformation modulus.
- The deformation modulus of drying HPC was smaller than the deformation modulus of sealed HPC given constant maturity.

8. SHRINKAGE

8.1 General

Autogenous, carbonation and drying shrinkage were investigated. The phenomenon called autogenous shrinkage is caused by the self-desiccation in HPC. The self-desiccation in turn occurs owing to chemical shrinkage of the mixing water when it becomes bound to the cement during hydration, **Persson (1997A)**. When the internal relative humidity decreased, the depression in the pore water also decreased, causing compression in the aggregate and the cement paste of the concrete, **Persson (1996C)**. The autogenous shrinkage thus causes self-stress in HPC. Chemical shrinkage of the mixing water also occurs in NSC during hydration. However, since the pores are larger in NSC, the chemical shrinkage hardly affects the self-desiccation at all, perhaps only by 2% RH, **Persson and Fagerlund (1997).**

8.2 Previous research on shrinkage of HPC

Roy and Larrard (1993) studied shrinkage of HPC and NSC at different w/c and with different amounts of silica fume. They found that the autogenous shrinkage increased at lower water-cement ratio, w/c. At $w/c \approx 0.3$ the autogenous shrinkage after 400 days was about 220 millionths. However, they observed the total shrinkage (autogenous and sorption) to be larger at higher w/c; for example about 600 millionths at $w/c \approx 0.6$. **Figure 8.1** shows shrinkage versus w/c with different amounts of silica fume, **Roy and Larrard (1993).** The results in **Figure 8.1** were obtained for specimens 1 m long (the diameter was 0.16 m) with strength varying between 46 and 101 MPa. The shrinkage measurements started at 2 days' age. The following conclusions were drawn:

- The autogenous shrinkage increased with decreasing water-cement ratio.
- The autogenous shrinkage increased when the concrete contained silica fume.
- The total shrinkage and the sorption shrinkage increased with increasing water-cement ratio.

Other French experiments were performed on 0.12 m diameter cylinders with a length of 0.24 m, **Sicard (1993). In** this case the water moisture losses were 1% by the weight of the concrete per year, which was quite much. The measurements of shrinkage started at an age of 1.2 days. In **Figure 8.2** the result of the autogenous shrinkage is shown versus time. The following conclusions were drawn:

- The autogenous shrinkage increased with decreasing water-cement ratio.
- The autogenous shrinkage was larger with limestone aggregate than with sandstone.
- The autogenous shrinkage was larger in concrete with silica fume than in HPC without silica fume.

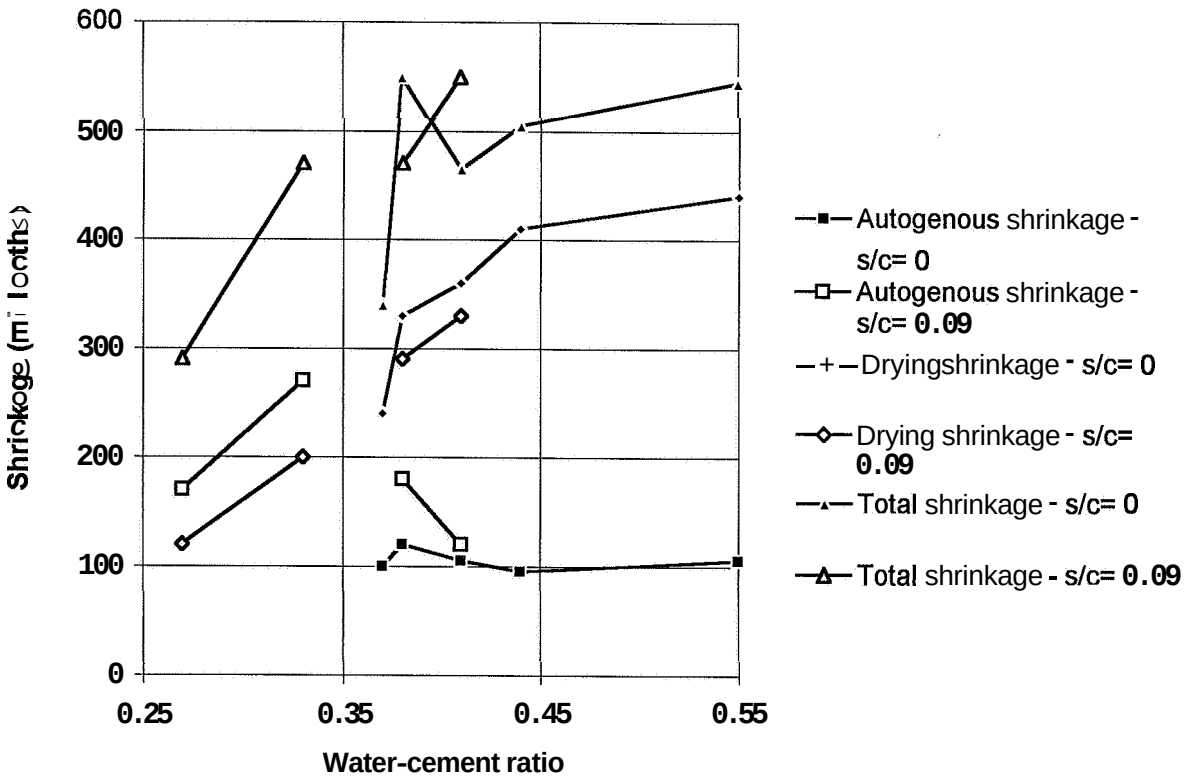

Figure 8.1-Shrinkage versus wlc. s/c = silica fume content, Roy & Larrard (1993).

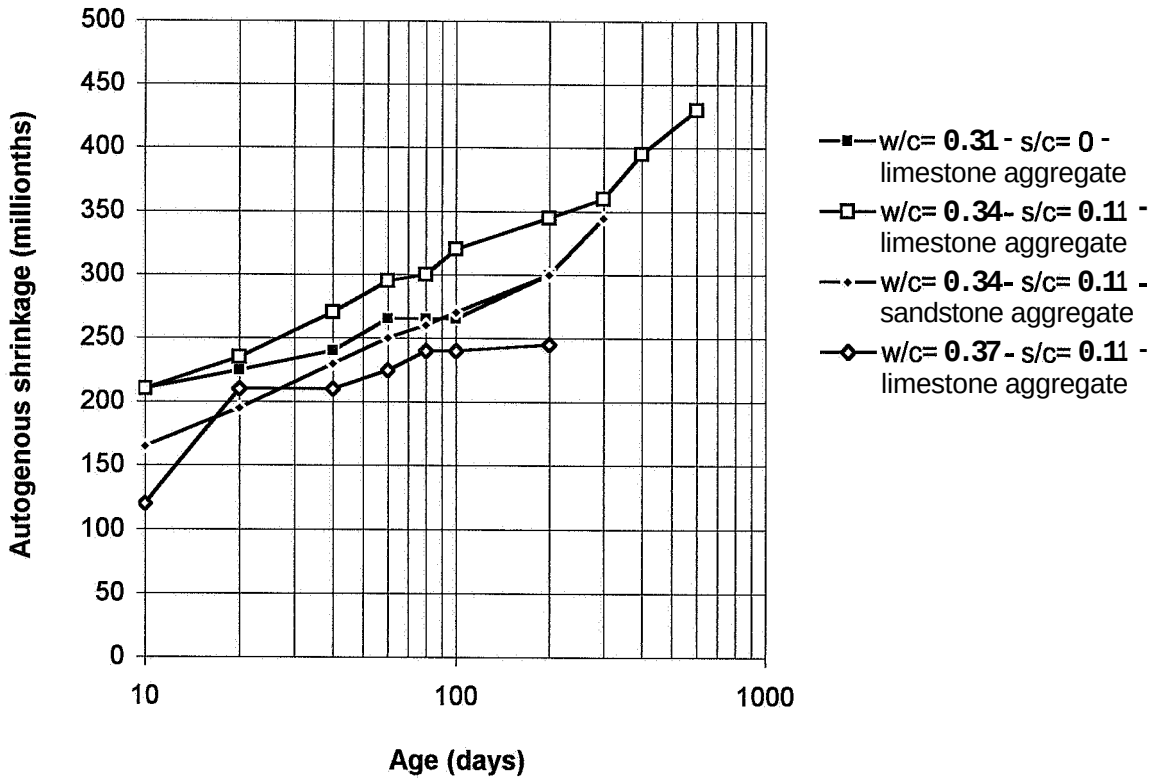

Figure 8.2 - Autogenous shrinkage versus time. s/c = silica fume, Sicard (1993).

Tazawa and Miyazawa (1993) studied shrinkage at very early ages by cast-in strain gauges. The specimen was 0.1 x 0.1 x 1.2 m. The concrete was cast in vinyl polymer plastic moulds allowing for movements of the concrete at early ages. The measurements started at ≈ 0.2 days' age. Figure 8.3 shows the shrinkage versus time at different w/c. The shrinkage increased with lower w/c and higher content of silica fume. The difference between autogenous and drying shrinkage was small.

8.3 Experimental method

General descriptions of material, preparation of specimens and chronology are given in Section 4. A total of 19 specimens for studies of autogenous shrinkage and 26 for studies of drying shrinkage cast of 8 different concretes were prepared as described in Table 5.1. Exactly the same batches of concrete were used as in the experiments on quasi-instantaneous loading. After demoulding and insulation by butyl rubber clothing (in the case of studies of autogenous shrinkage), 6 stainless steel screws were fixed into cast-in items in the cylinder 25 mm from each end. Measurements were taken on three sides of the cylinder on a length of 250 mm within 1 h of demoulding, Bazant and Carol (1993). The specimen was placed in a 20 °C climate chamber with a relative humidity, RH= 55%. Mechanical devices performed the measuring. Appendices 3-4 show the temperature at start of the measurement.

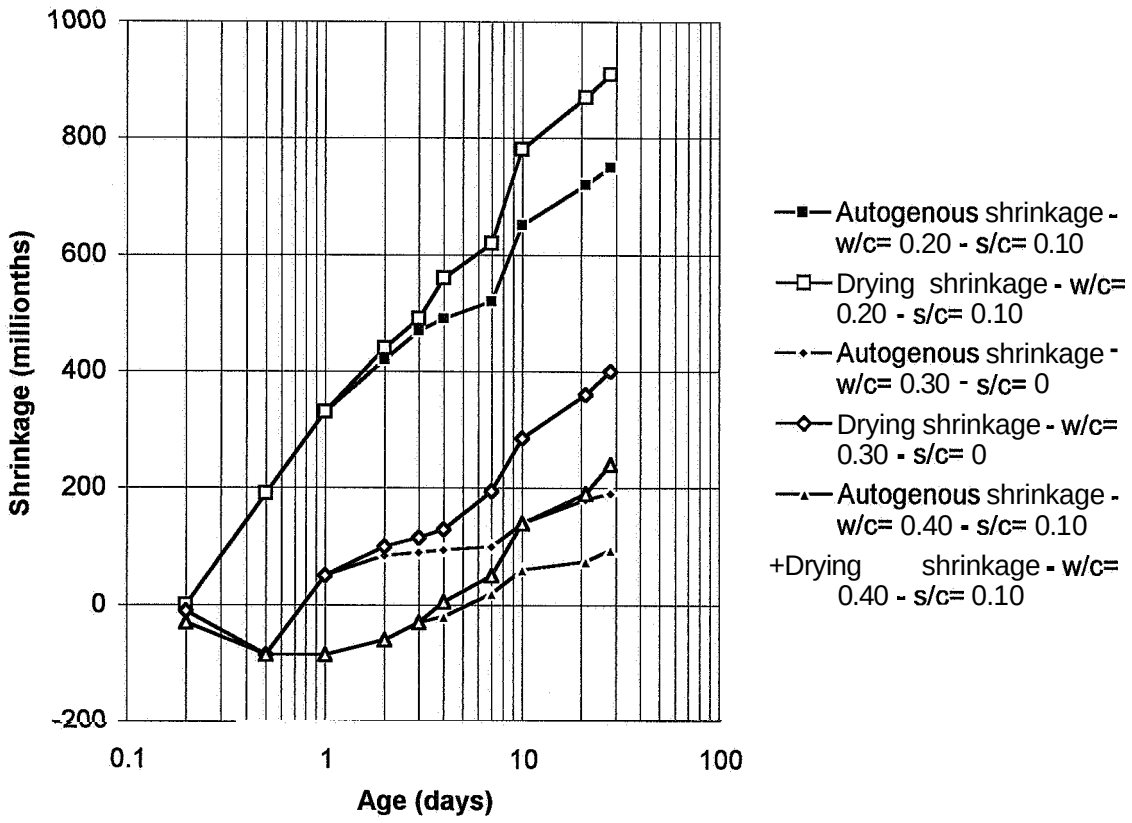

Figure 8.3 – Autogenous and drying shrinkage versus time at different w/c and varying content of silica fume, s/c, Tazawa and Miyazawa (1993).

8.4 Sources of error

Moisture losses and moisture absorption in insulation:

In spite of all the careful precautions some faults existed causing unforeseen weight losses. The specimens were continuously weighed to detect this loss. Possible absorption of water in the butyl rubber insulation perhaps affected the total weight of the specimen. The possible absorption of the butyl rubber had to be investigated.

Temperature movements:

Effects of hydration heat in particular were avoided by obtaining the first measurement at 20 "C. The temperature was followed by a cast-in thermo couple.

Variation of the mix proportions:

The different materials of the mix design were carefully weighed to avoid variations. However, the moisture of the gravel had to be calibrated after the batching as well which may cause alteration in the mixed proportions.

Carbonation:

Carbonation caused weight increase of the specimen and also shrinkage.

8.5 Results of the present study

Figure 8.4 shows a summary of the measured shrinkage of mix 6 versus age. **Figure 8.5** shows the relative loss of weight of the specimens (the ratio of weight loss, w_e, to the mixing water of the specimen, w) versus time. **Figure 8.6** shows the measured shrinkage versus the relative loss of weight. Symbols in **Figures 8.4 - 8.6.**

c denotes the content of cement (kg/m^3)
s denotes the content of silica fume (kg/m^3)
w denotes the mixing water of the concrete (kg/m^3)
w_e denotes the evaporated water or the absorbed carbon dioxide (kg/m^3)
.B.. denotes basic creep (sealed curing)
.D.. denotes drying creep (RH= 55%)
5... = HPC *mix,* **Table 5.1**
...01 = loading at 0.8 days' age with stresslcylinder strength = 0.84
...02 = loading at 2 days' age with stress/cylinder strength = 0.84
...03 = loading at 2 days' age with stresslcylinder strength = 0.42
...28 = loading at 28 days' age with stresslcylinder strength = 0.42

Appendix 8 shows the measured shrinkage, relative loss of weight of the specimens and the measured shrinkage versus the relative loss of weight of the 8 HPCs studied.

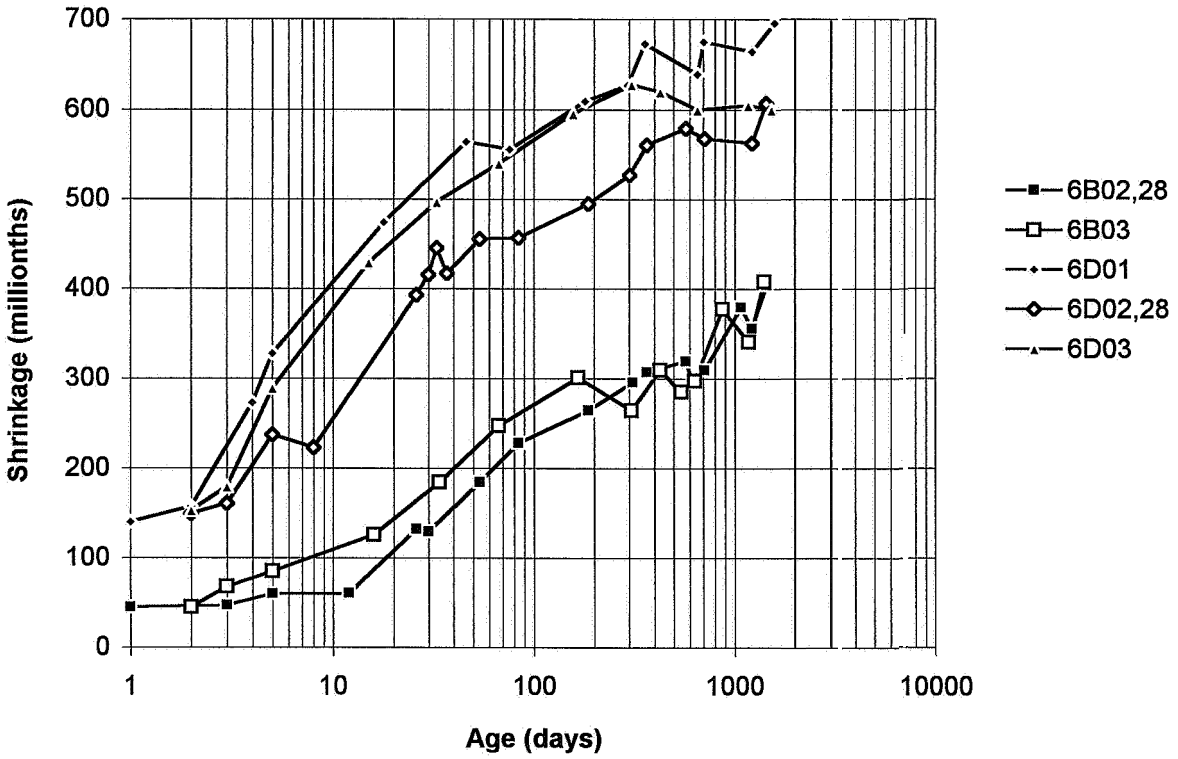

Figure 8.4 - Measured shrinkage of HPC mix 6. B= sealed curing, D= drying.

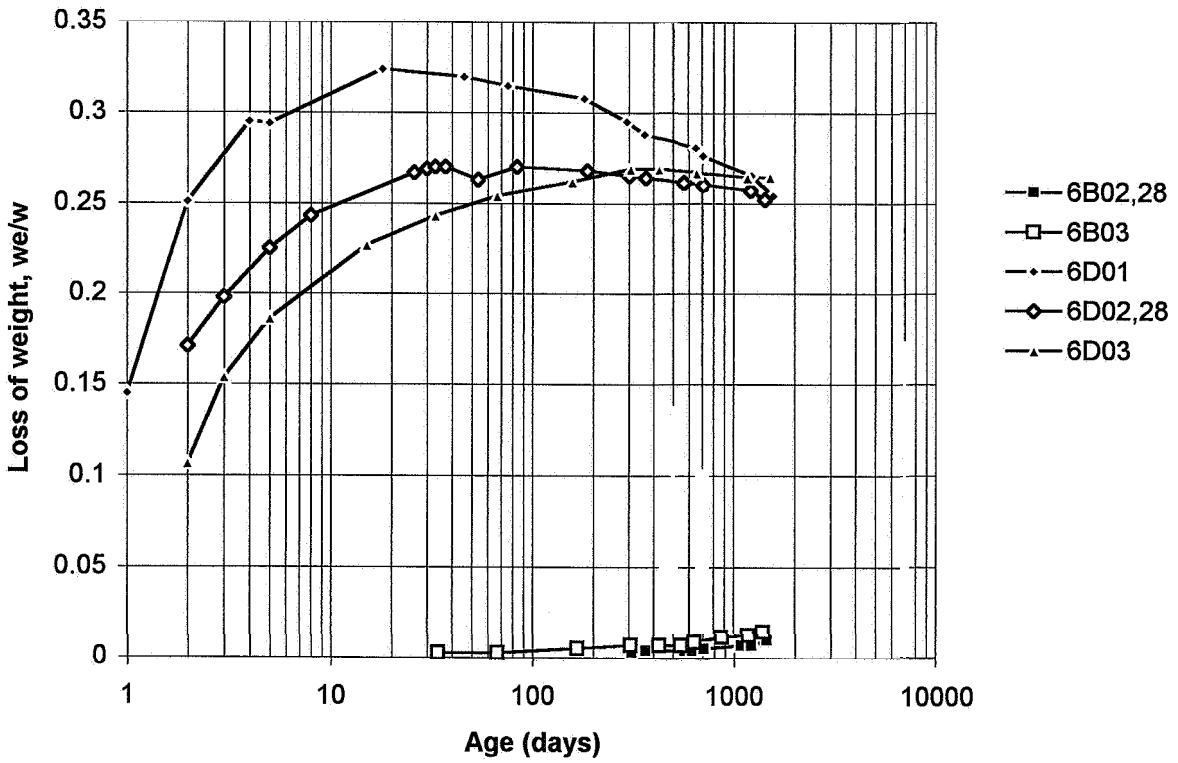

Figure 8.5 - Loss of weight of HPC mix 6 versus age. B= sealed curing, D= drying.

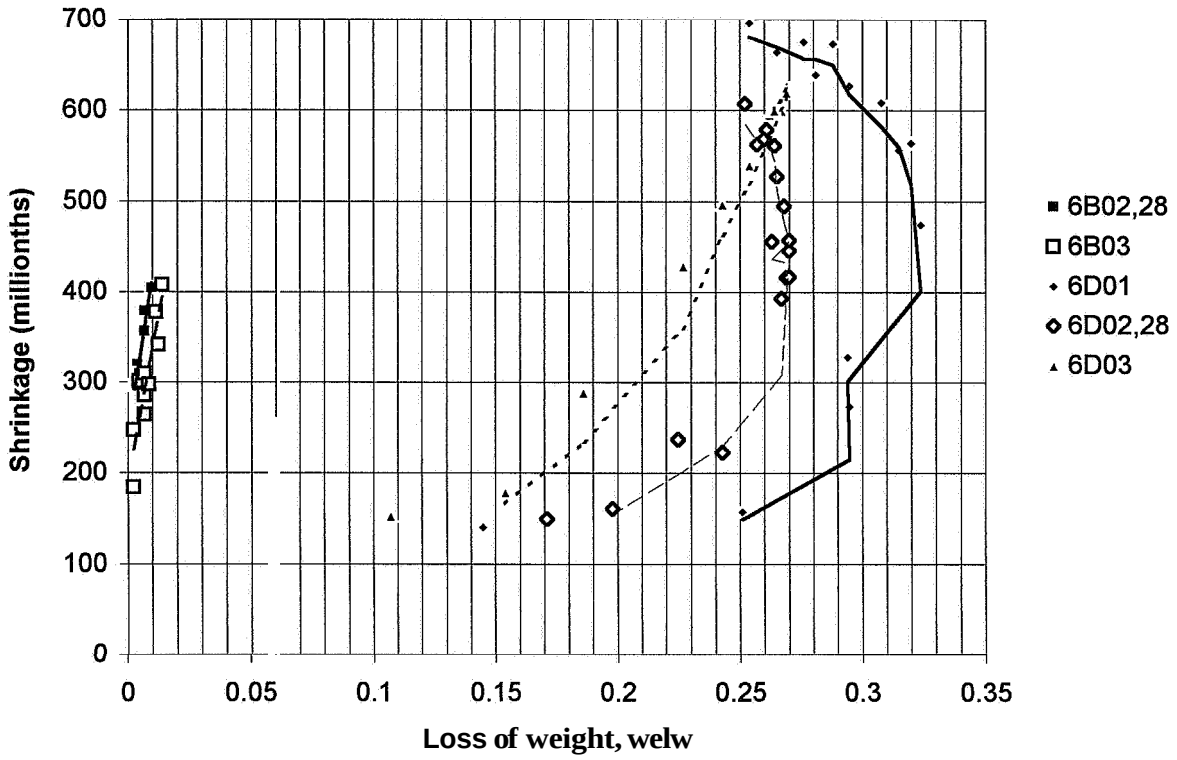

Figure **8.6** - Shrinkage of mix **6** versus loss of weight, w_e/w. w= mixing water, w_e= evaporated water, B= sealed curing, D= drying.

8.6 Accuracy

Loss of weight (moisture) and moisture absorption in the insulation:

Appendix 8, as mentioned above, gives all results of shrinkage studies and weighing. After about **1** month's age carbonation affected the weight of the drying specimens at **w/c > 0.30,** which probably caused a combination of drying and carbonation shrinkage. At low **w/c = 0.25** no increase of the weight was observed within **4** years. Absorption of water in the butyl rubber insulation existed at a high relative humidity only. Three rubber insulation tubes were first placed in an ambient relative humidity, RH = **40%.** After one week they were weighed and placed in RH = **55%.** No change of weight was observed at RH = **55%.** At **RH = 95%** the weight increased slightly but was hardly detectable, that is, **0.1** g of increased weight. Since the specimen contained **120** g of water the absorption was negligible.

Temperature movements:

A thermo couple was cast in the specimen and the temperature was followed as the first measurement was performed, **Appendices** 3-4. The maximum faults then would have been $4 \cdot 8 \cdot 10^{-6} = 32$ millionths, assuming the same effect of temperature on HPCs as on NSC. The temperature was followed as the first measurement was performed (a difference of **20** "C ± **1** "C reduced the fault to ≈ **16** millionths).

Variations in the mix design:

The variations in the mix design were normally small, less than w/c ± 0.01. Only for on eof the batches of concrete 6 a slightly larger difference was observed: w/c ≈ 0.285 instead of w/c = 0.30.

Stability of mechanical device:

The mechanical devices (Huggenberger and Proceq) were continuously calibrated with an INVAR rod and with a Mitutoyo micrometer. The reading of the device was within 0.004 mm, which was comparable to a maximum fault of 16 millionths.

Total accuracy:

The total fault of a temperature difference of ± 1°C and the fault of the mechanical device was fairly large, i.e. ≈ ± 16 ± 8 ≈ ± 24 millionths.

8.7 Analysis

8.7.1 Autogenous shrinkage

From a previous work on basic creep of HPC, **Persson (1995A)**, it was observed that the loss of weight for 14 cylinders used in the long-term creep studies was less than 0.7 g per specimen over a period of at least 1 year. (A 0.7 g loss of weight equals w_e/w= 0.006.) The specimens that were placed in the creep devices had steel plates at their ends with a joint sealing compound between the steel plate and the butyl-rubber clothing. However, the specimens used to study the autogenous shrinkage also had rubber clothing at their ends. The joint between the side and the end rubber clothing did not perform perfectly, which may have increased the loss of moisture. **Appendix** 8 show that even very small loss of weight may affect the measured shrinkage. Linear regressions were performed to obtain the measured shrinkage at no loss of weight (autogenous shrinkage). In **Figure** 8.7 the autogenous shrinkage after 4 years is given versus w/c. The type and amount of silica fume affected the autogenous shrinkage, **Figure** 8.8, which has also been observed by others, **Jensen and Hansen** (1995). **In Figure** 8.9 the autogenous shrinkage is given versus the internal relative humidity. The type and amount of silica fume clearly affects the autogenous shrinkage, **Figure** 8.10. (The internal relative humidity was obtained in the experiments and shown in **Appendix** 5.) Silica fume slurry had a larger fineness than granulated silica fume, which caused a larger shrinkage. The following correlations were obtained for the autogenous shrinkage, ε_B (per mil):

$$\varepsilon_B = k_s \cdot k_5 \cdot 1.42 \cdot [0.44-(w/c)] \quad (8.1)$$

$$\varepsilon_B = k_{s\emptyset} \cdot 1.75 \cdot (1-1.13 \cdot \emptyset) \quad (8.2)$$

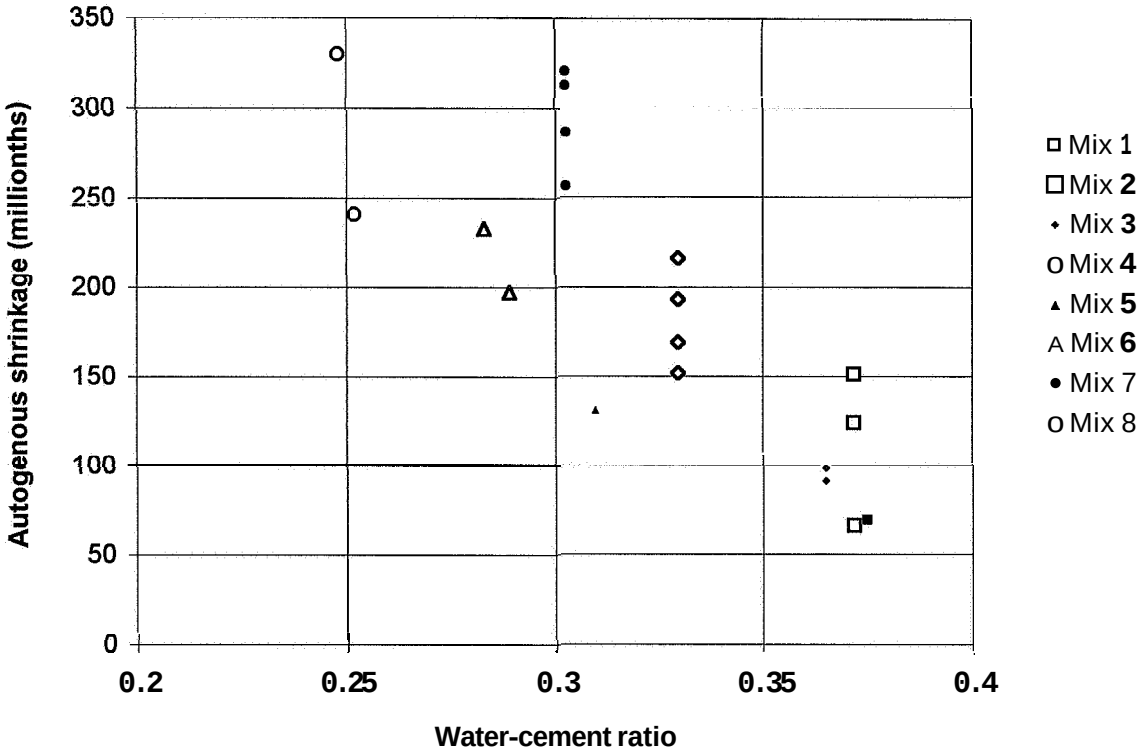

Figure 8.7 - Autogenous shrinkage versus w/c. The HPC mix is given, **Table 5.1**.

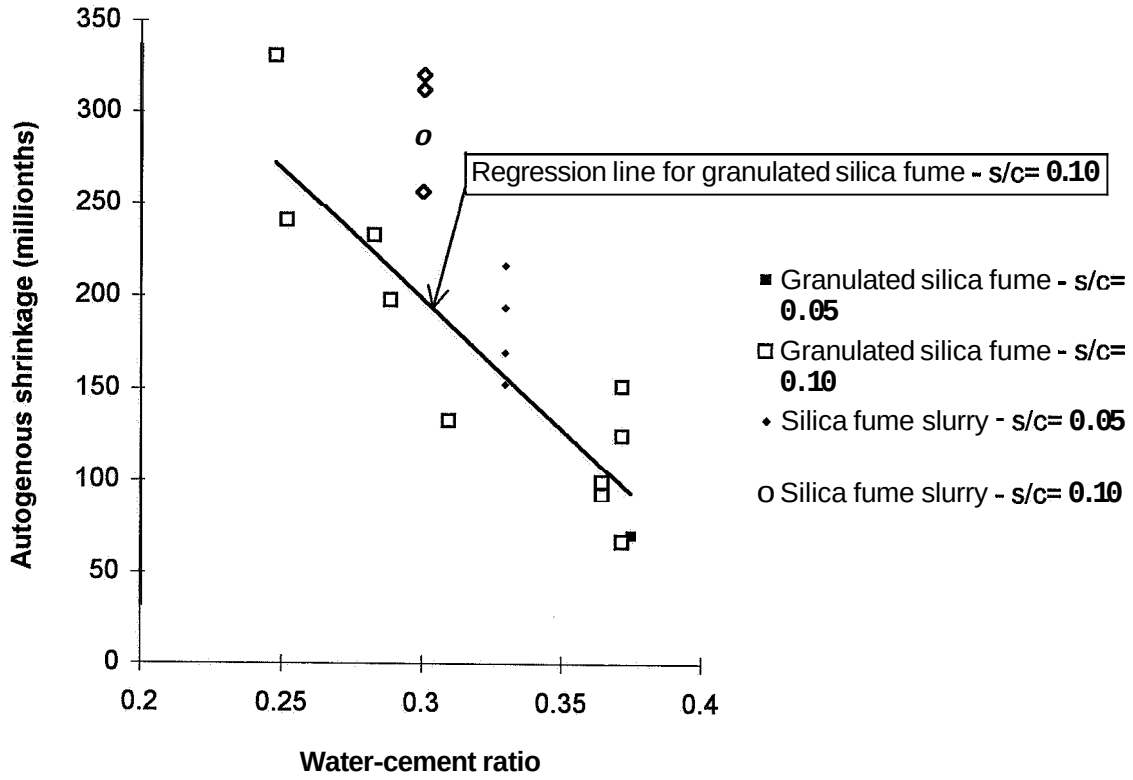

Figure 8.8 - Autogenous shrinkage versus w/c. Type and amount of silica fume.

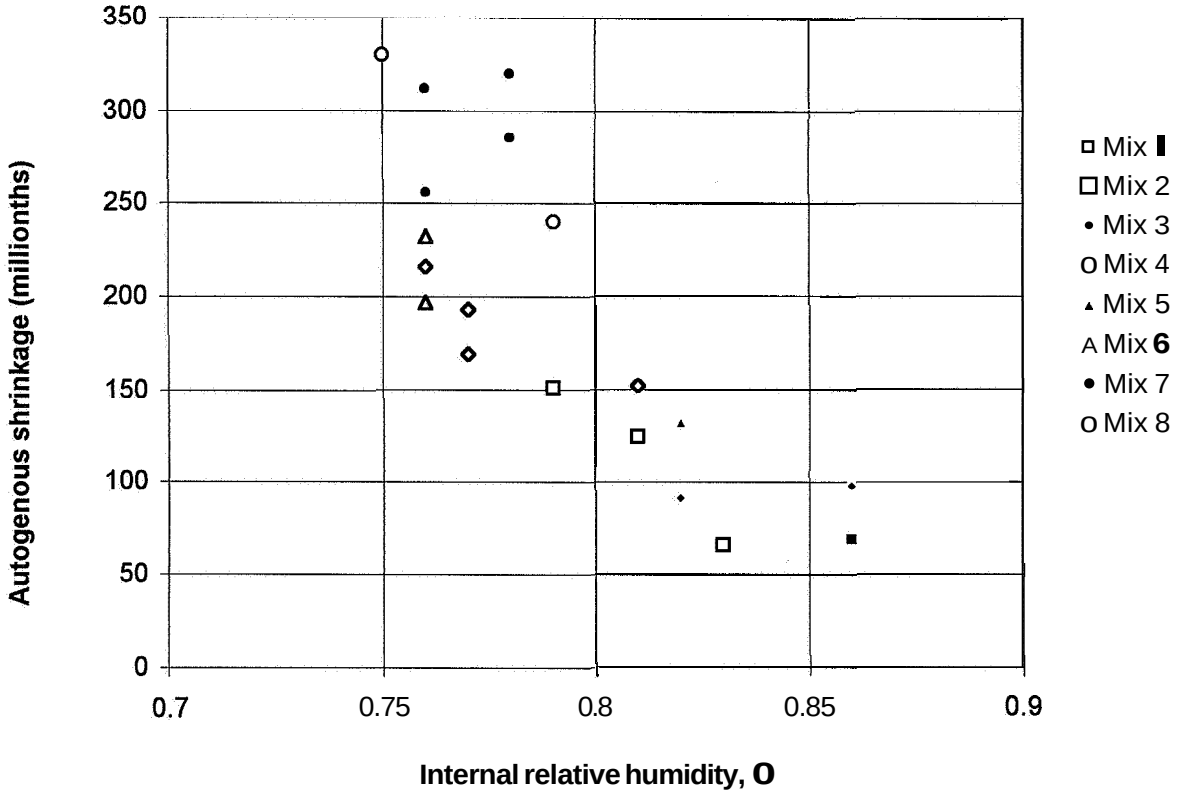

Figure 8.9 - Autogenous shrinkage versus internal relative humidity, O. HPC mix.

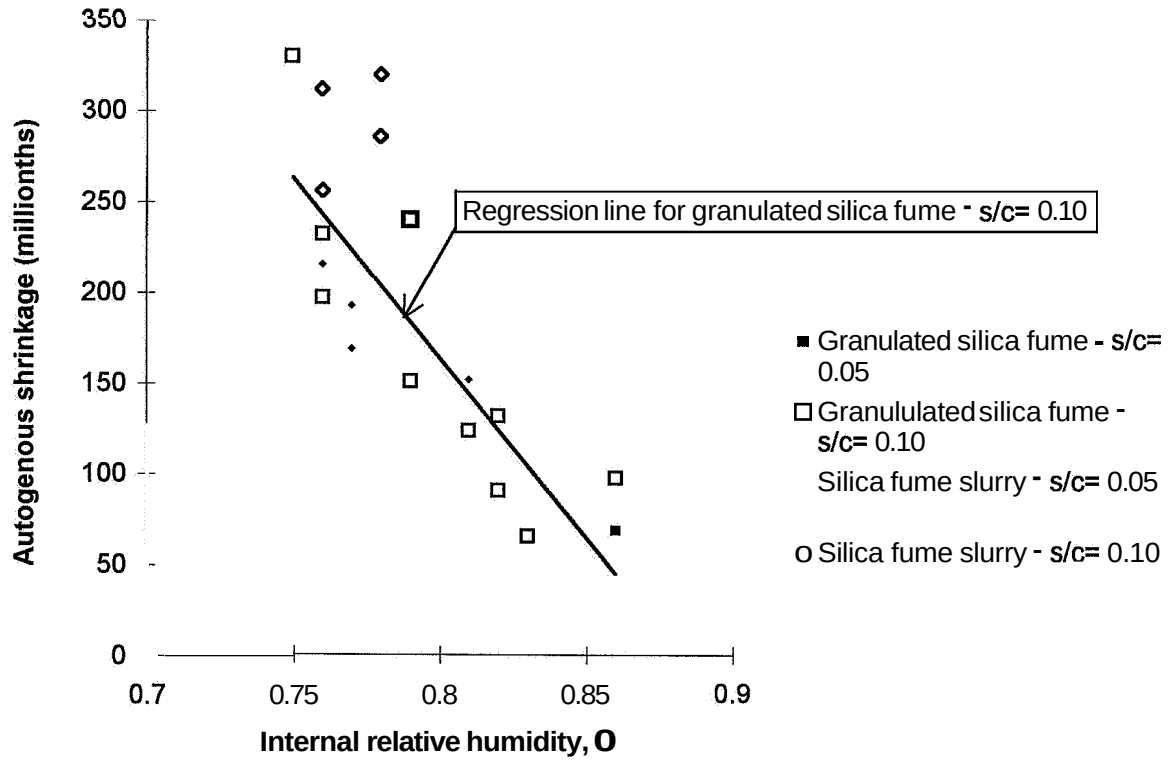

Figure 8.10 - Autogenous shrinkage versus O. Amount and type of silica fume.

k_s = 1.5 for silica fume slurry; k_s = 1 for HPC with granulated silica fume
$k_{s\Ø}$ = 1.3 for silica fume slurry; $k_{s\Ø}$ = 1 for HPC with granulated silica fume
k_5 = 0.78 for 5% silica fume; k_5 = 1 for HPC with 10% silica fume
O denotes the internal relative humidity {0.70<Ø<0.90}

8.7.2 Drying shrinkage of mature concrete

Small loss of weight was observed in the sealed specimens for reasons mentioned above. **Table** 8.1 shows the loss of weight recorded during a period of 3 years from 1.8-kg HPC specimen. Small loss of weight over a long period gave a simulation of the shrinkage of a large structure of mature HPC. On the left hand side of **Figure 8.6** the shrinkage of mature HPC is indicated versus the moisture losses, w_e/w. The inclinations of these regression lines gave the specific shrinkage of mature HPC versus w_e/w. **Appendix** 8 shows all relationships between relative loss of weight, i.e. the ratio of evaporated water to mixing water, w_e/w, which makes the study non-dimensional. **Figure** 8.11 shows the specific shrinkage (inclinations of **left-hand-**side regression lines in **Figure 8.6** and **Appendix** 8) versus the relative evaporated water, w_e/w. After transformation the following equation was obtained (per mil):

$$\varepsilon_D = k_{sD} \cdot 20 \cdot [1.1 \cdot (w_e/w) - (w_e/c)] \qquad (8.3)$$

c denotes the cement content of the concrete (kg/m^3)
k_{sD} = 0.4 for HPC with silica fume slurry; k_{sD} = 1 for granulated silica fume
w denotes the mixing water of the concrete (kg/m^3) {0< w_e/w<0.03}
w_e denotes the evaporated water from the concrete (kg/m^3) {0< w_e/w<0.03}
ε_D denotes the specific shrinkage related to the evaporated water (per mil)

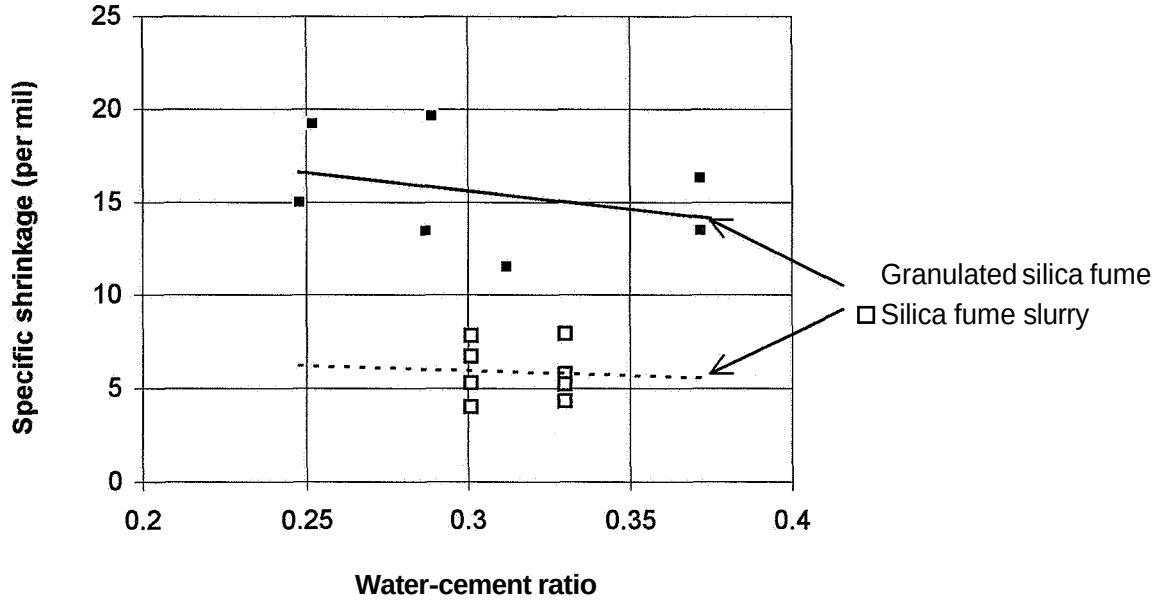

Figure 8.11 - Specific shrinkage versus w/c. Different types of silica fume.

Table 8.1 - Weight losses from 1.8-kg specimen (g).

Concrete	01	02	03	28
1	-	3.9	-	-
2	2.6	2.0	1.1	-
3	2.7	2.3	-	-
4[1)]	5.3	2.4	4.2	3.0
5	1.7	1.6	-	-
6	0.7	1.3	-	-
7[1)]	3.9	2.5	2.9	5.2
8	0.9	1.0	-	-

1) 4 years

Symbols in **Table** 8.1 :
5... = HPC **mix, Table** 5.1
...01 = loading at 0.8 days' age with stresslcylinder strength = 0.84
...02 = loading at 2 days' age with stresslcylinder strength = 0.84
...03 = loading at 2 days' age with stresslcylinder strength = 0.42
...28 = loading at 28 days' age with stresslcylinder strength = 0.42

8.7.3 Drying shrinkage of young concrete

The internal relative humidity, 0 , of the cylinder used for the measurements of shrinkage was obtained in the experiments and shown in **Appendix** 5 and **Figure** 5.24. Between 5 and 28 days' age O became less than 0.7, which ceased the effect of hydration and thus the autogenous shrinkage in the specimens. However, at 28 days' age O of the specimen was still about 5% larger than the ambient relative humidity. Another year of drying was required to obtain equilibrium between the internal and the ambient relative humidity, **Figure** 5.24. However, due to carbonation of the calcium hydroxide of the concrete, the loss of weight ceased at an age of the concrete that was dependent on wlc, **Figure** 8.12. [The water in the calcium hydroxide (molecule weight 74) was replaced by the carbon dioxide (molecule weight 100).] Sufficient silica fume to consume all the calcium hydroxide by the pozzolanic reaction was estimated. In NSC about 16% silica fume is required to consume all the calcium hydroxide, **Peterson** (1976):

$$3\ Ca(OH)_2 + 2\ SiO_2 = 3\ CaO.2\ SiO_2.3\ H_2O \qquad (8.4)$$

At lower wlc the required amount of silica fume, s_{rq}, to consume all the calcium hydroxide by the pozzolanic reaction also became smaller, **Powers & Brownyard (1946-1948)**, **Peterson** (1976):

$$s_{rq} \approx [(w/c)/0.39] \cdot 0.16 \approx 0.4 \cdot (w/c) \qquad (8.5)$$

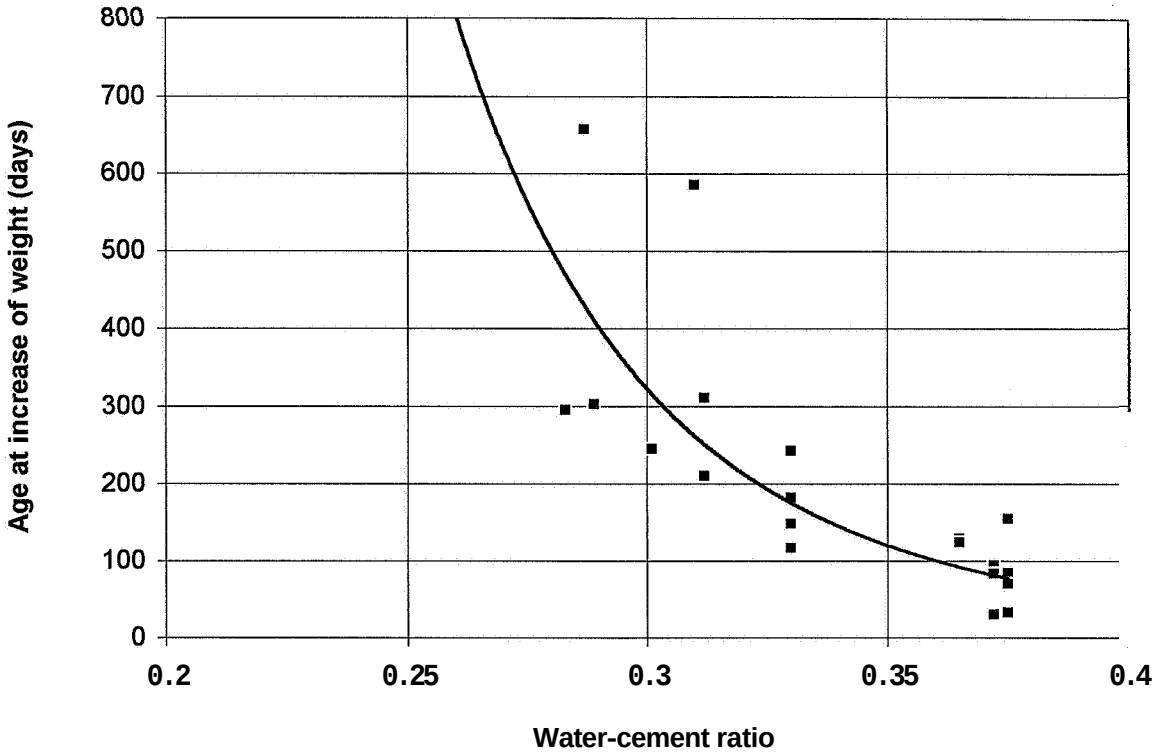

Figure 8.12 - Age at increase of weight due to carbonation versus w/c.

According to equation (8.5), carbonation does not occur at w/c= 0.25 and s/c= 0.10. This was confirmed by the experiments, **Figure** 8.12. At w/c= 0.3 some of the concretes did not carbonate, which indicated the required amount of silica fume to be slightly lower than estimated in equation (8.5). The following correlation was obtained for the age at carbonation, t_{ca} (days):

$$t_{ca} = 0.142 \cdot (w/c)^{-6.42} \qquad \{0.3<w/c<0.4\} \qquad (8.6)$$

For HPC with w/c<0.3, **Appendix** 8, when carbonation did not occur, the drying shrinkage, ε_{D1}, was correlated to the loss of weight with an equation (per mil):

$$\varepsilon_{D1} = 1.55 \cdot [(w/c)-0.219] \cdot e^{62.9 \cdot [0.423 \cdot (we/w)-(we/c)]} \qquad (8.7)$$

C denotes the cement content of the concrete (kg/m^3)
w denotes the mixing water of the concrete (kg/m^3) {0.25< w/c<0.30}
w_e denotes the evaporated water from the concrete (kg/m^3) {0<w_e/w<0.30}
ε_{D1} denotes the specific shrinkage related to the evaporated water (per mil)

However, for w/c> 0.3 the carbonation took place simultaneously with the drying of moisture. In this case the shrinkage was correlated to time, which made the equation dependent on the size of the specimen. The time of drying shrinkage was set according to equation **(8.6). Figure** 8.13 shows the rate of shrinkage (per mil/day).

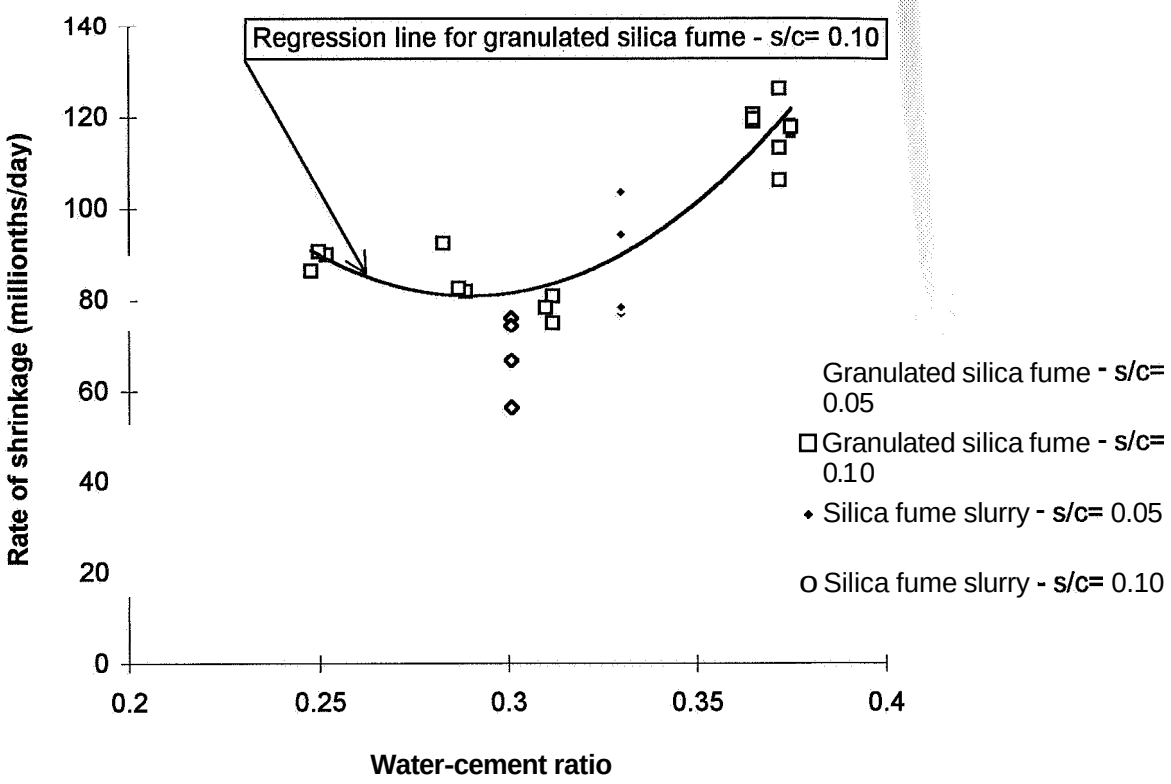

Figure 8.13 - Rate of drying shrinkage versus w/c. Type of silica fume is indicated.

From **Figure 8.13** the following equation was estimated:

$$d\varepsilon_{D2}/dt = k_s \cdot [5.65 \cdot (w/c)^2 - 3.28 \cdot (w/c) + 0.556]/t \qquad (8.8)$$

k_s =0.85 for concretes with silica fume slurry; k_s= 1 otherwise
t denotes age (days)
$d\varepsilon_{D2}/dt$ denotes rate of shrinkage (per mil /day) (diameter: 55 mm; length: 300 mm)

Equation (8.8) indicates that the rate of drying was lower for HPC with silica fume slurry than for concrete with granulated silica fume.

8.7.4 Carbonation shrinkage of mature concrete

At an age varying between 1 month and 2 years as described in equation (8.6) the specimens began to carbonate, which was recorded by weighing. Once the carbonation started, no decline of the internal relative humidity was recorded, **Figure 5.24. Appendix 8** show the carbonation shrinkage versus the loss of weight. **Figure 8.14** shows the carbonation rate versus w/c. It became feasible to describe the carbonation rate related to the mixing water:

$$d(w_c/w)/dt = 0.25\ (w/c - 0.25)/t \qquad (8.9)$$

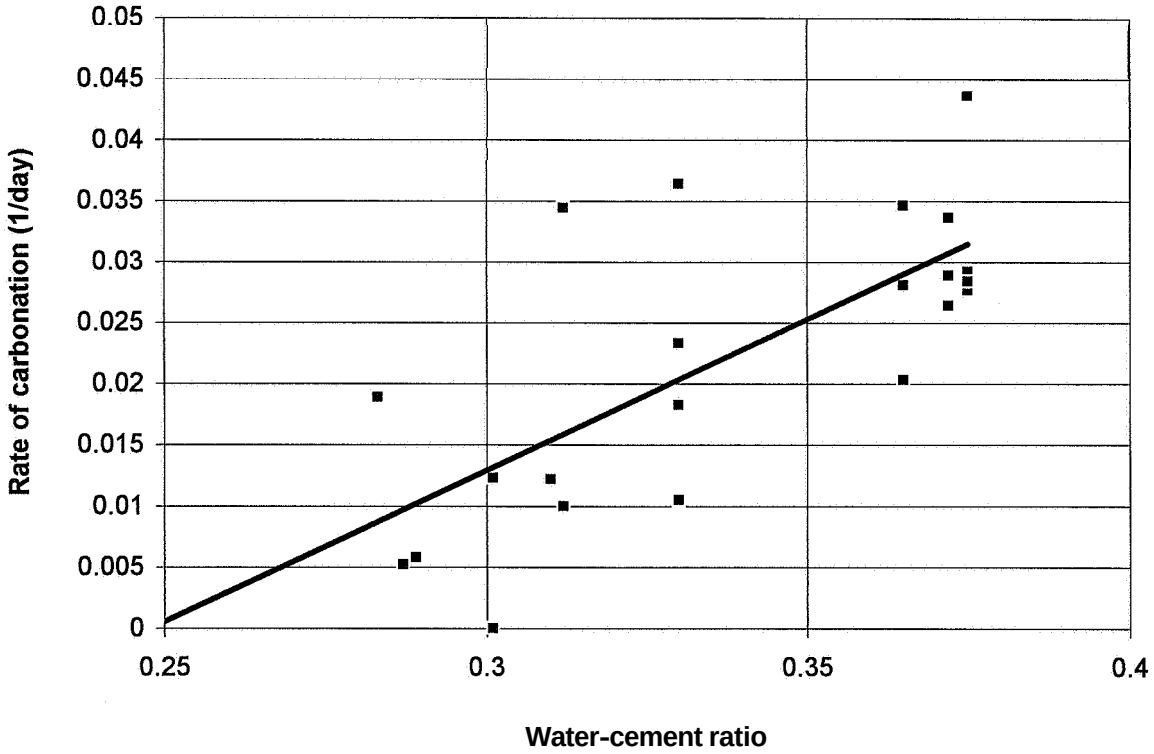

Figure 8.14 - Rate of carbonation versus w/c.

C	denotes the cement content of the concrete (kg/m^3)
t	denotes age (days)
W	denotes the mixing water of the concrete (kg/m^3) $\{0.25< w/c<0.40\}$
w_c	denotes carbonated weight (kg/m^3) $\{0.2< w_c/w<0.35)$
$\delta(w_c/w)/\delta t$	denotes the carbonation rate [(kg/kg)/day]

Equation (8.9) confirmed the previous results in equations (8.5) and (8.6), namely, that no carbonation occurred in a concrete with 10% silica fume and a water-cement ratio less than 0.25.

8.7.5 Total shrinkage

The studies were performed for at least 3 years (4 years for concretes 4 and 7), **Figure** 8.15:

$$\varepsilon=k\cdot 34\cdot[(w/c)^2-0.68\cdot(w/c)+0.13] \quad (8.10)$$

$$\varepsilon_B=k_B\cdot 1.5\cdot[0.43-(w/c)] \quad (8.11)$$

$$\varepsilon_C=0.85\cdot[(w/c)-0.25] \quad (8.12)$$

$$\varepsilon_D=33\cdot[(w/c)^2-0.654\cdot(w/c)+0.115] \quad (8.13)$$

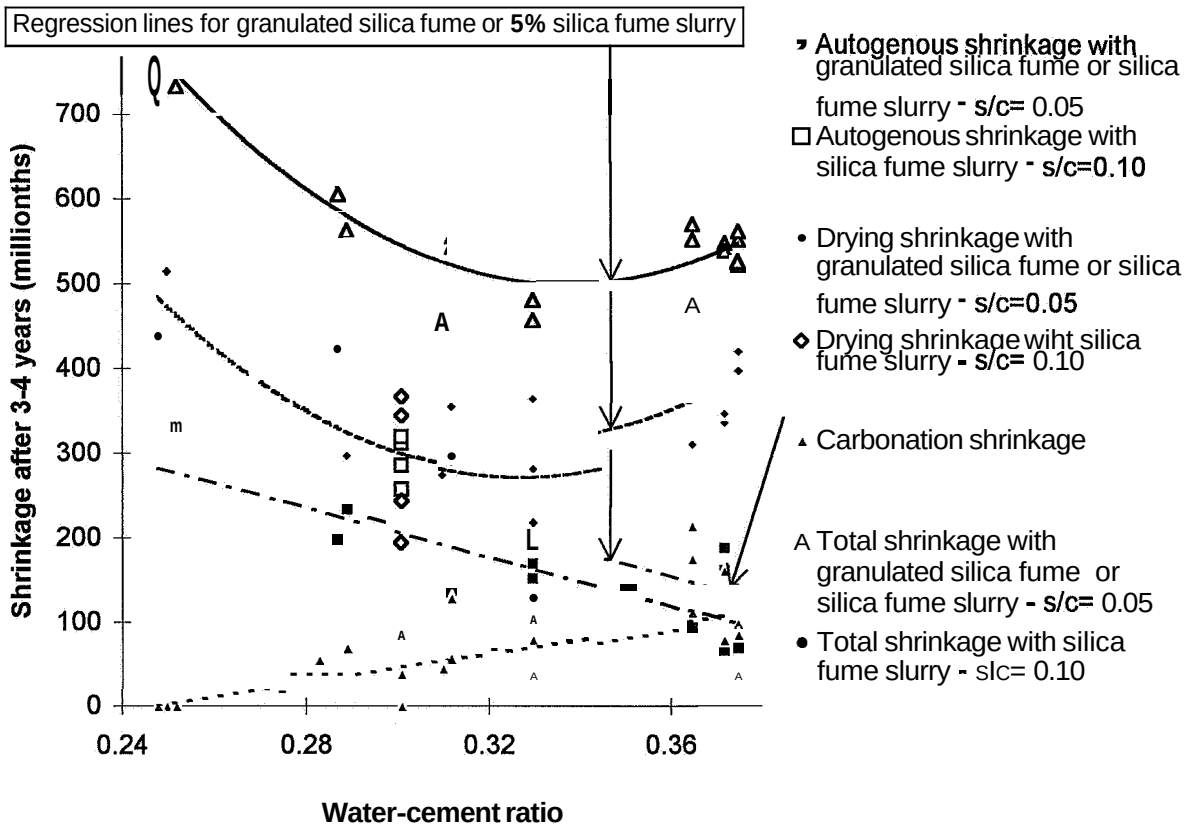

Figure 8.15 - Shrinkage versus the wlc. c= cement content; s= silica fume content.

k	=1.1 for **HPC** with 10% silica fume slurry; k=l for **HPC** with 10% granulated silica fume or 5% slurry
k_B	=1.5 for **HPC** with 10% silica fume slurry; k_B=1 for 10% granulated silica fume or 5% slurry
E, ε_B, ε_C, ε_D	denote total, basic (autogenous), carbonation and drying (per mil)

8.7.6 Comparison with other results

Table 8.2 shows a comparison with results according to other studies of the measured shrinkage. Obviously, according to **Table** 8.2, some of the results on autogenous shrinkage were significantly larger than the average result of autogenous shrinkage, probably due to losses of weight, **Table** 8.2, **Sicard (1993) and Persson (1995A)**. **Appendix** 8 (autogenous shrinkage after short-term creep) shows results from studies of 32 sealed HPC specimen, **Persson (1995A)**. Also these specimens exhibited some small losses of weight over time. The moisture losses were very small, only about 2 grams from a 2-kg specimen, but still the autogenous shrinkage seems to have been affected. It was feasible to correlate the autogenous shrinkage of the **HPC** specimen to the loss of weight. The autogenous shrinkage thus was defined as the shrinkage at no loss of weight at all. A linear regression between autogenous shrinkage and loss of weight was performed. **Figure 8.16** shows the autogenous shrinkage versus w/c of 50 specimens without loss of weight. The following equation was obtained between autogenous shrinkage, ε_{Bn}, and w/c (per mil):

Table 8.2 - Results of measured shrinkage for w/c= 0.3 and s/c= 0.1 (millionths).

Present study	**Roy & Larrard (1993)**	**Sicard (1993)**	**Tazawa & Miyazawa (1993,1997)**	**Persson (1995A)**	**Persson (1995A)**	**This study**	**This study**
Silica fume	Granu-lated	Granu-lated	G-ranulated	Granu-lated	Slurry	Granu-lated	Slurry
Age (days)	400	600	40	1000	1000	1200	1500
Auto-genous	220	430	200	320	380	195	295
Drying	160	-	200	-	-	300	285
Carbo-nation	-	-			-	45	30
Total	380	-	400	-	-	540	610
No weight losses						200	270

$$\varepsilon_{Bn} = k_{sn} \cdot k_{5n} \cdot 1.38 \cdot [0.45-(w/c)] \qquad (8.14)$$

ε_{Bn} denotes shrinkage in HPC with no loss of weight (per mil)
k_{sn} = 1.33 for HPC with silica fume slurry; k_{sn} = 1 with granulated silica fume
k_{5n} = 0.69 for HPC with 5% silica fume; k_{5n} = 1 for HPC with 10% silica fume

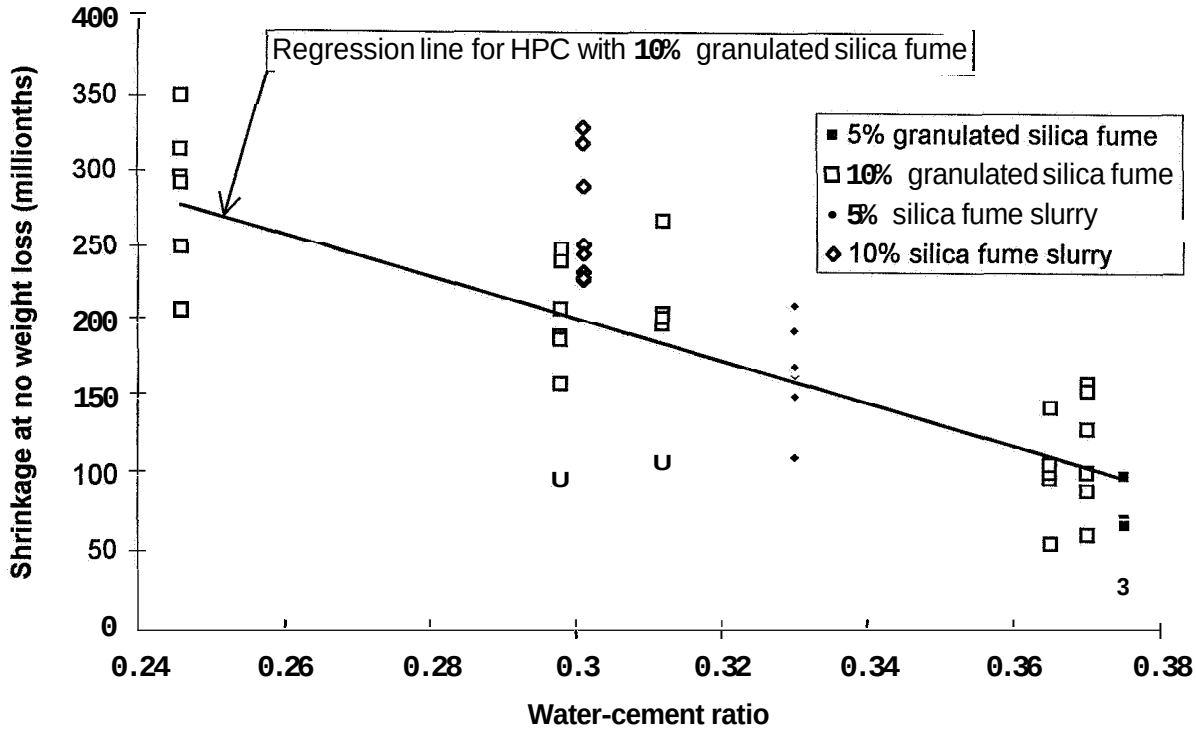

Figure 8.16 - Long-term autogenous shrinkage of HPC versus w/c at no weight loss.

8.7.7 Carbonation depth and shrinkage

No carbonation shrinkage and thus no carbonation of HPC was observed in HPC with w/c sufficiently low in combination with 10% granulated silica fume. Probably all calcium hydroxide was consumed in the pozzolanic interaction, giving no chemical component in HPC for the carbon dioxide in the air to carbonate. This observation was of course important for the durability of the HPC and a way to diminish the cover layer of the reinforcement. The way to verify the hypothesis concerning the carbonation of HPC mentioned above was to cut the specimen identical to the one used for measurements of autogenous shrinkage. For this purpose cylinders formerly used in the studies of quasi-instantaneous deformations were investigated. These cylinders originated fi-om the same batches as the specimens used for the studies of carbonation shrinkage, which were saved for future studies. The cylinders were cut in two halves, 150 mm in length. A solution of phenolphthalein was applied directly on the cut surface. The depth of carbonation was directly measured by microscope at 4 places on each cut part of the cylinder, in all 8 measurements. The difference in the measured carbonation depth of each HPC batch was little, within 1 mm. The average 5-year carbonation depth of the 8 measurements on each cylinder versus w/c is shown in **Figure 8.17.** The carbonation became astonishingly deep in HPC with w/c= 0.37. However, for HPC with w/c < 0.30 combined with 10% granulated silica fume no carbonation appeared even after 5 years. For HPC with silica fume slurry the w/c-limit for carbonation seemed to be larger. **Figure 8.18** shows the carbonation shrinkage versus the carbonation depth of the cylinder. The following equation was found between carbonation depth and carbonation shrinkage for 55-mm cylinder, ε_C (per mil):

$$\varepsilon_C = 0.005 \cdot d_c \cdot (1+0.14 \cdot d_c) \qquad (8.15)$$

d_c denotes the depth of carbonation for 55-mm cylinder (mm)

The size of the carbonation shrinkage also depended on the size of the cylinder. A small cylinder was more affected by carbonation shrinkage than a large one. Tensile stress at the surface was compensated by compression at the inner of the cylinder.

8.8 Conclusions

- Autogenous shrinkage was related to age, w/c, type and amount of silica fume.
- Autogenous shrinkage was related to the decline of internal relative humidity.
- Long-term drying shrinkage of mature HPC was related to the evaporated water.
- The conditions for carbonation were related to w/c and content of silica fume.
- Age at start of the carbonation of HPC was related to w/c.
- The drying shrinkage of young HPC was related to age and to the loss of weight.
- Carbonation shrinkage of HPC was related to age, w/c and depth of carbonation.
- Long-term shrinkage was related to age, w/c and type and content of silica fume.

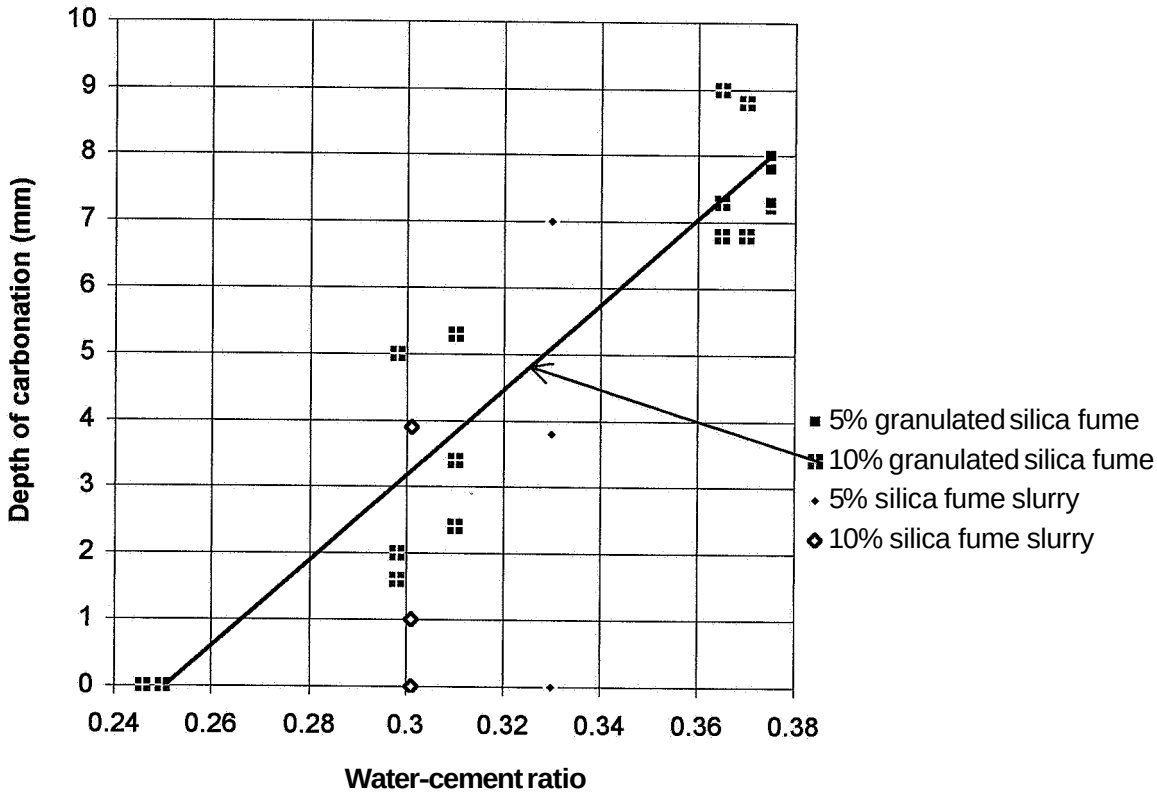

Figure **8.17** - 5-year carbonation depth versus w/c. Average of the **8** measurements.

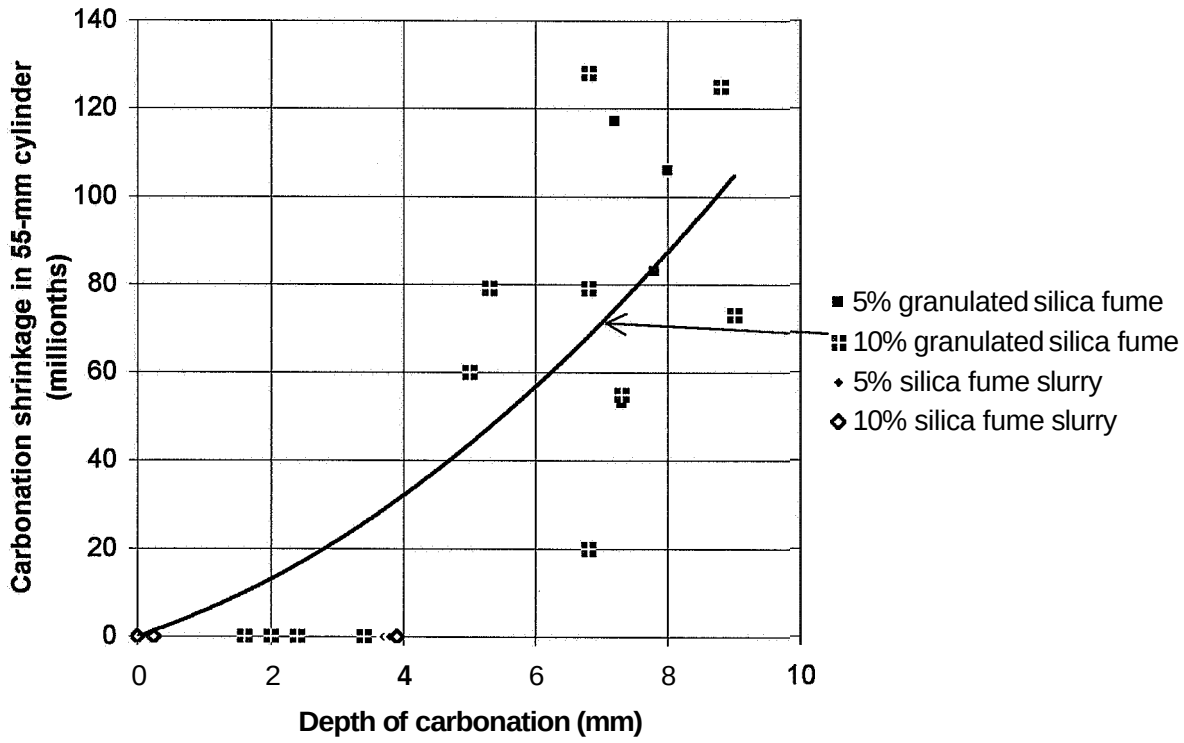

Figure **8.18** - Carbonation shrinkage versus the carbonation depth of the cylinder.

9. SHORT-TERM DEFORMATION

9.1 General

The quasi-instantaneous loading on air-cured or sealed HPC cylinders was immediately followed by studies of short-term deformation. At early age and/or at a high stress/strength ratio the plastic deformations probably dominate the short-term deformation. Loading on concrete is often rapidly transferred when prestressing is done. The prestressing wires are often cut with welding or grinding equipment which imposes a sudden loading on the concrete. One question of interest is whether this kind of loading causes larger creep deformation of the concrete than when the prestressing is slowly transferred to the concrete with hydraulic equipment. Finally, it was of interest to investigate short-term creep deformations of HPC concerning its continued prolongation with long-term creep deformations. The research was performed in an MTS machine. The conditions in Section 6 applied.

9.2 Experimental procedure

Cylinder specimens 300 mm long and 55 mm in diameter were also used in the experiment with short-term deformations. (The experiments were an extension of the quasi-instantaneous studies as described above.) The measurements were performed in an MTS machine on four points outside the specimen by Schlumberger displacement and gauging transducers (LVDT). The general layout is given in section **3.3** above. Materials, preparation of specimens and chronology are described in Section 4 above, and the concrete mix proportions are shown in **Table 5.1.** The measuring points were stiffly connected to the steel cast-in items by pin bolts of 3-mm diameter. The length between the longitudinal measuring points was 250 mm and between the transversal points 55.5 mm. The measurement was performed every 12 minutes by a computer. The testing room was air-conditioned to avoid displacements due to temperature movements. Furthermore the drying HPC cylinder was built into an insulated box as described above. The ambient climate of the HPC cylinder and its temperature was mainly stable, **Figure 6.1 and 6.2.**

9.3 Results

The shrinkage was reduced from the measured strain before the results were presented, Section **8. Figure 9.1** shows the compliance (specific deformation, ε/σ) of HPC mix 6 versus the loading time. **Figure 9.2** shows the short-term compliance of all mature concretes versus time. **Appendix 9** shows all the results of short-term compliance versus logarithmic time. The following symbols were used:

t denotes age of the concrete
t' denotes age of the concrete when loading
J(t,t´) denotes creep compliance (millionths/MPa)
5… = HPC mix 5, **Table** 5.1

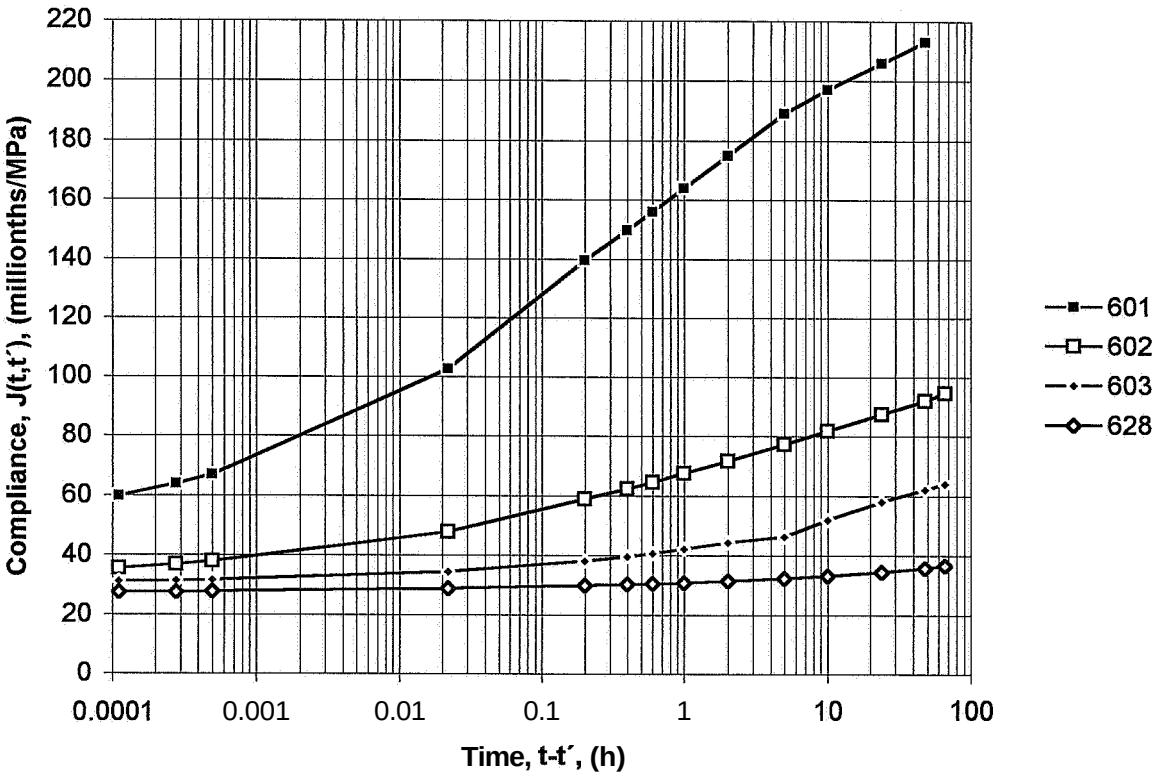

Figure 9.1 – Compliance of HPC mix 6 versus the loading time.

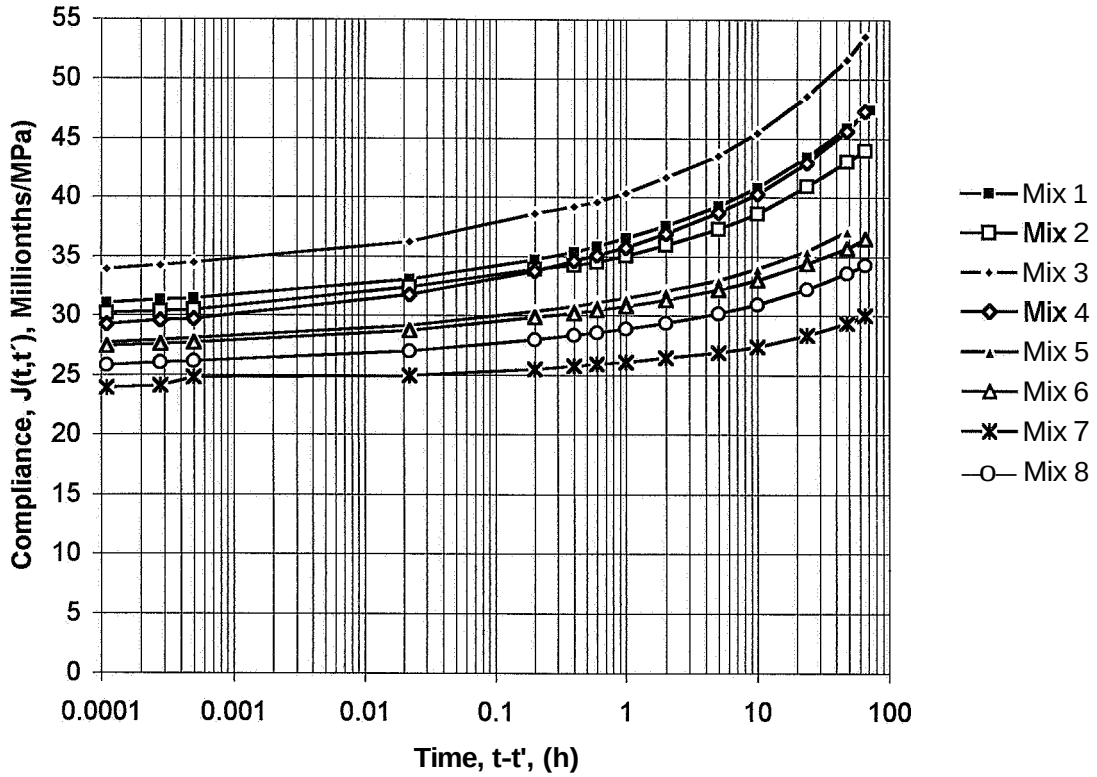

Figure 9.2 - Short-term compliance of all mature HPCs versus loading time.

...01 = loading at 0.8 days' age with stresslcylinder strength = 0.84
...02 = loading at 2 days' age with stresslcylinder strength = 0.84
...03 = loading at 2 days' age with stresslcylinder strength = 0.42
...28 = loading at 28 days' age with stresslcylinder strength = 0.42

9.4 Sources of error and accuracy

The following sources of error were taken into account:

- Level of loading
- Deformation errors of the LVDTs
- Eccentricity of loading
- Effects of lateral strain

The variations of the loading were kept within 0.01 kN, i.e. the stress variation was ± 0.004 MPa. The LVDTs were calibrated to an accuracy of ± 0.002 mm. The relative fault was obtained:

$$\delta J(t,t')/J(t,t') = \delta\varepsilon/\varepsilon - \delta\sigma/\sigma \qquad (6.5)$$

At 10 MPa stress the maximum fault was calculated according to equation (6.5): $\delta J(t,t')/J(t,t') = \delta\varepsilon/\varepsilon - \delta\sigma/\sigma = 0.00410.25 - 0.008110 = 0.008 \approx 0.01$ and was thus very small. The eccentricity, e, of the loading was calculated after 66 h of loading according to equations (6.6) - (6.12) adopting elastic conditions, **Table 9.1**. **Table 9.2** shows the stress during the 66 h of loading. The calculated eccentricity decreased substantially given that the concrete behaved more plastically at early ages than after 66 h, cp. **Table 6.2.** The effect of Poisson's ratio, u, will be studied at the unloading of the specimen. The compliance due to lateral strain decreased by a multiplication by $1- u^2$.

Table 9.1 - Loading eccentricity (mm)

Concrete	01	02	03	28
1	5.2	3	3.1	2.2
2	4.3	0.8	2.9	2.8
3	3.2	5.3	2.3	2.2
4	1.8	0	4.5	3.3
5	0.9	3	3.9	1
6	1.5	7.3	5.5	1
7	1.9	0.9	1.4	2.1
8	2.3	0.9	3.8	3.4

Table 9.2 - Stress during the short-term loading (MPa)

Concrete	01	02	03	28
1	14	18.6	7.8	20.7
2	14.4	26.4	13.2	25.8
3	16.2	18	12.9	17.4
4	13.9	22.4	14.4	26.7
5	22.8	27	18	31.8
6	18	36	17.4	33.3
7	21.8	37.9	20.2	35.4
8	21	40.6	19.5	35.4

9.5 Analyses

9.5.1 Stress and time dependence of HPC with air curing

The compliance during the testing period was separated into two parts: one part expressed the deformation due to the initial loading; the other part expressed creep:

$$J(t,t') = a_D \cdot \int d(t-t')/(t-t') + b = a_D \cdot \int d(t-t')/(t-t') + 1000/D_{t'} \qquad (6.13)$$

a_D denotes the drying creep compliance rate, **Table 9.3** [millionths/(MPa·h)]
b denotes the initial compliance 1 h after loading, **Table 9.4** (millionths/MPa)
t denotes the age of the concrete (h)
t' denotes the age of the concrete when loading (h)
$D_{t'}$ =1/b; denotes the deformation modulus at loading, see **Table 9.4** (GPa)
J(t,t') denotes the compliance (specific creep, millionths/MPa)

For correlation of the creep rate the initial compliance, b (millionths/MPa) was calculated by logarithmic regression from 0.4 s of loading until 66 h of loading. **Figure 9.3** shows the compliance rate versus the maturity of the concrete indicated as the relative 28-day strength, f_c/f_{c28}. The creep rate was dependent on the maturity and on the stress/strength level. **Figure 9.4** shows that the compliance rate decreased with w/c for mature HPC. The compliance rate was larger for HPC with air-entrainment. **Figure 9.4** also shows that the eccentricity had no effect on the compliance rate when specimens were loaded at 28 days' age. The following equation was obtained for the rate of short-term drying creep [millionths/(MPa·h)]:

$$a_D = 3.4 \cdot [(w/c)-0.13] \cdot s_{a5} + [0.3-11 \cdot (\sigma/f_c)] \cdot \ln(f_c/f_{c28}) \qquad \{0.25<w/c<0.40\} \qquad (9.1)$$

a_D denotes the rate of short-term drying creep of HPC [millionths/(MPa·h)]
f_c/f_{c28} denotes the relative 28-day strength at loading $\{0.3< f_c/f_{c28}<1\}$
s_{a5} =1.5 for 5% silica fume and/or air-entrainment; s_{a5}= 1 for 10% silica fume
σ/f_c denotes the stress/strength (100 mm cube) ratio at loading $\{0.3<\sigma/f_c<0.6\}$

Table 9.3 - Compliance rate within 66 h [millionths/(MPa·h)]

Concrete	01	02	03	28
1	4.83	5.11	3.41	1.16
2	6.13	4.76	3.14	0.936
3	6.93	6.02	2.97	1.3
4	11.2	7.65	3.18	1.21
5	4.57	3.6	2.51	0.625
6	12.53	4.46	2.27	0.611
7	8.85	4.1	2.16	0.378
8	8.99	4.5	2.96	0.564

Table 9.4 - Compliance 1 h after loading (millionths/MPa)

Concrete	01	02	03	28
1	102.5	84.9	64.5	39
2	92.8	81.3	66.2	36.8
3	107.5	95.1	58.5	43
4	154.3	103.7	56.3	37.9
5	78	61.3	60	32.4
6	164	70.5	46.5	31.8
7	121	65.1	44.2	26.8
8	113	64.6	49.9	29.9

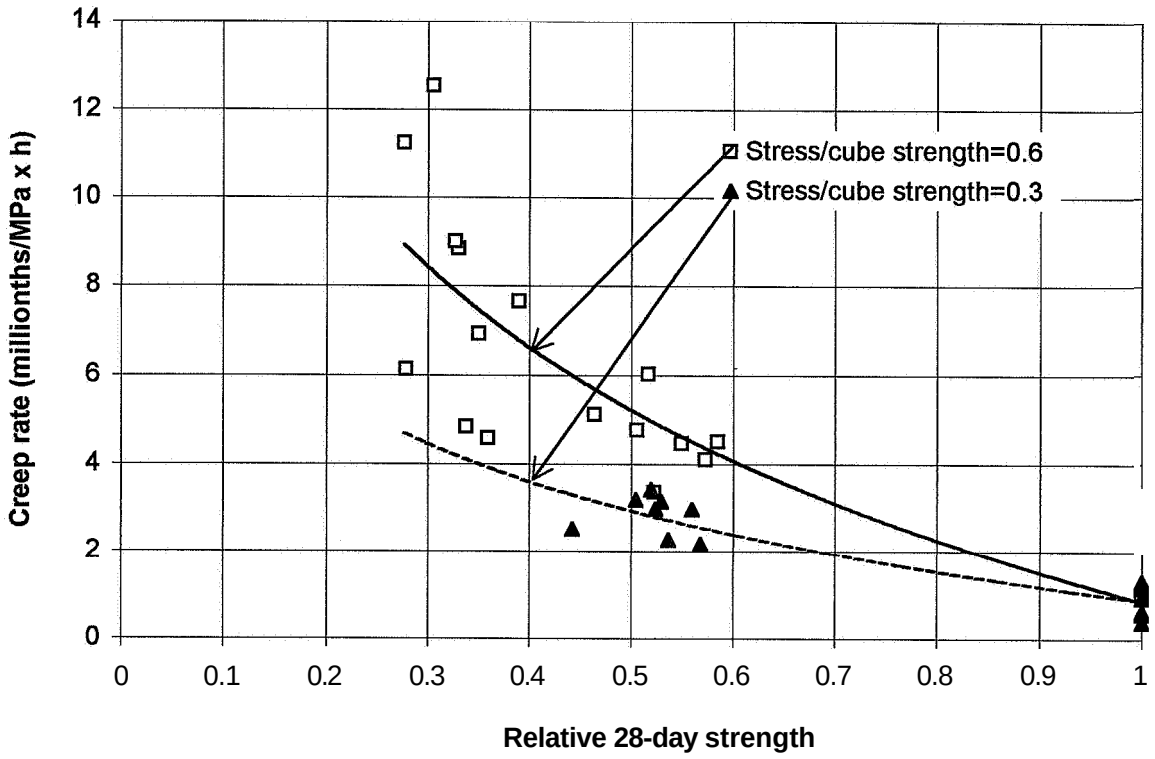

Figure 9.3 - Compliance rate of the HPC versus the maturity, f_c/f_{c28}.

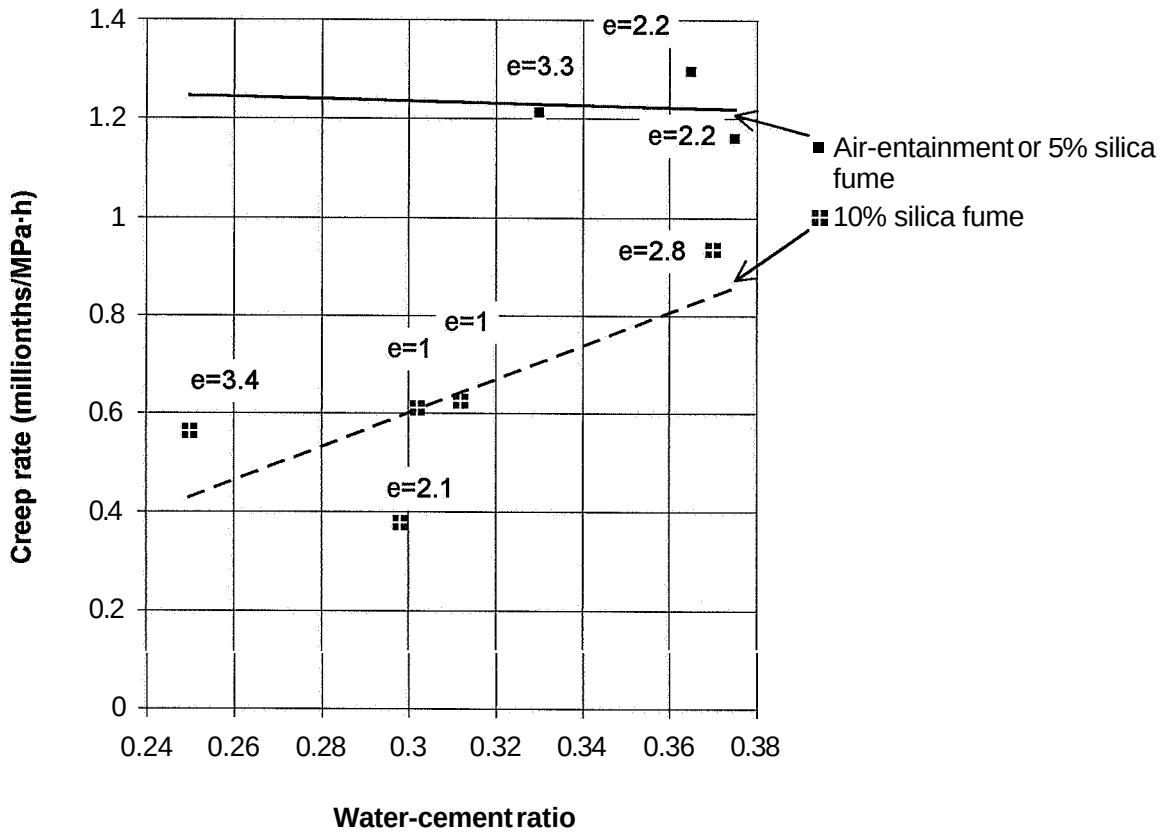

Figure 9.4 - Compliance rate for mature concrete versus the w/c. e= eccentricity.

9.5.2 Comparison with basic creep

Within the project short-term creep deformation studies also were performed on 32 sealed cylinders with constant moisture and temperature conditions, i.e. basic creep, **Persson (1995A)**. **Appendix 9** (sealed curing) provides the compliance of all tests of short-term creep of sealed HPC. **Figure 9.5** shows compliance versus relative 28-day strength when the loading was performed. The stress/strength levels 0.3 and 0.6 are indicated in **Figure 9.5.** However, the overlapping of relative strength, f_c/f_{c28}, where the creep was studied with a stress/strength level at both 0.3 and 0.6, was very little (actually it varied only between 0.4 and 0.55). The following equation was obtained for the creep rate of sealed HPC, a_B [millionths/(MPa·h)]:

$$a_B = 0.14\cdot[(w/c)+2.5]\cdot s_{a5} + [0.29-6.9\cdot(\sigma/f_c)]\cdot\ln(f_c/f_{c28}) \qquad (9.2)$$

a_B denotes the creep rate of sealed HPC [millionths/(MPa·h)]:

$\ln(f_c/f_{c28})$ denotes the natural logarithm of the relative strength when loading $\{0.4< f_c/f_{c28}<1$ for $\sigma/f_c=0.3$ and $0.15< f_c/f_{c28}<0.5$ for $\sigma/f_c=0.6\}$

s_{a5} =1.25 for HPCs with 5% silica fume or/and air-entrainment (10% silica fume); s_{a5}= 1 for HPC with 10% silica fume

σ/f_c denotes the stress/strength (100 mm cube) ratio at loading $(0.3<\sigma/f_c<0.6)$

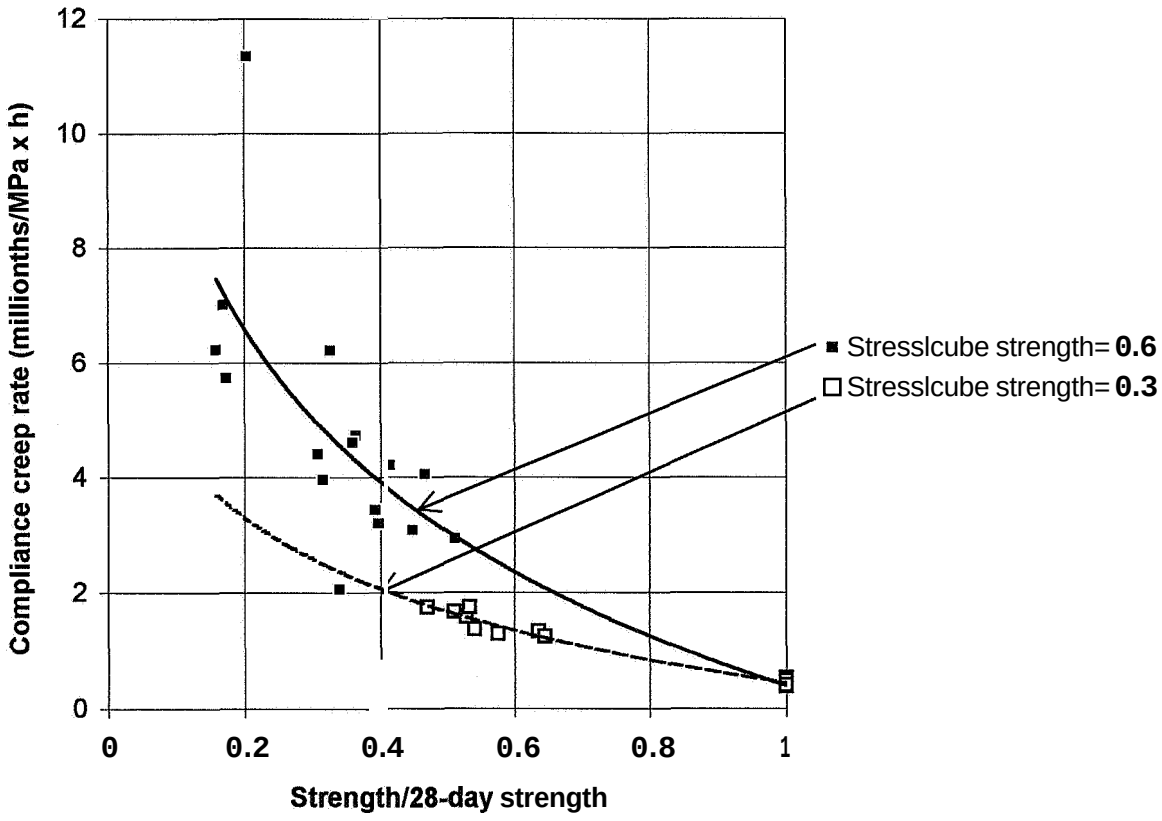

Figure 9.5- Creep compliance rate of sealed HPC versus the relative strength, f_c/f_{c28}.

9.5.3 Creep rate and moisture condition

With stress/strength level, $\sigma/f_c = 0.3$, $f_c/f_{c28}=0.5$ and w/c= 0.3 the creep rate of HPC was $a_D = 2.6$ [millionths/(MPa·h)] for drying creep and $a_B = 1.6$ for basic creep after 1 h in both cases. With stress/strength level, $\sigma/f_c = 0.6$, $f_c/f_{c28}=0.5$ and w/c= 0.3 the creep rate of HPC was $a_D = 3.8$ [millionths/(MPa·h)] for drying creep and $a_B = 3.1$ for basic creep after 1 h. The increase of the creep rate with air curing compared with sealed curing was explained by the moisture gradient of the specimen. During drying a certain amount of shrinkage occurred at the surface of the concrete, which caused an uneven distribution of stress in the cylinder. **Figure** 9.6 indicates the creep rate, a, versus the relative strength, f_c/f_{c28}, and the difference between the internal relative humidity of the inner part, $Ø_i$, and the surface, $Ø_s$, of the cylinder, $AO = Ø_i - Ø_s$, **Figure** 5.24. From **Figure** 9.6, the following equation was obtained:

$$a_{Ø0.3} = 0.52+1.6\cdot\Delta Ø -(3.6\cdot\Delta Ø+1.7)\cdot\ln(f_c/f_{c28}) \quad \{\sigma/f_c=0.3;\ 0.5< f_c/f_{c28}<1\} \qquad (9.3)$$

$$a_{Ø0.6} = 0.84-0.6\cdot\Delta Ø-(9.3\cdot\Delta Ø+3)\cdot\ln(f_c/f_{c28}) \quad \{\sigma/f_c=0.6;\ 0.15< f_c/f_{c28}<0.5\} \qquad (9.4)$$

$a_{Ø0.3}$ denotes the short creep rate of HPC with $\sigma/f_c=0.3$ [millionths/(MPa·h)]
$a_{Ø0.6}$ denotes the short creep rate of HPC with $\sigma/f_c=0.6$ [millionths/(MPa·h)]
$\ln(f_c/f_{c28})$ denotes the natural logarithm of the relative strength at loading
$A Ø = Ø_i - O$ difference in relative humidity of the inner part, $Ø_i$, and the surface, O,

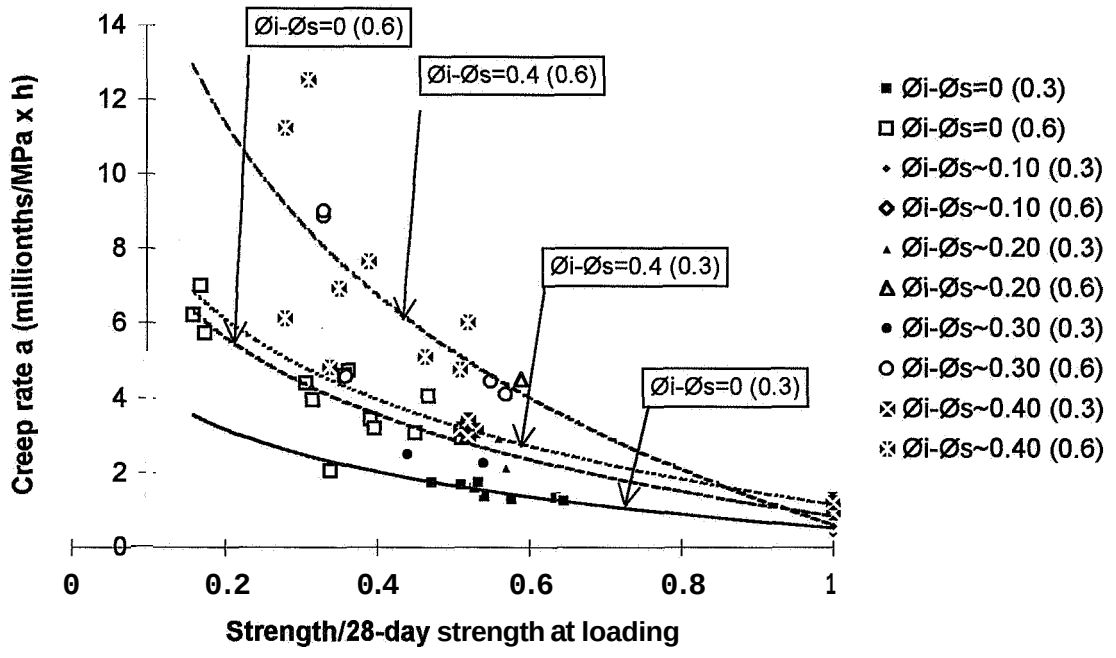

Figure 9.6 - Creep rate versus relative strength at loading with differences in relative humidity between surface and interior of the tested cylinder. ( )= stress/strength level when loading.

9.5.8 Creep rate and strength growth

It was of interest to obtain a relationship between creep and strength that was independent of time. The rate of strength growth was estimated in a logarithmic way like the rate of creep fiom age of loading until unloading. The strength at loading and unloading the specimens was obtained fiom **Appendix 5** (drying creep) and fiom **Persson (1995A)** on studies of exactly the same type of concretes (basic creep). All data on the strength development (air-cured and sealed specimens) are provided in **Appendix** 5. **Figures 9.7 and 9.8** show the rate of creep versus the rate of strength growth for drying and basic short-term creep respectively. From **Figures 9.7 and 9.8** the following general relationship was obtained for the rate of creep:

$$\frac{dJ(t,t')}{d(t-t')} = c \cdot e^{\frac{d}{f_{c28}} \cdot \frac{df_c}{d(t-t')}} \qquad \{0 < df_c/d(t-t') < 0.12\} \qquad (9.5)$$

c, d denote constants given in **Table 9.5** [millionths/(MPa·h)]
$df_c/d(t-t')$ denotes the strength growth during the loading time (MPa/h)
$dJ(t,t')/d(t-t')$ denotes the short-term creep rate during the loading time, t-t' [millionths/(MPa·h)]
f_{c28} denotes the 28-day strength (MPa)

Table 9.5 - Constants in equation (9.5)

Ambient conditions/stress level	Drying				Sealed			
Stress/strength level at loading	σ/f_c= 0.6		σ/f_c= 0.3		σ/f_c= 0.6		σ/f_c= 0.3	
Concrete	c	d	c	d	c	d	c	d
5% silica fume; air-entrainment (10% silica fume)	3.42	8.82	1.22	17.9	2.22	10.9	0.51	26
10% silica fume	2.9	10.2	0.67	22.8	2.15	9.64	0.41	28

9.5 Summary and conclusions

Short-term creep was studied during 66 h. The following conclusions were drawn:

- The rate of short term creep compliance of HPC was dependent on the relative strength at loading and on the stress level mainly.
- The eccentricity after 66 h of loading (less than 7 mm given elastic conditions) had no influence on the rate of creep.
- The rate of creep was about 50% larger with drying than with sealed curing.
- The type and amount of silica fume also affected the creep rate of HPC.
- The creep rate increased with air-entrainment in HPC.
- The short-term creep rate and the strength growth were also correlated.
- Finally, the rate of creep was related to the moisture gradient in the specimen.

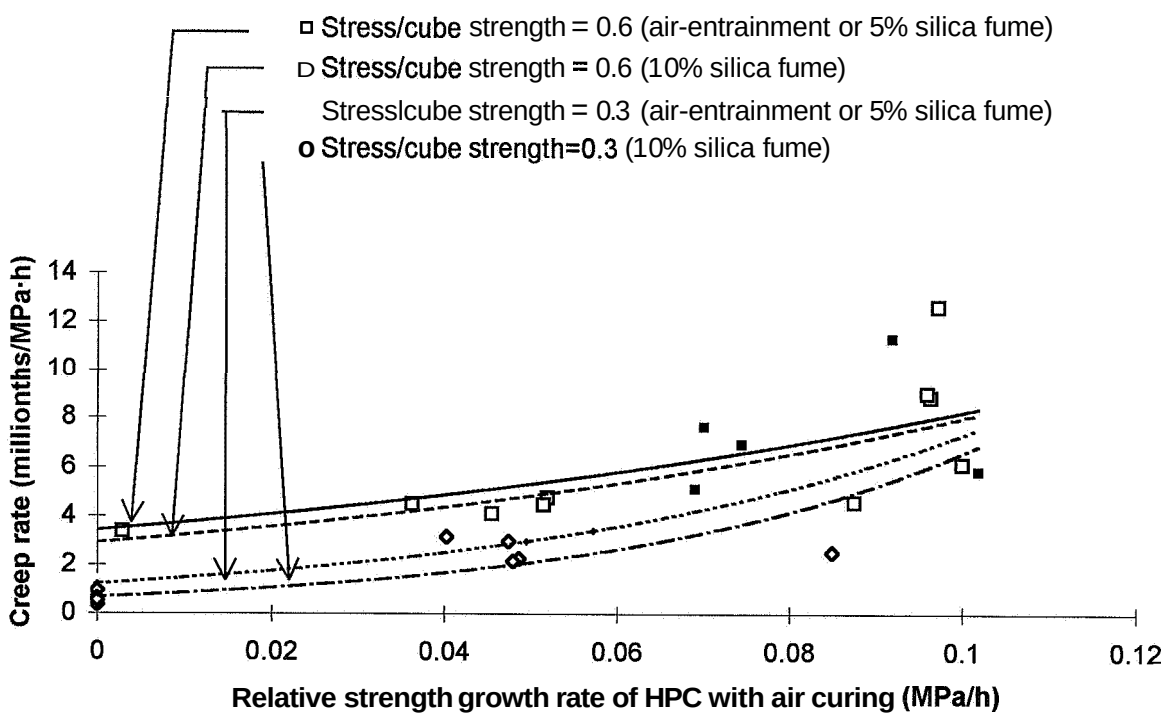

Figure 9.7 - Rate of creep versus the rate of strength growth with drying specimen.

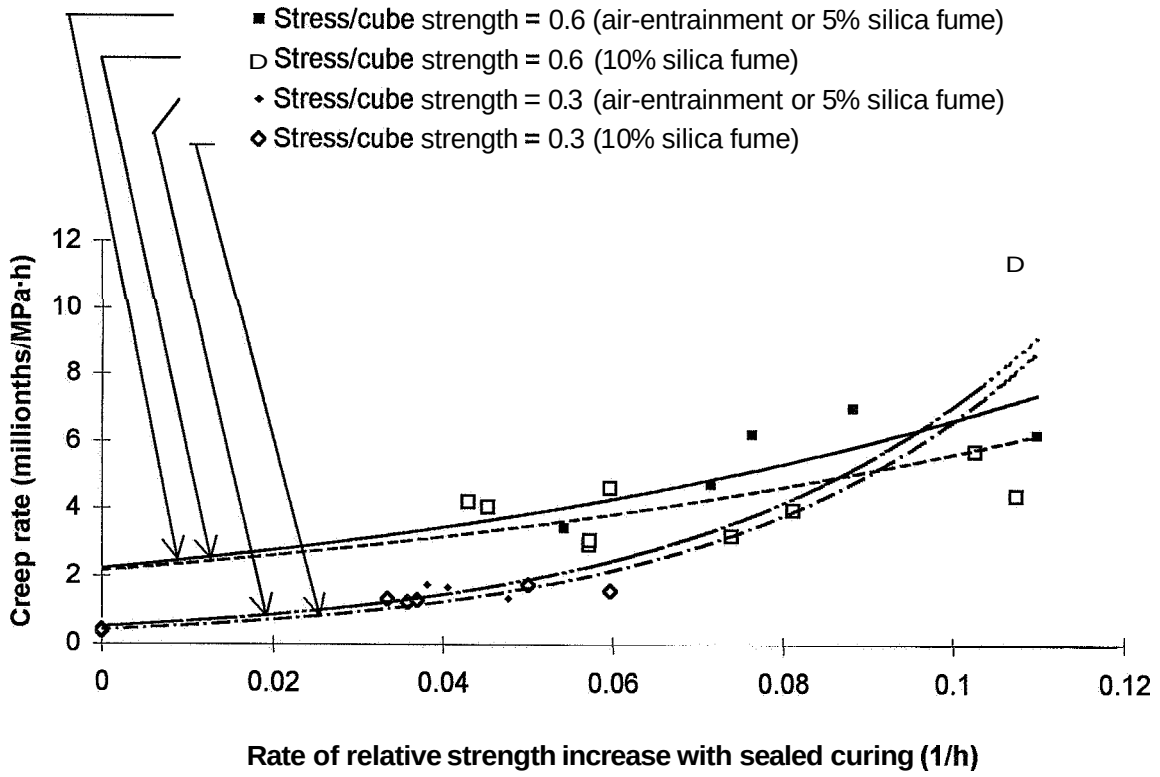

Figure 9.8 - Rate of creep versus the rate of strength growth with sealed specimen.

10. UNLOADING DEFORMATIONS AFTER SHORT-TERM LOADING

10.1 General

The short-term creep loading carried out for 66 h was immediately followed by studies of the deformations during unloading of the cylinder specimen. Studies of unloading took place in the MTS machine. From a practical point of view unloading deformations were of interest since these simulated the structural use of prestressed HPC. At first a prestressed structure obtains a high compressive stress in the zone of the prestressing tendons. Later on, in bent structural use, the opposite side of the structure becomes compressed. The zone of HPC where the tendons are situated subsequently obtains a lower stress. In some cases it even obtains cracks since the tendons secure the structural stability. It was thus of interest to study the deformations connected to the reloading situation in the structure, which was simulated by creep studies of HPC in the MTS machine. Both deformations immediately connected to the unloading and also any deformations following the unloading were interesting to study. The unloading tests also gave information about the modulus of elasticity, **Figure 1.1,** and deformation transversal to the cylinder.

10.2 Experimental

Specimen:

The same conditions applied as in Section 6 above. The drying specimen was placed in an insulated box in the MTS machine connected to a climate chamber, **Figure** 6.1 **and** 6.2. The testing room was air-conditioned to avoid displacements due to temperature movements when the specimen was transported before and after the tests in the MTS machine. Two cylinders were studied during repeated loading and unloading to verify the testing routine. Cylinder specimens as described in Section 6 were also used in the unloading experiments. Materials, preparation of specimen and chronology are given in Section 4 above and the HPC compositions are given in **Table** 5.1. The general layout is given in the Section 3.3 above. The hydraulic conditions in the MTS machine, i.e. the size of the pipes and the servo controlled accumulator, required an unloading period of about 1 s. Unloading procedure was thus not quasi-instantaneous like the loading described above.

Measurements:

The measurement was carried out in an MTS machine at four points outside the specimen by displacement and gauging transducers (LVDT). The measurement points were firmly connected to the steel cast-in items in the specimen by pin bolts of 3-mm diameter. The length between the longitudinal measurement points was 250 mm and between the transversal points 55.5 mm.

Repeated loading and unloading:

After a time of recovery, two specimens of concrete types 2 and 7 were utilised for repeated quasi-instantaneous loading and unloading with 3 minutes interval.

10.3 Results

Figure 10.1 shows a typical unloading deformation versus time. **Figure 10.2** shows the compliance of mature HPC versus time. **Appendix 10** provides the results of the resisting HPCs at unloading and results of repeated loading of mixes 2 and 7. The decrease of compliance of unloading is given in **Table 10.1** (millionths/MPa).

Table 10.1. Decline of compliance after 1 s of unloading (millionths/MPa)

Concrete/age	01	02	03	28	09	10	199	200
1	32.7	31.82	34.36	29.21	-	-	-	-
2	29.4	28.5	30.56	28.3	30.31	30.72	-	-
3	30.1	33.5	31.52	31.23	-	-	-	-
4	27.7	26.7	26.95	26.48	-	-	-	-
5	26.87	27.32	34.38	27.09	-	-	-	-
6	29	24.7	26.4	24.59	-	-	-	-
7	25.5	22.83	24.59	22.81	-	-	20.76	21.04
8	26.9	20.31	26.4	23.97	-	-	-	-

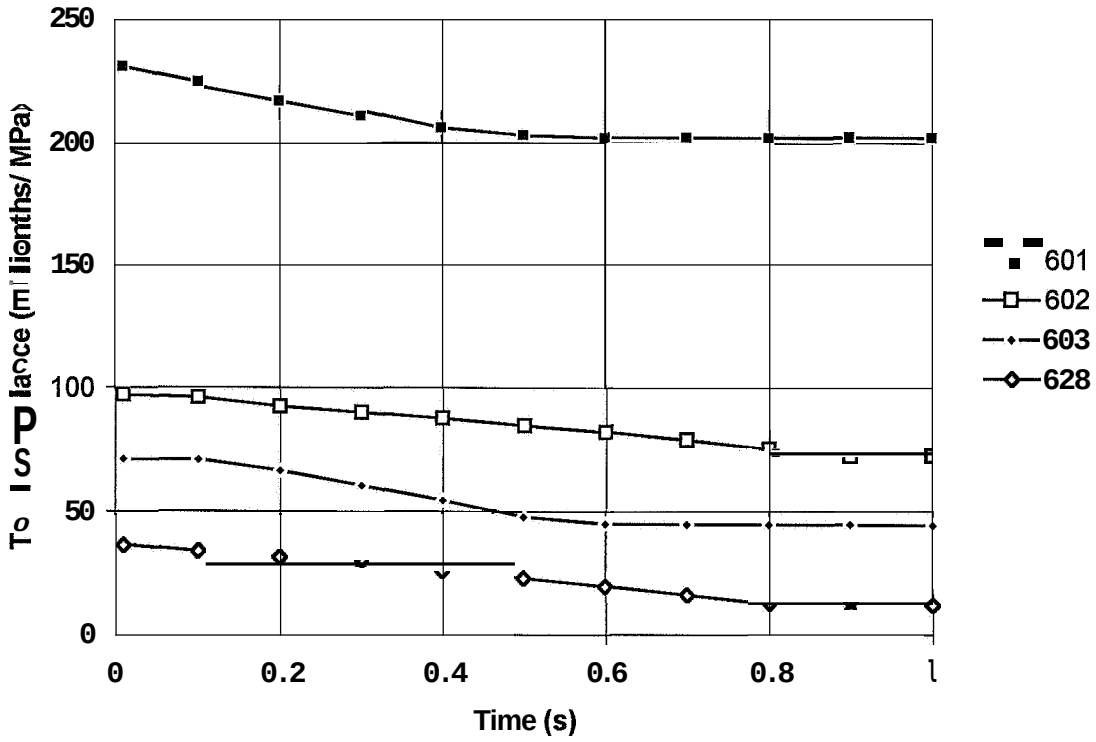

Figure 10.1 - Unloading deformation of mix 6 versus time.

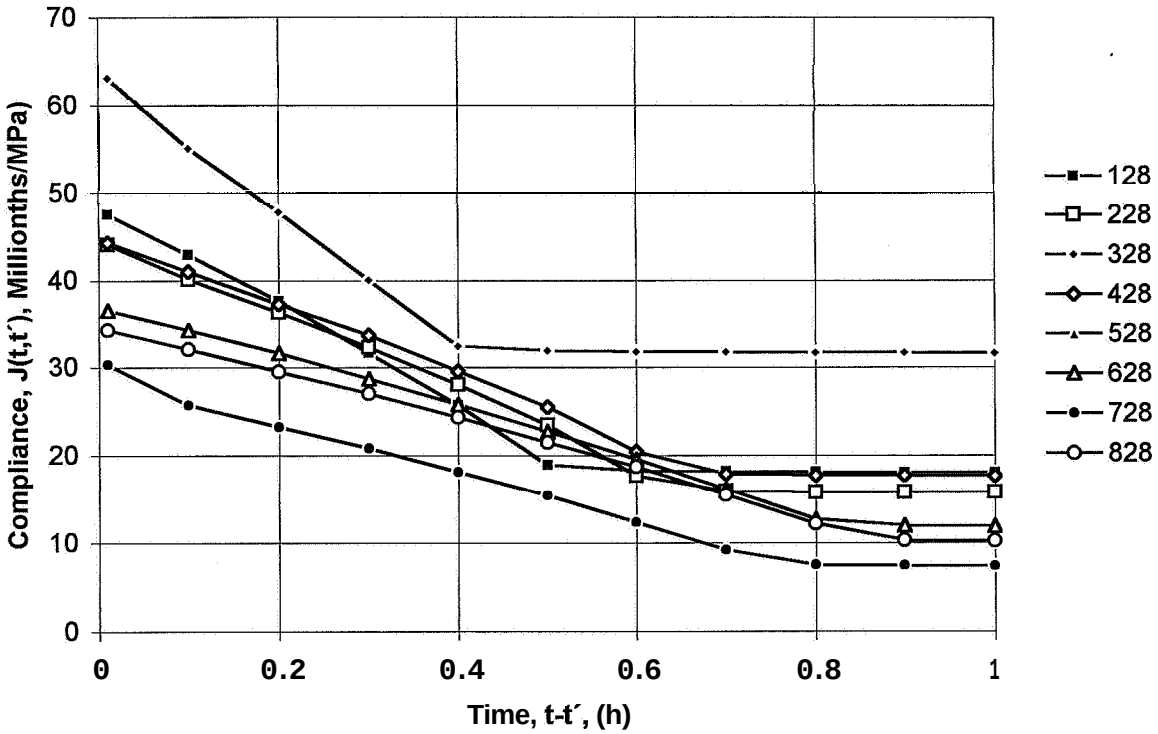

Figure 10.2 - Compliance at unloading of all mature HPCs versus time.

10.4 Sources of error and accuracy

The most essential sources of error were:

- Level of loading
- Deformation errors of the LVDTs
- Effects of lateral strain
- Recovery deformations during unloading due to the MTS machine.

Loading:

The loading was kept within 0.01 kN, i.e. within a stress variation of ± 0.004 MPa.

Deformations of the LVDTs:

The results with identical conditions coincided perfectly. The calibrations were performed to obtain an accuracy of ± 0.002 mm. After differentiation the maximum relative fault, $\delta J(t,t')/J(t,t')$, was obtained according to [$\delta \ln J(t,t')/\delta J(t,t')=1/J(t,t')$]:

$$\delta J(t, t')/J(t, t') = \delta\varepsilon/\varepsilon - \delta\sigma/\sigma \qquad (6.5)$$

At 10 MPa stress the maximum fault was calculated according to equation (6.5):

$\delta J(t,t')/J(t,t') = \delta\varepsilon/\varepsilon - \delta\sigma/\sigma = 0.00410.25 - 0.008/10 = 0.008 \approx 0.01$, thus very small.

Effect of lateral strain:

The effect of Poisson's ratio, u, will be shown in the analysis below. The reduction of compliance due to lateral strain would be decreased by a multiplication factor u^2.

Recovery deformations included in the unloading:

Owing to the hydraulics of the MTS machine, some of the recovery was included in the recorded deformation at unloading. However, the recovery was very slow. The unloading deformation was then defined within 1 s from the start of unloading, normally 0.1 s after the fast compliance rate at unloading changed into the slow deformation at recovery. The maximum compliance fault due to the slow unloading was estimated as 0.1 millionths/MPa.

10.5 Analyses

10.5.1 Elastic modulus of air-cured HPC

Figure 1.1 defines the elastic modulus (the inverted compliance at unloading, GPa):

$$E_{t'}=1000/\Delta J(t,t') \qquad (10.1)$$

$E_{t'}$ denotes the elastic modulus (GPa)
$\Delta J(t, t')$ denotes the difference in compliance at unloading (millionths/MPa)

Figure 10.3 shows the elastic modulus versus strength of mature HPC, which gives:

$$E_{Dma}=6.77\cdot(f_c)^{0.379} \qquad (10.2)$$

f_c denotes the compressive strength (MPa)
E_{Dma} denotes the elastic modulus of drying mature HPC (GPa)

Figure 10.3 shows the deformation modulus of mature HPC at different loading times, 0.01, 0.1 and 1 s as well. The deformation modulus of mature HPC at 0.01 s loading time coincided well with the elastic modulus at unloading. **Figure 10.3** also provides a comparison with the extension of the Model Code 90, MC 90, **Jaccoud and Leclercq (1995).** The MC 90 elastic modulus was about 1 GPa larger than the elastic modulus observed in the experimental, i.e. the difference compared with the experiments was small. The relationship of the elastic modulus and the compressive strength was clearly dependent on the maturity of the concrete when it was loaded. When a particular HPC was studied, the elastic modulus even increased at lower strength. 'When young concrete was loaded, the transition zone between aggregate and cement paste did not act particularly well. The majority of the compressive

strain of concrete at early ages was restrained by the cement paste, which caused viscous and plastic creep, **Figure 1.1.** Later on, during the ongoing hydration of the concrete, the quality of the transition zone was improved. At unloading the deformation was restrained by the aggregate. As a result of this restrain the elastic modulus increased for a particular concrete even at lower strength. The growth of the modulus confirmed the restraining effect of the aggregate dependent on the maturity of the concrete. The aggregate evidently acted as a reinforcement of the concrete during unloading at early ages. The tension of the aggregate in the concrete at the unloading of concrete that was loaded at an early age, may create a risk of cracking in the aggregate. The restraining effect of the aggregate in the concrete also caused a permanent deformation of, for example, prestressed structures. Even if the concrete was unloaded from stress, the deformation remained permanent due to maturity of the concrete when the concrete was prestressed. **Figure 10.4** shows the additional relative elastic modulus at unloading of young concrete versus the growth of strength from loading until unloading, Δf_c, compared to the 28-day strength, f_{c28}. From **Figure 10.4** the following correlation was obtained:

$$(E_{Dyo}/E_{Dma})=0.88+0.41\cdot(\sigma/f_c)+[0.38-0.81\cdot(\sigma/f_c)]\cdot(\Delta f_c/f_{c28}) \qquad (10.3)$$

E_{Dma} denotes the modulus of mature drying concrete (GPa)
E_{Dyo} denotes the elastic modulus of young drying concrete (GPa)

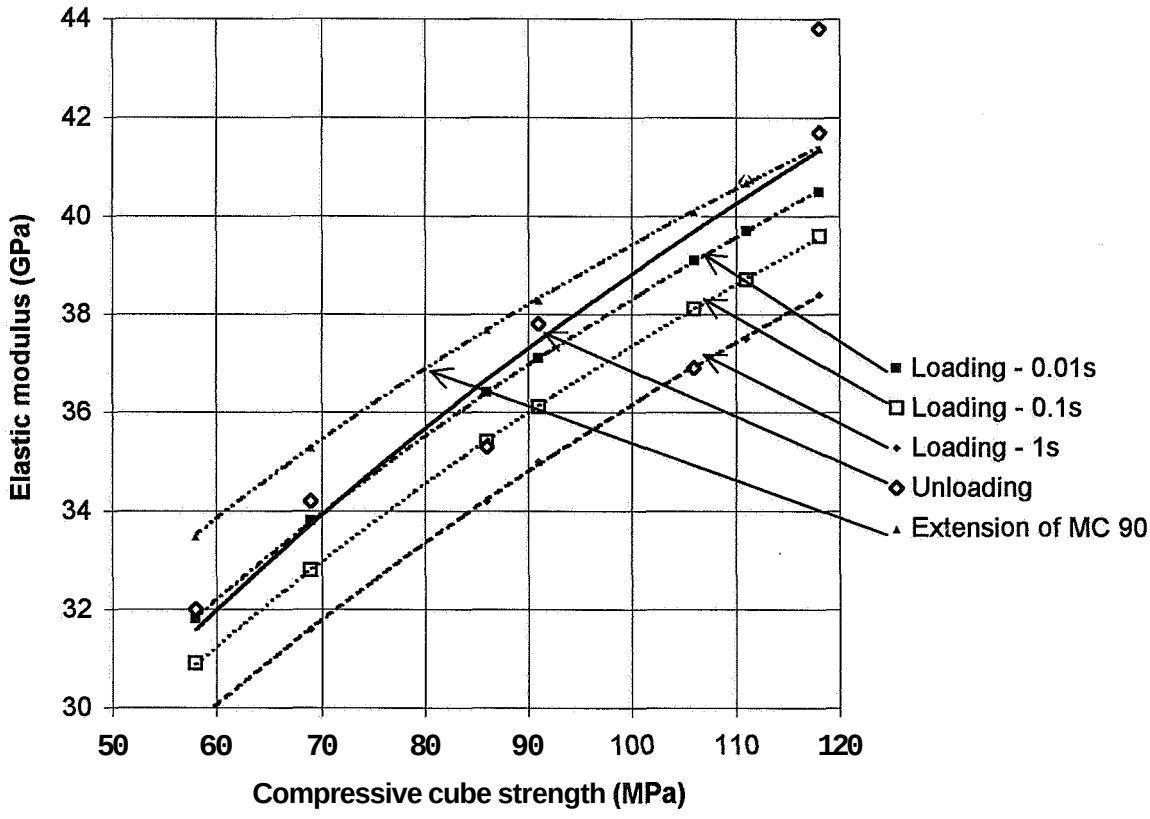

Figure 10.3 - The elastic modulus of mature concrete versus compressive strength.

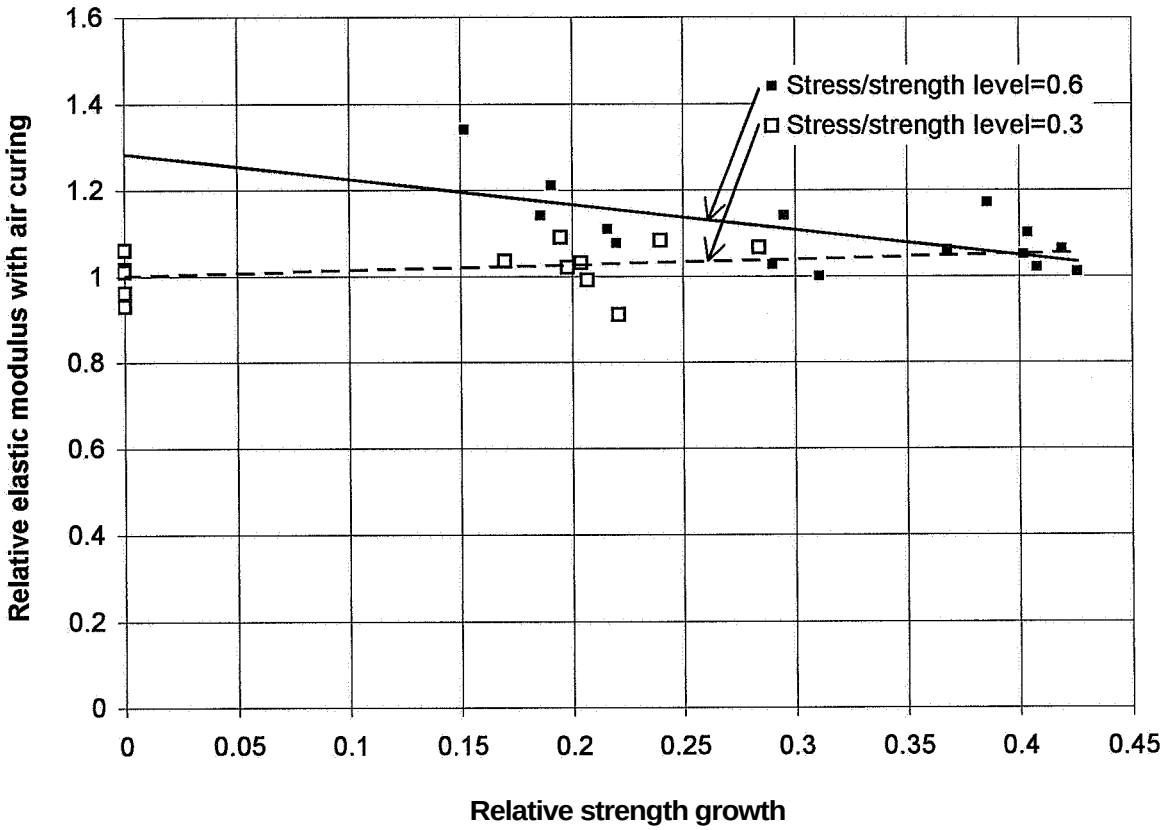

Figure 10.4 - Relative elastic modulus versus relative strength growth (increase of strength between loading and unloading compared with 28-day strength).

10.5.2 Comparison between elastic modulus with air and sealed curing

An identical procedure of unloading was used for studies of sealed specimens, Persson **(1995A)**, Appendix 10 (sealed curing). Figure 10.5 shows the elastic modulus at unloading. Figure 10.5 also shows the deformation modulus at 0.01, 0.1 and 1 s of loading. Like Figure 10.3, Figure 10.5 shows that the deformation modulus coincided well with the elastic modulus at 0.01 s loading time (the difference was less than 1 GPa). Figure 10.5 also indicates that the elastic modulus of mature HPC with sealed curing was substantially larger than the elastic modulus of drying HPC. Partly empty pores in drying HPC were more compressible, i.e. a lower elastic modulus was obtained during drying conditions. A comparison with the extension of Model Code 90, MC 90, Jaccoud and Leclercq **(1995)**, shows that all the results of the elastic modulus were larger with sealed curing than with air curing. The elastic modulus of sealed mature HPC (when measured within 1 s) was correlated in the following equation:

$$E_{Bma}=4.71\cdot(f_c)^{0.48} \qquad (10.4)$$

f_c denotes the compressive strength (MPa)
E_{Bma} denotes the elastic modulus at unloading of sealed mature HPC (GPa)

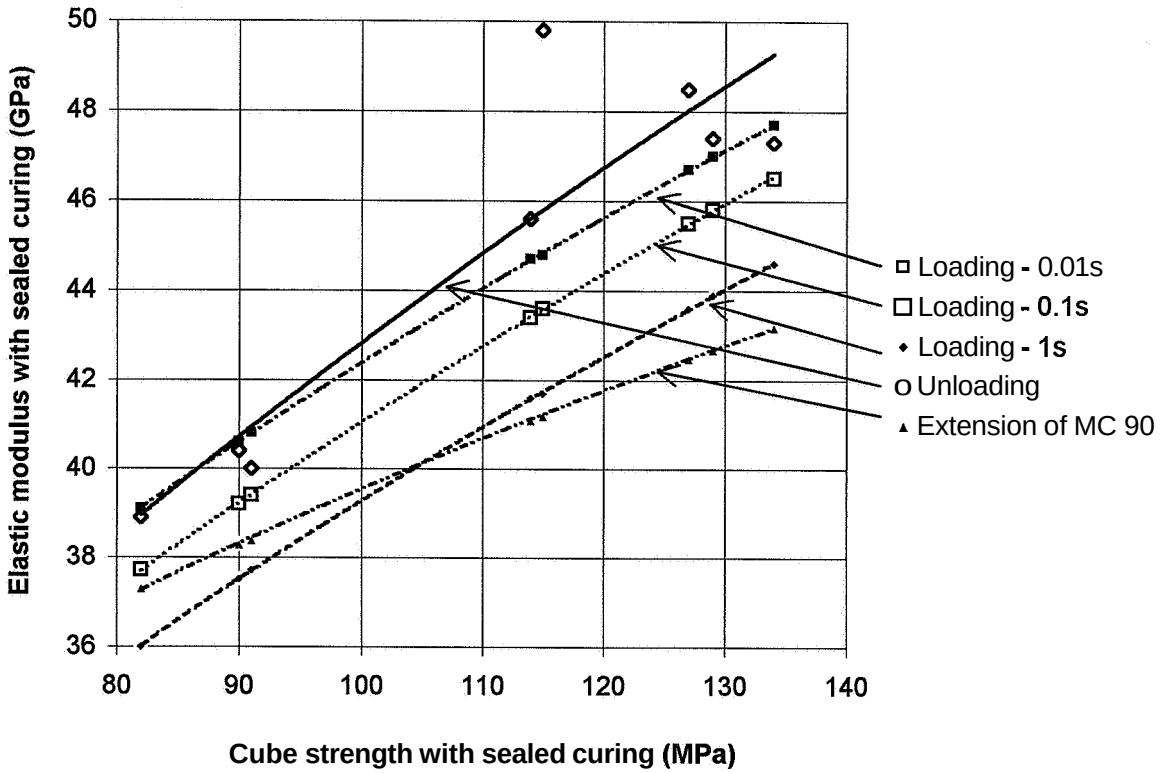

Figure 10.5 - The elastic modulus of sealed mature HPC versus the strength.

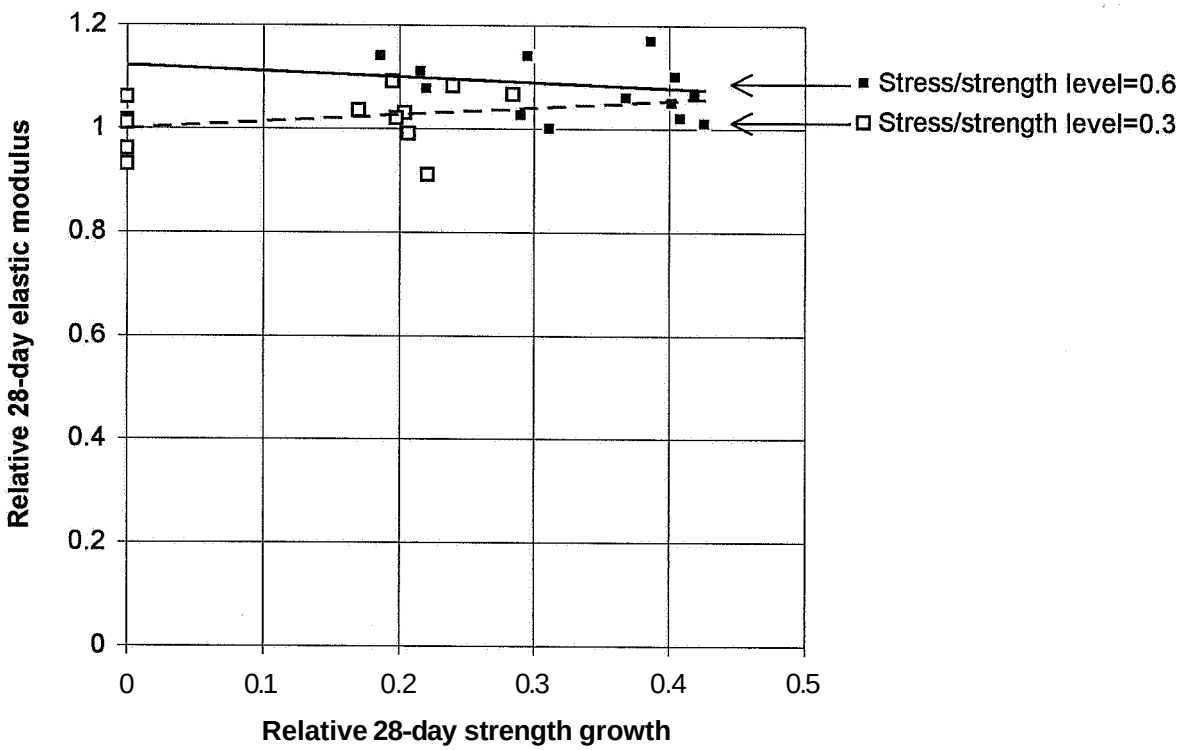

Figure 10.6 – Relative elastic modulus of sealed HPC vs. relative strength growth.

For sealed concrete, young when loading, a larger elastic modulus was obtained given a constant strength, **Figure** 10.6. The following correlation was obtained:

$$(E_{Byo}/E_{Bma}) = 0.87+0.4\cdot(\sigma/f_c)+[0.14-0.21\cdot(\sigma/f_c)]\cdot(\Delta f_c/f_{c28}) \qquad (10.5)$$

f_c denotes the strength at loading (MPa)
f_{c28} denotes the 28-day strength of HPC (MPa)
E_{Bma} denotes the modulus of sealed concrete mature when loading (GPa)
E_{Byo} denotes the elastic modulus of sealed concrete young when loading (GPa)
Δf_c denotes the strength growth between loading and unloading of HPC (MPa)
σ denotes the stress of HPC (MPa)

10.5.5 Effect of moisture on elastic deformations

The internal relative **humidity**, 0 , of the HPC in the creep tests was studied on drying cylinders, **Figure** 5.24 and **Appendix** 5 or on sealed cubes, **Persson (1995A)**, **Appendix** 10. The inverted compliance either 0.01 s after loading or 1 s after unloading was used as the elastic modulus, $E(f_c,Ø)$. From **Figure** 10.7, which shows results of about 130 tests, the following equation was obtained (GPa):

$$E(f_c,Ø)=10.3\cdot(1.45-Ø)\cdot(f_c)^{0.433\cdot(Ø+0.12)} \qquad (10.6)$$

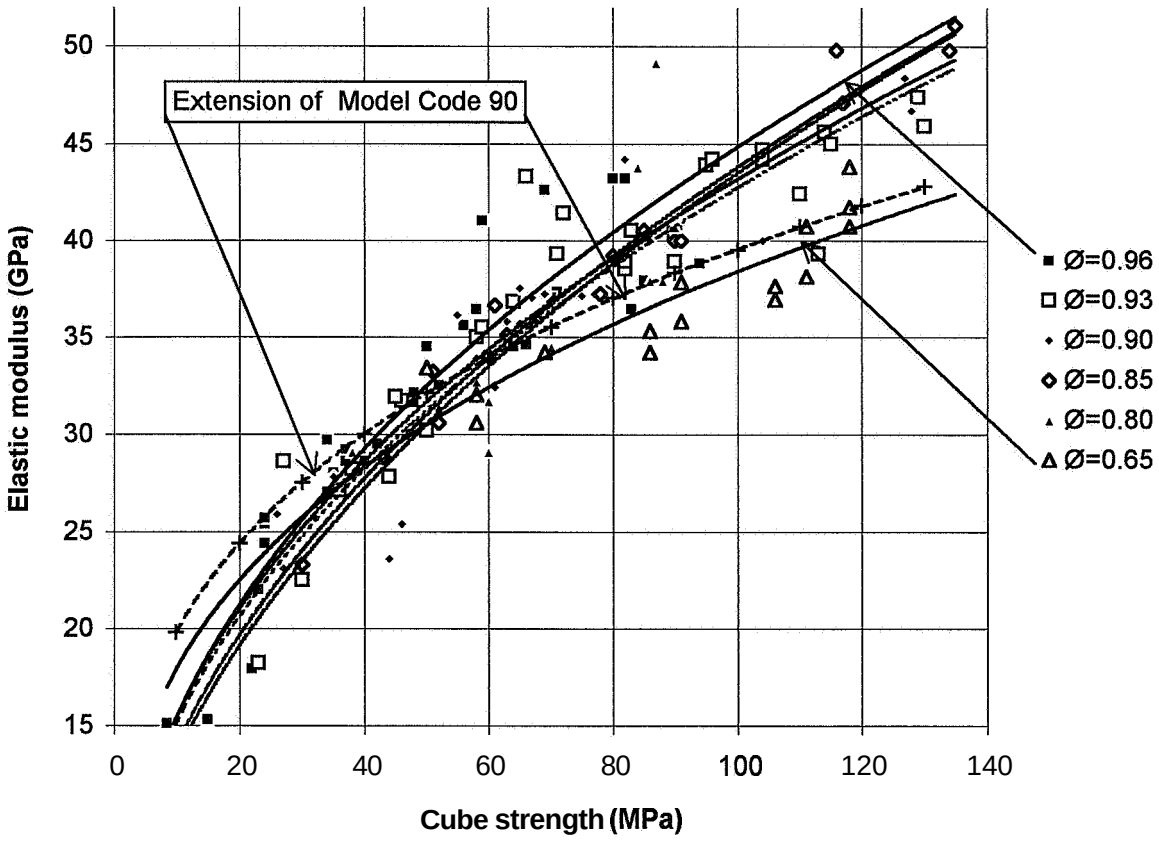

Figure 10.7 - Elastic modulus versus the strength. O = internal relative humidity.

10.6 Summary and conclusions

Several tests of the unloading deformations of HPC were performed, half of them on sealed concrete. The following conclusions were drawn:

- The experimental modulus of elasticity at unloading of air-cured mature HPC coincided well with the extension of Model Code 90.
- The experimental modulus of elasticity at unloading of air-cured mature HPC was about 10% smaller than with sealed HPC probably due to the larger mobility of the water in a drying structure.
- The experimental modulus of elasticity at unloading of HPC coincided well with the deformation modulus at loading of HPC given a loading time of 0.01 s.
- An HPC that was loaded young obtained a larger elastic modulus when unloaded than a mature HPC due to the ongoing hydration, with the strength held constant.
- The measured modulus of elasticity was related to the internal relative humidity by parallel tests on fragments of HPC.

1 POISSON'S RATIO AT SHORT-TERM LOADING

1 1 . General and previous studies of the Poisson's ratio on HPC

The lateral strain affected compliance during a creep test by an increase of u^2 where

$$\upsilon = \frac{\varepsilon_{lat}}{\varepsilon_{ax}} \qquad (11.1)$$

υ denotes Poisson's ratio
ε_{ax} denotes the axial deformation of the specimen
ε_{lat} denotes the lateral strain of the specimen during the creep test

Besides the compliance, the lateral strain also affected the size of the deformation modulus and the elastic modulus. Taking Poisson's ratio into account, these moduli will be reduced by u^2. For NSC Poisson's ratio, υ, was adopted to be around 0.18; the effect was then around **3%. Brooks (1993), Brooks and Hynes (1993)** calculated the Poisson's ratio for Compresit, formally known as Compact Reinforced Composite, CRC, **Bache (1987).** The calculations were based on experiments on plain HPC with a compressive strength (prisms 50 x 50 x 100 mm) of 159 MPa (elastic modulus: 58 GPa) and on fibre-reinforced (17% by mass) CRC with a compressive strength of 195 MPa (Young's modulus: 62 GPa). The w/c of the concrete was 0.22 (water-binder ratio = 0.18). The silica fume content was 24% calculated on the basis of the cement content. Poisson's ratio, υ= 0.19 for the plain concrete and υ= 0.22 for reinforced concrete was calculated. However, the elastic modulus of HPC in this study was smaller than the elastic modulus of CRC.

11.2 Experimental results

The lateral strains as well as the axial strain were studied during the 66 h short-term creep tests, Sections 6 and 10 above. The lateral strain was observed at one point of the specimen. The axial strain was studied on 3 sides of the specimen. Data on the strain were collected rapidly during the loading and at the unloading procedure. Data were collected over the first 2 seconds to obtain the Poisson's ratio. The lateral strain was also observed during the unloading of the short-term testing. Two Poisson's ratios, υ, were obtained for each concrete quality and each age, **Table 5.1,** one at loading and one at unloading after 66 h of creep. Normally the measured value of υ stabilised within 0.4 s at loading and 0.7 s from unloading, **Persson (1995A)**. However, to avoid dynamic effects on the u, the calculation of υ was performed for measurements at 1.5 s after loading and 1.8 s after unloading (the time of collected data being limited). Influence on υ of the type of silica fume or aggregate was observed. **Figure 11.1** shows Poisson's ratio at loading and unloading of drying HPC versus relative 28-day strength at loading and unloading.

11.3 Sources of error and accuracy

The main sources of error were:

- Deformation errors of the LVDTs
- Secondary effects of eccentricity of loading
- Temperature movements

Deformation errors of the LVDTs:

The calibration was performed to obtain an accuracy of ± 0.002 mm. However, the measurement accuracy of the LVDTs was within a displacement of ± 0.0005 mm. Poisson's ratio was evaluated according to equation (11.1). The logarithm was:

$$\ln \upsilon = \ln \varepsilon_{lat} - \ln \varepsilon_{ax} \qquad (11.2)$$

After differentiation the maximum relative fault, $\delta\upsilon/\upsilon$, was obtained ($\delta \ln\upsilon/\delta\upsilon=1/\upsilon$):

$$\delta\upsilon/\upsilon = \delta\, \varepsilon_{lat}/\varepsilon_{lat} - \delta\, \varepsilon_{ax}/\varepsilon_{ax} \qquad (11.3)$$

For a young concrete (type 3) the following relative fault, $\delta\upsilon/\upsilon$, was obtained: $\delta\upsilon/\upsilon = 0.0005/0.0030 - 0.000510.8315 = 0.1666 - 0.0006 \approx 0.17$, which was a fairly large relative fault. For a mature concrete (type 1) the following relative fault, $\delta\upsilon/\upsilon$, was obtained: $\delta\upsilon/\upsilon = 0.0005/0.0047 - 0.000510.4709 = 0.1065 - 0.0010 \approx 0.11$ which also was a fairly large relative fault. The reason for the large fault may be the small measured distance: 55.5 mm only. The calculated accuracy being low, the real accuracy was studied by means of 48 supplementary experiments on mature concrete, **Table** 5.1. **Table 11.1** gives the concrete properties of the study on long-term Poisson's ratio. **Figure** 11.2 shows the obtained long-term Poisson's ratio. The coefficient of variation was small, **Figure** 11.3, normally less than 0.04. The effect of type of silica fume or aggregate on Poisson's ratio was confirmed.

Table 11.1 - Properties of HPC of the study on long-term Poisson's ratio.

HPC mix	Age (days)	Stress, σ (MPa)	Strength, f_c (MPa)	f_c at 28 days' age, f_{c28} (MPa)	σ/f_c	f_c/f_{c28}
1	550	20.7	68	69	0.30	0.99
2	540	25.8	89	86	0.29	1.03
3	510	27	69	58	0.39	1.19
4	720	26.6	101	91	0.26	1.11
5	450	38.7	116	106	0.33	1.09
6	380	33.3	116	111	0.29	0.96
7	580	34.9	121	117	0.29	1.03
8	400	35.4	129	118	0.27	1.09

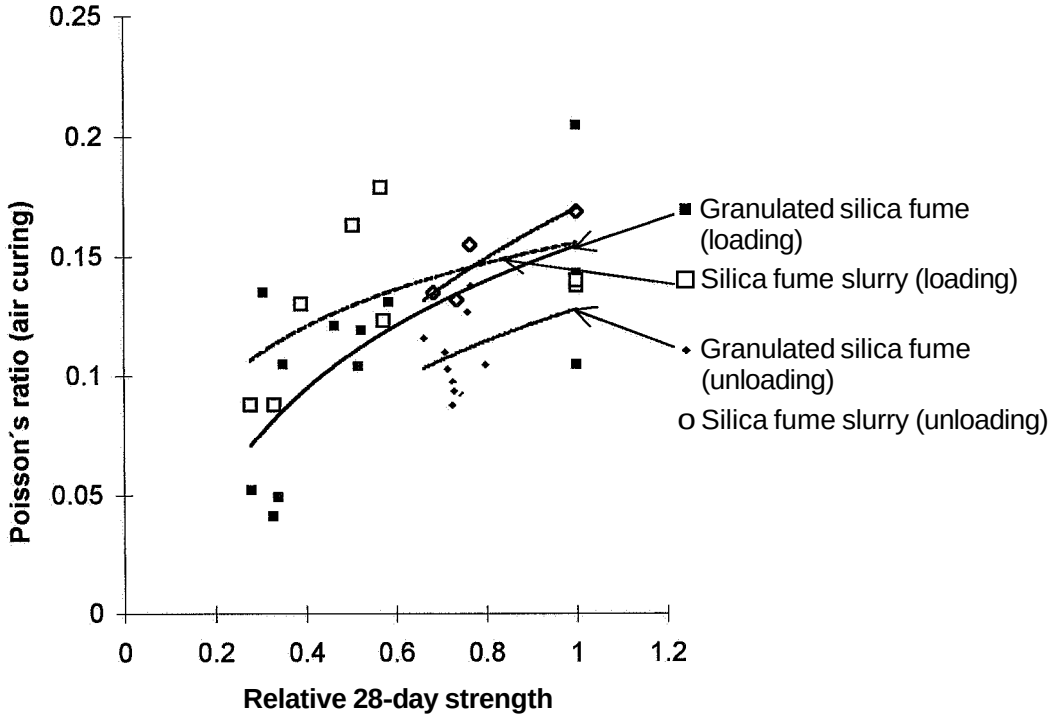

Figure 11.1 - Poisson's ratio of drying HPC versus the relative 28-day strength.

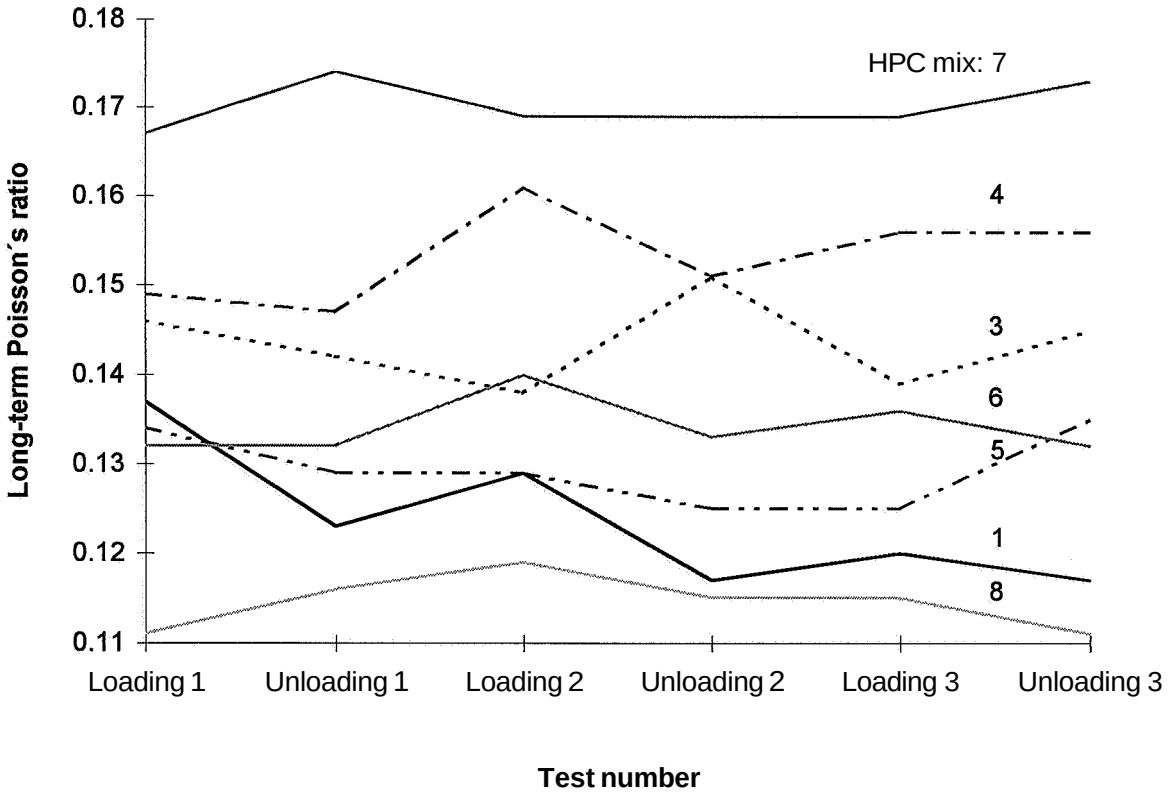

Figure 11.2 - Long-term Poisson's ratio. Type of HPC mix, **Tables 5.1 and 11.1**

Eccentricity at loading:

Eccentricity could not be avoided. Bending in the cylinder may also affect the lateral dimensions. The size of the effect of the bending could not be estimated since only one LVDT was utilised.

Temperature effects:

The measurement device was placed within the climate box in the MTS machine. However, to avoid any possible temperature effects on the measurement frame, only very short-term lateral displacements of the cylinder were calculated (within a 2 s period). It was possible also to study the incremental Poisson's ratio. Owing to possible effects of small alterations of the temperature, this possibility was not utilised.

11.4 Analysis

11.4.1 Drying concrete:

As shown in **Figure** 11.3, υ exhibited coefficients of variations generally less than 0.04, which is acceptable. From **Figure 11.1** a tendency of Poisson's ratio at loading or unloading of drying HPC, υ_D, was correlated to the maturity:

$$\upsilon_D = k_D \cdot [0.05 \cdot \ln(f_c/f_{c28}) + 0.13] \qquad \{0.2 < f_c/f_{c28} < 1\} \qquad (11.4)$$

f_c denotes the compressive strength of HPC at loading or unloading (MPa)
f_{c28} denotes the compressive strength of the concrete at 28 days (MPa)
ln denotes the natural logarithm
k_D =1.2 for HPC with silica fume slurry and granite (mix 4, 7), $k_D = 1$ otherwise
υ_D denotes Poisson's ratio at loading or unloading of drying HPC

11.4.2 Comparison with sealed concrete

Figure 11.4 shows results obtained from exactly the same type of experiments, **Persson (1995A), appendix 11 (sealed).** From **Figure 11.4** a tendency of Poisson's ratio at loading or unloading of sealed HPC, υ_B, was correlated to the maturity:

$$\upsilon_B = k_B \cdot [0.04 \cdot \ln(f_c/f_{c28}) + 0.14] \qquad \{0.2 < f_c/f_{c28} < 1\} \qquad (11.5)$$

f_c denotes the compressive strength of HPC at loading or unloading (MPa)
f_{c28} denotes the compressive strength of the concrete at 28 days (MPa)
ln denotes the natural logarithm
=1.4 for HPC with silica fume slurry and granite (mix 4, 7), $k_D = 1$ otherwise
υ_B denotes Poisson's ratio at loading or unloading of sealed HPC

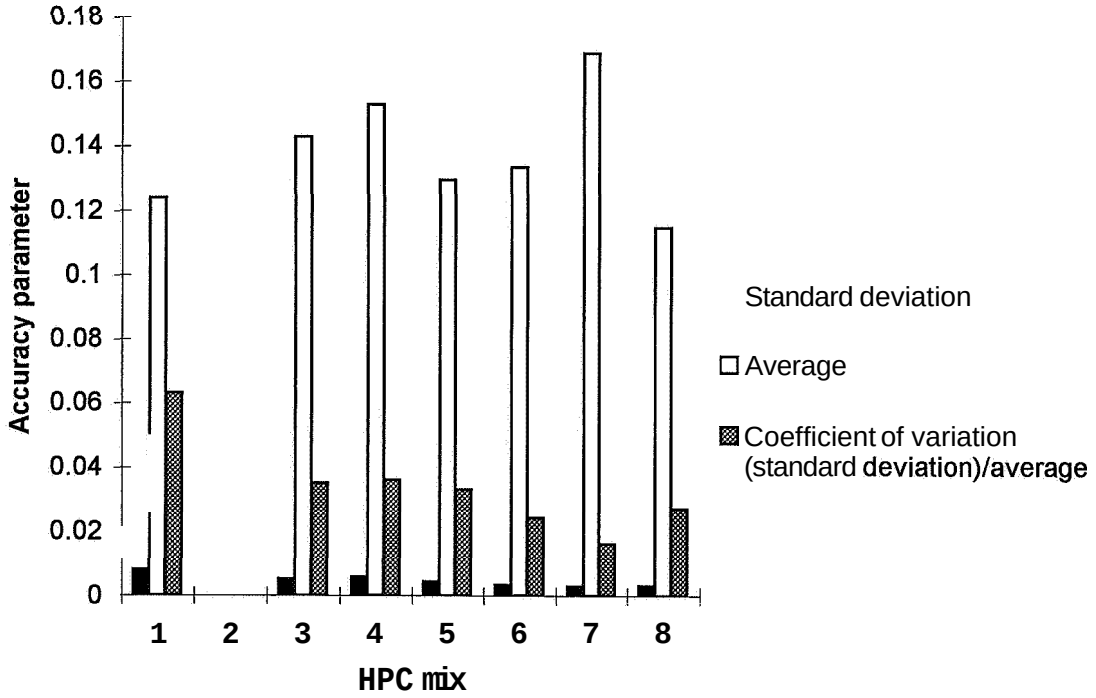

Figure 11.3- Standard deviation, average and variation coefficient of Poisson's ratio.

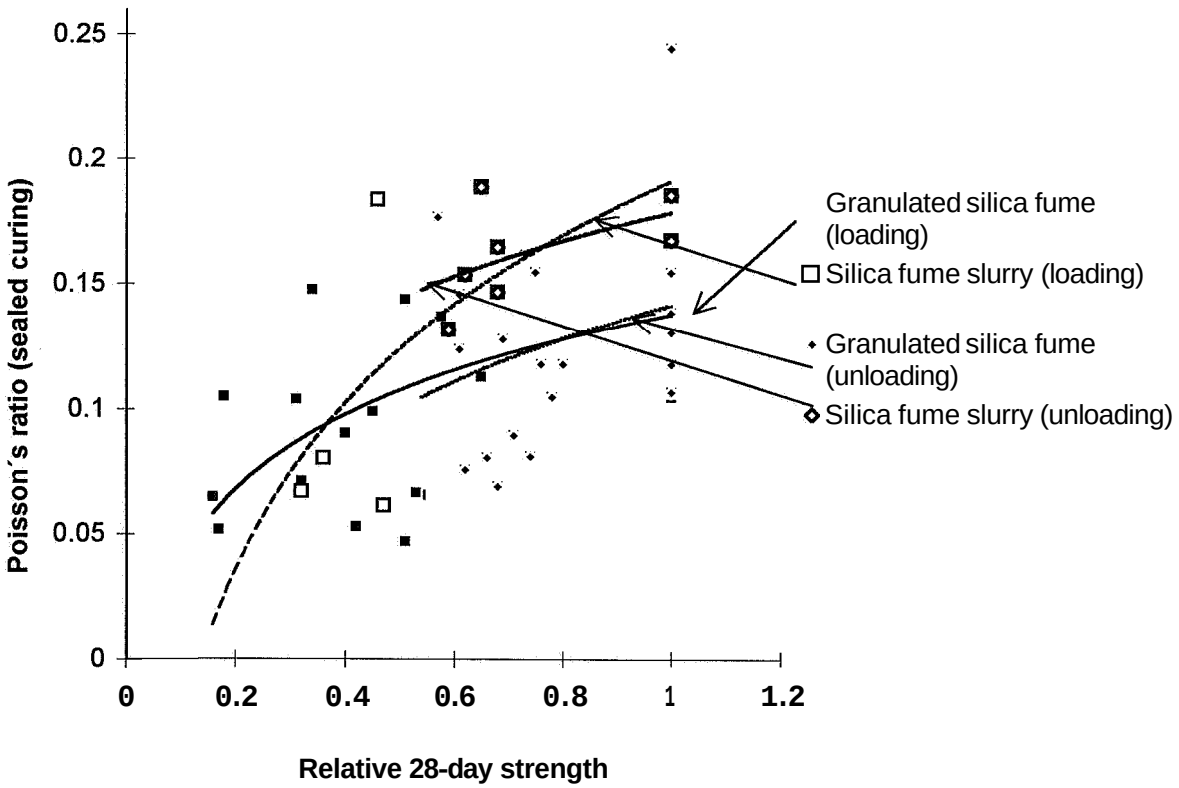

Figure 11.4 - Poisson's ratio of sealed HPC versus the relative 28-day strength.

11.4.3 Effect of moisture

As pointed out above, the obtained long-term υ was about 30% larger for HPC of mix 4 or 7 than for other HPCs, both for young HPC and for mature HPC. One reason for this observation may be the silica fume slurry in HPC mix 4 and 7, which initially caused a more rapid strength development of HPC than the granulated silica fume did, **Persson (1995A), Appendix 11 (sealed curing).** Another reason for the rise of υ may be the type of aggregate (granite in concrete 7 and special gravel in both HPC mix 4 and 7). The internal relative humidity, 0 , was studied on parallel specimens on each testing occasion. **Appendix 11** shows tendency curves of the effect of O on υ of young HPC versus the maturity. **Appendix l 1** shows υ of mature HPC versus 0 . These results were astonishing since υ of NSC rose with the humidity. The results may be related to the self-desiccation of HPC. Finally, tendency curves of υ versus strength of HPC are shown in **Appendix 11.** The tendency curves of υ were not correlated to the maturity, 0 , or to strength.

11.5 Summary and conclusions on studies of Poisson's ratio

A total of 178 tests of Poisson's ratio were carried out, of which 48 were on young HPC. Tests on young HPC exhibited low significance related to the maturity. One reason for the low significance was eccentricities at loading and unloading of the specimen. (The longitudinal strain was measured at three point but the tranversal only at one.) **Daerga and Elfgren (1991)** have shown that eccentricities often occur in HPC both during compression and tension. The tests on young HPC were supplemented by further loading and unloading tests on mature HPC. This study showed a coefficient of variation < 0.04, which was acceptable. The following conclusions were drawn:

- Poisson's ratio, υ, was found to be around u = 0.13 for mature drying HPC with quartzite sandstone and granulated silica fume. υ of a sealed mature HPC was about 0.01 larger.
- Poisson's ratio, υ, was found to be around υ = 0.16 for mature HPC with granite and silica fume slurry.
- About 50 supplementary tests confirmed these results of Poisson's ratio, υ, related to mature HPC.
- Poisson's ratio, υ, of young HPC exhibited low significance related to the maturity of HPC.
- At a current strength of half the 28-day strength, Poisson's ratio, u, became about 0.03 smaller than as mentioned above, i.e. υ = 0.10 (granulated slice fume slurry) and υ = 0.13 (silica fume slurry).
- Poisson's ratio, υ, of sealed young HPC was found to be about 0.03 smaller than Poisson's ratio, υ, of HPC with air curing.

12. MODULI OF ELASTICITY

12.1 General and previous research

A non-destructive testing method of the elastic modulus was of great interest for the purpose of studying damage in the concrete that was related to possible interior detriment due to, for example, freezing. The dynamic modulus of elasticity, E_{dyn}, of HPC was detected by the fundamental transverse frequency. A vibration was applied to the centre of the HPC specimen and the fundamental transverse frequency obtained at one end of the specimen. The evaluation of E_{dyn} was dependent on the weight, the shape of the specimen, the internal relative humidity and on Poisson's ratio. Xu **(1992)** studied the dynamic modulus of elasticity, E_{dyn}, on prisms of cement mortar stored at different ambient relative humidity and supposed to be equal to the internal relative humidity, **O.** A large dependence of **O** on E_{dyn} was found to exist, **Figure 12.1.** Between $\emptyset = 0.40$ and $\emptyset = 0.95$ E_{dyn} rose from 30 to around 36 GPa, i.e. ≈ 20%. It was the objective of the studies of dynamic modulus of elasticity to compare the results with the static modulus of elasticity (at unloading) and the deformation modulus obtained at loading of the HPC specimens. It was also the aim of the studies to correlate the influence of maturity and moisture on the measured dynamic modulus of elasticity.

12.2 Experimental

Right before the quasi-instantaneous testing of the deformation and elastic modulus of drying HPC in the MTS machine, the same specimen was tested related to E_{dyn}. Supplementary tests were also performed. During these tests conditions according to Section 6 and **Table 11.1** applied. The following testing procedure was used:

- The centre of the sides of the specimen was marked perpendicular to the direction of the cylinder specimen at curing. (Cylinder stored lying after casting developed air voids at the upper face.)
- The fundamental transverse frequency was detected by a pickup applied to the centre at one side of the concrete specimen.
- The driver (vibrator) was placed at one side of one end of the specimen.
- The weight and the shape of the specimen were measured.
- The internal relative humidity was measured on fragments from parallel specimens.
- The dynamic modulus was taken within ½ h of the quasi-instantaneous testing.
- Poisson's ratio was measured on the same specimen during the quasi-instantaneous testing.
- Repeated loading and unloading tests were performed with HPC according to **Table 11.1.**

The evaluation of E_{dyn} was carried out according to **ASTM** C **215-85:**

$$E_{dyn} = 0.00416 \cdot (L^3 \cdot T/d^4) \cdot W \cdot n^2 \qquad (12.1)$$

d denotes the diameter of the specimen (in.)
n denotes the fundamental transverse frequency (Hz)
E_{dyn} denotes the dynamic modulus of elasticity (GPa)
K ratio of gyration (=d/4 for cylinder)
L denotes the length (in.)
T =1.17 for υ=1/6 and K/L=0.046 [=55.5/(4·300]; T=1.17 for υ= 0.05; T=1.18 for υ= 0.25
W denotes the weight of the specimen (lb.)

Simplifications were done of equation (12.1):

$$E_{dyn} = 5.46 \cdot 10^{-6} \cdot G \cdot n^2 \qquad (12.2)$$

E_{dyn} denotes the dynamic modulus for a cylinder 300 mm long and 55.5 mm in diameter (GPa)
G denotes the weight (kg)
n denotes the fundamental transverse frequency (Hz)

12.3 Results

Table 12.1 shows results of the dynamic modulus of elasticity, E_{dyn}, for the different types of concrete, between 1 and 28 days' age. **Table 12.2** shows the internal relative humidity of fragments fiom parallel-tested cylinders. **Figures 12.2 and 12.3** show the compliance, σ/ε, at the first loading and first unloading of the cylinders respectively. **Appendix 12** shows the loading versus early loading time. **Appendix 12** also shows the compliance at loading and the compliance at unloading. **Table 12.3** shows the average deformation modulus, $D_{0.01}$, the elastic modulus, E_{stat}, at the repeated tests of mature HPC and E_{dyn} of the mature HPCs before the tests. The accuracy of the tests was evaluated and is stated.

Table 12.1 - Estimated elastic dynamic modulus, equation (12.2), (GPa).

Concrete	01	02	03	28
1	27.9	-	-	35.1
2	-	35.2	32.4	36.9
3	30.4	-	33.4	33.8
4	-	-	-	-
5	36.1	36.6	38.5	38.4
6	30.7	41.0	37.7	42.2
7	-	-	-	-
8	35.2	40.9	39.6	42.6

Table 12.2 –Internal relative humidity in fragments of parallel cylinders.

Concrete	01	02	03	28
1	0.93	0.90	0.90	0.65
2	0.96	0.93	0.90	0.65
3	0.90	0.85	0.85	0.65
4	0.96	0.96	0.96	0.65
5	0.93	0.93	0.90	0.65
6	0.93	0.90	0.90	0.65
7	0.93	0.90	0.90	0.65
8	0.90	0.90	0.90	0.65

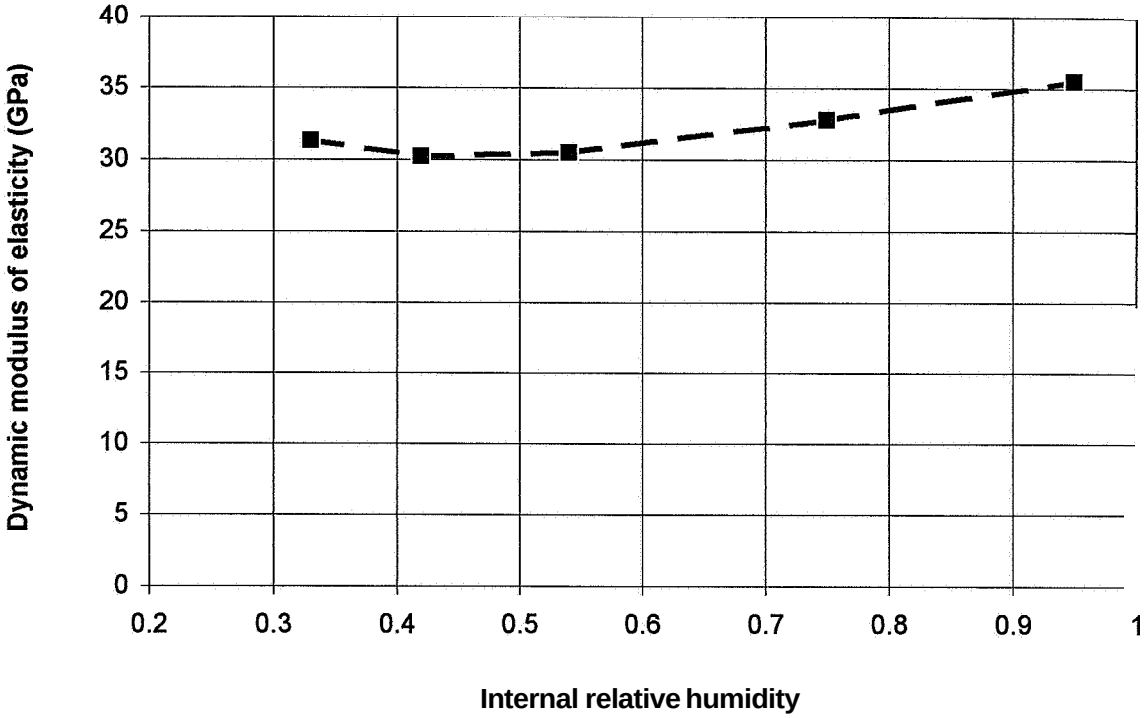

Figure 12.1 – Elastic dynamic modulus of cement mortar at different humidity, Xu (1992).

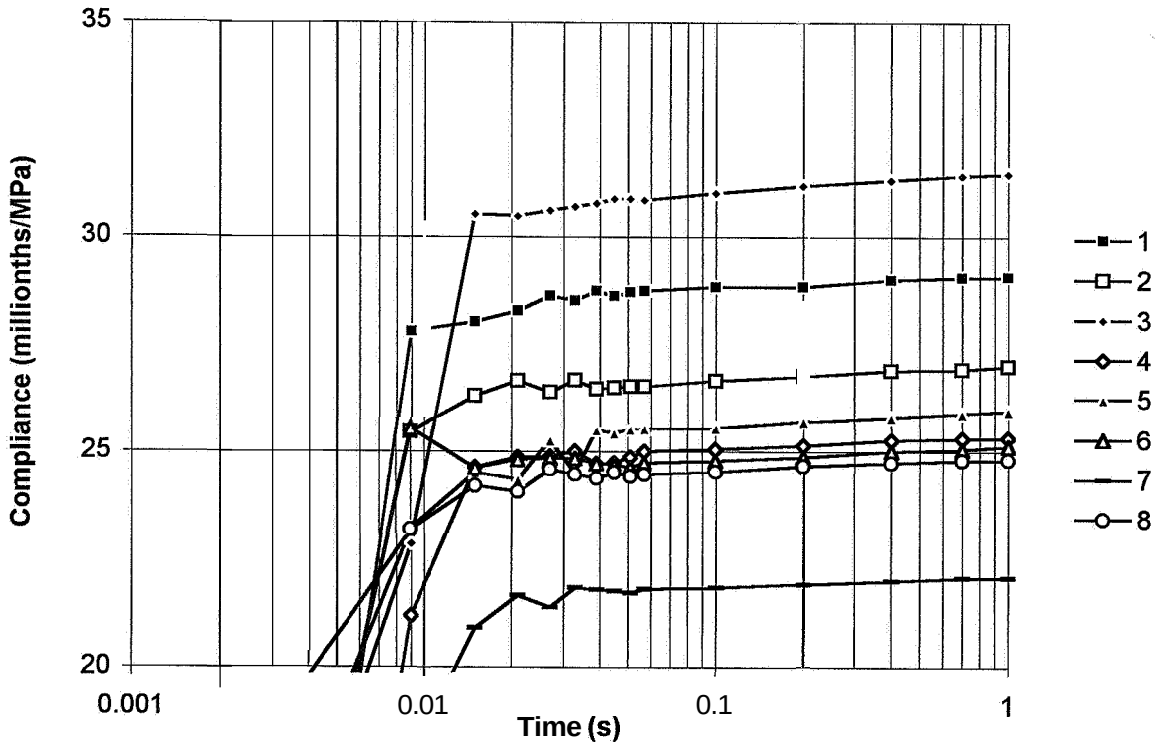

Figure 12.2 - Compliance at first loading versus loading time. HPC mix, **Table 5.1.**

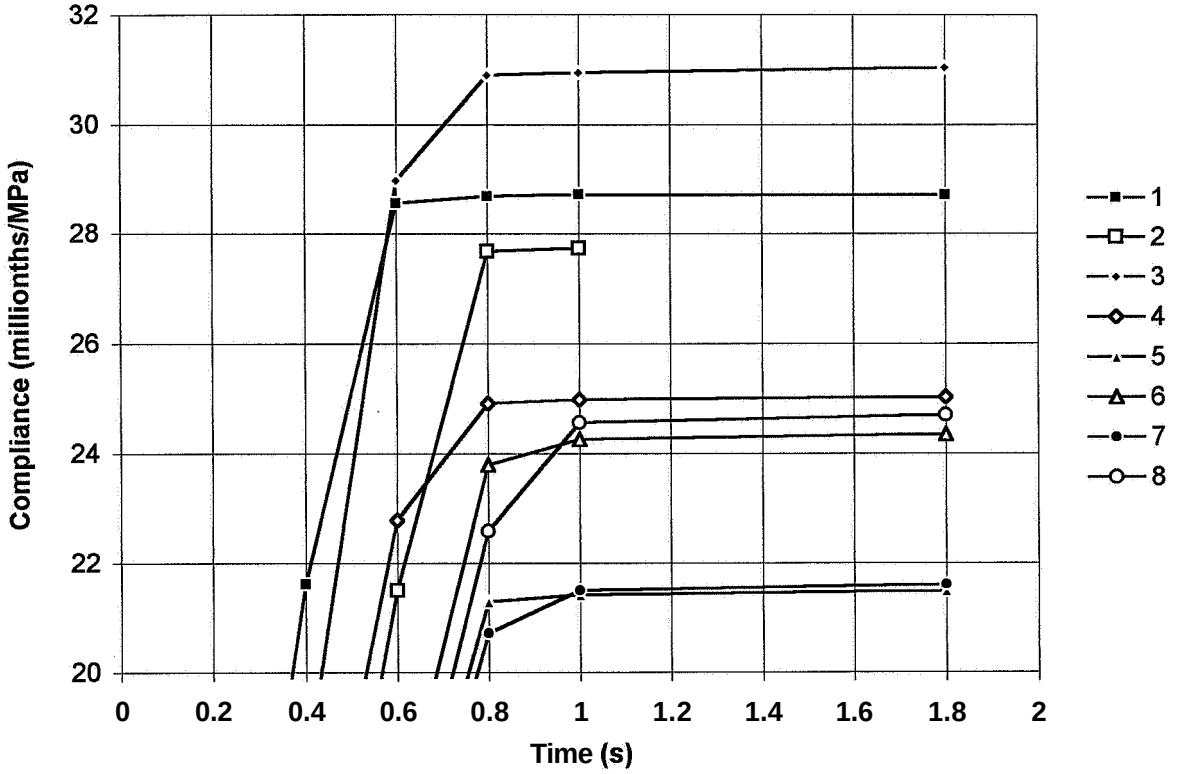

Figure 12.3 – Compliance at first unloading versus time. HPC mix, **Table 5.1.**

Table 12.3 - Deformation modulus, $D_{0.01}$, elastic modulus, E_{stat} and dynamic modulus of elasticity, E_{dyn}, after loadings and unloadings, testing accuracy (GPa).

Concrete	**128**	**228**	**328**	**428**	**528**	**628**	**728**	**828**
$D_{0.01}$ 0.01 s after loading	35.5	34.5	32.8	34.2	40.3	41.4	46.9	41.3
$D_{0.01}$, coefficient of variation	0.012	0.024	0.0035	0.01	0.0038	0.015	0.0075	0
E_{stat} 1 s after unloading	35.2	36.7	32.5	40.4	39.9	41.7	47.0	41.2
E_{stat}, coefficient of variation	0.013	0.014	0.012	0.011	0.012	0.0048	0.033	0.0061
Dynamic modulus, E_{dyn}	36.6	37	35.3	40.5	40.4	40.7	48.9	41.4

12.4 Sources of error and accuracy

The following sources of error were estimated:

- The pickup or the driver perhaps had a bad connection to the specimen.
- The weight was incorrect measured.
- The fundamental transverse frequency was incorrectly detected.
- Possible effect of varying internal relative humidity within the specimen.

Dynamic modulus of elasticity based on the fundamental transverse frequency:

The equipment used to obtain the fundamental transverse frequency was not calibrated. However, by the scale it was possible to obtain an accuracy of ± 10 Hz. The weighing was performed with an accuracy of ± 0.1g. The dynamic modulus of elasticity, E_{dyn}, was evaluated according to equation (12.1) above. The logarithm of equation (12.2) was evaluated:

$$\ln(E_{dyn}) = 5.46 \cdot 10^{-6} \cdot [\ln(G) \cdot + 2 \cdot \ln(n)] \qquad (12.3)$$

After differentiation the maximum relative fault, $\delta\upsilon/\upsilon$, was obtained ($\delta \ln\upsilon/\delta\upsilon = 1/\upsilon$):

$$\delta E_{dyn}/E_{dyn} = 6\ G/G + 2 \cdot \delta\ n/n \qquad (12.4)$$

For a young concrete (type 3) the following relative fault, $\delta E_{dyn}/E_{dyn}$, was obtained: $\delta E_{dyn}/E_{dyn} = 5.46 \cdot 10^{-6}\ (0.211770 + 2 \cdot 10/1780) = \approx 0.011$, which was a fairly small relative fault. For a mature concrete (type 1) the following relative fault, $\delta E_{dyn}/E_{dyn}$, was obtained: $\delta E_{dyn}/E_{dyn} = 0.211940 + 2 \cdot 10/1747 = 0.1065 - 0.0010 \approx 0.011$ (small).

Measurement of internal relative humidity:

The dew-point meters were calibrated according to **ASTM** E **104-85.** The same accuracy as with sealed concrete was obtained, i.e. ± 0.015, **Persson (1997C)**.

Measurement of the deformation modulus and the static modulus of elasticity:

The accuracy (coefficient of variation) was estimated in **Table 12.3.** The average coefficient of variation of the deformation modulus was 0.009 and the average coefficient of variation of the static modulus of elasticity was 0.013. These estimated faults were small.

12.5 Analyses

12.5.1 Deformation modulus, dynamic and static modulus of elasticity

Figure 12.4 shows the deformation modulus 0.01 s after loading, $D_{0.01}$, the dynamic modulus of elasticity, E_{dyn}, versus the elastic modulus at unloading, E_{stat} with the following correlations:

$$D_{0.01} = (1.04 - 8 \cdot 10^{-5} \cdot t) \cdot E_{stat} \qquad (12.5)$$

$$E_{dyn} = (1.04 - 4 \cdot 10^{-5} \cdot t) \cdot E_{stat} \qquad (12.6)$$

t denotes the age of the concrete (days, d)

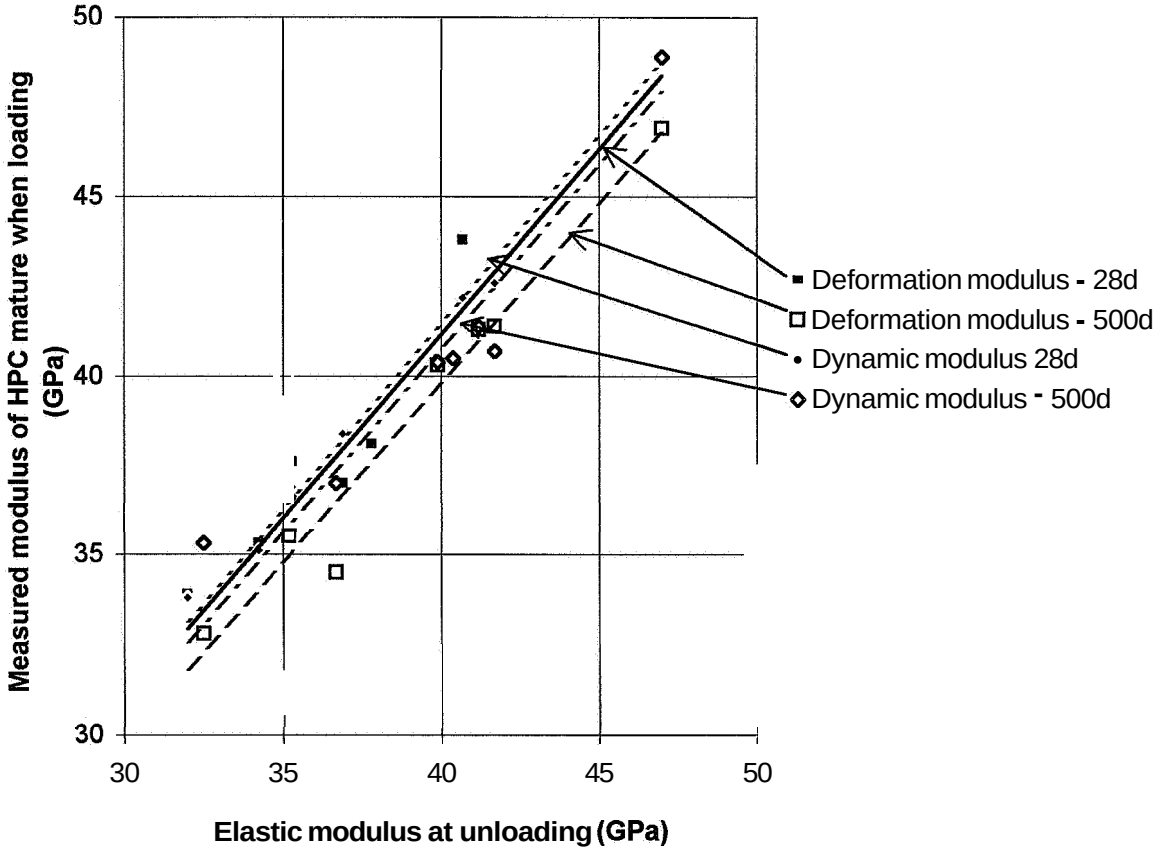

Figure 12.4 - Deformation and dynamic modulus versus elastic modulus. d = days.

12.5.2 Deformation, elastic dynamic and static modulus of young HPC

Figure 12.5 shows the dynamic modulus, E_{dyn}, versus the deformation modulus, $D_{0.01}$, at different internal relative humidity, 0 . The effect of high **O** was correlated:

$$E_{dyn} = 14.85 \cdot (Ø-0.537) \cdot (D_{0.01})^{1.208 \cdot (1.371-Ø)} \qquad \{0.65<Ø<0.9\} \qquad (12.7)$$

$D_{0.01}$ denotes the deformation modulus 0.01 s after loading (GPa)
E_{dyn} denotes the dynamic modulus of elasticity (GPa)

Correlation was made to the maturity when the HPC was tested, which also gave a relationship to the internal relative humidity (since young concrete exhibited high Ø). **Figure 12.6** shows the ratio of the dynamic modulus, E_{dyn}, to the deformation modulus, $D_{0.01}$, versus the relative 28-day strength, f_c/f_{c28}. The relative 28-day strength dominated the increase of the modulus (as much as 50%):

$$E_{dyn} = D_{0.01} \cdot [1.14-0.29 \cdot (\sigma/f_c)-0.0753 \cdot \ln(f_c/f_{c28}) \cdot (\sigma/f_c+4.08)] \qquad (12.8)$$

$D_{0.01}$ denotes the deformation modulus 0.01 s after loading (GPa)
E_{dyn} denotes the dynamic modulus of elasticity (GPa)

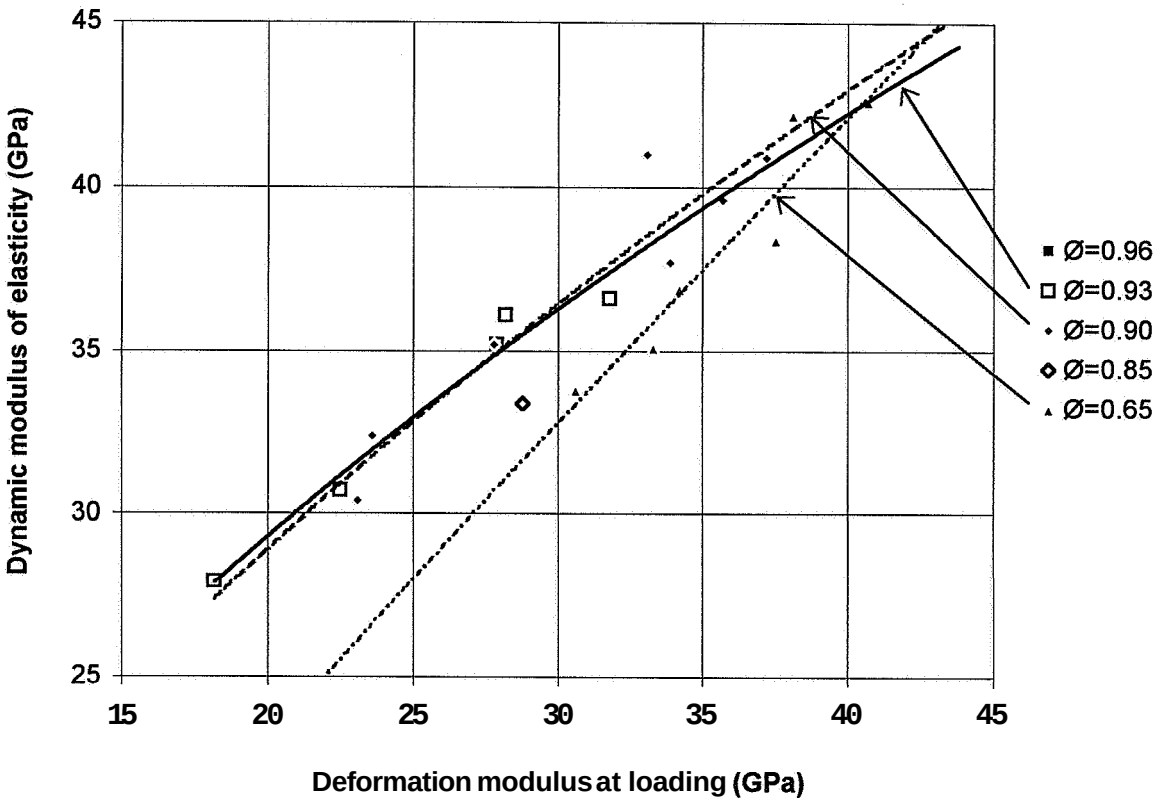

Figure 12.5 - Dynamic modulus versus deformation modulus at different humidity.

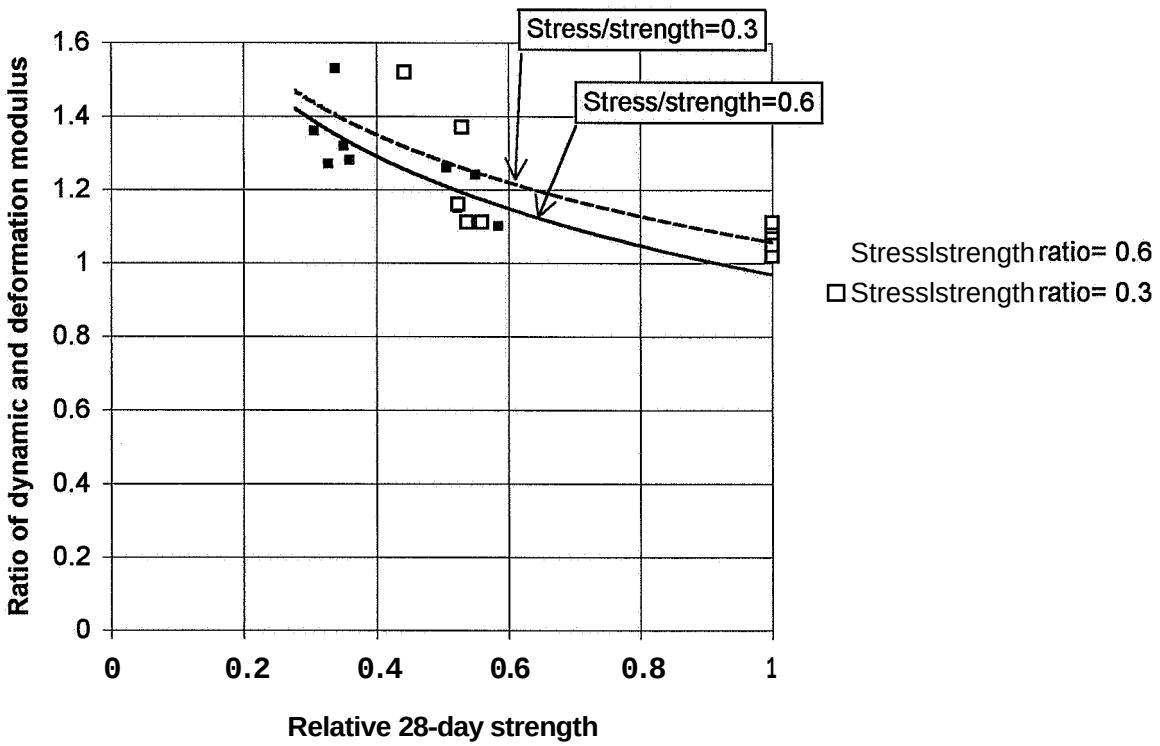

Figure 12.6 - Dynamic to deformation modulus versus relative 28-day strength.

12.5.3 Ageing effect on deformation, dynamic and elastic static modulus

The results on mature HPC described in **Table 11.1** were correlated to the ageing effect:

$$E_{dyn,t} = (E_{dyn}, 1) \cdot t^{0.0025} \quad (12.9)$$

$$D_{0.01,t} = (D_{0.01}, 1) \cdot t^{0.0135} \quad (12.10)$$

$$E_{stat,t} = (E_{stat}, 1) \cdot t^{0.0184} \quad (12.11)$$

t denotes age (months)
$D_{0.01}$ denotes the deformation modulus 0.01 s after loading (GPa)
E_{dyn} denotes the dynamic modulus of elasticity (GPa)
E_{stat} denotes the static modulus of elasticity at unloading (GPa)
1 denotes 1 month' s age

12.5.4 Strength effect on deformation, dynamic and elastic static modulus

Figure 12.7 shows the different moduli of mature HPC related to the cube strength. **Figure 12.7** also shows the proposed MC 90, from which slightly larger values of the elastic modulus were obtained than in the experiments carried out. The type of silica fume (granulated or slurry) had an effect on the size of the moduli and was thus indicated in the figure. As a comparison the proposed extension of Model Code 90, MC 90, **Jaccoud and Leclercq (1995),** was indicated in the figure. At 100 MPa E_{dyn} was 1% smaller, $D_{0.01}$ was 5% smaller and $D_{0.01}$ was 3% smaller than the value obtained according to the extended MC 90. The results on mature air-cured HPC described in **Table 11.1** were correlated to the cube strength:

$$E_{dyn} = k_{sl} \cdot 11.2 \cdot f_c^{0.272} \quad (12.12)$$

$$D_{0.01} = k_{sl} \cdot 7.47 \cdot f_c^{0.351} \quad (12.13)$$

$$E_{stat} = k_{sl} \cdot 8.1 \cdot f_c^{0.337} \quad (12.14)$$

f_c denotes the compressive strength of 100 mm cube at testing (MPa)
k_{sl} = 1.1 for HPC with silica fume slurry; k_{sl} = 1 with granulated silica fume
$D_{0.01}$ denotes the deformation modulus 0.01 s after loading (GPa)
E_{dyn} denotes the dynamic modulus of elasticity (GPa)
E_{stat} denotes the static modulus of elasticity at unloading (GPa)

Symbols in **Figure 12.7:**
Edyn denotes the dynamic modulus of elasticity (GPa)
Estat denotes the static modulus of elasticity at unloading (GPa)
MC 90 denotes Extension of Model Code 90

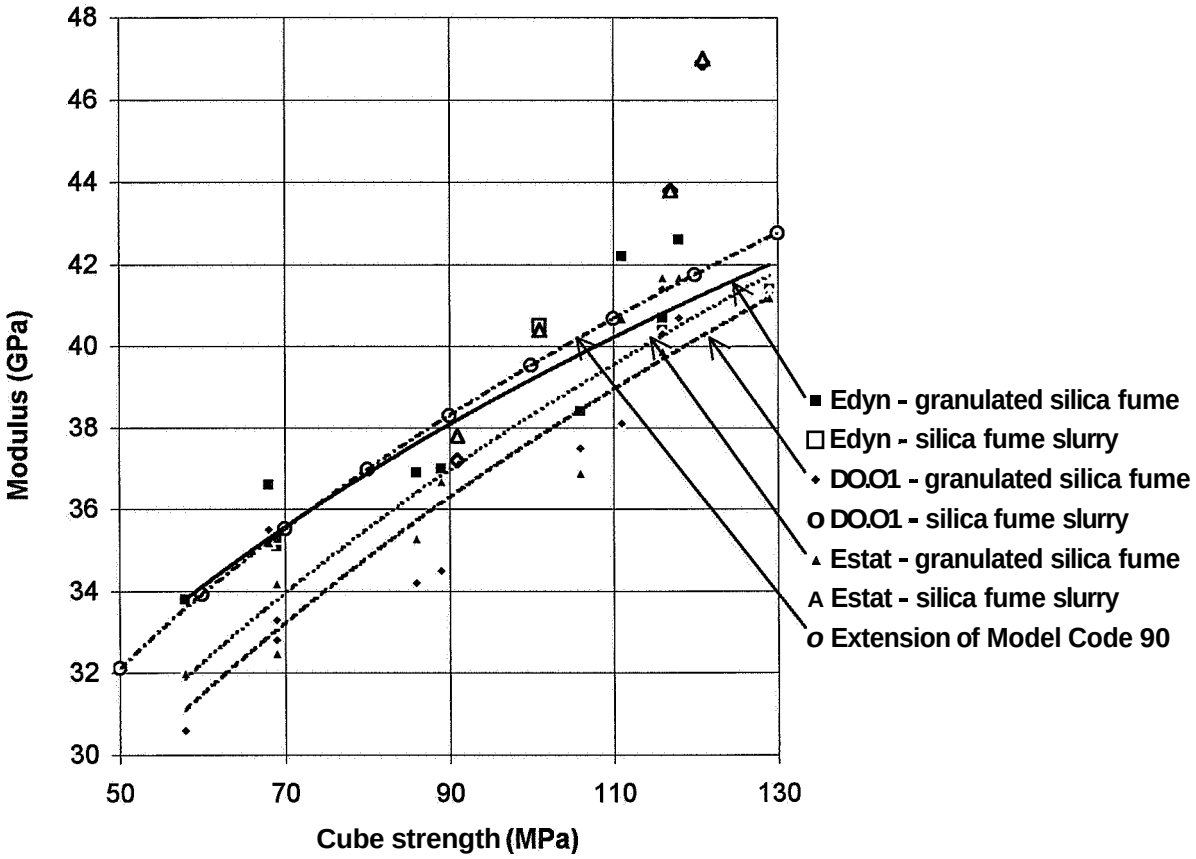

Figure 12.7 - Deformation modulus, $D_{0.01}$, dynamic modulus of elasticity, E_{dyn}, and the static elastic modulus at unloading, E_{stat}, versus the cube strength.

12 Summary and conclusions of the elastic dynamic modulus

Forty tests of the dynamic modulus of elasticity of drying HPC were compared with 50 loading and 50 unloading tests of young HPC (drying or sealed). The dynamic elastic modulus was also compared with 40 loading and 40 unloading tests of mature HPC with an age varying between 1 months and 2 years. Comparison was also made with MC 90. The following conclusions were drawn fiom (220 tests):

- The different moduli of drying, mature HPC coincided well within 4% of difference from the dynamic modulus of elasticity.
- The dynamic modulus of elasticity of young HPC overestimated the static modulus of elasticity by as much as 20% because of the high internal relative humidity in young concrete.
- The overestimation of the dynamic modulus of elasticity of young HPC compared to the static modulus of elasticity was also correlated to the maturity.
- The ageing effect of the modulus of elasticity between 1 and 24 months' age was estimated with an exponent of ≈ 0.02.
- The experimental dynamic modulus of elasticity of drying HPC coincided well with the proposed extension of Model Code 90.

13. RECOVERY DEFORMATIONS AFTER SHORT-TERM LOADING

13.1 General and previous research

The recovery of HPC after loading was normally related to micro-diffusion in the gel, **Bazant** (1993). During the period of creep an uneven pressure was built up in the gel pores. After unloading the moisture in the pores strove for equilibrium, i.e. moisture moved in the pores causing a stress release of the aggregate. Directly after unloading the aggregate was still under compression due to the external loading. The recovery was also called viscous deformation, **Figure** 1.1, or viscous elastic creep. Since the recovery was a pressure-related phenomenon it was most probable that the size of the recovery would be stress-related. Micro cracking was another explanation for the recovery. During the period of loading both the aggregate and the paste were subjected to compression. However, the creep deformation took place in the cement paste since a good-quality aggregate normally did not creep. Accordingly the compressive stress was larger in the aggregate than the stresses in the cement paste. After unloading, tensile stresses occurred in the paste but still compression in the aggregate. Since the cement paste was sensitive to tensile strain, micro cracking and relocation of binding in the gel perhaps caused the recovery. The recovery continued until the aggregate was fi-ee of compressive stresses. Studies of recovery gave the following mformation:

- Amount of viscous deformation
- Plastic deformation calculated as total deformation reduced by shrinkage, viscous and elastic deformation
- Share of recovery compared with the total deformation and period of recovery

Giovambattista and Zerbino (1993) studied the recovery of NSC with strength of 30 or 40 MPa after 10 years of loading. The aggregate consisted of river gravel or expanded clay. The share of recovery increased by the strength. At 30 MPa compressive strength the recovery was about 12% of the elastic deformation; at 40 MPa NSC the recovery was about 20% of the total elastic strain, **Figure** 13.1.

13.2 Experimental results

After the short-term testing as described in Section 9 the specimen was unloaded (Section 10) and moved fi-om the MTS machine after finishing the 66 hours of testing. The drying cylinder was then standing on a table in the air-conditioned box connected to the climate chamber with conditions as described in **Figures** 6.1 **and** 6.2 with the LVDT-equipment still firmly attached to it. The recovery was measured for at least 100 hours. A few concrete cylinders were measured for 200 additional hours to establish the extended recovery of the concrete. **Figure** 13.2 shows the recovery of mix 6 and **Figure** 13.3 shows the 100-hour recovery after unloading of

Symbols in **Figure 13.1:**

a) denotes concrete with 28-day cornpressive strength= 30 MPa,
b) denotes concrete with 28-day strength= 40 MPa.
EC denotes concrete with expanded clay
SRG denotes concrete with river gravel aggregate

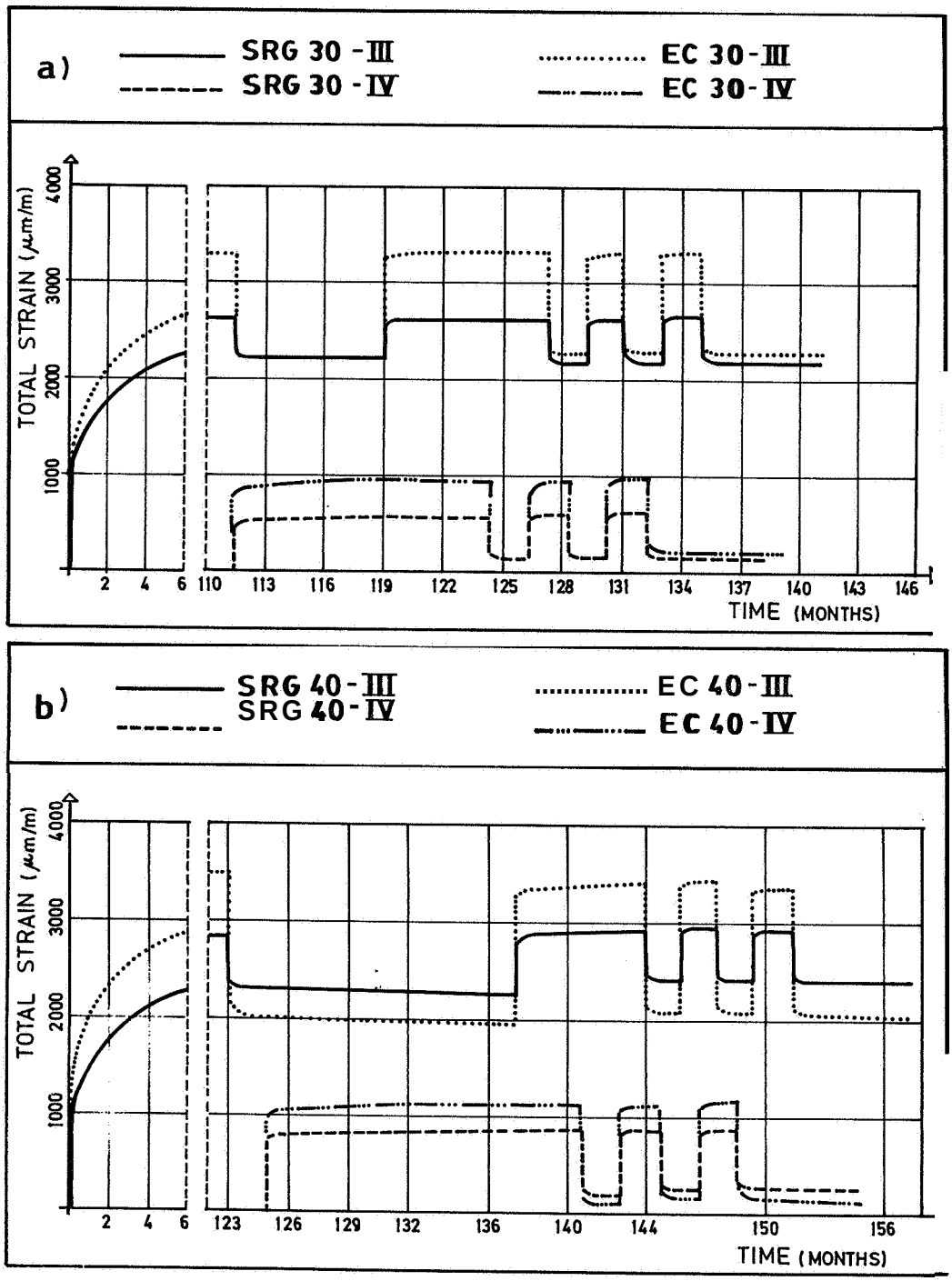

Figure 13.1 - Total strain versus time at long-term research, Giovambattista and Zerbino (1993).

concrete, 28-day-old when loading. The recovery of concrete, young when loading, seemed to be finished after about 100 h, **Figure 13.4.** However, for a 28-day-old concrete the recovery seemed to continue until 240 h. At 400 h of recovery the recovery certainly also stopped for HPC, mature when loading. **Appendix 13** shows recovery of all HPCs. Symbols in the figures:

5...= HPC mix, **Table 5.1**
...01= loading at 0.8 days' age with stresslcylinder strength = 0.84
...02= loading at 2 days' age with stresslcylinder strength = 0.84
...03= loading at 2 days' age with stresslcylinder strength = 0.42
...28= loading at 28 days' age with stresslcylinder strength = 0.42

13.3 Sources of error and accuracy

Some sources of error were detected and the accuracy estimated:

- Possible temperature movements in the cylinder during the period of recovery were avoided by the storage of the specimen in the climate chamber.
- Possible moisture movements were also avoided by the use of the climate chamber.
- The distance from the ends of the specimen to the measurement point was fairly small, which may cause some errors due to uneven stresses in the specimen, **Wittmann (1993).**
- The accuracy at unloading was discussed in **Section 10.4** above. These discussions concerning accuracy also apply to the accuracy during the recovery.

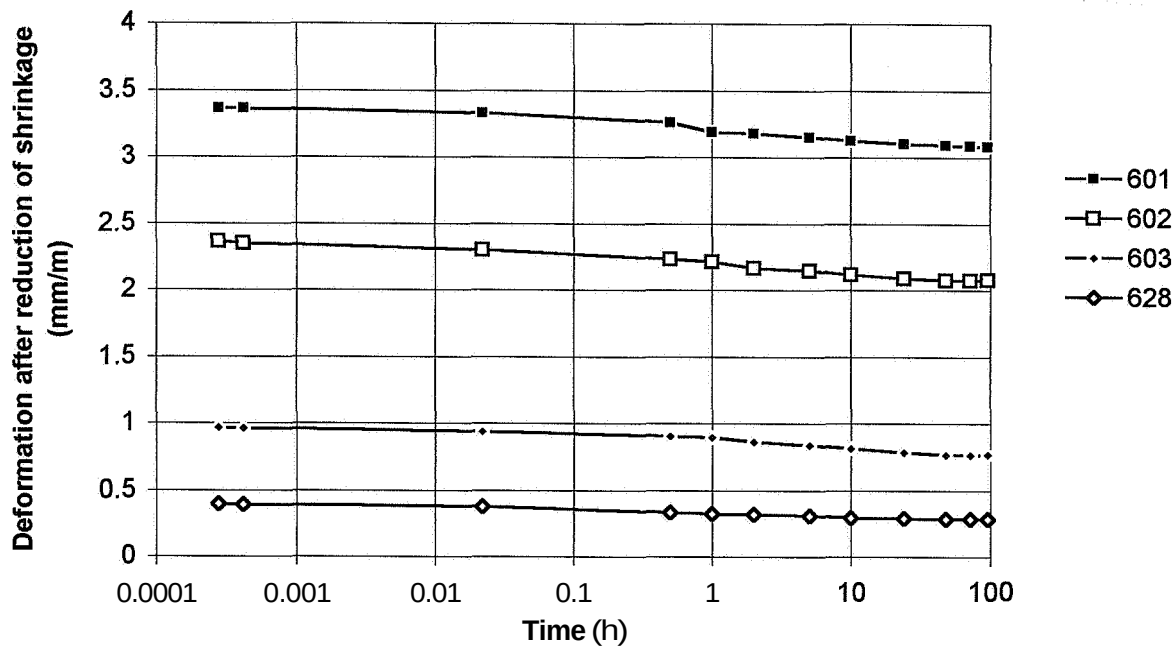

Figure 13.2 - The recovery of **mix** 6 versus time.

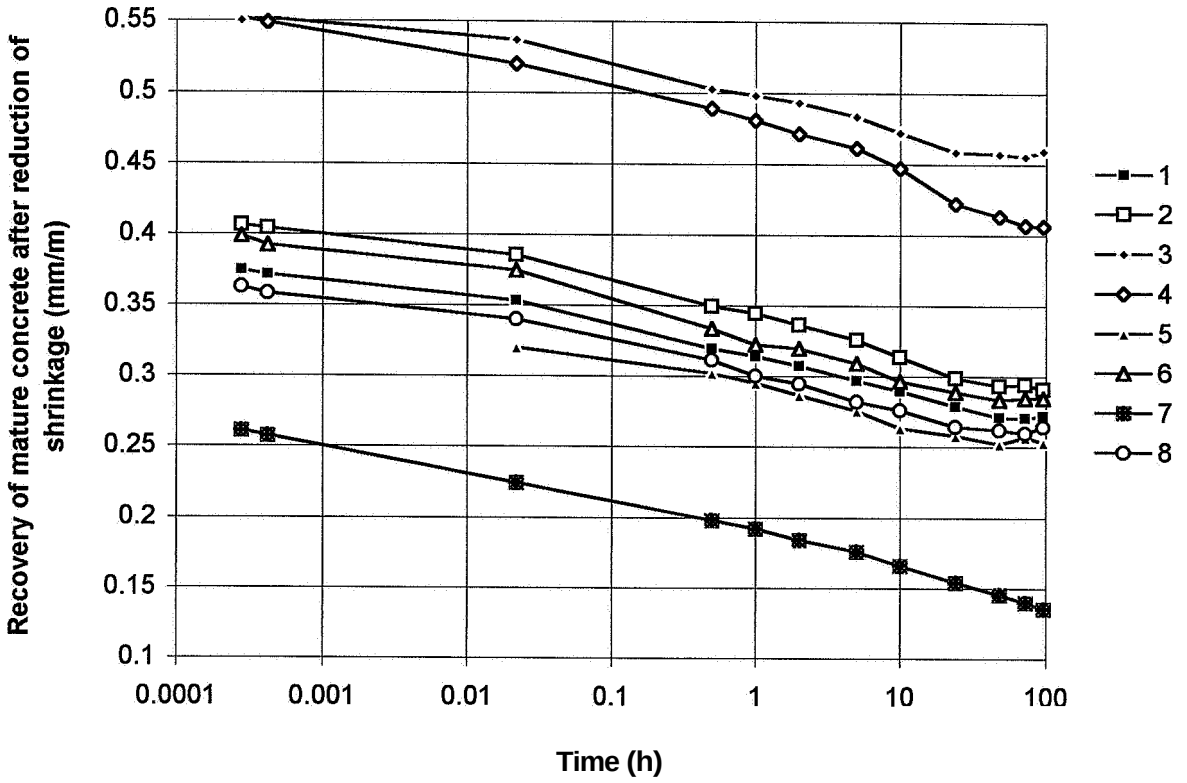

Figure 13.3 - Recovery 100 h after unloading of mature HPC (28 days' age).

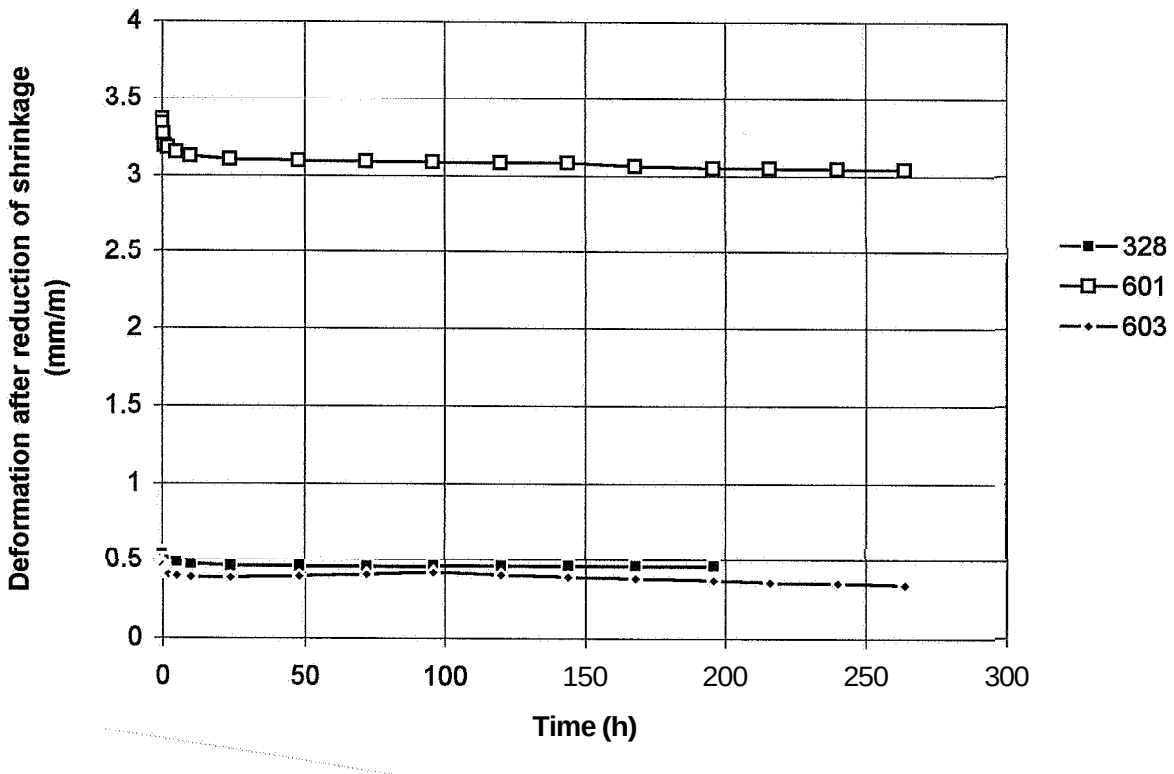

Figure 13.4 - Extended recovery of mixes 3 and 6, Table 5.1. 01 = age at loading.

13.4 Analyses

13.4.1 Concrete mature when loading

As pointed out above, the stress prior to unloading was the driving force for recovery. All HPCs were loaded to a stress/strength ratio = 0.30. **Figure 13.5** shows the elastic, plastic and viscous strain after 66 h of loading and 100 h of recovery versus the total stress, **Figure 1.1.** From **Figure 13.5** the following relationships were deduced related to the different strain (per mil):

$$\varepsilon_{el} = 410 \cdot \sigma \cdot (0.094 - \sigma) \qquad \{0.015 < \sigma < 0.045 \text{ GPa}\} \qquad (13.1)$$

$$\varepsilon_{pl} = 830 \cdot \sigma \cdot (0.042 - \sigma) \qquad \{0.015 < \sigma < 0.045 \text{ GPa}\} \qquad (13.2)$$

$$\varepsilon_{vi} = 144 \cdot \sigma \cdot (0.056 - \sigma) \qquad \{0.015 < \sigma < 0.045 \text{ GPa}\} \qquad (13.3)$$

ε_{el} denotes elastic strain of mature HPC after 66 h of loading and 100 h of recovery (per mil)

ε_{pl} denotes plastic strain of mature HPC after 66 h of loading and 100 h of recovery (per mil)

ε_{vi} denotes viscous strain of mature HPC after 66 h of loading and 100 h of recovery (per mil)

σ denotes the stress in the HPC (GPa) $\{0.015 < \sigma < 0.045 \text{ GPa}\}$

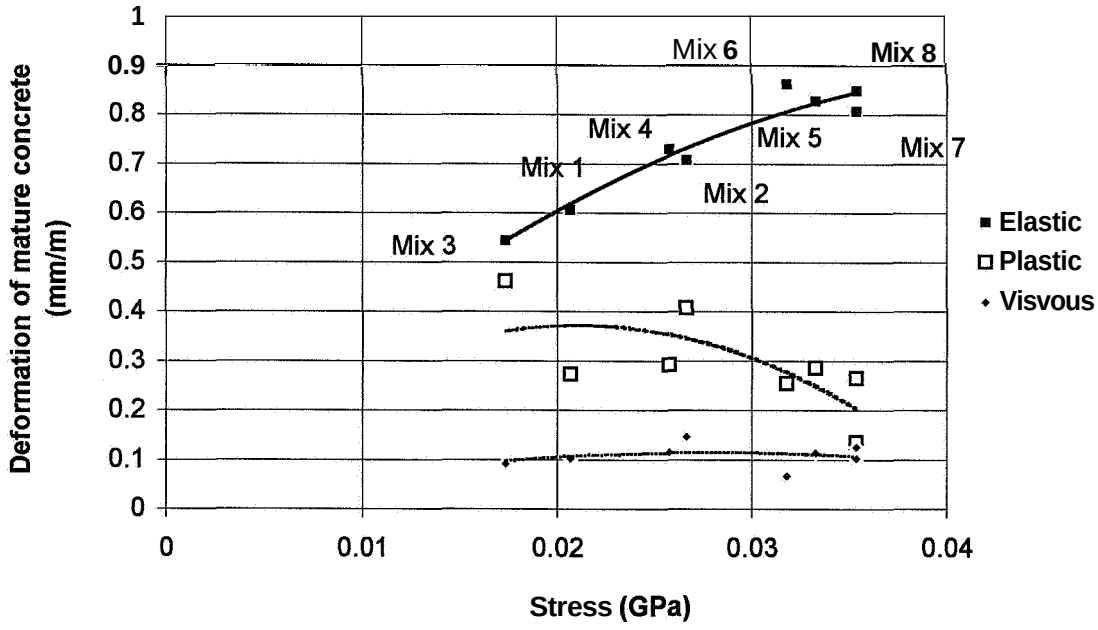

Figure 13.5 - Elastic, plastic and viscous strain after 66 h loading and 100 h recovery versus the total stress, **Figure 1.1.**

Figure 13.6 shows plastic and viscous strain after 66 h of loading and 100 h of recovery versus the elastic strain. From **Figure 13.6** the following correlations were obtained (per mil):

$$\varepsilon_{pl} = 1.4 \cdot \varepsilon_{el} \cdot (1 - \varepsilon_{el}) \qquad \{0.5 < \varepsilon_{el} < 0.9 \text{ per mil}\} \qquad (13.4)$$

$$\varepsilon_{vi} = 0.26 \cdot \varepsilon_{el} \cdot (1.3 - \varepsilon_{el}) \qquad \{0.5 < \varepsilon_{el} < 0.9 \text{ per mil}\} \qquad (13.5)$$

ε_{el} denotes elastic strain of mature HPC after 66 h of loading and 100 h of recovery (per mil)

ε_{pl} denotes plastic strain of mature HPC after 66 h of loading and 100 h of recovery (per mil)

ε_{vi} denotes viscous strain of mature HPC after 66 h of loading and 100 h of recovery (per mil)

However, equations (13.2) and (13.4) for plastic strain both exhibited a low significance, most probably due to the reduction of shrinkage measured on a parallel specimen. However, it was not possible to confirm that the shrinkage of unloaded parallel cast HPC specimen obtained the same shrinkage as the specimen during loading in the MTS machine, cp. **Bazant (1993).**

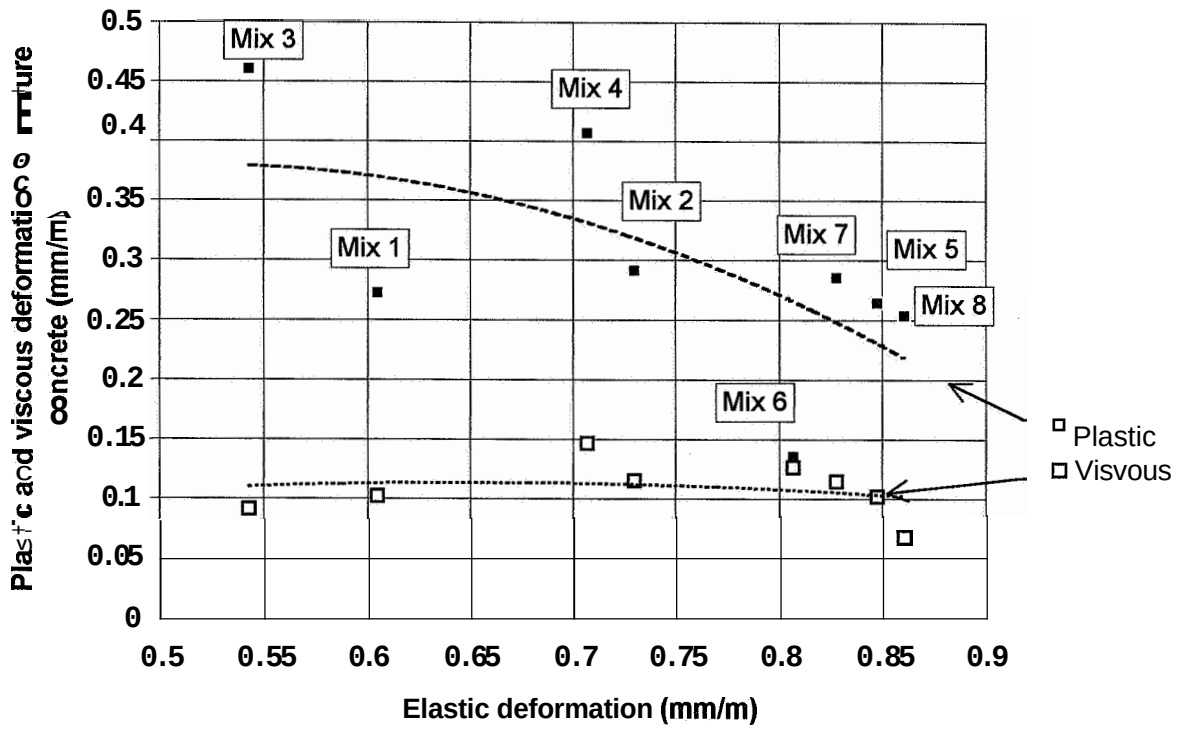

Figure 13.6 - Plastic and viscous strain of drying HPC, mature when loading, after 66 h of loading and 100 h of recovery versus the elastic strain.

13.4.2 Concrete loaded at early ages

The plastic strain of young HPC was dependent on the stress level, (σ/f_c), when the loading took place. In **Figure 13.7** the relative plastic strain of young HPC was correlated to the growth of strength between loading, lo, and unloading, un, of the concrete, i.e. $\delta f_c/f_{c28} = f_{c,un}/f_{c28} - f_{c,lo}/f_{c28}$:

$$\varepsilon_{pl}/\varepsilon_{el} = 1.45\cdot(\sigma/f_c) + [17.8\cdot(\sigma/f_c) - 2.9]\cdot(\delta f_c/f_{c28}) \qquad (13.6)$$

In Figure 13.8 the relative viscous strain was likewise correlated to the growth of strength:

$$\varepsilon_{vi}/\varepsilon_{el} = 0.89\cdot[(\delta f_c/f_{c28})+0.19)] \approx 0.9\cdot[(\delta f_c/f_{c28})+0.2)] \qquad (13.7)$$

13.4.3 Comparison with sealed concrete

Figure 13.9 shows the elastic, plastic and viscous elastic strain after 66 h of loading and 100 h of recovery, **Persson (1995A), Appendix 13 (sealed curing). Figure 13.9** gave the following correlations (per mil):

$$\varepsilon_{Bpl} = 0.04\cdot\varepsilon_{Bel}\cdot(5.5-\varepsilon_{Bel}) \qquad \{0.5<\varepsilon_{el}<0.9 \text{ per mil}\} \qquad (13.8)$$

$$\varepsilon_{Bvi} = 0.1\cdot\varepsilon_{Bel}\cdot(2.4-\varepsilon_{Bel}) \qquad \{0.5<\varepsilon_{el}<0.9 \text{ per mil}\} \qquad (13.9)$$

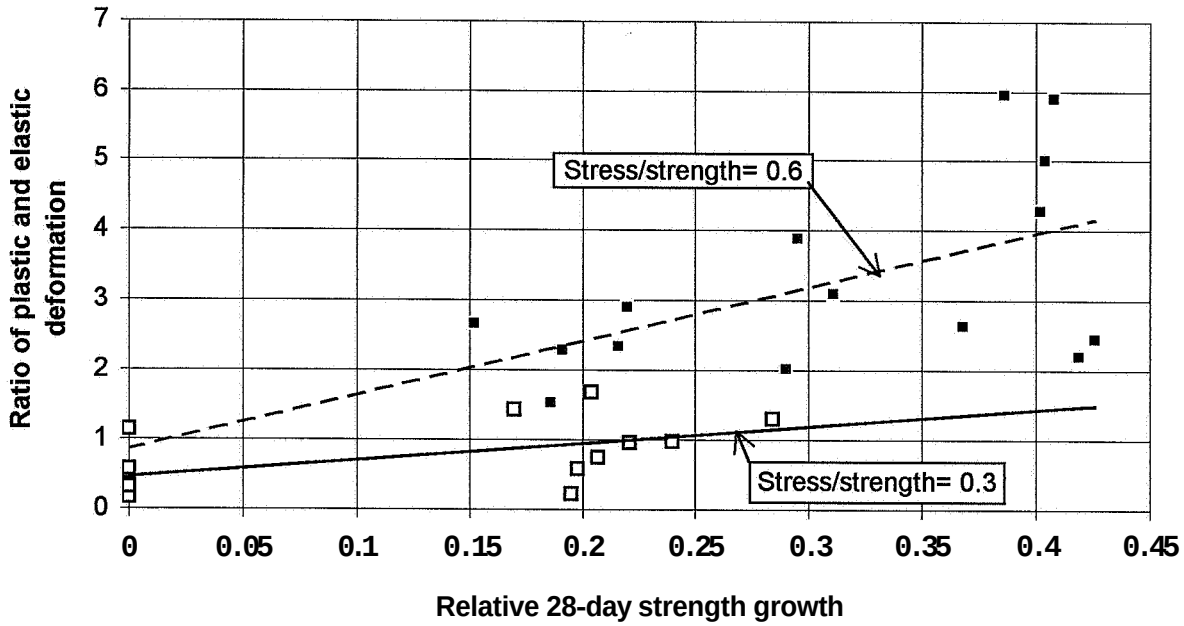

Figure 13.7 - Relative plastic strain of HPC, young when loading, versus the growth of strength between loading and unloading.

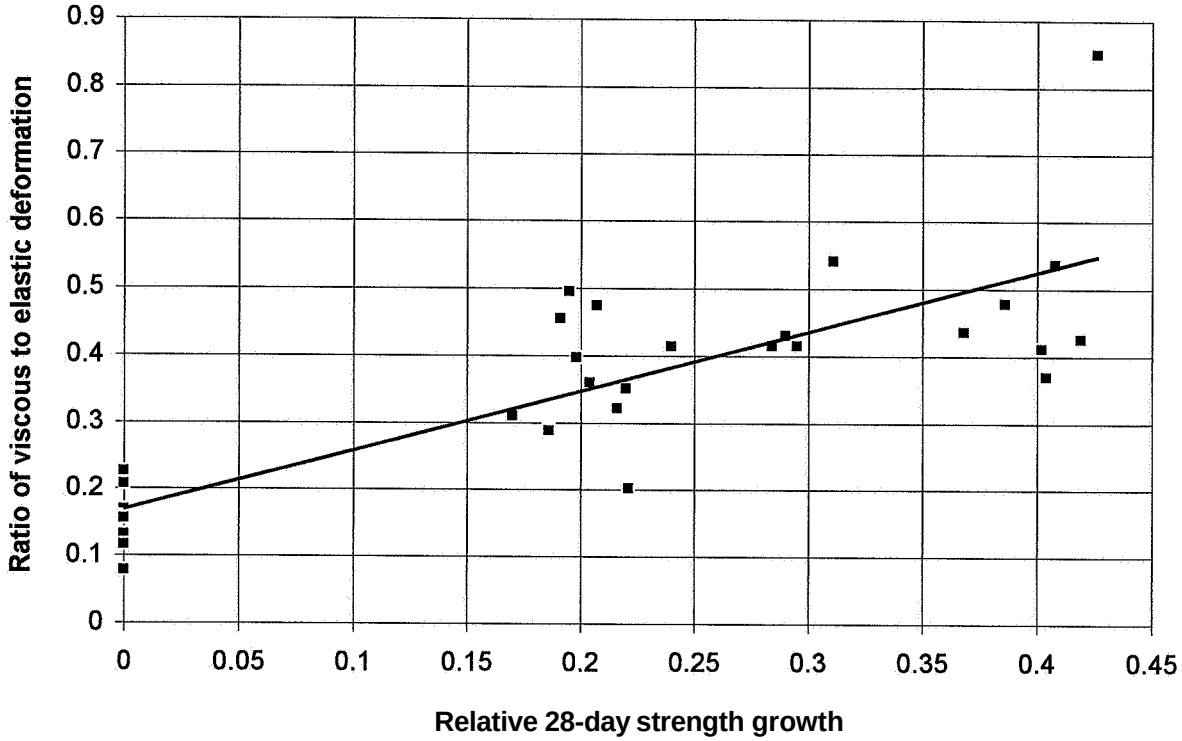

Figure 13.8 - Relative viscous strain of HPC, young when loading, versus the growth of strength.

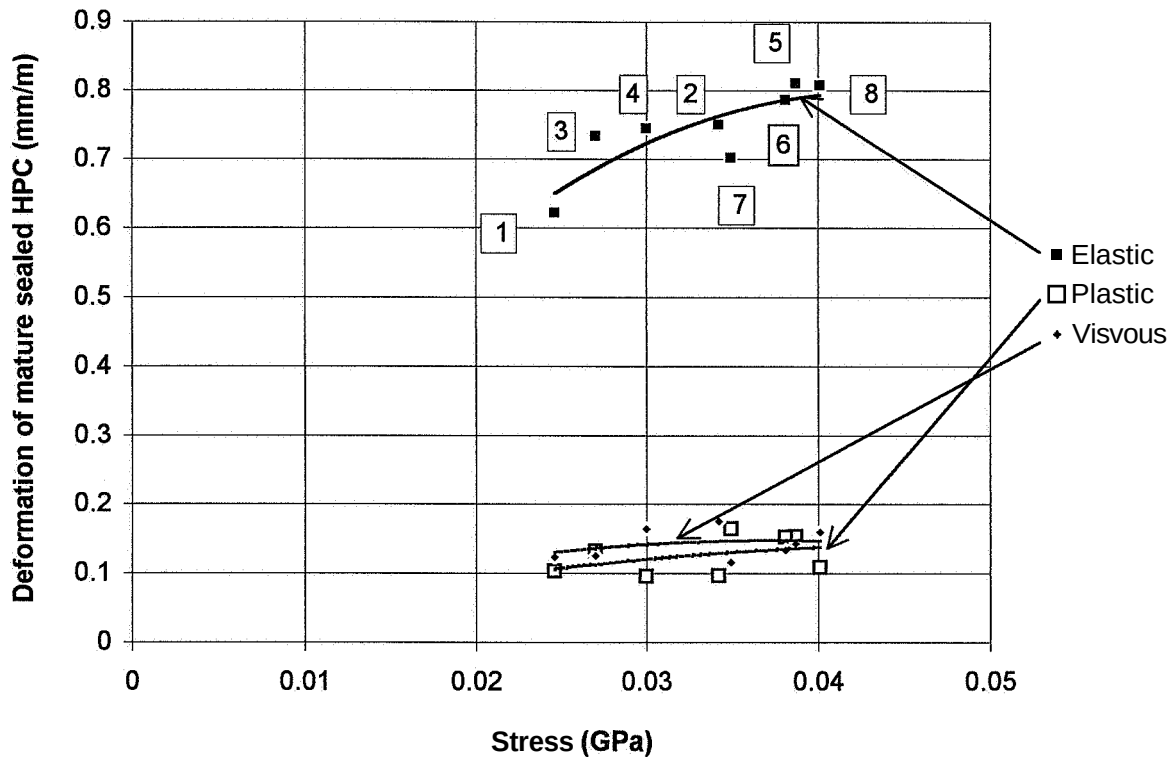

Figure 13.9 – Elastic, plastic and viscous strain of sealed HPC, mature when loading, versus stress. HPC mix is indicated, **Table 5.1**.

ε_{Bel} denotes elastic strain of sealed HPC after 66 h of loading and 100 h of recovery (per mil)

ε_{Bpl} denotes plastic strain of sealed HPC after 66 h of loading and 100 h of recovery (per mil)

ε_{Bvi} denotes viscous strain of sealed HPC after 66 h of loading and 100 h of recovery (per mil)

The plastic strain of young sealed HPC was dependent on the stress level, (σ/f_c), when the loading took place. In **Figure 13.10** the relative plastic strain of young HPC was correlated to the relative growth of strength between loading, lo, and unloading, un, of the concrete, i.e. $\delta f_c/f_{c28} = f_{c,un}/f_{c28} - f_{c,lo}/f_{c28}$. In **Figure 13.11** the relative viscous was also correlated to the growth of strength. **Appendix 13** shows the elastic, plastic and viscous strain of sealed HPC.

$$\varepsilon_{Bpl}/\varepsilon_{B_{el}} = 0.8\cdot(\sigma/f_c) + [17.3\cdot(\sigma/f_c) - 2.4]\cdot(\delta f_c/f_{c28}) \quad (13.10)$$

$$\varepsilon_{Bvi}/\varepsilon_{B_{el}} = 0.75\cdot(\delta f_c/f_{c28}+0.3) \quad (13.11)$$

ε_{Bel} denotes elastic strain after 66 h of loading and 100 h of recovery (per mil)

ε_{Bpl} denotes plastic strain after 66 h of loading and 100 h of recovery (per mil)

ε_{Bvi} denotes viscous strain after 66 h of loading and 100 h of recovery (per mil)

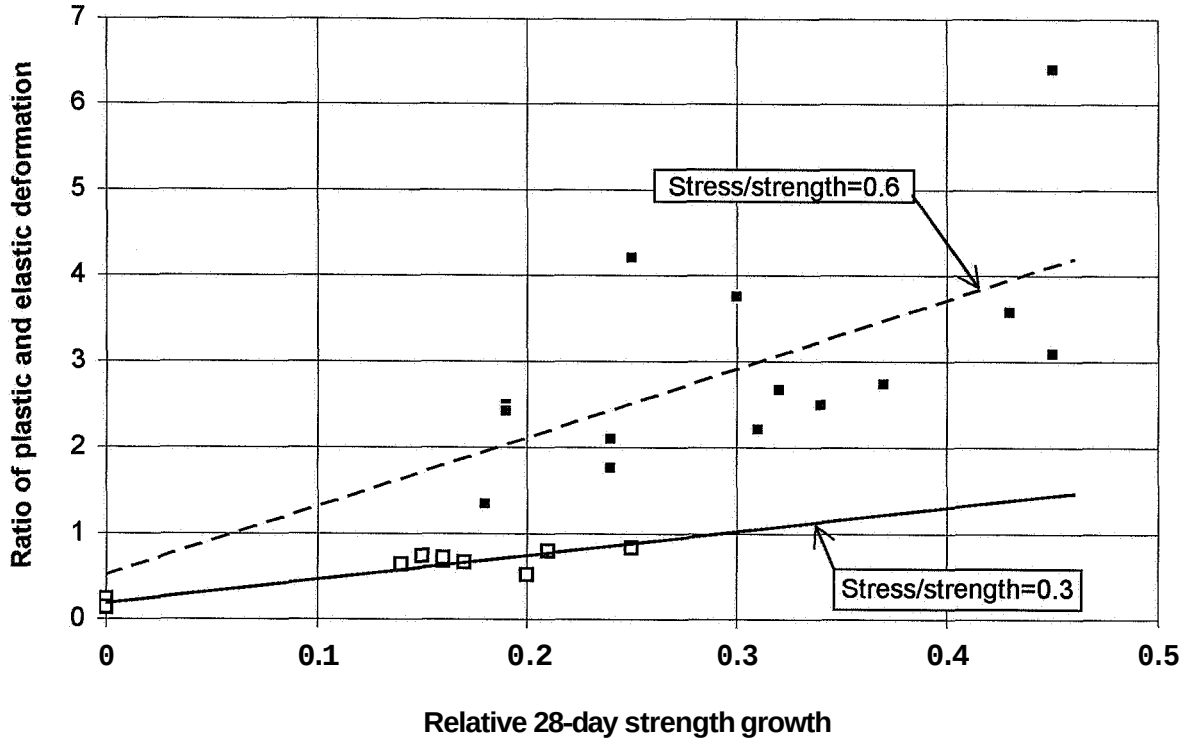

Figure 13.10 - Relative plastic strain of sealed young HPC versus strength growth.

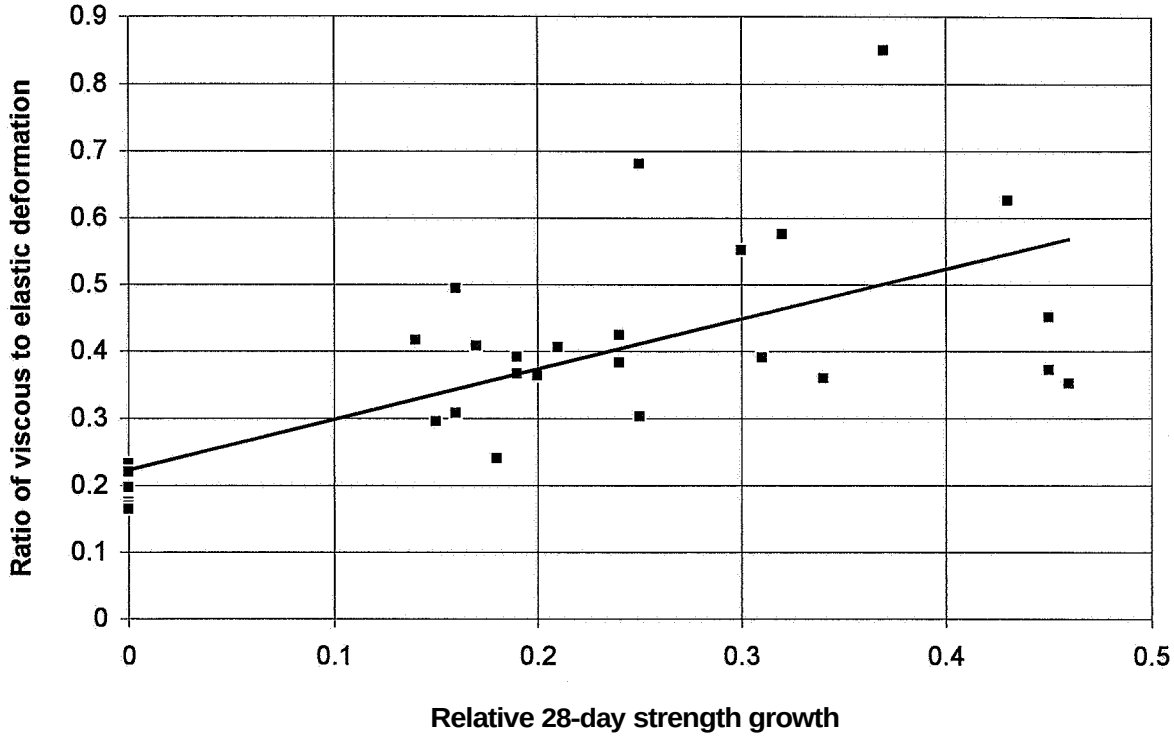

Figure 13.11 - Relative viscous strain of sealed young HPC versus strength growth.

Results of viscous deformation coincided well with results for NSC according to **Giovambattista and Zerbino (1993)**, i.e. viscous strain varying between 12% of the elastic strain (drying HPC) and 20% of the elastic strain (sealed HPC). The viscous strain of HPC was increasing with the stress likewise to results on NSC, **Giovambattista and Zerbino** (1993).

13.5 Summary and

The elastic strain studies of 32 drying and 32 sealed HPC cylinders during 66 h were followed by observations of viscous elastic strain and plastic (irreversible) strain during more than 100 h. The following conclusions were drawn:

- The viscous strain of air-cured mature HPC was equal to the viscous strain of sealed curing.
- The plastic strain of air-cured mature HPC was about three times as large as the viscous strain.
- The plastic strain of sealed mature HPC was about equal to the viscous strain.
- The viscous strain of young HPC was dependent on the strength growth during the loading.
- The plastic strain of young HPC was dependent both on the stress/strength level and on the strength growth from loading till unloading.
- Viscous strain varied between 12% (drying) and 20% of elastic strain (sealed).
- Viscous strain of HPC was increasing with the stress likewise to results on NSC.

14. LONG-TERM DEFORMATIONS

14.1 General and previous research

The main objective of the study was to establish knowledge of the long-term creep deformations of HPC. As defined in **Figure 1.1** above, the long-term creep deformations included elastic, viscous and plastic deformations. The strain was measured from the stress-fkee state. Then it was established after a period of fairly slow loading until constant stress was reached. The specimens were unloaded after at least 3 years to obtain the elastic, viscous and plastic component of the long-term creep. Parallel to the creep studies, the shrinkage was studied to reduce its influence on the creep.

In **Figure** 14.1 the steep line indicates the compliance (specific creep), ε/σ, versus the compressive strength of the concrete, **Bjerkeli et al.** (1989). However, the second line in **Figure** 14.1 indicates that the inverse of the initial "elastic" modulus does not follow the compliance in parallel. The resulting initial strain of concrete at a higher strength will then be larger than in a NSC at the same stress/strength ratio. The reference indicated in **Figure** 14.1, **Ngab et al.** (1981) shows an even lower compliance than **Bjerkeli et al.** (1989). **Müller and Kiittner** (1995) show the effect of the maturity of the concrete on the creep coefficient, **Figure** 14.2. Loading before 28 days' age increased the creep coefficient substantially, while loading at old ages decreased the creep coefficient to half the value that was obtained when the concrete was loaded at 28 days' age. The results of the present study indicated slightly smaller initial strain but slightly larger creep compliance.

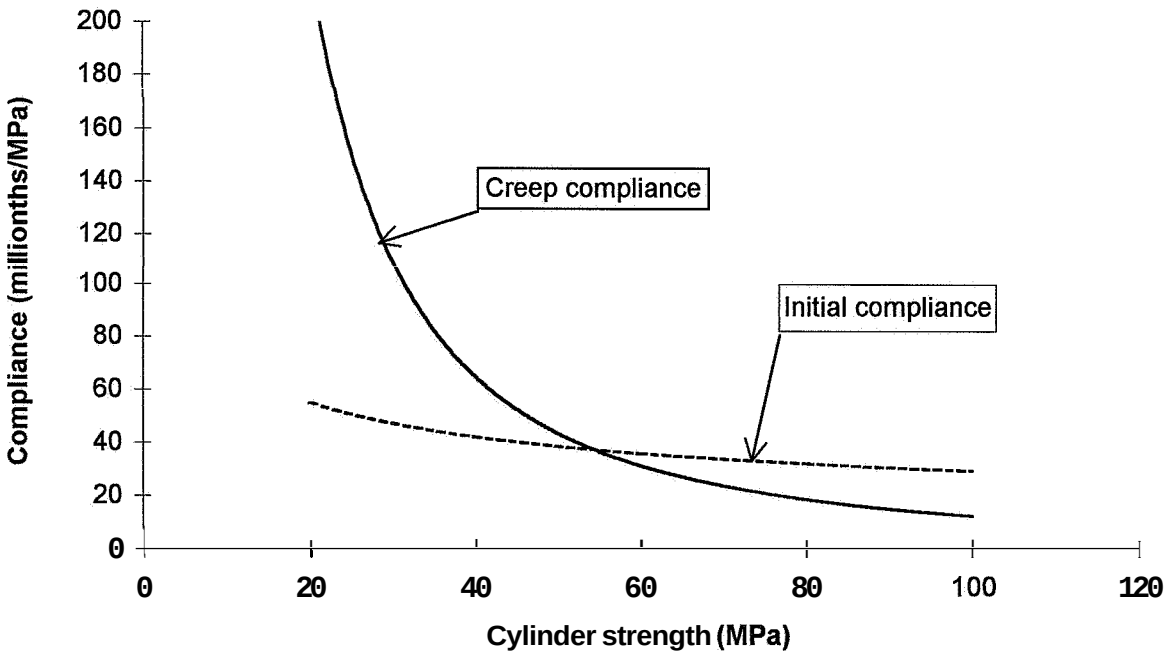

Figure 14.1 - Creep compliance (full line) and initial compliance (dotted line) versus cylinder strength, Bjerkeli et al. (1989), Ngab et al. (1981).

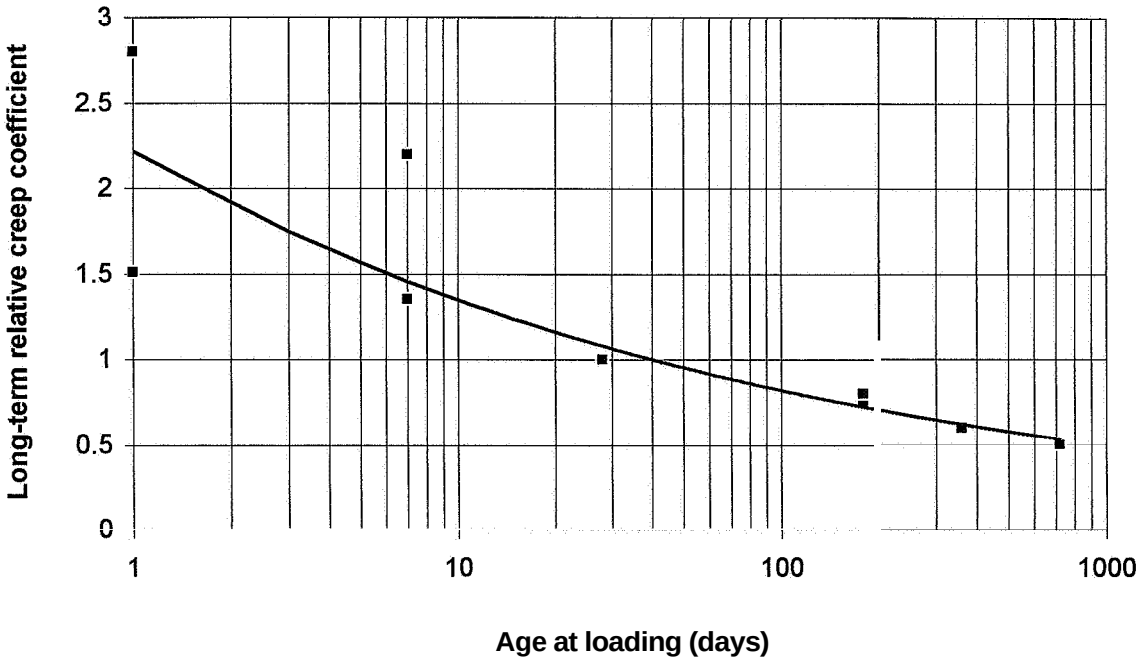

Figure 14.2- Creep coefficient of HPC versus loading age, Müller & Küttner (1995).

14.2 Experimental

14.2.1 Specimen

Figure 14.3 shows the specimen and the spring-loading device that were used. The 4 plate springs in the device acted as hinges, which decreased the possible eccentric loading in the device. The measurements were taken on **3** points of the specimen by Huggenberger or Proceq mechanical devices. The general layout is given in Section **3.3.** Materials, preparation of specimen and chronology are given in Section 4. The eight types of **mix** design are given in **Table** 5.1. At commencement of testing the age of the concrete was either 1 or 2 days (stress/cube strength level = 0.6) or 2 or 28 days (stress/cube strength level = 0.3). Air-cured and sealed HPCs were studied.

14.2.2 Preparation of loading device and location of specimen

Parallel to the start of the quasi-instantaneous loading, Section 6, in the MTS machine an identical specimen was placed in the spring-loading device, **Figure** 14.3, which also shows specimens for studies of strength and shrinkage. The weight of the specimen was taken before it was placed. The measuring points were stiffly connected to the steel cast-in items in the specimen by pin bolts of 3 mm diameter. The length between the longitudinal measuring points was 250 mm. The steel plates of the device were adjusted horizontal before the location of the specimen. The position of the cylinder was adjusted to avoid eccentricities in the device. The moisture stability in the sealed specimen was secured by sealing compound between the vulcanised 2 mm butyl-rubber of the specimen and the plate of the device.

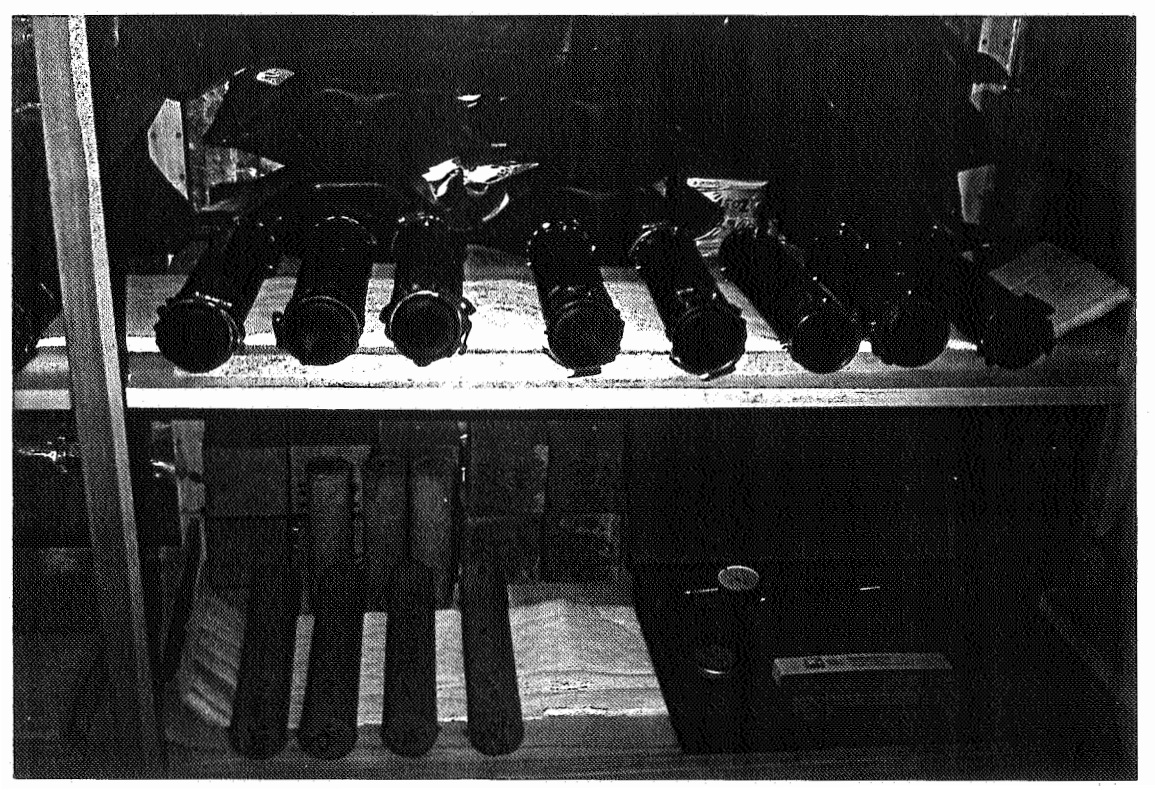

Figure 14.3 - Specimen and equipment used in the long-term experiments.

14.2.3 Commencement of testing

After commencement of the quasi-instantaneous loading of a drying HPC cylinder in the MTS machine, the following routine was carried out in the spring-loading device within a quarter of an hour:

- The position of the precision-turned screws in both sealed and drying cylinders was measured.
- The internal temperature of the cylinders was measured.
- The loading, identical to that in the MTS machine, was applied in the spring-loading devices; one device for a sealed HPC, another for the air-cured. The loading rate was about 1 MPa/s.
- The first measurements were recorded within 2 minutes of loading by the mechanical device.
- The loading was manually kept constant for an hour in the spring-loading devices.
- The second measurement was recorded.
- After 1 hour the nuts on the screws of the spring-loading were tightened until a 10% decrease of the loading was recorded on the display of the load cell in the device, **Figure 14.3.** This decrease of loading on the display corresponded to a constant length between the measurement point when the external loading was removed and only the spring acted.
- After 3 hours 90% of the specified loading of the specimen was applied in the load-cell.
- The nuts of the screws in the device were loosened.
- The external loading was adjusted to within $\pm$ 0.05 kN.
- The measurement was recorded between the 6 screws on both the cylinders.
- No decrease of loading then occurred, cp. above.

14.2.4 Continual measurements

At about 10 and 16 h, 1 day, 2 , 4, 8, 16 days, 1 month, 2, 4, 8,12, 18, 24, 30, 36 and (in some cases) 48 months after commencement of testing, the following measurement routine applied:

- The measurement between the screws of the cylinder was established with tightened screws on the spring-loading device.
- 90% of the specified loading of the specimen was applied in the load-cell.
- The nuts of the screws in the device were loosened.
- The loading was adjusted to within $\pm$ 0.05 kN.
- The measurement was recorded between the 6 screws on the cylinder.
- The nuts on the screws of the spring-loading were tightened until a 10% decrease of the loading was recorded on the display of the load cell in the device. This decrease of loading on the display corresponded to a constant

length between the measurement point when the external loading was removed and only the spring acted.
- The pressure of the jack in the device was released.
- The measurement between the screws of the cylinder was established with tightened screws.

14.2.5 Unloading of specimen

- After at least 3 years of loading all specimens, **Table** 4.5, were unloaded according to the following procedure:
- The measurement between the turned screws of the concrete cylinder was established with tightened screws on the spring-loading device.
- 90% of the specified loading of the specimen was applied in the load-cell.
- The nuts of the screws in the device were well loosened.
- The loading was adjusted to within $\pm$ 0.05 kN.
- The measurement was recorded between the *6* screws on the cylinder.
- The concrete cylinder was unloaded.
- The measurement was recorded between the *6* screws on the cylinder within 1 minute of unloading (long-term elastic deformation, **Figure** 1.1).
- The measurements were also taken 2 minutes and 2 weeks after unloading (in order to separate viscous and plastic deformation).
- The cylinder was weighed to establish the moisture losses.

14.2.6 Loading level

Tables 14.1-14.6 show the cube strength when the specimens were loaded and unloaded. **Tables** 14.7-14.8 show the stress during loading and, finally, **Table 14.9-**14.14 show the stress/strength at loading, at 28 days' age and at unloading of the cylinders, **Persson (1995A)** and section 5. Concretes of type 1, 4 and 7 were cast on different occasions related to air curing and sealed curing. All other HPCs were cast parallel, i.e. HPC from the same batch was used in parallel tests of short-term and long-term drying creep (air curing) and long-term basic creep (sealed curing). The stress-level shown in **Tables** 14.9-14.14 above was related to the cube strength, f_{ccube}. The stress-level that was related to the current cylinder strength was substantially higher. Equation (5.8) above gives a good estimation of the cylinder strength, $f_{ccyl} = 0.71 \cdot f_{ccube}$ (cube strength). Symbols:

B= sealed curing (basic creep)
D= air curing (drying creep)
6...= HPC mix, **Table** 5.1
...01= loading at 0.8 days' age with stresslcylinder strength = 0.84
...02= loading at 2 days' age with stress/cylinder strength = 0.84
...03= loading at 2 days' age with stresslcylinder strength = 0.42
...28= loading at 28 days' age with stresslcylinder strength = 0.42

Table 14.1. - Strength at loading with air curing (MPa).

Concrete	01	02	03	28
1	23	32	26	69
2	24	44	44	86
3	27	30	43	58
4	23	37	48	91
5	38	45	60	106
6	30	61	58	111
7	36	63	67	118
8	35	69	65	118

Table 14.2. - Strength at loading with sealed curing (MPa).

Concrete	01	02	03	28
1	14.1	23.5	52	82
2	24	44	44	101
3	27	30	43	79
4	37	34	55.5	91
5	38	45	60	126
6	30	61	58	136
7	41.5	58	59.5	116
8	35	69	74	132

Table 14.3. - Strength at 28 days with air curing (MPa).

Concrete	01	02	03	28
1	68	69	50	69
2	86	87	83	86
3	77	58	82	58
4	83	95	95	91
5	106	86	104	106
6	98	111	108	111
7	109	110	118	118
8	107	118	116	118

Table 14.4 - Strength at 28 days with sealed curing (MPa).

Concrete	01	02	03	28
1	50	60	96	82
2	101	108	101	101
3	99	79	106	79
4	102	106	104	91
5	126	113	125	126
6	122	136	120	136
7	119	126	126	116
8	128	132	127	132

Table 14.5 - Strength at unloading with air curing (MPa).

Concrete	01	02	03	28
1	72	66	54	69
2	91	-	88	91
3	-	69	85	69
4	91	99	95	100
5	116	93	118	116
6	106	116	113	116
7	118	122	123	123
8	120	129	127	129

Table 14.6 - Strength at unloading with sealed curing (MPa).

Concrete	01	02	03	28
1	66	71	112	101
2	117	118	123	117
3	105	105	118	105
4	113	118	113	112
5	131	126	125	131
6	144	141	130	141
7	132	132	129	128
8	145	154	137	154

14.3 Results

Figure 14.4 shows the reduced compliance, ε/σ, of concrete 6 versus time. **Figure 14.5** shows the reduced compliance, ε/σ, versus time when unloading concrete 6. **Appendix 14** shows the reduced compliance of all HPCs in the creep tests. Symbols used in Figures and Tables:

Table **14.7**-Stress during long-term loading with air curing (MPa).

Concrete	01	02	03	28
1	14	18.6	7.8	20.7
2	14.4	26.4	13	25.8
3	16.2	18	12.9	17.4
4	13.9	22.4	14.4	26.7
5	22.8	27	18	31.8
6	18	36	17.4	33.3
7	21.8	37.9	20.2	35.4
8	21	40.6	19.5	35.4

Table 14.8 - Stress during long-term loading with sealed curing (MPa).

Concrete	01	02	03	28
1	8.5	14.1	15.6	24.6
2	14.4	26.4	13	25.8
3	16.2	18	12.9	17.4
4	22.2	20.4	16.7	30
5	22.8	27	18	31.8
6	18	36	17.4	33.3
7	24.9	34.8	19.9	34.9
8	21	40.6	19.5	35.4

Table **14.9**- Stresslstrength-levelat loading of long-term creep tests with air curing.

Concrete	01	02	03	28
1	**0.61**	**0.58**	**0.30**	**0.30**
2	0.60	0.60	0.30	0.30
3	0.60	0.60	0.30	0.30
4	0.60	0.61	0.30	0.29
5	0.60	0.60	0.30	0.30
6	0.60	0.59	0.30	0.30
7	0.61	0.60	0.30	0.30
8	0.60	0.59	0.30	0.30

Table **14.10-Stresslstrength-level**at loading of long-term creep tests with sealed curing.

Concrete	01	02	03	28
1	**0.60**	**0.60**	**0.30**	**0.30**
2	0.60	0.60	0.30	0.26
3	0.60	0.60	0.30	0.22
4	0.60	0.60	0.30	0.33
5	0.60	0.60	0.30	0.25
6	0.60	0.59	0.30	0.25
7	0.60	0.60	0.33	0.30
8	0.60	0.59	0.26	0.27

Table **14.ll** - Stresslstrength-levelof long-term creep tests with air curing at **28** days' age.

Concrete	01	02	03	28
1	0.21	0.27	0.16	0.30
2	0.17	0.30	0.16	0.30
3	0.21	0.31	0.16	0.30
4	0.17	0.24	0.15	0.29
5	0.22	0.32	0.17	0.30
6	0.18	0.32	0.16	0.30
7	0.20	0.35	0.17	0.30
8	0.20	0.34	0.17	0.30

Table **14.12**- Stresslstrength-levelof long-term creep tests with sealed curing at **28** days' age.

Concrete	01	02	03	28
1	0.17	0.24	0.16	0.30
2	0.14	0.24	0.13	0.26
3	0.16	0.23	0.12	0.22
4	0.22	0.19	0.16	0.33
5	0.18	0.24	0.14	0.25
6	0.15	0.26	0.15	0.25
7	0.21	0.28	0.16	0.30
8	0.16	0.31	0.15	0.27

6.. = HPC mix, Table 5.1
...01= loading at **0.8** days' age with stresslcylinder strength = **0.84**
...02= loading at **2** days' age with stresslcylinder strength = **0.84**
...03= loading at **2** days' age with stresslcylinder strength = **0.42**
...28= loading at **28** days' age with stresslcylinder strength = **0.42**

Table **14.13-** Stresslstrength-levelat unloading of long-term creep tests with air curing.

Concrete	01	02	03	28
1	**0.194**	**0.282**	**0.144**	**0.300**
2	**0.158**	**-**	**0.148**	**0.284**
3	-	0.260	0.152	0.252
4	0.153	0.226	0.152	0.267
5	0.197	0.290	0.153	0.274
6	0.170	0.310	0.179	0.287
7	0.185	0.311	0.164	0.288
8	0.175	0.317	0.154	0.274

Table **14.14-Stresslstrength-level**at unloading of long-term loading with sealed curing.

Concrete	01	02	03	28
1	**0.129**	**0.199**	**0.139**	**0.244**
2	**0.123**	**0.224**	**0.106**	**0.221**
3	**0.154**	**0.171**	**0.109**	**0.166**
4	0.196	0.173	0.148	0.268
5	0.174	0.214	0.144	0.243
6	0.125	0.255	0.134	0.236
7	0.189	0.264	0.154	0.273
8	0.149	0.264	0.142	0.230

Symbols used in **Figures 14.4 and 14.5:**

B= sealed curing (basic creep)
D= air curing (drying creep)
6.. = HPC mix, **Table 5.1**
…01= loading at **0.8** days' age with stresslcylinder strength = **0.84**
…02= loading at **2** days' age with stresslcylinder strength = **0.84**
…03= loading at **2** days' age with stresslcylinder strength = **0.42**
…28= loading at **28** days' age with stresslcylinder strength = **0.42**

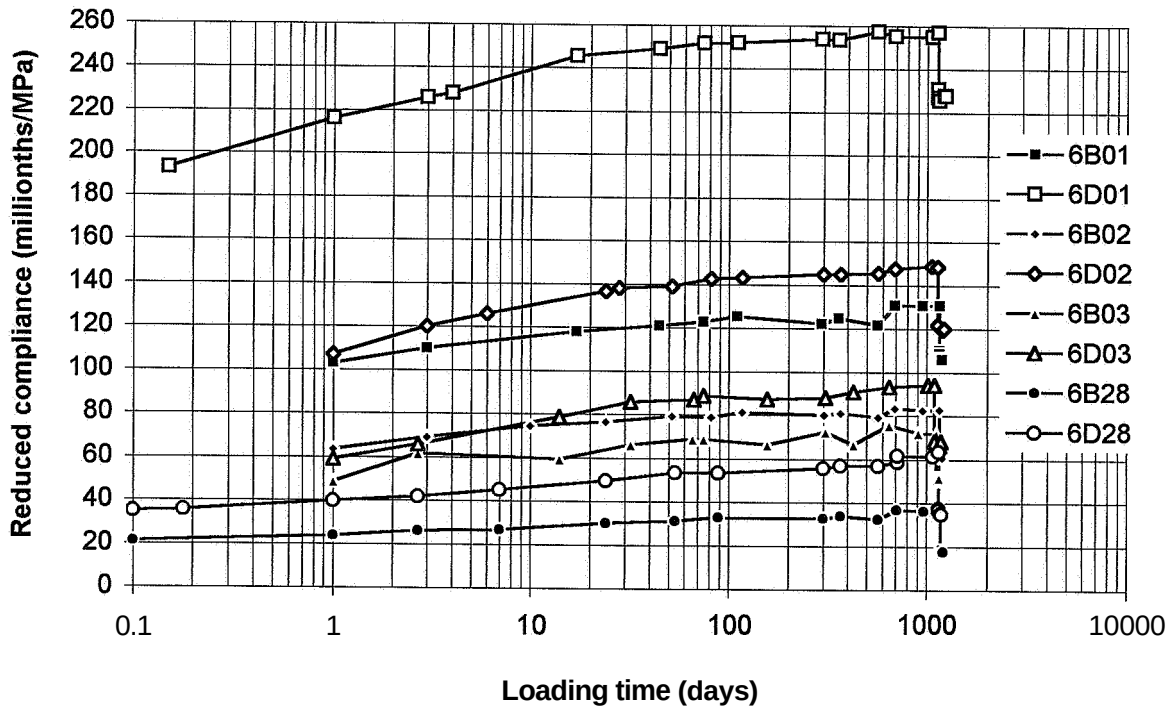

Figure **14.4-** Reduced compliance (regarding shrinkage) of mix **6** versus time.

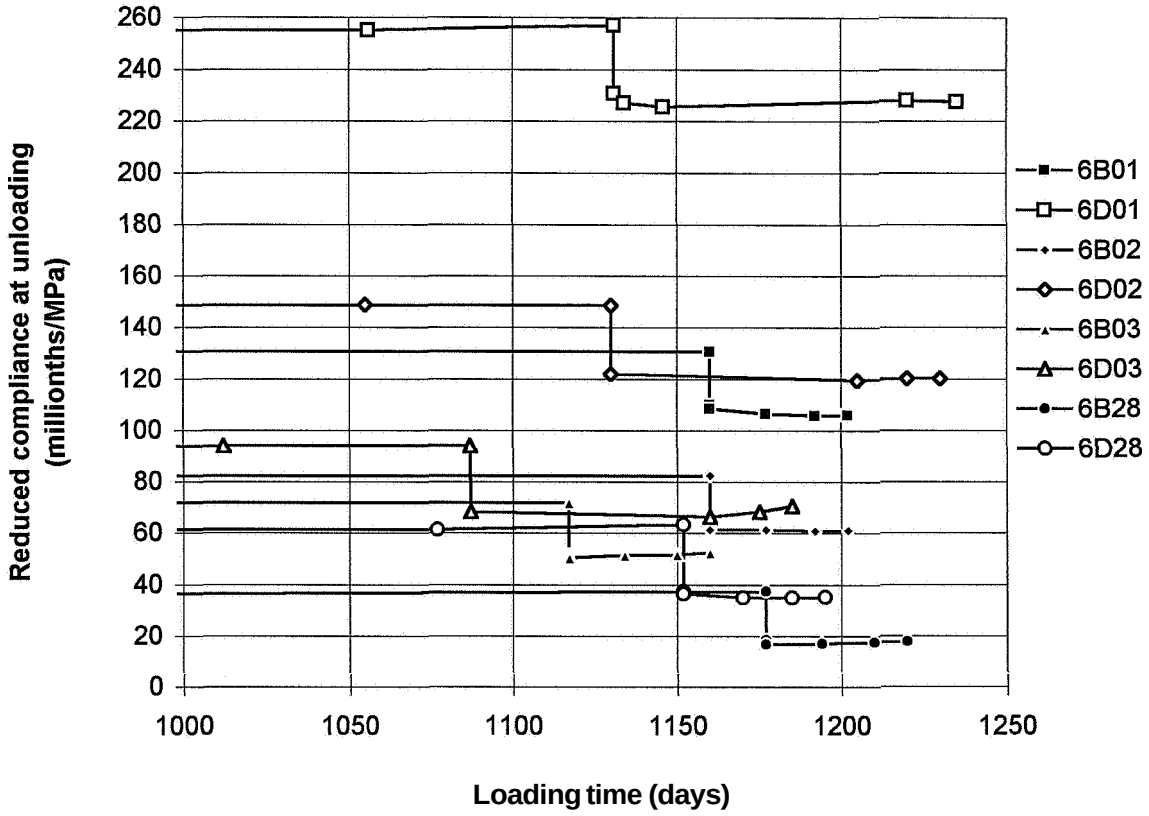

Figure 14.5 - Reduced compliance of HPC mix 6 at unloading versus time.

14.4 Sources of error and accuracy

14.4.1 Loading in the spring-loading device

A precision load-cell, which kept the loading within 0.05 kN, was used while the measurements were done. The load-level between the measurements was calculated using the elastic modulus. The variation of the loading when measuring was kept within ± 0.05 kN, corresponding to a stress variation of ± 0.04 MPa. The accuracy of the loading at measuring was thus fairly good. Between the measurement the maximum variation of loading was estimated as ± 3% at the commencement of the tests (high rate of creep) and as ± 1% at end of the long-term tests (low creep rate).

14.4.2 Deformations of mechanical devices

Calibrations with a Mitutoyo micrometer showed that the measurements were within ± 0.002 mm. The calibrations of the mechanical devices were performed to obtain an accuracy of ± 0.002 mm. The compliance, J(t,t'), was evaluated:

$$J(t,t') = \varepsilon/\sigma \qquad (14.1)$$

ε denotes the concrete deformation (millionths)
σ denotes the compressive stress (MPa)

The total accuracy was $\delta J(t,t')/J(t,t')$. The logarithm of equation (6.3) was:

$$\ln J(t,t') = \ln \varepsilon - \ln \sigma \qquad (14.2)$$

After differentiation the relative fault was obtained $[\delta \ln J(t,t')/\delta J(t,t') = 1/J(t,t')]$:

$$\delta J(t,t')/J(t,t') = \delta\varepsilon/\varepsilon - \delta\sigma/\sigma \qquad (14.3)$$

At 10 MPa stress the maximum fault was small according to equation (6.5) ≈ 0.03.

14.4.3 Eccentricity of loading and loading rate

The eccentricity was calculated at each loading. The eccentricity was normally within ≈ 5 mm. Adopting elastic conditions, the eccentricity, e, was calculated:

$$e = \sqrt{e_x^2 + e_y^2} \qquad (14.4)$$

$$e_x = \frac{a}{\Delta l}\left(\Delta l_1 - \frac{\Delta l_2}{2} - \frac{\Delta l_3}{2}\right) \qquad (14.5)$$

$$e_y = \frac{a \cdot \sqrt{3}}{\Delta l \cdot 2}(\Delta l_2 - \Delta l_3) \qquad (14.6)$$

$$\Delta l = \Delta l_1 + \Delta l_2 + \Delta l_3 \qquad (14.7)$$

a denotes the centre distance of the mechanical devices

Δl_i denotes deformation of mechanical device i

As was observed in Section 6 the maximal acceptable eccentricity would be 16 mm at a stress/strength ratio = 0.3 and 4.5 mm at a stress/strength ratio = 0.6. In **Tables** 14.15-14.18 the estimated eccentricities at long-term loading providing elastic conditions are given (mm). The eccentricity of the loading was more or less acceptable given that the concrete behaved more plastically at early ages. The reason for the eccentricities was probably the type of early curing of the cylinders. The cylinders were lying on their side, which may have caused the aggregate to move towards the bottom of the mould and the cement paste in the opposite direction. The reason for this kind of curing was to obtain plane and parallel ends in the specimen. Capping of the ends was not possible due to the large stresses in the concrete. In Sections 6 and 7 above it has been shown that the measured eccentricities did not affect either the creep rate or the deformation modulus after short-term loading. One way to detect the effect of eccentricity on creep was to compare the compliance between short-term and long-term loading after 2.7 days. **Figure** 14.6 shows the long-term compliance versus the short-term at eccentricities, e, varying between e=O and e=15 mm.

Table 14.15 - Eccentricities at loading of long-term creep tests of HPC with air curing.

Concrete	01	02	03	28
1	8.9	3.6	1.4	3.1
2	3.8	4.5	8.2	8.5
3	14.7	5.1	4.7	11.5
4	4	4.6	3.1	5
5	7	11.9	2.4	1.6
6	4	3.7	4.1	3.1
7	2.4	4.2	9.4	5.5
8	7	0.5	9.6	3.2

Table 14.16 - Eccentricities at loading of long-term tests of HPC loading with sealed curing.

Concrete	01	02	03	28
1	0.8	0.7	3.4	4.7
2	0.8	9	1.2	7.9
3	4.8	15.2	4.4	8.2
4	7.6	1	9.1	3.7
5	0	2.5	12	2.2
6	6.5	4.5	6	4.4
7	5.6	4.3	11	6
8	5.7	5.1	11.6	2.8

Table 14.17 - Eccentricities at unloading of long-term creep tests of HPC with air curing.

Concrete	01	02	03	28
1	6	6	3.2	3.4
2	8.8	1.5	5.2	3.7
3	7.2	4.6	7.2	5.4
4	5.4	3	5.5	3.3
5	1.8	11.9	6.6	4.1
6	5.4	1.6	11	1.8
7	5.4	5.4	12.6	6
8	7.7	0.3	6.5	2.2

Table 14.18 - Eccentricities at unloading of long-term creep tests of sealed HPC.

Concrete	01	02	03	28
1	6.6	3.7	3	7.2
2	5.5	3.7	13.3	3
3	1.8	11.1	3.3	12.1
4	5.3	2	8	10.8
5	8.4	7.4	7.3	1.1
6	9.5	6.9	11	2.6
7	4.6	5.5	7.2	6.3
8	12.5	7.4	5.3	9.8

The eccentricity did not systematically influence the measured long-term compliance. Concretes 328 and 502 exhibited e=12, which resulted in about 20% larger long-term compliance than short-term. Concrete 301 exhibited e=15 mm but in this case the long-term compliance was equal to the short-term. **Figure 14.6** also shows that the rate of loading (about 1700 MPa/s at quasi-instantaneous loading and 1 MPa/s at long-term loading) did not affect the compliance after 66 h. (The loading was applied without a load-peak, cp. Sections *6* and 12 and **Appendices 6 and 12.)**

14.4.4 Effects of lateral strain

The effect of the Poisson's ratio was obtained in Section 11 above. The decrease of the compliance owing to Poisson's ratio was estimated to $\upsilon^2 \approx 0.02$, i.e. very little.

14.4.5 Weight losses of specimens with sealed curing during the creep

The weight of the specimens was obtained before and after the long-term tests. **Tables 14.19 and 14.20** provide the weight losses during the test period. Specimens used for creep tests and for studies of shrinkage were identically moisture insulated.

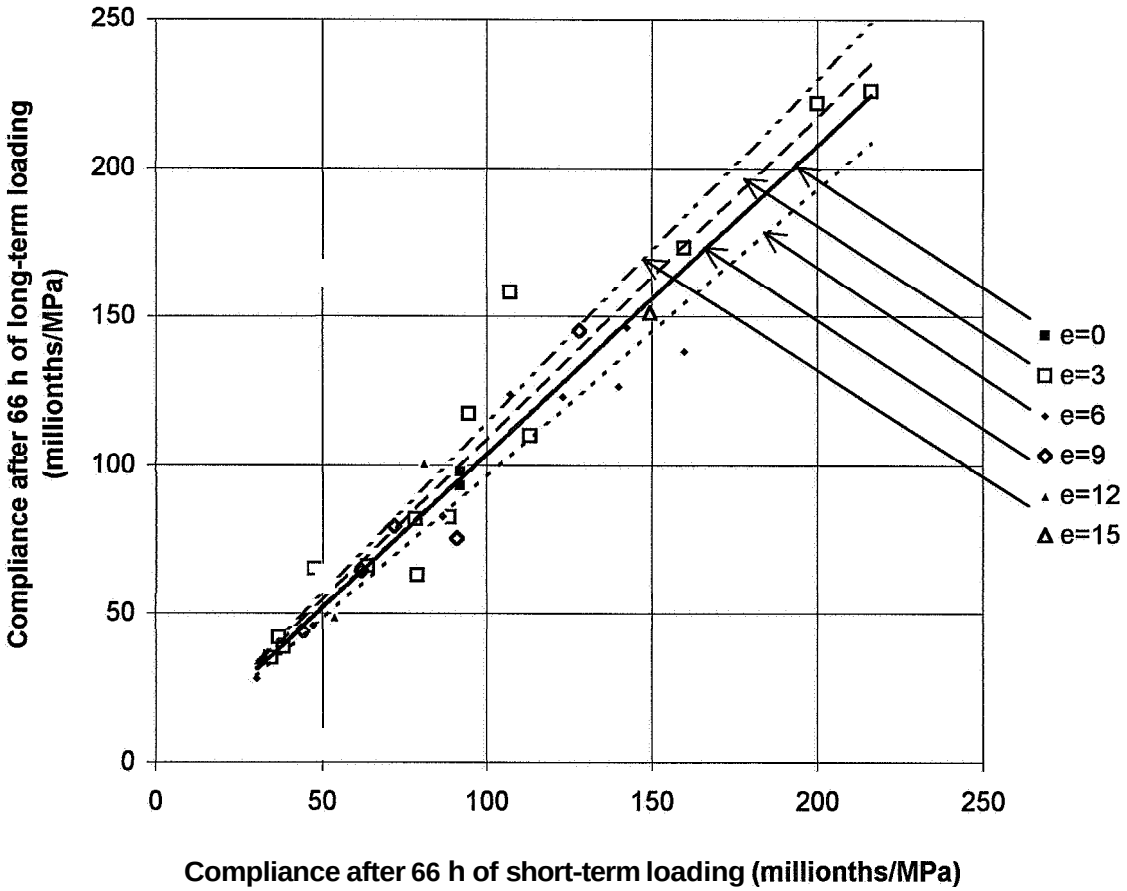

Figure 14.6 - Long-term compliance after 66 h of loading versus the short-term compliance likewise after 66 h of loading at varying eccentricities, e (mm).

Table 14.19 - Relative loss of weight with air curing, w_e/w.

Concrete	01	02	03	28
1	0.147	0.052	0.195	-0.082
2	0.159	0.058	0.029	-0.063
3	0.235	0	0.049	-0.092
4	0.212	0.237	0.235	-0.036
5	-	0.077	-	0.005
6	0.125	0.058	0.168	-0.008
7	0.202	0.166	0.189	0.060
8	-	0.088	-	0.038

Table 14.20 - Relative loss of weight with sealed curing, w_e/w.

Concrete	01	02	03	28
1	-	0.085	0.034	0.042
2	0.05	0.035	0.028	0.055
3	0.025	0.078	0.033	0.028
4	0.034	0.053	0.044	0.023
5	0.032	0.030	0.025	0.018
6	0.038	0.012	0.038	0.017
7	0.029	0.027	0.045	0.027
8	0.013	0.053	-	10.032

w= mixing water, w_e= evaporated water from loading until unloading

Sealed specimens lost less than 3 g of moisture over 3 years. The long-term losses of weight were of the same magnitude as the losses of weight during the shrinkage tests, Section 8. The reduction of shrinkage strain from the creep strain was thus accurate. The specimens with air curing decreased in weight until about 28 days' age. Then the weight increased due to carbonation, cp. the 28-day specimens.

14.5 Analysis of long-term creep

14.5.1 Stress and time dependence with air curing

The compliance, J(t,t′), was separated into two parts: one part expressed the deformation due to the initial loading; the other part expressed the creep of loading:

$$J(t,t') = 1000/D_{t'} + a_D \cdot \int d(t-t')/(t-t') \qquad (14.8)$$

a_D denotes compliance rate with air curing [millionths/(MPa·day)]
t denotes age of the concrete (days)
t' denotes age at loading (days)
$D_{t'}$ denotes the deformation modulus at loading, Section 7 above (GPa)
J(t,t′) denotes the compliance (specific creep, millionths/MPa)

Appendix 14 was used to correlate the stress and time dependence with air curing. **Figure 14.7** shows the compliance rate of mature HPC versus w/c. The eccentricity had no effect on the creep rate, **Figure 14.7. Figure 14.8** shows the creep rate of HPC young at loading versus the relative 28-day strength, f_c/f_{c28}, at loading. The following equation was obtained for the creep rate, a_D:

$$a_D = k_{ai} \cdot 513 \cdot [(w/c)^2 - 0.6 \cdot (w/c) + 0.0959] - k_{as} [1.83 + 2.37 \cdot (\sigma/f_c)] \cdot \ln(f_c/f_{c28}) \qquad (14.9)$$

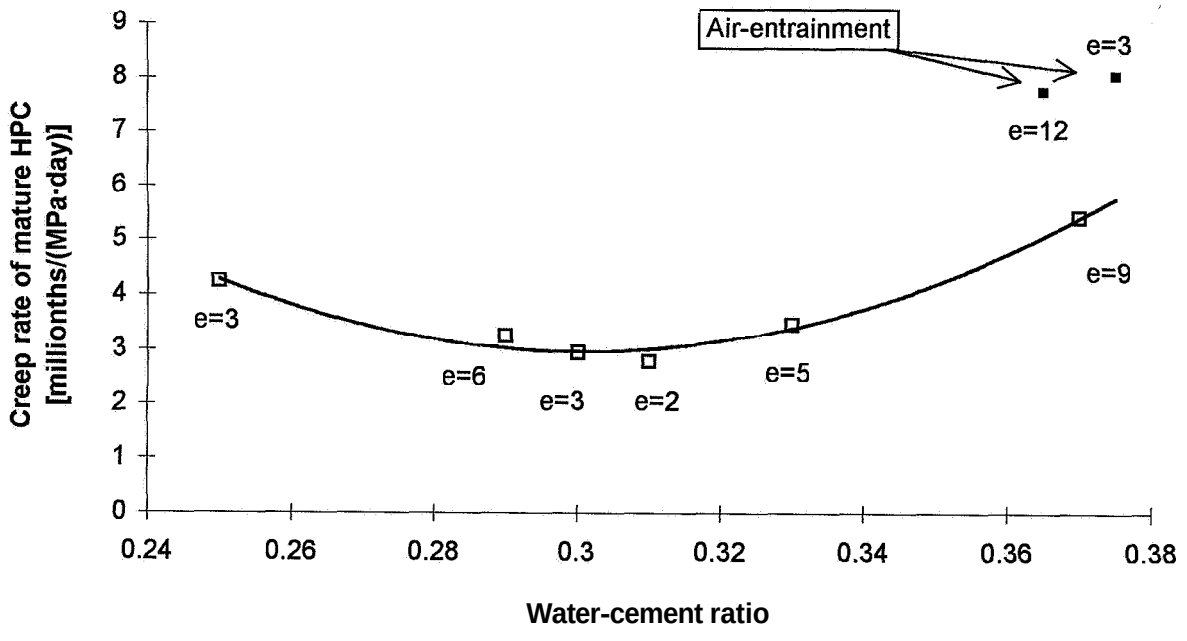

Figure 14.7 - Compliance rate of mature drying HPC versus w/c. e= eccentricity at loading (mm).

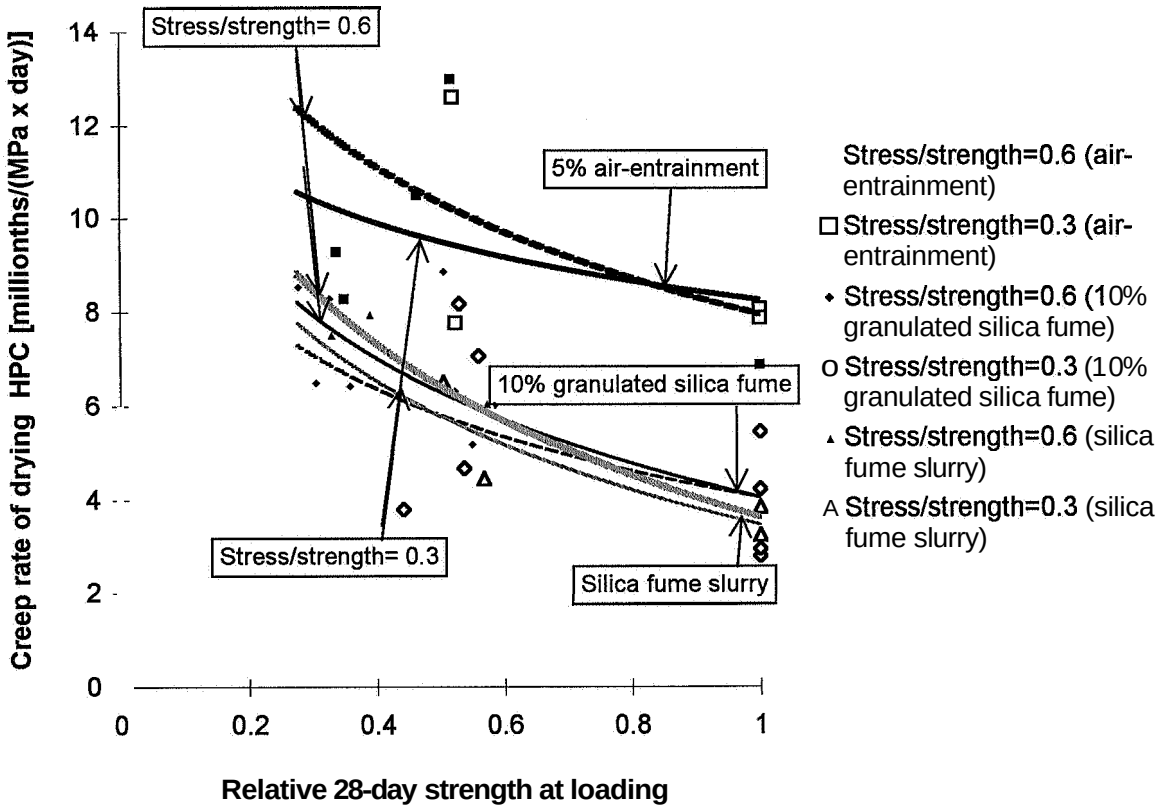

Figure 14.8 - Creep rate of air-cured HPC, young when loading, versus relative 28-day strength.

a_D denotes compliance rate with air curing [millionths/(MPa·day)]
f_c denotes cube strength at loading (MPa)
f_{c28} denotes 28-day cube strength (MPa)
k_{as} = 0.8 for HPC with 5% air-entrainment; k_{as} = 1.3 for HPC with silica fume slurry, k_{as} = 1 otherwise
k_{ai} = 1.5 for HPC with 5% air-entrainment; k_{ai} = 1 otherwise

14.5.2 Stress and time dependence with sealed curing

The compliance during 4 years was separated into two parts: one part expressed the deformation due to the initial loading; the other part expressed the creep of loading:

$$J(t,t') = 1000/D_{t'} + a_B \cdot \int d(t-t')/(t-t') \qquad (14.10)$$

a_B denotes compliance rate with sealed curing [millionths/(MPa·day)]
t denotes age of the concrete (days)
t' denotes age at loading (days)
$D_{t'}$ denotes the deformation modulus at loading, Section 7 above (GPa)
$J(t,t')$ denotes the compliance (specific creep, millionths/MPa)

Appendix 14 was used to correlate the stress and time dependence with sealed curing. **Figure** 14.9 shows the compliance rate of mature HPC versus the water-cement ratio, w/c. The eccentricity at loading is indicated in **Figure** 14.9. The eccentricity had no effect on the creep rate. **Figure** 14.10 shows the creep rate of HPC young at loading versus the relative 28-day strength, f_c/f_{c28} at loading. The following equation was obtained for the creep rate, a_B:

$$a_B = k_{s5} \cdot 231 \cdot [(w/c)^2 - 0.594 \cdot (w/c) + 0.0952] - k_{s5} [2.83 - 3 \cdot (\sigma/f_c)] \cdot \ln(f_c/f_{c28}) \quad (14.11)$$

a_B denotes compliance rate with sealed curing [millionths/(MPa·day)]
f_c/f_{c28} denotes the relative 28-day strength at loading $\{0.3 < f_c/f_{c28} < 1\}$
k_{s5} = 1.5 for HPC with 5% silica fume or 10% silica fume slurry; $k_{s5} = 1$ otherwise

14.5.3 Dependence on strength growth

It was of interest to obtain a relationship between creep and strength that was independent of time. The rate of strength growth was estimated logarithmically as was the rate of creep from age of loading until unloading. The strength of the specimens when loaded and unloaded was obtained from **Appendix** 5 and from **Tables** 14.1-14.6 above on studies of exactly the same type of concretes. **Figures** 14.11 **and** 14.12 show the rate of long-term creep of drying and sealed HPC versus the rate of strength growth between loading and unloading of the specimen.

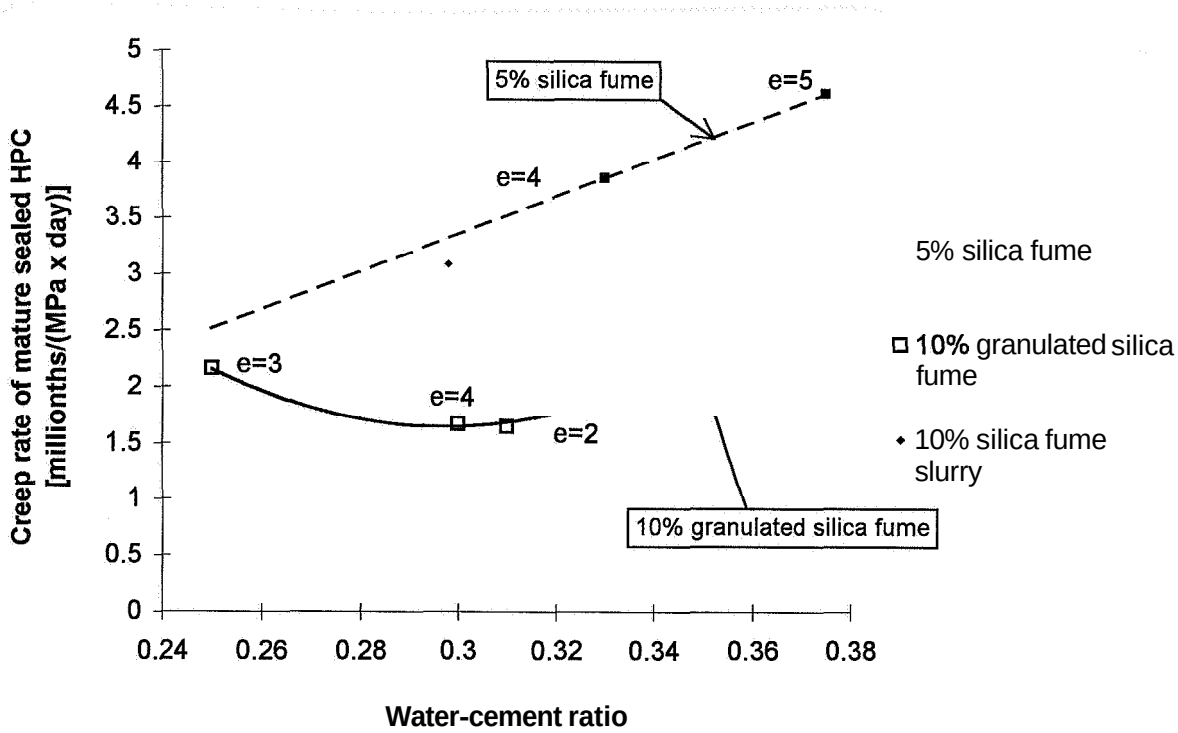

Figure 14.9 - Compliance rate of sealed mature HPC versus w/c. e= eccentricity at loading (mm).

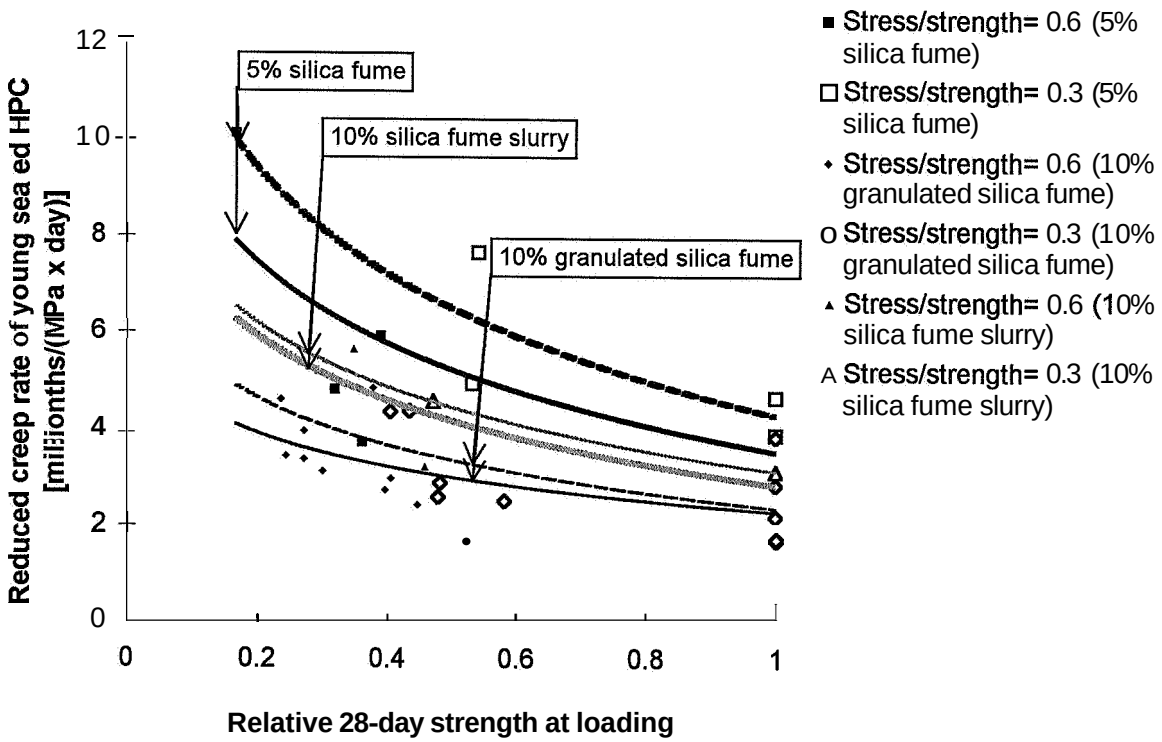

Figure 14.10 - Compliance rate of sealed HPC young at loading versus relative 28-day strength. Full line denotes stress/strength ratio, $\sigma/f_c = 0.3$. Dotted line: $\sigma/f_c = 0.6$.

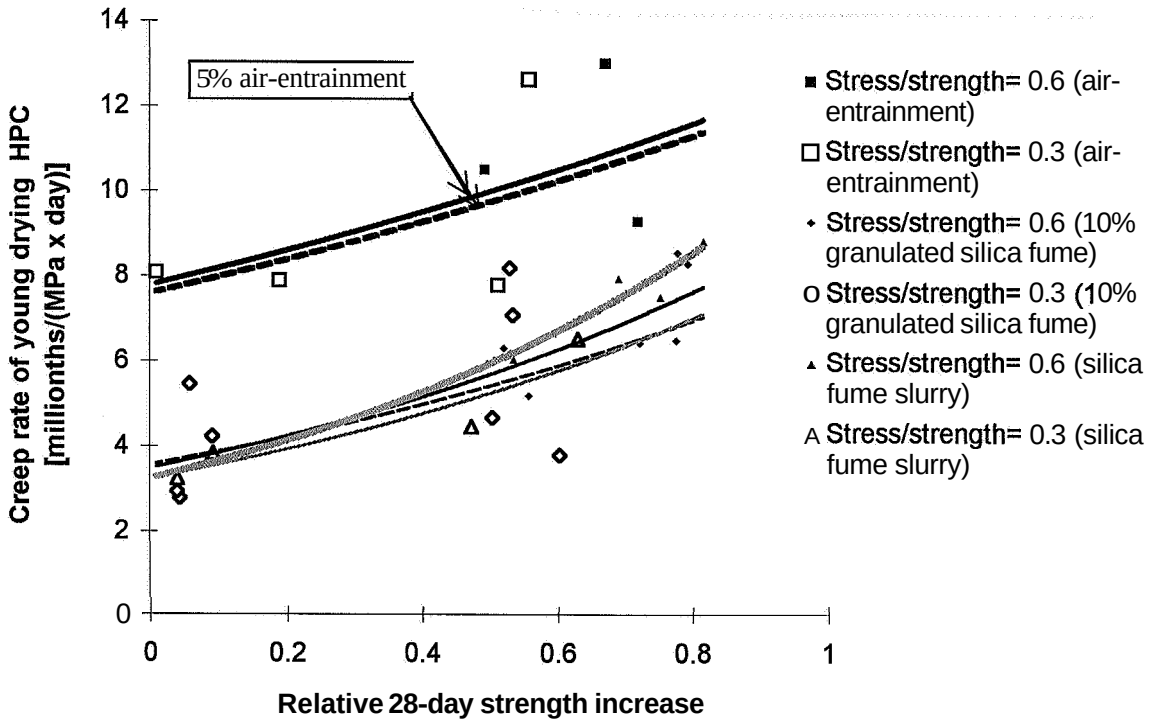

Figure 14.11 - Creep rate of air-cured HPC versus the rate of strength growth.

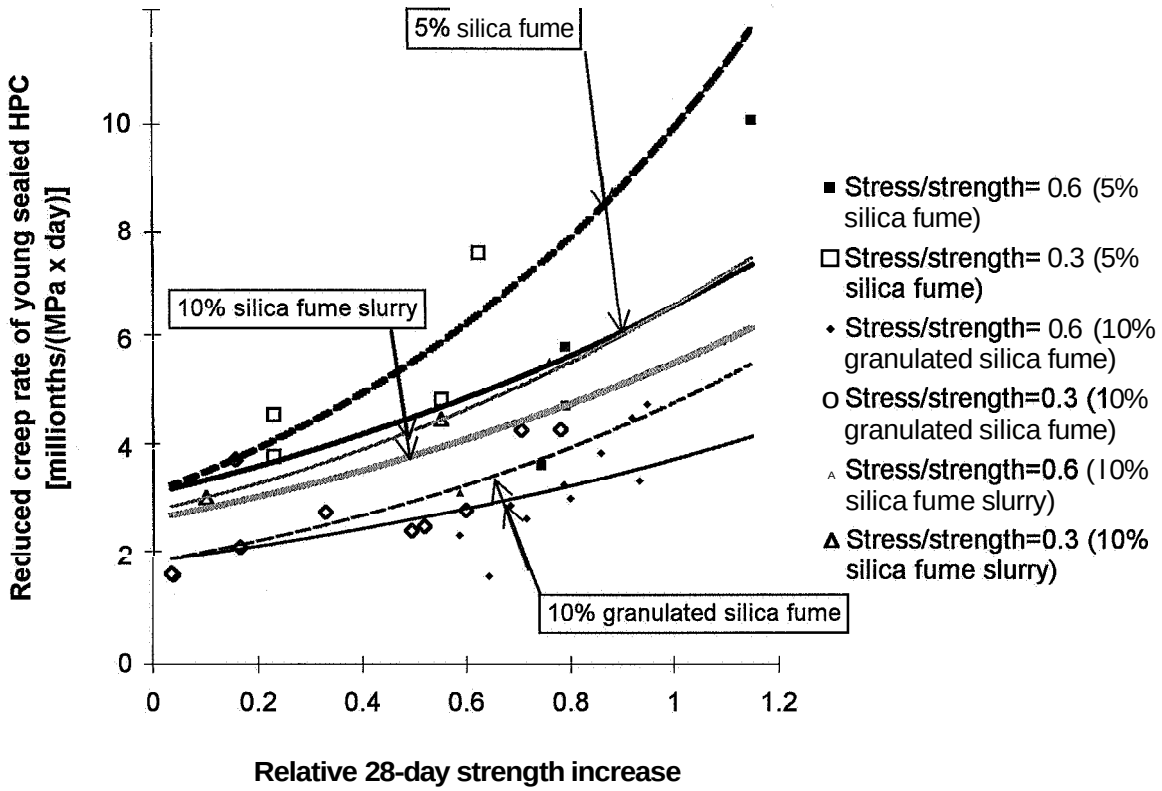

Figure 14.12 - Creep rate of sealed HPC versus the rate of strength growth.

From **Figures 14.11 and 14.12** the following relationships were obtained:

$$J_D(t,t') = 1000/D_{t'} + a_{Dm} \cdot e^{0.48 \cdot kD \cdot [(\sigma/fc) + 1.44] \cdot (dfc/fc28)} \cdot \int d(t-t')/(t-t') \qquad (14.12)$$

$$J_{Dai}(t,t') = 1000/D_{t'} + a_{Dm} \cdot e^{0.5 \cdot (dfc/fc28)} \cdot \int d(t-t')/(t-t') \qquad (14.13)$$

$$a_{Dm} = k_{ais} \cdot 513 \cdot [(w/c)^2 - 0.6 \cdot (w/c) + 0.0959] \qquad (14.14)$$

$$J_B(t,t') = 1000/D_{t'} + a_{Bm} \cdot e^{0.82 \cdot kB \cdot [1.44 - (\sigma/fc)] \cdot (dfc/fc28)} \cdot \int d(t-t')/(t-t') \qquad (14.15)$$

$$a_{Bm} = k_{s5} \cdot 231 \cdot [(w/c)^2 - 0.594 \cdot (w/c) + 0.0952] \qquad (14.16)$$

a_{Bm} denotes compliance rate of sealed mature HPC [millionths/(MPa·day)]
a_{Dm} denotes compliance rate of air-cured mature HPC [millionths/(MPa·day)]
ai denotes 5% air-entrainment
df_c denotes relative 28-day strength increase between loading and unloading
k_{ais} = 1.5 for HPC with 5% air-entrainment; k_{ais} = 0.8 for HPC with silica fume slurry; k_{ais}=1 otherwise
k_{s5} = 1.5 for HPC with 5% silica fume or for HPC with 10% silica fume slurry; k_{s5} = 1 otherwise

k_B = **1.14** for HPC with 5% air-entrainment; k_B = **0.97** for silica fume slurry; k_B = **1** otherwise
k_D = **1.2** for HPC with silica fume slurry; k_D = **1** otherwise
f_c denotes compressive strength at loading (MPa)
s denotes silica fume slurry
t denotes age of the concrete (days)
t' denotes age at loading (days)
B denotes sealed curing
D denotes air curing
$D_{t'}$ denotes the deformation modulus at loading, Section 7 (GPa)
J(t,t') denotes the compliance (specific creep, millionths/MPa)

14.5.4 Dependence on internal relative humidity

The increased creep rate during drying was explained by the moisture distribution of the specimen. During the drying a certain amount of shrinkage occurred at the surface of the concrete, which caused an uneven distribution of stress in the cylinder. **Figure 14.13** shows the creep rate versus the relative strength, f_c/f_{c28}, at loading and the difference between the internal relative humidity of the inner part, $Ø_i$, and the surface, $Ø_s$, of the cylinder (= ambient relative humidity), $AO = Ø_i - 0$,. From **Figure 14.13** the following correlation was calculated (millionths/MPa·h):

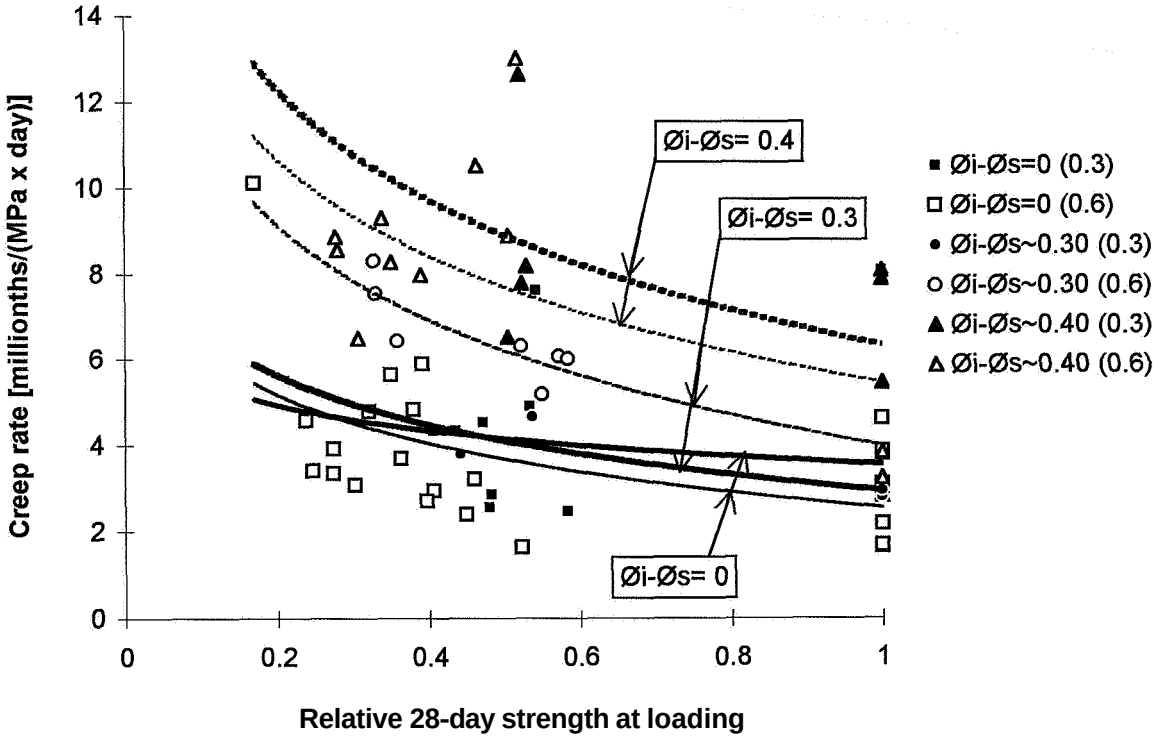

Figure **14.13** - Creep rate versus relative strength at loading. Difference between internal relative humidity of inner part, $Ø_i$, and surface, $Ø_s$, at loading. Dotted line: stresslstrength = **0.6.** Solid line: stresslstrength = 0.3. ( )= stresslstrength ratio.

$$J_{0.3}(t,t') = 1000/D_{t'} + [a_{Bm} - 6.1\cdot(\Delta\emptyset + 0.11)\cdot\ln(f_c/f_{c28})]\cdot\int d(t-t')/(t-t') \quad \{\sigma/f_c = 0.3;\ 0.5 < f_c/f_{c28} < 1\} \qquad (14.17)$$

$$J_{0.6}(t,t') = 1000/D_{t'} + [a_{Bm} - 4.3\cdot(\Delta\emptyset + 0.39)\cdot\ln(f_c/f_{c28})]\cdot\int d(t-t')/(t-t') \quad \{\sigma/f_c = 0.6;\ 0.2 < f_c/f_{c28} < 0.5\} \qquad (14.18)$$

a_{Bm}	denotes compliance rate of sealed mature HPC, equation (4.16)
f_c/f_{c28}	denotes the relative 28-day strength at loading
$J(t,t')$	denotes the compliance (specific creep, millionths/MPa)
$A\emptyset = \emptyset_i - O$,	denotes difference in internal relative humidity between the inner part of the cylinder at loading and the surface of the cylinder
0.3	denotes relative stress/strength-level at loading, $\sigma/f_c = 0.3$
0.6	denotes relative stress/strength-level at loading, $\sigma/f_c = 0.6$

However, after about 1 month of creep almost no difference existed in relative humidity between the ambient climate and the internal part of the drying cylinders, **Figure 5.24. Figure 14.14** shows the creep rate versus the internal relative humidity of the cylinders after 1 month. No correlation of creep rate versus relative humidity was possible owing to low significance in **Figure 14.14.**

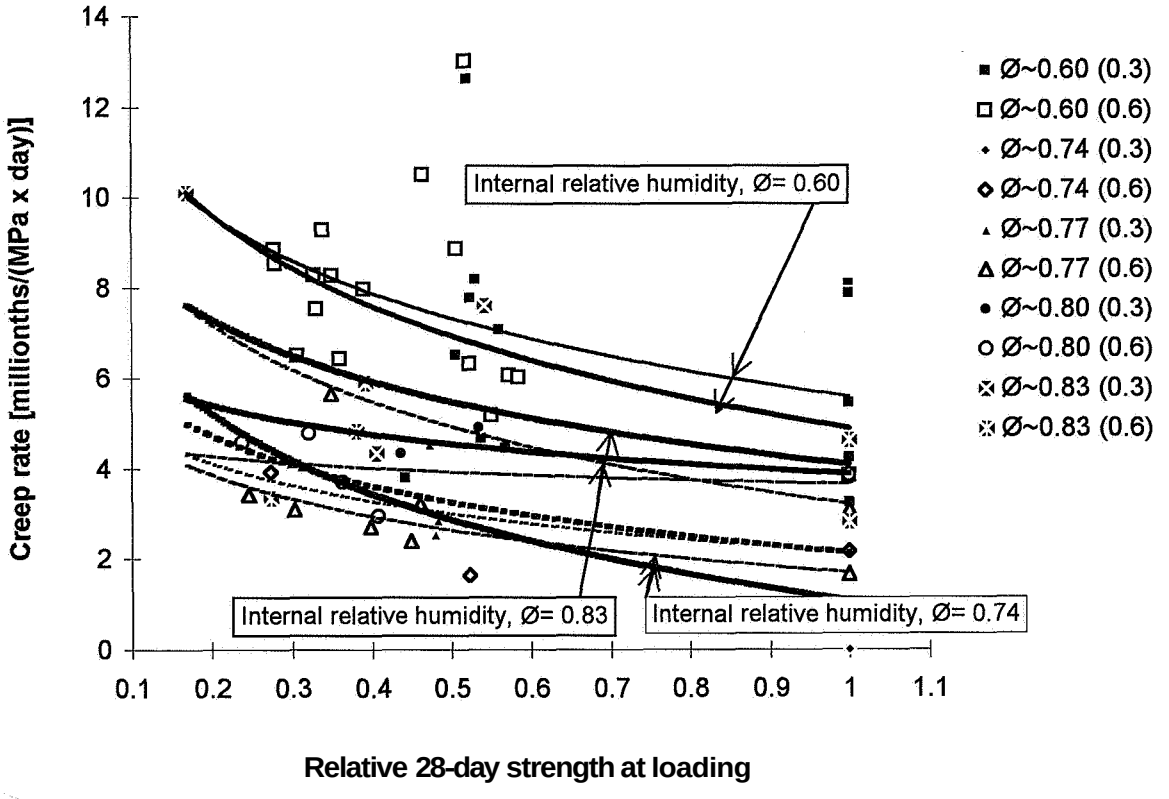

Figure 14.14 - Creep rate versus internal relative humidity of the cylinders after 1 month. Thin line: stresslstrength = 0.6. Solid line: stress/strength = 0.3.

14.5.5 Elasticity

All concretes were unloaded at an age varying between 3 and 4 years. Simultaneously the deformation, the mechanical properties and the weight of the concrete were established, Section 5. **Tables** 14.19-20 give the difference in compliance at unloading, $\Delta J(t,t')$, (millionths/MPa). The long-term elastic modulus was defined as the inverted compliance at unloading, **Figure 1.1.**

$$E_{t-t'} = \frac{1000}{\Delta J(t,t')} \qquad (14.19)$$

$E_{t-t'}$ denotes the long-term modulus of elasticity (GPa)
$\Delta J_l(t,t')$ denotes the difference in compliance at unloading (millionths/MPa)

Table 14.19 - Compliance at unloading of air-cured HPC (millionths/MPa).

Concrete	**01**	**02**	**03**	**28**
1	33.9	31.7	36.1	32.7
2	29.7	31.4	31.0	35.1
3	31.7	35.7	30.2	33.7
4	24.9	28.1	27.1	27.2
5	28.3	28.7	30.5	27.0
6	26.2	26.6	25.6	26.1
7	26.1	22.7	21.7	22
8	24.4	26.1	24.8	24.4

Table 14.20 - Compliance at unloading of sealed HPC (millionths/MPa).

Concrete	01	02	03	28
1	26.1	25	25.3	21.6
2	20.3	19.8	20.2	22.1
3	20	24.3	22.3	21.6
4	20.2	22.8	20.7	20.6
5	20	21	20	20.2
6	20.6	21	20.3	19
7	22.4	21.6	23.3	22.1
8	20.8	23.5	23.4	22.4

Symbols in the Figures and Tables:

B= sealed curing
D= air curing
6…= HPC mix, **Table** 5.1
…01= loading at 0.8 days' age with stresslcylinder strength = 0.84
…02= loading at 2 days' age with stresslcylinder strength = 0.84
…03= loading at 2 days' age with stresslcylinder strength = 0.42
…28= loading at 28 days' age with stresslcylinder strength = 0.42

In Figure 14.15 the elastic modulus is shown versus the current cube strength. **Figure** 14.16 shows the elastic modulus of concrete that was mature at loading versus the strength. From **Figure** 14.16, which shows the elastic modulus of HPC that was mature at loading, no influence of air-entrainment nor of kind of silica fume was observed. As reported in Section 10 above, the strain at unloading was dependent on the maturity of HPC at loading. **Figure** 14.15 shows an almost constant correlation between the elastic modulus and strength of drying concrete taking into account the strength at unloading, f_{cun}, and the age at loading, t' (GPa):

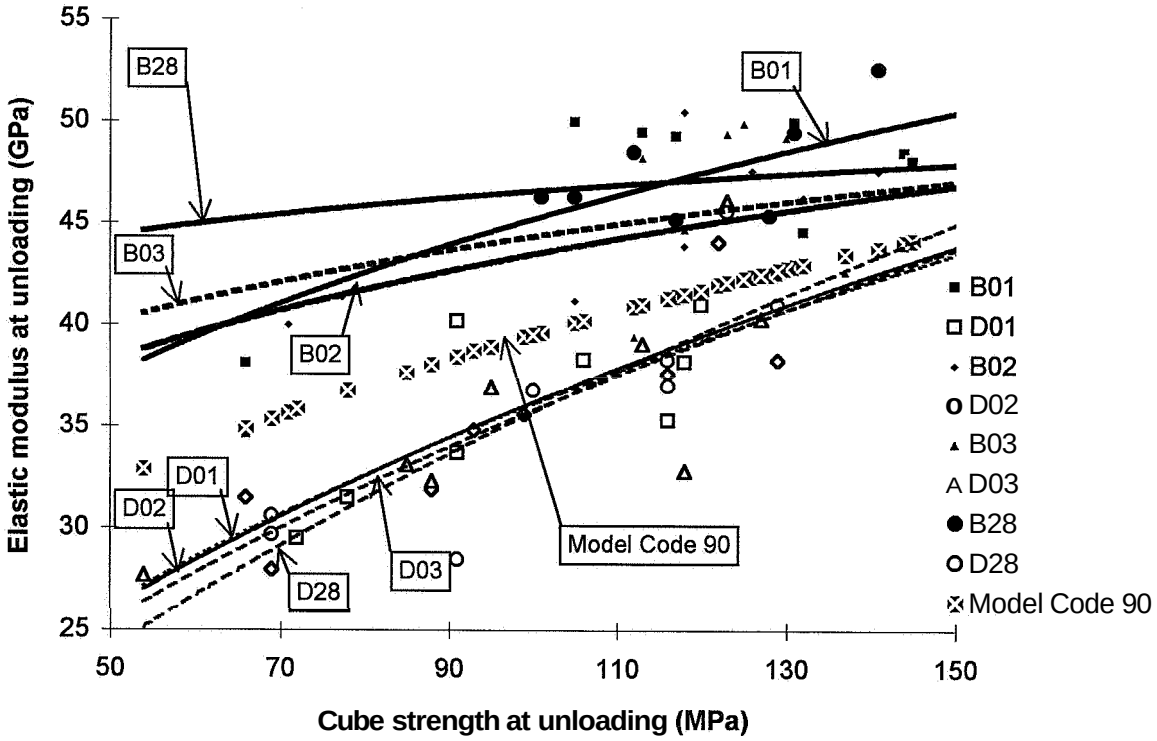

Figure **14.15** - Elastic modulus versus of the current cube strength at unloading. Comparison with the extension of Model Code 90. B= sealed curing, D= air curing.

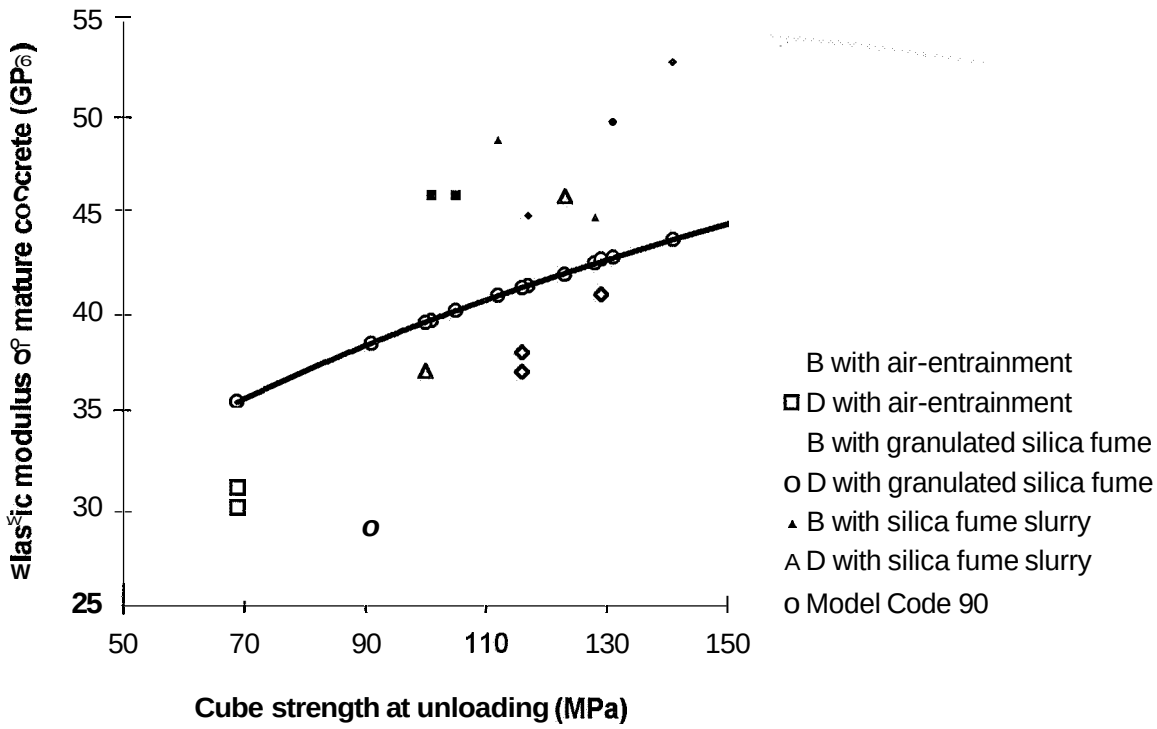

Figure **14.16** - Elastic modulus of concrete that was mature at loading versus the strength. Symbols besides those given above: B= sealed curing, D= air curing.

$$E_D = 0.0543\cdot(76\text{-}t')\cdot(f_{cun})^{0.0035\cdot(t'+134)} \quad \{1<t'<28 \text{ days}\} \quad (14.20)$$

f_{cun} denotes the compressive cube strength at unloading (MPa)
t' denotes the age at loading (days)
E_D denotes the elastic modulus of drymg concrete (GPa)

The elastic modulus of drying HPC was about 5 GPa less than the extension of Model Code 90, **Jaccoud and Leclerq** (1995). The elastic modulus was also smaller in the present long-term experiments than in the short-term creep, Section 10, probably due to the fact that the HPC had been drying for at least 3 years. Sealed HPC exhibited about 8 MPa larger elastic modulus than Model Code 90 perhaps since pores filled to a higher degree prevent movements of moisture especially at early ages. The dependence on age was explained by the self-desiccation of the HPC that partly emptied the pores and allowed for moisture movements in the structure. From **Figure** 14.15 the following correlation between the elastic modulus and strength of sealed concrete was calculated (GPa):

$$E_B = 6.02\cdot[2.4+\ln(t')]\cdot(f_{cun})^{0.0545\cdot[4.37-\ln(t')]} \quad \{1<t'<28 \text{ days}\} \quad (14.21)$$

f_{cun} denotes the compressive cube strength at unloading (MPa)
t' denotes the age at loading (days)
E_B denotes the elastic modulus of sealed concrete (GPa)

As mentioned above and also shown in section 10, the elastic modulus was dependent on the internal relative humidity at unloading. **Figure** 14.17 shows the elastic modulus versus unloading strength at different relative humidity, O. The following equations were calculated (GPa):

$$E_{\emptyset = 0.60} \approx 3.6\cdot\sqrt{f_{cun}} \quad (14.22)$$

$$E_{\emptyset = \approx 0.80} \approx 17.6\cdot(f_{cun})^{0.2} \quad (14.23)$$

f_{cun} denotes the compressive cube strength at unloading (MPa)

14.5.6 Viscous-elastic and viscous-plastic compliance compared with elastic compliance ["creep coefficient", Bazant (1995)]

From a practical point of view it was of great interest and essential to relate the different kinds of creep such as viscous-plasticity and viscous-elasticity to the elasticity at unloading. From this comparison different kinds of creep coefficients may be evaluated dependent on definition. **Appendix** 14 give the compliance of the long-term creep at unloading. **Tables** 14.21-14.22 give the difference in compliance between 1 minute and 1 month after unloading (viscous-elasticity). **Tables** 14.23-14.24 shows the remaining compliance 1 month after unloading (viscous-plasticity). Symbols in the tables are given above.

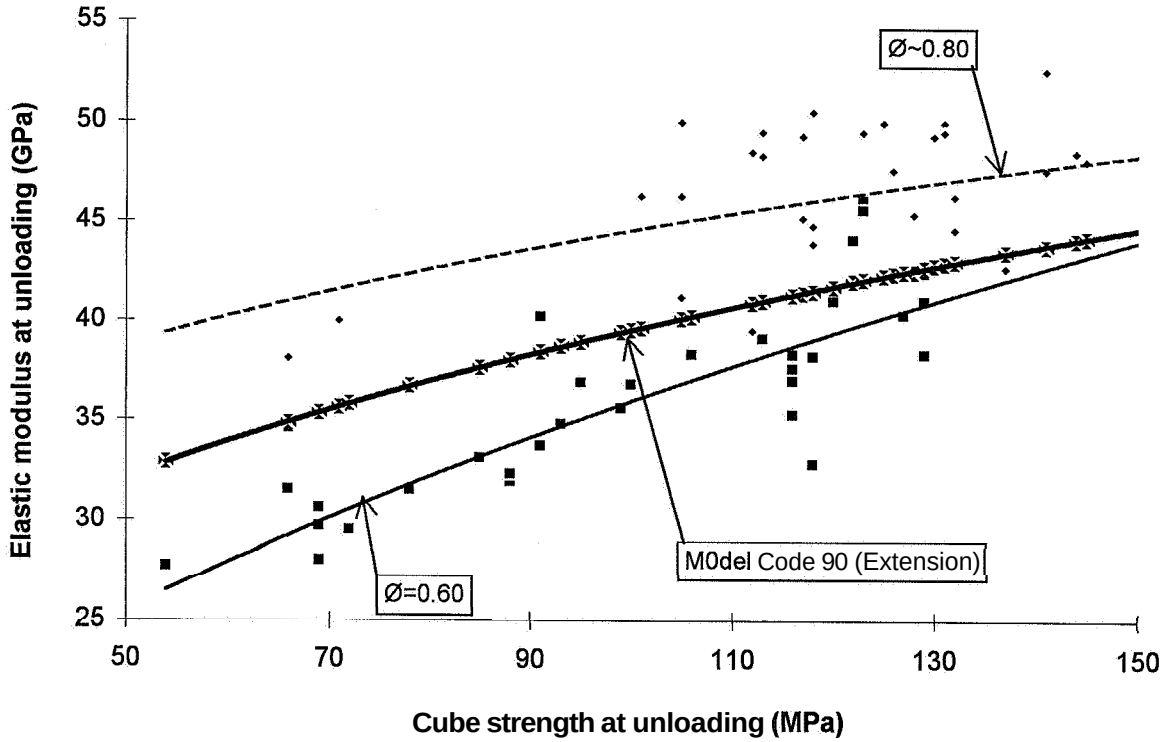

Figure 14.17 – Elastic modulus at unloading versus strength. Relative humidity, **O.**

Table 14.21 - Difference in compliance of HPC with air curing 1 month after unloading (viscous-elasticity) (millionths/MPa).

Concrete	01	02	03	28
1	3.4	8.9	9.6	4
2	5.4	4.1	4.6	5.1
3	5.6	6.8	1.7	4.6
4	6	0.3	0.5	0.4
5	0.3	4.8	-3	0.5
6	3.2	1.7	0	0.5
7	1.2	0	-0.2	0.4
8	2.1	0.9	1.1	0

Table 14.22 - Difference in compliance of HPC with sealed curing 1 month after unloading (viscous-elasticity) (millionths/MPa).

Concrete	01	02	03	28
1	-1.6	8	8.8	2.7
2	3.9	3.4	0.2	2.8
3	0.3	-0.5	0.5	2.2
4	5	0.8	2.5	2
5	3.5	3.1	1.5	1.52
6	2.8	0.7	-0.1	1
7	2.7	1.4	1.4	1.2
8	1.7	1.9	1.2	0.8

6…= HPC mix, **Table 5.1**
…01= loading at 0.8 days' age with stresslcylinder strength = 0.84
…02= loading at 2 days' age with stresslcylinder strength = 0.84
…03= loading at 2 days' age with stresslcylinder strength = 0.42
…28= loading at 28 days' age with stresslcylinder strength = 0.42

Mature concrete was analysed first. **Figure 14.18** gives the compliance at unloading of concrete that was mature at loading.

Table **14.23** - Remaining compliance **1** month after unloading of air-cured HPC (viscous-plasticity, millionths/MPa).

Concrete	01	02	03	28
1	141	133	130	82.1
2	173	144	91.9	39.6
3	161	156	94.7	70.3
4	240	165	86.1	41.3
5	124	111	55	28.5
6	228	121	68.3	34.8
7	194	95	69.2	23.6
8	143	96.1	91.9	36.2

Table **14.24** - Remaining compliance **1** month after unloading in HPC with sealed curing (viscous-plasticity, millionths/MPa).

Concrete	01	02	03	28
1	176	91	59.7	35.7
2	95.6	70.8	61	35.4
3	117	89.4	65.7	24.9
4	137	115	62.5	40.6
5	89.1	59.6	48.2	14.2
6	106	60.9	51.6	17.5
7	121	79.1	61.6	25.5
8	86.3	39.1	35.8	15.8

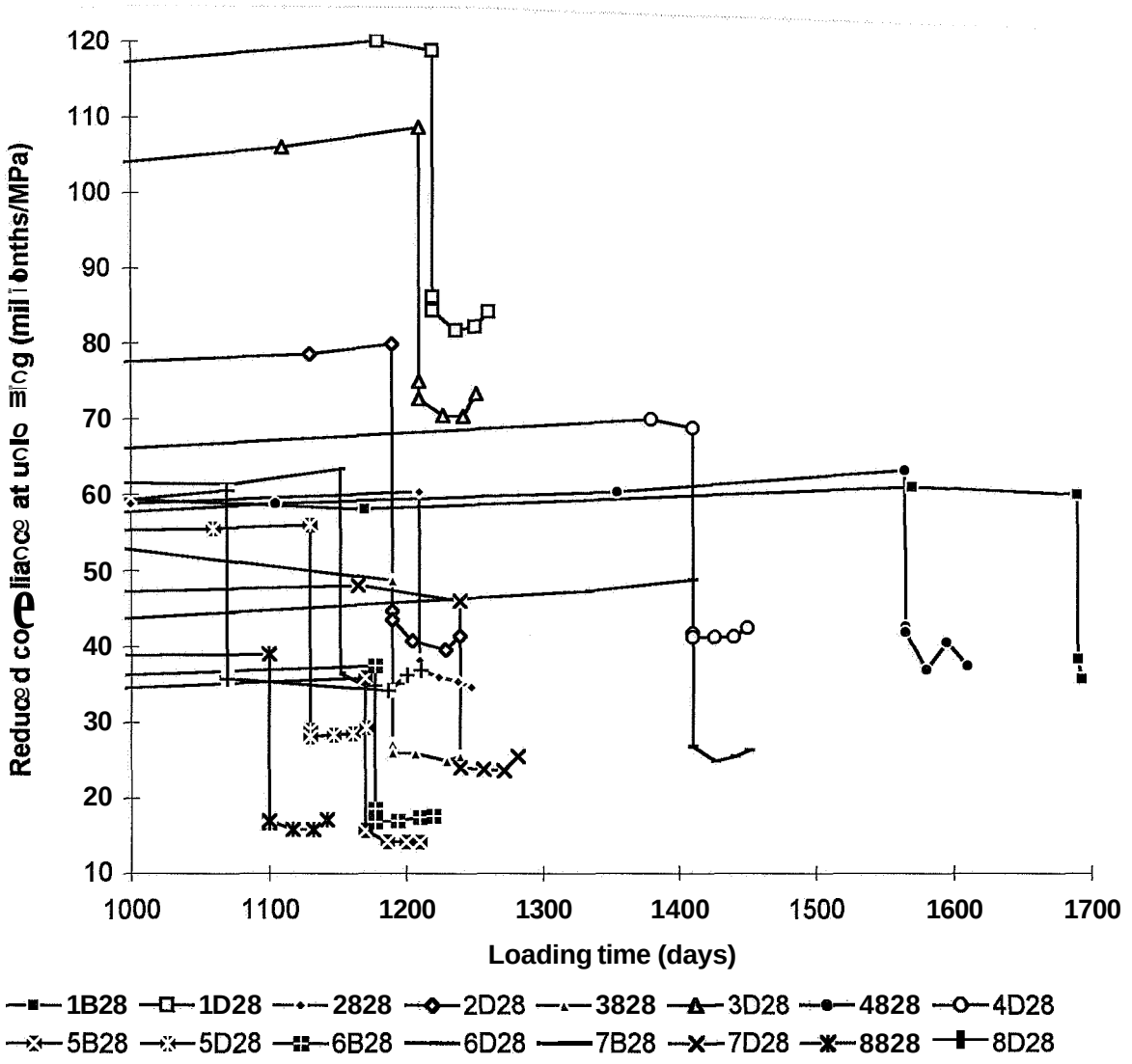

Figure **14.18** - Compliance at unloading of HPCs that were mature when loaded.

Figures 14.19-14.22 give the ratio of viscous-plastic compliance or viscous-elastic compliance to the elastic compliance at unloading with air curing and sealed curing. The eccentricity at unloading is shown in **Figures 14.19-14.20.** The eccentricity did not affect the compliance ratio. Besides w/c the compliance ratio of air-cured mature HPC was affected by the amount of silica fume and of air-entrainment, **Figure 14.19.** The air-entrainment and the amount of silica fume probably affected the early drying of the specimens. The effect of air-entrainment was partly reduced in young drying HPC, which obtained a lower compliance ratio than HPC without air-entrainment, **Figure 14.21.** The stress/strength ratio had an affect on the early age compliance ratio since the drying shrinkage caused an uneven stress distribution in the specimen (shrinkage in the surface). At stress/strength ratio *0.6* the linear relationship between stress and strain was thus exceeded. HPC with silica fume slurry exhibited a larger early compliance ratio than HPC with granulated silica fume, probably due to the greater fineness. Besides w/c the compliance ratio of mature sealed HPC was affected by the type of silica fume, probably due to the larger fineness of silica fume slurry, Section 5, **Figure 14.20.** The type of silica fume probably affected the early self-desiccation of the specimens, cp. equation (5.37), **Persson (1996D)**. The stress/strength ratio had only a small effect on the early age compliance ratio with sealed curing since the autogenous shrinkage caused an even stress distribution in the specimen (no additional shrinkage at the surface).

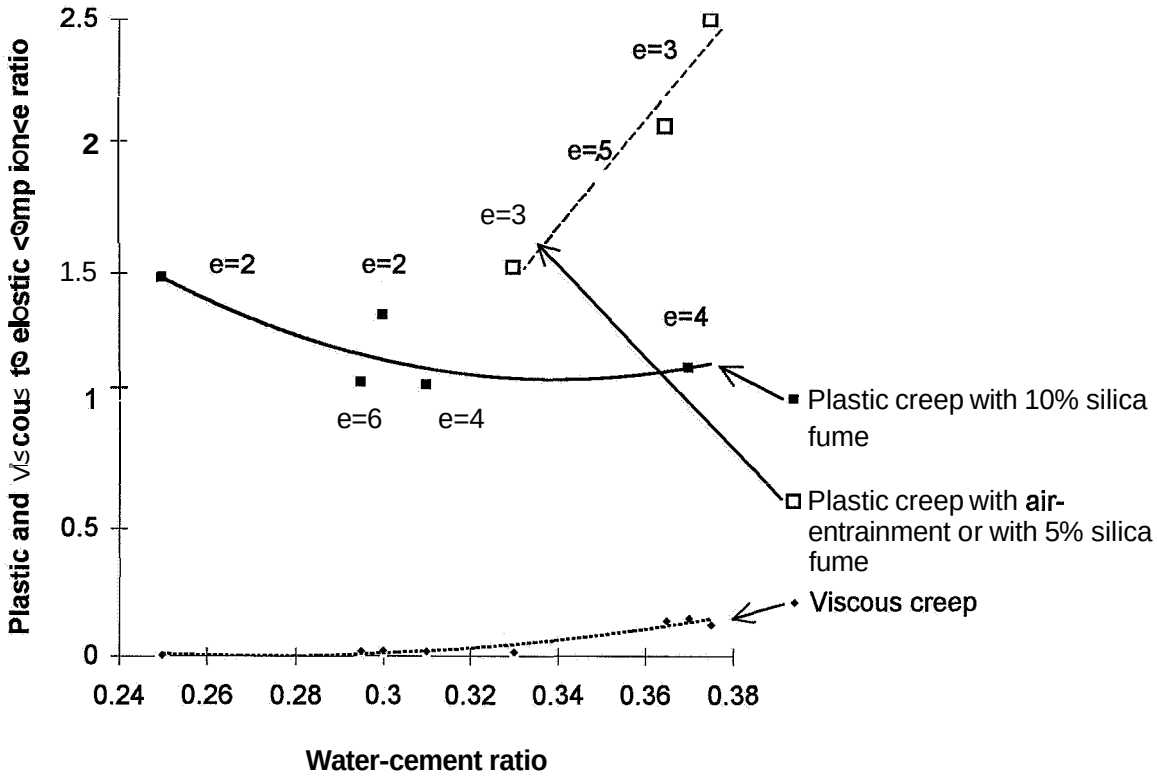

Figure 14.19 - Ratio of plastic or viscous compliance to elastic compliance versus w/c. Unloading of mature HPC with air curing. e= eccentricity (mm).

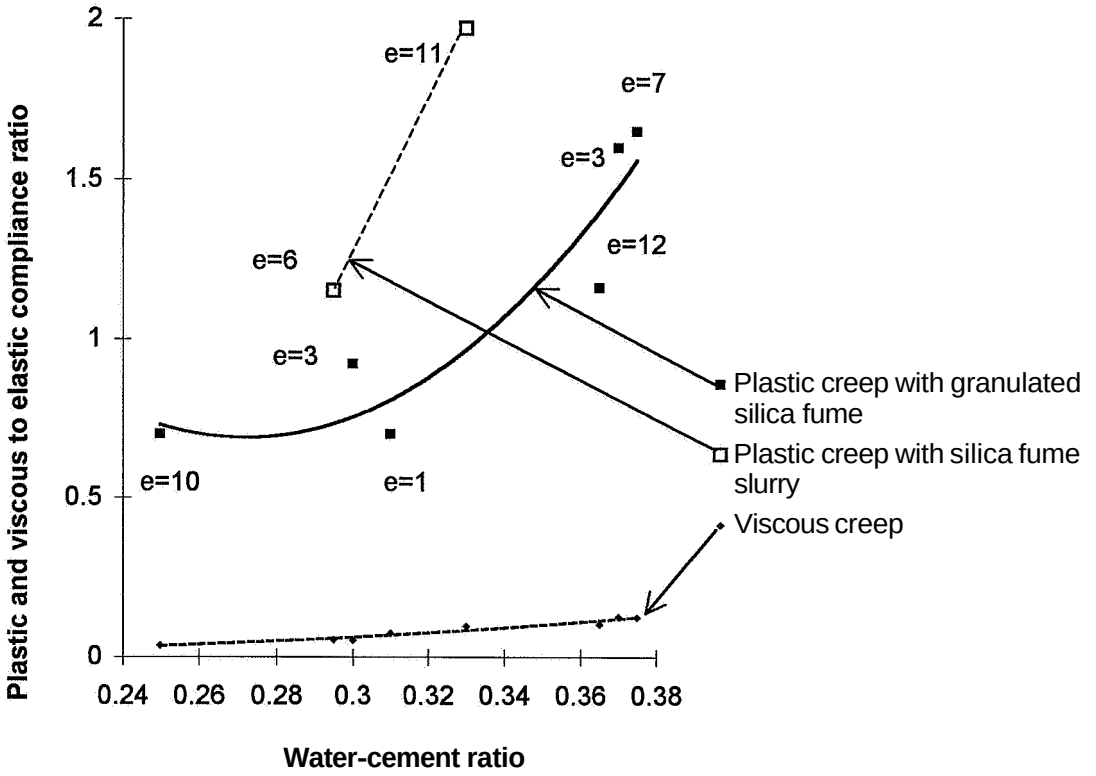

Figure 14.20 - Ratio of plastic or viscous compliance to the elastic compliance versus w/c. Unloading of mature HPC with sealed curing. e= eccentricity (mm).

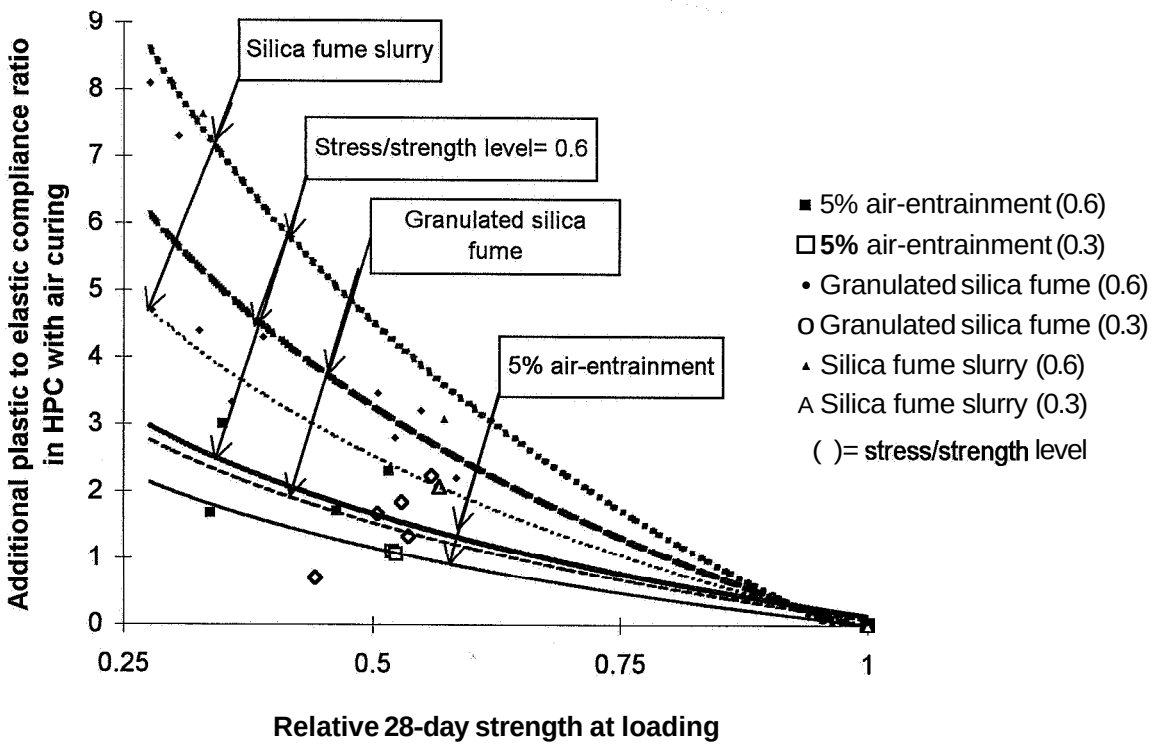

Figure 14.21 - Ratio of additional plastic to the elastic compliance versus relative 28-day strength. Unloading of HPC with air curing, young when loading.

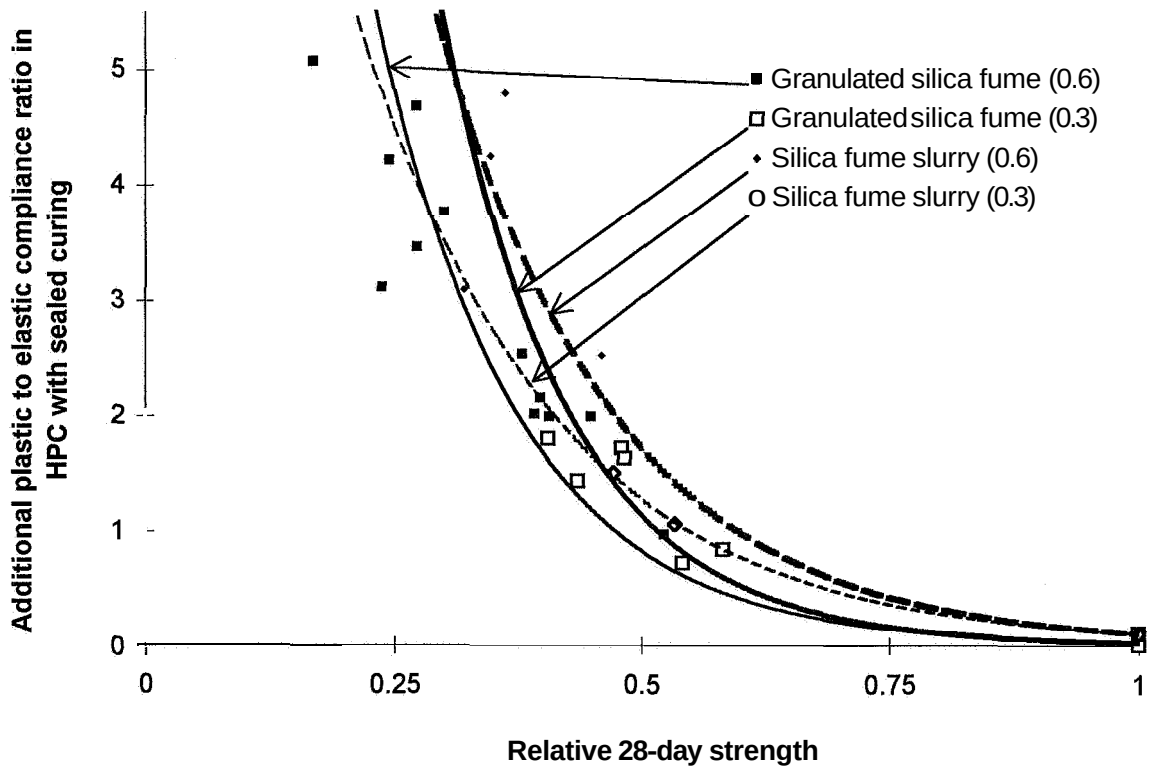

Figure 14.22 - Ratio of additional plastic to elastic compliance versus relative 28-day strength. Unloading of sealed HPC, young when loading.

HPC with silica fume slurry exhibited a slightly larger early compliance ratio than HPC with granulated silica fume for the reason mentioned above. From the discussion above and **Figures** 14.19-14.22 the following equations were calculated:

$$(J_{pl}/J_{el})_D = 50 \cdot k_{mai} \cdot k_{m5} \cdot [(w/c)^2 - 0.68 \cdot (w/c) + 0.1372] - 7.8\, k_{yai} \cdot k_{ysl} \cdot (\sigma/f_c) \cdot \ln(f_c/f_{c28}) \quad (14.24)$$

$$(J_{pl}/J_{el})_B = 82 \cdot k_{msl} \cdot [(w/c)^2 - 0.544 \cdot (w/c) + 0.0824] + 49 \cdot (\sigma/f_c) \cdot k_{ysl} \cdot e^{-6.77 \cdot k \cdot [(\sigma/fc) + 0.451] \cdot (fc/fc28)} \quad (14.25)$$

$$J_{vi}/J_{el} = 0.75 \cdot k_{mD} \cdot [(w/c) - 0.25] - k_{yD} \cdot \ln(f_c/f_{c28}) \quad (14.26)$$

ai denotes 5% air-entrainment
m denotes mature HPC
f_c denotes compressive strength at loading (MPa)
f_{c28} denotes compressive strength at 28 days' age (MPa)
$[k, k_{mai}, k_{msl}, k_{mD}, k_{m5}, k_{yai}, k_{ysl}, k_{yD}]$
denotes constants given in **Table** 14.24 (k=1 otherwise).
sl denotes silica fume slurry
y denotes HPC young when loading
B, D denote sealed and air curing respectively

J_{pl}/J_{el} denotes ratio of viscous-plastic compliance to the elastic compliance at unloading

J_{vi}/J_{el} denotes ratio of viscous-elastic compliance to the elastic compliance at unloading

σ denotes stress (MPa)

5 denotes HPC with 5% silica fume

Table 14.24 - Constants in equations (14.24) and (14.25) (k=1 otherwise).

Constant	k (slurry)	k_{mai}	k_{msl}	k_{mD}	k_{m5}	k_{yai}	k_{ysl}	k_{yD}
Air curing	-	1.38	-	1.66	1.33	0.52	1.48	0
Sealed curing	1.1	-	1.56	1	-	-	2	-0.06

The viscous-elastic part of the compliance was small and hardly detectable at w/c< 0.35.

14.5.6 Basic creep rate compared with another model

As indicated above, a knowledge of the long-term basic creep rate was of the utmost importance for the lifetime of a concrete structure. Present codes often underestimate the effect of the creep, most probably due to low creep rate assumption, **Sakata (1993).** As proposed, the basic creep may be separated into one part related to creep and another part consisting of the initial deformations, **Bazant (1995).** It was therefore essential to describe the slope of the creep function, i.e. the creep rate. From the eight long-term creep tests carried out as a part of the project the long-term creep rate, dC(t,28)/dt, for mature concrete was expressed in relation to the 28-day strength, **Persson (1995A), Persson (1997B) and Appendix 14 (sealed curing)** [millionths/(MPa·day)]:

$$\frac{dC(t,28)}{dt} = k \cdot 0.25 \cdot (f_{c28})^{-0.84} \cdot (t-28)^{k\cdot(0.19\cdot f_{c28}-0.81)} \qquad (14.27)$$

dC(t,28)/dt denotes the long-term creep rate for HPC mature when loading [millionths/(MPa·day)]

f_{c28} denotes 28-day cube strength (GPa) $\{0.085<f_{c28}<0.145$ GPa$\}$

k k= 0.92 for HPC with 5% silica fume; k= 1 for 10% silica fume

t denotes the age (days); $\{28<t<720$ days$\}$

The long-term creep rate of concrete, young at loading, dC(t,t′)/dt, varied mainly with the relative 28-day strength of the concrete. In this case, 24 tests of HPC were available for analysis. The long-term term studies indicated that, even after a long time, the creep rate of a concrete, young at loading, was higher than that of a HPC that was mature at loading. The creep rate was expressed as, **Persson (1995A), Persson (1997B) and Appendix 14 (sealed curing)** [millionths/(MPa·day)]:

$$\frac{dC(t,t')}{dt} = 11 \cdot e^{-2\cdot(f_c/f_{c28})} \cdot (t-t')^{0.95\cdot f_{c28}\cdot[\ln(f_c/f_{c28})-0.54]-0.72} \qquad (14.28)$$

$dC(t,t')/dt$	denotes the long-term creep rate of HPC, that was young at loading
f_c	denotes cube strength at loading (GPa)
f_{c28}	denotes 28-day cube strength (GPa) $\{0.085<f_{c28}<0.145$ GPa$\}$
t	denotes age (days) $\{2<t<720$ days$)$
t'	denotes the age at loading (t> t') (days) $\{0.8<t'<3$days$\}$

Equations (14.27) and (14.28) were compared with the well-known model for estimation of the creep rate called B_3, **Bazant (1995)** using the concretes in this study. The creep rate of concrete in model B_3, dC_0/dt, was simplified and transformed as follows, **Hedenblad (1996)** [millionths/(psi·day)]:

$$\frac{dC_0(t,t')}{dt} = \frac{45.11\cdot\sqrt{c}\cdot\left[1/\sqrt{t}+0.29\cdot(w/c)^4\right]}{(f'_c)^{0.9}\cdot\left[(t-t')+(t-t')^{0.9}\right]} + \frac{0.14}{t\cdot(a/c)^{0.7}} \qquad (14.29)$$

a	denotes the aggregate content (lb/ft^3)
c	denotes the cement content in the concrete (lb/ft^3)
f'_c	denotes the cylinder strength (psi)
dC_0/dt	denotes the creep rate of the concrete [millionths/(psi·day)]
t	denotes the age of the concrete (days)
t'	denotes the age at loading (days)
w	denotes the water content at mixing (lb/ft^3)

In the comparisons a stress to strength ratio at loading of the concrete, $\sigma/f_c = 0.3$ (based on the cube strength, f_c) was studied. Both young concrete (2 days' age) and mature concrete (28 days' age) were used in the comparison. Model B_3 applied for $\sigma/f'_c < 0.4$ (cylinder strength, f_c). The cylinder strength, f_c, of 32 cylinders was correlated to cube strength, E„ **Figure 5.5** (MPa):

$$f'_c = 0.71\cdot f_c \qquad (5.8)$$

The stress/cylinder strength ratio at loading of the specimens in the study was then calculated: $\sigma/f'_c = 0.41$. **Figure 14.23** shows the creep rate estimated according to equations (14.27), (14.28) and (14.29) versus the measured creep, **Persson (1995A), Persson (1997B) and Bazant (1995) and Appendix 14 (sealed curing).** The precise estimations according to the equations are given in **Table 14.25.** Symbols used in Table 14.25:

a	denotes the aggregate content (lb/ft^3)
ai	denotes 5% air-entrainment
c	denotes the cement content (1b/ft^3)
f_{c28}	denotes the 28-day cube strength (MPa)

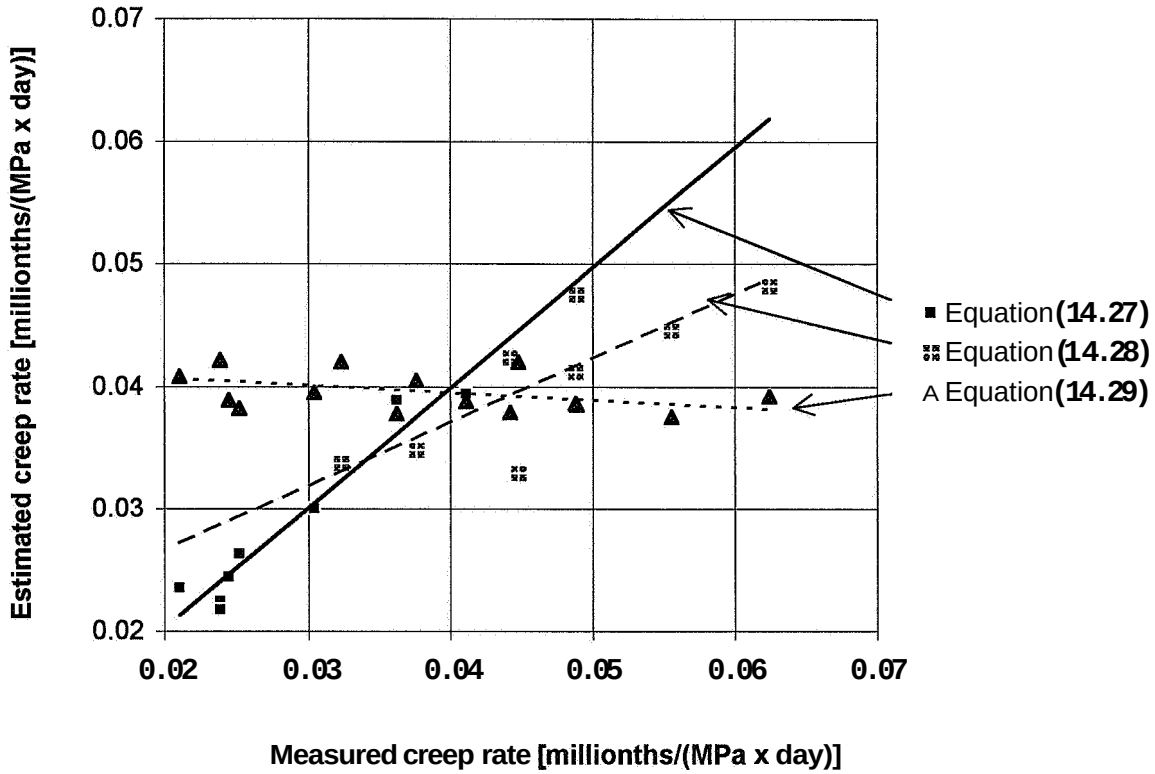

Figure 14.23 - Estimated creep rate [equations (14.27) - (14.29)] versus measured.

f'_c denotes the 28-day cylinder strength (psi)
..g.. denotes granulated silica fume
k denotes a parameter in equation (14.27) above
..s.. denotes silica fume slurry
t denotes the age of the concrete at estimation of the creep rate (days)
t' denotes the age of the concrete at loading (days)
B_3 denotes the creep formula given in equation (14.29) above
Eq. (1) denotes equation (14.27)
Eq. (2) denotes equation (14.28)
Eq. (3) denotes equation (14.29)
Ref. denotes measured creep rate, **Persson (1995A), Persson (1997B) and Appendix 14 (sealed curing)**
σ denotes the stress on the concrete
$\omega = \sigma/f_{c28}$
…5 denotes 5% silica fume calculated on the basis of cement content
25… denotes w/c= 0.25

The estimations according to equation (14.29) gave a decreasing estimated creep rate with increasing measured creep rate, which was in contrast to equations (14.27) and (14.28) and also in disagreement with other research results, cp. **Figure 14.2, Miiller and Kiittner (1995).** One reason for this divergence may be the dominating right-hand part of model B_3, **Bazant (1995):**

Table 14.25 - Estimation of creep rate of HPC [equations (14.27) - (14.29)].

Mix	f'_c	c	w/c	t	t´	t-t´	a/c	B_3-Eq. (3)	B_3-Eq. (3)	k	Eq. (1)	ϖ	Eq. (2)	Ref.
Sort	psi	lb /ft^3	%	d	d	d	-	psi^{-10}	MPa^{-8}	-	MPa^{-8}	-	MPa^{-8}	MPa^{-8}
38g5ai	9200	33	38	210	28	182	4.07	2.68	3.88	0.92	3.94	1	-	4.11
38g5ai	9200	33	38	210	2	208	4.07	2.67	3.85	0.92	-	0.54	4.75	4.89
37g10	11300	28	37	210	28	182	4.18	2.63	3.82	1	2.63	1	-	2.52
37g10	11300	28	37	210	2	208	4.18	2.62	3.79	1	-	0.53	4.24	4.42
36g10ai	9500	28	37	210	28	182	3.92	2.72	3.95	1	3	1	-	3.04
36g10ai	9500	28	37	210	2	208	3.92	2.70	3.92	1	-	0.51	4.82	6.24
33s5	10400	28	33	210	28	182	4.15	2.61	3.78	0.92	3.89	1	-	3.62
33s5	10400	28	33	210	2	208	4.15	2.59	3.75	0.92	-	0.53	4.46	5.56
31g10	13100	31	31	210	28	182	3.67	2.81	4.08	1	2.35	1	-	2.11
31g10	13100	31	31	210	2	208	3.67	2.79	4.05	1	-	0.64	3.48	3.76
30g10	14100	33	30	210	28	182	3.47	2.91	4.21	1	2.24	1	-	2.39
30g10	14100	33	30	210	2	208	3.47	2.89	4.2	1	-	0.65	3.29	4.48
29s10	12600	30	30	210	28	182	39.2	2.69	3.89	1	2.44	1	-	2.45
20s10	12600	30	30	210	2	208	3.92	2.67	3.86	1	-	0.47	4.12	4.88
25g10	14700	34	25	210	28	182	3.45	2.91	4.22	1	2.17	1	-	2.39
25g10	14700	34	25	210	2	208	3.45	2.89	4.2	1	-	0.58	3.37	3.23

$$\left[\frac{dC_0(t,t')}{dt}\right]_{tac} = \frac{0.14}{t\cdot(a/c)^{0.7}} \qquad (14.30)$$

a/c denotes the aggregate to cement ratio
dC_0/dt denotes the creep rate of the concrete [millionths/(psi·day)]
t denotes the age of the concrete (days)

About 96% of the creep rate calculated according to equation (14.29) depended on the right-hand part shown in equation (14.30), which meant that the strength of the concrete had almost no effect on the creep rate. The strength at loading played an important role when estimating the creep, **Müller and Kiittner (1995), Figure 14.2.** Equation (14.29) only depended on the age of the HPC being studied and also on the aggregate content, a/c. In order to estimate the affect of the aggregate and other mix design properties of HPC on the measured creep rate in the present study, an extended parameter study was carried out, **Figure 14.24 and Table 14.26. Table 14.26** shows the accuracy parameter R^2, equation (14.31) for the creep rate of mature HPC at 210 days' age related to the parameters mentioned above. Strength, f_c, was concluded the most significant parameter for the creep rate.

$$R^2 = 1 - \frac{\sum(Y_i - Y_m)^2}{(\sum Y_i^2) - \frac{(\sum Y_i)^2}{n}} \qquad (14.31)$$

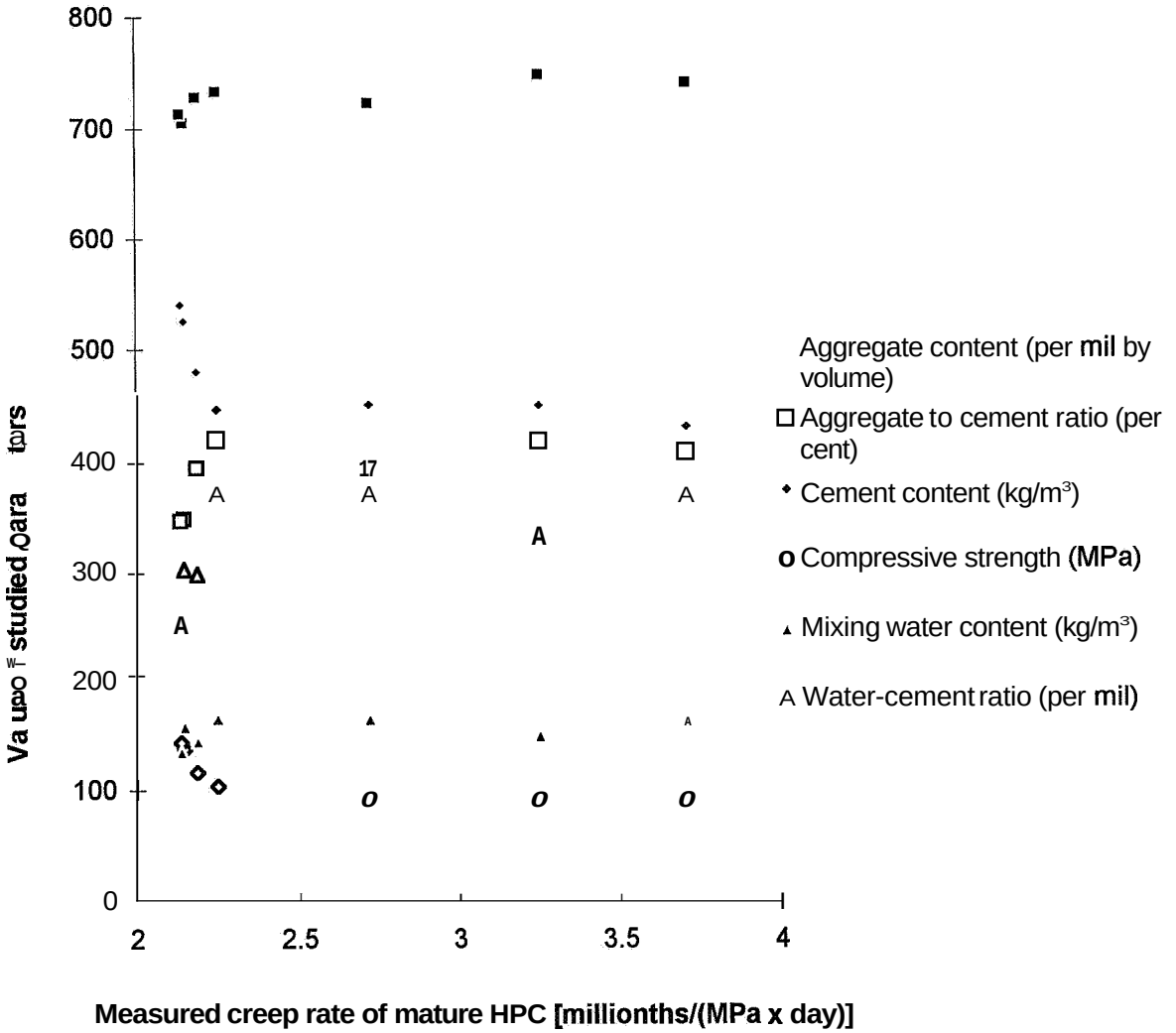

Figure **14.24** - Parameters affecting creep rate of HPC. Symbols are given above.

Table **14.26** - Accuracy parameter R^2 of the creep rate for HPC, **210** days' age.

Accuracy/ studied parameter	**a (per mil by volume)**	**a/c (per cent)**	**c (kg/m^3)**	**f_c (MPa)**	**w (kg/m^3)**	**w/c (per mil)**
R^2	**0.62**	**0.37**	**0.51**	**0.66**	**0.07**	**0.34**

Symbols in **Figure 14.24 and Table 14.26:**

a denotes aggregate content (per mil by volume)
a/c denotes ratio of aggregate to cement (%)
c denotes cement content (kg/m^3)
f_c denotes compressive strength (MPa)
n denotes the number of measured values
w denotes water content (kg/m^3)
Y_i denotes the measured value
Y_m denotes the average measured value

14.6 Summary and conclusions

A total of 32 air-cured and 52 sealed specimens were studied over a minimum period of 1100 days up to 1700 days. Traditional spring-loading devices were used. The studies took place in a climate chamber with extremely accurate relative humidity and temperature. The loading was slowly applied by hydraulic equipment with the control of a precision load-cell. The loading was controlled at each time of measurement.

Measurement were also carried out without any external loading in order to control the loading-level in the device, which varied ± 3% as a maximum. The measurements were taken mechanically. The mechanically measured deformations of HPCs in the spring-loading devices coincided reasonably well with the deformations of specimens that were measured by LVDTs in parallel tests. The measurements were taken on three sides of the specimen which made it possible to obtain the eccentricity of the loading given elastic conditions (mature concrete). The eccentricity was also obtained at the unloading of the specimens (elastic conditions). Owing to the way of curing the specimens (lying) the eccentricity sometimes was quite large given elastic conditions. However, the eccentricity did not significantly influence the amount of deformation. One explanation was perhaps that elastic conditions did not exist at early ages but rather plastic.

After the measurement period the specimens were rapidly unloaded and the elastic deformation established within 1 minute. The viscous deformation was studied over 1 month. Finally, the plastic deformation (the remaining) was obtained. Parallel tests of compressive strength, hydration and internal relative humidity were carried out during the whole time of the creep study. The specimens were weighed before and after the measurement period. Comparison was performed with other research. The following conclusions were drawn:

- Loading time, w/c, air-entrainment, and type of silica fume, stress/strength level, and strength at loading and 28-day strength mainly influenced the long-term creep of HPC with air curing.
- Loading time, w/c, and amount of silica fume, type of silica fume, stress/strength level, and strength at loading and 28-day strength mainly influenced the long-term creep of HPC with sealed curing.
- The rate of creep was also related to the strength growth rate of HPC.
- The rate of creep of mature drying HPC increased with air-entrainment and was dependent on amount and type of silica fume.
- The rate of creep of young drying HPC was dependent on air-entrainment, the amount and type of silica fume.
- The creep rate of sealed HPC was dependent on air-entrainment and amount of silica fume.
- The rate of creep in HPC was related to the internal relative humidity of HPC.

- The elastic modulus of HPC with air curing that was obtained in the present study was about 5 GPa smaller than the elastic modulus estimated according to the proposed extension of Model Code 90.
- The elastic modulus of HPC with sealed curing that was obtained in the present study was about 8 GPa larger than the elastic modulus estimated according to the proposed extension of Model Code 90. These results were explained by the increased immobility of water in sealed specimens compared with drying HPC.
- The viscous-elastic partition of creep was small (hardly detectable) at w/c < 0.35.
- Time, w/c, air-entrainment, and type of silica fume, stresslstrengthlevel, and strength at loading and 28-day strength influenced the long-term plastic compliance to elastic compliance ratio of HPC with air curing mainly.
- Time, w/c, and type of silica fume, stresslstrengthlevel, and strength at loading and 28-day strength influenced the long-term plastic compliance to elastic compliance ratio of HPC with sealed curing mainly.
- The creep rate of the HPC estimated according to equations evaluated within these studies, decreased with increasing compressive strength, which was in contrast to another well-known model.
- The proposed equations agreed reasonably well with the experimental results.

15. CREEP AND SHRINKAGE AFTER HEAT CURING

15.1 General

From a practical point of view, it was of great interest to study creep of HPC after heat curing. HPC of mix 6, Table 5.1, was studied at various temperatures, Figure 15.1. The temperature during the fist day was chosen to reflect a curing period in a large HPC structure. After the fist day HPC was studied at different temperatures.

15.2 Experimental

The tested HPC cylinder was built into a climate box within the MTS machine. The same loading and unloading procedures were used as applied in the short-term studies above, Sections 6-13. HPC of mix 6 was cured at about 48 °C for 16 h and then tested at various temperatures, Figure 15.1. The loading on the HPC cylinders was applied at 1 day's age. The cylinders were unloaded after 66 h.

Parallel to the tests in the MTS machine long-term tests of heated HPC of mix 6 were performed. The spring-loading devices used for the long-term studies initially were placed in same climate chamber as was supplying the MTS machine, i.e. the same temperature was obtained in the specimen at the short-term and at the beginning of the long-term tests. After the heat curing for 16 h + 66 h, the creep of the cylinders was studied at 20 °C, sealed or air-cured, for 3 years.

15.3 Result of short-term creep

The climate chamber that was used to maintain the relative humidity and temperature in the MTS machine was connected to another chamber in which cubes of 100 mm were placed in order to study the mechanical properties of the HPC. Figure 15.2 gives the compressive strength of HPC type 6. One day of heat curing at 48 °C reduced the strength at 28 days' age by about 10%. The heat-cured HPCs obtained the same strength after 1 day of curing, as did HPCs cured at 20 °C after about 2 days. Figures 15.3-15.5 give the hydration, internal relative humidity, RH, and weight losses of the heated HPC of mix 6. The heat-cured HPCs obtained lower relative hydration and also initially a lower RH than the HPCs cured at normal temperature, which explained the resulting lower strength at 28 days' age. Figure 15.6 shows the shrinkage of the HPC after heat curing according to Figure 15.1. Figure 15.7 shows the shrinkage versus the weight losses, i.e. a combination of Figures 15.5 and 15.6. Figure 15.8 shows the total compliance reduced by the shrinkage versus loading time at various curing temperatures. Symbols that were used in the figures:

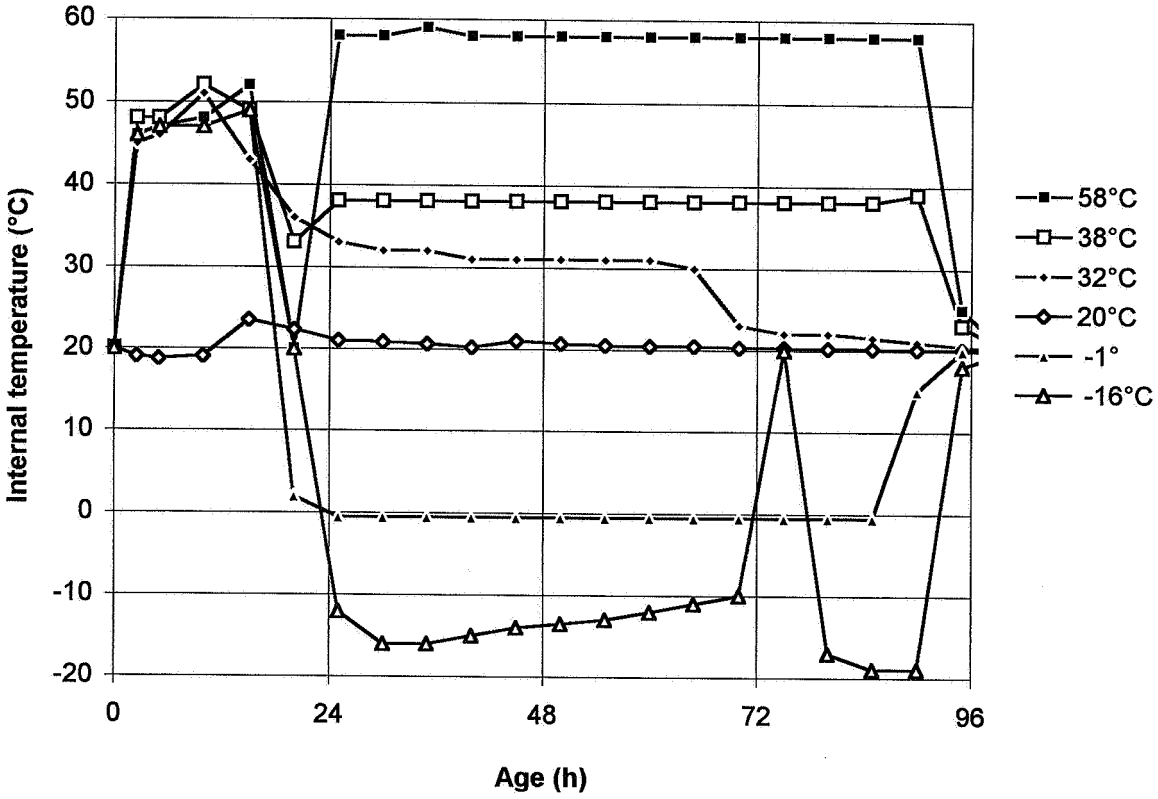

Figure 15.1 - Temperatures of testing HPC of **mix** 6 (fist cured at 48 °C for 16 h).

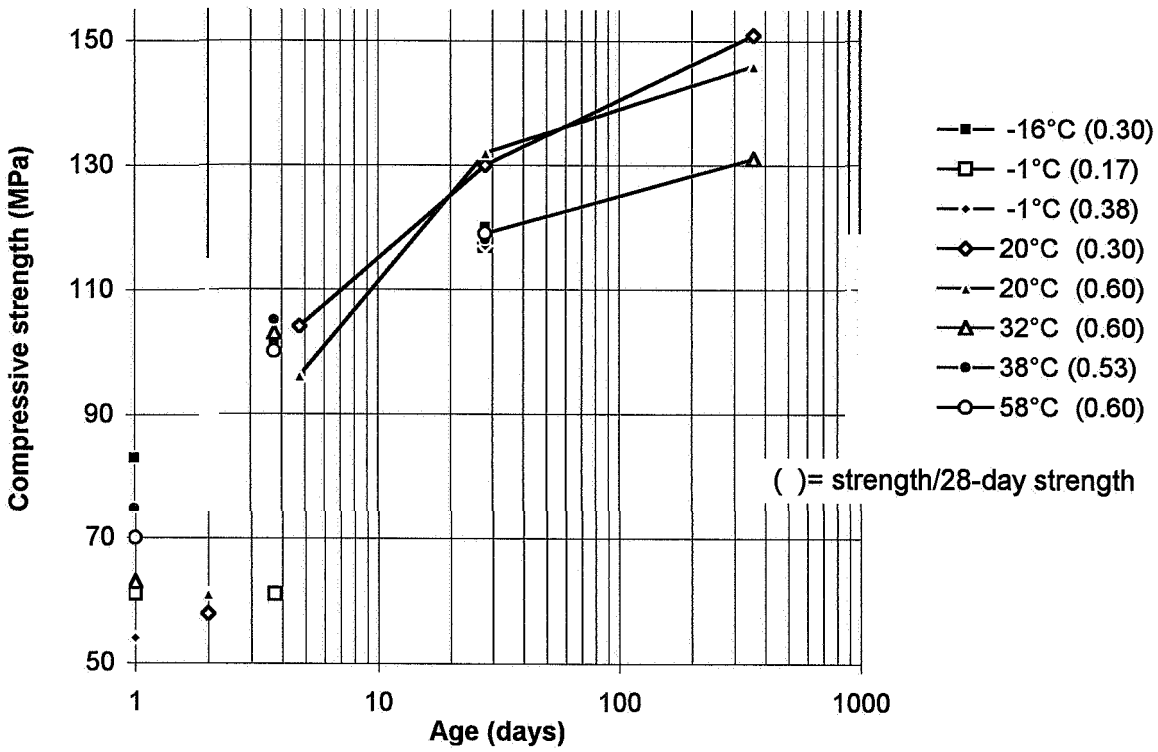

Figure 15.2 - Strength of HPC of **mix** 6 cured at various temperatures.

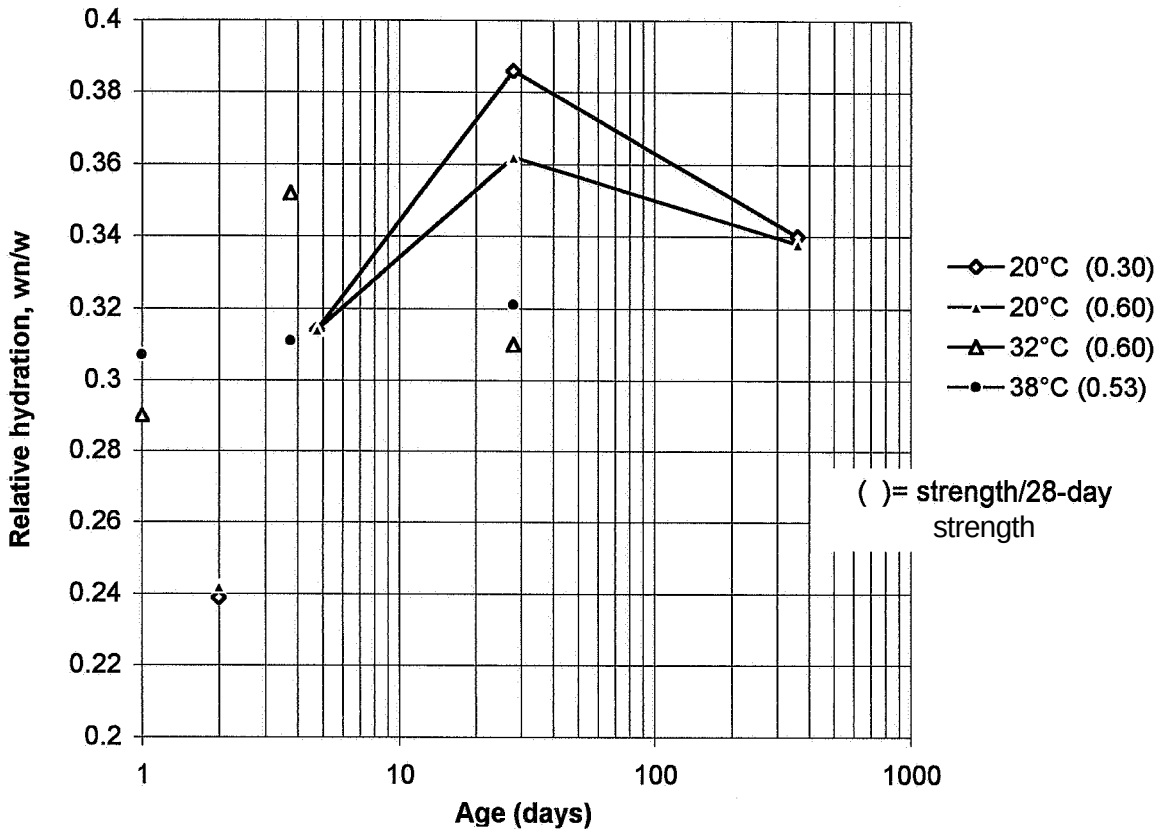

Figure 15.3 - Relative hydration during tests at different temperatures.

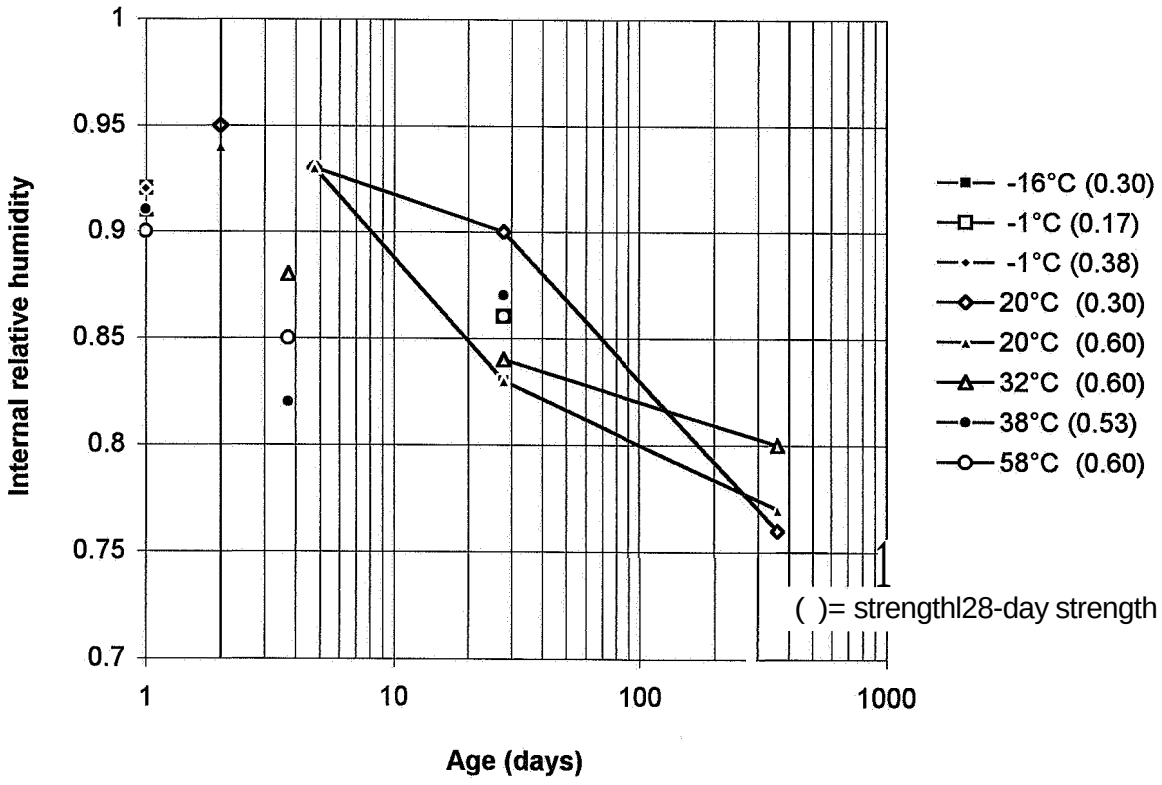

Figure 15.4 - Relative humidity during tests at different temperatures.

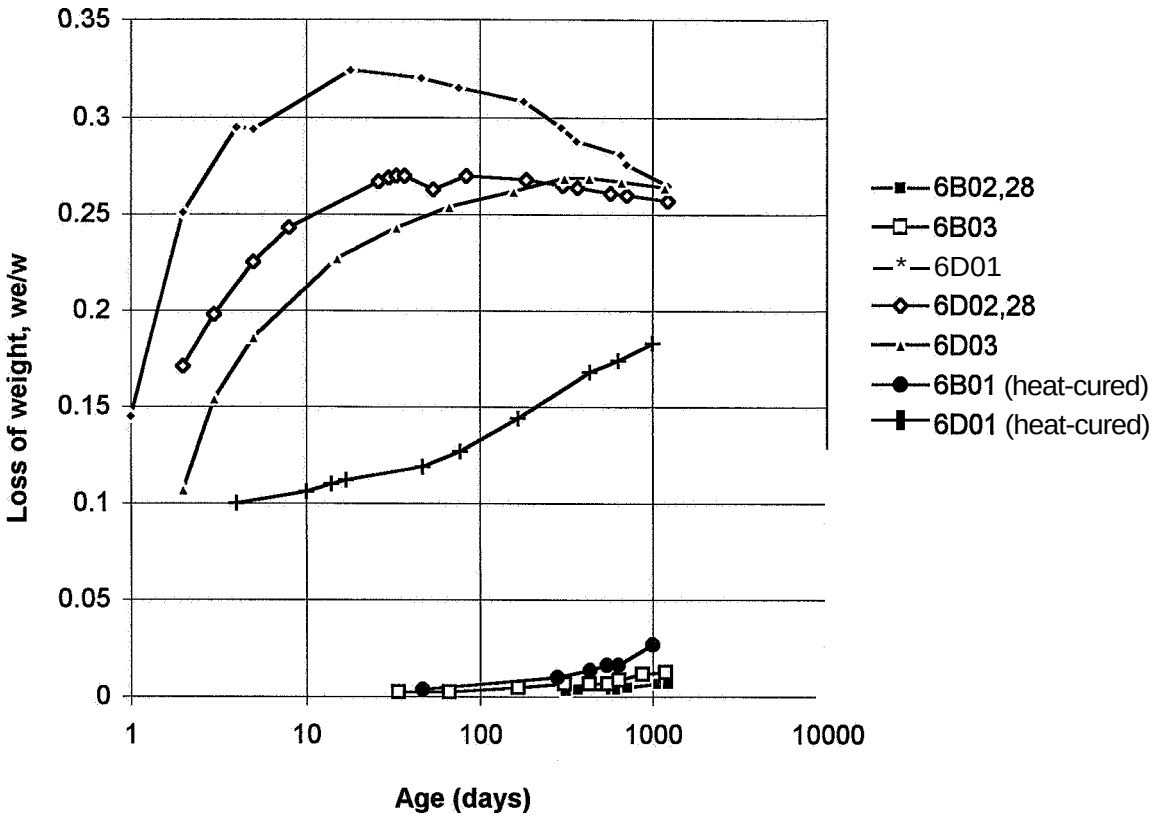

Figure 15.5 - Weight losses of HPC of mix 6 during tests at different temperatures.

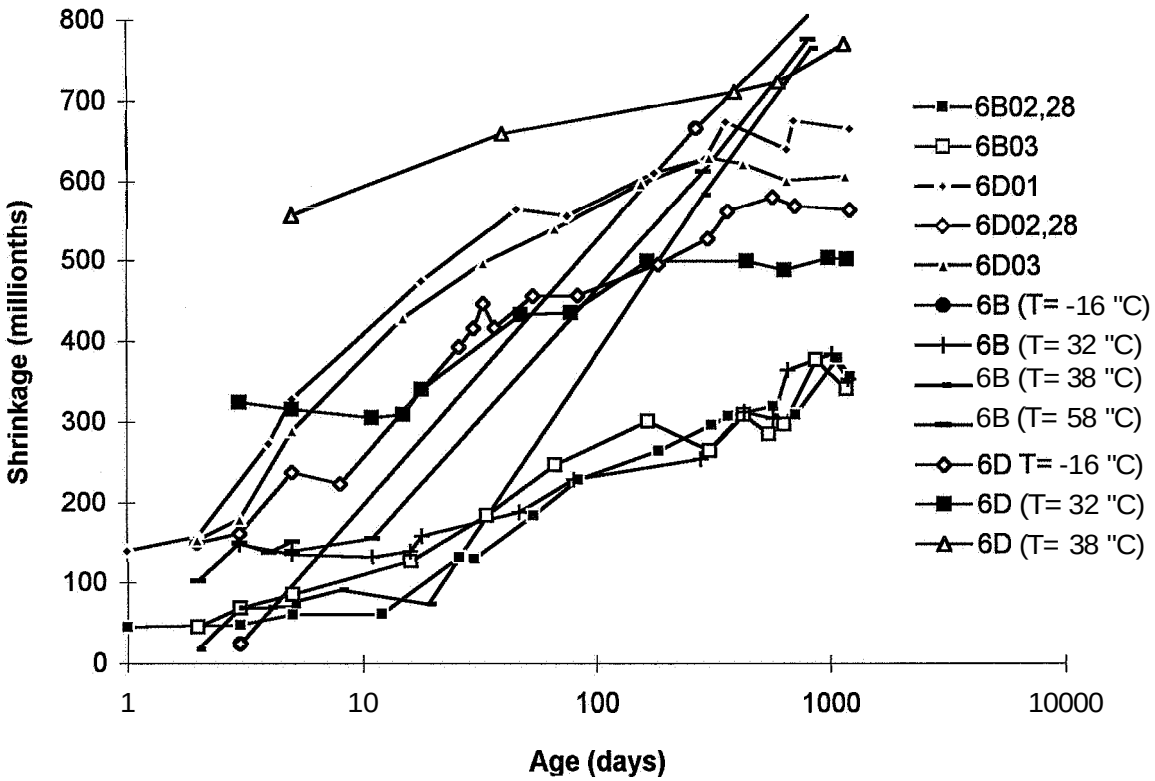

Figure 15.6 - Shrinkage in HPC of mix *6* during tests at different temperatures.

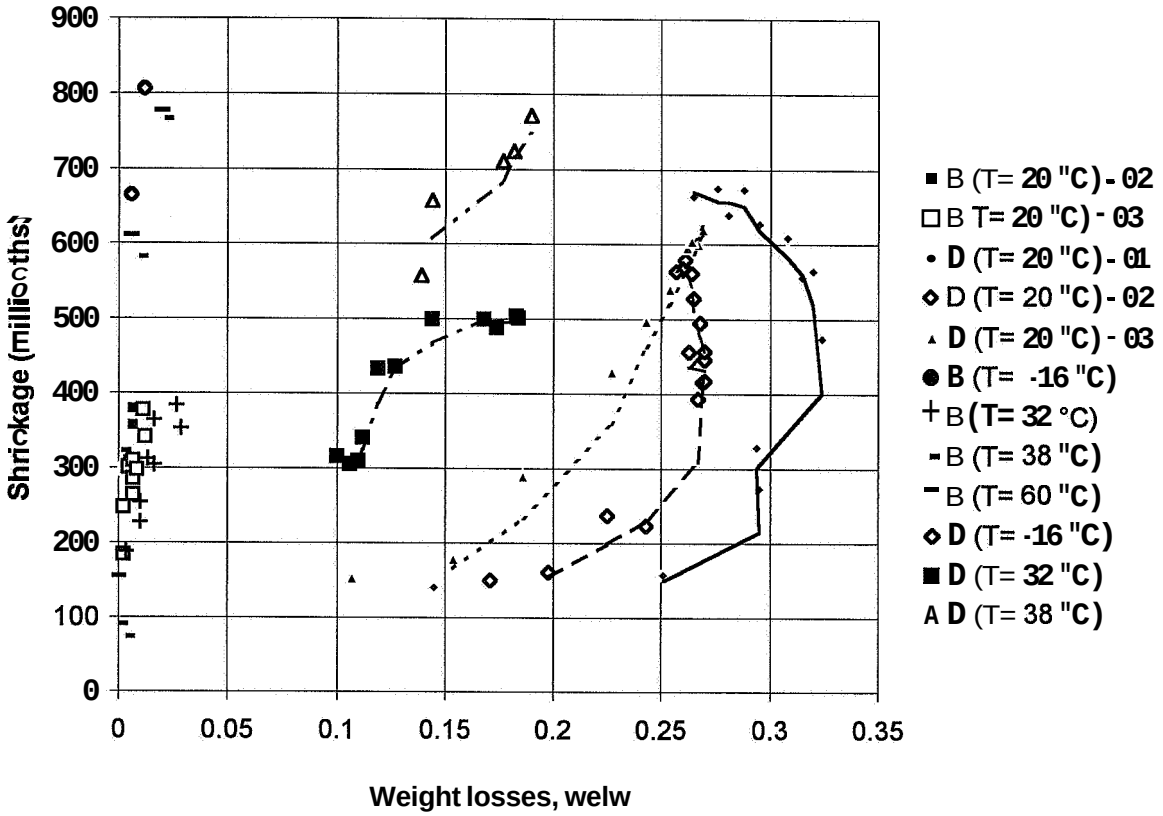

Figure 15.7- Shrinkage versus loss of weight in HPC of **mix** *6* after heat curing.

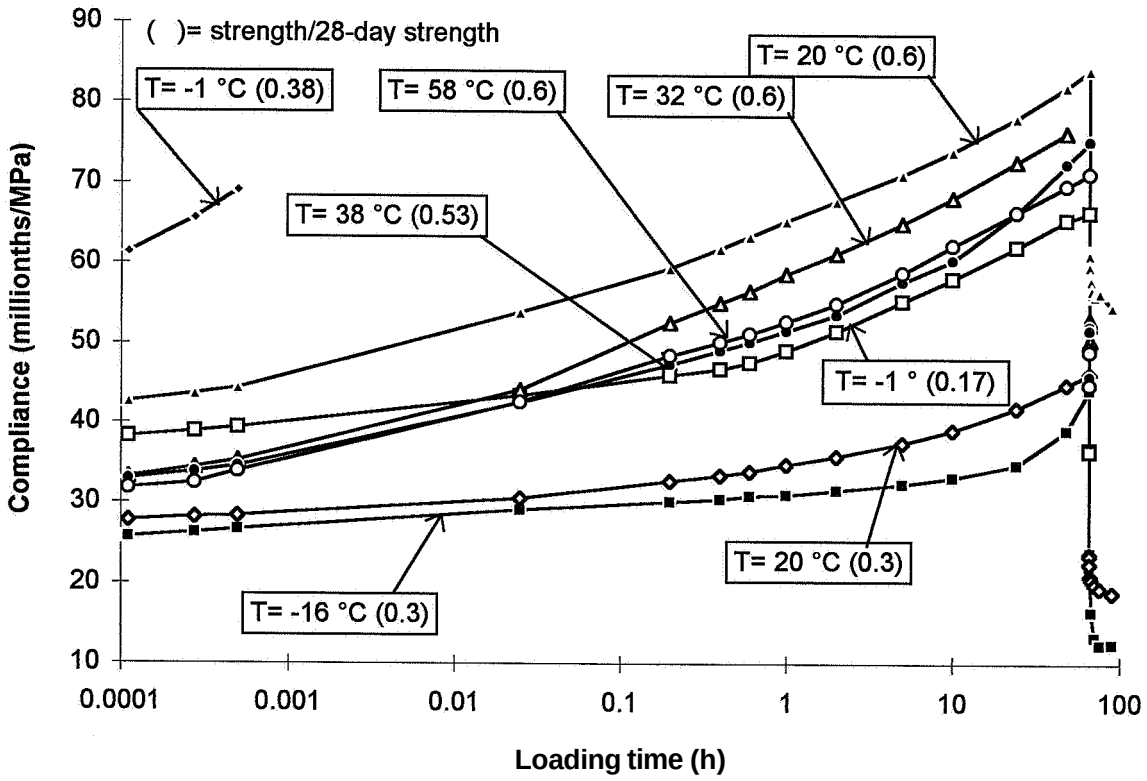

Figure 15.8 - Compliance of **mix** *6* reduced **by** shrinkage versus loading time.

B	denotes sealed curing (basic creep)
D	denotes air curing (drying creep)
T	denotes the internal temperature of the cylinder ("C)
6...=	HPC mix, Table 5.1
...02	denotes batch number
(0.30)	denotes stresslcube strength at loading, $\sigma/f_c = 0.30$

15.4 Analysis of short-term creep after heat curing

Some variations in the temperature were observed during the creep test at -16 °C. At -1 "C rapid failures of the specimens were observed both at $\sigma/f_c = 0.6$ and at $\sigma/f_c = 0.38$. At -1 "C the short-term tests only were carried out at a stress to cube strength ratio, $\sigma/f_c = 0.17$. Remaining tests at temperatures other than -1 "C were carried out at $\sigma/f_c = 0.3$ (-16 °C) or at $\sigma/f_c \approx 0.6$ (32°, 38" and 58 "C). As a reference creep results from HPC of mix 6 cured at 20 °C and loaded at 1 and 2 days' age are shown in **Figure 15.8.** The failures of the specimens at -1 °C were probably due to formation of some salts only stable at this temperature, **Stark (1995, 1997), Stark and Bollmann (1995), Stark (1996).** However, more research is required to co m this hypothetical failure mechanism that occurred during creep tests of HPC at -1 "C only. **Figure 15.9** shows the creep rate versus the stress to strength ratio at loading. **Figure 15.10** shows the creep rate versus the temperature of the specimen. The creep rate of HPC at -1 °C was substantially larger than at other temperatures. The following equations for the creep rate were calculated:

$$dJ/dt = (\sigma/f_c)\cdot 0.55[1+13\cdot(\sigma/f_c)]/(t-t') \quad \{0.30<\sigma/f_c<0.60 \text{ except for } T=-1\ "C\} \quad (15.1)$$

$$(dJ/dt)_{-1^\circ} = (\sigma/f_c)\cdot 13/(t-t') \quad \{0.17<\sigma/f_c<0.38\} \quad (15.2)$$

$$(dJ/dt) = (\sigma/f_c)\cdot[T\cdot 0.021\cdot(1-\sigma/f_c)+0.3\cdot(1+23.3\cdot\sigma/f_c)]/(t-t')$$

$$\{0.30<\sigma/f_c<0.60\ ,-20<T<60\ "C \text{ except for } T=-1\ "C\} \quad (15.3)$$

Symbols in **Figures 15.8-15.9** and **in** equations (15.1)- (15.3):

dJ/dt	denotes the creep rate at temperatures other than -1 "C [millionths/(MPa·h)]
$(dJ/dt)_{-1^\circ}$	denotes the creep rate of HPC at [millionths/(MPa·h)]
t-t'	denotes the loading time (days)
T	denotes the temperature of the HPC (-20 < T < 60 "C)

The stresslstrength ratio at loading turned out to be more important as regards the creep rate than the temperature did. The effect of temperature shown in **Figure 15.10** was related to the stresslstrength levels. At 20 "C the study was carried out both at stresslstrength = 0.3 and =0.6 at loading. The creep rate rose accordingly.

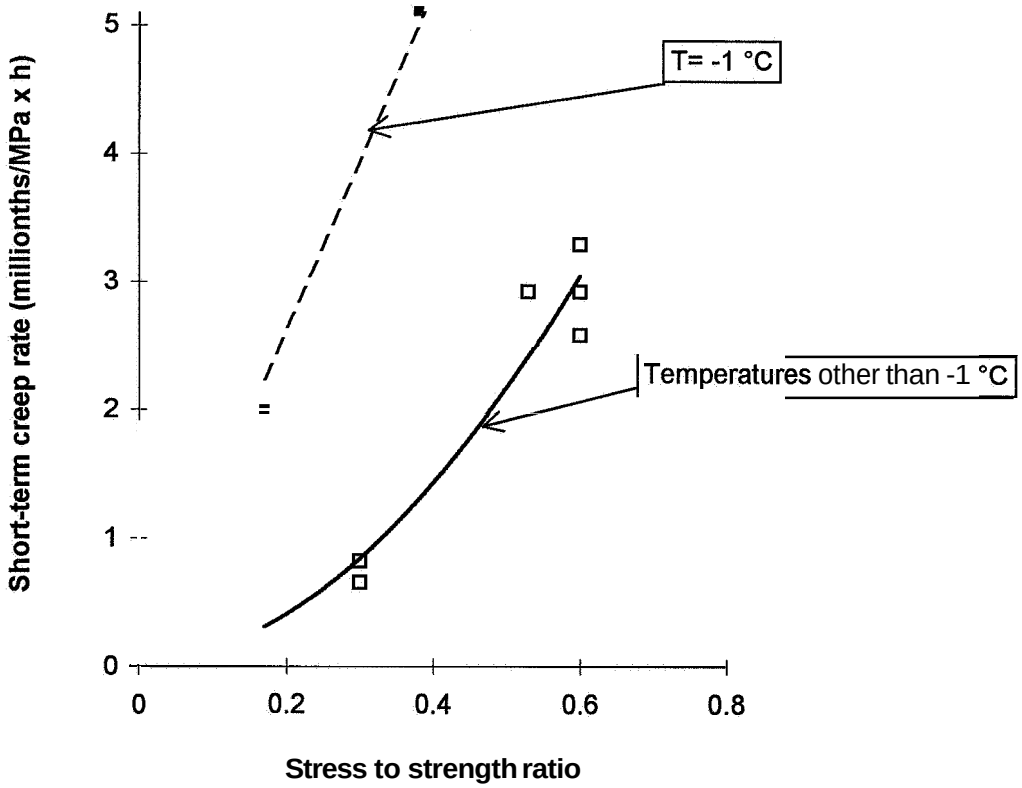

Figure 15.9 - Creep rate of heated HPC versus the stress to strength ratio at loading.

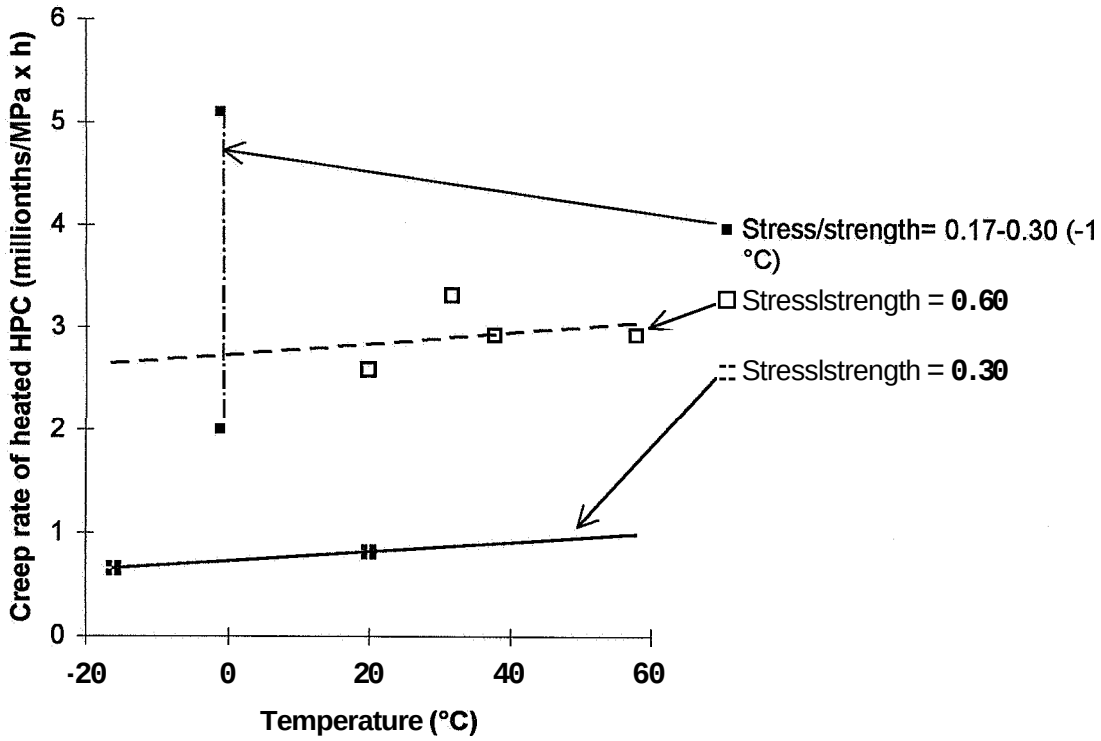

Figure 15.10 - Short-term creep rate versus the temperature of the specimen.

15.5 Analysis of long-term deformations after heat curing

After 1 day of heat curing at 48 "C the curing was carried out at 32 "C for 2.7 days, both related to short-term creep and shrinkage. During the short-term creep test in the MTS machine parallel long-term test were started up in a climate chamber with exactly the same climate as in the MTS machine. However, during the first 2.7 days only an initial temperature of 32 "C was studied regarding long-term deformations. After this period the creep studies were carried out at 20 °C for more than 1000 days. **Figure 15.2** shows the long-term strength of the HPC, i.e. about 13% lower strength after 1 year and heat curing compared with curing at 20 °C. The lower hydration after heat curing partly expressed the lower strength, cp. **Figures 15.2 and 15.3.**

Another explanation for the lower strength after heat curing was the lower RH, **Figure 15.4.** At both 4 and 28 days' age the RH was about 5% lower after heat curing than after curing at 20 "C, leaving less water in the HPC available for development of hydration and strength, **Persson (19963).** The long-term weight losses were substantially lower after heat curing at 48 °C than after curing at 20 "C, **Figure 15.5.** Moreover HPC cured at 20 °C started to increase in weight after above 28 days' age, probably due to carbonation, cp. Section 8 above. No such increase of weight was observed after heated curing of HPC, probably indicating that no carbonation occurred. The heat curing probably created a more dense surface of HPC, which delayed the transport of carbon dioxide, or, alternatively, the surface of HPC obtained too low a relative humidity for carbonation to occur, cp. Section 8 above. (Carbonation requires both air and moisture to occur.)

Less drying occurred in heat-cured HPC than in HPC cured at 20 "C: about 19% of the mixing water evaporated over 1000 days but about 26% from HPC cured at 20 "C. **Figure 15.7** seems to confirm these results. In order to study the shrinkage after heated curing it was essential to know the coefficient of thermal dilatation at various temperatures. **Figure 15.11** shows that the coefficient of thermal dilatation on average was about 0.01 per mil/°C, although slightly increasing with the temperature. From **Figure 15.11** the following coefficient of thermal dilatation was obtained:

$$\alpha_T = (9.8+0.014\cdot\Delta T)\cdot 10^{-6} \qquad \{-20<T<60\ "C) \qquad (15.4)$$

α_T denotes the coefficient of thermal dilatation {m/(m·°C)}
AT denotes the change in temperature ("C)

The long-term autogenous shrinkage over 1000 days was about 0.35 per mil after curing at 20 "C but twice as large after heat curing (about 0.7 per mil), **Figure 15.7.** The reason for this observation is unknown. **Figure 15.7** also shows that the drying shrinkage over 1000 days was about 0.6 per mil after curing at 20 °C and about 0.7 per mil after heat curing, results which coincided well with the correlations

presented in Section **8** above. The reduced long-term creep compliance is shown in **Figure 15.12.** (The shrinkage strain has been reduced fiom the creep strain.) The creep rate with sealed curing increased with the increase of curing temperature, **Table 15.1,** which coincides well with **Figure 15.10.** However, the opposite effect of the temperature was observed with air curing, **Table 15.1.** Then the creep rate decreased after heat curing mainly owing to the different amount of evaporable water. About 19% of the mixing water evaporated fiom the heated HPC over 1000 days and about 26% fiom HPC cured at 20 °C.

The driving force for drying shrinkage is evaporation of water, i.e. decrease of RH, which in turn decreases the underpressure in the pore water, **Figure 15.13.** Since **RH** decreased much more in the 20 "C-cured specimen a larger creep rate was observed than in heat-cured HPC. The creep rate for heated HPC was independent of the curing condition since the decrease of RH was in the same order for the two curing conditions.

Table 15.1 - Reduced long-term creep rate [millionths/(days·MPa)]

Conditions	**Cured at 20 °C**	**Heat-cured**
Sealed curing	2.1	3.8
Air curing	7	3.9

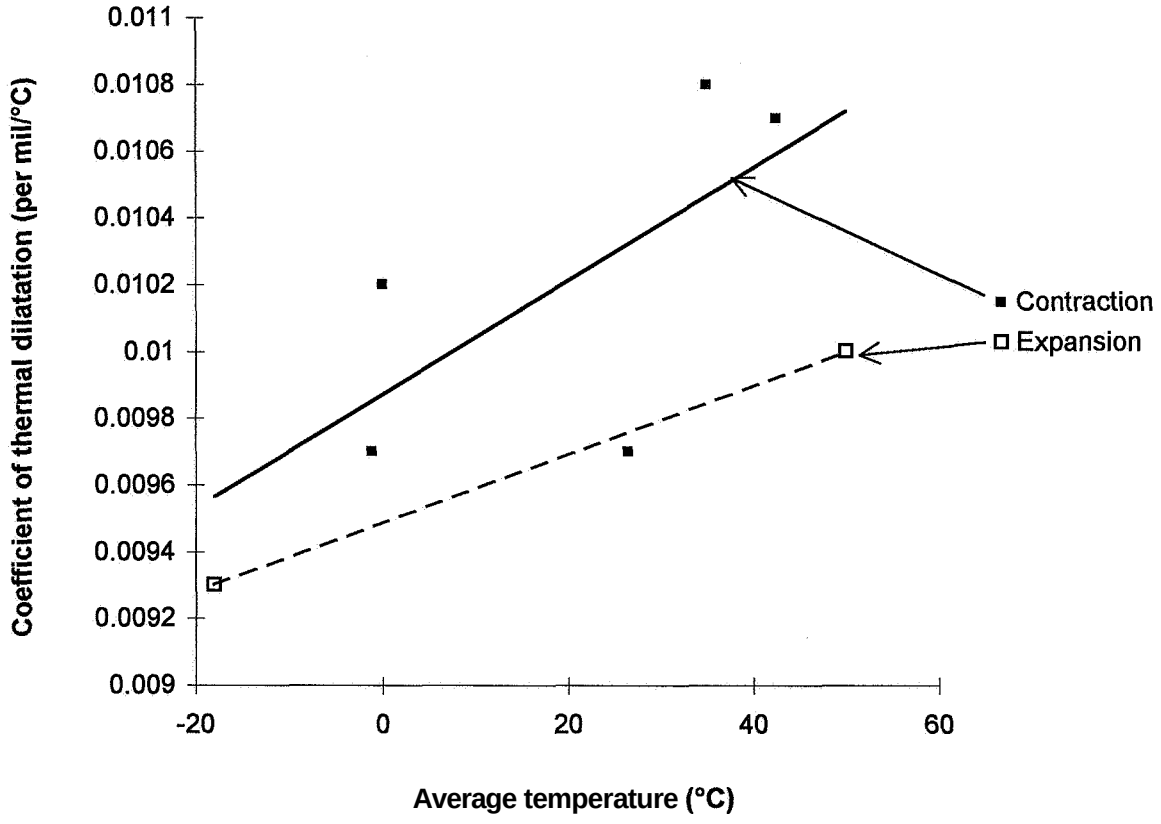

Figure 15.11 - Coefficient of thermal dilatation versus the average internal temperature.

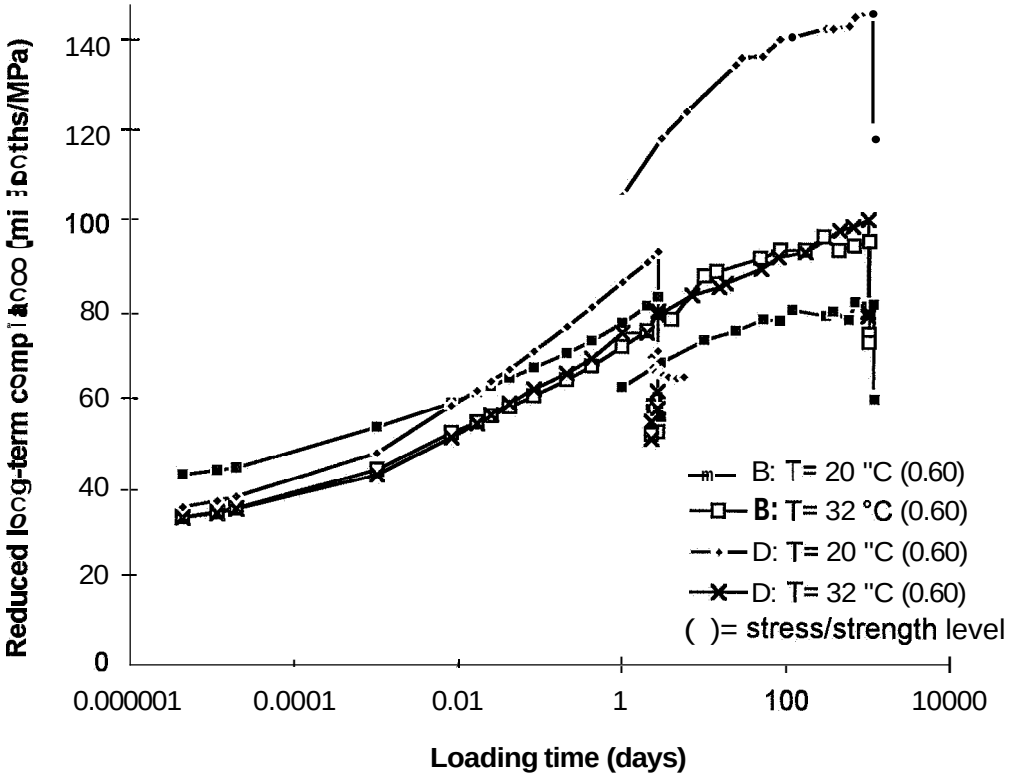

Figure 15.12 - Reduced long-term shrinkage versus the loading time.

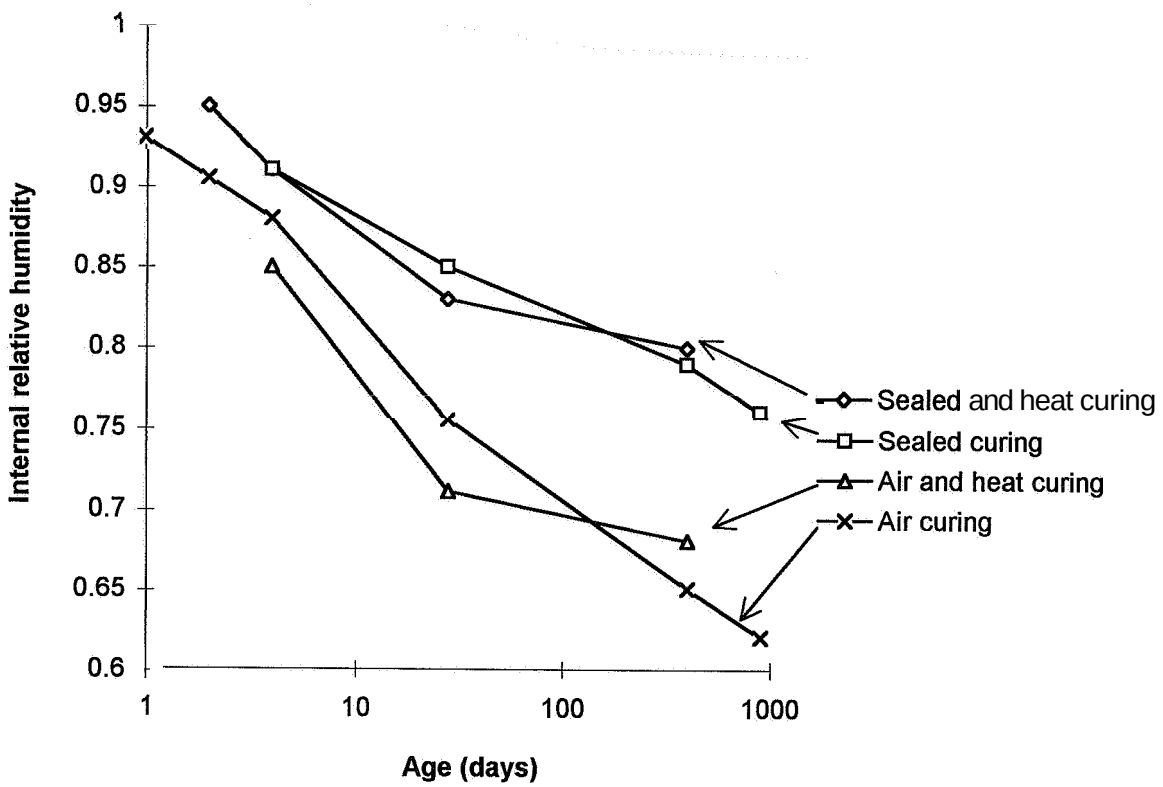

Figure 15.13 - Internal relative humidity of long-term creep tests.

15.6 Summary and conclusions

Short-term creep of five HPCs was studied at temperatures varying between -16 and 58 "C. The rate of creep was correlated to the temperature except for -1 °C at which temperature rapid failures were observed during the creep tests, probably owing to formation of salts in the HPC. The salts were only stable at this particular temperature. This hypothesis still is to be confirmed by further research. Long-term creep of HPC after heat curing was studied for more than 1000 days. Parallel studies were carried out related to strength, hydration, internal relative humidity weight losses and shrinkage. The following conclusions were drawn:

- The creep rate of HPC during short-term creep increased both with the stress to strength ratio and with the temperature. Much larger creep rate was observed at -1 "C than at other temperatures when the stress to strength ratio was held constant.
- The long-term creep rate with sealed curing also increased with the increase of curing temperature, which coincided well with the findings of short-term creep tests. The opposite effect of the temperature was observed with air curing since the creep rate decreased after heat curing mainly due to the different amount of evaporable water.
- The long-term autogenous shrinkage over 1000 days was about 0.35 per mil after curing at 20 °C but twice as large after heat curing (about 0.7 per mil). The reason for this observation is unknown. The drying shrinkage over 1000 days was about 0.6 per mil after curing at 20 °C and about 0.7 per mil after heat curing, results which coincided well with the correlations presented above.

16. DIMENSIONAL EFFECT ON CREEP AND SHRINKAGE

16.1 General

It was of great interest to study the dimensional influence on creep and shrinkage of HPC. **Bazant and Baweja (1995)** give a general approach regarding the influence of the size of the structure on creep and shrinkage, **Figure 2.2.** The approach is based on moisture transports in the concrete. It is known for NSC that the rate of drying shrinkage increases with lower half the hydraulic radius of the construction, i.e. at lower VIA (V = volume and A = cross-section area). However, since the final drying shrinkage is more or less independent of the size of the construction, the time of drying shrinkage is shorter at lower VIA when the ambient climate is held constant. The autogenous shrinkage is not dependent on specimen size. Since drying creep is partly affected by the drying shrinkage, drying creep too becomes size-dependent. It was the purpose of this study to compare creep and shrinkage of 55-mm cylinders with the same properties of cylinders 100 mm in diameter.

16.2 Materials and experimental methods

16.2.1 Aggregate, cement and studied HPCs

Tables 16.1-16.2 shows the main properties of the aggregate and the cement and **Table 16.3** the mix design (wlc = 0.37). The natural sand had 0.8% ignition losses and the silica fume 2.3% ignition losses (granulated, specific surface: 17.5 m^2/g).

16.2.2 Preparation of specimens

Ten cylinders 100 mm in diameter and 500 mm in length of each HPC were cast and sealed cured for 16 h at 20 °C. Six cast-in items were placed in each cylinder. After demoulding 4-mm stainless screws were connected to the cast-in items and fixed with nuts to the surface of the specimen. A measurement cup was ground into the head of the screws. Half the specimens were sealed cured with adhesive aluminium foil directly after demoulding. The specimens were weighed before the measurements started. Eight specimens of each HPC were placed in a traditional creep device. Two specimens per HPC were used to study shrinkage. Cubes with 100 mm sides were used to study compressive strength and internal relative humidity, RH. The cubes were sealed in the same way as the cylinders (half of the specimens were drymg). The ambient climate was provided by a climate chamber with 20 ± 0.5 °C and ambient RH = 55± 3%.

Table 16.1 - Characteristics of the aggregate.

Material1 characteristics	**Elastic modulus**	**Compressive strength**	**Split tensile strength**	**Ignition losses**
Quartzite sandstone	60 GPa	332 MPa	15 MPa	0.3%

Table 16.2 - Chemical composition and the main characteristics of the cement.

X-ray fluorescence analysis	**(%)**
CaO	64.9
SiO_2	22.2
Al_2O_3	3.36
Fe_2O_3	4.78
MgO	0.91
ICP-analysis	**(%)**
K_2O	0.56
Na_2O	0.04
LECO apparatus	**(%)**
Ignition losses at 950 °C	0.6
SO_3	2.0
Physical properties	
Specific surface according to Blaine	302 m^2/kg
Density	3220 kg/m^3
Setting time	
Vicat	135 min.
Water	26.0%
Standard test (prisms 40x40x160 mm)	**(MPa)**
1 day	11.0
2 days	20.2
7 days	35.8
28 days	52.6

Table 16.3 - Mix design of studied HPCs with w/c= 0.37 (kg/m^3 dry material).

Material	**101**	**103**
Quartzite sandstone, 11-16 mm	455	910
Quartzite sandstone, 8-11 mm	455	
Natural sand, Åstorp 0-8	880	790
Granulated silica fume	22	44
Cement	445	440
Air-entraining agent (vinsole resin)	0.02	0.04
Water	162	161
Superplasticiser (melamine formaldehyde)	3.3	4.8
Air-content (% by total volume)	2.4	14.3
Density (kg/m^3)	2430	2350
Slump (mm)	140	170

16.2.3 Loading and measurements

The measurement points were placed at a distance of 300 mm. The first measurement was taken directly after preparation. After testing the compressive strength the force of the creep device was set at a maximum of 0.6 of the compressive strength or 196 kN (25 MPa). The required time of loading was about 2 minutes. The first measurement was taken within 3 minutes fiom the start of loading. Initially the loading was controlled with a container of nitrogen gas that was connected to the hydraulic oil pressure of the jack in the spring-loading device. The load level was controlled with a precision load-cell. After a couple of days the loading was maintained by four springs in the device. The age of the HPC at loading varied between 2 and 28 days, i.e. the stress/cube strength varied between 25 and 50% at loading. Mechanical measurement devices were used. The measurement device was calibrated with an INVAR rod. The accuracy of the measurement was ± 0.002 mm and of the loading ± 3% over time. At loading the load-cell and the jack provided the precise loading with a high accuracy (± 0.1 kN).

16.2.4 Internal relative humidity, RH

Fragments fiom strength tests were used to study RH. Pieces of HPC fiom the inner part of the cube were placed in a glass tube, which was tightened with a rubber plug. After 24 h a dew point meter was entered into the glass tube and tightened with an expanding rubber ring around the glass. A golden mirror of the dew point meter was heated and cooled continuously. At the precise (decreasing) temperature of the dew point the reflection of light flash was interrupted on the golden mirror due to condensation of moisture of the air around the dew point meter. The air around the mirror was connected to the air in the capillary pores of the HPC. The same RH was obtained in the dew point meter as in the HPC provided the measurement time was set sufficiently long (at 22 h). It was important to calibrate the dew point meter. The calibrations were performed according to ASTM E 104-85 with solutions of salt at 33.1, 75.5, 85.1, 94.6 and 97.6% RH, which RH was slightly temperature-dependent.

16.2.5 Unloading procedure

After about 10 months of loading the elastic, viscous and plastic deformations were observed after the specimens were unloaded. The first measurement was taken 2 minutes after unloading. The measuring then continued until no more viscous deformation was observed. The weight.of the specimen was measured.

16.3 Results

Figures 16.1 and 16.2 show the development of strength and internal relative humidity, RH, in 100-mm cubes. In **Table 16.4** the stress to cube strength ratio used at loading is shown. RH of drymg cubes was mainly dependent on the hydraulic radius of the specimen. Half the hydraulic radius, VIA, of the cubes was 0.017 m for the cubes but V/A= 0.025 m for the 100 mm cylinder specimen. The cylinders in the main research on creep and shrinkage had V/A= 0.014 m. Shrinkage of 100 mm cylinders versus time and shrinkage of the same type of cylinders versus moisture losses is shown in **Figures 16.3 and 16.4.** The moisture losses, w_e, have been related to the original amount of mixing water, w. Finally the compliance, i.e. the specific deformation after reduction of shrinkage of cylinders subjected to sustained constant loading, is shown in **Figures 16.5 and 16.6.**

16.4 Analysis

16.4.1 Shrinkage

The amount and rate of autogenous shrinkage was more or less independent of the size specimen, cp. **Appendices 8.1 and 8.3** with **Figure 16.3.** The majority of the autogenous shrinkage stopped after 100 days. However the drying shrinkage was size-dependent. Cylinders 55 mm in diameter (V/A= 0.014 m) obtained drymg shrinkage for about 1 month before the carbonation shrinkage started. Cylinders 100 mm in diameter (V/A= 0.025 m) exhibited drying shrinkage for 100 days before any carbonation shrinkage (increase of weight) was observed, **Persson (1997A)**, cp. **Appendices 8.1, 8.3, 8.17** and **8.19** with **Figures 16.2, 16.3** and **16.4. Figure 16.7** shows the rate of drymg shrinkage versus half the hydraulic radius of the specimen. From **Figure 16.7** the following correlation was obtained between the drymg shrinkage rate, half the hydraulic radius, VIA, and age of the HPC:

$$d\varepsilon/dt = 0.0073 \cdot (V/A)^{-0.66}/t \qquad \{0.014<V/A<0.025\} \qquad (16.1)$$

$d\varepsilon/dt$	denotes the drying shrinkage rate (millionths/day)
t	denotes age (days)
A	denotes the area of the specimen (m^2)
V	denotes the volume of the specimen (m^2)
VIA	denotes half the hydraulic radius (m)

Symbols used in the figures:

B	denotes sealed curing
D	denotes air curing
1011	HPC mix (101..) and 28 days' age when loading (...28)

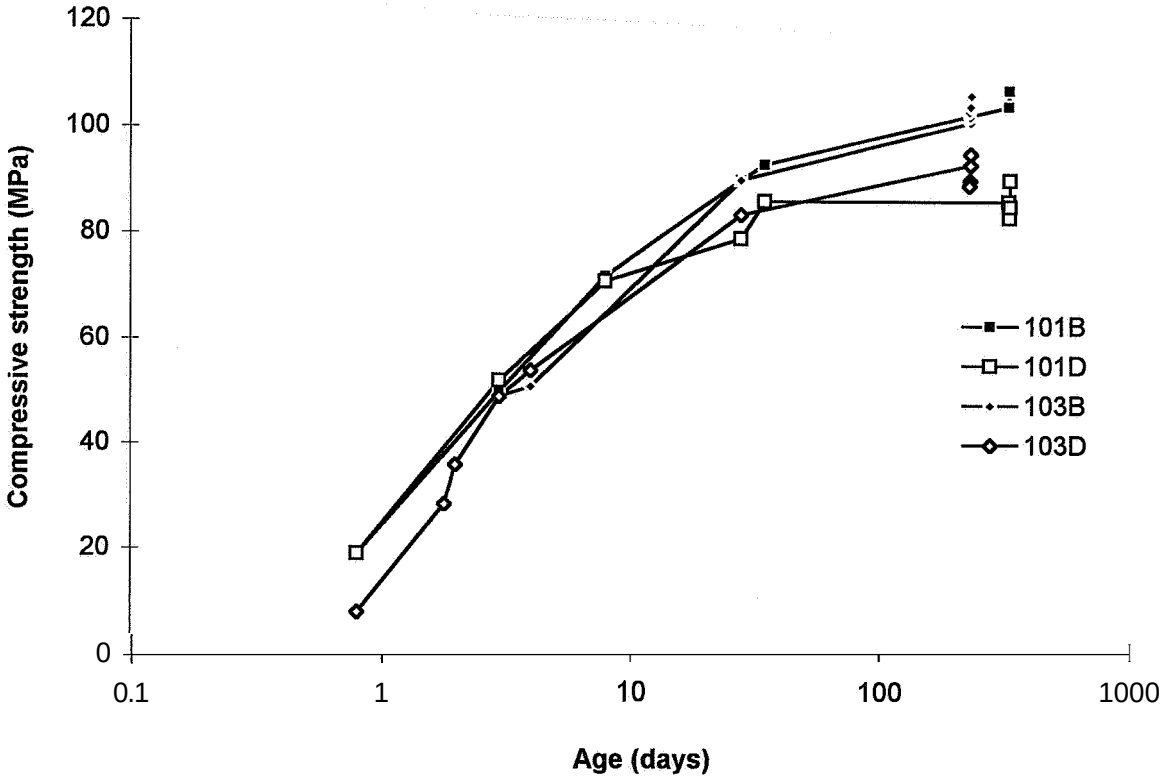

Figure 16.1 - Compressive cube strength versus time.

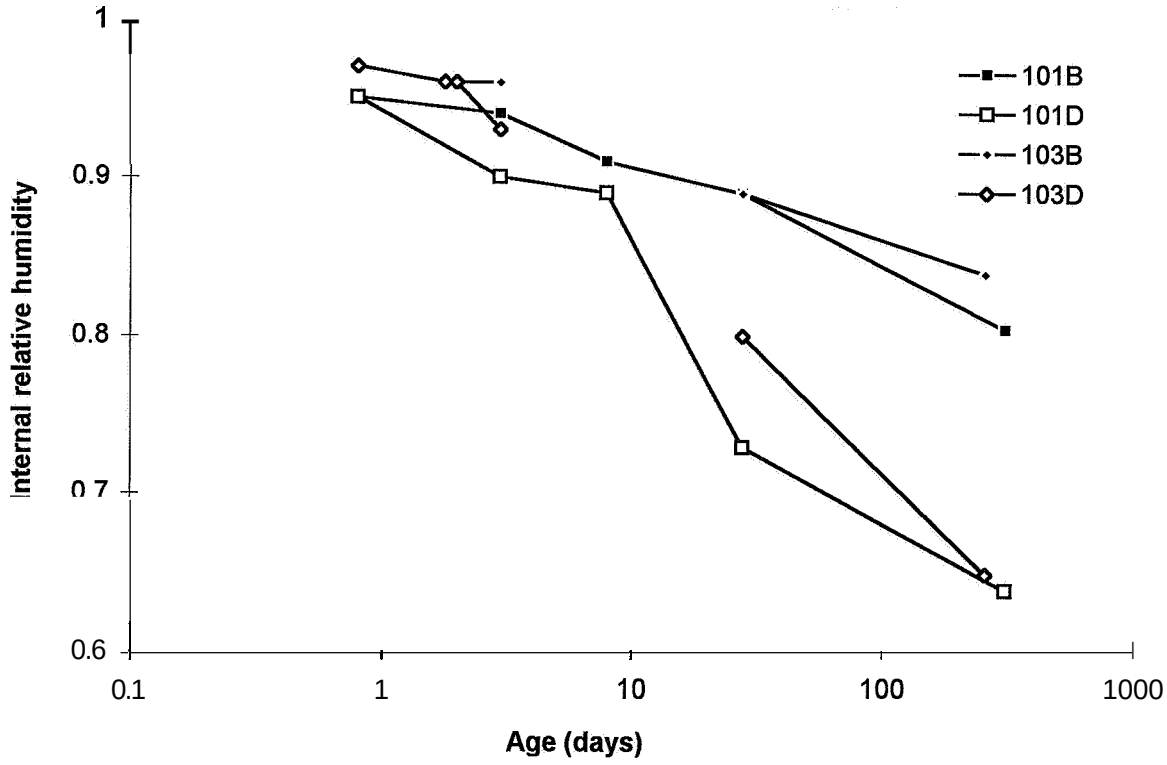

Figure 16.2 - Internal relative humidity of cubes versus time, symbols given above.

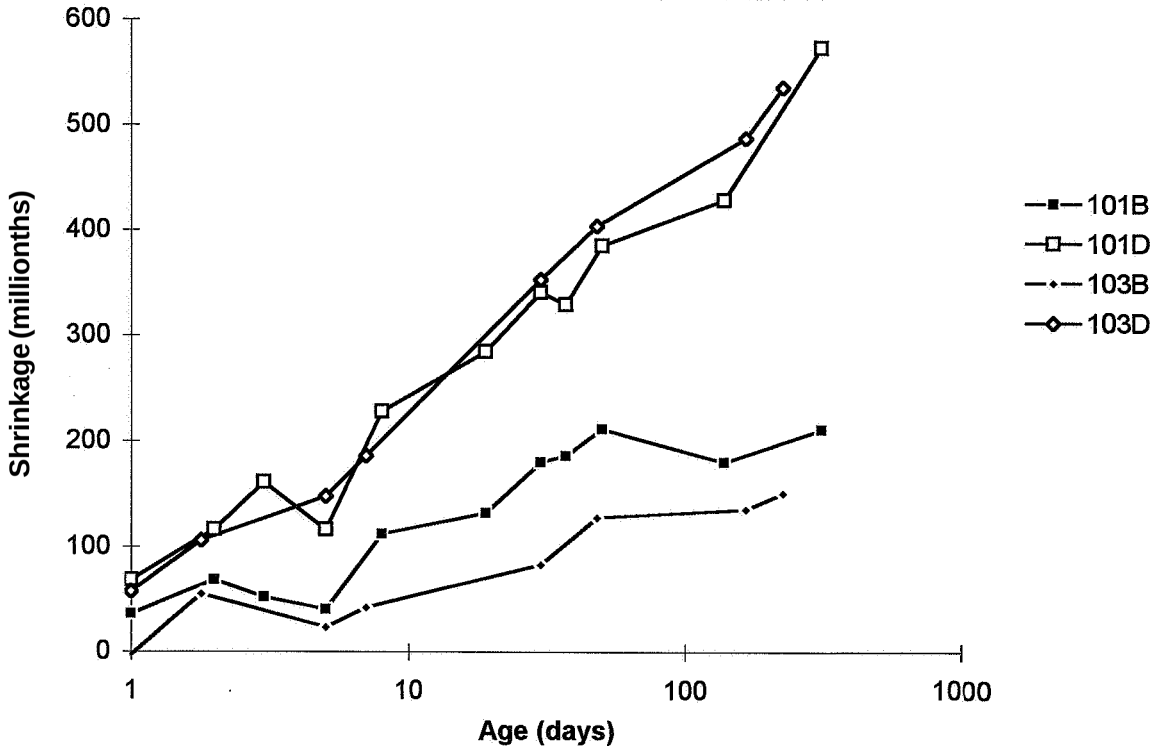

Fig ıre 16.3 - Shrinkage of HPCs versus time. The symbols are given above.

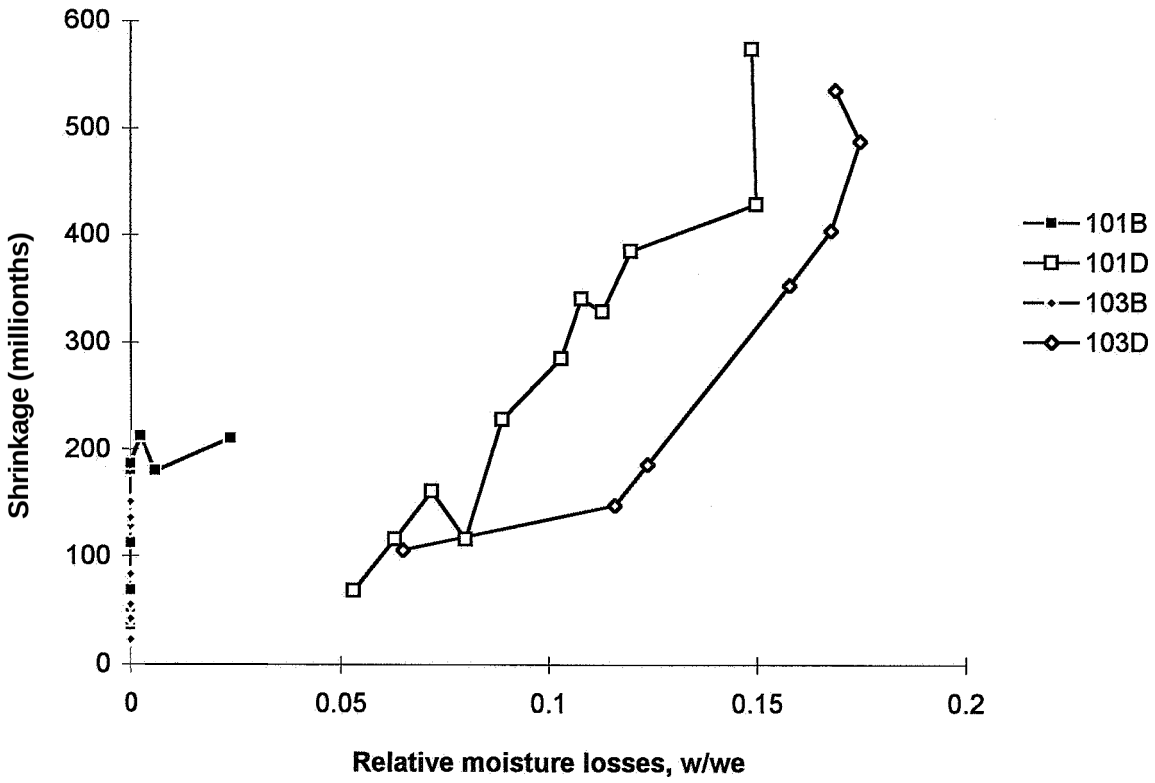

Figure 16.4 - Shrinkage versus relative moisture losses, w_e/w, symbols given above.

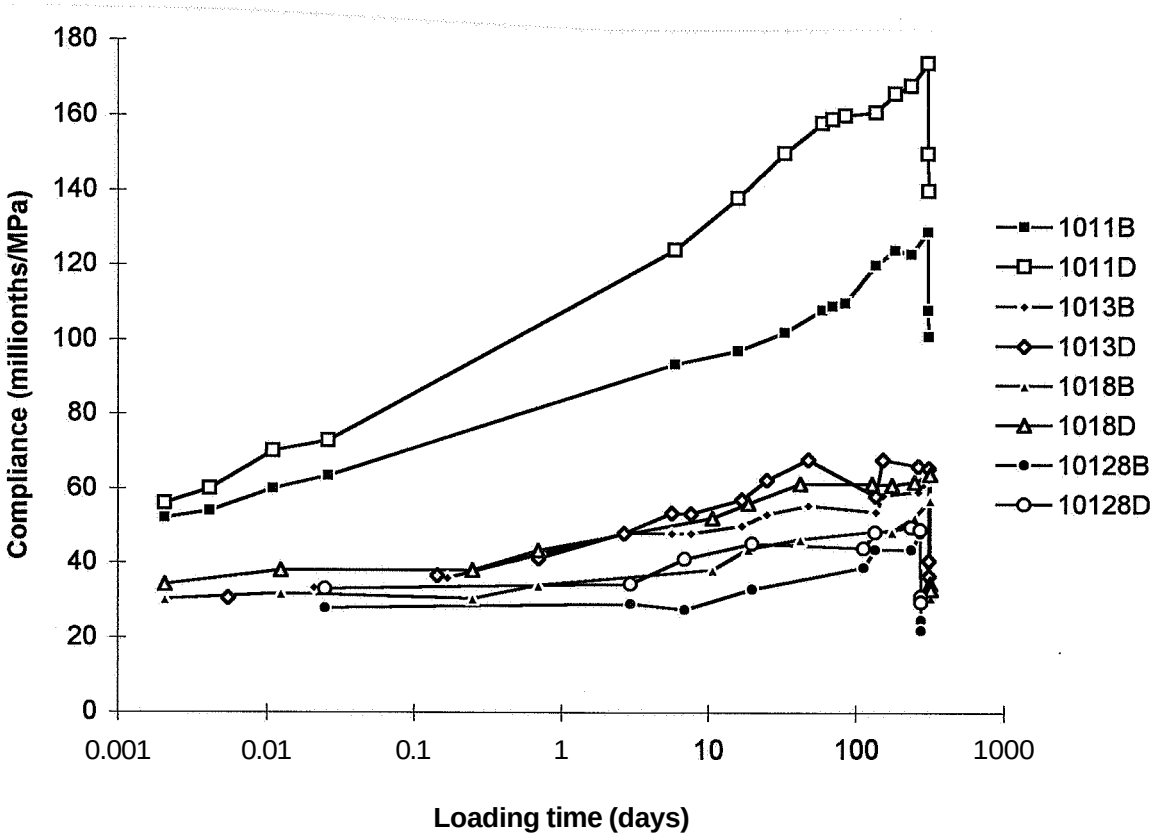

Figure 16.5 - Compliance of HPC 101 versus time. The symbols were given above.

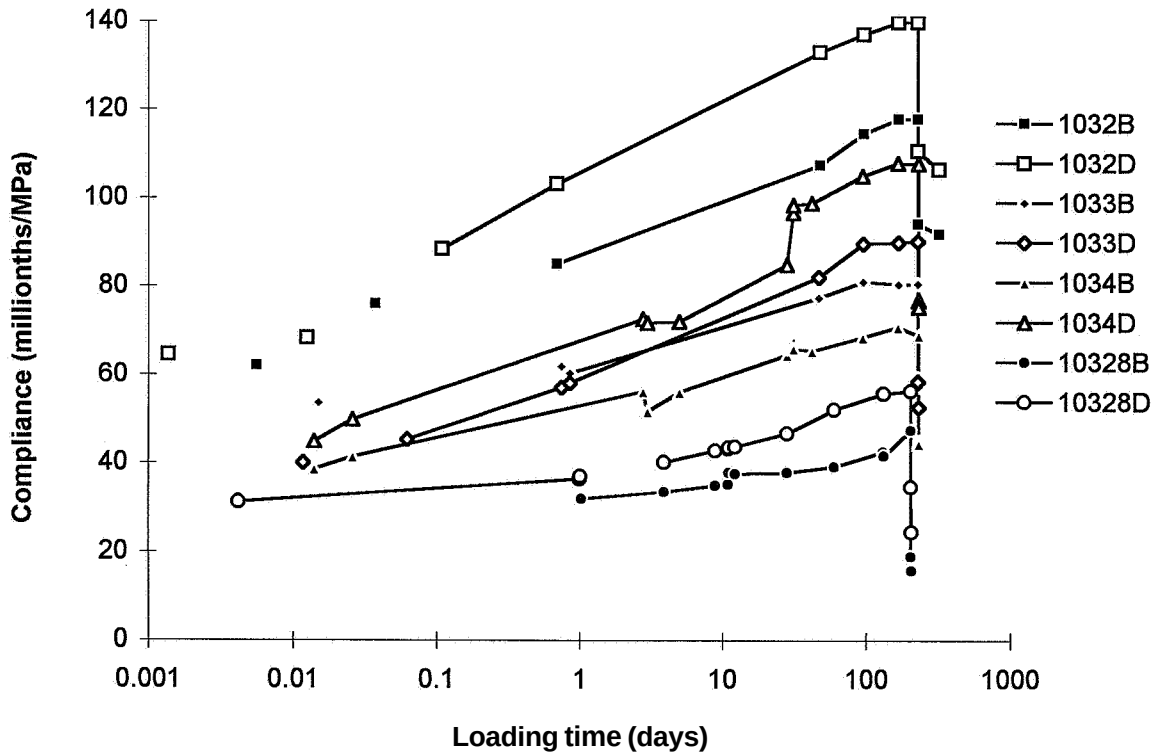

Figure 16.6 - Compliance of HPC 103 versus time. The symbols were given above.

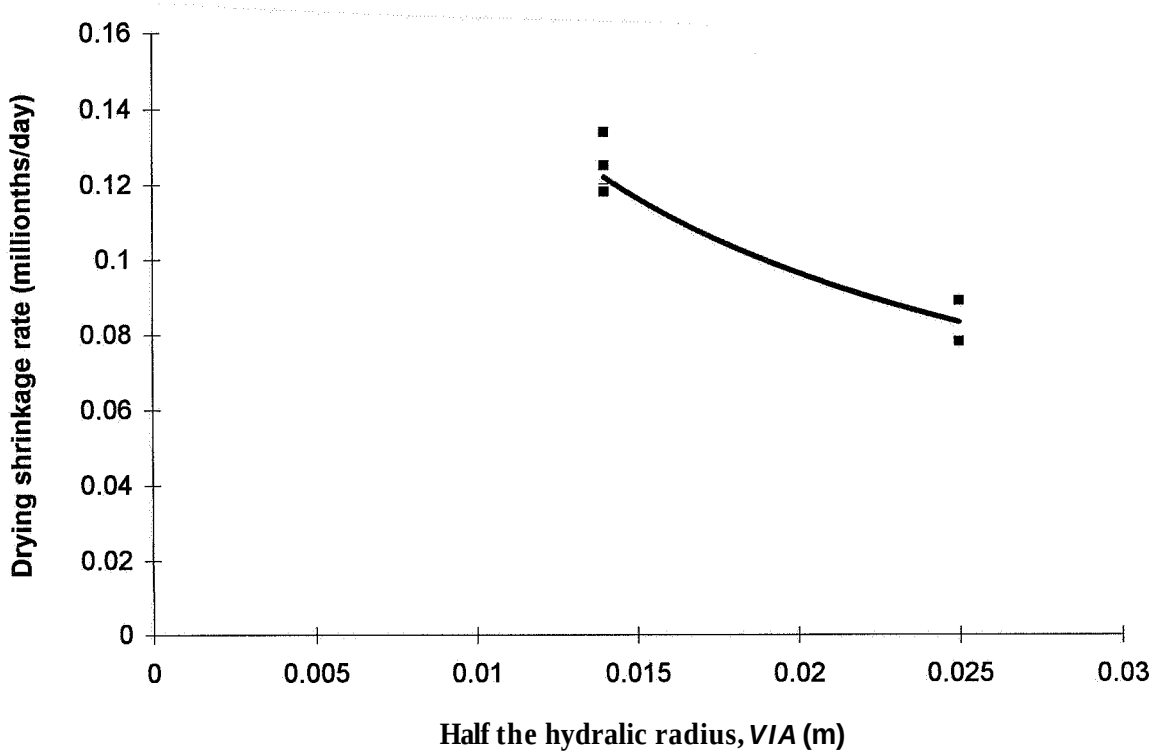

Figure 16.7 - Rate of drying shrinkage versus half the hydraulic radius, VIA.

16.4.2 Creep compliance

The measured creep compliance was reduced by the measured shrinkage. The measured creep compliance was compared with the calculated creep compliance according to equations (6.13), (9.1), (9.2), (14.8), (14.9), (14.10) and (14.11).

$$J(t,t')_{sh} = a \cdot \int d(t-t')/(t-t') + b = a_{sh} \cdot \int d(t-t')/(t-t') + 1000/D_{t'} \qquad (6.13)$$

$$a_{Dsh} = 3.4 \cdot [(w/c)-0.13] \cdot s_{Da5} + [0.3-11 \cdot (\sigma/f_c)] \cdot \ln(f_c/f_{c28}) \{0.25<w/c<0.40\} \qquad (9.1)$$

$$a_{Bsh} = 0.14 \cdot [(w/c)+2.5] \cdot s_{Ba5} + [0.29-6.9 \cdot (\sigma/f_c)] \cdot \ln(f_c/f_{c28}) \qquad (9.2)$$

a_{sh}	denotes the short-term compliance rate [millionths/(MPa·h)]
a_{Bsh}	denotes short-term basic creep rate [millionths/(MPa·h)]
a_{Dsh}	denotes short-term drying creep rate [millionths/(MPa·h)]
b	denotes the initial compliance 1 s after loading (millionths/MPa)
f_c/f_{c28}	denotes the relative 28-day strength at loading $\{0.4< f_c/f_{c28}<1$ for $\sigma/f_c=0.3$ and $0.15< f_c/f_{c28}<0.5$ for $\sigma/f_c=0.6\}$
s_{Ba5}	=1.25 for HPC with 5% silica fume or/and air-entrainment combined with 10% silica fume; s_{Ba5}= 1 for HPC with 10% silica fume
s_{Da5}	=1.5 for HPC with 5% silica fume and/or air-entrainment; s_{Da5}= 1 for HPC with 10% silica fume

t	denotes the age of the concrete (h)
t'	denotes the age of the concrete when loading (h)
$D_{t'}$	denotes the deformation modulus 1 h after loading, Section 7 (GPa)
$J(t,t')_{sh}$	denotes the short-term compliance (specific creep, millionths/MPa)
σ/f_c	denotes the stress/cube strength ratio when loading $\{0.3<\sigma/f_c<0.6\}$

$$J(t,t')_{Dlo} = 1000/D_{t'} + a_{Dlo} \cdot \int d(t-t')/(t-t') \quad (14.8)$$

$$a_{Dlo} = k_{ai} \cdot 513 \cdot [(w/c)^2 - 0.6 \cdot (w/c) + 0.0959] - k_{as} [1.83 + 2.37 \cdot (\sigma/f_c)] \cdot \ln(f_c/f_{c28}) \quad (14.9)$$

a_{Dlo}	denotes the long-term creep rate with air curing [millionths/(MPa·day)]
k_{ai}	= 1.5 for HPC with 5% air-entrainment; $k_{ai} = k_{as} = 1$ otherwise
k_{as}	=O.8 for HPC with 5% air-entrainment; k_{as} = 1.3 silica fume slurry
t	denotes age of the concrete (days)
t'	denotes age at loading (days)
$D_{t,}$	denotes the deformation modulus at loading, Section 7 (GPa)
$J(t,t')_{Dlo}$	denotes the long-term drying creep compliance (millionths/MPa)

$$J(t,t')_{Blo} = 1000/D_{t'} + a_{Blo} \cdot \int d(t-t')/(t-t') \quad (14.10)$$

a_{Blo}	denotes long-term basic creep compliance rate with sealed curing [millionths/(MPa·day)]
t	denotes age of the concrete (days)
t'	denotes age at loading (days)
$D_{t'}$	denotes the deformation modulus at loading, Section 7 (GPa)
$J(t,t')_{Blo}$	denotes the long-term basic creep compliance (millionths/MPa)

$$a_{Blo} = k_{s5} \cdot 231 \cdot [(w/c)^2 - 0.594 \cdot (w/c) + 0.0952] - k_{s5} [2.83 - 3 \cdot (\sigma/f_c)] \cdot \ln(f_c/f_{c28}) \quad (14.11)$$

a_{Blo}	denotes long-term creep rate with sealed curing [millionths/(MPa·day)]
f_c/f_{c28}	denotes the relative 28-day strength at loading $\{0.3< f_c/f_{c28}<1\}$
k_{s5}	= 1.5 for HPC with 5% silica fume or 10% silica fume slurry; $k_{s5}=1$ otherwise

Table 16.4 provides details concerning the parameters of the equations. The effect of the size of the cylinder (55 or 100 mm) was taken into account when choosing half the hydraulic radius, i.e. the volume to area ratio of the specimens (V/A), **Table 16.5.** The measured deformation at 100 s of loading was estimated with logarithmic extrapolation of all values of the creep compliance less than 10 days' age. **Figure 16.8** shows estimated compliance, $J_{est.}$, versus the measured compliance according to equation:

$$J_{est.} = J_B + [V/A)_{ø55}/(V/A)_{ø100}] \cdot (J_D - J_B) = J_B + (d_{ø55}/d_{ø100}) \cdot (J_D - J_B) = J_B + 0.555 \cdot (J_D - J_B) \quad (16.2)$$

Table 16.4 – Parameters of equations (9.1), (9.2), (14.9) and (14.11).

No	Age (d)	σ/f_c	f_c/f_{c28}	ln (f_c/f_{c28})	s_{a5}	a_{sh}	$\int_{0.028}^{65} dt/t$	J_{sh}	k_{ai}	k_{s5}	a_{lo}	$\int_{27}^{d} dt/t$	J_{lo}	J_{tot}
1011B	312	0.57	0.21	-1.57	1.25	6.22	7.76	48	1	1.5	6.91	4.75	33	81
1011D	312	0.59	0.23	-1.47	1.5	10.3	7.76	80	1.5	0.9	11.5	4.75	55	135
1013B	313	0.29	0.57	-0.56	1.25	1.46	7.76	7.4	-	1.5	6	4.75	28	36
1013D	313	0.29	0.63	-0.46	1.5	2.55	7.76	20	1.25	0.9	7.97	4.75	38	58
1018B	308	0.30	0.78	-0.25	1.25	0.95	7.76	7.4	-	1.5	5.03	4.75	24	31
1018D	308	0.30	0.87	-0.14	1.5	1.64	7.76	13	1.25	0.9	7.25	4.75	34	47
10128B	288	0.27	1	0	1.25	0.5	7.76	3.9	-	1.5	4.3	4.65	20	24
10128D	288	0.30	1	0	1.5	1.22	7.76	9.5	1.25	0.9	6.93	4.65	33	42
1032B	230	0.60	0.40	-0.92	1.25	4.0	7.76	31	-	1	3.80	4.44	17	48
1032D	230	0.60	0.43	-0.84	1.5	6.51	7.76	51	1.5	0.8	10.5	4.44	47	97
1033B	231	0.29	0.54	-0.62	1.25	1.56	7.76	12	-	1	4.06	4.44	18	30
1033D	231	0.29	0.59	-0.53	1.5	2.75	7.76	21	1.5	0.8	9.38	4.44	42	63
1034B	232	0.48	0.58	-0.54	1.25	2.13	7.76	17	-	1	3.6	4.44	16	32
1034D	232	0.48	0.63	-0.46	1.5	4.6	7.76	36	1.5	0.8	9.4	4.44	42	77
10328B	208	0.28	1	0	1.25	0.5	7.76	3.9	-	1.5	2.84	4.33	12	16
10328D	208	0.30	1	0	1.5	1.22	7.76	9.5	1.25	0.8	8.31	4.33	36	46

Table 16.5 - Measured and estimated creep compliance after 100s (millionths/MPa).

No	$J_{mea.}$	J_{100s}	$J_{creep}= J_{mea.} - J_{100s}$	$J_{est.}$
1011B	129	48	81	81
1011D	174	49	125	111
1013B	63	24	39	36
1013D	66	23	43	48
1018B	57	29	28	31
1018D	64	32	32	40
10128B	48	28	20	24
10128D	49	29	20	34
1032B	118	57	61	48
1032D	140	59	81	71
1033B	81	42	39	30
1033D	90	29	61	48
1034B	69	33	36	32
1034D	108	36	72	57
10328B	47	31	16	16
10328D	56	29	27	32

d denotes diameter of cylinder (mm)

J_B denotes estimated compliance of sealed cylinder 55 mm in diameter at

J_D denotes estimated compliance at drying of cylinder 55 mm in diameter

The following equation was obtained between estimated and measured compliance:

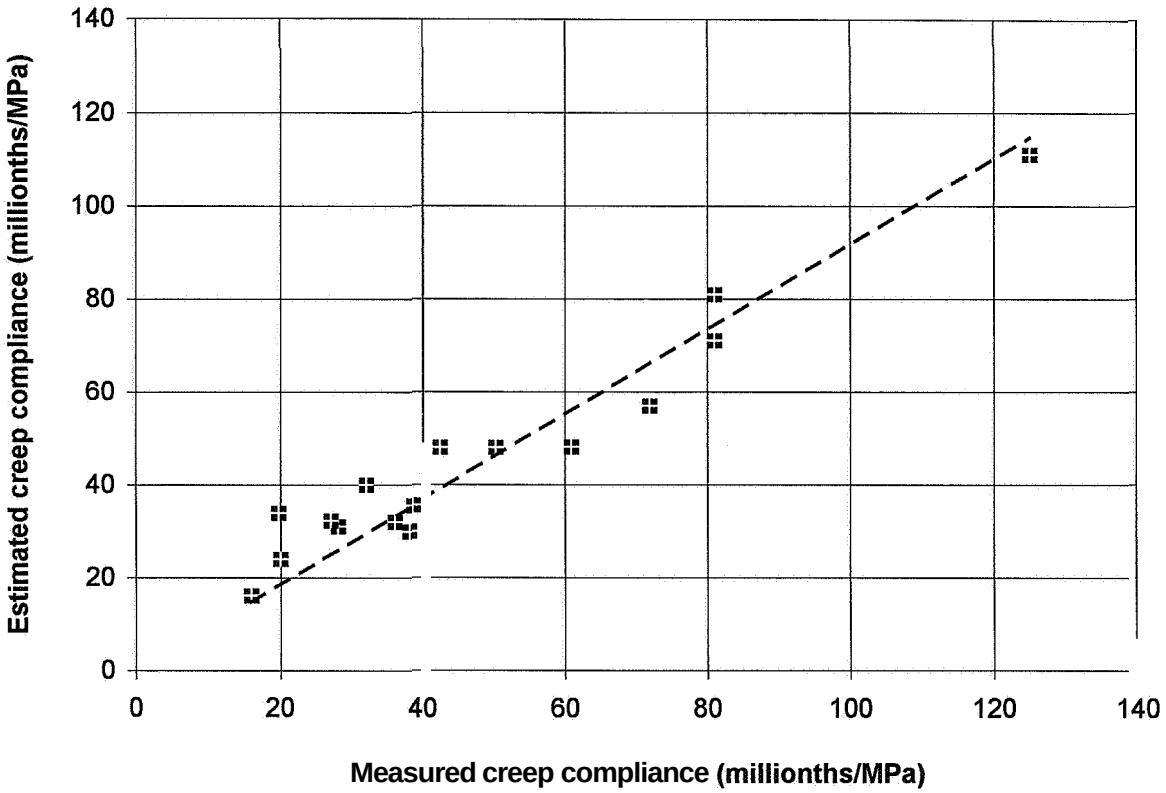

Figure 16.8 - Estimated compliance versus measured compliance.

$$J_{est.} = 0.92 \cdot J_{mea.} \qquad (16.3)$$

$J_{est.}$ denotes the creep compliance estimated according to equation (6.13), (9.1), (9.2), (14.8), (14.9), (14.10), (14.11) and (16.2) (millionths/MPa)

$J_{mea.}$ denotes the measured creep compliance (millionths/MPa)

According to equation (16.3), the estimated creep compliance coincided reasonably well with the estimated compliance taking in account half the hydraulic radius of the specimen according to equation (16.2).

16.5 Summary and conclusions of dimensional study

The results and analysis of the creep and shrinkage investigation presented above performed on more than 100 cylinders 55 mm in diameter were compared with tests on 20 cylinders 100 mm in diameter. The following conclusions were drawn:

- The autogenous shrinkage was independent of size.
- The drying creep rate was correlated to the hydraulic radius of the specimen. The creep compliance studied on cylinders 100 mm in diameter coincided well with the results of creep studies performed on cylinders 55 mm in diameter taking into account half the hydraulic radius of the specimens.

17. FIELD STUDIES

17.1 General

From a practical point of view it was of great interest to confirm the laboratory studies by a few field studies. The high stress/strength levels achieved in the laboratory research were difficult to simulate in structures affected by gravity force only. The field studies were therefore carried out on prestressed constructions. Two types of beams were studied: hat beams mainly prestressed at the bottom flange and square beams, symmetrically prestressed, i.e. prestressed pillars. It was the objective of the field studies to compare the field studies with the laboratory studies.

17.2 Experimental

Specimen and materials:

The width of the hat beam was 350 mm and the height was 300 mm. The height of the flange was 160 mm and thus the height of the web was 140 mm. The web had a width of 170 mm. In the flange 18 pieces of prestressed strands were placed. The web contained 2 strands, **Figure 17.1**. The strands had a diameter of 12.5 mm and were tensioned to a force of 135 kN each. HPC was poured into the mould and cured. After a curing period varying between 18 and 42 h the strands were cut outside the mould and thus the force from the strands was transferred to the HPC. Due to elastic strain and creep strain of the HPC the force of the strands continuously diminished. Some relaxation of the strands also occurred which also lowered the force. Since the force was unsymmetrically related to the section of the beams, some overestimation was made to establish the resulting stress.

The square beams had a size of 200x200 mm and were prestressed by alternatively 12 or 16 pieces of 12.5 mm strands. The strands were symmetrically placed in the beam, **Figure 17.1.** The initial force of the strands varied between 90 and 135 kN before prestressing of the HPC. The force was hydraulically transferred to the HPC after a curing period varying between 2 and 4 days. Thus the stress in the HPC beams became more or less symmetrically distributed.

The mix proportions, etc. of the HPCs in the hat beams are given in **Table 17.1** (kg/m^3 dry material, etc.). After pouring, the HPC was heated in the mould. The cubes that were used to obtain the strength were placed in a hot box. The temperature in the box was adjusted to obtain the same heat development as the beam. The target value for the strength of the HPC was 80 MPa before prestressing was performed. Some hat beams were insulated by butyl-rubber cloth to study basic creep (B). The remaining beams were placed in a climate with a relative humidity of about 45% (D). All beams were studied at 20 °C after initial curing at about 48 "C. The mix proportions, etc. of the HPCs in the square beams are given in **Table 17.2** (kg/m^3 dry material, etc.).

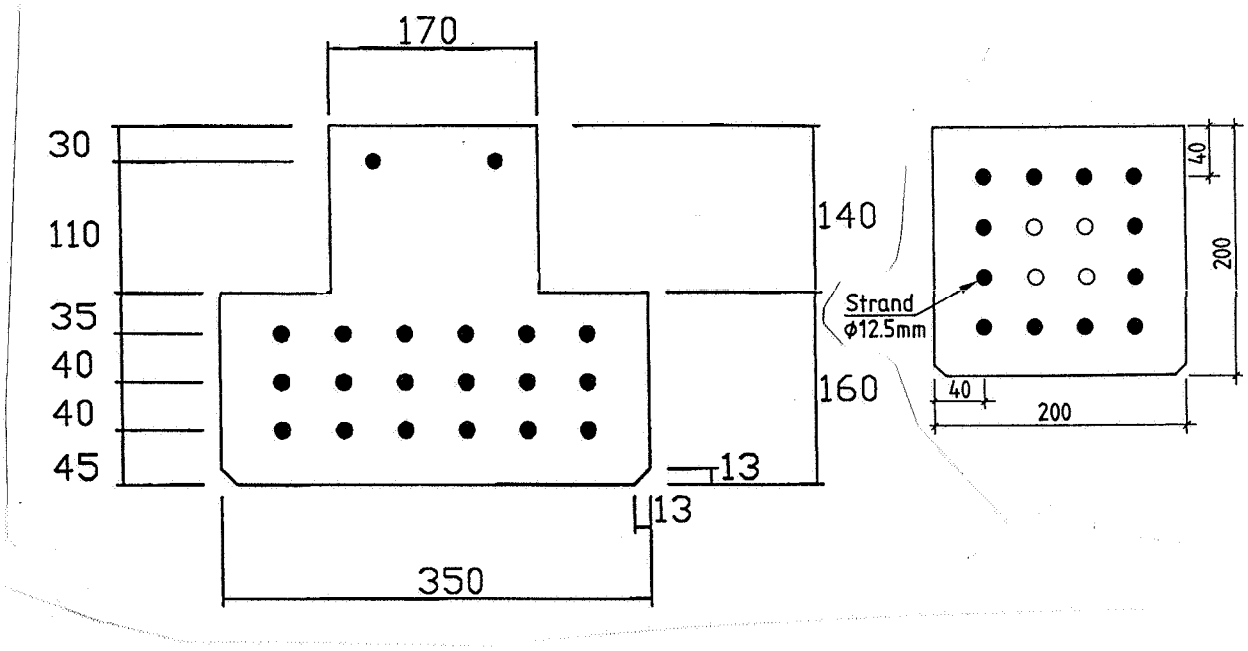

Figure 17.1 – Section of beams. • = strands in all beams. o = strands in some beams.

Table 17.1 - Mix proportions, etc. of HPCs in hat beams (kg/m^3 dry material, etc.).

Material/ mix	**1**	**2**	**3**	**4**	**5**
Coarse aggregate 8-16 mm	1043	1024	990	990	970
Gravel 0-8 mm	617	736	708	708	715
Filler	118	-	90	90	87
Cement, c, low-alkali (404 m^2/kg Blaine)	510	512	510	511	429[1)]+ 76[2)]
Silica fume, s (fineness 17.5 m^2/g)	51	56	51	51	50
Superplasticiser	9	9.6	7	7	12.1
w/c	0.28	0.27	0.30	0.30	0.28
s/c	0.10	0.11	0.10	0.10	0.10
Density	2510	2475	2510	2510	2483
Age at loading (h)	18	42	22	20	20
Strength at loading (100-mm cube, MPa)	70	87	83	85	78
Strength at 28 days' age (MPa)	122	130	122	125	110

1) 302 m^2/kg Blaine, 2) ≈1000 m^2/kg Blaine, w= mixing water including moisture

The cubes that were used to obtain the strength development of the square beams were placed in an insulated box on top of the beam but inside the mould. The box was not insulated towards the beam. The cubes thus obtained the same heat development as the beam did. Different target values for the strength of the HPC before prestressing were used dependent on the force applied by the strands. Initially the HPC was cured in the steel mould. Plastic foil and 60 mm of heat insulation covered the top of the HPC. About 12 h before prestressing the beams were cooled to 20 °C. After prestressing the beams were cured at the same temperature as before (20 °C) but uncovered. After 1 h of measurement the beams were placed in an ambient climate of ≈ 45% relative humidity at 20 °C temperature.

Table 17.2 - Mix proportions, etc. of HPC in square beams (kg/m^3 dry material).

Material/ mix	3230	3240	3730	3740	3750
Coarse aggregate 12-16 mm	425	425	425	380	380
Coarse aggregate 8-12 mm	425	425	425	380	380
Coarse aggregate 4-8 mm	325	325	325	190	190
Gravel 0-8 mm	775	775	775	790	790
Fibre	1-4	1-4	0-2	0-2	0-2
Cement, c, low-alkali (302 m^2/kg Blaine)	500	500	500	480	480
Silica fume, s (fineness 17.5 m^2/g)	35	35	35	33	33
Superplasticiser, melamine formaldehyde	10	10	10	4.8	4.8
w/c	0.32	0.32	0.37	0.37	0.37
s/c	0.07	0.07	0.07	0.07	0.07
Density	2500	2500	2500	2390	2390
Age at loading (h)	69	65	48	71	92
Strength at loading (150-mm cube, MPa)	57-69	62-72	42-46	49-55	56-62
Strength at 28 days' age (MPa)	62-88[1)]	100-105[1)]	77-88[1)]	81-89[1)]	85-88[1)]

1) details are given in the estimations below

Later after about 1 week the square beams were placed at a lower temperature. The final measurement was performed at a temperature of 20 "C. The coefficient of thermal dilatation was assumed to be 0.01 per mil/°C. The HPCs in the square beams contained either 0, 1, 2 or 4 kg/m^3 polypropylene plastic fibre in order to prevent spalling of the HPC surface in the event of fire temperatures. In the mix proportions the fibre additive was indicated after the mix no. For example: 37..2 indicates water-cement ratio, w/c = 0.37 and a fibre content of 2 kg/m^3. The figure in between indicated the target 28-day load level, σ/f_{c28}, at loading (prestressing, %/10). The distribution of particles in the fresh HPC was of great importance for the workability of the HPC and the possibility to pour HPC in a structure, **Persson (1995B)**. **Figure 17.2** shows the cumulated material in the HPC including cement and the ideal distribution of particles for HPC with a 28-day strength of 120 MPa.

Experimental methods:

The autogenous shrinkage and the drying shrinkage were measured for all the HPCs studied. The cylinder had a length of 300 mm and a diameter of 55.5 mm. The cylinders were cast on site and then transported to the laboratory where the HPC was demoulded. One cylinder of each batch of HPC was insulated by 2 mm butyl-rubber cloth; one cylinder was left unprepared. Cast-in items were placed 25 mm fiom the ends of the 300-mm cylinder. After demoulding, stainless ground screws were placed in the cast-in items. The cylinders were placed in a 20 °C air-conditioned room with an ambient relative humidity of 55%. The first measurement took place after the HPC reached the same temperature as the ambient climate room. Measurements at three sides of the cylinders started at about 20 hours' age.

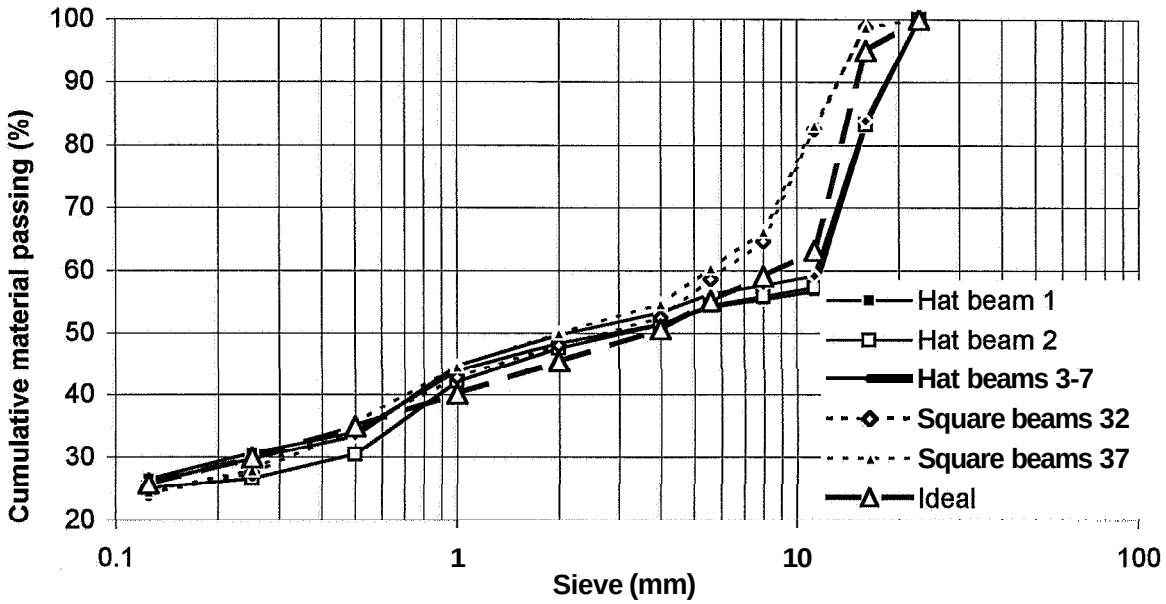

Figure 17.2 - Grading curve (cumulated material passing) in fresh HPC versus sieve.

The measurement device (Proceq) was calibrated to an INVAR rod, cp. laboratory experiments. The measurements were carried out for 3 years. The weight of the cylinder was obtained parallel to the measurement of length to control losses of moisture fiom the specimen. In case of hat beams a part of the beam was insulated by 2-mm butyl-rubber cloth. The drying shrinkage was obtained on the remaining part of the beam in an ambient climate of about 55% relative humidity. Cast-in items of steel were placed in the flange of the hat beam. The distance fiom the bottom and the top of the flange to the cast-in item was 25 mm. The horizontal distance between the cast-in items was 250 mm. After demoulding, the beam consoles were fixed to the cast-in items. The measurement was carried out by LVDTs in the same way as described in the laboratory experiments. The LVDTs were calibrated before the measurement took place. A computer collected the strain data. In the case of square beam, cast-in items of steel were placed in the top of the beam. The distance fiom the side of the beam to the cast-in item was 100 mm. The horizontal distance between the cast-in items parallel to the beam was 250 mm. After demoulding, the beam consoles were fixed to the cast-in items. The measurement was carried out by LVDTs in the same way as described above. The LVDTs were calibrated before each measurement took place. A computer automatically collected the strain data. After 1 h the LVDT-measurements were replaced by mechanical measurements in stainless ground screws, that were placed in the cast-in items In the case of square beam, cast-in plastic pipes were placed at the top of the beam reaching the centre of the square section in order to measure the internal relative humidity. The pipe was tightened with a rubber plug between the measurements. During the measurement of internal relative humidity the dew-point meter (calibrated according to ASTM E 104-85) was placed in the pipe for at least 16 h. The instrument was covered with a hood to avoid temperature changes.

17.3 Results

Figure 17.3 shows the results of internal relative humidity in the square beams. **Figure 17.4** shows the shrinkage of cylinders. The observed total strain (including shrinkage) of the hat beams at the middle height of the flange is shown in **Figure 17.5.** The observed total strain at the middle upper edge of the square beams is shown in **Figures 17.6-17.10. Figure 17.11** shows the moisture losses versus time. **Figure 17.12** shows the shrinkage versus moisture losses of all beams.

17.4 Sources of error and accuracy

The main sources of error were:

- Temperature difference between the beam and the LVDTs the instrument during measurement of internal relative humidity.
- Uneven deformation of the surface and the inner part of the beam.
- Delayed start of the tests of shrinkage.
  Moisture losses in studies of basic creep.
- Differences between measured strength and strength obtained in the beams.
- Differences in ambient climate of beams and specimens for shrinkage studies.

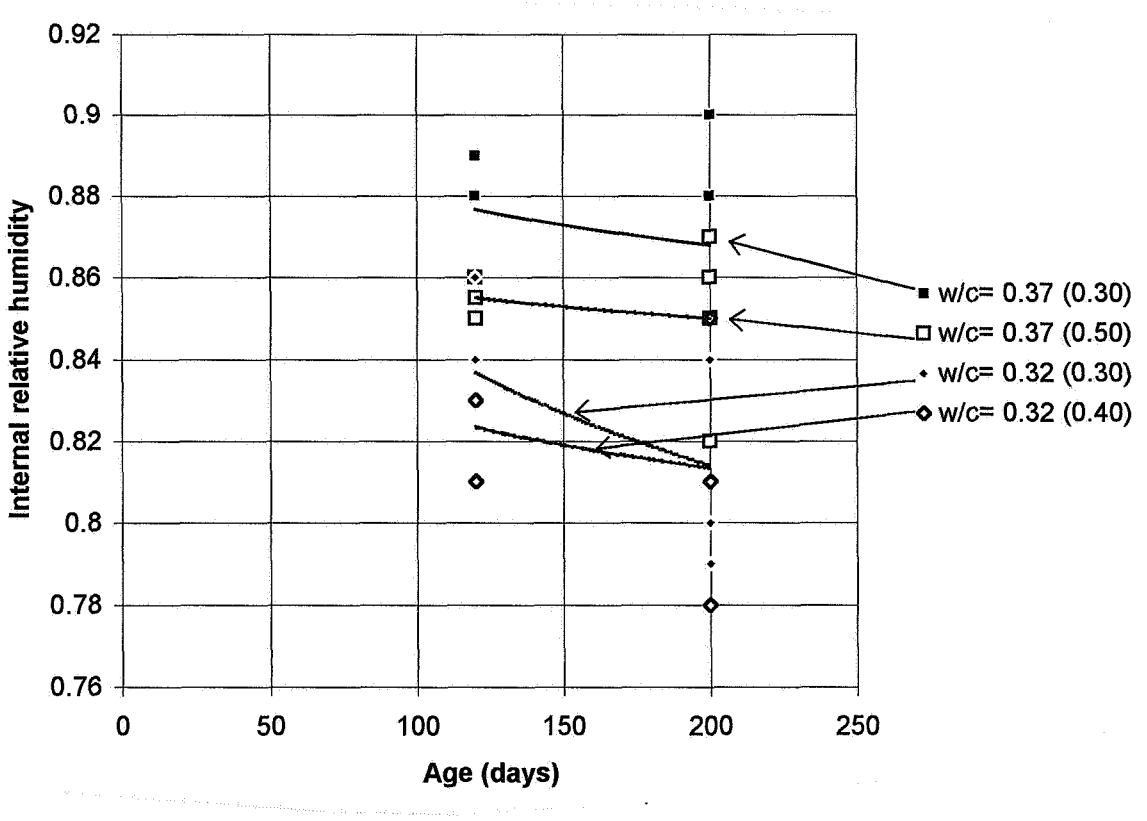

Figure 17.3 – Internal relative humidity in square beams. ( )= stress/strength level.

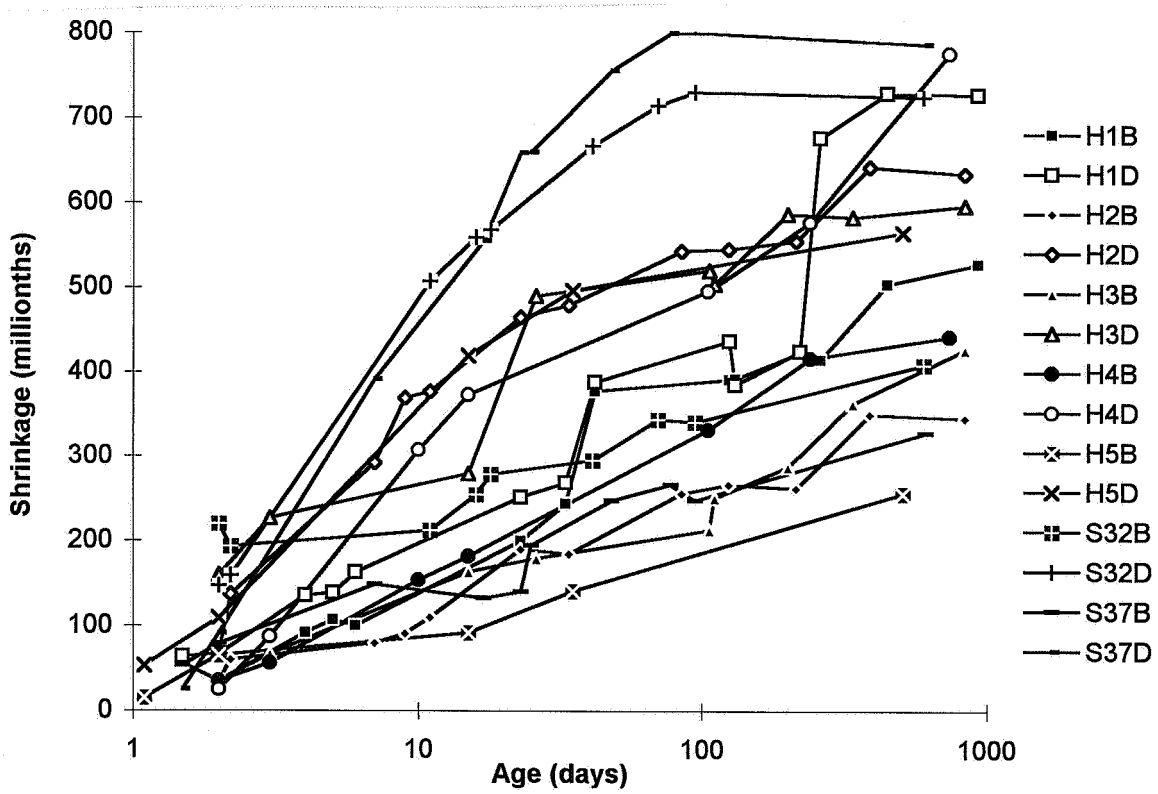

Figure 17.4 - Shrinkage of cylinders versus age. B = sealed curing, D = air curing (drying), H= hat beam, S= square beam, 37= water-cement ratio, wlc (per cent).

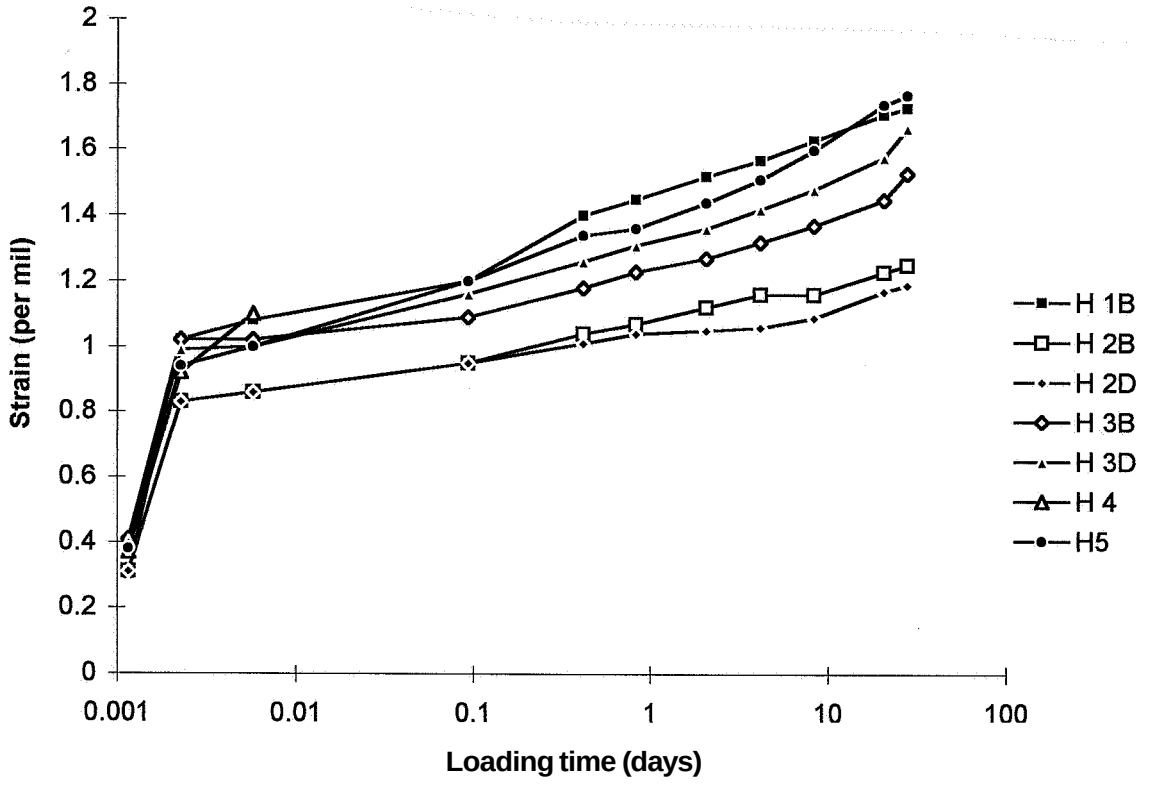

Figure 17.5 Measured strain of hat beams versus time. B= sealed, D= drying.

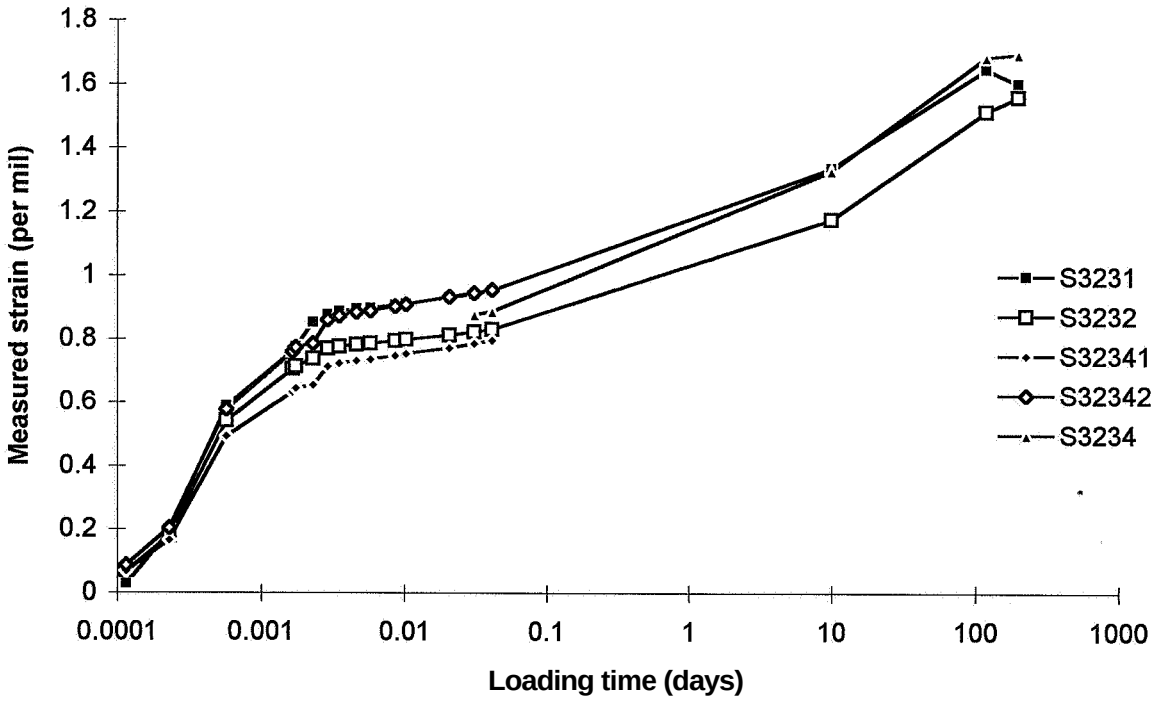

Figure 17.6 - Measured total strain of beams S323 at the middle top versus loading time. S= square beam; 32...=w/c; ..3.= amount of plastic fibre; ...4= batch no.

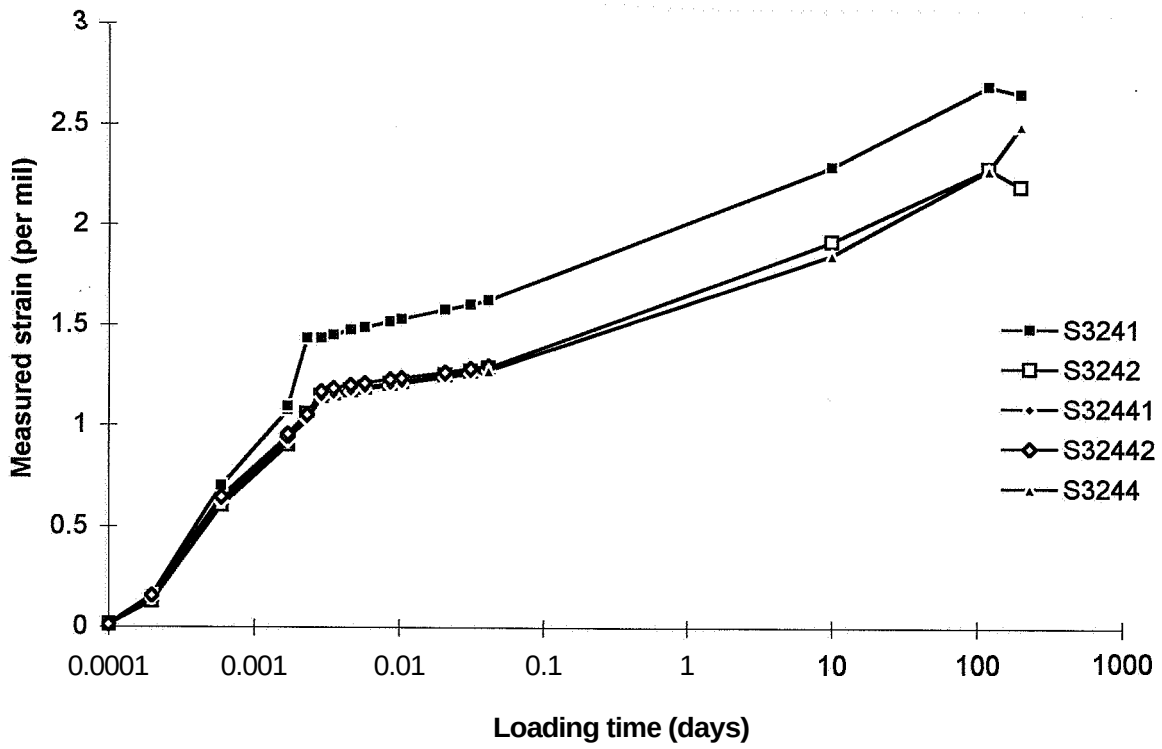

Figure 17.7 - Measured total strain of beams S324 at the middle top versus loading time. S= square beam; 32...=w/c; ..3.= amount of plastic fibre; ...4= batch no.

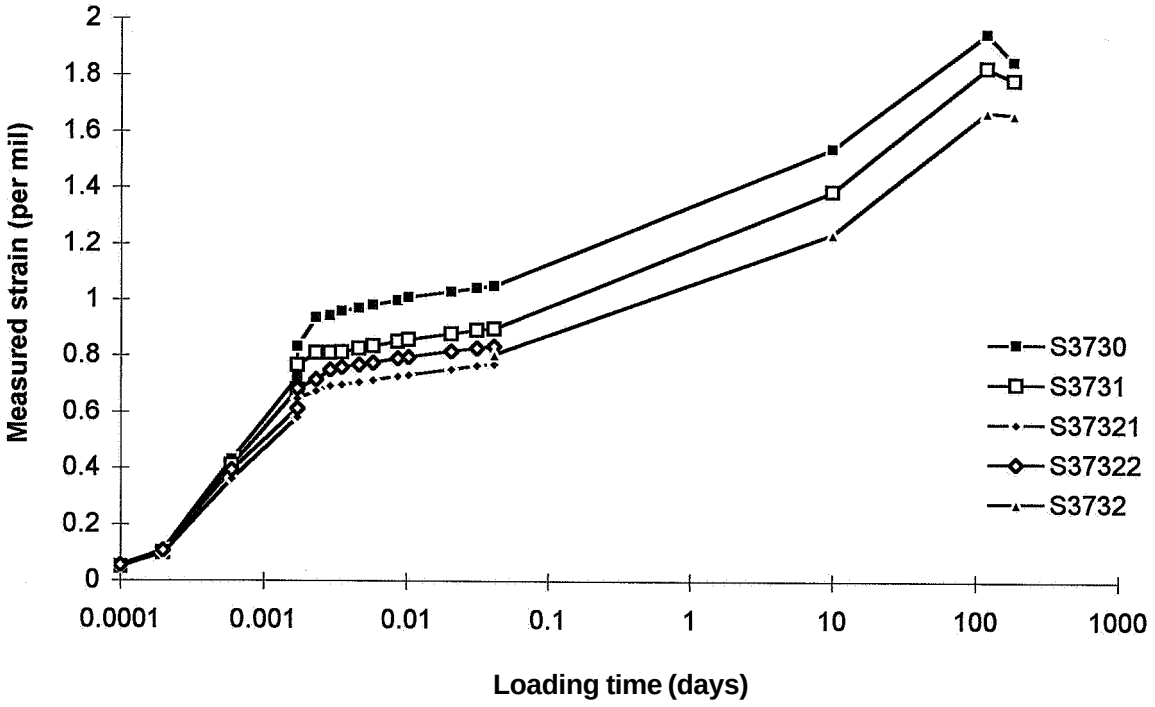

Figure 17.8 - Measured total strain beam S373 at the middle top versus loading time. S= square beam; 32...=w/c; ..3.= amount of plastic fibre; ...4= batch no.

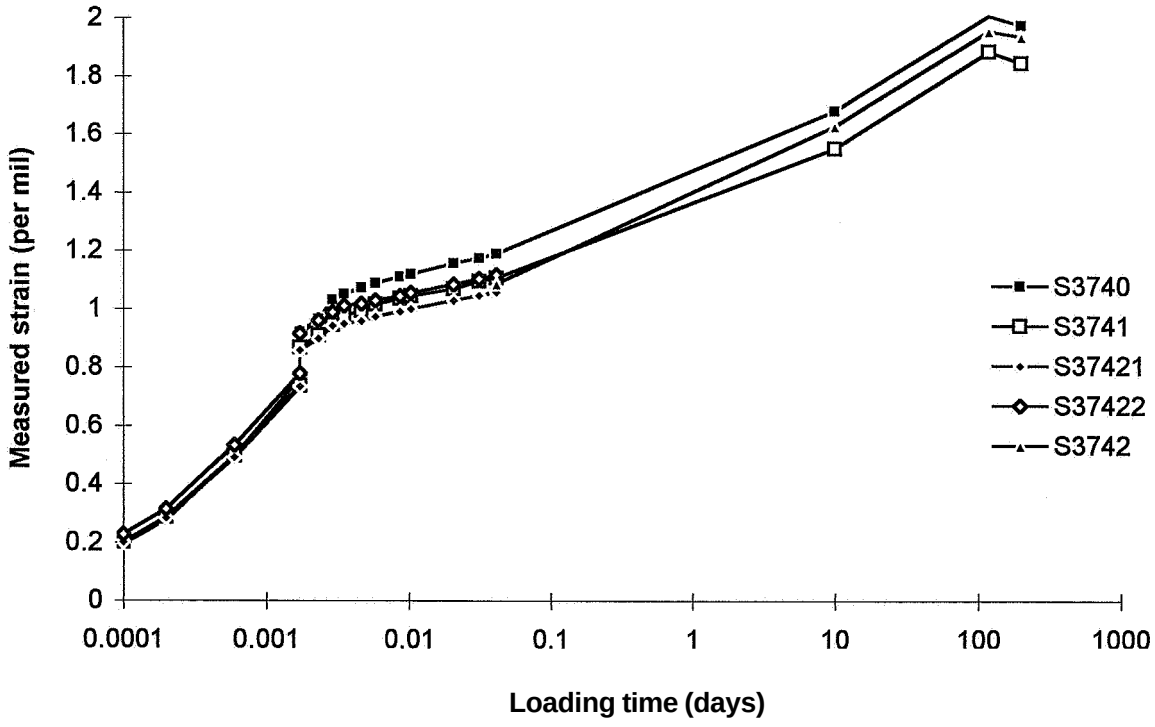

Figure 17.9 - Measured total strain of beams S374 at the middle top versus loading time. S= square beam; 32...=w/c; ..3.= amount of plastic fibre; ...4= batch no.

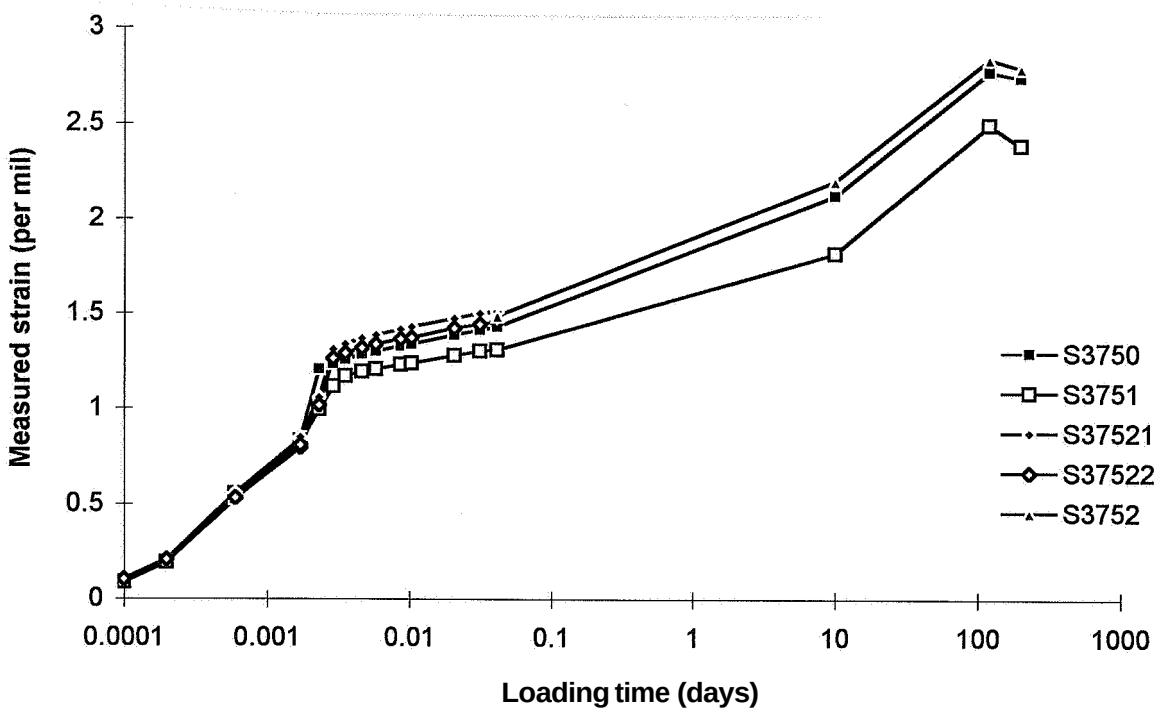

Figure 17.10 - Measured total strain beam S375 at the middle top versus loading time. S= square beam; *32*..=w/c; ..3.= amount of plastic fibre; ...4= batch no.

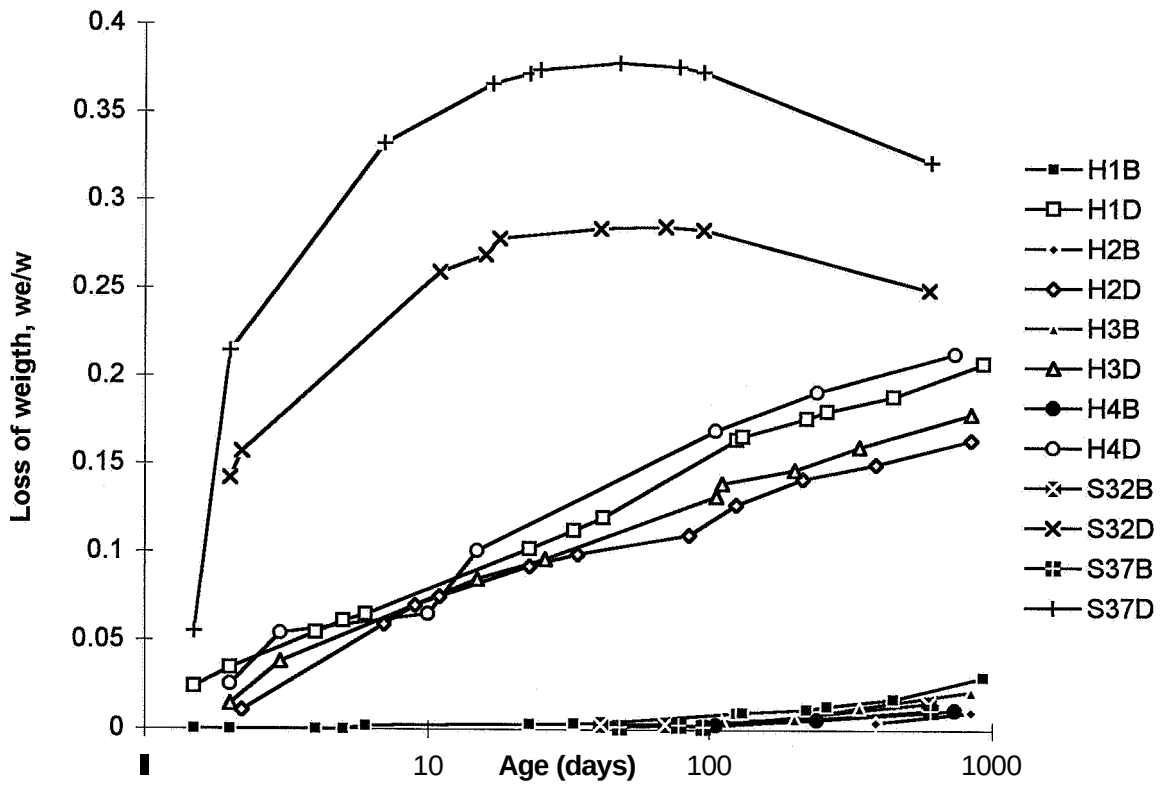

Figure 17.11 Moisture losses versus time. B= sealed curing, D= air curing.

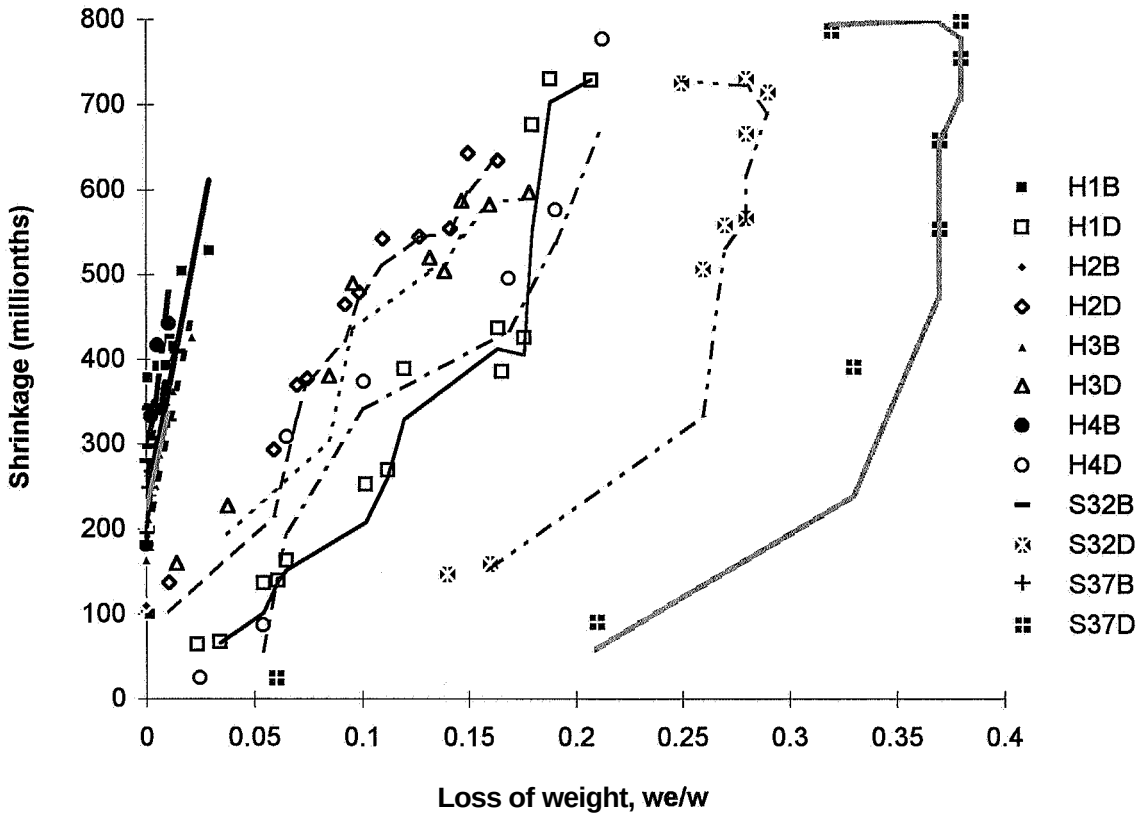

Figure 17.12 - Shrinkage versus moisture losses, we/w. B= sealed curing, D= air curing, H2= hat beam 2, S= square beam, 32= water-cement ratio, w/c (per cent).

The maximum temperature of the hat beam at unloading was about 30 "C. However, the LVDTs were 20 "C at the start of measurement, which cause a fault. The fault increased the measured strain, i.e. large creep strain was measured including some temperature differences. The fault in the strain then became about 0.10 per mil assuming that the coefficient of thermal dilatation was 0.010 per mil/°C. At 30 MPa stress in the HPC, the fault was less than 4 millionths/MPa.

The square beam was cooled to 20 °C before the prestressing of the HPC was performed. In an extensive investigation of the influence of the moisture profile on the measured shrinkage, **Alvaredo and Wittmann (1993)**, it was pointed out that the way of measurement was of great importance for obtaining a correct strain. If the measurement points were placed at the surface, the measured shrinkage became larger than the average shrinkage of the beam, due to the shrinkage of the surface. The maximum measured fault could be estimated as the difference between drying shrinkage and the autogenous shrinkage. At 28 days' age this difference was about 0.18 per mil calculated as an average on the beams H1, H2 and H3. The fault of compliance then was less then 6 millionths/MPa at 30 MPa stress in the HPC.

Due to the required time of transport of specimens from the site to the laboratory, the start of the shrinkage measurements was delayed for beam H2 and H3. The measured autogenous shrinkage then became about 0.05 per mil lower than when the measurements started at 1 day's age. This fault was also small. The moisture

losses of the insulated specimen were also much smaller than losses of moisture in drying specimen and also much smaller than the initial amount of water. The compressive strength was obtained for one beam of each stress/strength level only. However, due to different admixture of plastic fibre in the beams the mixing was continued during the addition of plastic fibre, which may have influenced the compressive strength, perhaps ± 5 MPa. Some differences certainly existed between the ambient climate in the laboratory, where the shrinkage was measured, and the industry where the beams were cured, perhaps as much as ± 10% RH, internal relative humidity. The strain was mainly measured at 20 °C or recalculated to 20 °C accordant a thermal coefficient of dilatation of 0.01 per mil/°C, cp. equation (15.4).

17.5 Analysis

17.5.1 Effect of elasticity during relaxation and estimated shrinkage

Equation (14.23) and **Figure 17.3** were used to compensate for the decline of forces in the strands during the creep deformations (named elastic effect; millionths/MPa): $\Delta J_E = (\Delta\sigma/\sigma)\cdot(1000/E_\varnothing)$. As regards shrinkage **Figure 17.12** shows shrinkage versus the loss of moisture. The autogenous shrinkage was estimated at the left of **Figure 17.12.** (A linear regression was carried out and the autogenous shrinkage estimated at no loss of weight.) The long-term drying shrinkage (excluding autogenous shrinkage) was estimated at an age before the specimen increased in weight due to carbonation. The results of carbonation shrinkage from Section 8 above were co rmed by the present field study, i.e. no carbonation shrinkage occurred provided $w/c \leq 0.30$ and $s/c \geq 0.10$, where c denotes the cement content, s denotes the content of silica fume and w denotes the amount of mixing water. **Figure 17.13** shows the shrinkage estimated according to equations (8.10)-(8.13) versus measured shrinkage. The estimation of shrinkage according to equations (8.10)-(8.13) is also shown in **Table 17.3.** Another possibility the estimate the shrinkage was by the measured internal relative humidity, 0 , **Figure 7.3** and equation (8.2). However, **O** in the beams was about 1% lower than **O** estimated according to equation (5.39, self-desiccation). It was then concluded to be more accurate to use the measured shrinkage for the calculation of the reduction of the compliance owing to shrinkage.

Table 17.3 - Estimated shrinkage according to equations (8.10)-(8.13) (per mil).

Type of shrinkage	w/c=0.27	w/c=0.28	w/c=0.30	w/c=0.32	w/c=0.37
Total	0.66	0.61	0.54	0.50	0.52
Autogenous	0.24	0.23	0.20	0.17	0.09
Carbonation	0.02	0.03	0.04	0.06	0.10
Drying	0.37	0.34	0.29	0.27	0.33

$$\varepsilon = k\cdot 34\cdot[(w/c)^2 - 0.68\cdot(w/c) + 0.13] \qquad (8.10)$$

$$\varepsilon_B = k_B\cdot 1.5\cdot[0.43 - (w/c)] \qquad (8.11)$$

$$\varepsilon_C = 0.85 \cdot [(w/c) - 0.25] \quad (8.12)$$

$$\varepsilon_D = 33 \cdot [(w/c)^2 - 0.654 \cdot (w/c) + 0.115] \quad (8.13)$$

k = 1.1 for HPC with 10% silica fume slurry; k = 1 for HPC with 10 % granulated silica fume or 5% slurry

k_B = 1.5 for HPC with 10% silica fume slurry; k_B = 1 for HPC with 10 % granulated silica fume or 5% slurry

E, ε_B, ε_C, ε_D denotes total, autogenous, carbonation and drying shrinkage (per mil)

From **Figure 7.13** it was observed that the estimated shrinkage was smaller than the measured shrinkage. Total, autogenous and carbonation shrinkage was 20% smaller and the drying shrinkage 30% smaller than the measured. One reason for this observation is probably that another type of cement was used in some of the studied HPCs (with w/c varying between 0.27 and 0.30). According to **Miyazawa and Tazawa (1997),** the type of cement influences the amount of shrinkage in HPC. Larger shrinkage was observed with higher fineness of the cement. In this field study the fineness was Blaine 404 m^2/kg but in the laboratory study presented in Section 8 the cement fineness was only Blaine 302 m^2/kg. In the remaining HPCs (with w/c varying between 0.32 and 0.37) the unfavourable grading curve of the fresh HPC perhaps affected the size of shrinkage owing to lower workability in the fresh state, i.e. the compaction of a plastic concrete becomes more difficult.

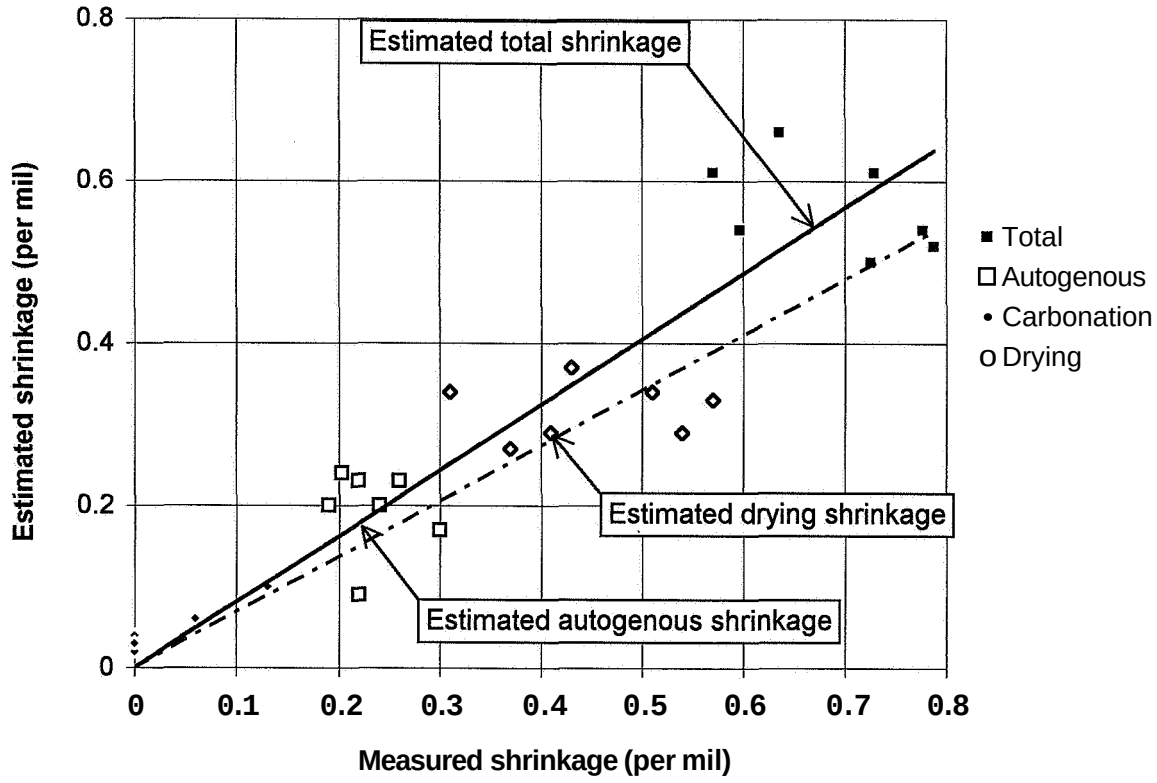

Figure 17.13 - Estimated shrinkage versus measured shrinkage in the field studies.

17.5.2 Creep compliance of hat beams

The measured strain of HPC in hat beams is shown in **Figure 17.5** above. To compare the field results with the laboratory results in Sections 9 and 14 estimations of the compliance, J (millionths/MPa) were expressed by the following equation:

$$J = \varepsilon/\sigma \qquad (17.1)$$

J denotes the compliance (millionths/MPa)
E denotes the measured strain (millionths)
σ denotes the stress of HPC (MPa)

The calculations of the stresses in the HPC were based on **Hurst (1988)** mainly. The forces were estimated according to the following equations:

$$F_i = n_i \cdot (F_0 - \varepsilon_i \cdot E_{st} \cdot A_{st}) \qquad (17.2)$$

$$F_{total} = \sum_{1}^{4} F_i \qquad (17.3)$$

A_{st} denotes area of a strand
n_i denotes number of strands in layer i
E_{st} denotes elastic modulus of strands
F_i denotes forces of strands in layer i
F_{total} denotes total force of strands
F_0 denotes the initial force in the strands before prestressing of the concrete
ε_i denotes specific deformation of beams at level of strand layer i

The stresses of the concrete flange were estimated according to:

$$\sigma_u = F_{total}/A_c - F_{total} \cdot e_F/W_u \qquad (17.4)$$

$$\sigma_b = F_{total}/A_c - F_{total} \cdot e_F/W_b \qquad (17.5)$$

$$\sigma = 0.5 \cdot (\sigma_u + \sigma_b) \qquad (17.6)$$

e_F denotes the eccentricity of the prestressing force compared with concrete area
A, denotes the concrete area
F_{total} denotes total force of strands
W_b denotes the deviation moment related to the bottom edge of the flange
W, denotes the deviation moment related to the upper edge of the flange
σ_b stresses in the concrete at bottom edge of the flange
σ_u stresses in the concrete at upper edge of the flange

Table 17.4 provides forces, stresses of the strands and compliance of HPC after relaxation. The comparison with laboratory studies was carried out with equations (6.13), (9.1), (9.2), (14.8), (14.9), (14.10) and (14.11).

$$J(t,t')_{sh} = a \cdot \int d(t-t')/(t-t') + b = a_{sh} \cdot \int d(t-t')/(t-t') + 1000/D_{t'} \qquad (6.13)$$

a_{sh} denotes the short-term compliance rate, **Table 6.3** [millionths/(MPa·h)]
b denotes the initial compliance 1 h after loading, **Table 6.4** (millionths/MPa)
t denotes the age of the concrete (h)
t' denotes the age of the concrete when loading (s)
$D_{t'}$ denotes the deformation modulus after 1 h of loading, see Section 7 (GPa)
$J(t,t')_{sh}$ denotes the short-term compliance (specific creep, millionths/MPa)

$$a_{Dsh} = 3.4 \cdot [(w/c)-0.13] \cdot s_{Da5} + [0.3-11 \cdot (\sigma/f_c)] \cdot \ln(f_c/f_{c28}) \quad \{0.25<w/c<0.40\} \qquad (9.1)$$

a_{Dsh} denotes short-term drying creep rate [millionths/(MPa·h)]
f_c/f_{c28} denotes the relative 28-day strength at loading $\{0.3< f_c/f_{c28}<1\}$
s_{Da5} =1.5 for HPC with 5% silica fume and/or air-entrainment; s_{Da5}= 1 for HPC with 10% silica fume
σ/f_c denotes the stress/strength (100 mm cube) ratio at loading $\{0.3<\sigma/f_c<0.6\}$

$$a_{Bsh} = 0.14 \cdot [(w/c)+2.5] \cdot s_{Ba5} + [0.29-6.9 \cdot (\sigma/f_c)] \cdot \ln(f_c/f_{c28}) \qquad (9.2)$$

a_{Bsh} denotes short-term basic creep rate [millionths/(MPa·h)]
σ/f_c denotes the stress/strength (100 mm cube) ratio at loading $\{0.3<\sigma/f_c<0.6\}$
f_c/f_{c28} denotes relative strength $\{0.4< f_c/f_{c28}<1$ for $\sigma/f_c = 0.3$ and $0.15< f_c/f_{c28}<0.5$ for $\sigma/f_c = 0.6)$
s_{Ba5} =1.25 for concrete with 5% silica fume or/and air-entrainment (10% silica fume); s_{Ba5}= 1 for 10% silica fume

$$J(t,t')_{Dlo} = 1000/D_{t'} + a_{Dlo} \cdot \int d(t-t')/(t-t') \qquad (14.8)$$

a_{Dlo} denotes long-term drying creep compliance rate with air curing [millionths/(MPa·day)]
t denotes age of the concrete (days)
t' denotes age at loading (days)
$D_{t'}$ denotes the deformation modulus at loading, Section 7 above (GPa)
$J(t,t')_{Dlo}$ denotes the long-term drying creep compliance (millionths/MPa)

$$a_{Dlo} = k_{ai} \cdot 513 \cdot [(w/c)^2 - 0.6 \cdot (w/c) + 0.0959] - k_{as} [1.83 + 2.37 \cdot (\sigma/f_c)] \cdot \ln(f_c/f_{c28}) \qquad (14.9)$$

a_{Dlo} denotes long-term drying creep compliance rate with air curing [millionths/(MPa·day)]

Table 17.4 - Forces, stresses of strands and compliance after relaxation (kN, MPa).

Force; stress/hat beam	H 1D	H2B	H2D	H3B	H3D	H4D	H 5D
Force in strands 100 s after prestressing (kN)	2290	2370	2370	2300	2300	2335	2304
28 d after prestressing (kN)	2005	2200	2150	2094	2039	-	1999
Stress in HPC 100 s after prestressing (MPa)	33.9	35.1	35.1	34	33	33.5	33.6
28 d after prestressing (MPa)	29.2	32.7	31.9	30.9	30	-	29.1
Compliance 100s after prestressing, J_{100} (millionths/MPa)	31	23.7	23.7	30	30	27.5	29.8
28 d after prestressing (millionths/MPa)	61.2	38.2	43.6	49.5	55.5	-	60.8
Elastic effect (millionths/MPa)	2.9	1.4	1.9	1.9	1.9	-	2.9
Reduction of compliance at 28 days' age due to shrinkage (millionths/MPa)	7.6 (8.9)	5.7	5.7 (14.4)	5.8	5.8 (16.3)	-	4.8 (17.1)
Resulting 28d compliance (excluding compliance at 100 s of loading, elastic effect and shrinkage; millionths/MPa)	25.5 (24.2)	10.2	16.1 (7.4)	15.6	21.6 (11.1)	-	29.1 (16.8)
Estimated 28 d compliance (excluding compliance at 100 s of loading and shrinkage; millionths/MPa)	22.5 (39.7)	17	17 (27.2)	15.5	15.5 (24.9)	-	18.5 (29.8)

B = basic creep; D = drying creep = ( ); d= loading time (days); s= seconds.

k_{as} = 0.8 for HPC with 5% air-entrainment; k_{as} = 1.3 for silica fume slurry
k_{ai} = 1.5 for HPC with 5% air-entrainment; $k_{ai} = k_{as} = 1$ otherwise

$$J(t,t')_{Blo} = 1000/D_{t'} + a_{Blo} \cdot \int d(t-t')/(t-t') \qquad (14.10)$$

a_{Blo} denotes long-term basic creep compliance rate with sealed curing [millionths/(MPa·day)]
t denotes age of the concrete (days)
t' denotes age at loading (days)
$D_{t'}$ denotes the deformation modulus at loading, Section 7 above (GPa)
$J(t,t')_{Blo}$ denotes the long-term basic creep compliance (millionths/MPa)

$$a_{Blo} = k_{s5} \cdot 231 \cdot [(w/c)^2 - 0.594 \cdot (w/c) + 0.0952] - k_{s5} \cdot [2.83 - 3 \cdot (\sigma/f_c)] \cdot \ln(f_c/f_{c28}) \qquad (14.11)$$

a_{Blo} denotes long-term basic creep compliance rate with sealed curing [millionths/(MPa·day)]
f_c/f_{c28} denotes the relative 28-day strength at loading $\{0.3 < f_c/f_{c28} < 1\}$
k_{s5} = 1.5 for 5% silica fume or 10% silica fume slurry; $k_{s5} = 1$ otherwise

Table 17.5 provides detailed information concerning the parameters of the equations. The size of the beam compared with the cylinders used in the laboratory studies was taken into account by half the hydraulic radius of the specimens (VIA).

Table 17.5 - Parameters of equations (6.13), (9.1)-(9.2), (14.8)-(14.11). $k_{s5}= s_{a5}=1$.

No	w/c	$(w/c)^2$	σ/f_c	f_c/f_{c28}	ln (f_c/f_{c28})	a_{sh}	$\int_{0.028}^{66} dt/t$	J_{sh}	a_{lo}	$\int_{2.7}^{28} dt/t$	J_{lo}	J_{tot}
1B	0.28	0.0784	0.48	0.57	-0.56	2.15	7.76	16.7	2.46	2.34	5.76	23
1D	0.28	0.0784	0.48	0.57	-0.56	3.30	7.76	25.6	6.03	2.34	14.1	40
2B	0.27	0.0729	0.40	0.67	-0.40	1.43	7.76	11.3	2.44	2.34	5.69	17
2D	0.27	0.0729	0.40	0.67	-0.40	2.11	7.76	16.4	4.60	2.34	10.8	27
3B	0.30	0.09	0.36	0.68	-0.385	1.3	7.76	10.1	2.98	2.34	5.36	16
3D	0.30	0.09	0.36	0.68	-0.385	1.99	7.76	15.4	4.06	2.34	9.50	25
5B	0.28	0.0784	0.38	0.71	-0.50	1.62	7.76	12.6	2.52	2.34	5.91	19
5D	0.28	0.0784	0.38	0.71	-0.50	2.45	7.76	19.0	4.60	2.34	10.8	30

B= basic creep; D= drying creep

Figure 17.14 shows the compliance estimated according to the equations given above and based on laboratory studies versus creep measured in hat beams of independent field studies [f: "+" is used when estimating the compliance (increase of compliance); "-" is used when calculating the resulting compliance (decrease)].

$$J_{beam} = J_B \pm [(V/A)_{cyl}/ (V/A)_{beam}]\cdot(J_D-J_B) \qquad (17.7)$$

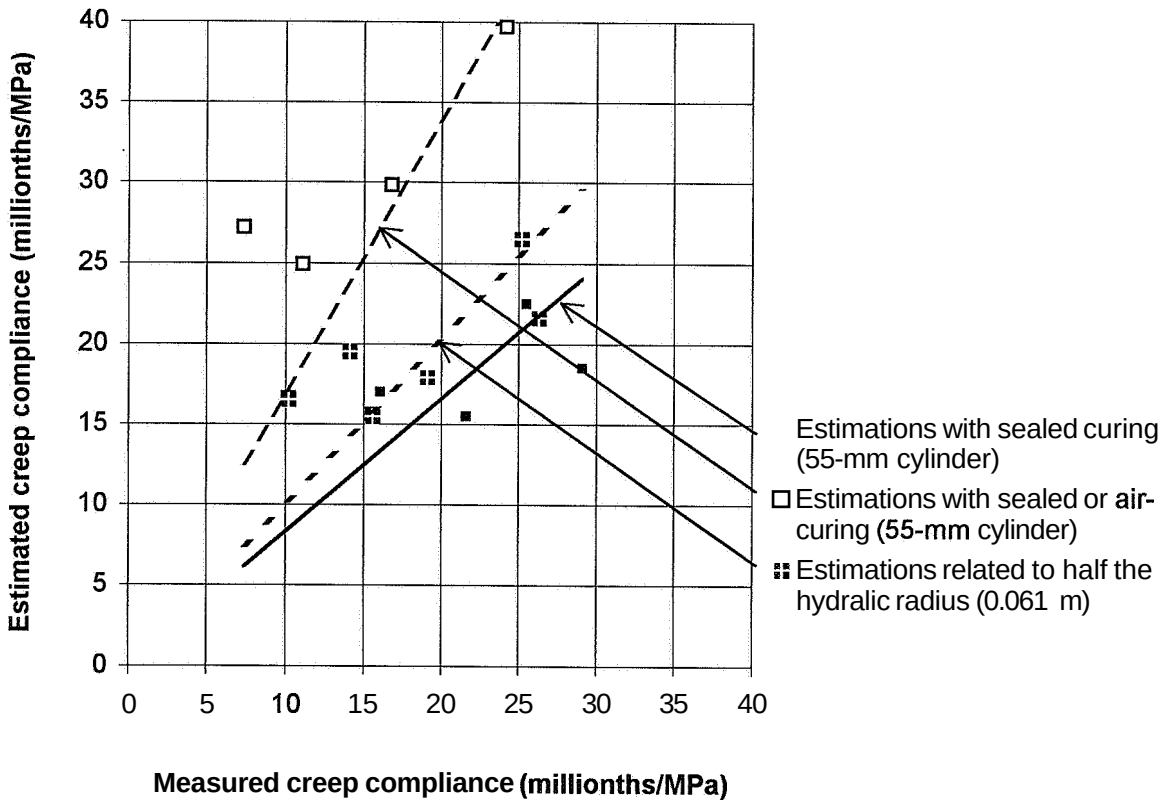

Figure 17.14 - Estimated creep compliance versus measured creep in hat beams.

Notations in equation (17.7):

A denotes the cross section area of the specimen
J_{beam} denotes the compliance of the beam taking in account the size effect
J_B denotes compliance of sealed cylinder 55 mm in diameter at
J_D denotes compliance at drying of cylinder 55 mm in diameter
V denotes the area of the specimen
VIA = 0.014 m for cylinder specimens, = 0.061 m for hat beam, **Figure 17.1**

Figure 17.14 also shows the compliance calculated only for drying cylinder, which resulted in an overestimation of about 69%. When the estimation was carried according to basic creep only, the underestimation became about 18%. When equation (17.7) was used the estimated compliance coincided reasonably well with the measured compliance (an overestimation of about 1%).

17.5.3 Creep compliance of square beams

Some beams were identical as regards the structural properties, in which case only the average results are presented. **Tables 17.6-17.8** show the structural properties of the square beams S32. **Table 17.9-17.12** show the structural properties of the beams S37. The estimations of the creep were carried out with equations (6.13), (9.1), (9.2), (14.8), (14.9), (14.10) and (14.11). **Figure 17.15** shows the estimated creep compliance versus the measured creep compliance, i.e. the compliance was reduced by the creep compliance 100 s after loading and by the shrinkage. The elastic effect was added accordant Section 17.5.1. The creep compliance was adjusted according to equation (17.7), which takes into account half the hydraulic radius of the specimen. Half the hydraulic radius of the square beam was 0.05 m. The estimated creep and measured creep was compared with the following equation:

$$J_{est.} = f \cdot J_{mea.} \qquad (17.8)$$

Table 17.13 provides the correction parameter f of the estimated creep compared with the measured creep. On average the correction parameter, $f_{av.} = 0.95$, was obtained, which is reasonably good, cp. **Figure 2.1.** It was decreasing with loading time, i.e. the ambient climate seemed to have an influence.

17.5.4 Deformation modulus

The deformation modulus after 100 s of loading was compared with the deformation modulus estimated according to equations (6.13), (7.8) and (9.2) given above.

$$D_{ba}(f_c;t\text{-}t';\sigma/f_c)= \{6.06-3.02\cdot(\sigma/f_c)-[0.44-0.51\cdot(\sigma/f_c)]\cdot\ln(t\text{-}t')\}\cdot(f_c)^{0.42+0.061\cdot(\sigma/fc)-\,0.039\cdot(\sigma/fc-0.5)\cdot\ln(t\text{-}t')} \qquad (17.9)$$

Table 17.6 - Forces, stresses, compliance and reduction of shrinkage of beams S32.

Property/beam	**3231**	**3232**	**3234[1)]**	**3241**	**3242**	**3244[1)]**
Force (kN) in strands at 100 s	1082	1108	1102	1512	1601	1596
10 d after prestressing	972	1010	974	1236	1353	1364
200 d after prestressing	908	919	886	1120	1266	1170
Stress (MPa) in HPC after 100 s	28	29	28	39	42	42
10 d after prestressing	25	26	25	32	35	36
200 d after prestressing	23	23.7	22.6	28.9	32.5	30.1
Compliance (millionths/MPa) after 100s	31.4	26.7	27.8	35.9	27.2	27.6
10 d after prestressing	54	45	53	71	54	53
200 d after prestressing	68.5	66	64.9	91.7	67.5	82.7
Elastic effect (millionths/MPa) at 10d	2.5	2.4	2.5	4	3.7	3.2
200 d after prestressing	1.9	2.3	2.2	2.2	1.6	3.6
Reduction of compliance (millionths/MPa) for shrinkage after 10 d	8.5 (22)	8.5 (22)	8.5 (22)	7 (16)	6 (14.5)	6 (14)
200 d after prestressing	17 (32)	17 (32)	17 (32)	13 (25)	12 (23)	13 (24)
Resulting; creep compliance (millionths/MPa) at 10d	17 (4)	11 (-2)	19 (6)	32 (23)	25 (16)	22 (14)
200 d after prestressing	23 (8)	24 (9)	22 (7)	45 (33)	31 (20)	46 (35)
Estimated creep compliance 10 d after prestressing	112.7 (20.6)	9.2 (14.8)	8.8 (15.2)	23.2 (38.9)	20.2 (33.7)	18.9 (31.6)
200 d after prestressing (millionths/MPa)	21.0 (32.3)	16.5 (25.2)	15.2 (25.6)	31.7 (53.4)	28.8 (47.4)	27.4 (44.9)

[1)] average of 2 beams; d= loading time (days); s= seconds; (....)= drying shrinkage.

Table 17.7 - Parameters of beam S323 in equations (6.13), (9.1), (9.2), (14.8), (14.9), (14.10) and (14.11); w/c = 0.32; $(w/c)^2 = 0.1024$.

No	**Age**	σ/f_c	f_c/f_{c28}	$\ln(f_c/f_{c28})$	s_{a5}	a_{sh}	$\int_{0.028}^{\infty} d\dot{t}$	J_{sh}	k_{s5}	a_{lo}	$\int_{27}^{d} d\dot{t}/t$	J_{lo}	J_{tot}
3231B	10 d	0.41	0.78	-0.24	1.15	1.06	7.76	8.25	1.3	2.76	1.61	4.44	12.7
3231D	10 d	0.41	0.78	-0.24	1.3	1.84	7.76	14.3	-	3.90	1.61	6.28	20.6
3232B	10 d	0.39	0.91	-0.09	1.15	0.67	7.76	5.2	1.3	2.46	1.61	4.0	9.2
3232D	10 d	0.39	0.91	-0.09	1.3	1.19	7.76	9.2	-	3.48	1.61	5.6	14.8
3234B	10 d	0.49	0.92	-0.08	1.15	0.70	7.76	5.4	1.3	2.12	1.61	3.4	8.8
3234D	10 d	0.49	0.92	-0.08	1.3	1.24	7.76	9.6	-	3.47	1.61	5.6	15.2
3231B	200 d	0.41	0.78	-0.24	1.15	1.06	7.76	8.25	1.3	2.76	4.61	12.7	21.0
3231D	200 d	0.41	0.78	-0.24	1.3	1.84	7.76	14.3	-	3.90	4.61	18.0	32.3
3232B	200 d	0.39	0.91	-0.09	1.15	0.67	7.76	5.2	1.3	2.46	4.61	11.3	16.5
3232D	200 d	0.39	0.91	-0.09	1.3	1.19	7.76	9.2	-	3.48	4.61	16.0	25.2
3234B	200 d	0.49	0.92	-0.08	1.15	0.70	7.76	5.4	1.3	2.12	4.61	9.8	15.2
3234D	200 d	0.49	0.92	-0.08	1.3	1.24	7.76	9.6	-	3.47	4.61	16.0	25.6

d= loading time (days); B= basic creep; D= drying creep

Table 17.8 - Parameters of beam S324 in equations (6.13), (9.1), (9.2), (14.8), (14.9), (14.10) and (14.11); w/c = 0.32; $(w/c)^2 = 0.1024$.

No	Age	σ/f_c	f_c/f_{c28}	$\ln(f_c/f_{c28})$	s_{a5}	a_{sh}	$\int_{0.028}^{66} dt/t$	J_{sh}	k_{s5}	a_{lo}	$\int_{2.7}^{d} dt/$	J_{lo}	J_{tot}
3241B	10 d	0.63	0.62	-0.48	1.15	2.40	7.76	18.6	1.3	2.85	1.61	4.58	23.2
3241D	10 d	0.63	0.62	-0.48	1.3	4.01	7.76	31.1	-	4.83	1.61	7.76	38.9
3242B	10 d	0.58	0.66	-0.42	1.15	2.01	7.76	15.6	1.3	2.86	1.61	4.60	20.2
3242D	10 d	0.58	0.66	-0.42	1.3	3.38	7.76	26.3	-	4.58	1.61	7.37	33.7
3244B	10 d	0.58	0.69	-0.38	1.15	1.87	7.76	14.5	1.3	2.80	1.61	4.40	18.9
3244D	10 d	0.58	0.69	-0.38	1.3	3.14	7.76	24.4	-	4.45	1.61	7.16	31.6
3241B	200 d	0.63	0.62	-0.48	1.15	2.40	7.76	18.6	1.3	2.85	4.61	13.1	31.7
3241D	200 d	0.63	0.62	-0.48	1.3	4.01	7.76	31.1	-	4.83	4.61	22.3	53.4
3242B	200 d	0.58	0.66	-0.42	1.15	2.01	7.76	15.6	1.3	2.86	4.61	13.2	28.8
3242D	200 d	0.58	0.66	-0.42	1.3	3.38	7.76	26.3	-	4.58	4.61	21.1	47.4
3244B	200 d	0.58	0.69	-0.38	1.15	1.87	7.76	14.5	1.3	2.80	4.61	12.9	27.4
3244D	200 d	0.58	0.69	-0.38	1.3	3.14	7.76	24.4	-	4.45	4.61	20.5	44.9

d= loading time (days); B= basic creep; D= drying creep

Table 17.9 - Forces, stresses, compliance (millionths/MPa), etcetera for beams S37.

Property/beam	3730	3731	3732[1)]	3740	3741	3742[1)]	3750	3751	3752[1)]
Force (kN) after 100 s	857	888	910	1111	1130	1136	1327	1347	1319
10 d after prestressing	713	750	769	907	950	924	1116	1188	1097
200 d after prestressing	639	655	684	813	856	826	968	1052	956
Stress (MPa) at 100 s	22	23	23	29	30	30	34	35	34
10 d after prestressing	18	19	20	24	25	24	29	31	28
200 d after prestressing	16	17	18	21	22	21	25	27	25
Compliance at 100s	43	35	31	36	33	32	36	33	37
10 d after prestressing	84	72	66	71	63	68	74	59	78
200 d of prestressing	113	106	95	94	84	91	110	88	114
Elastic effect at 10d	4.3	4.2	3.9	4.1	4	4.8	3.5	2.7	4.2
200 d after prestressing	2.6	2.5	2.4	3	3	3	3.3	3.3	2.6
Reduction for shrinkage after 10 d (mill./MPa)	8 (22)	8 (21)	7 (20)	6 (17)	6 (16)	6 (17)	5 (14)	5 (13)	5 (14)
200 d after prestressing	15 (47)	15 (47)	14 (46)	12 (38)	11 (36)	12 (38)	10 (32)	9 (30)	10 (32)
Resulting compliance (millionths/MPa, 10 d)	37 (23)	33 (20)	31 (18)	33 (22)	28 (18)	35 (24)	37 (28)	24 (16)	40 (31)
200 d after prestressing	58 (24)	59 (27)	52 (20)	51 (23)	43 (18)	50 (24)	67 (45)	49 (28)	70 (48)
Estimated creep compliance after 10 d	126.6 (46)	128.5 (49)	127.2 (47)	125.3 (44)	(23.7 (41)	124.9 (43)	24.1 (42)	121.1 (37)	20.3 (35)
200 d after prestressing (millionths/MPa)	40.8 (68)	42.9 (72)	41.6 (69)	38.7 (65)	37.1 (62)	38.1 (65)	37.0 (63)	33.9 (57)	32.9 (55)

1) average of 2 beams; d= loading time (days); s= seconds; (....)= drying shrinkage.

Table 17.10 - Parameters of beam S373 in equations. wlc = 0.37; $(w/c)^2 = 0.1369$.

NO	Age	σ/f_c	f_c/f_{c28}	ln (f_c/f_{c28})	s_{a5}	a_{sh}	$\int_{0.028}^{66} dt/t$	J_{sh}	k_{s5}	a_{lo}	$\int_{27}^{d} dt/$	Jlo	Jtot
3730B	10 d	0.52	0.55	-0.61	1.15	2.46	7.76	19.1	1.3	4.7	1.61	7.6	27
37301)	10 d	0.52	0.55	-0.61	1.3	4.36	7.76	33.8	-	7.4	1.61	11.9	46
3731B	10 d	0.53	0.52	-0.66	1.15	2.68	7.76	20.8	1.3	4.8	1.61	7.74	29
32311)	10 d	0.53	0.52	-0.66	1.3	4.70	7.76	36.6	-	7.7	1.61	12.5	49
3732B	10 d	0.50	0.52	-0.65	1.15	2.51	7.76	19.5	1.3	4.8	1.61	7.7	28
37321)	10 d	0.50	0.52	-0.65	1.3	4.44	7.76	34.5	-	7.5	1.61	12.1	47
3730B	200 d	0.52	0.55	-0.61	1.15	2.46	7.76	19.1	1.3	4.7	4.61	21.7	41
37301)	200d	0.52	0.55	-0.61	1.3	4.36	7.76	33.8	-	7.4	4.61	34.1	68
3731B	200d	0.53	0.52	-0.66	1.15	2.68	7.76	20.8	1.3	4.8	4.61	22.1	43
3231D	200 d	0.53	0.52	-0.66	1.3	4.70	7.76	36.6	-	7.7	4.61	35.7	72
3732B	200d	0.50	0.52	-0.65	1.15	2.51	7.76	19.5	1.3	4.8	4.61	22.1	42
37321)	200 d	0.50	0.52	-0.65	1.3	4.44	7.76	34.5	-	7.5	4.61	34.6	69

d= days' age; B= basic creep; D= drying creep

Table 17.11 - Parameters of beam S374 in equations (6.13), (9.1), (9.2), (14.8), (14.9), (14.10) and (14.11); w/c = 0.37; $(w/c)^2 = 0.1369$.

Beam	Age	σ/f_c	f_c/f_{c28}	ln (f_c/f_{c28})	s_{a5}	a_{sh}	$\int_{0.028}^{66} dt/$	J_{sh}	k_{s5}	a_{lo}	$\int_{27}^{d} dt/$	J_{lo}	J_{tot}
3740B	10 d	0.59	0.60	-0.50	1.15	2.35	7.76	18.2	1.3	4.44	1.61	7.1	25
3740D	10 d	0.59	0.60	-0.50	1.3	4.16	7.76	32.2	-	7.15	1.61	11.5	44
3741B	10 d	0.55	0.62	-0.48	1.15	2.14	7.76	16.6	1.3	4.44	1.61	7.1	24
3241D	10 d	0.55	0.62	-0.48	1.3	3.82	7.76	29.6	-	7.04	1.61	11.3	41
3742B	10 d	0.59	0.61	-0.49	1.15	2.31	7.76	17.9	1.3	4.38	1.61	7.04	25
3742D	10 d	0.59	0.61	-0.49	1.3	4.09	7.76	31.8	-	7.12	1.61	11.5	43
3740B	200 d	0.59	0.60	-0.50	1.15	2.35	7.76	18.2	1.3	4.44	4.61	20.5	39
3740D	200 d	0.59	0.60	-0.50	1.3	4.16	7.76	32.2	-	7.15	4.61	33	65
3741B	200 d	0.55	0.62	-0.48	1.15	2.14	7.76	16.6	1.3	4.44	4.61	20.5	37
3241D	200 d	0.55	0.62	-0.48	1.3	3.82	7.76	29.6	-	7.04	4.61	32.5	62
3742B	200 d	0.59	0.61	-0.49	1.15	2.31	7.76	17.9	1.3	4.38	4.61	20.2	38
3742D	200 d	0.59	0.61	-0.49	1.3	4.09	7.76	31.8	-	7.12	4.61	32.8	65

d= days' age; B= basic creep; D= drying creep

t-t' denotes the loading time

First of all the compliance at 1s loading time was estimated according to equation (7.8). Then the additional compliance between 1s and 100s was calculated according to equations (6.13) and (9.2). **Table 17.14** shows the estimations of the 100-S deformation modulus and calculations of the measured deformation modulus.

Table 17.12 - Parameters of beam S375 in equations (6.13), (9.1), (9.2), (14.8), (14.9), (14.10) and (14.11); w/c = 0.37; $(w/c)^2 = 0.1369$.

Beam	Age	σ/f_c	f_c/f_{c28}	ln (f_c/f_{c28})	s_{a5}	a_{sh}	$\int_{0.028}^{66} dt/$	J_{sh}	k_{s5}	a_{lo}	$\int_{2.7}^{d} dt/$	J_{lo}	J_{tot}
3750B	10 d	0.61	0.60	-0.45	1.15	2.21	7.76	17.2	1.3	4.29	1.61	6.9	24.1
3750D	10 d	0.61	0.64	-0.45	1.3	3.95	7.76	30.6	-	7.01	1.61	11.3	41.9
3751B	10 d	0.57	0.68	-0.38	1.15	1.84	7.76	14.3	1.3	4.25	1.61	6.84	21.1
3251D	10 d	0.57	0.68	-0.38	1.3	3.32	7.76	25.8	-	6.75	1.61	10.9	36.7
3752B	10 d	0.57	0.71	-0.35	1.15	1.74	7.76	13.5	1.3	4.21	1.61	6.78	20.3
3752D	10 d	0.57	0.71	-0.35	1.3	3.15	7.76	24.4	-	6.65	1.61	10.7	35.1
3750B	200 d	0.61	0.60	-0.45	1.15	2.21	7.76	17.2	1.3	4.29	4.61	19.8	37.0
3750D	200 d	0.61	0.64	-0.45	1.3	3.95	7.76	30.6	-	7.01	4.61	32.3	62.9
3751B	200 d	0.57	0.68	-0.38	1.15	1.84	7.76	14.3	1.3	4.25	4.61	19.6	33.9
3251D	200 d	0.57	0.68	-0.38	1.3	3.32	7.76	25.8	-	6.75	4.61	31.1	56.9
3752B	200 d	0.57	0.71	-0.35	1.15	1.74	7.76	13.5	1.3	4.21	4.61	19.4	32.9
3752D	200 d	0.57	0.71	-0.35	1.3	3.15	7.76	24.4	-	6.65	4.61	30.7	55.1

d= days' age; B= basic creep; D= drying creep

Table 17.13 - Correction parameter for estimated measured creep, eq. (17.8).

Studied object	Hat beams	Square beams			
w/c	0.27<w/c<0.30	w/c= 0.32	w/c= 0.32	w/c= 0.37	w/c= 0.37
Loading time (d)	28 d	10 d	200 d	10 d	200 d
Parameter f	1.01	1.01	0.94	0.96	0.91

Figure 17.16 shows the estimated deformation modulus of the HPCs 100 s after loading versus the measured deformation modulus. Given constant strength, f_c, the estimated deformation modulus was smaller in HPC with plastic fibre than in plain HPC, **Table 17.15.** Normally plastic fibres have no or very little effect on the mechanical properties of HPC. **Figure 17.18** shows that the plastic fibre had little or no effect on the estimated creep compliance of the studied HPCs compared with the measured compliance given ≤ 1 kg/m^3. **Figure 17.17** shows a good correlation between the amount of plastic fibre and the relative deformation modulus:

$$D_{fib.} = D_{nof.} \cdot (1 + 0.0523 \cdot f) \qquad (17.10)$$

f denotes the amount of plastic fibre (kg/m^3)
$D_{fib.}$ denotes the deformation modulus of HPC with plastic fibre
$D_{nof.}$ denotes the deformation modulus of HPC with no plastic fibre

Table 17.15 - Ratio of deformation modulus according to equation (17.9) to deformation modulus measured 100s after loading (constant strength).

Amount of plastic fibre (kg/m^3)	0	1	2	4
Estimated relative deformation modulus (constant strength)	0.93	0.88	0.81	0.76

Table 17.14 - Deformation modulus calculated according to equation (17.9) and measured deformation modulus 100 s after loading; s_{a5}= 1.15.

Beam	σ/f_c	f_c (MPa)	D_{1s} (MPa)	J_{1s} (mill./ MPa)	ΔJ_{100s} (mill./ MPa)	J_{100s} (mill./ MPa)	$D_{est.}$ (GPa)	$D_{mea.}$ (GPa)	ΔD (GPa)
H1B	0.48	70	31	32.3	2.1	34.4	29.1	32.3	3.2
H2B	0.40	87	34.4	29.1	2.1	31.2	32.1	(42)	(10)
H2D	0.40	87	34.4	29.1	2.1	31.2	32.1	(42)	(10)
H3B	0.36	83	34.5	29	2.1	31.1	32.2	33.3	1.1
H3D	0.36	83	34.5	29	2.1	31.1	32.2	33.3	1.1
H4D	0.39	85	34.9	28.7	2.1	30.8	32.5	36.4	3.9
H5D	0.38	78	33.2	30.1	2.1	32.2	31.1	33.6	2.5
S3231	0.41	69	31.6	31.6	2.1	33.7	29.7	31.9	2.2
S3232	0.39	75	33.1	30.2	2.1	32.3	31.0	37.5	6.5
S3234	0.49	57	28.1	35.6	2.1	37.7	26.5	36.0	9.5
S3241	0.63	62	27.4	36.5	2.1	38.6	25.9	27.9	2.0
S3242	0.58	72	30	33.3	2.1	35.4	28.2	36.8	8.6
S3244	0.58	72	30	33.3	2.1	35.4	28.2	36.2	8
S3730	0.52	42	24.2	41.3	2.1	43.2	23.1	23.3	0.2
S3731	0.53	43	24.3	41.1	2.1	43.2	23.1	28.6	5.5
S3732	0.50	46	25.5	39.3	2.1	41.4	24.2	32.3	8.1
S3740	0.59	49	25.5	39.2	2.1	41.3	24.2	27.8	3.6
S3741	0.55	55	27.0	37	2.1	39.1	25.6	30.3	4.7
S3742	0.59	51	25.6	39.1	2.1	41.2	24.3	31.3	7
S3750	0.61	56	26.2	38.2	2.1	40.3	24.8	27.8	3.0
S3751	0.57	62	28.2	35.5	2.1	37.6	26.6	30.3	3.7
S3752	0.57	60	27.8	35.9	2.1	38.0	26.3	27.0	0.7

17.6 Summary and conclusions

Two types of beams, i.e. "hat" beams and square beams, were studied up to 200 days. The measured strain was compared with estimated strain according to several equations given above. The objective was to compare the results on creep and shrinkage obtained in the laboratory with the results on the beams. The following conclusions were drawn:

- The estimated deformation modulus was 7% smaller than the measured deformation modulus when the compressive strength was held constant.
- Addition of plastic fibre in **HPC** tended to increase the deformation modulus when the compressive strength was held constant.
- The estimated creep compliance of 7 hat beams made of **HPC** was about 1% larger than the measured compliance.
- The estimated creep compliance of 20 square **HPC** beams coincided reasonably well with the measured compliance given ≤ 1 kg/m^3 plastic fibre in the **HPC**.

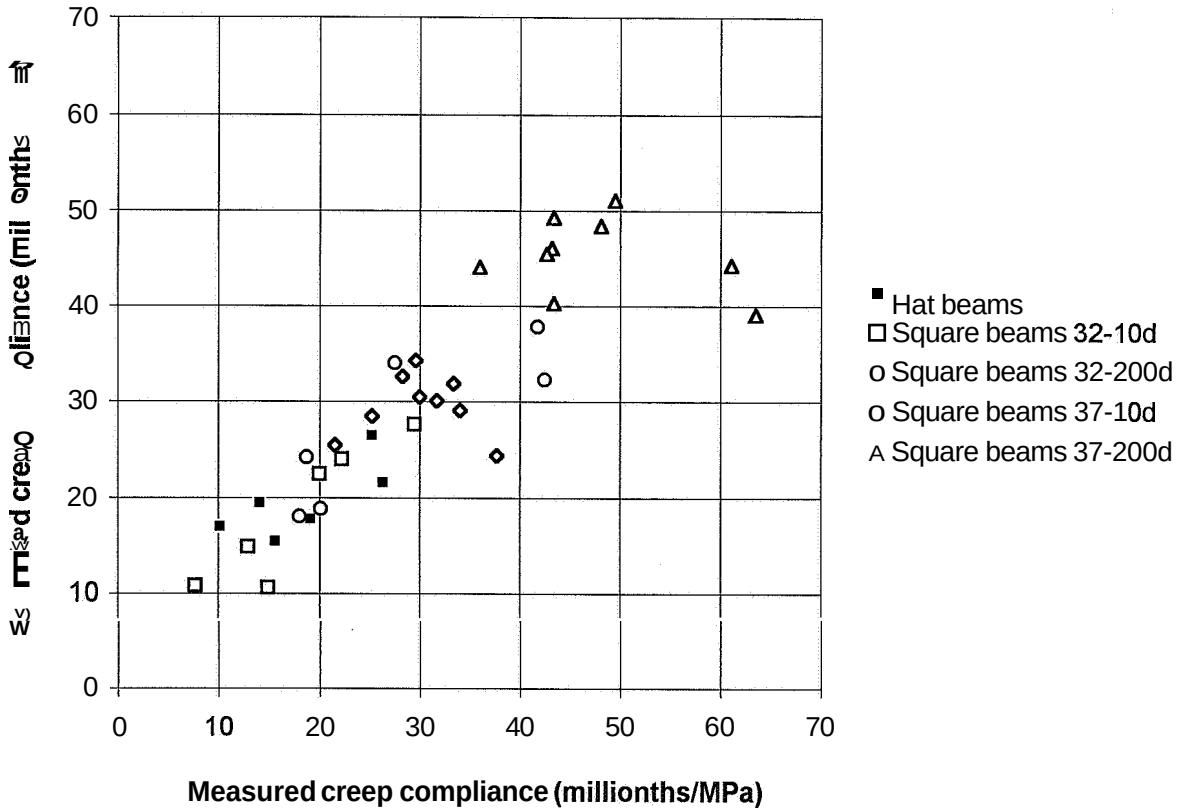

Figure 17.15 - Estimated creep compliance versus measured creep compliance of beams in field studies. Loading time is indicated. d= days' age, 32= w/c (per cent).

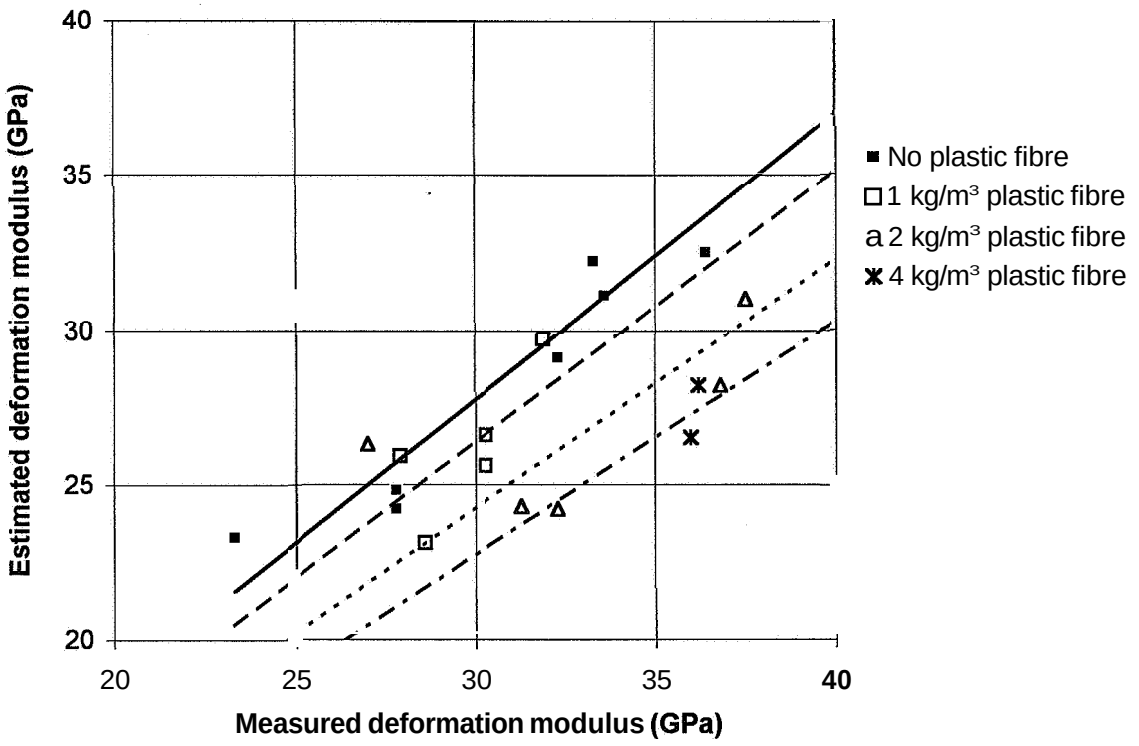

Figure 17.16 - Estimated deformation modulus versus measured modulus.

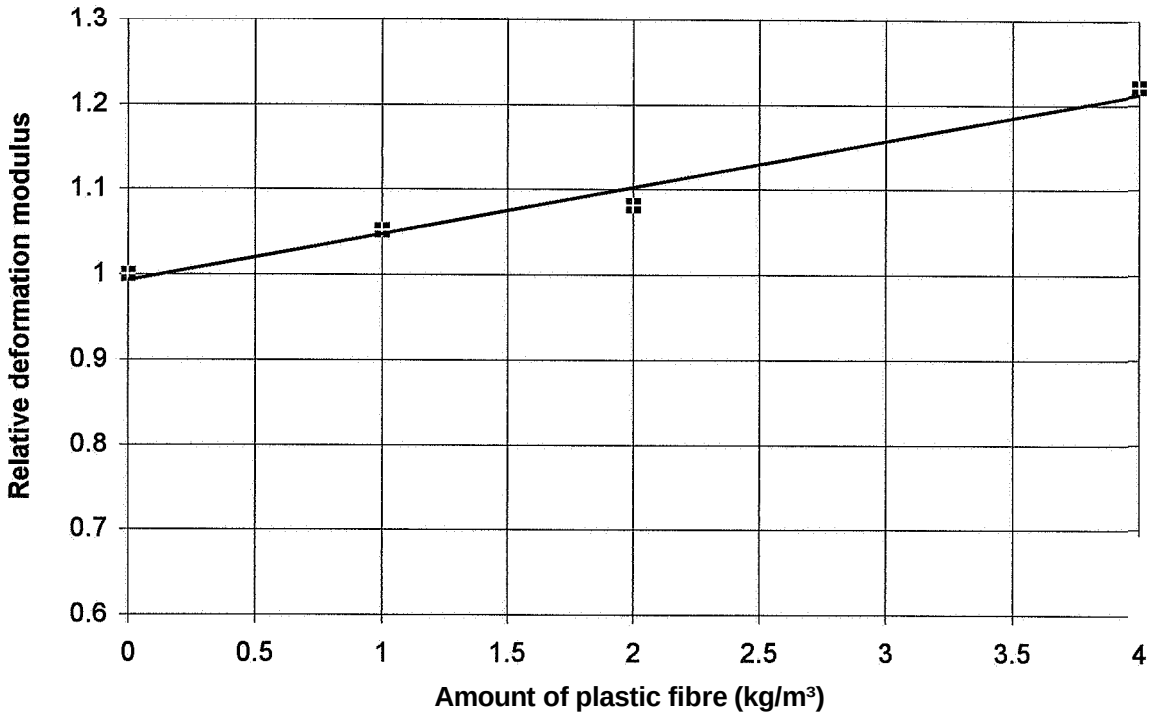

Figure 17.17 - Relative deformation modulus versus amount of plastic fibre.

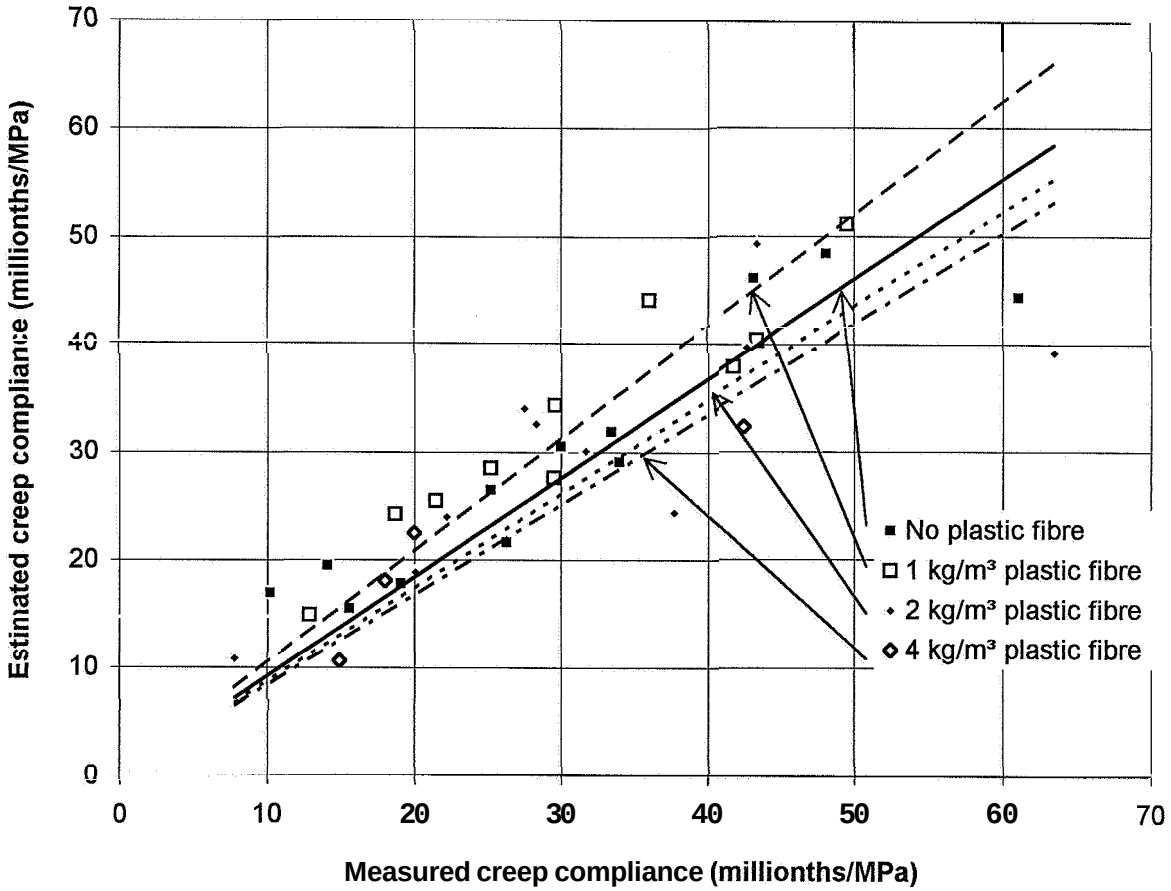

Figure 17.18 - Estimated creep compliance versus measured creep compliance.

18. STRENGTH AFTER LONG-TERM LOADING

18.1 General and experimental

The long-term creep rate observed in Section 14 above was dependent on the age of HPC when loading. HPC that was loaded at early ages exhibited a larger long-term creep rate than HPC that was loaded in the mature state. Perhaps the high stresslcylinder strength level affected the long-term strength of the loaded HPC and thus also the long-term stability of the structure where HPC was used. After the long-term creep studies the sealed cylinders in the tests were investigated as regards strength. Parallel cast sealed cylinders that were used in studies of autogenous shrinkage were also investigated as regards strength. The moisture condition of the HPC perhaps affected the results of the strength tests, **Persson (1997D)**. After the strength tests were performed, HPC pieces were collected in glass tubes. After 1 day the HPC pieces then were used to measure the relative humidity, 0 , Section 5.

18.2 Results and discussion

Table 18.1 gives O of the tested specimens, which followed the self-desiccation curves, cp. Section 5. On average Ø= 0.70 of loaded specimen and Ø= 0.69 of specimen with no loading was obtained. The moisture state did not affect the result of the strength tests. **Figure 18.1** shows the ratio of the strength of cylinders after loading and the strength of unloaded cylinders versus the relative 28-day strength at loading. The type of mix did not affect the result. **Figure 18.2** shows the ratio of the strength of cylinders after loading and the strength of unloaded cylinders versus the relative 28-day strength at loading. The stresslstrength level is indicated. The ratio of the strength of cylinders after loading and the strength of unloaded cylinders increased with the relative 28-day strength at loading. HPC, that was loaded mature state, obtained about 10% larger strength after long-term loading than HPC without loading. With the stresslstrength level = 0.3 the following equation was obtained:

$$f_{clo}/f_{cun} = 0.4 \cdot (f_c/f_{c28}) + 0.73 \qquad \{\sigma/f_c = 0.3;\ 0.5 < f_c/f_{c28} < 1\} \qquad (18.1)$$

f_c denotes strength at loading (MPa)
f_{clo} denotes long-term strength of loaded specimen (MPa)
f_{cun} denotes long-term strength of unloaded specimen (MPa)
f_{c28} denotes 28-day strength (MPa)

High stresslstrength-level at early ages did not decrease the long-term strength of HPC. At low stresslstrength-level the long-term strength increased ≈ 10% after long-term loading compared with the strength of unloaded HPC. Symbols in **Table 18.1:**
…01= loading at 0.8 days' age with stresslcylinder strength = 0.84
…02= loading at 2 days' age with stresslcylinder strength = 0.84
…03= loading at 2 days' age with stresslcylinder strength = 0.42
…28= loading at 28 days' age with stresslcylinder strength = 0.42

Table 18.1 - Internal relative humidity of specimens (lo= loaded; un= no loading).

Mix/ batch	1 lo	1 un	2 lo	2 un	3 lo	3 un	5 lo	5 un	6 lo	6 un	8 lo	8 un
01	0.63	0.73	0.69	0.67	0.62	0.73	0.72	0.71	0.70	0.69	0.68	0.65
02	0.81	0.74	0.64	0.69	0.64	-	0.72	0.74	0.69	0.66	0.64	0.68
03	0.67	0.83	0.71	0.68	0.70	0.66	0.71	0.71	0.71	0.71	0.66	0.68
28	-	0.74	0.81	0.72	0.72	0.64	0.70	0.70	0.71	0.70	0.58	0.67

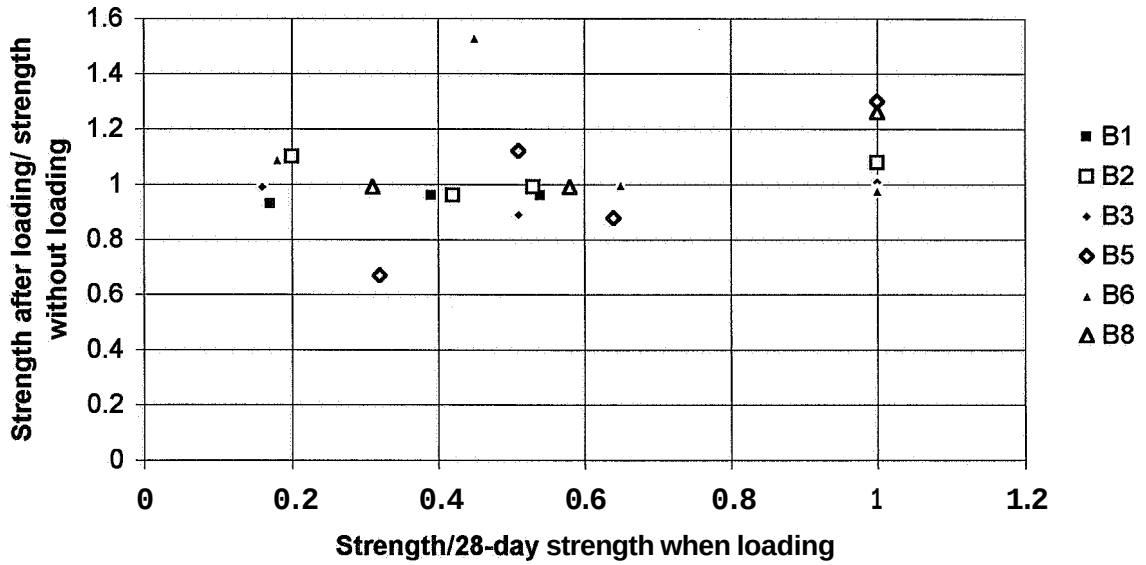

Figure 18.1 - Strength of loaded cylinder to strength of unloaded cylinders versus the relative 28-day strength at loading. B= sealed curing; 1= **mix (Table 5.1).**

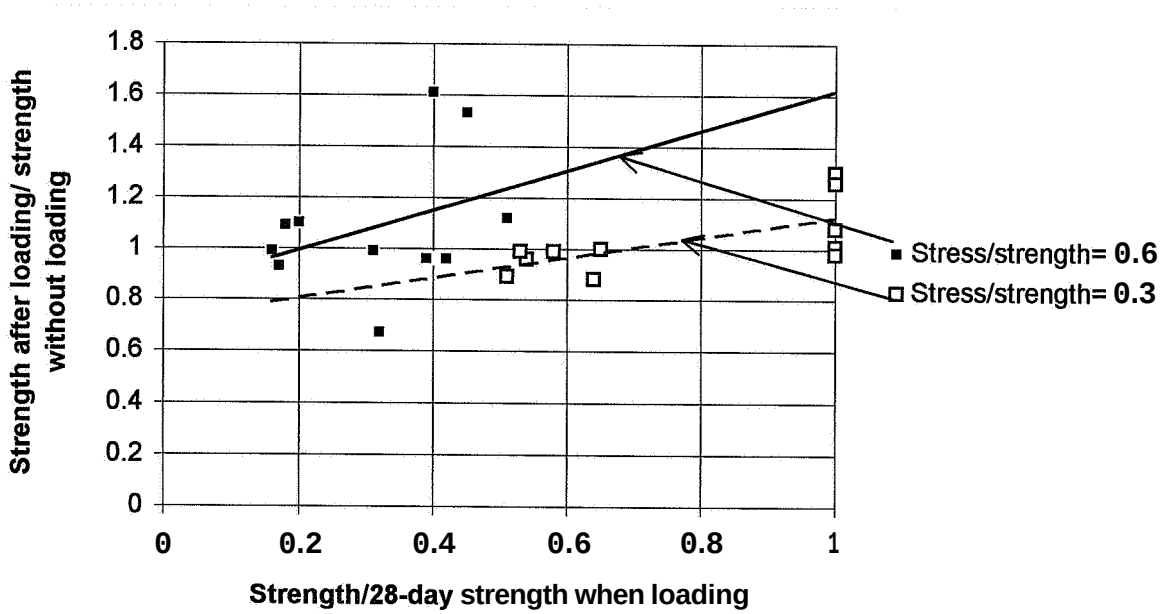

Figure 18.2 - Strength of loaded cylinder to strength of unloaded cylinders versus the relative 28-day strength at loading at different stress/strength level at loading.

19. EVALUATION OF SUGGESTED PREDICTION FORMULAS

19.1 General

After the comparison between the results of the field tests and the laboratory studies was performed, further evaluation of the suggested prediction formulas was done. The results after use of all the suggested prediction formulas seemed to coincide reasonably well with laboratory data. The accuracy factor (R^2) of the suggested prediction formulas is given. The estimations also gave the possibility to demonstrate the use of the mentioned equations in concrete design. However, it must be emphasised that the suggested formulas apply only for the HPCs tested under the conditions given in this study. Other size of specimen, other types of material, loading levels, other ambient climate, and so forth, most certainly will give other quasi-instantaneous and long-term properties of the HPC.

19.2 Method

Equations of principal interest in this report were summarised and the most of the estimations performed for four typical kinds of HPC, that are given in **Table 19.1.** **Table 19.2** gives the characteristics of the cement, silica fume, and aggregate.

Table 19.1 – Concretes studied in the estimations

HPC	w/c	s/c	Type of silica fume	Aggregate
1	0.27	0.10	Granulated	Quartzite
2	0.27	0.10	Slurry	Granite
3	0.37	0.05	Granulated	Quartzite
4	0.37	0.05	Slurry	Granite

Symbols in Table 19.1:

c denotes the cement content (kg/m^3)
s denotes the content of silica fume (kg/m^3)
w denotes the amount of mixing water including moisture (kg/m^3)

Table 19.2 - Characteristics of cement, silica fume and aggregate in the estimations.

Material	Elastic modulus	Compressive strength	Split strength	Specific surface	Ignition losses
Low-alkali cement	-	-	-	302 m^2/kg	0.63%
Granulated silica fume	-	-	-	17.5 m^2/g	2.3%
Silica fume slurry	-	-	-	22.5 m^2/g	1.9%
Quartzite sandstone,	60 GPa	330 MPa	15 MPa		0.3%
Granite	61 GPa	150 MPa	10 MPa		1.7%

19.3 Strength

19.3.1 Efficiency factor of silica fume:

Table 19.3 gives estimations of the strength efficiency factor of 10% silica fume that was calculated on the basis of the cement content according to equation (5.2):

$$k_{sc} = 0.113 \cdot [4.44 - \ln(t)] \cdot (w/c)^{-0.056 \cdot [\ln(t)+35]}$$

{1<t< 90 months; 0.24<w/c<0.48; R^2= 0.86) (5.2)

k_{sc} denotes the efficiency factor of silica fume related to compressive strength of sealed cylinders; 80 mm in length and 40 mm in diameter, equation (5.1)
t denotes age (months)

Table 19.3 - Estimation of the strength efficiency factor of silica fume.

t (months)	w/c	k_{sc}
3	0.27	***5.2***
3	0.37	2.7
30	0.27	1.7
30	0.37	1

19.3.2 Compressive strength and split tensile strength

Table 19.4 gives estimations of the relationship between compressive and split tensile strength at sealed curing done on the basis of the following equations:

$$f_{sp,s} = [0.281 - 0.0144 \cdot \ln(t)] \cdot (f_c)^{0.744+0.0109 \cdot \ln(t)}$$

{30<f_c<150 MPa; 1<t<90 months; R^2= 0.66) (5.3)

$$f_{sp} = [0.144 + 0.0084 \cdot \ln(t)] \cdot (f_c)^{0.902-0.0165 \cdot \ln(t)}$$

{30<f_c<150 MPa; 1<t<90 months; R^2= 0.69) (5.4)

f_c denotes the compressive strength (MPa)
f_{sp} denotes the split tensile strength (MPa)
ln (t) denotes the natural logarithm of age, t (months)
s denotes 10% silica fume calculated on the basis of the cement content

Table 19.4 – Estimations of compressive and split tensile strength at sealed curing.

t (months)	w/c	s/c	f_c (MPa)	f_{sp} (MPa)
3	0.27	0.10	120	10.1
3	0.37	0.05	80	7.3[1)]
30	0.27	0.10	130	7.6
30	0.37	0.05	90	6.7[1)]

1) average of equations (5.3) and (5.4)

19.3.3 Compressive strength

Table 19.5 gives estimations of compressive strength on the basis of the following equations:

$f_{cB}=21.5\cdot k_a\cdot k_s\cdot[5.75+\ln(t)-11.5\cdot(w/c)]$ {0.8<t<28 days; R^2= 0.79) (5.5)

$f_{cD}=30\cdot k_a\cdot k_s\cdot\{2.6+[1-1.2\cdot(w/c)]\cdot\ln(t)-3.9\cdot(w/c)\}$ {0.8<t<28 days; R^2= 0.76} (5.6)

f_{cB} denotes the strength with sealed curing (basic creep)
f_{cD} denotes the strength of **HPC** with air curing (drying creep)
k_a = 0.88 in **HPC** with 5% air-entrainment; k_a = 1 without air-entrainment
k_s = 0.77 in **HPC** 5% silica fume; k_s = 1 in concrete with 10% silica fume
ln (t) denotes the natural logarithm of the age of the **HPC** {0.8<t<28 days)

Table 19.5 - Estimations of compressive strength.

t (days)	w/c	s/c	Air-entrainment (%)	f_{cB} (MPa)	f_{cD} (MPa)
3	0.27	0.10	1	81	69
3	0.37	0.05	1	42	41
3	0.37	0.05	5	37	36
28	0.27	0.10	1	154	138
28	0.37	0.05	1	99	85
28	0.37	0.05	5	87	74

19.3.4 Influence of air curing on the strength:

Table 19.6 gives 100-mm cubes strength of with air curing related to sealed curing.

$f_{cD}= a\cdot[0.93-0.36\cdot(w/c)]\cdot f_{cB}$ {R^2= 0.80} (5.7)

f_{cB} denotes the cylinder strength with sealed curing (basic creep)
f_{cD} denotes the cylinder strength with air curing (drying creep)
a = 1.1 in **HPC** with silica fume slurry; a= 0.94 with 5% silica fume; a= 1 in concrete with 10% granulated silica fume.

Table 19.6 – The 100-mm cubes strength related to type of curing, sealed or air.

t (days)	w/c	s/c	Type of silica fume silica fume	f_{cB} (MPa)	f_{cD} (MPa)
3	0.27	0.10	Granulated	81	68
3	0.37	0.05	Granulated	42	32
3	0.37	0.05	Slurry	46	35
28	0.27	0.10	Granulated	154	128
28	0.37	0.05	Granulated	99	74
28	0.37	0.05	Slurry	109	81

19.4 Hydration

19.4.1 Sealed curing

Table 19.7 gives the strength, f_{cB}, according to the following expressions:

$$f_{cB} = 3.3 \cdot k_5 \, (w/c)^{-4.63} \cdot [(w_n/w) - 5.2 \cdot k_a \cdot k_5 \cdot e^{-11 \cdot (w/c)}] \qquad \{R^2 = 0.67\} \quad (5.27)$$

$$f_{cBsl} = 600 \cdot [(w_n/w) - 0.052] \qquad \{R^2 = 0.97\} \quad (5.28)$$

e denotes the natural logarithm
k_a =2.2 for air-entrained HPC, k_a= 1 otherwise (except with 10% silica slurry)
k_5 =0.72 for HPC with 5% silica fume, k_5= 1 otherwise (except for silica slurry)
sl denotes 10% silica fume slurry
w_n/w denotes the relative hydration (non-evaporable water to mixing water)

Table 19.7 - Strength related to hydration with sealed curing.

w/c	w_n/w	s/c	Air-entrainment (%)	Type of silica fume	f_{cB} (MPa)
0.27	0.3	0.10	1	Granulated	47
0.27	0.3	0.10	1	Slurry	149
0.37	0.3	0.05	1	Granulated	56
0.37	0.3	0.05	5	Granulated	83
0.37	0.5	0.05	1	Granulated	104

19.4.2 Air curing

Table 19.8 gives the relative hydration and strength, f_{cD}, of HPC with air curing:

$$f_{cD} = 530 \cdot k_a \cdot k_5 \cdot [(w_n/w) - k_a \cdot 0.14] \qquad \{R^2 = 0.86\} \quad (5.31)$$

$$f_{cDsl} = 510 \cdot [(w_n/w) - 0.015] \qquad \{R^2 = 0.97\} \quad (5.32)$$

k_a =0.6 for HPC with 5% air-entraining, k_a= 1 otherwise
k_5 =0.8 for HPC with 5% silica fume slurry, k_{sl}= 1 otherwise
sl denotes 10% silica fume slurry
w_n/w denotes the relative hydration (non-evaporable water to mixing water)

Table 19.8 - Relative hydration and strength of HPC with air curing:

w_n/w	w/c	s/c	Air-entrainment (%)	Type of silica fume	f_{cD} (MPa)
0.2	0.27	0.10	1	Granulated	32
0.2	0.27	0.10	1	Slurry	94
0.2	0.37	0.05	1	Granulated	25
0.2	0.37	0.05	5	Granulated	15
0.4	10.27	0.10	1	Granulated	1138

19.5 Internal relative humidity

19.5.1 Sealed curing

Table 19.9 gives the internal relative humidity calculated with the equations:

$$Ø(t,w/c)_s = 1.13\,[1-0.065\cdot\ln(t)]\cdot(w/c)^{0.24\cdot[1-0.1\cdot\ln(t)]} \qquad \{R^2= 0.76\} \quad (5.35)$$

$$Ø(t,w/c) = 1.09\cdot(w/c)^{0.17\cdot(1+0.0451\cdot t)} \qquad \{R^2= 0.54\} \quad (5.36)$$

t denotes the age of the concrete {1<t <15 months}
w/c denotes the water-cement ratio {0.22<w/c <0.58 }
s denotes 10% silica fume
$Ø(t,w/c)$ denotes RH in sealed-cured Portland cement concrete with sealed curing
$Ø(t,w/c)_s$ denotes RH in sealed-cured concrete with 10% silica fume

Table 19.9 - Internal relative humidity, Ø, in sealed HPC

t (months)	w/c	s/c	Ø
1	0.27	0.10	0.83
1	0.37	0.05	0.91[1)]
3	0.27	0.10	0.79
3	0.37	0.05	0.87[1)]
30	0.27	0.10	0.72
30	0.37	0.05	0.74[1)]

1) average of 0 and 10% silica fume

Table 19.10 gives Ø in sealed HPC calculated with the equation:

$$Ø(wbr_{eff}, t) = 0.38\cdot[w/(c+2\cdot s) + 2.4 - 0.1\cdot\ln t] + \Delta Ø_{sl} \qquad \{R^2= 0.83\} \quad (5.37)$$

c denotes the cement content in the concrete (kg/m^3)
s denotes the content of silica fume in the concrete (kg/m^3)
t denotes the age of the concrete {1<t<1000 days}
w denotes the water content in the concrete (kg/m^3)
$\Delta Ø_{sl}$ = - 0.035 for 5-10% silica fume slurry at age, t≤ 28 days

Table 19.10 - Internal relative humidity, Ø, in sealed HPC

t (days)	w/c	s/c	Ø	$Ø_{sl}$
28	0.27	0.10	0.87	0.83
28	0.37	0.05	0.91	0.87
90	0.27	0.10	0.83	0.83
90	0.37	0.05	0.87	0.87
900	0.27	0.10	0.74	0.74
900	0.37	0.05	0.78	0.78

Table 19.11 the internal relative humidity in **HPC** calculated with the equation:

$$Ø = 0.965 \cdot t^{0.0188} \cdot (w/c)^{0.0331 \cdot \ln(t)+0.0505}$$

{1<t<1000 days; 0.25<w/c<0.38; R^2= 0.53) (5.39)

Table 19.11 - Internal relative humidity, 0 , in sealed **HPC.**

t (days)	w/c	s/c	Ø
28	0.27	0.10	0.83
28	0.37	0.05	0.88
90	0.27	0.10	0.81
90	0.37	0.05	0.86
900	0.27	0.10	0.76
900	0.37	0.05	0.83

Table 19.12 gives the relative humidity correlated to the relative hydration , w_n/w:

$$Ø = 1.2 \cdot [(w/c)-0.467] \cdot \ln(w_n/w)+0.637 \cdot (w/c)+0.536$$

{0.25<w/c<0.38; 0.10< w_n/w<0.60; R^2= 0.28} (5.40)

Table 19.12 - The relative humidity, 0 , in **HPC** with sealed curing.

w/c	w_n/w	O
0.27	0.2	1.0
0.27	0.4	0.92
0.27	0.6	0.83
0.37	0.2	0.96
0.37	0.4	0.88
0.37	0.6	0.83

19.5.2 Air curing

Table 19.13 gives **RH** in the inner part of 100-mm cubes calculated with equation:

$$O = 1.193.t^{-0.0883} \cdot (w/c)^{-0.0155 \cdot \ln(t)+0.1937}$$

{1<t<1000 days; 0.25<w/c<0.38; R^2= 0.46) (5.39)

Table 19.13 - Internal relative humidity, 0 , in sealed **HPC.**

t (days)	w/c	s/c	O
28	0.27	0.10	0.74
28	0.37	0.05	0.77
90	0.27	0.10	0.68
90	0.37	0.05	0.71
900	0.27	0.10	0.58
900	0.37	0.05	0.60

19.6 Quasi-instantaneous creep compliance

19.6.1 Air curing

Table 19.14 gives the drying creep compliance during the first second (from 0.01 s of loading) calculated according to the following two equations:

$$J(t,t') = a \cdot \int d(t-t')/(t-t') + b = a \cdot \int d(t-t')/(t-t') + 1000/D_{t'} \qquad (6.13)$$

a	denotes the compliance rate, **Table 6.3** [millionths/(MPa·s)]
b	denotes initial compliance 1 s after loading, **Table 6.4** (millionths/MPa)
t	denotes the age of the concrete (s)
t'	denotes the age of the concrete at loading (s)
t-t'	denotes loading time (s)
$D_{t'}$	denotes the deformation modulus after 1 s of loading (GPa)
J(t,t')	denotes the compliance (specific creep, millionths/MPa)

$$a_D = [0.37-0.23\cdot(\sigma/f_c)]\cdot s_{a5} + [1.2-5.5\cdot(\sigma/f_c)]\cdot \ln(f_c/f_{c28}) \qquad \{R^2 = 0.78) \ (6.14)$$

a_D	denotes the compliance rate with air curing [millionths/(MPa·s)]
$\ln(f_c/f_{c28})$	denotes the natural logarithm of the relative 28-day cube strength
s_{a5}	=1.1 for HPC with 5% silica fume or/and air-entrainment; s_{a5}= 1 for HPC with 10% silica fume and no air-entrainment
σ/f_c	denotes the stress/cube strength ratio at loading $\{0.3<\sigma/f_c<0.6\}$

Table 19.14 - Drying creep compliance during the first second (from 0.01 s).

f_c/f_{c28}	σ/f_c	Amount of silica fume (%)	a_D [millionths/(MPa·s)]	J(t,t')-1/$D_{t-t'}$ (millionths/MPa)
0.3	0.3	5	0.87	4
0.3	0.3	10	0.84	3.9
0.3	0.6	10	2.75	12.7
0.65	0.3	5	0.52	2.4
0.65	0.3	10	0.49	2.3
0.65	0.6	10	1.13	4.2
1	0.3	5	0.33	1.5
1	0.3	10	0.30	1.4
1	0.6	10	0.23	1.1

19.6.2 Sealed curing

Table 19.15 gives the first second of compliance according to equation (6.13) and

$$a_B = [0.18+0.42\cdot(\sigma/f_c)]\cdot s_5 + [0.12-2\cdot(\sigma/f_c)]\cdot \ln(f_c/f_{c28}) \qquad \{R^2 = 0.68) \ (6.15)$$

a_B denotes the compliance rate with sealed curing [millionths/(MPa·s)]
f_c/f_{c28} relative strength level{σ/f_c=0.3: 0.4<f_c/f_{c28}<1; σ/f_c=0.6: 0.15<f_c/f_{c28}<0.5}
$\ln(f_c/f_{c28})$ denotes the natural logarithm of the relative 28-day cube strength
s_5 =1.5 for HPC with 5% silica fume; s_5= 1 for 10% silica fume
σ/f_c denotes the stress/cube strength ratio at loading {0.3<σ/f_c<0.6}

Table 19.15 - Sealed creep compliance during the first second (from 0.01 s).

f_c/f_{c28}	σ/f_c	Amount of silica fume (%)	a_D [millionths/(MPa·s)]	$J(t,t')-1/D_{t-t'}$ (millionths/MPa)
0.3	0.3	5	0.87	4
0.3	0.3	10	0.84	3.9
0.3	0.6	10	2.75	12.7
0.65	0.3	5	0.52	2.4
0.65	0.3	10	0.49	2.3
0.65	0.6	10	1.13	4.2
1	0.3	5	0.33	1.5
1	0.3	10	0.30	1.4
1	0.6	10	0.23	1.1

19.6.3 Influence of internal relative humidity

Table 19.16 gives the creep rate during according to the following equation:

$$a_{0.3}=0.30-0.04\cdot\Delta\emptyset-(0.48+0.02\cdot\Delta\emptyset)\cdot\ln(f_c/f_{c28}) \quad \{\sigma/f_c=0.3;\ 0.4< f_c/f_{c28}<1;\ R^2=0.60\} \qquad (6.16)$$

$$a_{0.6}=0.43-2.7\cdot\Delta\emptyset-(1.07+5.14\cdot\Delta\emptyset)\cdot\ln(f_c/f_{c28}) \quad \{\sigma/f_c=0.6;\ 0.15< f_c/f_{c28}<0.5;\ R^2=0.60\} \qquad (6.17)$$

$a_{0.3}$ denotes the creep rate with stress/strength = 0.3 [millionths/(MPa·s)]
$\ln(f_c/f_{c28})$ denotes the natural logarithm of the relative strength/28-day strength
AO denotes the difference between the internal relative humidity of the inner part, $\emptyset_i$, and the surface, $\emptyset_s$, of the cylinder

Table 19.16 - Creep rate during the first second of loading (from 0.01s).

f_c/f_{c28}	AØ	$a_{0.3}$ [millionths/(MPa·s)]	$a_{0.6}$ [millionths/(MPa·s)]
0.3	0.15	0.8	2.2
0.3	0.30	0.8	2.8
0.65	0.15	0.4	0.8
0.65	0.30	0.4	0.8
1	0.15	0.3	-[1]
1	0.30	0.3	-[1]

1) out of the limits of equation (6.17)

19.7 Deformation modulus

19.7.1 Air curing

Tables 19.17 - 19.19 gives the deformation modulus of HPC with air curing determined according to the following equations:

$$D_D = a \cdot (f_c)^b \qquad \{R^2 = 0.74\text{-}0.85\} \qquad (7.2)$$

$$D_D = [c \cdot \ln(t\text{-}t') + d] \cdot (f_c)^{e \cdot \ln(t-t')+f} \qquad \{0.01 < t\text{-}t' < 1s;\ R^2 = 0.73\} \qquad (7.3)$$

$$D_D(f_c; t\text{-}t'; \sigma/f_c) = \{10.7 - 12.8 \cdot (\sigma/f_c) - [0.15 + 0.29 \cdot (\sigma/f_c)] \cdot \ln(t\text{-}t')\} \cdot (f_c)^{0.18 + 0.61 \cdot (\sigma/fc) + 0.022 \cdot (\sigma/fc - 0.1) \cdot \ln(t-t')}$$
$$\{R^2 = 0.73\} \qquad (7.4)$$

a, b, c, d, e, f denotes constants given in **Table 7.3** and **Table 7.4**

f_c denotes the cube strength at loading (MPa) $\{20 < f_c < 120$ MPa$\}$

$\ln(t\text{-}t')$ denotes the natural logarithm of the time elapsed from loading

$t\text{-}t'$ denotes loading time (s)

D_D denotes the deformation modulus of HPC with air curing, (GPa)

σ/f_c denotes the stress to cube strength ratio at loading $\{0.3 < \sigma/f_c < 0.6\}$

Table 7.3 - Constants a and b of equation (7.2)

Loading time, t-t′(s)	**Stress/strength level, σ/f_c = 0.6**		**Stress/strength level, σ/f_c = 0.3**	
Constant	a	b	a	b
0.01	4.55	0.4947	8	0.3402
0.1	3.81	0.5155	7.45	0.35
1	3.04	0.5453	6.89	0.3606

Table 7.4 - Constants c, d, e and f

Stresslstrength level, σ/f_c = 0.6		**Stresslstrength level, σ/f_c = 0.3**	
c	0.328	c	-0.241
d	3.05	d	6.89
e	0.011	e	0.0044
f	0.544	f	0.361

Table 19.17 - Deformation modulus of air-cured HPC according to equation (7.2).

Loading time (s)	**Compressive strength (MPa)**	**Stresslstrength level**	**Deformation modulus (GPa)**
0.01s	80	0.3	35.5
0.01s	120	0.3	40.8
0.01s	120	**0.6**	48.6
1s	80	0.3	33.5
1s	120	0.3	38.7
1s	120	0.6	41.4

Table 19.18 - Deformation modulus of air-cured **HPC** according to equation (7.3).

Loading time (s)	Compressive strength (MPa)	Stresslstrength level	Deformation modulus (GPa)
0.01s	80	0.3	35.6
0.01s	120	0.3	40.9
0.01s	120	0.6	48.4
1s	80	0.3	33.5
1s	120	0.3	38.8
1s	120	0.6	41.2

Table 19.19 - Deformation modulus of air-cured **HPC** according to equation (7.4).

Loading time (s)	Compressive strength (MPa)	Stress/strength level	Deformation modulus (GPa)
0.01s	80	0.3	35.7
0.01s	120	0.3	41.0
0.01s	120	0.6	48.3
1s	80	0.3	33.7
1s	120	0.3	39.0
1s	120	0.6	41.2

19.7.2 Sealed curing

Table 19.20 gives the deformation modulus, D_B, according to equation (7.5):

$$D_B(f_c;t\text{-}t') = 0.43 \cdot [7.9 - \ln(t\text{-}t')] \cdot (f_c)^{0.17 \cdot [3.14 + 0.1 \cdot \ln(t\text{-}t')]} \quad \{0.01 < t\text{-}t' < 1s;\ R^2 = 0.92\} \quad (7.5)$$

$\ln(t\text{-}t')$ denotes the natural logarithm of the time elapsed from loading

Table 19.20 - Deformation modulus of air-cured HPC according to equation (7.5).

Loading time (s)	Compressive strength (MPa)	Deformation modulus (GPa)
0.01s	80	39.6
0.01s	120	47.6
1s	80	35.2
1s	120	43.8

Tables 19.21 - 19.23 show the deformation modulus, D_B, of HPC with sealed curing computed according to the equations (7.6) – (7.8) with constants a, b, c, d, e, f given in **Table** 7.5 and **Table 7.6:**

$$D_B = a \cdot (f_c)^b \quad \{10 < f_c < 140\ \text{MPa};\ R^2 = 0.74\text{-}0.95\} \quad (7.6)$$

$$D_B = [c \cdot \ln(t\text{-}t') + d] \cdot (f_c)^{e \cdot \ln(t\text{-}t') + f} \quad \{0.01 < t\text{-}t' < 1s;\ R^2 = 0.66\} \quad (7.7)$$

$$D_B(f_c;t\text{-}t';\sigma/f_c) = \{6.06\text{-}3.02\cdot(\sigma/f_c)\text{-}[0.44\text{-}0.51\cdot(\sigma/f_c)]\cdot\ln(t\text{-}t')\}\cdot(f_c)^{0.42+0.061\cdot(\sigma/fc)-\ 0.039\cdot(\sigma/fc-0.5)\cdot\ln(t\text{-}t')} \quad \{R^2 = 0.66\} \qquad (7.8)$$

$\ln(t\text{-}t')$ denotes the natural logarithm of the time elapsed from loading

Table 7.5 - Constants a and b of equation (7.6)

Loading time, t-t′(s)	Stress/strength level, $\sigma/f_c = 0.6$		Stress/strength level, $\sigma/f_c = 0.3$	
Constant	a	b	a	b
0.01	4.89	0.4813	6.59	0.4041
0.1	4.58	0.4682	5.64	0.4309
1	4.25	0.4595	5.25	0.4369

Table 7.6 - Constants c, d, e and f

Stress/strength level, $\sigma/f_c = 0.6$		Stress/strength level, $\sigma/f_c = 0.3$	
c	-0.139	c	-0.291
d	4.25	d	5.16
e	-0.0047	e	0.0071
f	0.459	f	0.440

Table 19.21 - Deformation modulus of sealed **HPC** according to equation (7.6).

Loading time (s)	Compressive strength (MPa)	Stress/strength level	Deformation modulus (GPa)
0.01s	80	0.3	38.7
0.01s	120	0.3	45.6
0.01s	120	0.6	49.0
1s	80	0.3	35.6
1s	120	0.3	42.5
1s	120	0.6	38.4

Table 19.22 - Deformation modulus of sealed **HPC** according to equation (7.7).

Loading time (s)	Compressive strength (MPa)	Stress/strength level	Deformation modulus (GPa)
0.01s	80	0.3	38.7
0.01s	120	0.3	45.7
0.01s	120	0.6	48.8
1s	80	0.3	35.5
1s	120	0.3	42.4
1s	120	0.6	38.3

Table 19.23- Deformation modulus of sealed **HPC** according to equation (7.8).

Loading time (s)	Compressive strength (MPa)	Stresslstrength level	Deformation modulus (GPa)
0.01s	80	0.3	37.7
0.01s	120	0.3	44.4
0.01s	120	0.6	47.2
1s	80	0.3	35.2
1s	120	0.3	42.0
1s	120	0.6	37.8

19.8 Shrinkage

19.8.1 Autogenous shrinkage

Table 19.24 gives the autogenous shrinkage counted from equations (8.1)-(8.2):

$$\varepsilon_B = k_s \cdot k_5 \cdot 1.42 \cdot [0.44-(w/c)] \qquad \{R^2 = 0.80\} \quad (8.1)$$

$$\varepsilon_B = k_{s\emptyset} \cdot 1.75 \cdot (1-1.13 \cdot \emptyset) \qquad \{R^2 = 0.72\} \quad (8.2)$$

k_s = 1.5 for silica fume slurry; k_s = 1 for granulated silica fume
$k_{s\emptyset}$ = 1.3 for silica fume slurry; $k_{s\emptyset}$ = 1 for granulated silica fume
k_5 = 0.78 for 5% silica fume; k_5 = 1 for 1% silica fume
w/c denotes the water-cement ratio {0.2<w/c<0.4}
O denotes the internal relative humidity {0.70<Ø<0.90}

Table 19.24 - Autogenous shrinkage according to the equations (8.1) - (8.2):

w/c	O	Type of silica fume	Amount of silica fume	Equation (8.1, per mil)	Equation (8.2, per mil)
0.27	0.76	Granulated	5%	0.19	0.25
0.27	0.76	Granulated	10%	0.24	0.25
0.27	0.76	Slurry	10%	0.36	0.32
0.37	0.83	Granulated	5%	0.08	0.11
10.37	10.83	Slurry	15%	0.12	0.14

19.8.2 Drying shrinkage

Table 19.25 gives the drying shrinkage of mature **HPC** versus the evaporated water:

$$\varepsilon_D = k_{sD} \cdot 20 \cdot [1.1 \cdot (w_e/w) - (w_e/c)] \qquad \{R^2 = 0.18\} \quad (8.3)$$

c denotes the cement content of the concrete (kglm^3)
k_{sD} = 0.4 for **HPC** with silica fume slurry; k_{sD} = 1 for granulated silica fume
w denotes the mixing water of the concrete (kglm^3) {0< w_e/w<0.03}
w_e denotes the evaporated water from the concrete (kglm^3) {0< w_e/w<0.03}
ε_D denotes the specific shrinkage related to the evaporated water (per mil)

Table 19.25 - Drying shrinkage of mature HPC versus the evaporated water.

w_e/w	w_e/c	Type of silica fume	ε_D (per mil)
0.03	0.01	Granulated	0.46
0.03	0.01	Slurry	0.18

Table 19.26 gives the drying shrinkage for **HPC** with w/c<0.3:

$$\varepsilon_{D1} = 1.55\cdot[(w/c)-0.219]\cdot e^{62.9\cdot[0.423\cdot(we/w)-(we/c)]} \quad \{R^2 = 0.80\} \quad (8.7)$$

c denotes the cement content of the concrete (kg/m^3)
w denotes the mixing water of the concrete (kg/m^3) {0.25< w/c<0.30}
w_e denotes the evaporated water from the concrete (kg/m^3) {0<w_e/w<0.30}
ε_{D1} denotes the specific shrinkage related to the evaporated water (per mil)

Table 19.26 - Drying shrinkage for HPC with w/c< 0.3.

w/c	we/w	we/c	ε_{D1}(per mil)
0.25	0.25	0.08	0.16
0.25	0.35	0.12	0.29
0.30	0.35	0.12	0.73

19.8.3 Total shrinkage

Table 19.27 shows the total shrinkage after at least 3 years estimated according to:

$$\varepsilon = k\cdot 34\cdot[(w/c)^2-0.68\cdot(w/c)+0.13] \quad \{R^2 = 0.80\} \quad (8.10)$$

$$\varepsilon_B = k_B\cdot 1.5\cdot[0.43-(w/c)] \quad \{R^2 = 0.75\} \quad (8.11)$$

$$\varepsilon_C = 0.85\cdot[(w/c)-0.25] \quad \{R^2 = 0.49\} \quad (8.12)$$

$$\varepsilon_D = 33\cdot[(w/c)^2-0.654\cdot(w/c)+0.115] \quad \{R^2 = 0.52\} \quad (8.13)$$

k =1.1 for **HPC** with 10% silica fume slurry; k=1 for **HPC** with 10% granulated silica fume or 5% silica fume slurry
k_B =1.5 (10% silica fume slurry); k_B=1 (10% granulated silica fume or 5% slurry)
E, ε_B, ε_C, ε_D denote total, basic (autogenous), carbonation and drying (per mil)

Table 19.27 - Shrinkage after at least 3 years according to equations (8.10)-(8.13).

w/c	Type of silica fume	Amount of silica fume (%)	ε (per mil)	ε_B (per mil)	ε_C (per mil)	ε_D (per mil)
0.27	Granulated	10	0.66	0.24	0.02	0.38
0.27	Slurry	5	0.66	0.24	0.02	0.38
0.27	Slurry	10	0.72	0.36	0.02	0.38
0.37	Granulated	10	0.52	0.09	0.10	0.33
0.37	Slurry	5	0.52	0.09	0.10	0.33
0.37	Slurry	10	0.57	0.14	0.10	0.33

19.8.4 Shrinkage at constant weight (no loss of weight)

Table 19.28 gives the shrinkage at no loss of weight according to equation (8.14):

$$\varepsilon_{Bn} = k_{sn} \cdot k_{5n} \cdot 1.38 \cdot [0.45-(w/c)] \quad \{R^2 = 0.67\} \quad (8.14)$$

ε_{Bn} denotes shrinkage in HPC with no loss of weight (autogenous, per mil)
k_{sn} = 1.33 for HPC with silica fume slurry; k_{sn} = 1 with granulated silica fume
k_{5n} = 0.69 for HPC with 5% silica fume; k_{5n} = 1 for HPC with 10% silica fume

Table 19.28 - Autogenous shrinkage according to the equations (8.14)

w/c	Type of silica fume	Amount of silica fume	ε_{Bn} (per mil)
0.27	Granulated	5%	0.17
0.27	Granulated	10%	0.25
0.27	Slurry	10%	0.33
0.37	Granulated	5%	0.08
0.37	Granulated	10%	0.11
0.37	Slurry	5%	0.15

19.9 Short-term deformation

19.9.1 Drying short-term creep compliance

Table 19.29 shows creep according to equation (6.13) and the following equation:

$$a_D = 3.4 \cdot [(w/c)-0.13] \cdot s_{a5} + [0.3-11 \cdot (\sigma/f_c)] \cdot \ln(f_c/f_{c28}) \quad \{0.25<w/c<0.40;\ R^2 = 0.73\} \quad (9.1)$$

a_D denotes the rate of short-term drying creep of HPC [millionths/(MPa·h)]
f_c/f_{c28} denotes the relative 28-day strength at loading $\{0.3< f_c/f_{c28}<1\}$
s_{a5} =1.5 for 5% silica fume and/or air-entrainment; s_{a5} = 1 for 10% silica fume
σ/f_c denotes the stress/strength (100 mm cube) ratio at loading $\{0.3<\sigma/f_c<0.6\}$

Table 19.29 – Compliance from 1 s till 66-h of loading according to equation (9.1).

w/c	f_c/f_{c28}	σ/f_c	Amount of silica fume (%)	Compliance (millionths/MPa)
0.27	0.3	0.3	5	4.3·12.4= 53
		0.3	10	4.1·12.4= 50
		0.6	10	8·12.4= 99
	0.6	0.3	10	2·12.4= 24
		0.6	10	3.7·12.4= 46
	1	0.3	5	0.56·12.4= 6.9
		0.3	10	0.37·12.4= 4.6
0.37	0.3	0.3	5	4.8·12.4= 59
	0.6	0.3	5	2.8·12.4= 34
	1	0.3	5	1.2·12.4= 15

19.9.2 Basic short-term creep compliance

Table 19.30 shows creep according to equation (6.13) and to following equation:

$a_B = 0.14\cdot[(w/c)+2.5]\cdot s_{a5} + [0.29-6.9\cdot(\sigma/f_c)]\cdot\ln(f_c/f_{c28})$ $\{R^2 = 0.83\}$ (9.2)

a_B denotes the creep rate of sealed HPC [millionths/(MPa·h)]:
$\ln(f_c/f_{c28})$ denotes the natural logarithm of the relative strength when loading $\{0.4< f_c/f_{c28}<1$ for $\sigma/f_c=0.3$ and $0.15< f_c/f_{c28}<0.5$ for $\sigma/f_c=0.6\}$
s_{a5} =1.25 for HPCs with 5% silica fume or/and air-entrainment (10% silica fume); s_{a5}= 1 for HPC with 10% silica fume
σ/f_c denotes the stress/strength (100 mm cube) ratio at loading $\{0.3<\sigma/f_c<0.6\}$

Table 19.30 – Compliance from 1 s till 66-h of loading according to equation (9.2).

w/c	f_c/f_{c28}	σ/f_c	Amount of silica fume (%)	66-h compliance (millionths/MPa)
0.27	0.3	0.3	5	2.6·12.4= 32
		0.3	10	2.5·12.4= 31
		0.6	10	5·12.4= 62
	0.6	0.3	10	1.3·12.4= 16
		0.6	10	2.4·12.4= 29
	1	0.3	5	0.49·12.4= 6.1
		0.3	10	0.39·12.4= 4.8
0.37	0.3	0.3	5	2.6·12.4= 32.6
	0.6	0.3	5	1.4·12.4= 17.4
	1	0.3	5	0.5·12.4= 6.2

19.9.3 Short-term creep and internal relative humidity

Table 19.31 gives the creep rate estimated according to equations (9.3)-9.4):

$a_{Ø0.3} = 0.52+1.6\cdot\Delta Ø-(3.6\cdot\Delta Ø+1.7)\cdot\ln(f_c/f_{c28})$ $\{\sigma/f_c=0.3;\ 0.5< f_c/f_{c28}<1;\ R^2=0.93\}$ (9.3)

$a_{Ø0.6} = 0.84-0.6\cdot\Delta Ø-(9.3\cdot\Delta Ø+3)\cdot\ln(f_c/f_{c28})$ $\{\sigma/f_c=0.6;\ 0.15<f_c/f_{c28}<0.5;\ R^2=0.51\}$ (9.4)

$a_{Ø0.3}$ denotes the short creep rate of HPC with $\sigma/f_c=0.3$ [millionths/(MPa·h)]
$a_{Ø0.6}$ denotes the short creep rate of HPC with $\sigma/f_c=0.6$ [millionths/(MPa·h)]
$\ln(f_c/f_{c28})$ denotes the natural logarithm of the relative strength at loading
$\Delta Ø = Ø_i - O$, difference in relative humidity of the inner part, $Ø_i$, and the surface, O,

Table 19.31 - Creep rate estimated according to equations (9.3)-9.4).

f_c/f_{c28}	ΔO	Equation (9.3)	Equation (9.3)
0.6	0.30	1.6	3.6
1	0.15	0.9	0.8

19.10 Elastic modulus

19.10.1 Air-cured HPC

Table 19.32 shows the elastic modulus estimated according to equation (10.2):

$$E_{Dma}=6.77\cdot(f_c)^{0.379} \qquad (R^2= 0.87) \quad (10.2)$$

f_c denotes the compressive strength (MPa)
E_{Dma} denotes the elastic modulus versus strength of mature drying HPC (GPa)

Table 19.32 - Elastic modulus of mature drying HPC according to equation (10.2).

f_c (MPa)	80	90	100	110	120	130	140	150
E_{Dma} (GPa)	35.6	37.3	38.8	40.2	41.6	42.8	44.1	45.2

Table 9.33 shows the relative elastic modulus of young HPC compared to the 28-day elastic modulus of mature HPC estimated according to equation (10.3):

$$(E_{Dyo}/E_{Dma})=0.88+0.41\cdot(\sigma/f_c)+[0.38-0.81\cdot(\sigma/f_c)]\cdot(\Delta f_c/f_{c28}) \qquad \{R^2= 0.25\} \quad (10.3)$$

f_c denotes the strength at loading of young concrete (MPa)
f_{c28} denotes the 28-day strength (MPa)
E_{Dma} denotes the modulus of mature drying concrete (GPa)
E_{Dyo} denotes the elastic modulus of young drying concrete (GPa)
Δf_c denotes the growth of strength from loading until unloading (MPa)
σ denotes the stress of the concrete (MPa)

Table 9.33 - Relative elastic modulus of drying HPC according to equation (10.3).

$\Delta f_c/f_{c28}$	σ/f_c	E_{Dyo}/E_{Dma}
0	0.3	1.00
0	0.6	1.13
0.2	0.3	1.01
0.2	0.6	1.11
0.4	0.3	1.06
0.4	0.6	1.08

19.10.2 Sealed HPC

Table 19.34 shows the elastic modulus estimated according to equation (10.4):

$$E_{Bma}=4.71\cdot(f_c)^{0.48} \qquad \{R^2= 0.85) \quad (10.4)$$

f_c denotes the compressive strength (MPa)
E_{Bma} denotes the elastic modulus of mature sealed HPC (GPa)

Table 19.34 - Elastic modulus of mature sealed HPC according to equation (10.4).

f_c (MPa)	80	90	100	110	120	130	140	150
E_{Dma} (GPa)	38.6	40.8	43.0	45.0	46.9	48.7	50.5	52.2

Table 9.35 shows the relative elastic modulus of young sealed HPC compared to the 28-day elastic modulus of mature HPC estimated according to equation (10.3):

$$(E_{Byo}/E_{Bma}) = 0.87+0.4\cdot(\sigma/f_c)+[0.14-0.21\cdot(\sigma/f_c)]\cdot(\Delta f_c/f_{c28}) \qquad \{R^2= 0.19\} \quad (10.5)$$

f_c/f_{c28} denotes the ratio of strength at loading and the 28-day strength E_{Bma} denotes the modulus of mature sealed concrete (GPa)
E_{Byo} denotes the elastic modulus of young sealed concrete (GPa)
Δf_c denotes the strength growth between loading and unloading of HPC (MPa)
a denotes the stress of HPC (MPa)

Table 9.35 - Relative elastic modulus according to equation (10.3).

$\Delta f_c/f_{c28}$	σ/f_c	E_{Byo}/E_{Bma}
0	0.3	1.00
0	0.6	1.11
0.2	0.3	1.03
0.2	0.6	1.11
0.4	0.3	1.02
0.4	0.6	1.11

19.10.3 Effect of moisture on elastic modulus

Table 19.36 shows result of elastic modulus estimated according to equation (10.6):

$$E(f_c,Ø)=10.3\cdot(1.45-Ø)\cdot(f_c)^{0.433\cdot(Ø+0.12)} \qquad \{R^2= 0.83\} \quad (10.6)$$

f_c denotes the strength at loading (MPa)
O denotes the internal relative humidity

Table 19.36 - Result of elastic modulus estimated according to equation (10.6).

f_c (MPa)	O	$E(f_c,Ø)$ (GPa)
80	0.65	35.5
80	0.95	39.2
100	0.65	38.3
100	0.95	43.5
120	0.65	40.7
120	0.95	47.3
140	0.65	42.8
140	0.95	50.8

19.11 Possion's ratio

Table 19.37 gives Poisson's ratio estimated according to equations (11.4)- (11.5):

$$\upsilon_B = k_B \cdot [0.04 \cdot \ln(f_c/f_{c28}) + 0.14] \qquad \{R^2 = 0.15\} \quad (11.5)$$

$$\upsilon_D = k_D \cdot [0.05 \cdot \ln(f_c/f_{c28}) + 0.13] \qquad \{R^2 = 0.25\} \quad (11.4)$$

f_c denotes the compressive strength at loading or unloading (MPa)
f_{c28} denotes the compressive strength at 28 days's age (MPa)
ln denotes the natural logarithm
k_B =1.4 for HPC with silica fume slurry and granite (mix 4, 7); k_D = 1 otherwise
k_D =1.2 for HPC with silica fume slurry and granite (mix 4, 7); k_D = 1 otherwise
υ_B denotes Poisson's ratio at loading or unloading of sealed HPC
υ_D denotes Poisson's ratio at loading or unloading of drying HPC

Table 19.37 - Poisson's ratio estimated according to equations (11.4)- (11.5).

f_c/f_{c28}	Type of aggregate	Type of silica fume	υ_B	υ_D
0.3	Granite	Slurry	0.13	0.08
0.3	Quartzite	Granulated	0.09	0.07
0.65	Granite	Slurry	0.17	0.13
0.65	Quartzite	Granulated	0.12	0.11
1	Granite	Slurry	0.20	0.16
1	Quartzite	Granulated	0.14	0.13

19.12 Dynamic modulus of elasticity

19.12.1 Deformation modulus, dynamic and static modulus of elasticity

Table 19.38 gives the different kinds of elastic modulus estimated according to:

$$D_{0.01} = (1.04 - 8 \cdot 10^{-5} \cdot t) \cdot E_{stat} \qquad \{R^2 = 0.89\} \quad (12.5)$$

$$E_{dyn} = (1.04 - 4 \cdot 10^{-5} \cdot t) \cdot E_{stat} \qquad \{R^2 = 0.95\} \quad (12.6)$$

t denotes the age of the concrete (days)
$D_{0.01}$ denotes the deformation modulus at loading (GPa)
E_{dyn} denotes the dynamic modulus of elasticity (GPa)
$E_{,}$ denotes the static modulus of elasticity at unloading (GPa)

Table 19.38 - Elastic modulus estimated according to equations (12.5) – (12.6).

E_{stat} (GPa)	Age (days)	$D_{0.01}$ (GPa)	E_{dyn} (GPa)
35	28	36.3	36.4
35	500	35	35.7
40	28	41.5	41.6
40	500	40	40.8
45	28	46.7	46.7
45	500	45	45.9

19.12.2 Deformation, elastic dynamic and static modulus of young HPC

Table 19.39 gives the effect of moisture on the dynamic modulus of elasticity:

$$E_{dyn} = 14.85\cdot(Ø-0.537)\cdot(D_{0.01})^{1.208\cdot(1.371-Ø)} \qquad \{0.65<Ø<0.9;\ R^2= 0.93\} \quad (12.7)$$

$D_{0.01}$ denotes the deformation modulus 0.01 s after loading (GPa)
E_{dyn} denotes the dynamic modulus of elasticity (GPa)
O denotes the internal relative humidity

Table 19.39 - The dynamic modulus estimated according to equation (12.7).

$D_{0.01}$ (GPa)	Ø	E_{dyn} (GPa)
35	*0.65*	37.1
35	0.90	40.8
40	0.65	41.7
40	0.90	44.0
45	0.65	46.2
45	0.90	47.0

Table 19.40 gives the effect of relative 28-day strength on the dynamic modulus:

$$E_{dyn} = D_{0.01}\cdot[1.14-0.29\cdot(\sigma/f_c)-0.0753\cdot\ln(f_c/f_{c28})\cdot(\sigma/f_c+4.08)] \qquad \{R^2= 0.54\} \quad (12.8)$$

$D_{0.01}$ denotes the deformation modulus 0.01 s after loading (GPa)
E_{dyn} denotes the dynamic modulus of elasticity (GPa)

Table 19.40 - The effect of relative 28-day strength on the dynamic modulus.

$D_{0.01}$ (GPa)	f_c/f_{c28}	σ/f_c	E_{dyn}(GPa)
35	0.3	0.3	50.7
40	0.3	0.3	58
40	0.3	0.6	55.6
40	0.65	0.6	44.7
40	1	0.3	42.1
45	1	0.3	47.4

19.12.3 Ageing effect on deformation, dynamic and elastic static modulus

Table 19.41 gives an ageing effect on mature HPC described in equations (12.9-11):

$$E_{dyn,t} = (E_{dyn}, 1)\cdot t^{0.0025} \quad (12.9)$$

$$D_{0.01,t} = (D_{0.01}, 1)\cdot t^{0.0135} \quad (12.10)$$

$$E_{stat,t} = (E_{stat}, 1)\cdot t^{0.0184} \quad (12.11)$$

t denotes age (months)
$D_{0.01}$ denotes the deformation modulus 0.01 s after loading (GPa)
E_{dyn} denotes the dynamic modulus of elasticity (GPa)
E_{stat} denotes the static modulus of elasticity at unloading (GPa)

Table 19.41 - Ageing effect on mature HPC described in equations (12.9) – (12.11).

Age (months)	$D_{0.01}$ (GPa)	E_{dyn} (GPa)	E_{stat} (GPa)
1	41.5	41.6	40
12	42.9	41.8	41.9
24	43.3	41.9	42.4

19.12.4 Strength effect on deformation, dynamic and elastic modulus

Table 19.42 gives an effect of strength estimated according to equations (12.12-14):

$$E_{dyn} = k_{sl}\cdot 11.2\, f_c^{0.272} \quad \{R^2 = 0.89\} \quad (12.12)$$

$$D_{0.01} = k_{sl}\cdot 7.47\cdot f_c^{0.351} \quad \{R^2 = 0.88\} \quad (12.13)$$

$$E_{stat} = k_{sl}\cdot 8.1\, f_c^{0.337} \quad \{R^2 = 0.89\} \quad (12.14)$$

f_c denotes the compressive strength of 100 mm cube at testing (MPa)
k_{sl} = 1.1 for HPC with silica fume slurry; k_{sl} = 1 for granulated silica fume
$D_{0.01}$ denotes the deformation modulus 0.01 s after loading (GPa)
E_{dyn} denotes the dynamic modulus of elasticity (GPa)
E_{stat} denotes the static modulus of elasticity at unloading (GPa)

Table 19.42 - Effect of cube strength estimated according to equations (12.12-14).

f_c (MPa)	$D_{0.01}$ (GPa)	E_{dyn} (GPa)	E_{stat} (GPa)
80	34.8	36.9	35.5
90	36.2	38.1	36.9
100	37.6	39.2	38.2
110	38.9	40.2	39.5
120	40.1	41.2	40.7

19.13 Recovery deformations

19.13.1 Mature concrete

Table 19.43 gives plastic and viscous recovery of mature **HPC** after *66* **h** of loading and 100 h of recovery estimated according to the following equations (per mil):

$\varepsilon_{pl} = 1.4 \cdot \varepsilon_{el} \cdot (1-\varepsilon_{el})$ $\{R^2 = 0.37\}$ (13.4)

$\varepsilon_{vi} = 0.26 \cdot \varepsilon_{el} \cdot (1.3-\varepsilon_{el})$ $\{R^2 = 0.16\}$ (13.5)

$\varepsilon_{Bpl} = 0.04 \cdot \varepsilon_{Bel} \cdot (5.5-\varepsilon_{Bel})$ $\{R^2 = 0.52\}$ (13.8)

$\varepsilon_{Bvi} = 0.1 \cdot \varepsilon_{Bel} \cdot (2.4-\varepsilon_{Bel})$ $\{R^2 = 0.25\}$ (13.9)

ε_{el} denotes elastic strain of drying **HPC**
ε_{pl} denotes plastic strain of drying **HPC**
ε_{vi} denotes viscous strain of drying **HPC**
ε_{Bel} denotes elastic strain of sealed **HPC**
ε_{Bpl} denotes plastic strain of sealed **HPC**
ε_{Bvi} denotes viscous strain of sealed **HPC**

Table 19.43 - Recovery according to equations (13.4), (13.5), (13.8) and (13.9).

ε_{el}(per mil)	ε_{pl}(per mil)	ε_{vi}(per mil)	ε_{Bel}(per mil)	ε_{Bpl}(per mil)	ε_{Bvi}(per mil)
0.5	0.35	0.10	0.5	0.10	0.10
0.6	0.34	0.11	0.6	0.12	0.11
0.7	0.29	0.11	0.7	0.13	0.12
0.8	0.22	0.10	0.8	0.15	0.13

19.13.2 Young concrete

Table 19.44 gives plastic and viscous recovery of young **HPC** after *66* **h** of loading and 100 h of recovery estimated according to the following equations (per mil):

$\varepsilon_{pl}/\varepsilon_{el} = 1.45 \cdot (\sigma/f_c) + [17.8 \cdot (\sigma/f_c) - 2.9] \cdot (\delta f_c/f_{c28})$ $\{R^2 = 0.32\}$ (13.6)

$\varepsilon_{vi}/\varepsilon_{el} = 0.89 \cdot [(\delta f_c/f_{c28}) + 0.19)] \approx 0.9 \cdot [(\delta f_c/f_{c28}) + 0.2)]$ $\{R^2 = 0.66\}$ (13.7)

$\varepsilon_{Bpl}/\varepsilon_{B_{el}} = 0.8 \cdot (\sigma/f_c) + [17.3 \cdot (\sigma/f_c) - 2.4] \cdot (\delta f_c/f_{c28})$ $\{R^2 = 0.64\}$ (13.10)

$\varepsilon_{Bvi}/\varepsilon_{B_{el}} = 0.75 \cdot (\delta f_c/f_{c28} + 0.3)$ $\{R^2 = 0.49\}$ (13.11)

f_c denotes current strength (MPa)
f_c denotes 28-day strength (MPa)
$\delta f_c/f_{c28} = f_{c,un}/f_{c28} - f_{c,lo}/f_{c28}$ (growth of strength between loading, lo, and unloading, un)
ε_{el} denotes elastic strain of drying HPC
ε_{pl} denotes plastic strain of drying HPC
ε_{vi} denotes viscous strain of drying HPC
ε_{Bel} denotes elastic strain of sealed HPC
ε_{Bpl} denotes plastic strain of sealed HPC
ε_{Bvi} denotes viscous strain of sealed HPC
σ/f_c stress level

Table 19.44 - Recovery according to equations (13.6), (13.7), (13.10) and (13.11).

$\delta f_c/f_{c28}$	σ/f_c	$\varepsilon_{pl}/\varepsilon_{el}$	$\varepsilon_{vi}/\varepsilon_{el}$	$\varepsilon_{Bpl}/\varepsilon_{B_{el}}$	$\varepsilon_{Bvi}/\varepsilon_{B_{el}}$
0.2	0.3	0.92	0.35	0.80	0.38
0.2	0.6	2.4	0.35	2.1	0.38
0.4	0.3	1.4	0.53	1.3	0.53
0.4	0.6	4	0.53	3.7	0.53

19.14 Long-term deformations

19.14.1 Air curing

Table 19.45 gives the long-term creep rate estimated with the following equation:

$$a_D = k_{ai} \cdot 513 \cdot [(w/c)^2 - 0.6 \cdot (w/c) + 0.09591 - k_{as} [1.83 + 2.37 \cdot (\sigma/f_c)] \cdot \ln(f_c/f_{c28}) \quad \{R^2=0.71\} \quad (14.9)$$

a_D denotes compliance rate with air curing [millionths/(MPa·day)]
f_c denotes cube strength at loading (MPa)
f_{c28} denotes 28-day cube strength (MPa)
k_{as} =0.8 with 5% air-entrainment; k_{as} = 1.3 with silica fume slurry, k_{as}=1 otherwise
k_{ai} = 1.5 for HPC with 5% air-entrainment; k_{ai} =1 otherwise

Table 19.45 - Long-term creep rate estimated with the equation (14.9).

w/c	f_c/f_{c28}	σ/f_c	Air-entrainment (%)	Silica fume	a_D (millionths/MPa·day)
0.27	0.3	0.6	1	Granulated	7.4
0.27	0.65	0.6	1	Granulated	4.9
0.27	0.65	0.6	1	Slurry	5.3
0.27	1	0.3	1	Granulated	3.5
0.37	0.65	0.6	1	Granulated	7.4
0.37	0.65	0.6	5	Granulated	10.2
0.37	1	0.3	1	Granulated	6.1

19.14.2 Sealed curing

Table **19.46** gives the long-term creep rate estimated with the following equation:

$$a_B = k_{s5}\cdot 231\cdot[(w/c)^2 - 0.594\cdot(w/c) + 0.0952] - k_{s5}\,[2.83 - 3\cdot(\sigma/f_c)]\cdot\ln(f_c/f_{c28}) \quad \{R^2 = 0.67\} \quad (14.11)$$

a_B denotes compliance rate with sealed curing [millionths/(MPa·day)]
f_c/f_{c28} denotes the relative 28-day strength at loading $\{0.3 < f_c/f_{c28} < 1\}$
k_{s5} = 1.5 with 5% silica fume or 10% silica fume slurry; k_{s5}=1 otherwise

Table 19.46 - Long-term creep rate estimated with the equation (14.11).

w/c	f_c/f_{c28}	σ/f_c	Silica fume	a_B [millionths/(MPa·day)]
0.27	0.3	0.6	10% granulated	3.1
0.27	0.65	0.6	10% granulated	2.3
0.27	0.65	0.6	10% slurry	3.5
0.27	1	0.3	10% granulated	1.9
0.37	0.65	0.6	5% granulated	4.9
0.37	0.65	0.6	10% granulated	3.3
0.37	1	0.3	10% granulated	2.9

19.14.3 Dependence on strength growth

Table **19.47** gives the compliance from 100 s until 1000 days' age of loading calculated according the equations (14.12) – (14.16):

$$J_D(t,t') = 1000/D_{t'} + a_{Dm}\cdot e^{0.48\cdot kD\cdot[(\sigma/fc) + 1.44]\cdot(dfc/fc28)}\cdot\int d(t-t')/(t-t') \quad \{R^2 = 0.53\} \quad (14.12)$$

$$J_{Dai}(t,t') = 1000/D_{t'} + a_{Dm}\cdot e^{0.5\cdot(dfc/fc28)}\cdot\int d(t-t')/(t-t') \quad \{R^2 = 0.44\} \quad (14.13)$$

$$a_{Dm} = k_{ais}\cdot 513\cdot[(w/c)^2 - 0.6\cdot(w/c) + 0.0959] \quad \{R^2 = 0.98\} \quad (14.14)$$

$$J_B(t,t') = 1000/D_{t'} + a_{Bm}\cdot e^{0.82\cdot k_B\cdot[1.44 - (\sigma/fc)]\cdot(dfc/fc28)}\cdot\int d(t-t')/(t-t') \quad \{R^2 = 0.50\} \quad (14.15)$$

$$a_{Bm} = k_{s5}\cdot 231\cdot[(w/c)^2 - 0.594\cdot(w/c) + 0.0952] \quad \{R^2 = 0.99\} \quad (14.16)$$

a_{Bm} denotes compliance rate of sealed mature HPC [millionths/(MPa·day)]
a_{Dm} denotes compliance rate of air-cured mature HPC [millionths/(MPa·day)]
ai denotes 5% air-entrainment
df_c denotes relative 28-day strength increase between loading and unloading
k_{ais} = 1.5 for 5% air-entrainment; k_{ais} =0.8 for silica fume slurry; k_{ais}=1 otherwise

k_{s5} = 1.5 for HPC with 5% silica fume or for HPC with 10% silica fume slurry; k_{s5}=1 otherwise
k_B =1.14 for HPC with 5% air-entrainment; k_B= 0.969 for silica fume slurry; k_B= 1 otherwise
k_D = 1.2 for HPC with silica fume slurry; k_D=1 otherwise
f_c denotes compressive strength at loading (MPa)
s denotes silica fume slurry
t denotes age of the concrete (days)
t′ denotes age at loading (days)
B denotes sealed curing
D denotes air curing
$D_{t'}$ denotes the deformation modulus at loading, Section 7 above (GPa)
J(t,t′) denotes the compliance (specific creep, millionths/MPa)

Table 19.47 - Creep from 100 s until 1000 days' age, equations (14.12) – (14.16).

w/c	df_c/f_{c28}	σ/f_c	Air (%)	Type of silica fume	Silica fume	$J_D(t,t')$ (millionths/MPa)	$J_B(t,t')$ (millionths/MPa)
0.27	0	0.3	1	Granulated	10%	37	19
0.27	0.3	0.3	1	Granulated	10%	45	23
0.27	0.3	0.6	1	Granulated	10%	47	22
0.27	0.3	0.6	1	Slurry	10%	40	33
0.27	0.6	0.3	1	Granulated	10%	57	30
0.27	0.6	0.6	1	Granulated	10%	63	27
0.37	0	0.3	1	Granulated	5%	58	45
0.37	0.3	0.3	1	Granulated	5%	71	57
0.37	0.3	0.6	1	Granulated	5%	74	53
0.37	0.3	0.6	1	Slurry	5%	63	53
0.37	0.6	0.3	1	Granulated	5%	89	72
0.37	0.6	0.6	1	Granulated	5%	100	64
0.37	0.6	0.6	5	Granulated	5%	112	69

19.4.4 Dependence on internal relative humidity

Table 19.48 gives the compliance from 100 s until 1000 days' age of loading according to equations (14.16), (14.17) and (14.18):

$$J_{0.3}(t,t') = 1000/D_{t'} + [a_{Bm} - 6.1\cdot(\Delta\emptyset + 0.11)\cdot\ln(f_c/f_{c28})]\cdot\int d(t-t')/(t-t')$$

$$\{\sigma/f_c = 0.3;\ 0.5 < f_c/f_{c28} < 1;\ R^2 = 0.29\} \qquad (14.17)$$

$$J_{0.6}(t,t') = 1000/D_{t'} + [a_{Bm} - 4.3\cdot(\Delta\emptyset + 0.39)\cdot\ln(f_c/f_{c28})]\cdot\int d(t-t')/(t-t')$$

$$\{\sigma/f_c = 0.6;\ 0.2 < f_c/f_{c28} < 0.5;\ R^2 = 0.28\} \qquad (14.18)$$

a_{Bm} denotes compliance rate of sealed mature HPC, equation (4.16)
f_c/f_{c28} denotes the relative 28-day strength at loading
J(t,t′) denotes the compliance (specific creep, millionths/MPa)
A O $= Ø_i - O$, denotes difference in internal relative humidity between the inner part of the cylinder at loading and the surface of the cylinder
0.3 denotes relative stresslstrength-level at loading, $\sigma/f_c = 0.3$
0.6 denotes relative stresslstrength-level at loading, $\sigma/f_c = 0.6$

Table 19.48 - Compliance from 100 s until 1000 days's age according to equations (14.16), (14.17) and (14.18).

w/c	f_c/f_{c28}	A O	Type of silica fume	Amount of silica fume	J0.3(t,t′) (millionths/MPa)	$J_{0.6}$(t,t′) (millionths/MPa)
0.27	0.3	0.2	Granulated	10%	42	51
0.27	0.3	0.4	Granulated	10%	58	62
0.27	0.3	0.4	Slurry	10%	67	71
0.27	0.65	0.2	Granulated	10%	27	30
0.27	0.65	0.4	Granulated	10%	33	34
0.27	1	0.2	Granulated	10%	19	19
0.37	0.3	0.2	Granulated	5%	69	77
0.37	10.3	10.4	Granulated	15%	84	88
0.37	0.3	0.4	Slurry	5%	84	88
0.37	0.65	0.2	Granulated	5%	54	56
0.37	0.65	0.4	Granulated	5%	59	60
0.37	1	0.4	Granulated	5%	45	45

19.4.5 Elastic modulus

Table 19.49 gives the elastic modulus related to age at loading and compressive strength at unloading according to equations (14.20) and (14.21):

$$E_D = 0.0543\cdot(76-t')\cdot(f_{cun})^{0.0035\cdot(t'+134)} \quad \{1<t'<28 \text{ days; } R^2= 0.62) \quad (14.20)$$

$$E_B = 6.02\cdot[2.4+\ln(t')]\cdot(f_{cun})^{0.0545\cdot[4.37-\ln(t')]} \quad \{1<t'<28 \text{ days; } R^2= 0.20\} \quad (14.21)$$

f_{cun} denotes the compressive cube strength at unloading (MPa)
t' denotes the age at loading (days)
E_B denotes the elastic modulus of sealed concrete (GPa)
E_D denotes the elastic modulus of drying concrete (GPa)

19.4.6 Plastic and viscous compliance related to the elastic compliance

Table 19.50 gives the plastic and viscous compliance related to the elastic compliance at unloading, all estimated according to equations (14.24)- (14.26):

Table 19.49 - Elastic modulus according to equations (14.20) and (14.21).

Age at loading, t´ (days)	Strength at unloading, f_{cun} (MPa)	E_D (GPa)	E_B (GPa)
2	80	32.2	44.5
2	110	37.4	47.4
2	140	42.0	49.8
7	80	32.4	46.4
7	110	37.9	48.4
7	140	42.7	49.9
28	80	31.1	44.0
28	110	37.2	44.8
28	140	42.7	45.5

$$(J_{pl}/J_{el})_D = 50\cdot k_{mai}\cdot k_{m5}\cdot[(w/c)^2-0.68\cdot(w/c)+0.1372]-7.8\, k_{yai}\cdot k_{ysl}\cdot(\sigma/fc)\cdot\ln(f_c/f_{c28}) \quad \{R^2=0.72\} \quad (14.24)$$

$$(J_{pl}/J_{el})_B = 82\cdot k_{msl}\cdot[(w/c)^2-0.544\cdot(w/c)+0.0824]+49\cdot(\sigma/fc)\cdot k_{ysl}\cdot e^{-6.77\cdot k\cdot[(\sigma/fc)+0.451]\cdot(fc/fc28)} \quad \{R^2=0.79\} \quad (14.25)$$

$$J_{vi}/J_{el} = 0.75\cdot k_{mD}\cdot[(w/c)-0.25]-k_{yD}\cdot\ln(f_c/f_{c28}) \quad \{R^2=0.85\} \quad (14.26)$$

ai denotes 5% air-entrainment
m denotes mature HPC
f_c denotes compressive strength at loading (MPa)
f_{c28} denotes compressive strength at 28 days' age (MPa)
[k, k_{mai}, k_{msl}, k_{mD}, k_{m5}, k_{yai}, k_{ysl}, k_{yD}] constants in **Table 14.24** (k=1 otherwise).
sl denotes silica fume slurry
y denotes HPC young when loading
B, D denotes sealed and air curing respectively
J_{pl}/J_{el} denotes ratio of viscous-plastic compliance to the elastic compliance
J_{vi}/J_{el} denotes ratio of viscous-elastic compliance to the elastic compliance
o denotes stress (MPa)
5 denotes HPC with 5% silica fume

Table 19.50 – Relative plastic and viscous compliance, equations (14.24)- (14.26):

w/c	f_c/f_{c28}	σ/fc	Air (%)	s/c (%)	Silica fume	$(J_{pl}/J_{el})_D$	$(J_{pl}/J_{el})_B$	J_{vi}/J_{elB}
0.27	0.3	0.6	1	10	Granulated	6.9	4.2	0.09
0.27	0.65	0.3	1	10	Granulated	2.3	1.2	0.04
0.27	0.65	0.3	1	10	Slurry	2.8	1.5	0.04
0.27	0.65	0.6	1	10	Granulated	3.3	1.0	0.04
0.27	1	0.3	1	10	Granulated	1.3	0.7	0.02
0.37	0.3	0.6	1	5	Granulated	7.1	5.0	0.16
0.37	0.65	0.6	1	5	Granulated	2.5	1.8	0.12
0.37	1	0.3	1	5	Granulated	1.5	1.5	0.09
0.37	1	0.3	1	5	Slurry	2.0	2.3	0.09

REFERENCES

P Acker (1993). Creep and Shrinkage of Concrete. Proceedings of the Fifth International RILEM Symposium on Creep and Shrinkage in Barcelona. RILEM 1993. E & FN Spon. London. 1993. Pp. 3-14.

A M Alvaredo and F H Wittmann (1993). Shrinkage as Influenced by Strain Softening and Crack Formation. Proceedings of the Fifth International RILEM Symposium on Creep and Shrinkage in Barcelona. RILEM 1993. E & FN Spon. London. 1993. Pp. 103-114.

ASTM C 215-85 (1985). Standard Test Method for Fundamental Transverse, Longitudinal, and Torsional Frequencies of Concrete Specimens. ASTM. Philadelphia. 1985. Pp. 119-122.

ASTM E 104-85 (1985). Standard Practice for Maintaining Constant Relative Humidity by Means of Aqueous Solutions. ASTM. Philadelphia. 1985. Pp. 33,637.

E Atlassi (1993). Effect of Moisture on the Compressive Strength of High Performance Concrete. Proceedings at the 3rd Symposium of High-Strength Concrete. Lillehammer. 1993. Ed. by I Holand and E Sellevold. 1993. Pp. 646-653.

H H Bache (1987). Compact Reinforced Composite, Basic Principles. CBL Report No. 41. Aalborg Portland. Denmark. 1987.

Z P Bazant (1993). New Test Method to Separate Microcracking from Drying Creep. Proceedings of the Fifth International RILEM Symposium on Creep and Shrinkage in Barcelona. RILEM 1993. E & FN Spon. London. 1993. Pp. 77-82.

Z P Bazant (1995). Creep and Shrinkage Prediction Model for Analysis and Design of Concrete Structures - Model B_3. Guidelines for Formulation of Creep and Shrinkage Prediction Models. RILEM Technical Committee 107. Materials and Structures. 1995. E & FN Spon. London. 1993. Pp. 357-365.

Z P Bazant; S Baweja (1995). Justifications and Refinements of Model B_3 for Concrete Creep and Shrinkage. 1. Statistics and Sensitivity. Materials and Structures. Vol. 28. London. 1995. Pp. 415-430.

Z P Bazant; I Carol (1993). Preliminary Guidelines and Recommendations for Characterising Creep and Shrinkage in Structural Design Codes. Proceedings of the Fifth International RILEM Symposium on Creep and Shrinkage in Barcelona. RILEM 1993. E & FN Spon. 1993. London. Pp. 805-829.

L Bjerkeli; A Tomaszewics; J J Jensen (1989). Deformation Properties and Ductility of High-Strength Concrete. 2nd International Symposium on Applications of High-Strength Concrete. Berkeley. ACI SP-121. 1989. Ed. by H Weston. 1993. Pp. 215-238.

J Brooks (1993). The Influence of Steel Fibre Reinforcement on Compressive Strength and Deformation of Ultra High Strength Cement-Silica Fume Mortar Matrix. Proceedings at the 3rd Symposium of High-Strength Concrete in Lillehammer. 1993. Ed. by I Holand and E Sellevold. 1993. Pp. 1024-1032.

J Brooks; J P Hynes (1993). Creep and Shrinkage of Ultra High-Strength Silica Fume Concrete. Proceedings of the Fifth International RILEM Symposium on Creep and Shrinkage in Barcelona. RILEM 1993. E & FN Spon. 1993. London. Pp. 493-498.

J Byfors (1980). Plain Concrete at Early Ages. Report FO 3:80. The Swedish Cement and Concrete Research Institute. Stockholm. 1980. Pp. 40-43.

P A Daerga; L Elfgren (1991). "Draghiillfasthet hos hogpresterande betong". Tensile Strength of High-Performance Concrete. Bygg & Teknik 7/91. Stockholm. 1991. Pp. 25-26. (In *Swedish.*)

M Emborg (1989). Thermal Stresses in Concrete Structures at Early Ages. Doctoral Thesis. Report 1989:73D. Division of Structural Engineering. Luleå University of Technology. Luleii. 1989. Pp. 77-99.

R H Evans (1958). Effect of Rate of Loading on Some Mechanical Properties of Concrete. Proceedings of the Conference of Behaviour of Non-metallic Brittle Materials. Ed. by W H Walton Butterworths Sc. London. 1958. Pp. 175-192.

G Fagerlund (1972). Relationship between the Porosity and the Mechanical Properties of Materials. Report 26. Division of Building Physics. Lund Institute of Technology. Lund. 1972.

G Fagerlund (1987). Relations between the Strength and the Degree of Hydration or Porosity of Cement Paste, Cement Mortar and Concrete. Cementa Report T 87023. Danderyd. 1987. 57 pp.

A Giovambattista; R Zerbino (1993). Creep of Concrete after 10 years of Loading. Proceedings of the Fifth International RILEM Symposium on Creep and Shrinkage in Barcelona. RILEM 1993. E & FN Spon. London. 1993. Pp. 51-62.

T C Hansen (1966). Theories of Multiphase Material Applied to Concrete, Cement Mortar and Cement Paste. Report 39. The Cement and Concrete Research Institute, CBI. Stockholm. 1966. Pp. 22.

M Hassanzadeh (1994). Fracture Mechanical Properties of High-Performance Concrete. Report M4:05. Lund Institute of Technology. Division of Building Materials. 1994. Pp. 8-13.

G Hedenblad (1996). Personal Communication. Division of Building Materials. Lund Institute of Technology. University of Lund. Lund. 1996.

M K Hurst (1988). Prestressed Concrete Design. Nanyang Technological Institute, Singapore. Chapman and Hall. London. 1998. Pp. 48-67.

J-P Jaccoud; A Leclercq (1995). Some Aspects Concerning Extension of Present Design Rules to HPC-structures. Material Properties and Design. Proceedings of the Fourth Weimar Workshop on High Performance Concrete held at Hochschule für Architektur und Bauwesen (HAB). Weimar. Ed. by F H Wittmann, P Schwesinger. Freiburg and Unterengstringen. 1995. Pp. 341-357.

O M Jensen; P F Hansen (1995). Autogenous Relative Humidity Change in Silica Fume-modified Cement Paste. Advances in Cement Research. 1995, 7. No. 25. Pp. 33-38.

S J Lokhorst; K van Breugel (1993). The Effect of Microstructural Development on Creep and Relaxation of Hardening Concrete. Proceedings of the Fifth International RILEM Symposium on Creep and Shrinkage in Barcelona. RILEM 1993. E & FN Spon. London. 1993. Pp. 145-150.

H S Müller; Küttner (1995). Characteristics and Prediction of Creep of High Performance Concrete. Material Properties and Design. Proceedings of the Fourth Weimar Workshop on High Performance Concrete held at Hochschule für Architektur und Bauwesen (HAB). Weimar. Ed. by F H Wittmann, P Schwesinger. Freiburg and Unterengstringen. 1995. Pp. 145-162.

H S Müller; M Pristl (1993). Creep and Shrinkage of Concrete at Variable Ambient Conditions. Proceedings of the Fifth International RILEM Symposium on Creep and Shrinkage in Barcelona. RILEM 1993. E & FN Spon. London. 1993. Pp. 15-26.

A Ngab; A Nilson; F Slate (1981). Creep of HPC. ACI Journal. 1981. Pp. 255-261.

A Nielsen (1972). Rheology of Building Materials. Doctoral Thesis. Document D6:1972. National Swedish Building Research. Stockholm. 1972. Pp. 25-53.

L O Nilsson (1987). Temperature Effects in Relative Humidity Measurements on Concrete - Preliminary Studies. The Moisture Research Group Informs. Report 1987:1. The Swedish Council of Building Research. Stockholm. 1987. Pp. 84.

K Norling Mjörnell (1994). Self-desiccation in Concrete. Report P-94:2. Division of Building Materials. Chalmers University of Technology. Gothenburg. 1994. Pp. 21.

V Penttala; P Häyrinen (1992). "Höghållfast betong och dess anv~dningsmojligheter.'High-Strength Concrete and Its Possible Applications. The Building Calendar 1992. The Swedish Building Contractors. Helsinki. 1992. Pp. 684. *(In Swedish.)*

D Perraton; F de Larrard; P C Aitcin (1994). Additional Data on the Strength Retrogression of Air-cured Silica Fume Concretes. 2nd CANMETIACI Conference on Durability of Concrete. Nice. 1994. Pp. 2-14.

B Persson (1992A). "Hogpresterande betongs hydratation, struktur och hållfasthet". Hydration, Structure and Strength of HPC. Report TVBM-1009. Lund Inst. of Techn. Div. Building Materials. Lund. 1992. Pp. 75-97; 99-123. *(In Swedish.)*

B Persson (1992B). Proportions of High-Performance Concrete. Report M6:01. Lund Institute of Technology. Division of Building Materials. Lund. 1992. Pp. 1-8.

B Persson (1992C). Pre-tests of High-Performance Concrete. Report M6:02. Lund Institute of Technology. Division of Building Materials. Lund. 1992. Pp. 1-11.

B Persson (1992D). Programme for Long-term Investigations of HPC. Report M6:04. Lund Institute of Technology. Div. Building Materials. 1992. Lund. 18 pp.

B Persson (1993A). Self-desiccating High-Strength Concrete Slabs. Proceedings at the 3rd Symposium of High-Strength Concrete in Lillehammer. 1993. Ed. by I Holand and E Sellevold. 1993. Pp. 882-889.

B Persson (1993B). Workability of the National Recipe in the HPC Programme. Report M6:09. Lund Inst. of Techn. Div. Building Materials. Lund. 1993. 12 pp.

B Persson (1995A). Basic Creep of High Performance Concrete. Report M6:14. Lund Institute of Technology. Division Building Materials. Lund. 1995. 292 pp.

B Persson (1995B). "Ideal partikelfördelning i färsk betong." Ideal Distribution of Particles in Fresh Concrete. Report TVBM-7090. Lund Institute of Technology. Division Building Materials. Lund. 1995. 10 pp. *(In Swedish.)*

B Persson (1996A). Pozzolanic Interaction Between Portland Cement and Silica Fume in Concrete. Report TVBM-7105. Lund Inst. of Techn. Div. Building Materials. Lund. Sixth CANMET/ACI/JCI International Conference on Fly Ash, Silica Fume, Slag and Natural Pozzolans in Concrete. Bangkok. 1998. Pp. 631-660.

B Persson (1996B). Self-desiccation and Its Importance in Concrete Technology. Materials and Structures. Vol. 30. RILEM. 1996. Pp. 293-305.

B Persson (1996C). (Early) basic creep of HPC. 4th International Symposium on the Utilisation of HPC. Paris. 1996. Ed. by F Larrard and R Lacroix. Pp. 405-414.

B Persson (1996D). Moisture in Concrete Subjected to Different Kinds of Curing. Materials and Structures. Vol. 30. RILEM 1996. Pp. 533-544.

B Persson (1996E). Hydration and Strength of HPC. Advanced Cement Based Material. Vol. 3. 1996. Pp. 107-123.

B Persson (1997A). Long-term shrinkage of HPC. Proc. of the 10th Int. Congress on the Chemistry of Cement. Contr. 2ii073. Gothenburg. 1997. Ed. by H Justnes. 9 pp.

B Persson (1997B). Basic Deformations of HPC. Nordic Concrete Research. Vol. 20. 1997. Pp. 59-74.

P Persson (1997C). Influence of Cement Type, Silica Fume, Water-cement Ratio and Moderate Shift of Temperature on Self-desiccation in Concrete. Report U97.17. Lund Institute of Technology. Div. Building Materials. Lund. 1994. 20 pp.

B Persson (1997D). Long-term Effect of Silica Fume on the Principal Properties of Low-temperature-cured Ceramics. CCR. Vol. 27. 1997. Pp. 1667-1680.

B Persson; F Berlin (1994). Programme CREEP for Estimation of the Creep Coefficient. Report M6:18. Lund Inst. of Techn. Div. Building Materials. 1994.

B Persson; G Fagerlund (1997). Self-desiccation and Its Importance in Concrete Technology. Report TVBM-3075. Lund Institute of Technology. Div. Building Materials. Lund. 1997. 255 pp.

O. Peterson (1976). Interaction between Silica Fume and Standard Portland Cement in Mortar and Concrete. Cementa Ltd. Malmö. 1976. 8 pp.

T C Powers; T L Brownyard (1946-1948). Studies of Physical Properties of Hardened Portland Cement Paste. Research Laboratories. PCA. Bulletin 22. 1948. Pp. 473-488, 845-864.

V Randall; K Foot (1989). High-Strength Concrete for Pacific First Centre. Concrete International. 1989. Pp. 14-16.

A M Rosenberg; J M Gaidis (1989). A New Mineral Admixture for High Strength Concrete. Concrete International. 1989. Pp. 31-36.

R le Roy; F de Larrard (1993). Creep and shrinkage of High-Strength Concrete. Proceedings of the Fifth International RILEM Symposium on Creep and Shrinkage in Barcelona. RILEM 1993. E & FN Spon. London. 1993. Pp. 500-508.

K Sakata (1993). Prediction of Concrete Creep and Shrinkage. Proceedings of the Fifth International RILEM Symposium on Creep and Shrinkage in Barcelona. 1993. E & FN Spon. 1993. Pp. 649-654.

P Schwesinger (1996). Prüfanlage zur Untersuchung des Lang- und Kurzzeitverhaltens Mechanisch, Thermisch und Hygrisch beanspruchter Baustoffe und Konstruktionselemente. Fakultät Bauingenieurwesen. Bauhaus-Universitat Weimar. Weimar. 1996. Pp. 1-2.

A Scordelis (1991). Analysis of Structural Concrete Systems. Proceedings of the International Association for Bridge and Structural Engineering Colloquium. Stuttgart. 1991. Pp. 265-266.

A Scordelis (1993). The Importance of Creep and Shrinkage in the Analysis, Design and Construction of Concrete Structures. Opening lecture. Fifth International RILEM Symposium. on Creep and Shrinkage in Barcelona. RILEM 1993.

E J Sellevold (1959). Unelastic Behaviour of Hardened Portland Cement Paste. Technical Report no 113. Department of Civil Engineering. Stanford University. 1959.267 pp.

H Shkoukani; J C Walraven (1993). Creep and Relaxation of Concrete Subjected to Imposed Thermal Deformations. Proceedings of the Fifth International RILEM Symposium on Creep and Shrinkage in Barcelona. RILEM 1993. E & FN Spon. London. 1993. Pp. 45-50.

V Sicard (1993). Origènes et Propriétés des Déformations de Retrait et de Fluage de Bétons a Hautes Performances a Partir de 28 heures de Durcissement. Materiaux et Durabilité de Constructions. INSA-UPS no. 201. Toulouse. 1993. Pp. 55-81.

J Stark (1995, 1997). Formation of Unstable Salts at O°C. Personal Communication. Weimar. 1995 and 1997.

J Stark (1996). Zusammenhänge zwischen Zementhydration und Dauerhaftigkeit von Beton. Hochschule fiir Architektur und Bauwesen Weimar. Festkolloquium am 31. Mai 1996. Universität - GH - Siegen, Labor fiir Bau- und Werkstoffchernie: Siegen. Germany. 1996. Pp. 5-21.

J Stark; K Bollmann (1995). Untersuchungen zur Bildung von Oberflächenrissen in Betonfahrbahndecken. Hochschule für Architektur und Bauwesen Weimar. Bulletin 6/7. Vol. 41. Wissenschaftige Zeichnung von Hochschule für Architektur und Bauwesen: Weirnar. 1995. Pp. 65-74.

E Tazawa; S Miyazawa (1993). Autogenous Shrinkage of Concrete and Its Importance in Concrete Technology. Proceedings of the Fifth International RILEM Symposium on Creep. 1993. Pp. 159-168.

E Tazawa; S Miyazawa (1997). Influence of Cement Composition on Autogenous Shrinkage of Concrete. Proceedings of the 10th International Congress on the Chemistry of Cement. Gothenburg. 2ii071. 1997. 8 pp.

F H Wittmann (1993). On the Influence of Stress on Shrinkage of Concrete. Proceedings of the Fifth RILEM Symposium on Creep in Concrete. Barcelona. 1993. E & FN Spon. London. 1993. Pp. 151-157.

A Xu (1992). Structure of Hardened Cement-fly Ash Systems and Their Related Properties. Report P-92:7. Division of Building Materials. Chalmers University of Technology. Gothenburg. 1992. Pp. IV: 15-19.

APPENDIX 1. GRADING CURVES OF AGGREGATE AND GRANULOMETRY OF CEMENTS

Appendix 1.1 - Grading curves of the aggregate
Appendix 1.2 - Granulometry of Degerhamn Standard cement and P400 cement

Appendix 1.1 - Grading curves of the aggregate

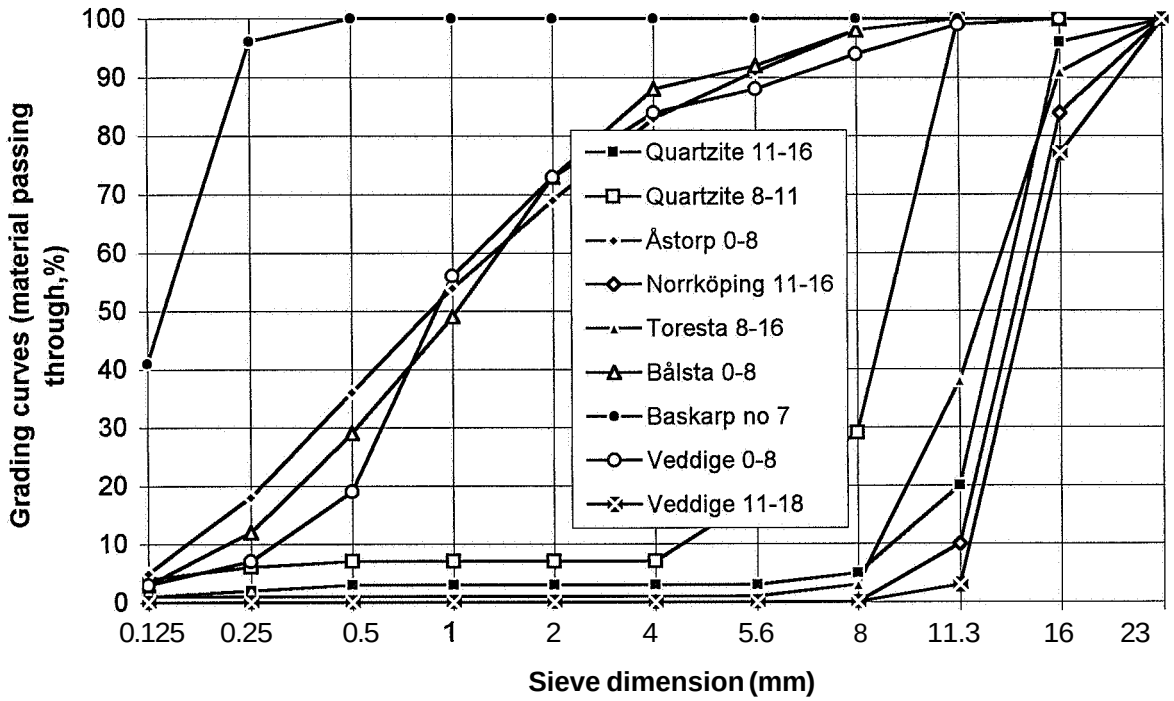

Appendix 1.2 - Granulometry of Degerhamn Standard and P400 cement

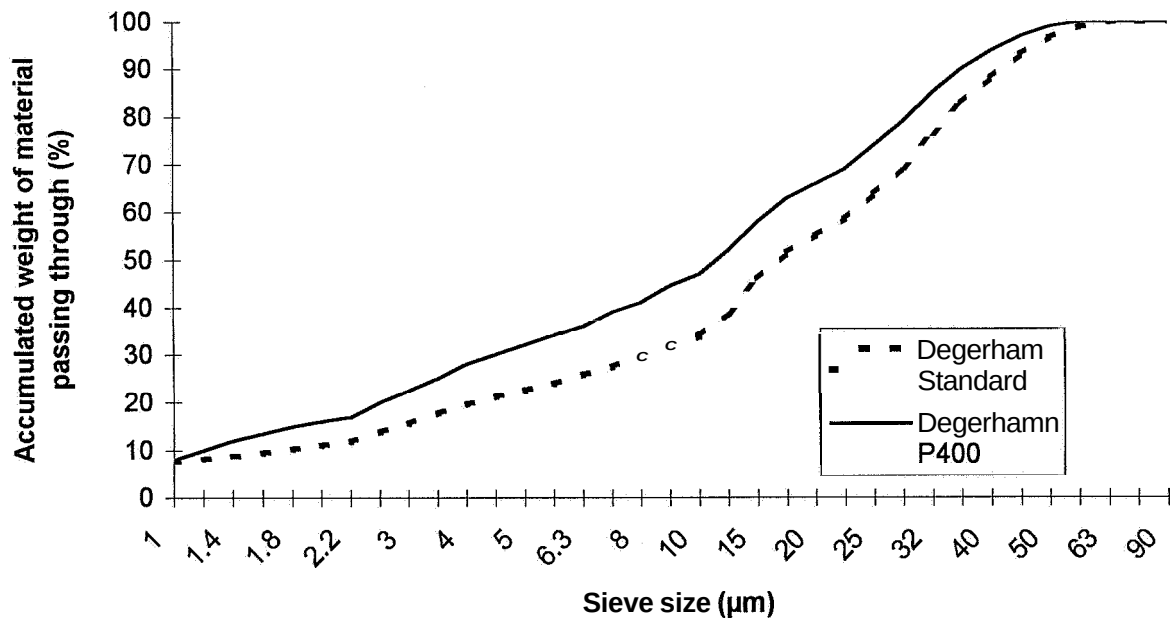

APPENDIX. 2. GRADING CURVES OF FRESH CONCRETE

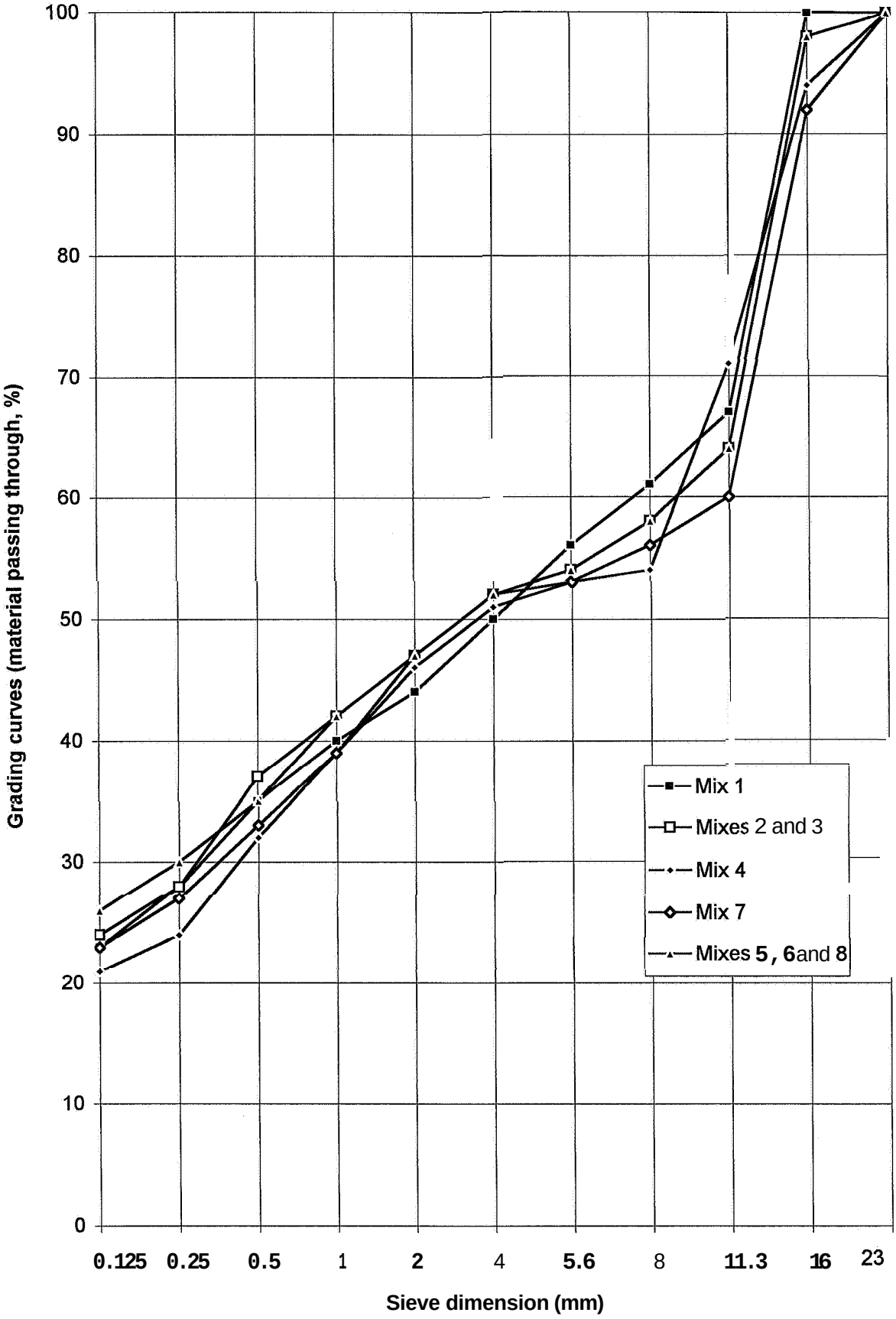

APPENDIX 3. TEMPERATURE OF CUBES AND CYLINDERS

Appendix 3.1 - Mix 7 (M, cube and cylinder)
Appendix 3.2 - Mix 8 (cylinders, 1503= basic creep, 1513= drying creep)

Symbols:
M= with granulated silica fume
03= batch number

Appendix 3.1 – Temperature of mix 7 (M, cube and cylinder)

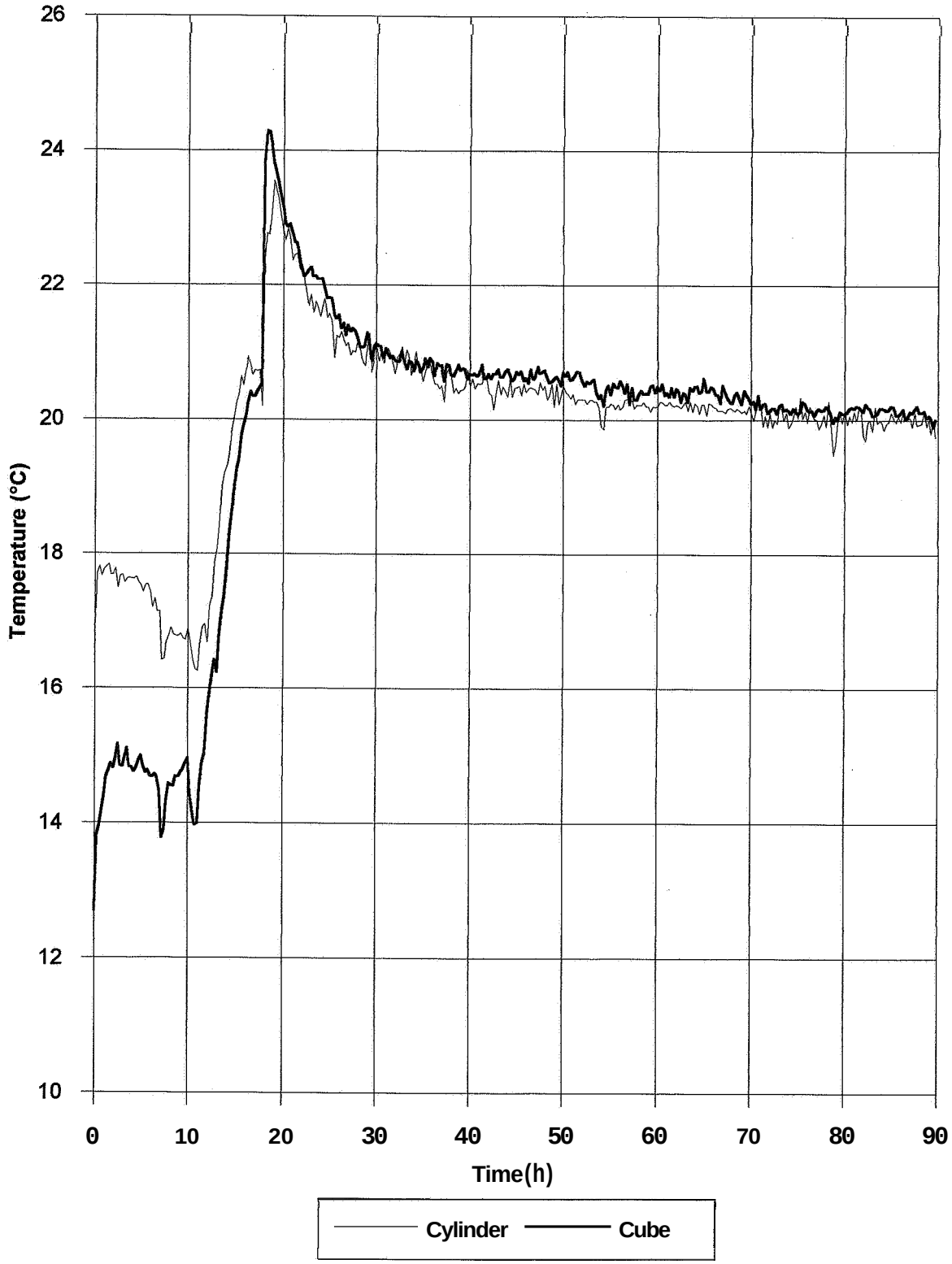

Appendix 3.2 - Temperature of mix 8 (cylinders, 1503= basic creep, 1513= drying creep)

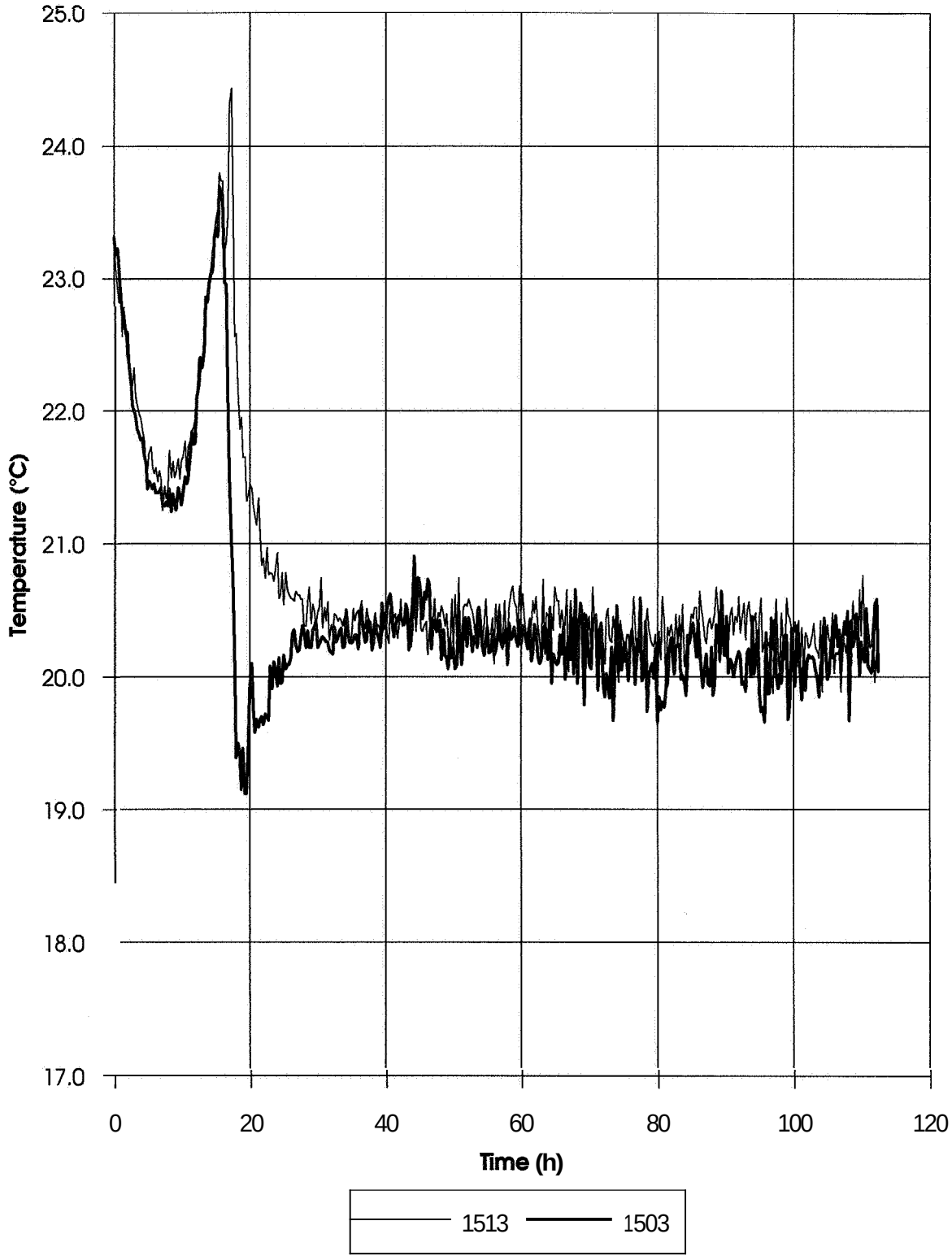

APPENDIX 4. TEMPERATURE OF CUBES AND CYLINDERS SUBJECTED TO AIR CURING

Appendix 4.1 - Temperature of mix 2 batch 3

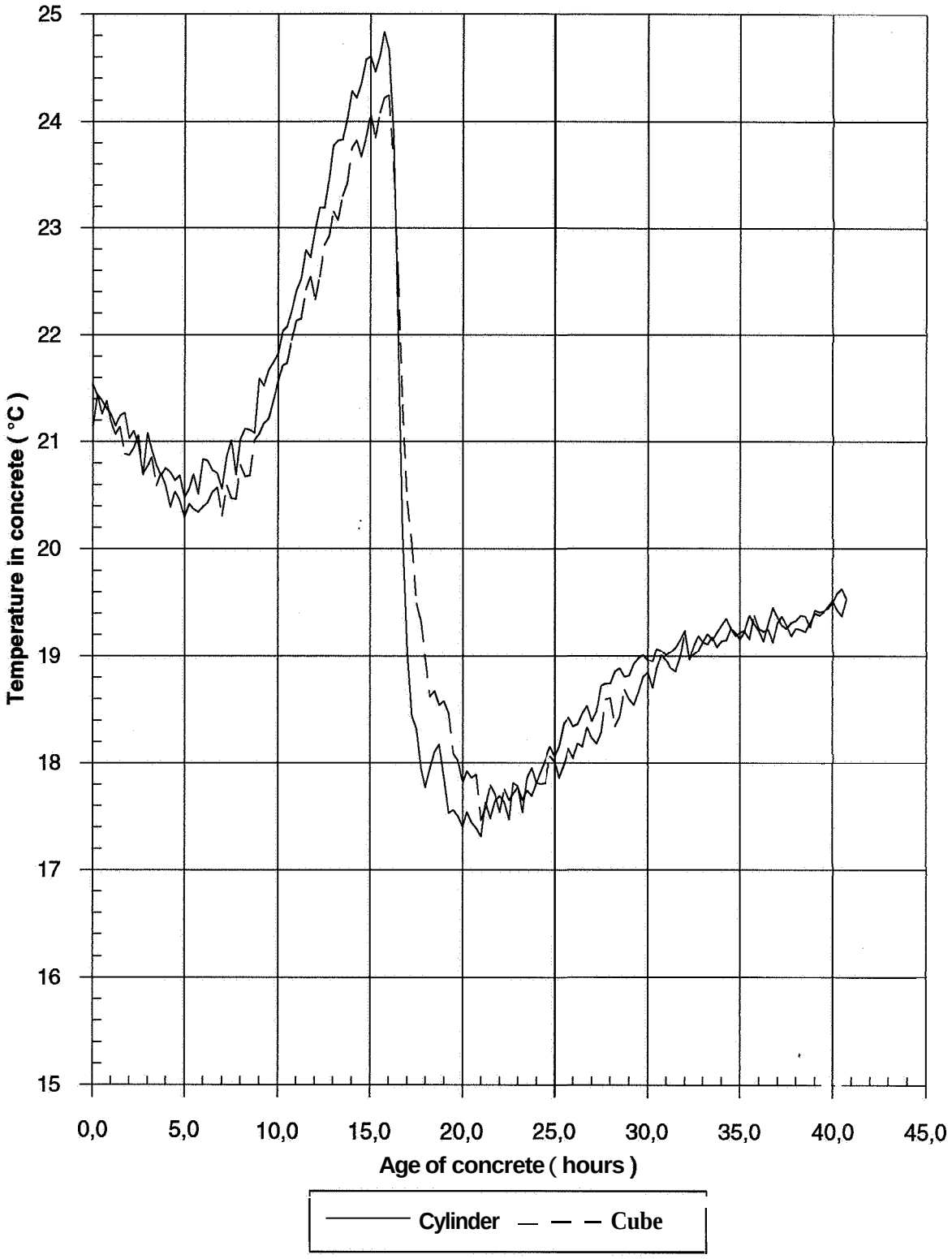

Appendix 4.2 - Temperature of mix 5 batch 1

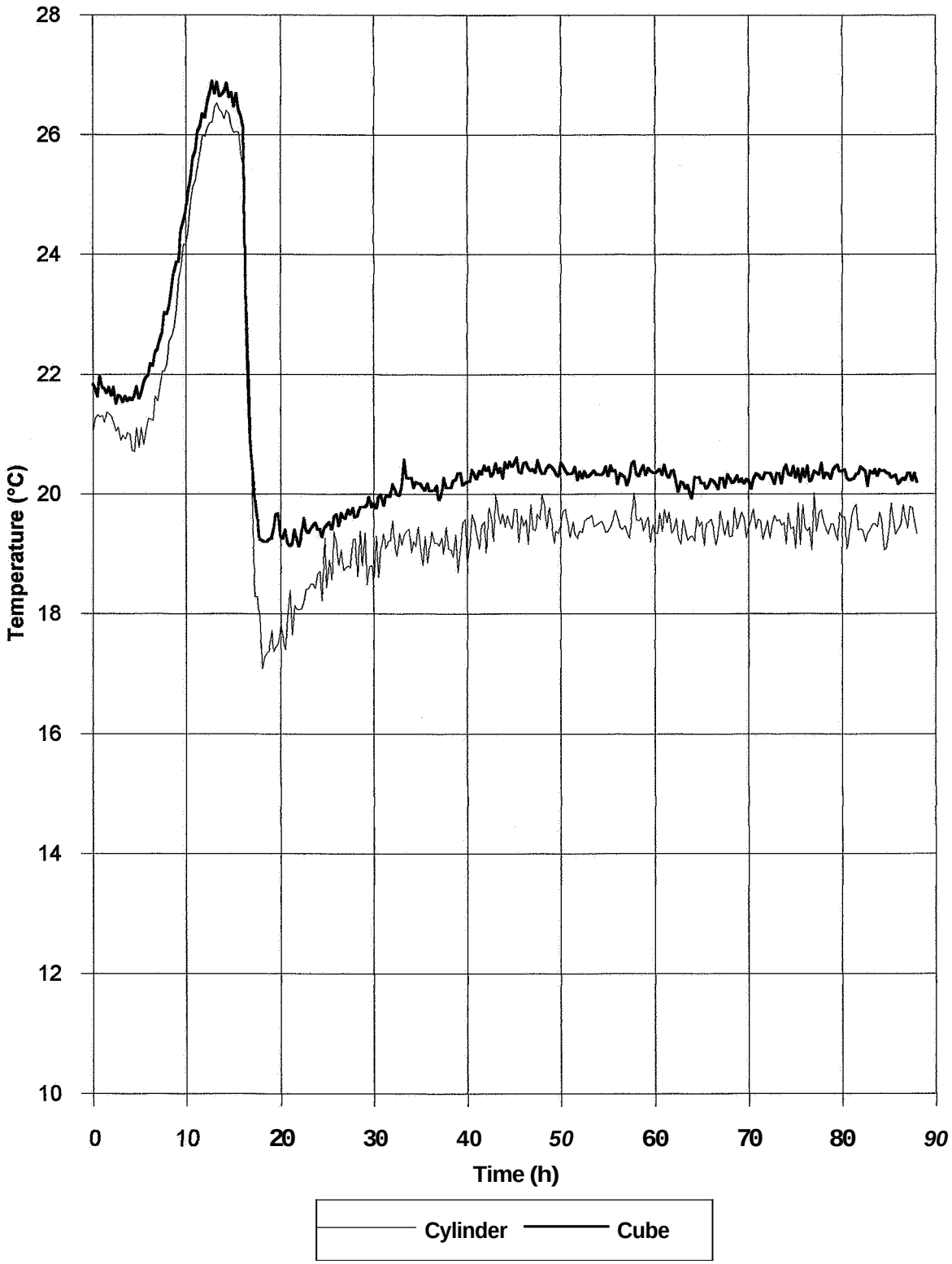

Appendix 4.3 - Temperature of mix 5 batch 2

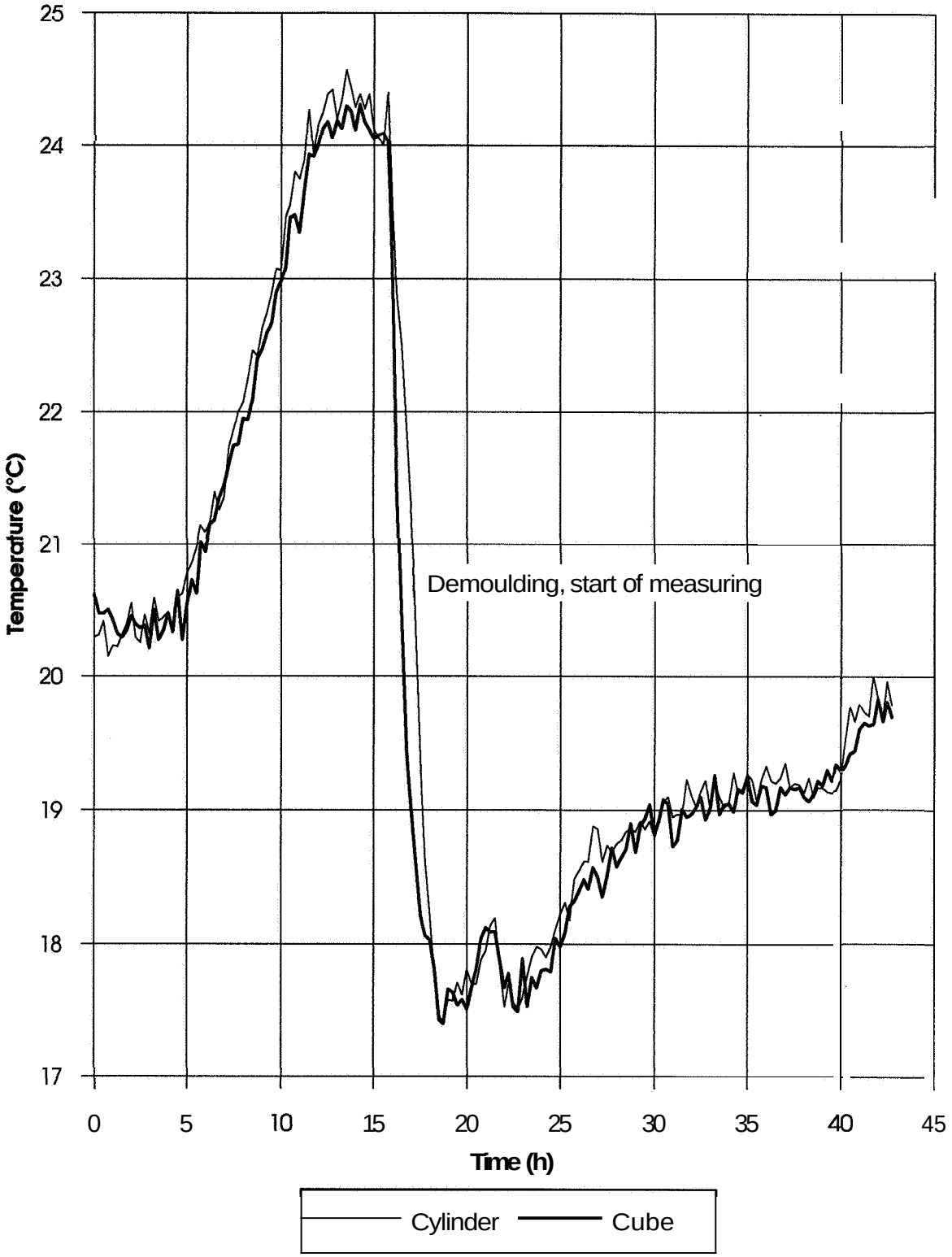

Appendix 4.4 - Temperature of mix 6 batch 2

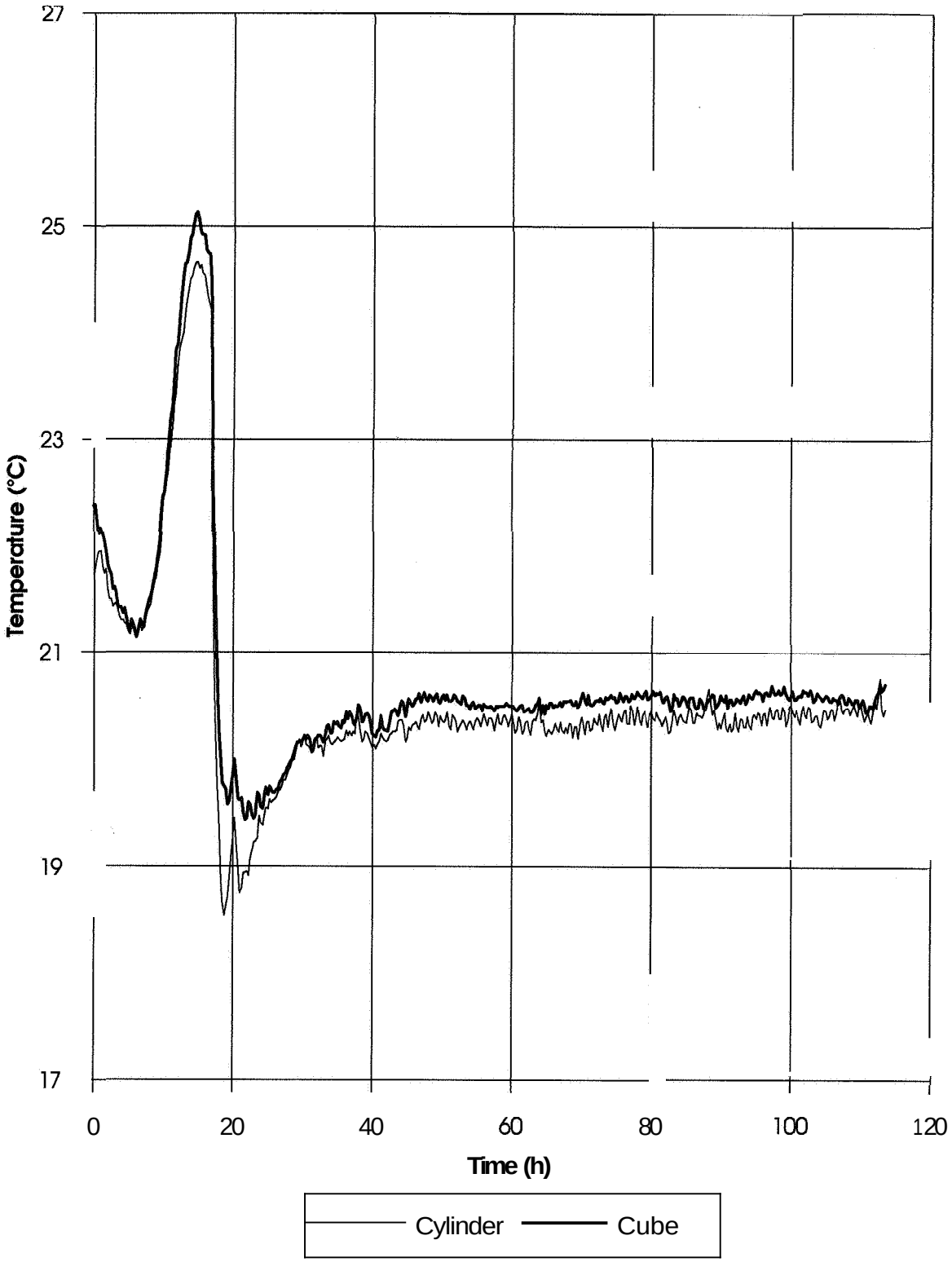

APPENDIX 5. PROPERTIES OF STUDIED CONCRETES

Symbols:

.....C**.....**	cylinder subjected to air curing (drying creep)
….I.…	interior of specimen
….S**.…**	surface of specimen
..B.....	Basic creep (cube subjected to sealed curing)
..D**.....**	Drying creep (cube subjected to air curing)
6..	concrete *mix* **6 (Table 5.1)**
...01	age at loading: 1 day; stresslcylinder strength ratio: **0.84**
...02	age at loading: 2 days; stresslcylinder strength ratio: **0.84**
...03	age at loading: **2** days; stresslcylinder strength ratio: **0.42**
...28	age at loading: **28** days; stresslcylinder strength ratio: **0.42**

Appendix 5.1 - Compressive strength of mix 1

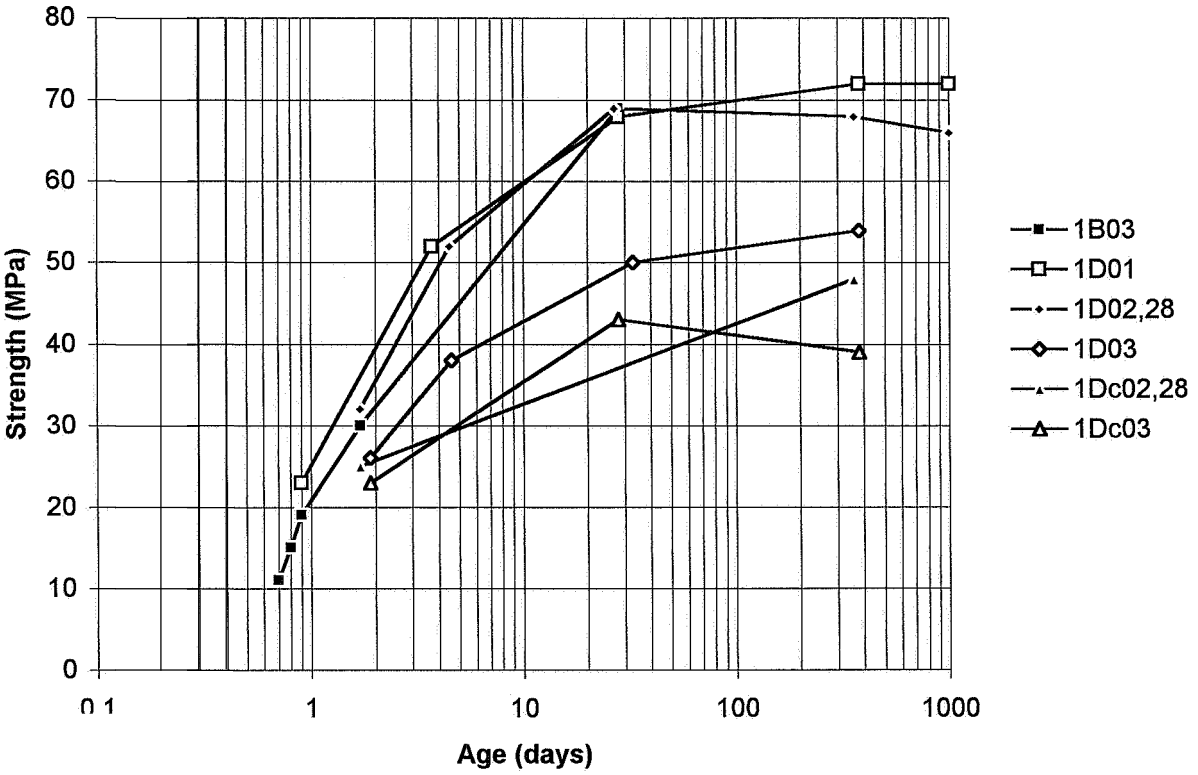

Appendix 5.2 - Compressive strength of mix 2

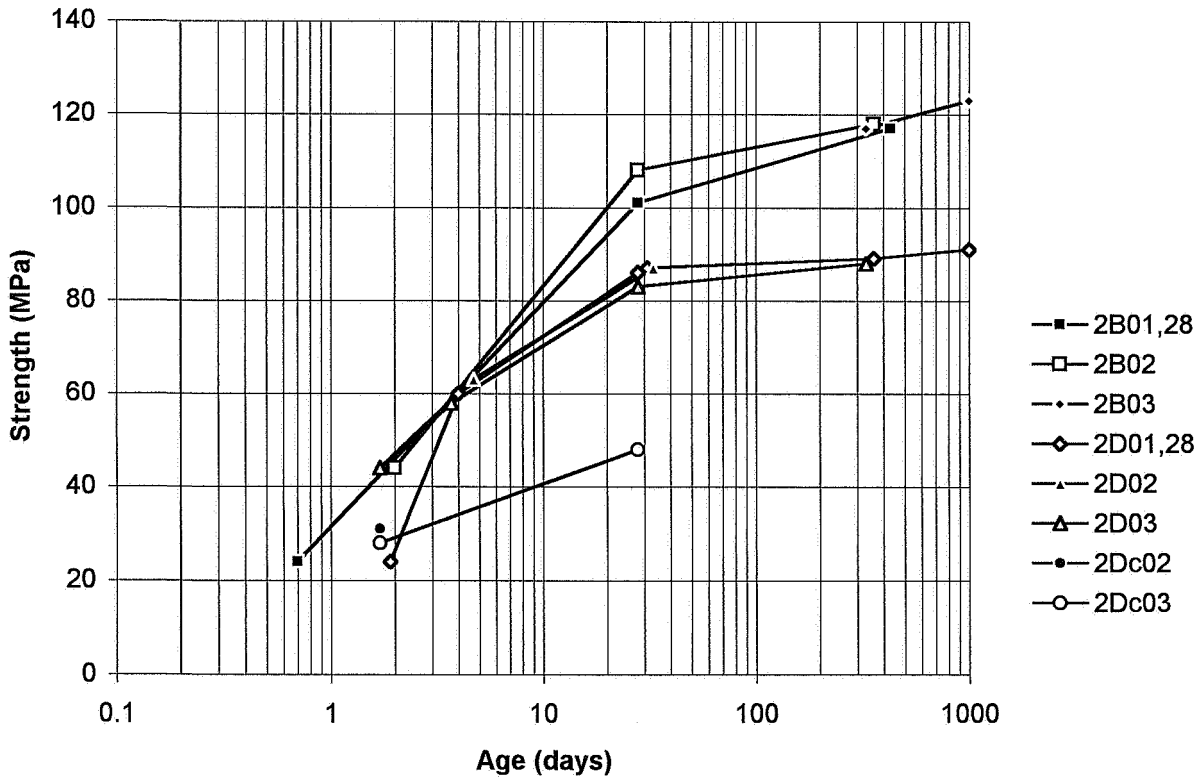

Appendix 5.3 - Compressive strength of mix 3

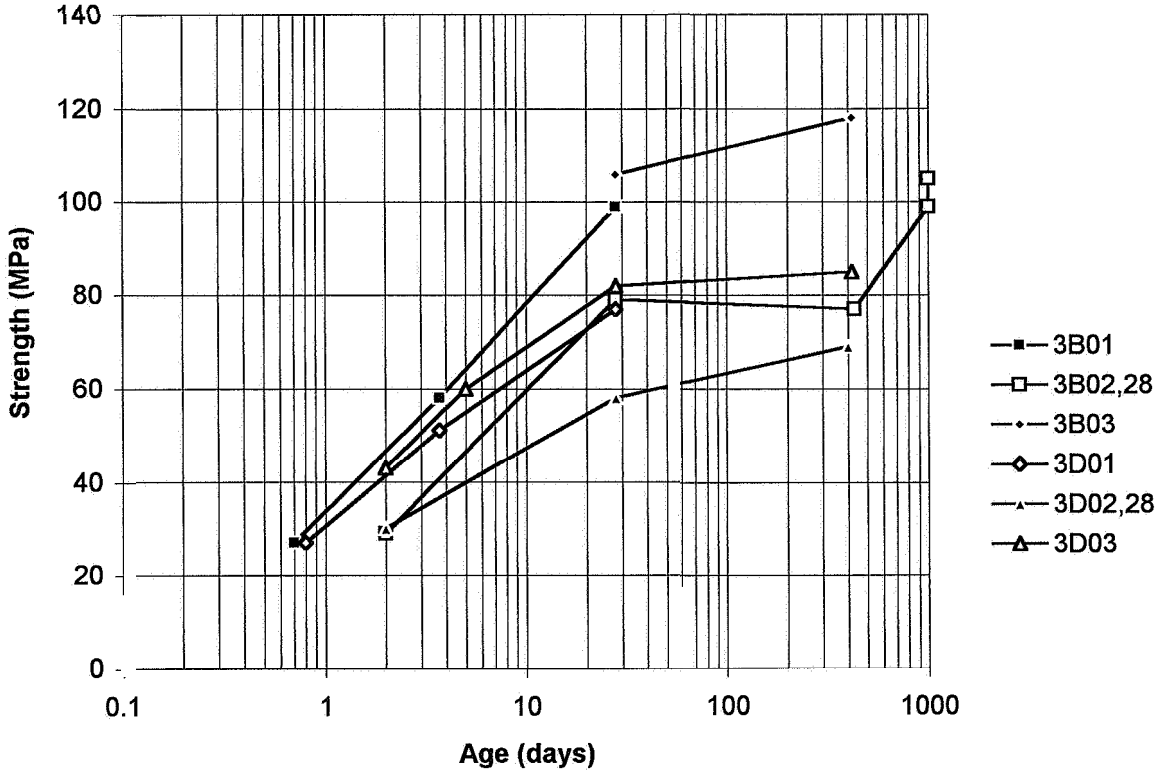

Appendix 5.4 - Compressive strength of mix 4

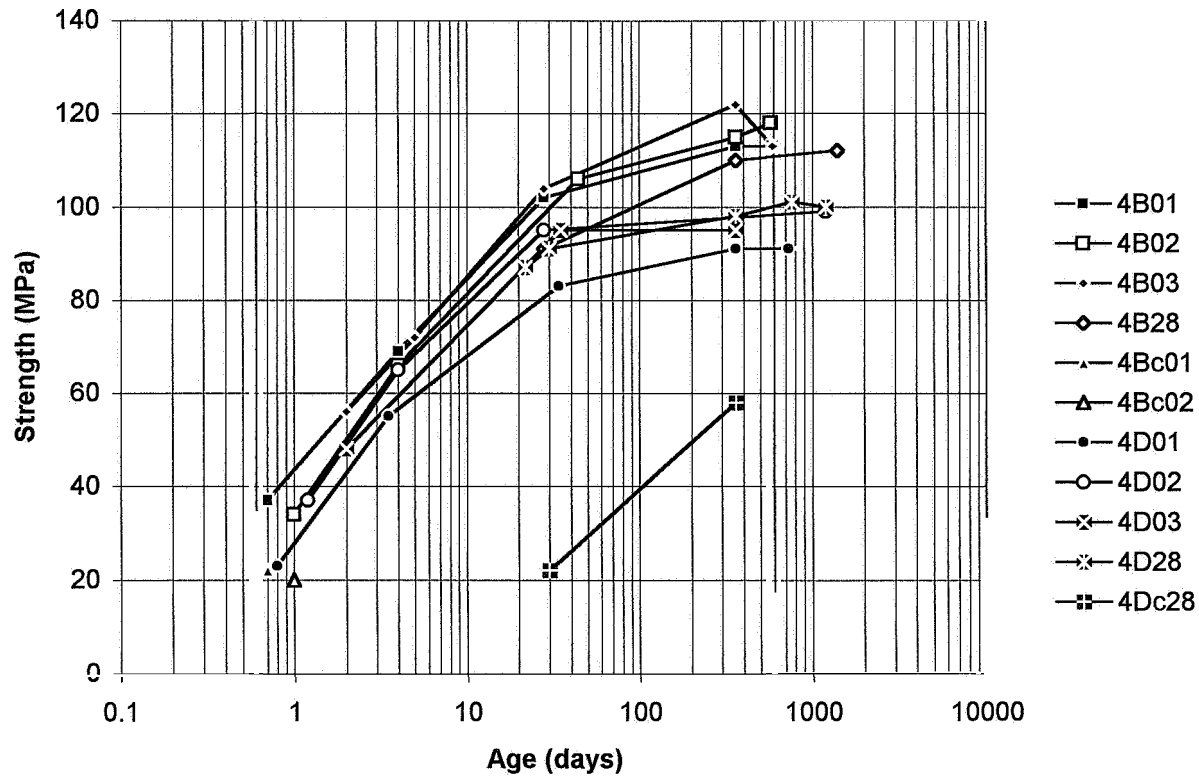

Appendix 5.5 - Compressive strength of mix 5

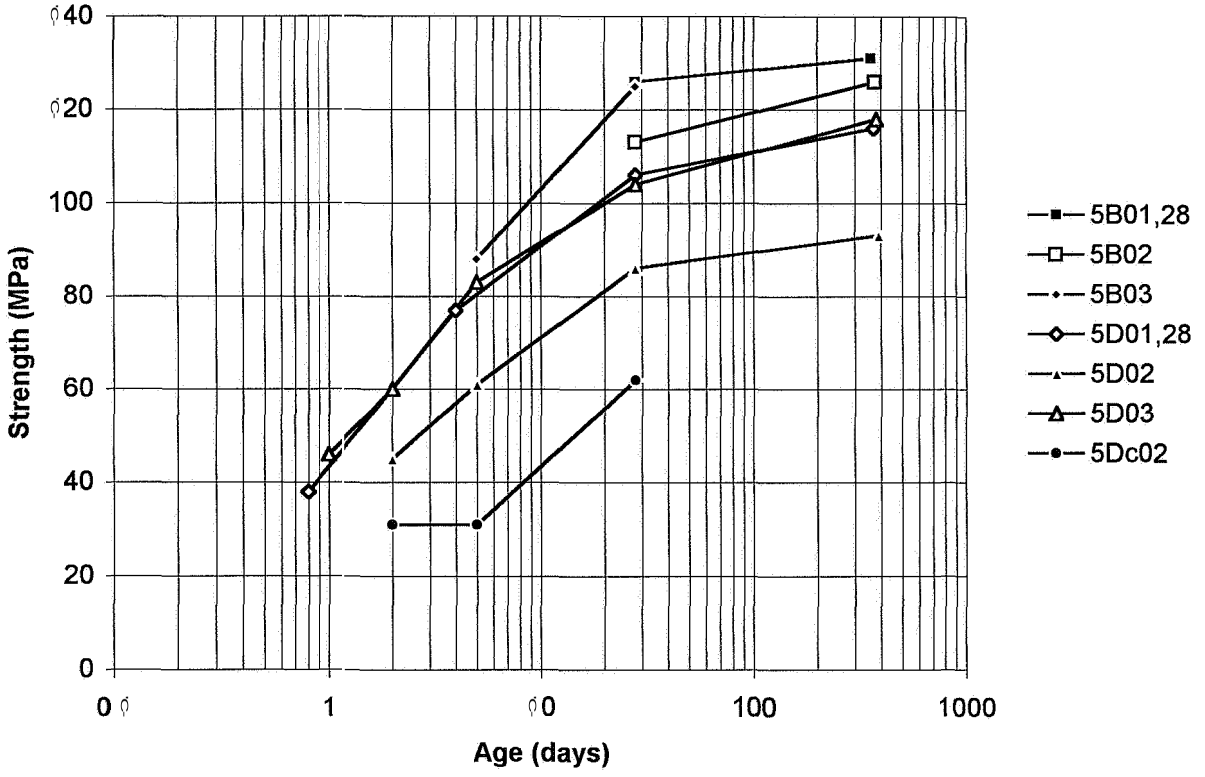

Appendix 5.6 - Compressive strength of mix 6

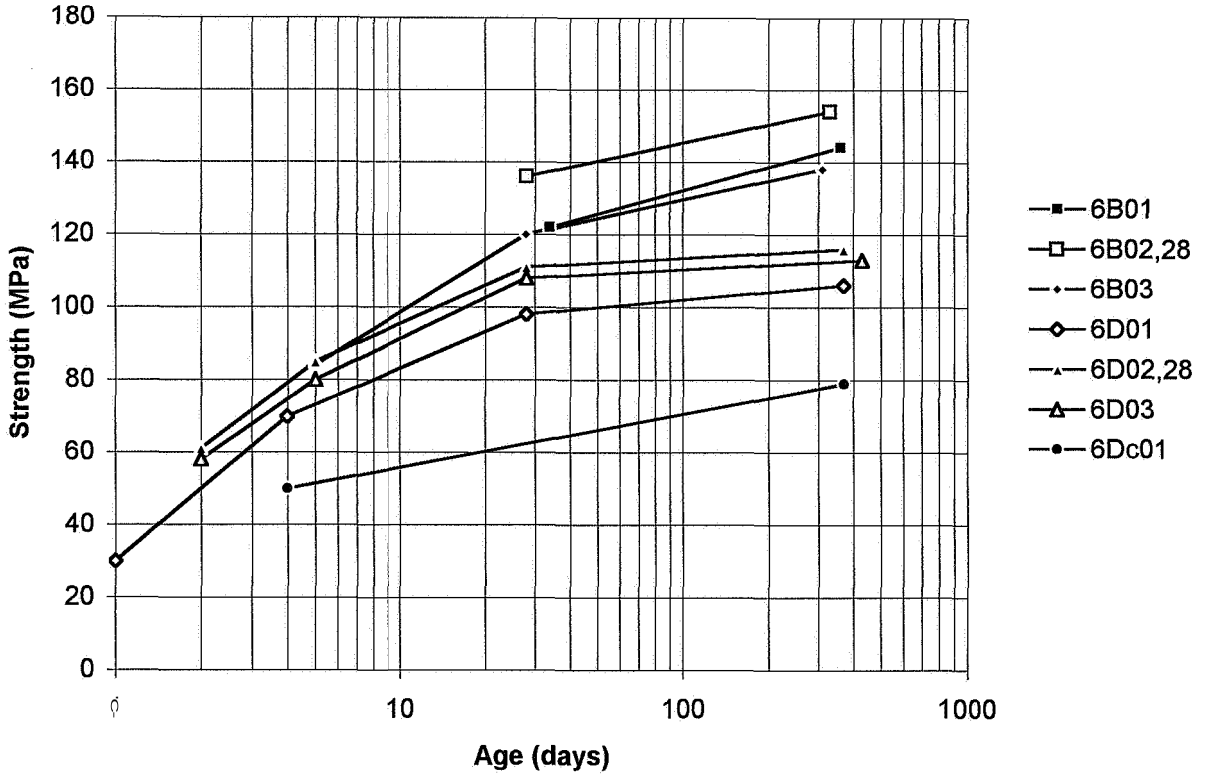

Appendix 5.7 - Compressive strength of mix 7

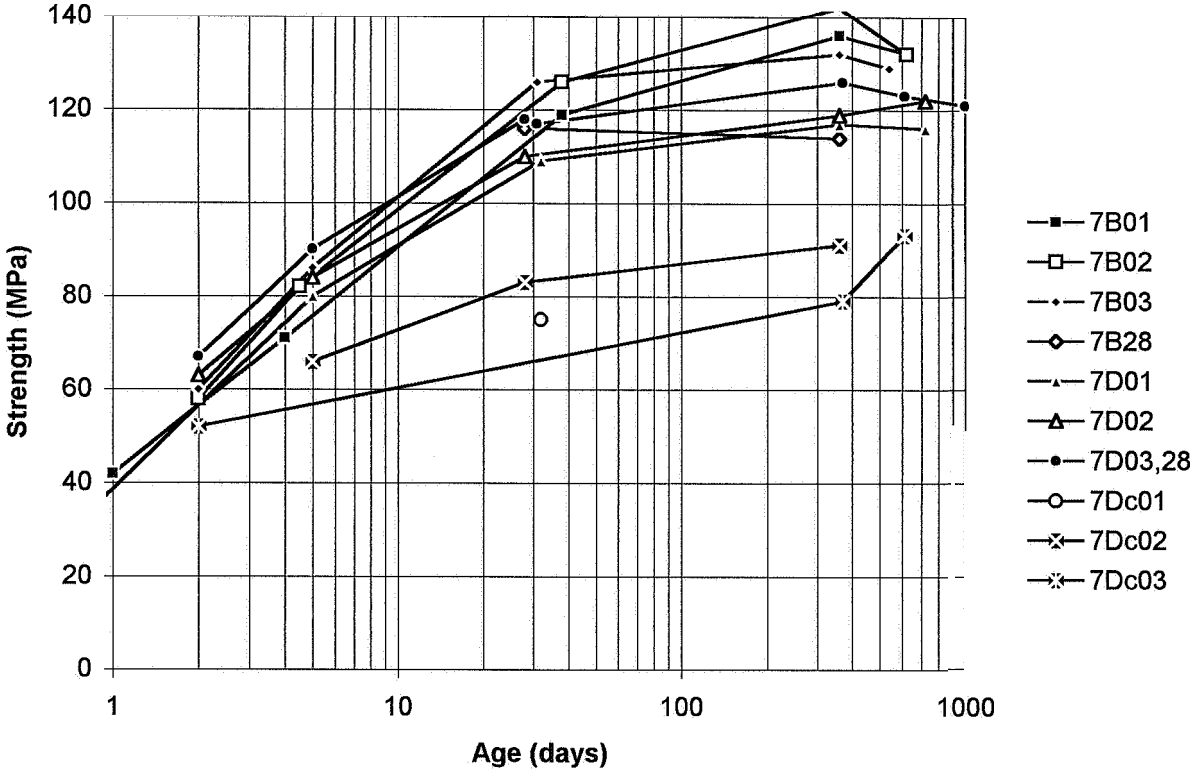

Appendix 5.8 - Compressive strength of mix 8

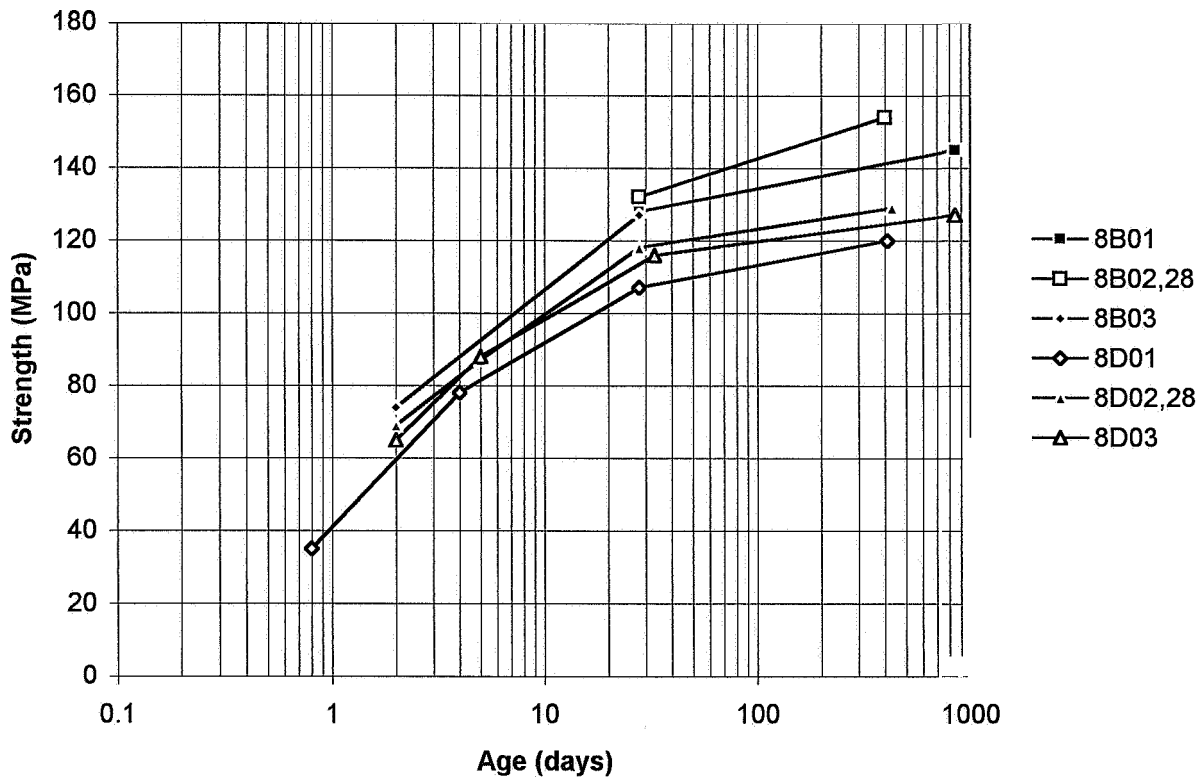

Appendix 5.9 - Compressive strength of mix 1 at short-term creep subjected to sealed curing

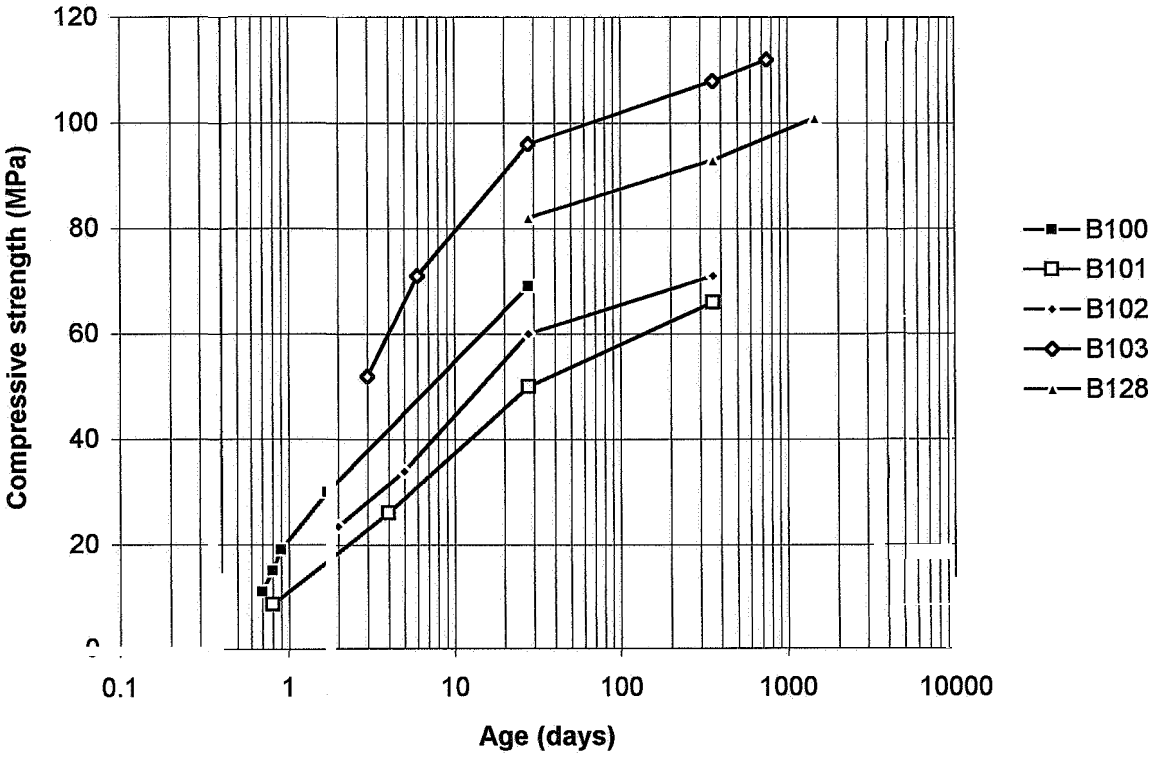

Appendix 5.10 - Compressive strength of mix 2 at short-term creep subjected to sealed curing

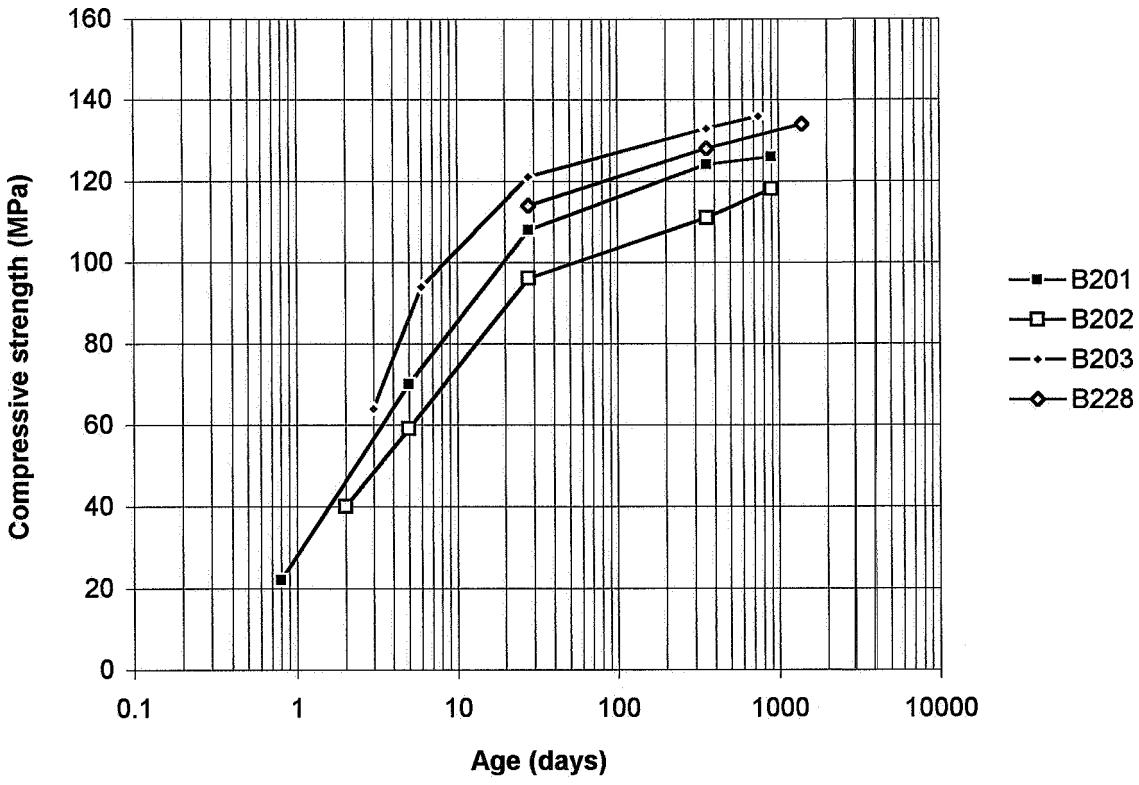

Appendix 5.11 - Compressive strength of mix 3 at short-term creep subiected to sealed curing:

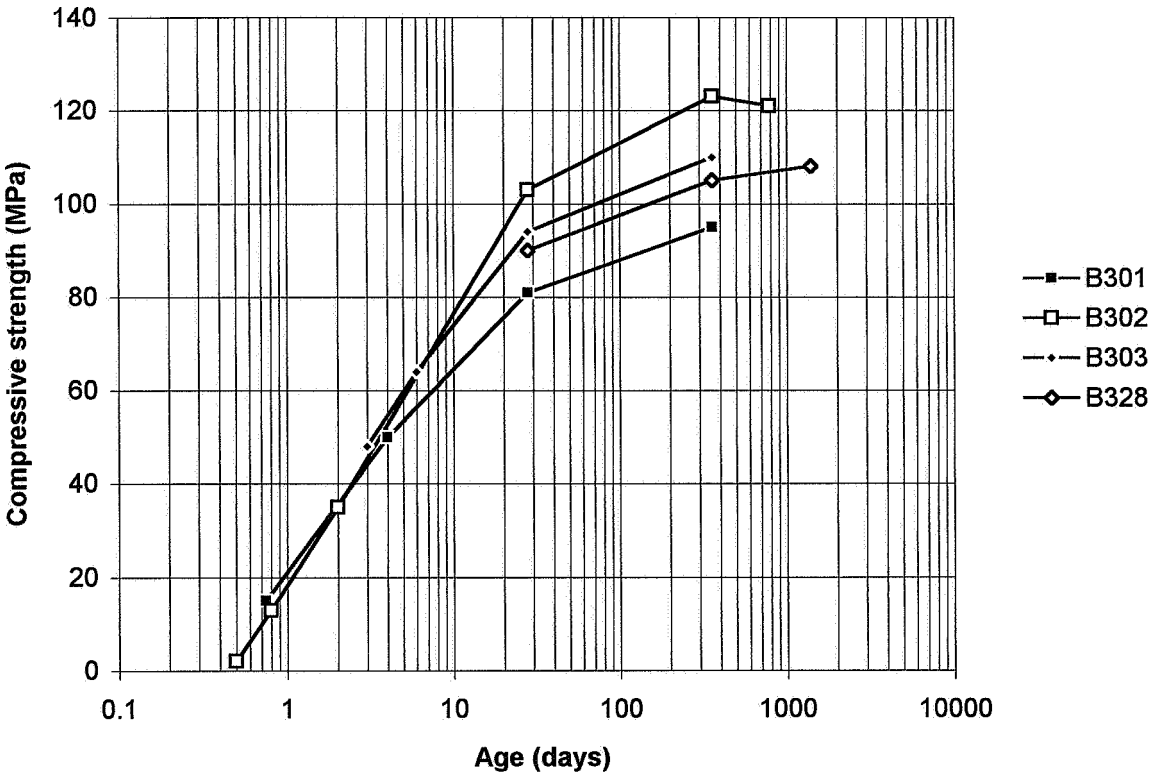

Appendix 5.12 - Compressive strength of mix 4 at short-term creep subiected to sealed curing:

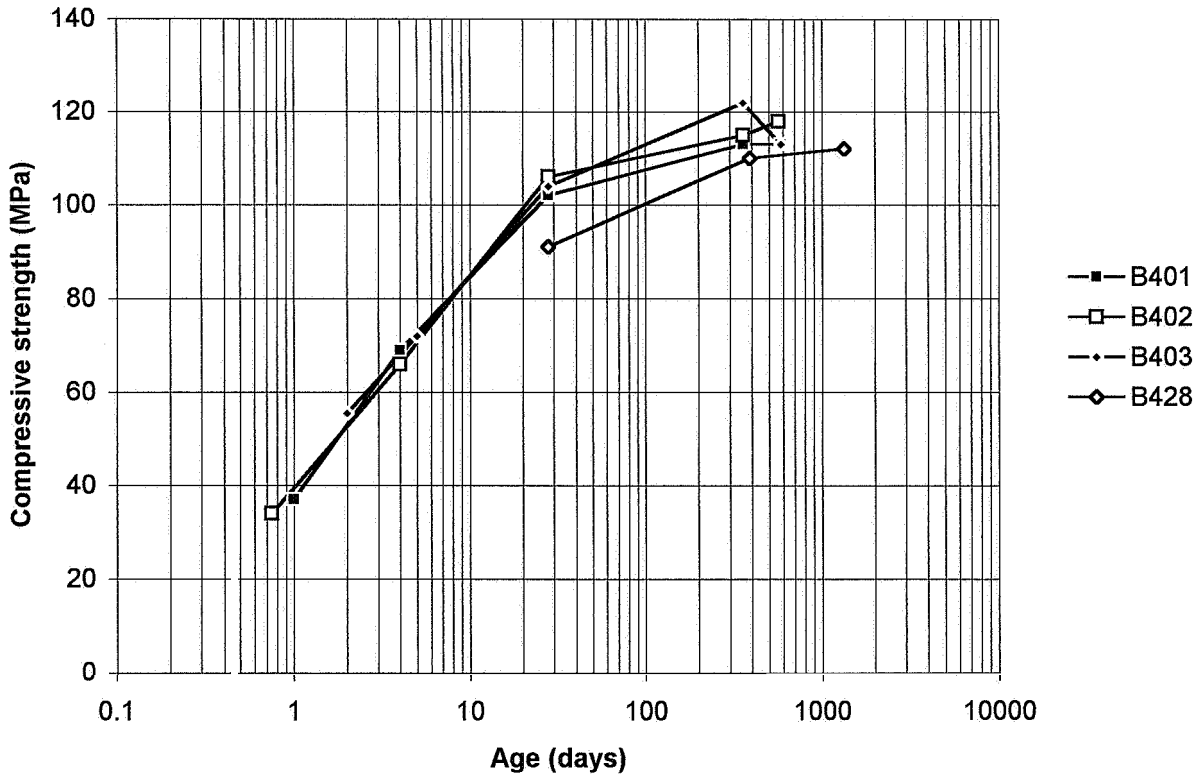

Appendix 5.13 - Compressive strength of mix 5 at short-term creep subjected to sealed curing

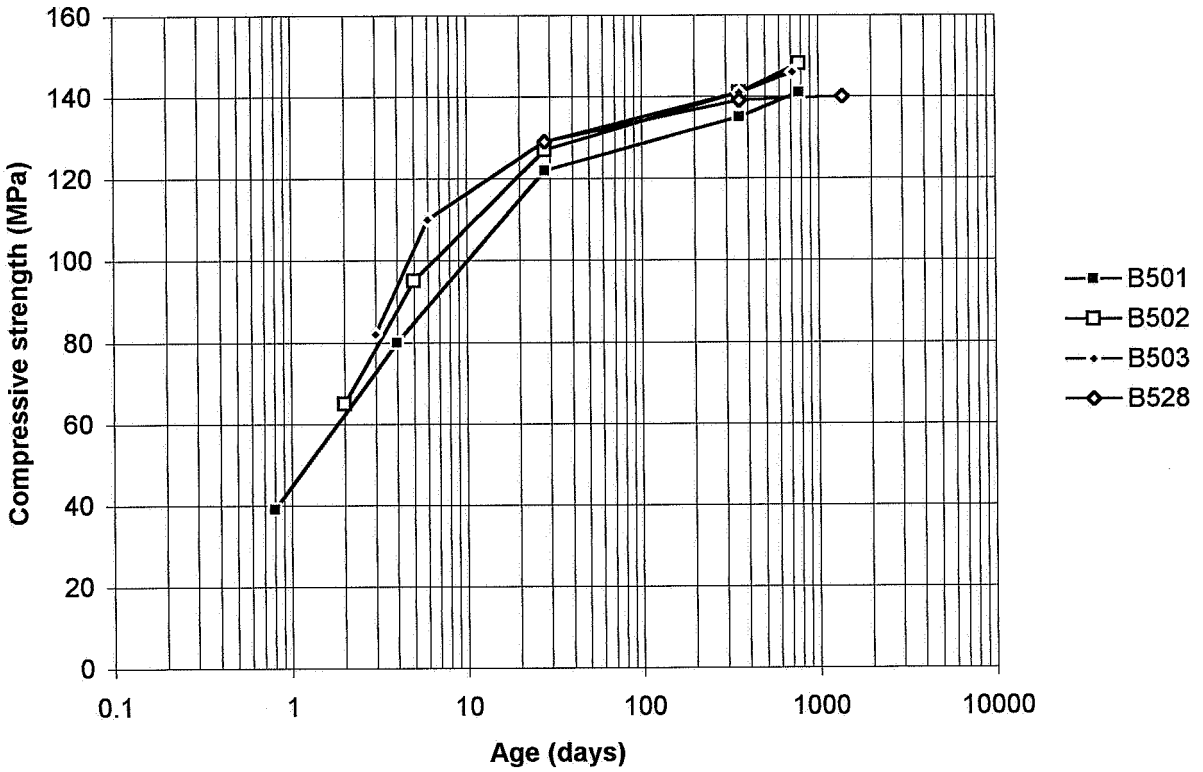

Appendix 5.14 - Compressive strength of mix 6 at short-term creep subjected to sealed curing

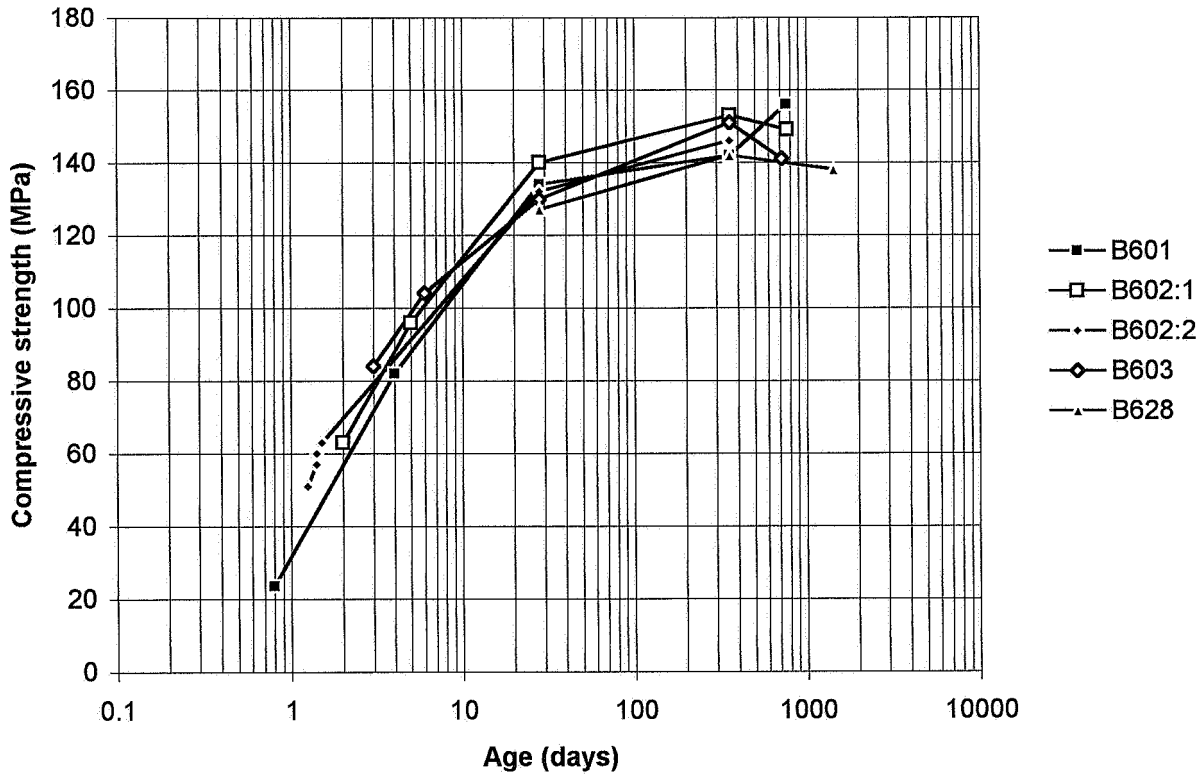

Appendix 5.15 - Compressive strength of mix 7 at short-term creep subiected to sealed curing

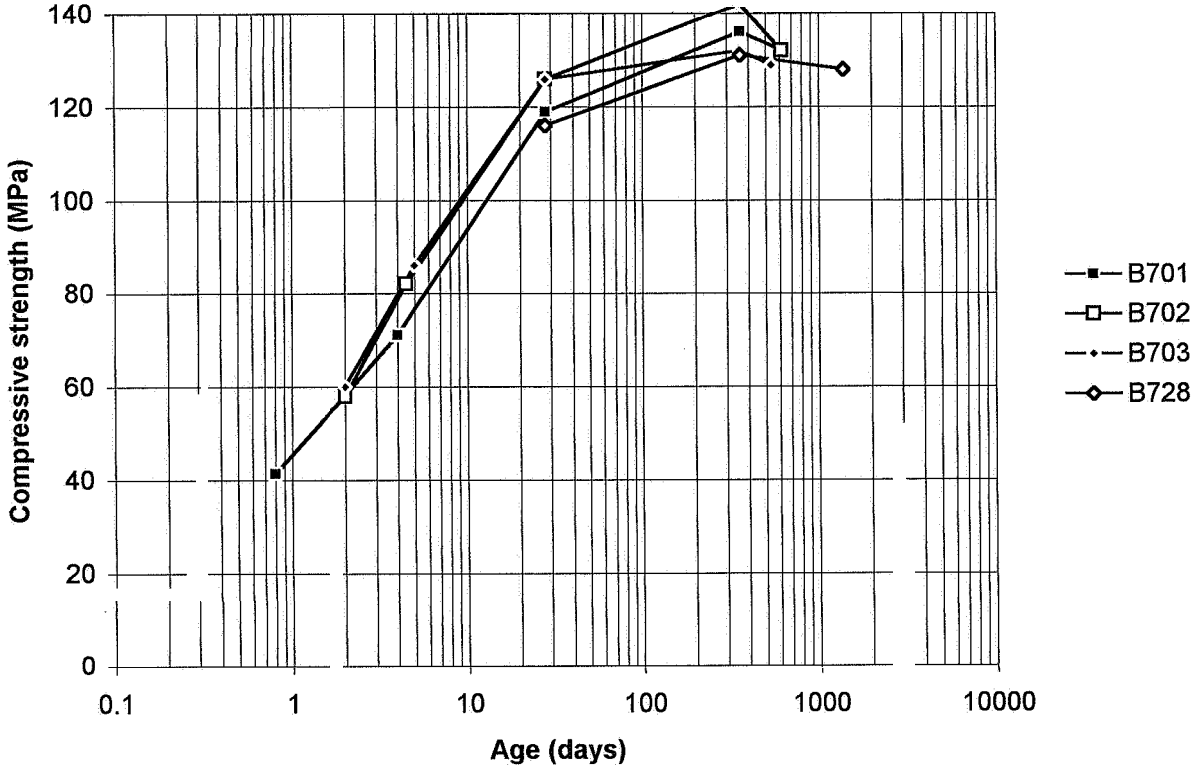

Appendix 5.16 - Compressive strength of mix 8 at short-term creep subiected to sealed curing

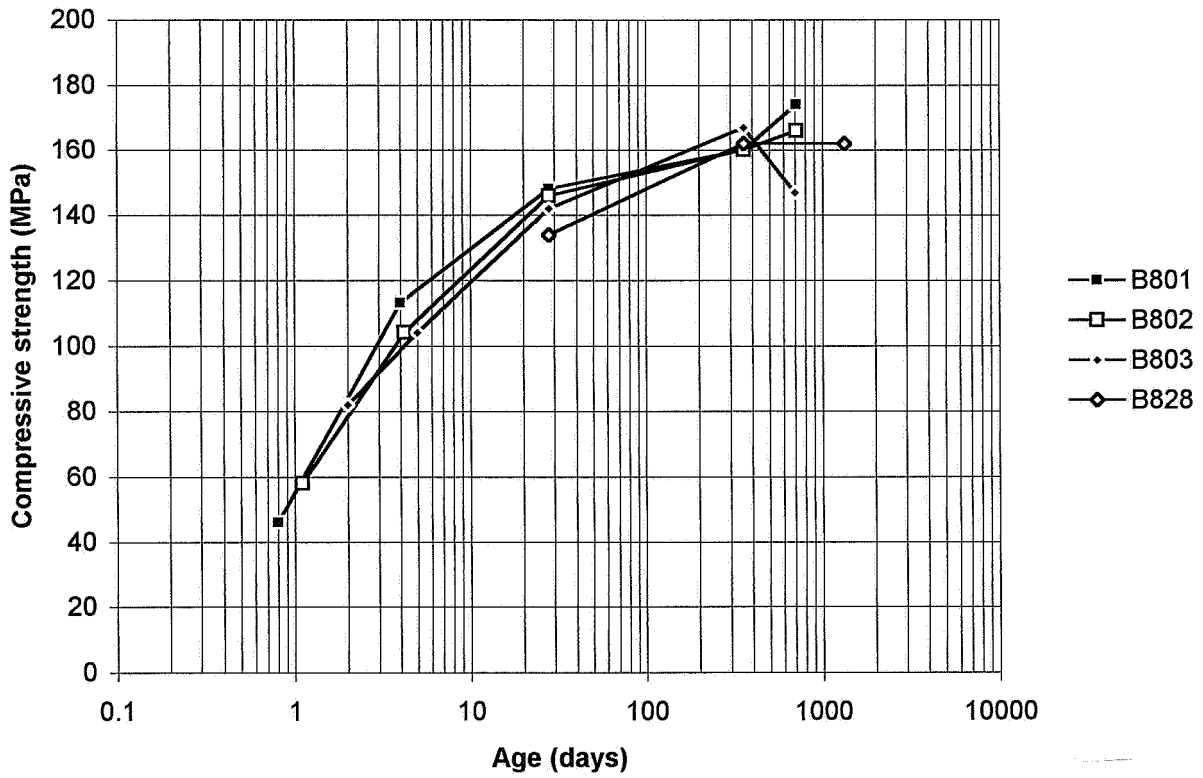

Appendix 5.17 - Hydration of mix 1

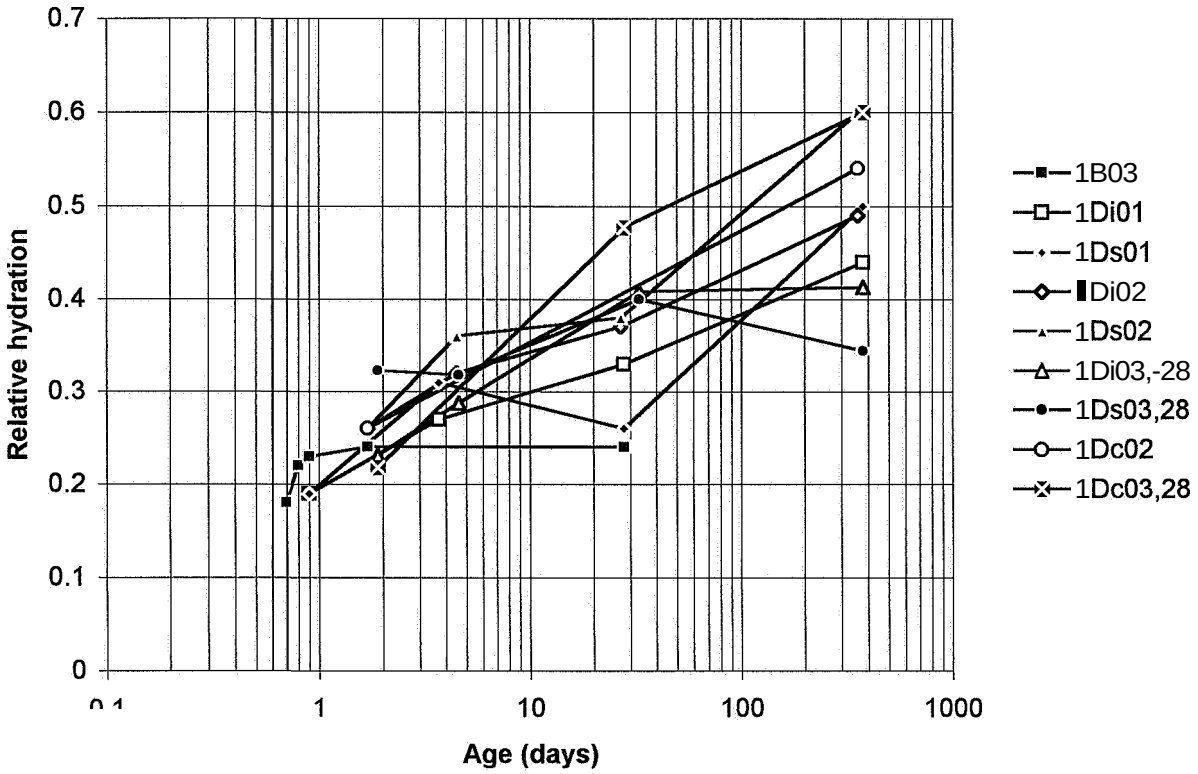

Appendix 5.18 - Hydration of mix 2

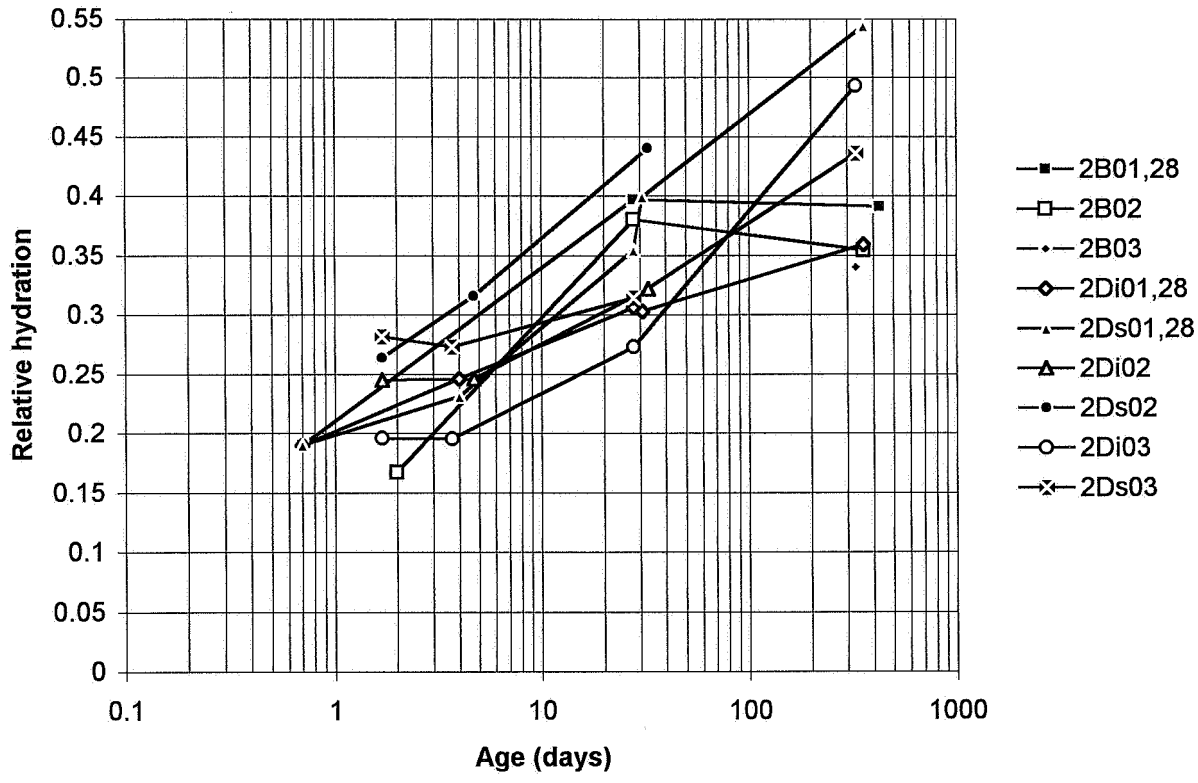

Appendix 5.19 - Hydration of mix 3

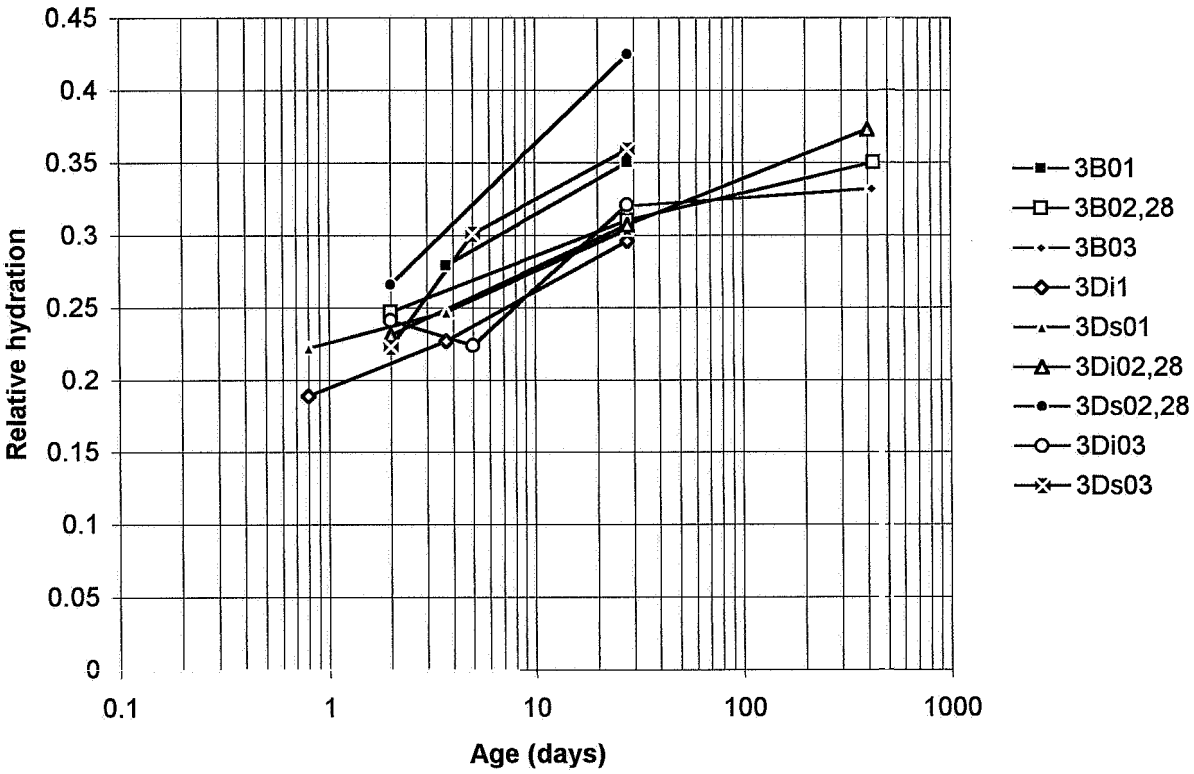

Appendix 5.20 - Hydration of mix 4

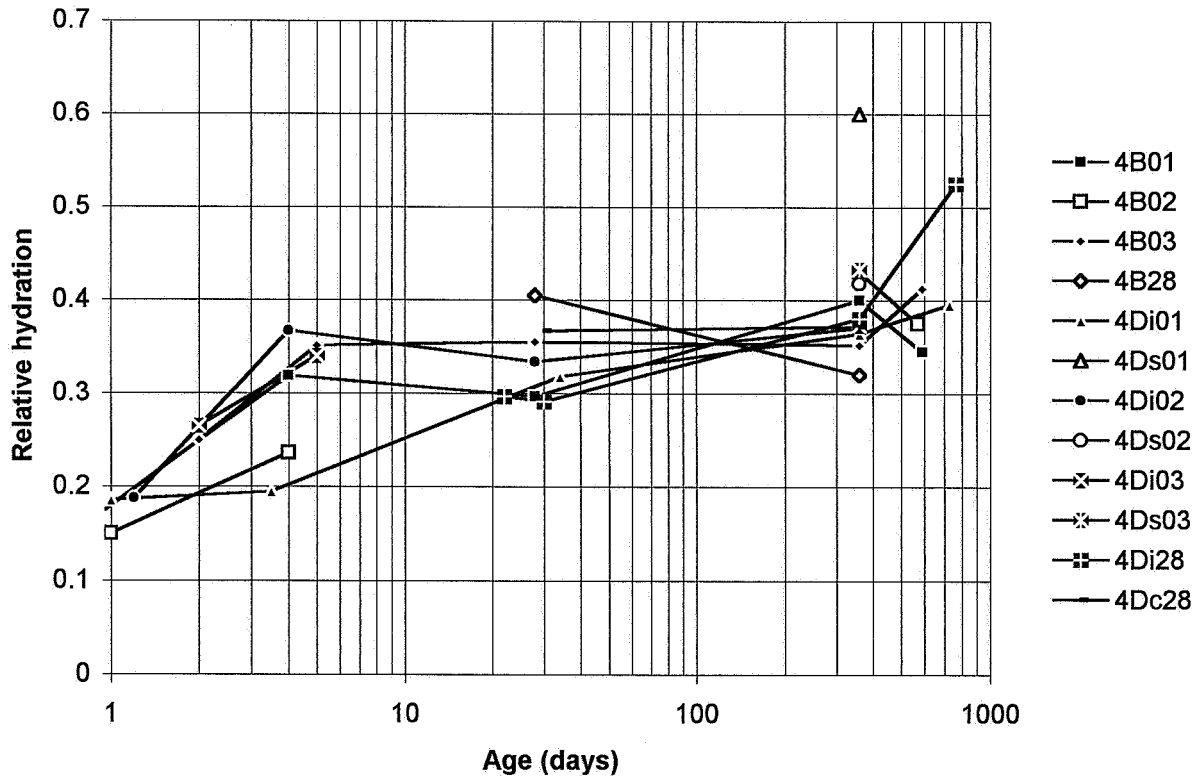

Appendix 5.21 - Hydration of mix 5

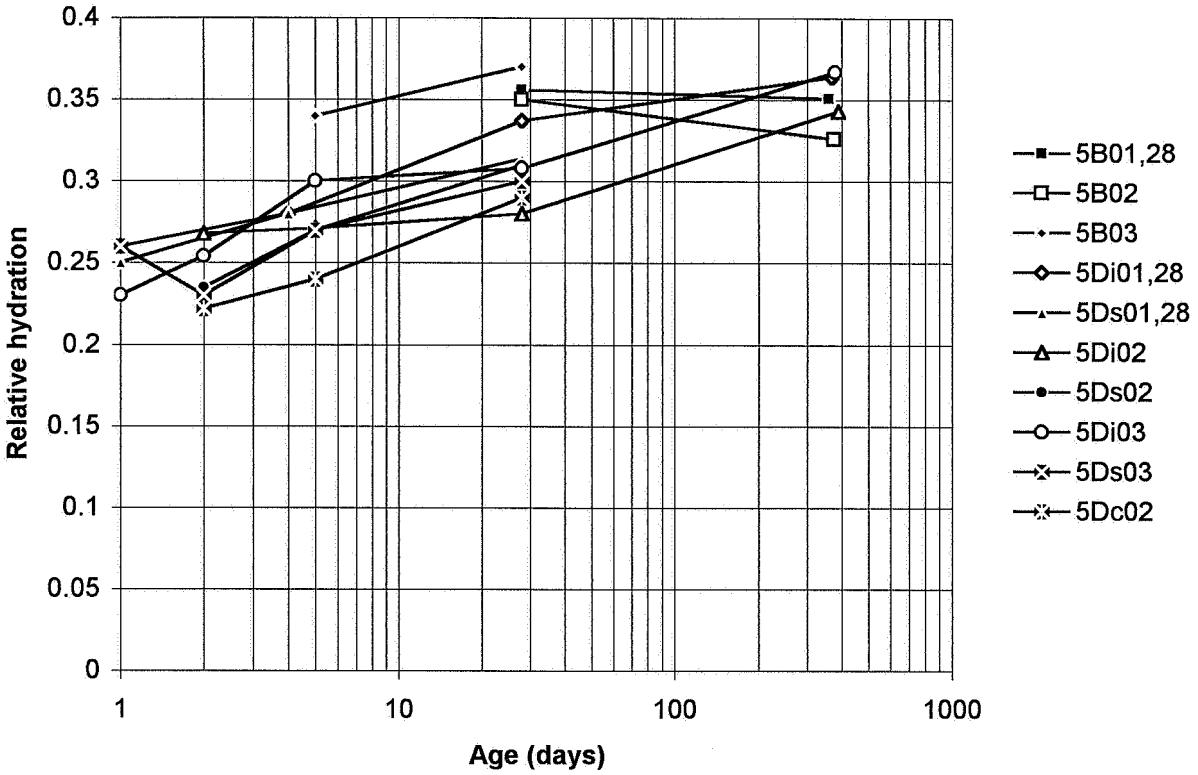

Appendix 5.22 - Hydration of mix 6

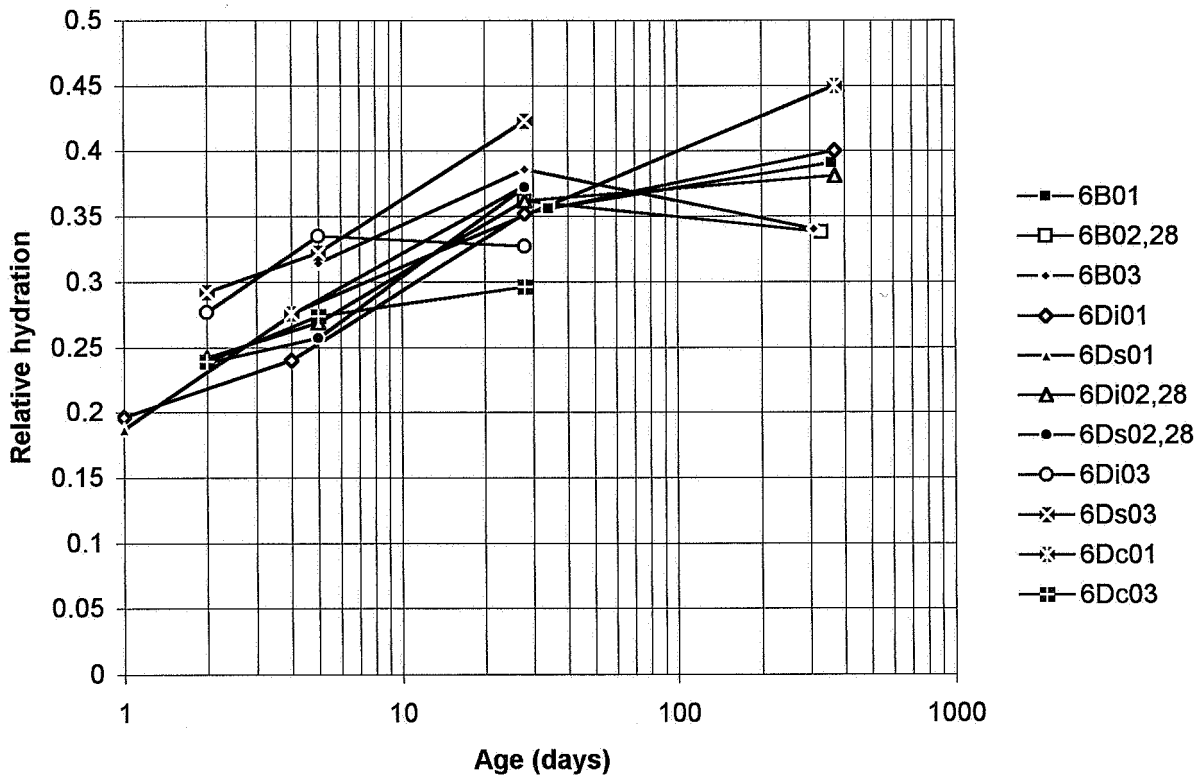

Appendix 5.23 - Hydration of mix 7

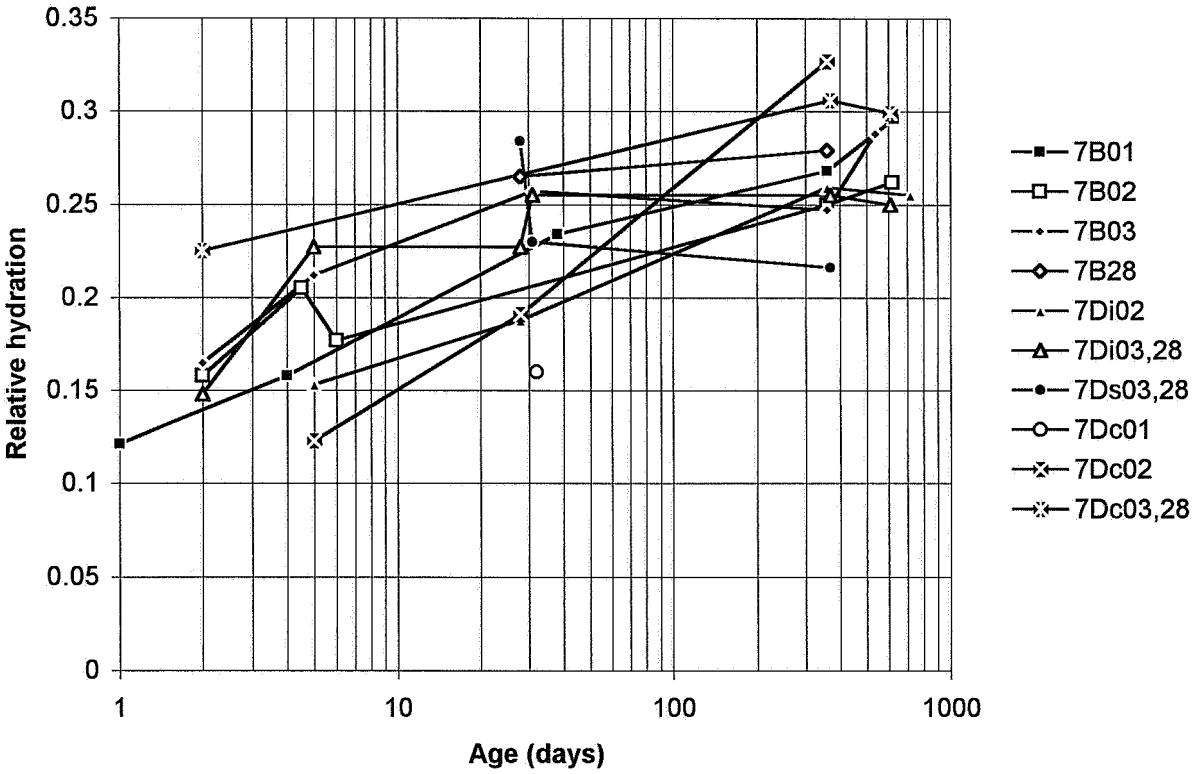

Appendix 5.24 - Hydration of mix 8

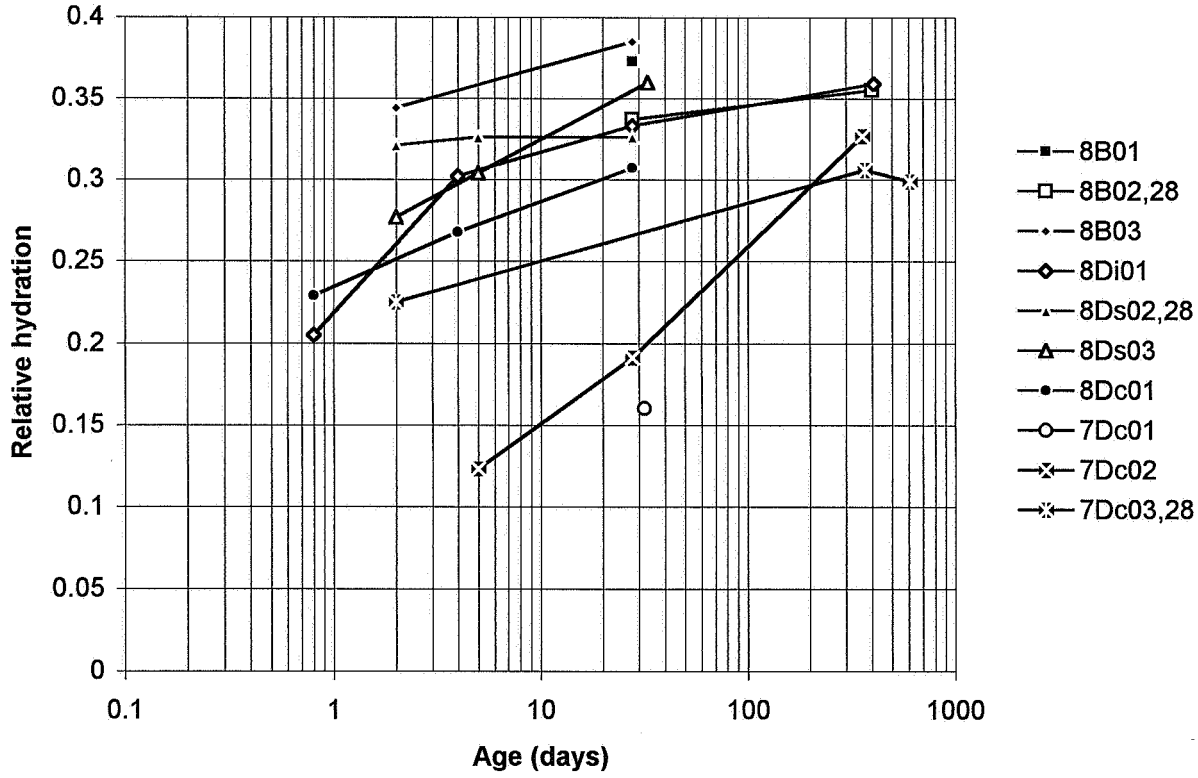

Appendix 5.25 - Hydration of mix 1 at short-term creep subjected to sealed curing:

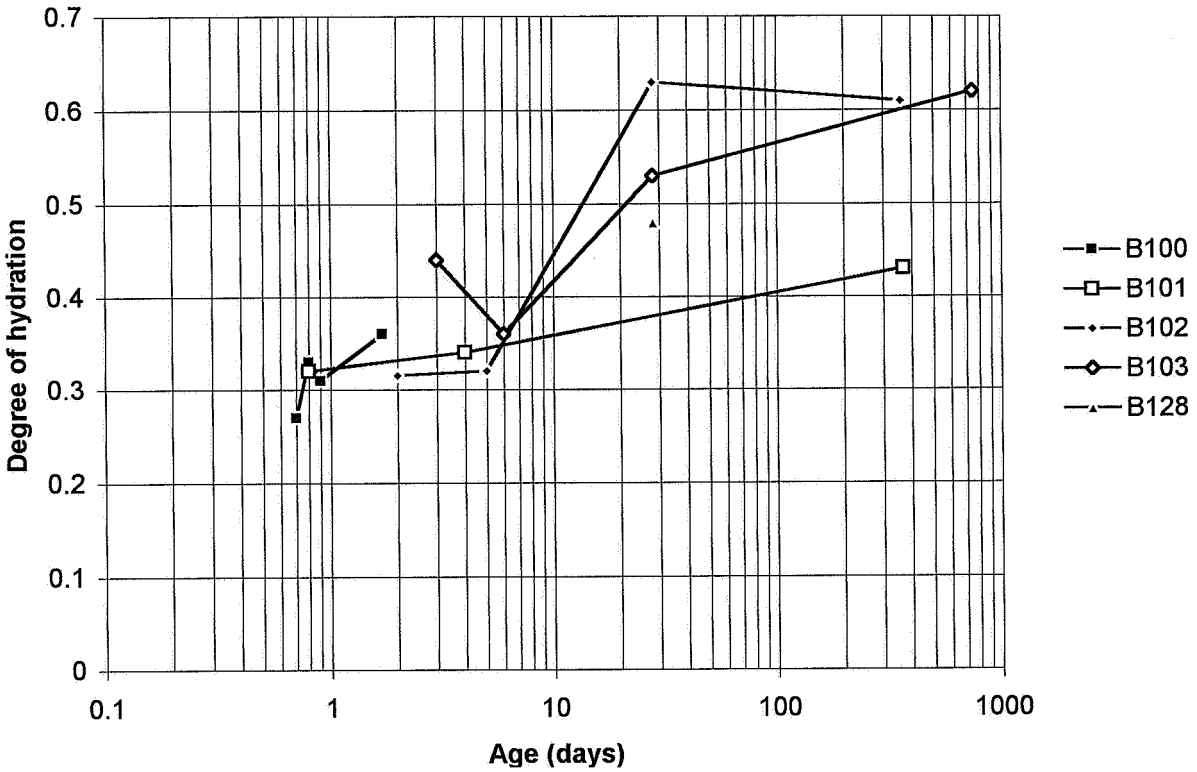

Appendix 5.26 - Hydration of mix 2 at short-term creep subjected to sealed curing

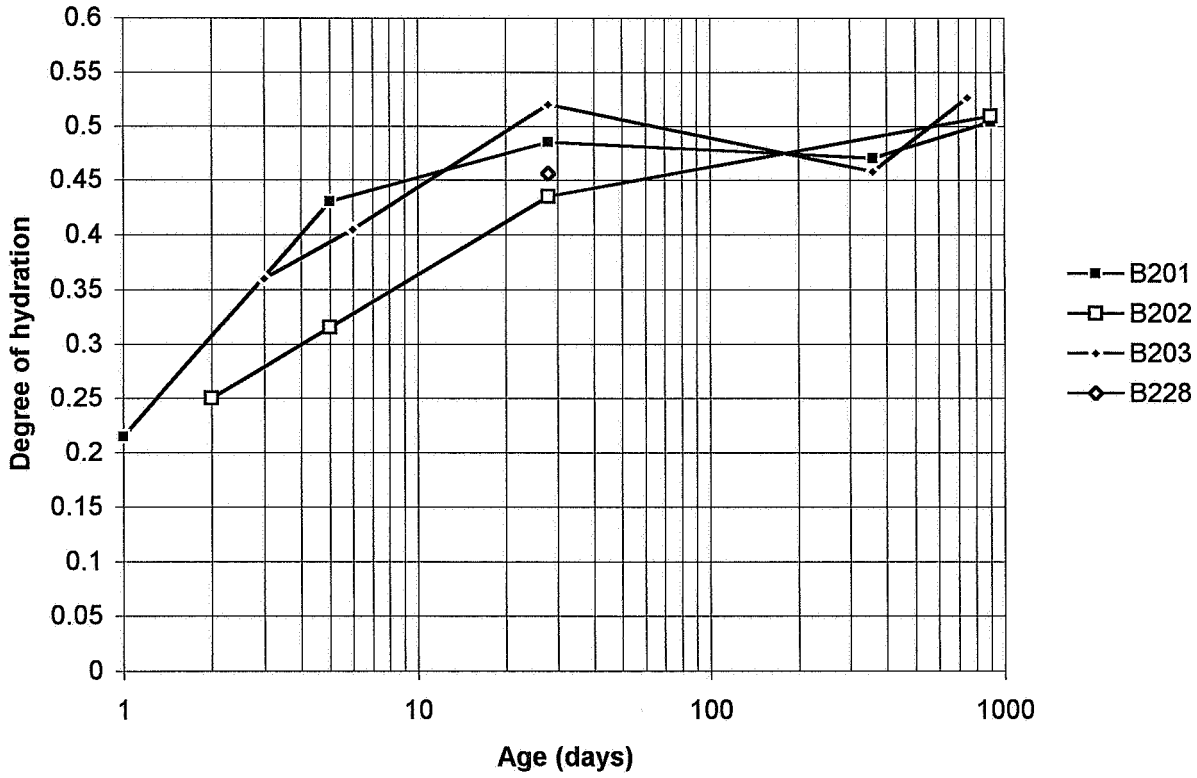

ppen 5.27 - Hydration f mix 3 at short-term cr subjected to s curing

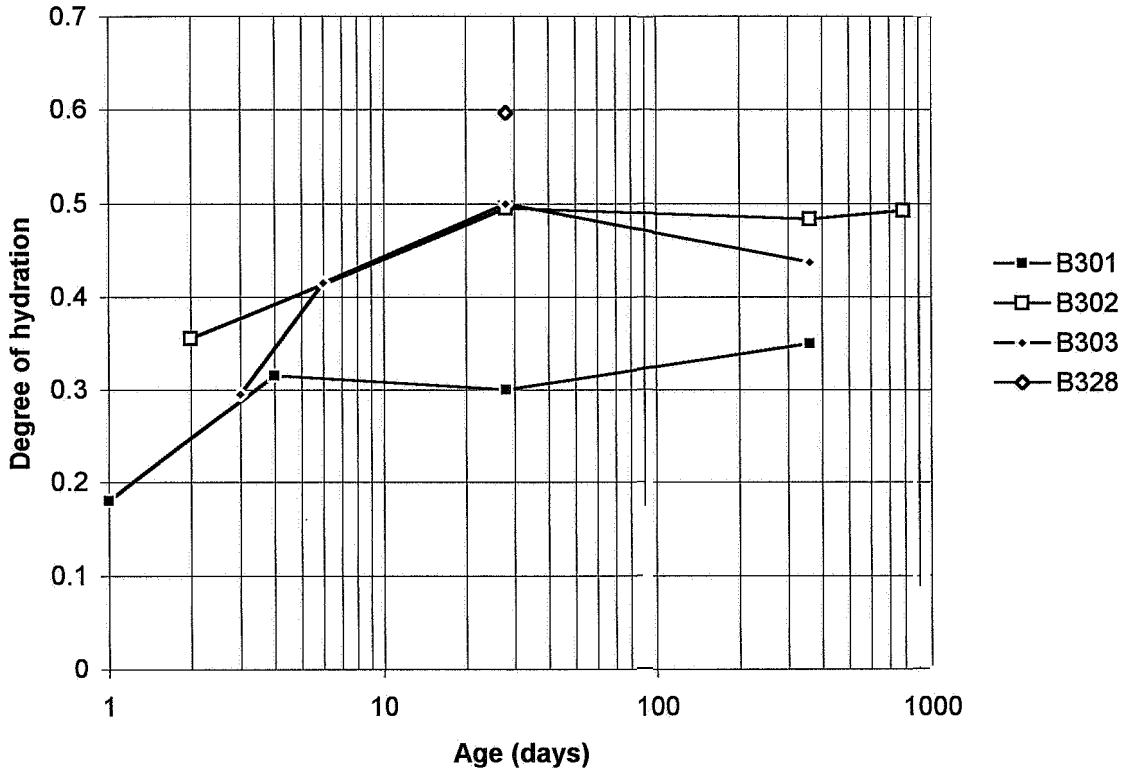

Appendix 5.28 - Hydration of mix 4 at short-term creep subjected to sealed curing

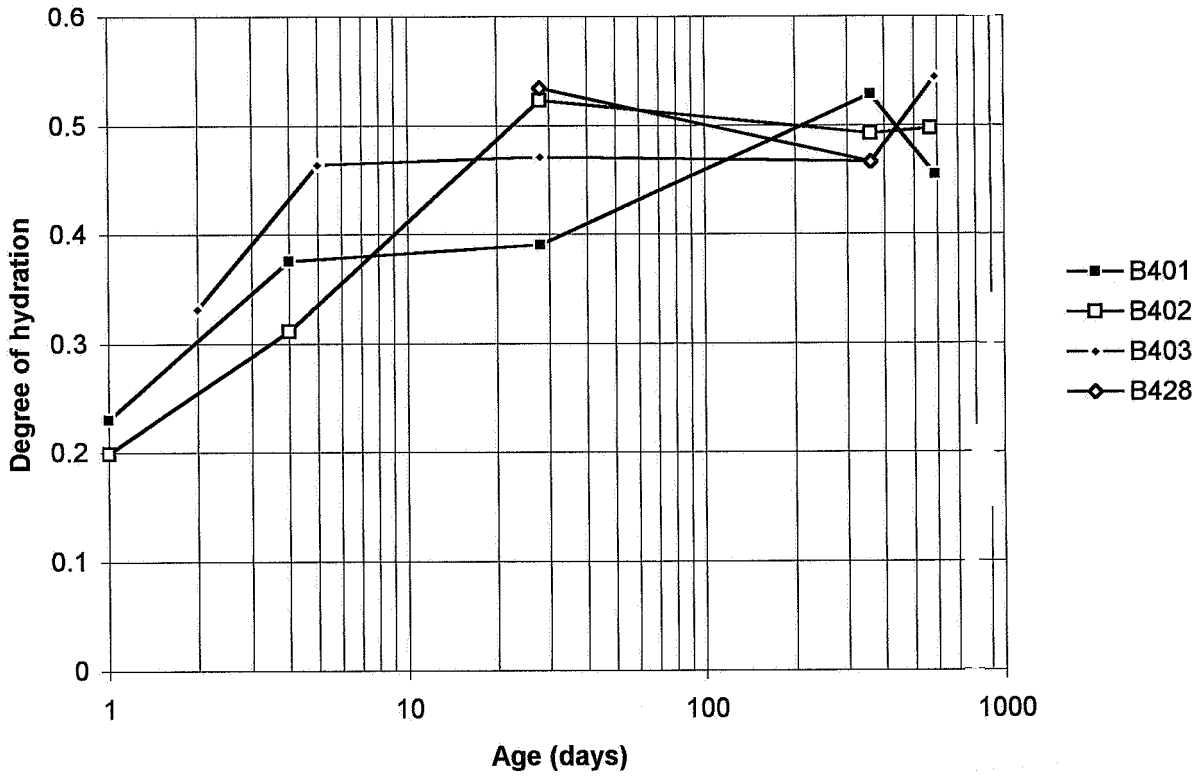

Appendix 5.29 - Hydration of mix 5 at short-term creep subjected to sealed curing

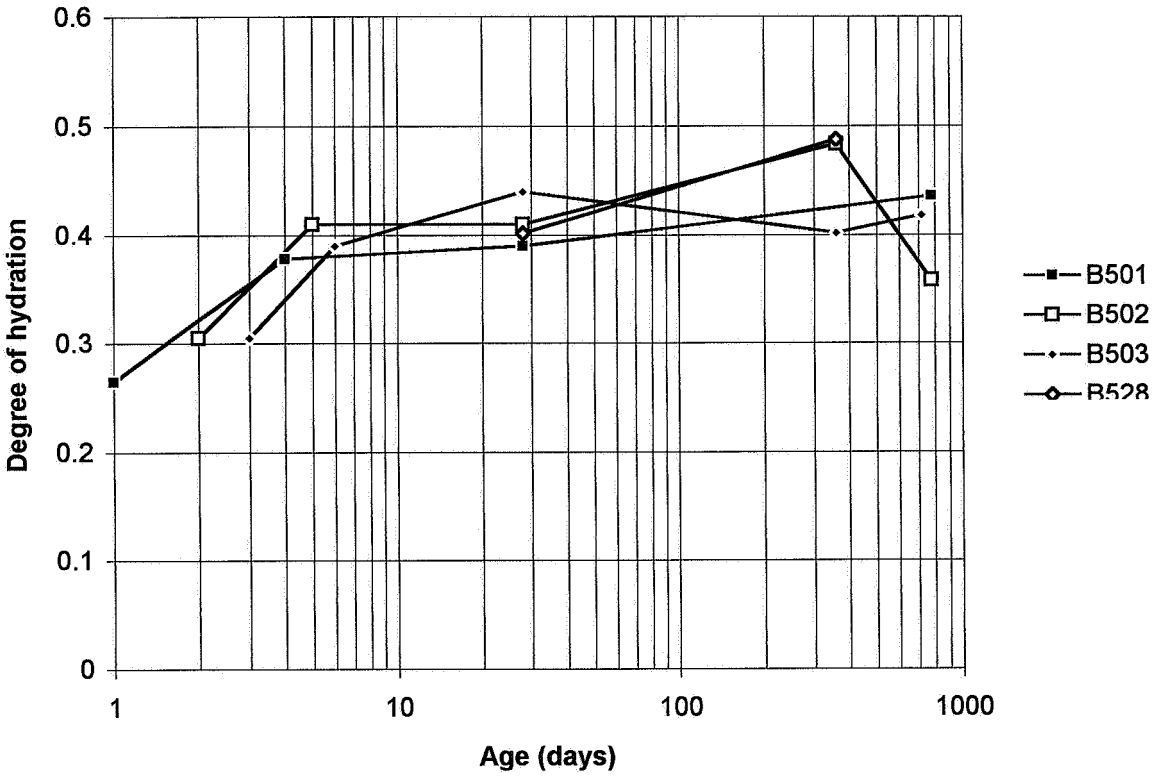

Appendix 5.30 - Hydration of mix 6 at short-term creep subjected to sealed curing

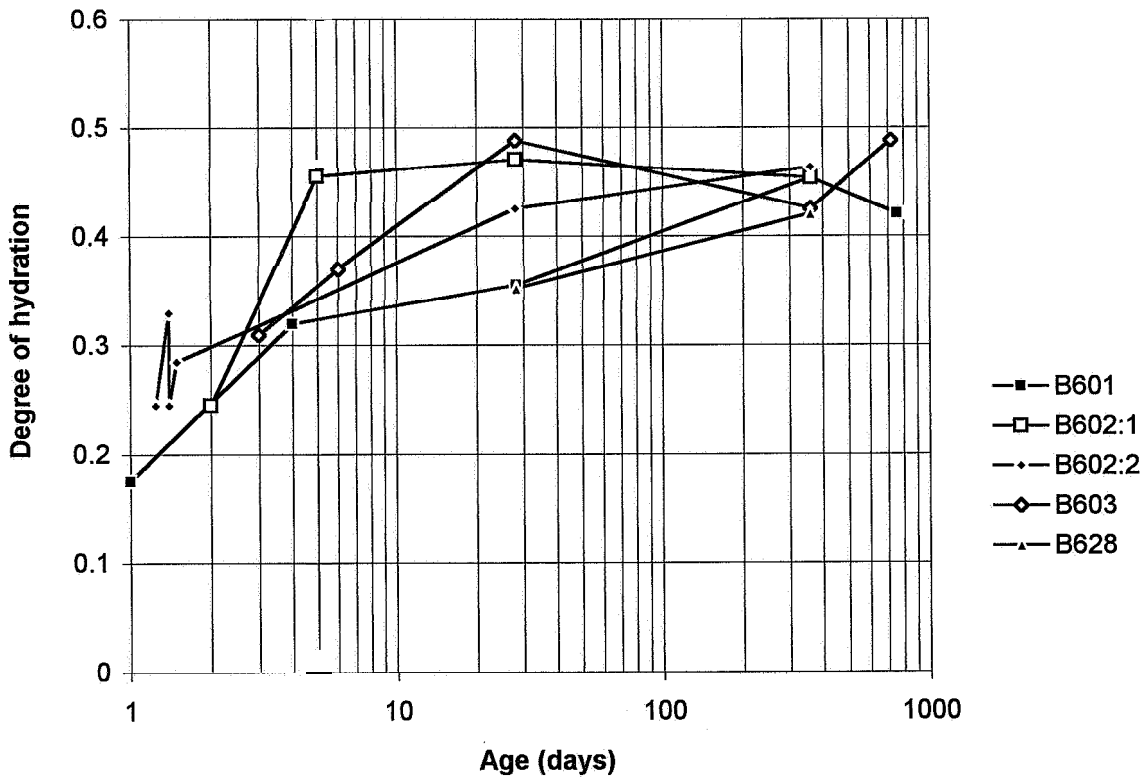

Appendix 5.31 - Hydration of mix 7 at short-term creep subjected to sealed curing

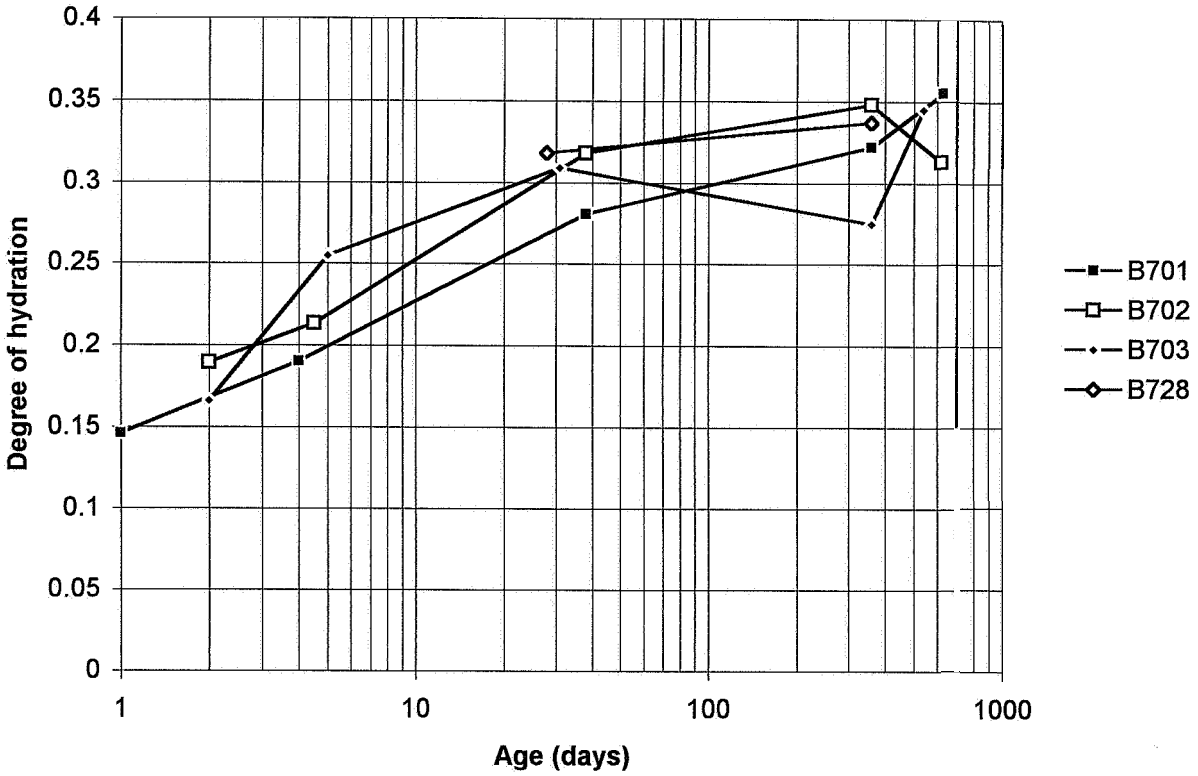

Appendix 5.32 - Hydrat of mix 8 at short term creep subje to sealed curing

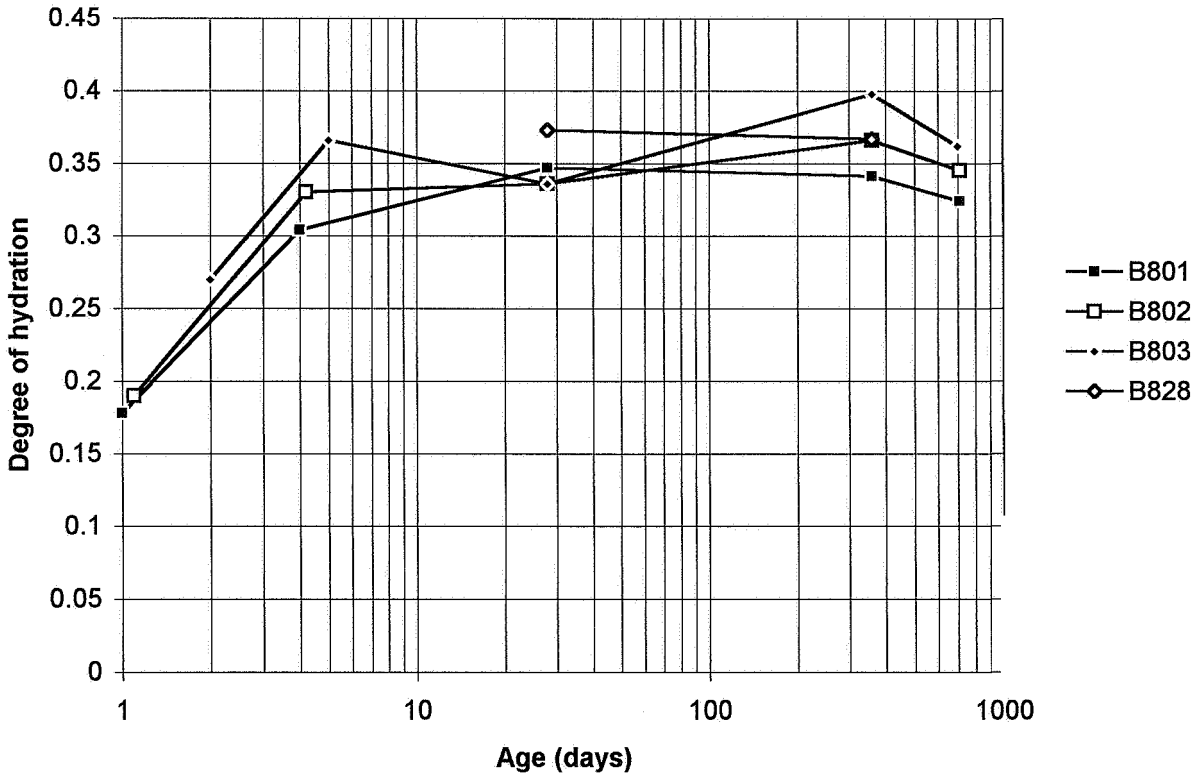

Appendix 5.33 - Internal relative humidity of mix 1

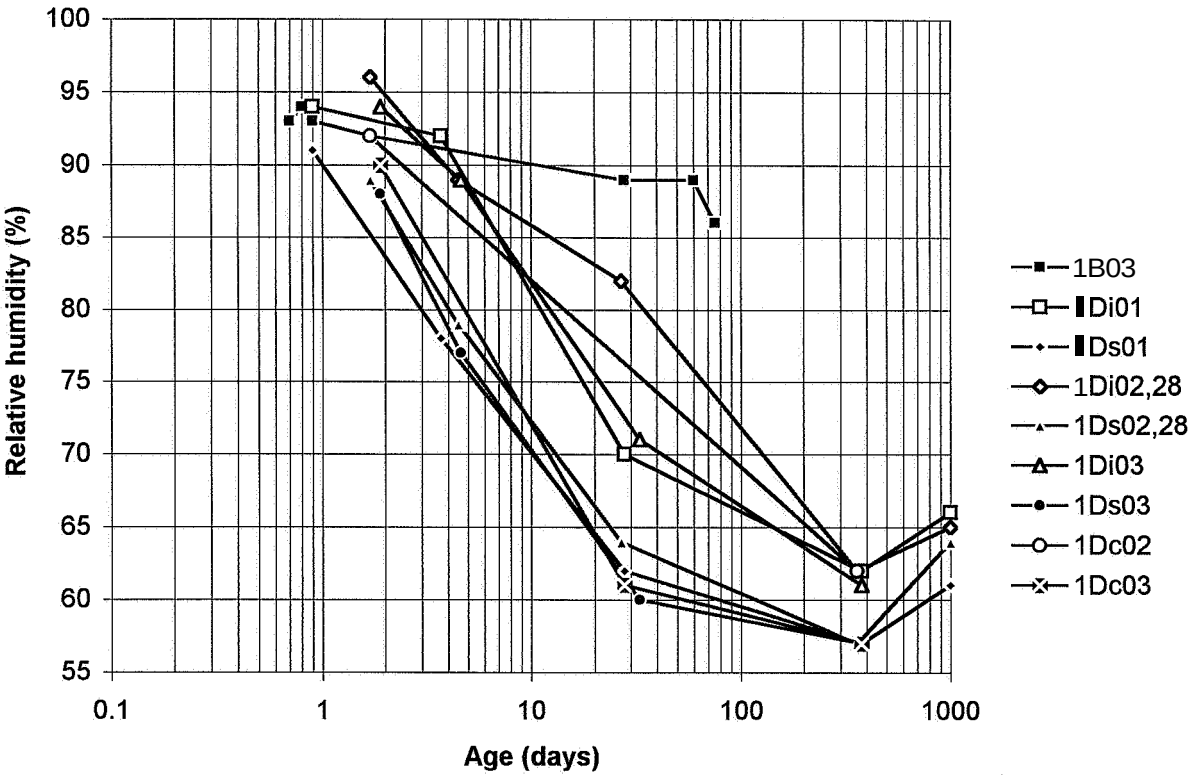

Appendix 5.34 - Internal relative humidity of mix 2

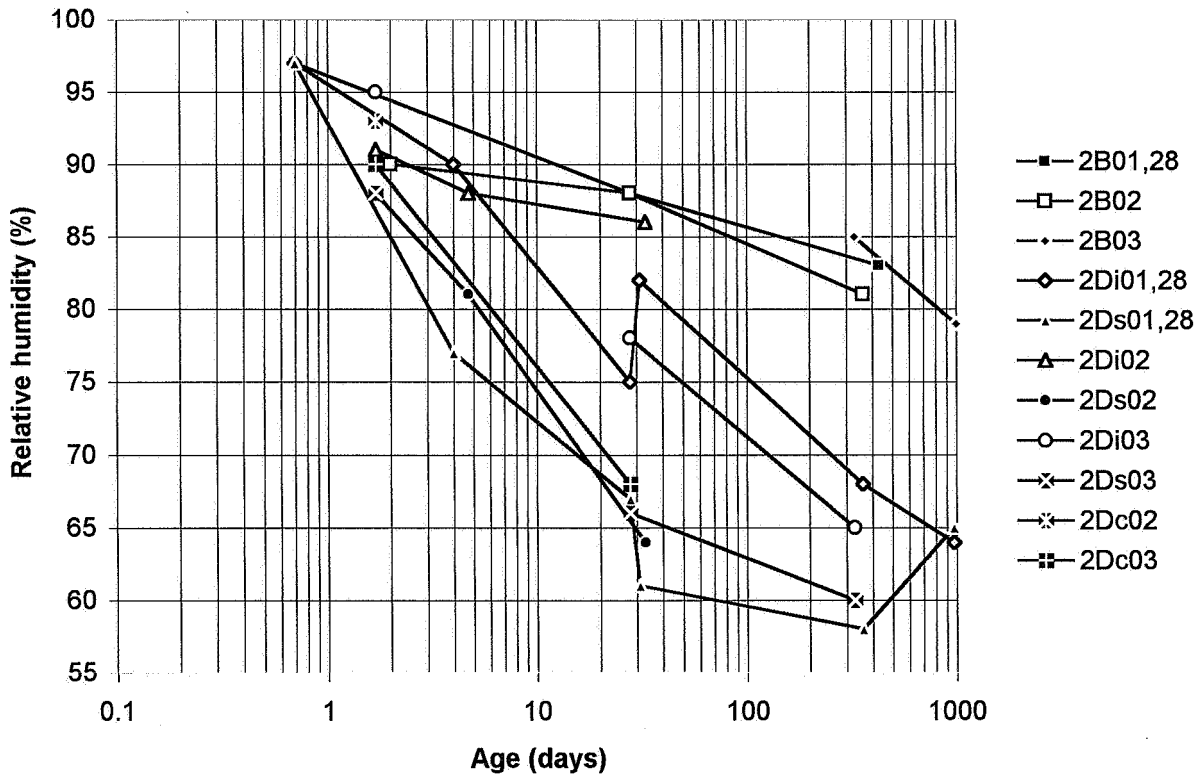

Appendix 5.35 - Internal relative humidity of mix 3

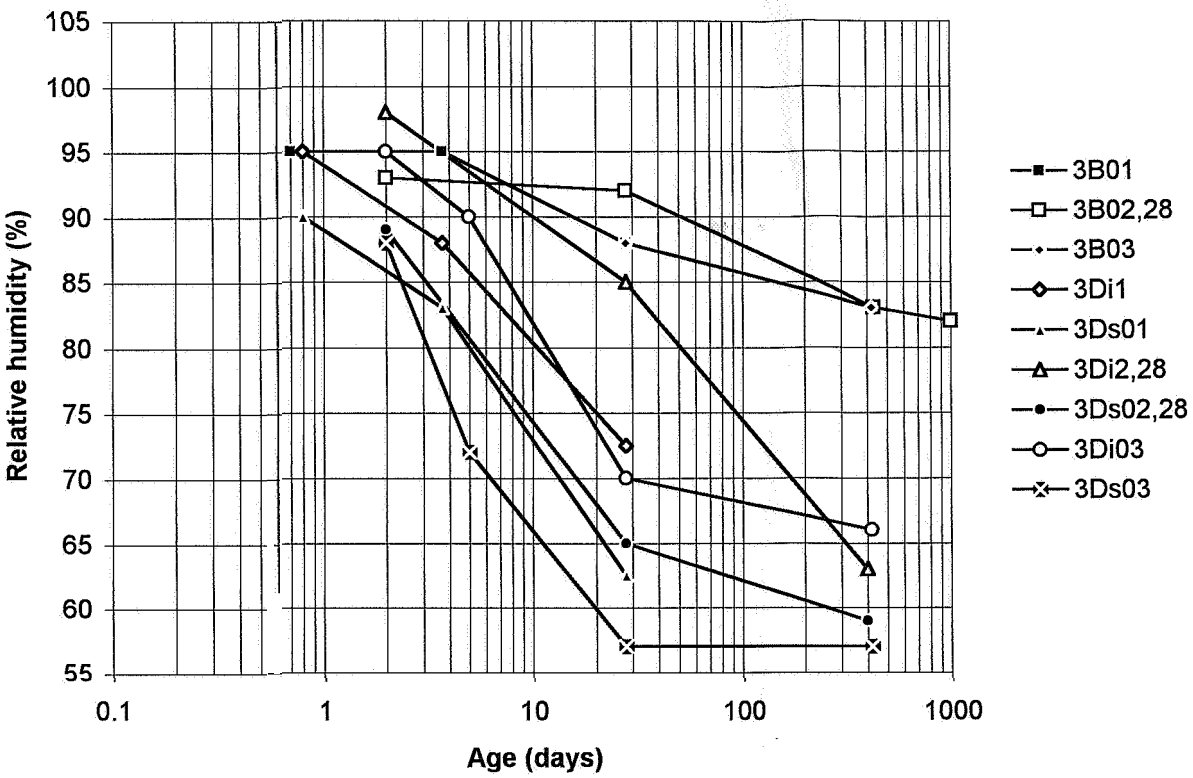

Appendix 5.36 - Internal relative humidity of mix 4

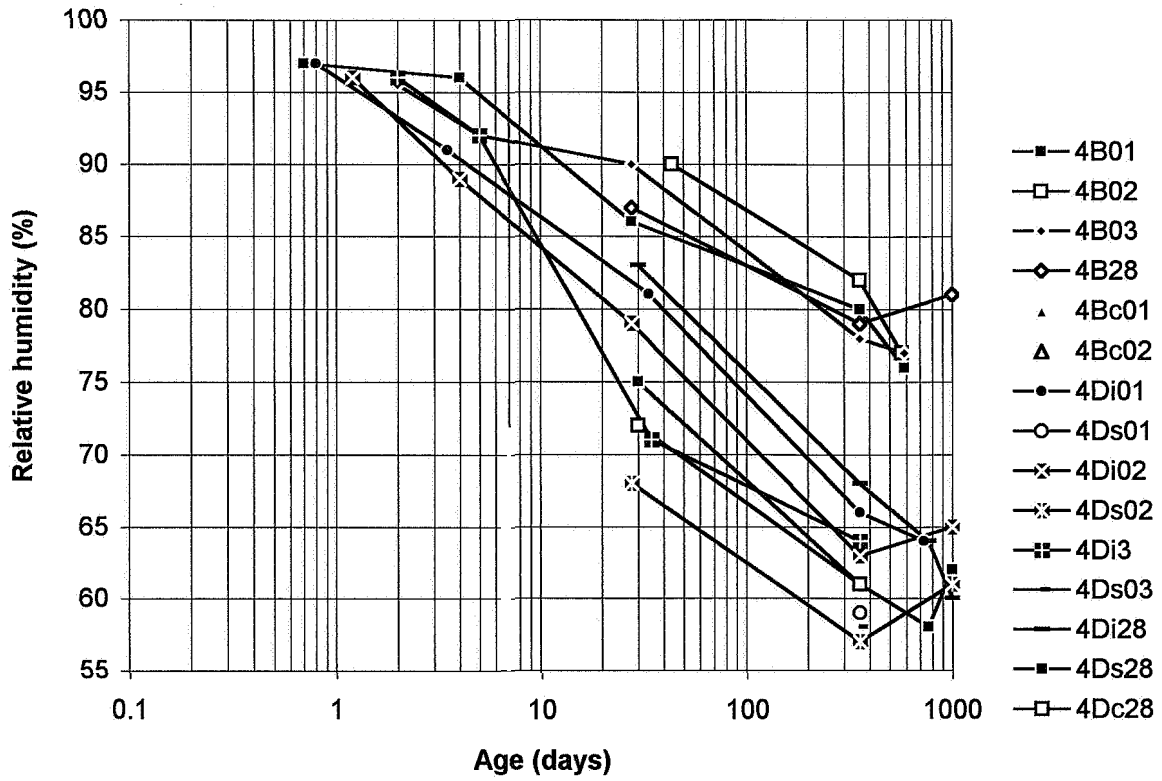

Appendix 5. 7 - Internal elativ t of mix 5

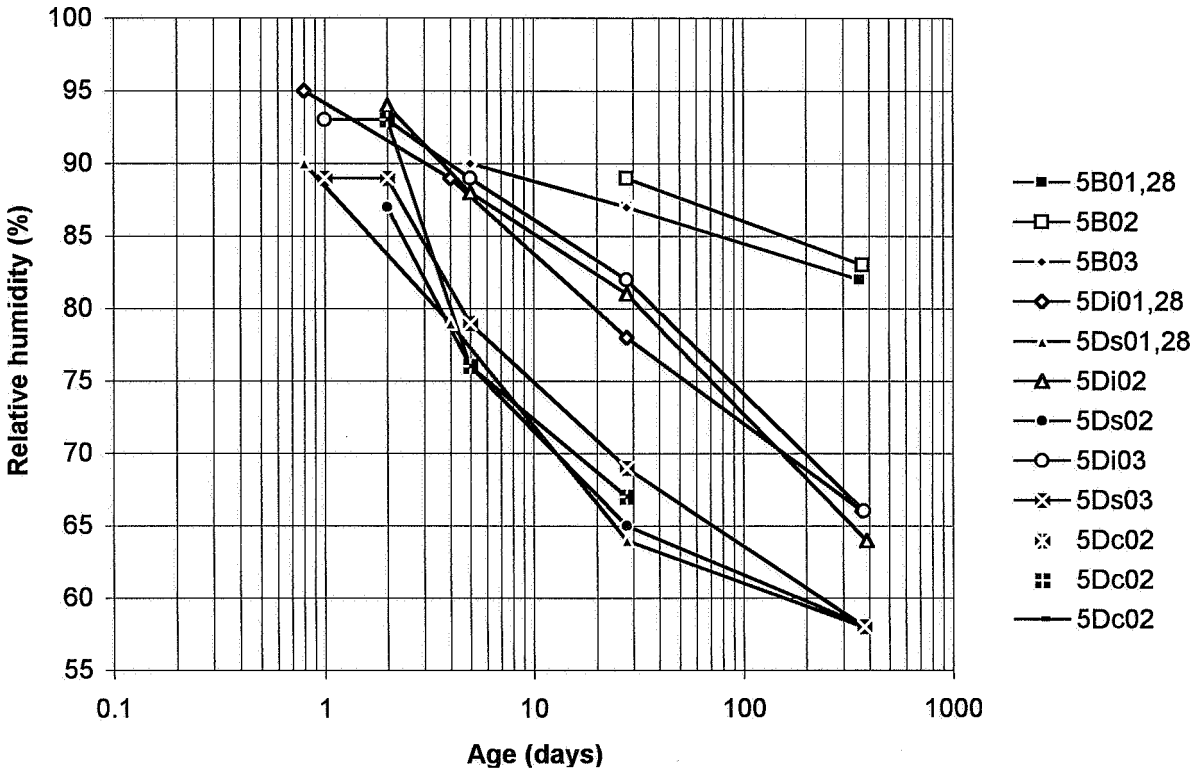

Appendix 5.38 - Internal relative humiditv of mix 6

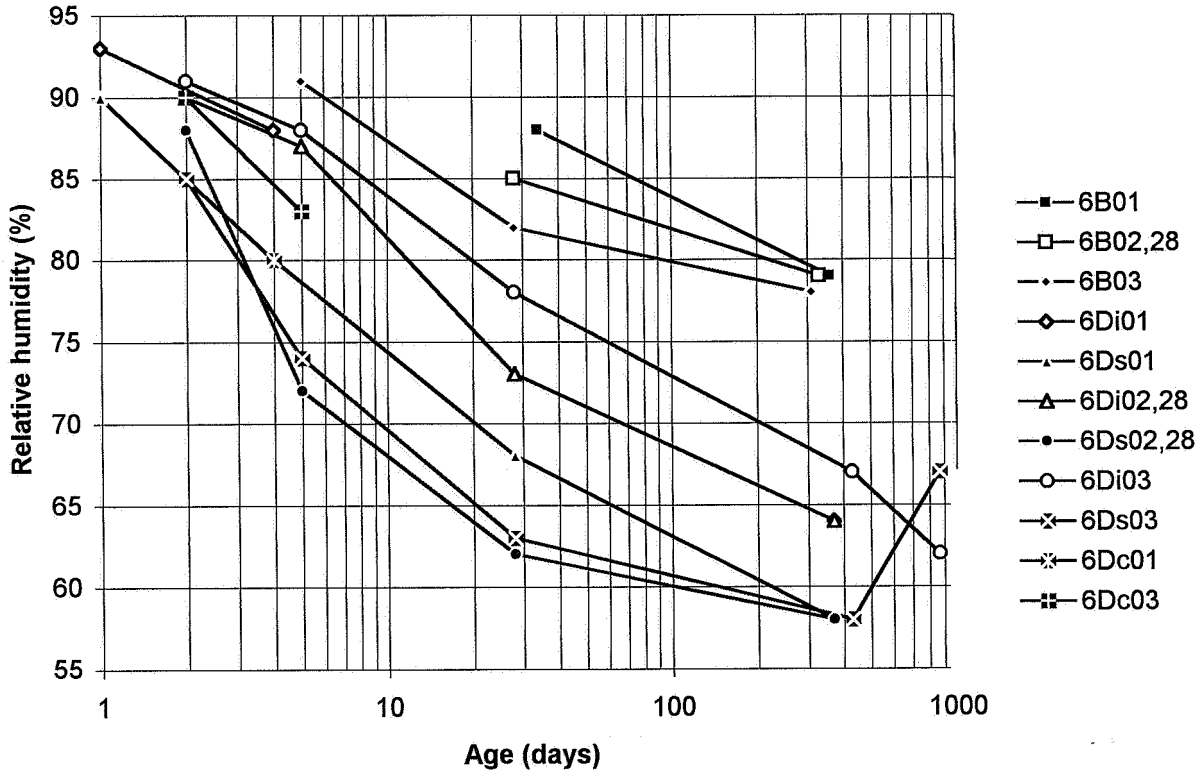

Appendix 5.39 - Internal relative humidity of mix 7

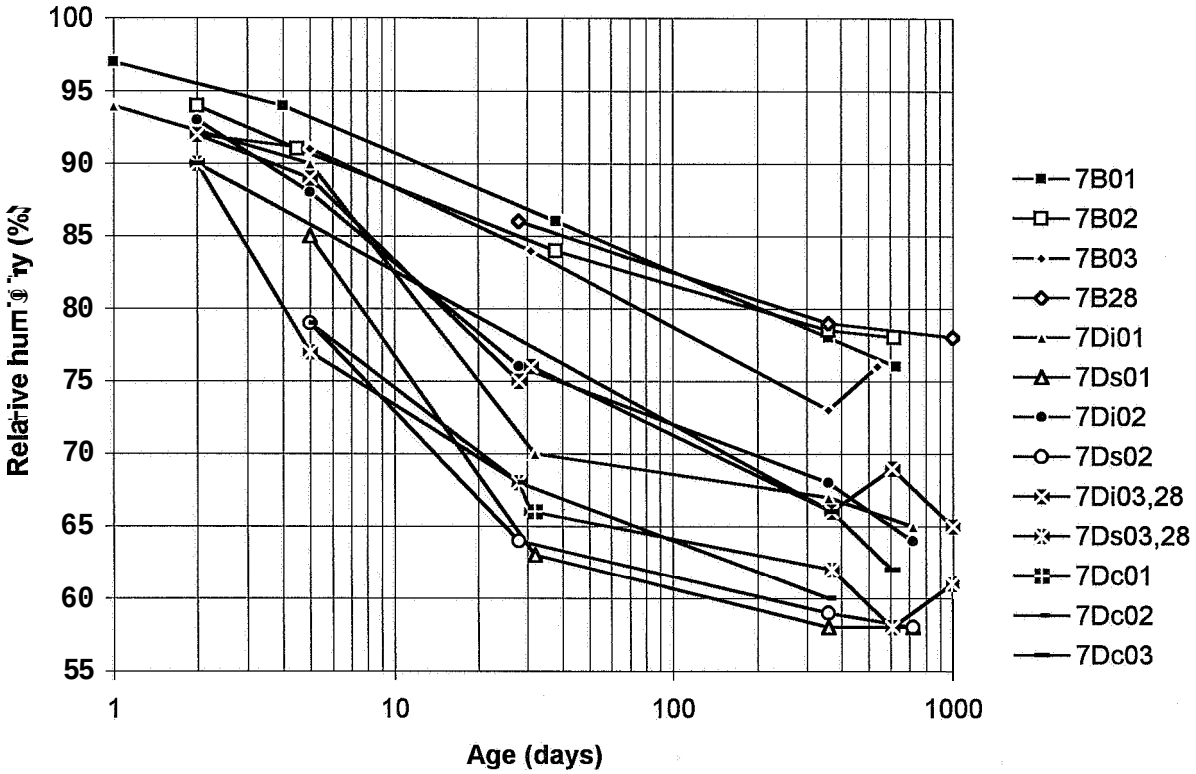

Appendix 5.40 - [illegible] of mix 8

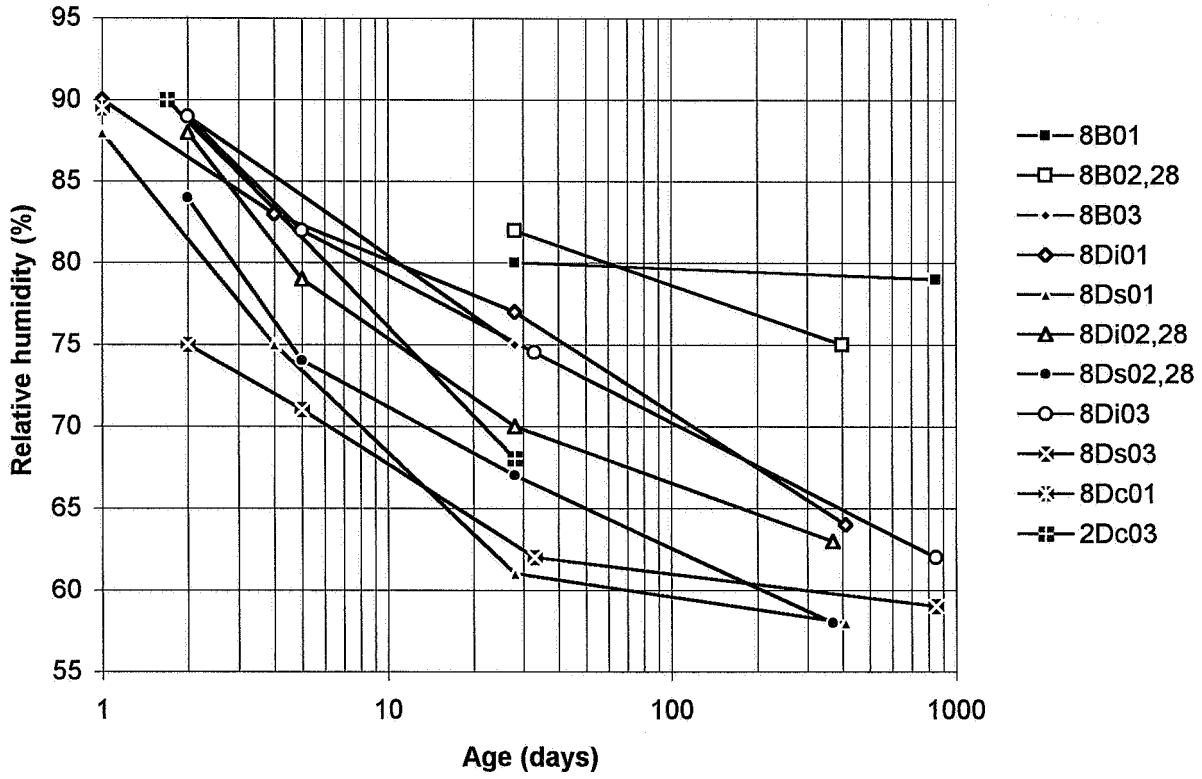

Appendix 5.41 - Internal relative humidity of mix 1 at short-term creep subjected to sealed curing

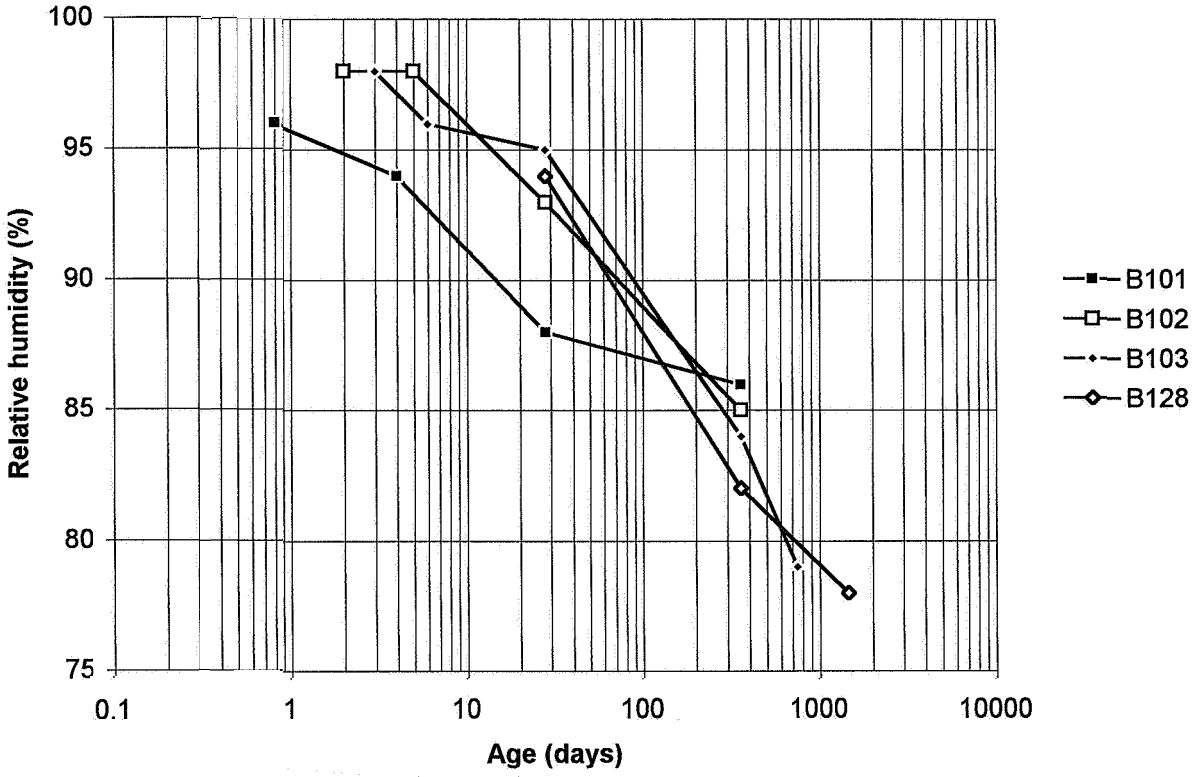

Appendix 5.42 - Internal relative humidity of mix 2 at short-term creep subjected to sealed curing

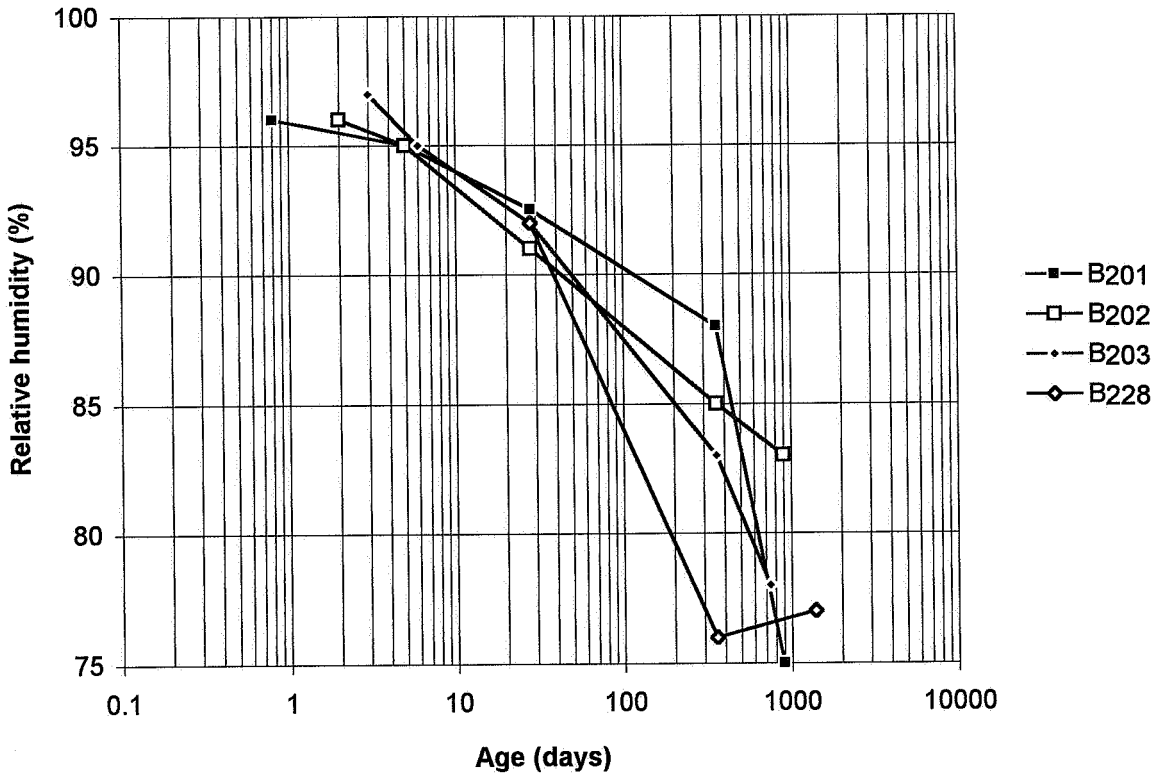

Appendix 5.43 - Internal relative humidity of mix 3 at short-term creep subjected to sealed curing

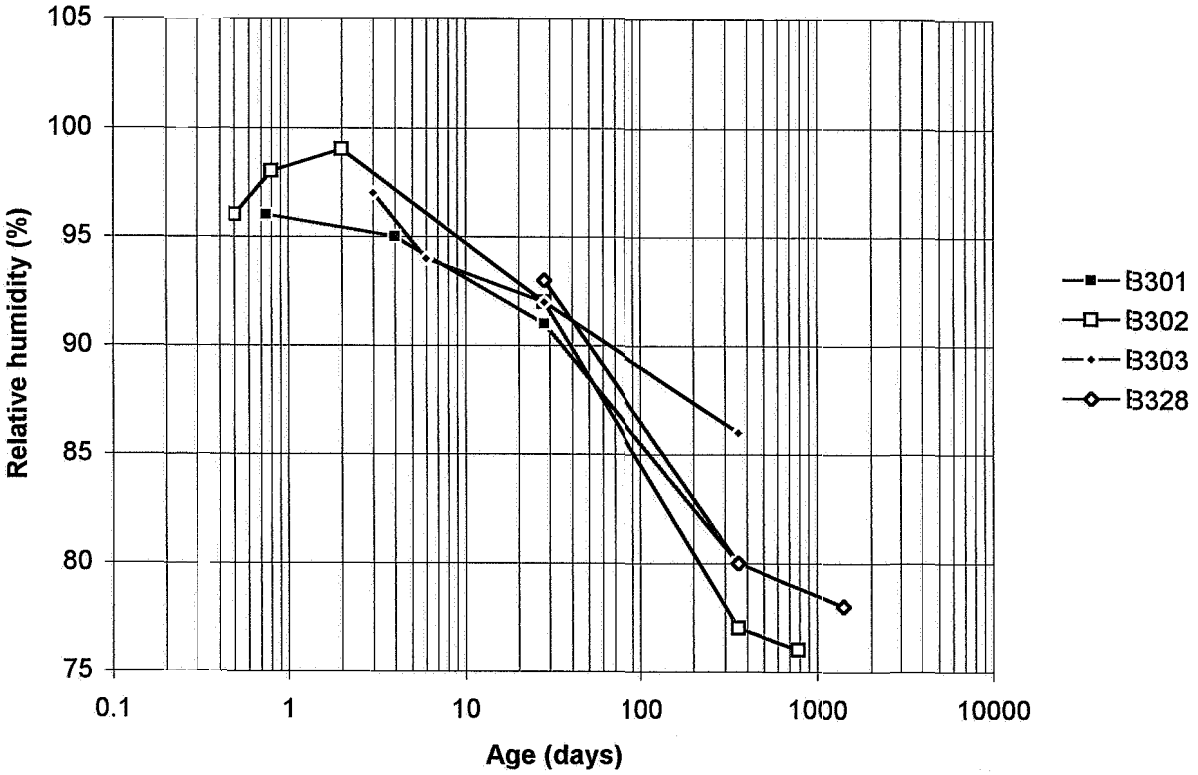

Appendix 5.44 - Internal relative humidity of mix 4 at short-term creep subjected to sealed curing

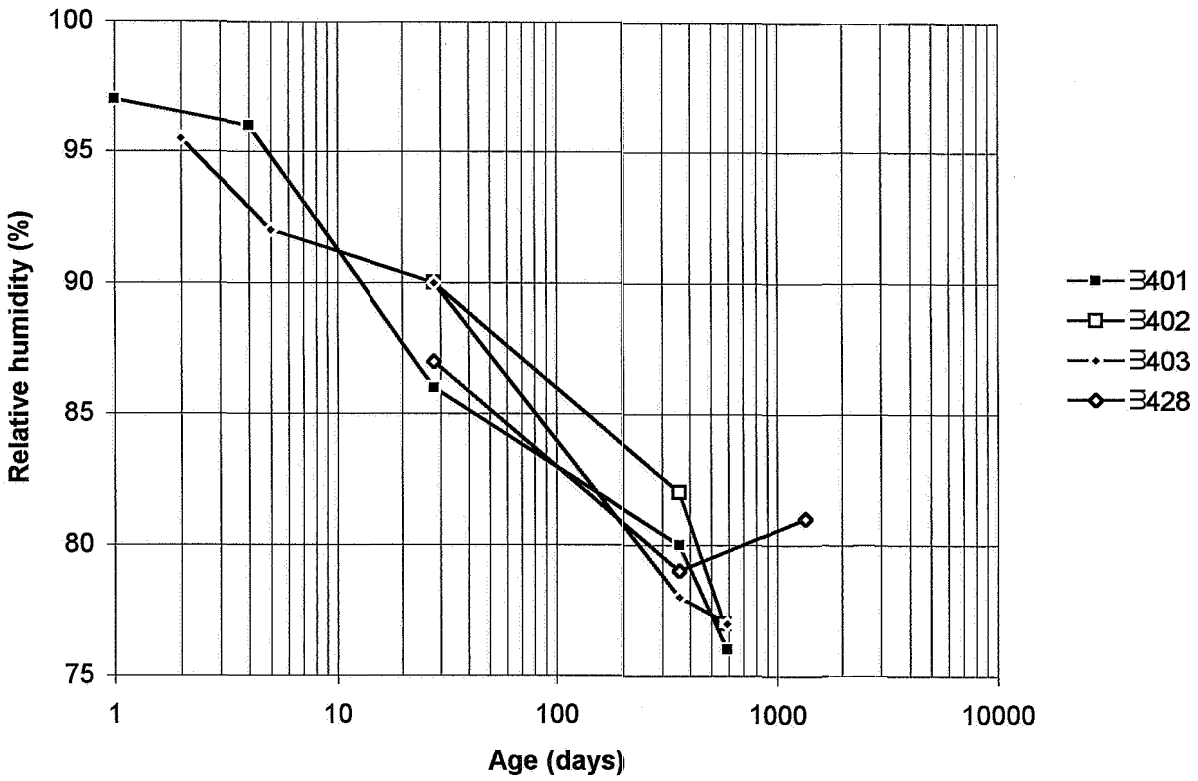

ɔendix 5.45 - Internal relative humidity of mix 5 at short-term creep jected to sealed curing

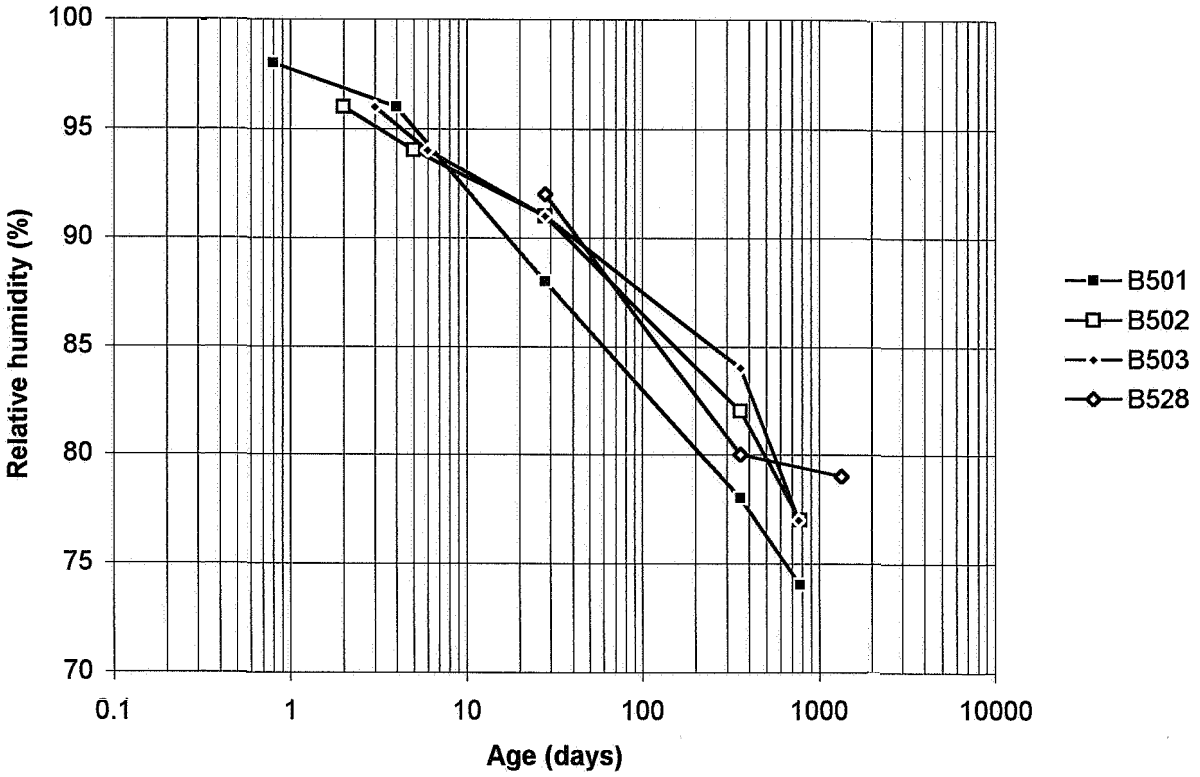

Appendix 5.46 - Internal relative humidity of mix 6 at short-term creep subjected to sealed curing

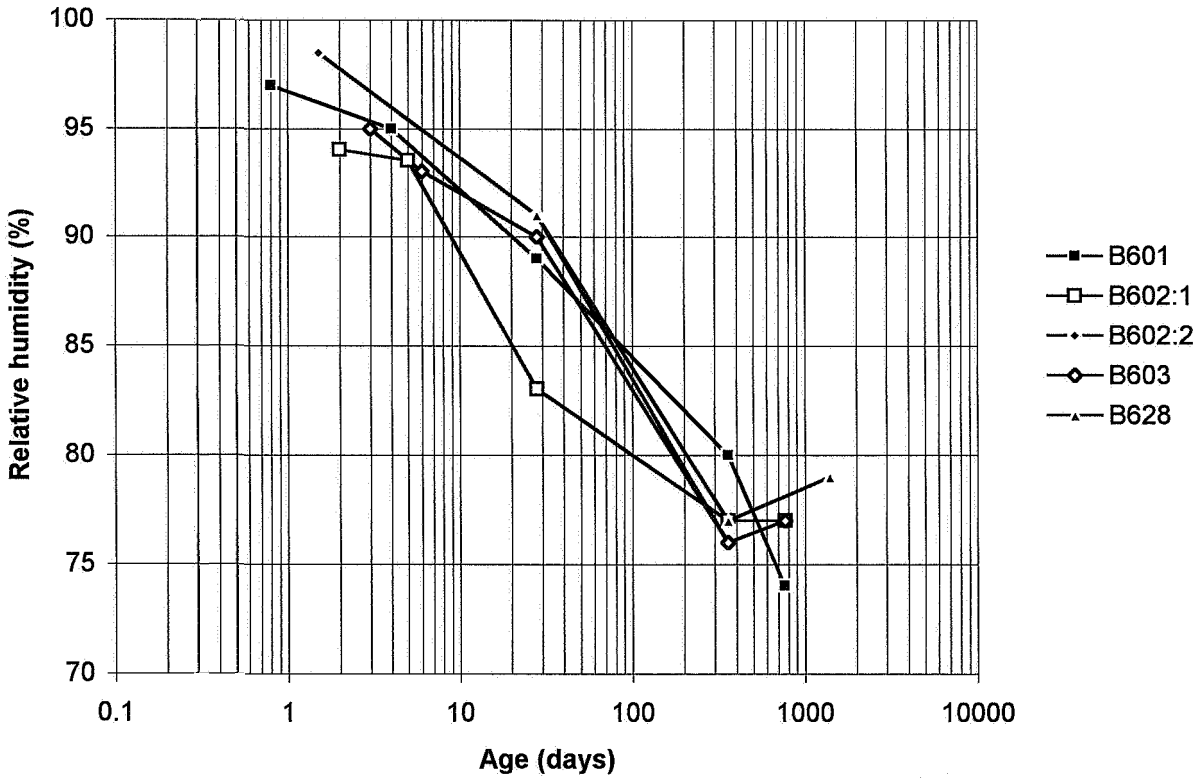

Appendix 5.47 - Internal relative humidity of mix 7 at short-term creep subjected to sealed curing

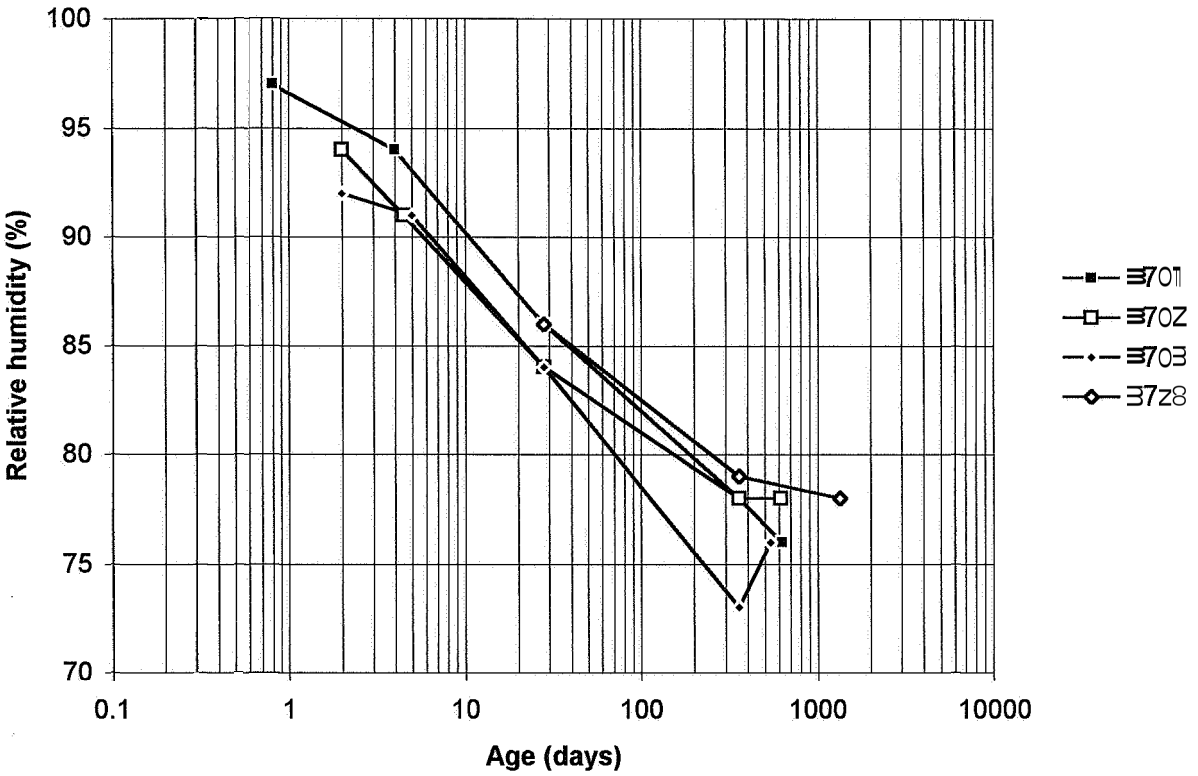

ɔendix 5.48 - Internal relative humidity of mix 8 at short-term creep jected to sealed curing

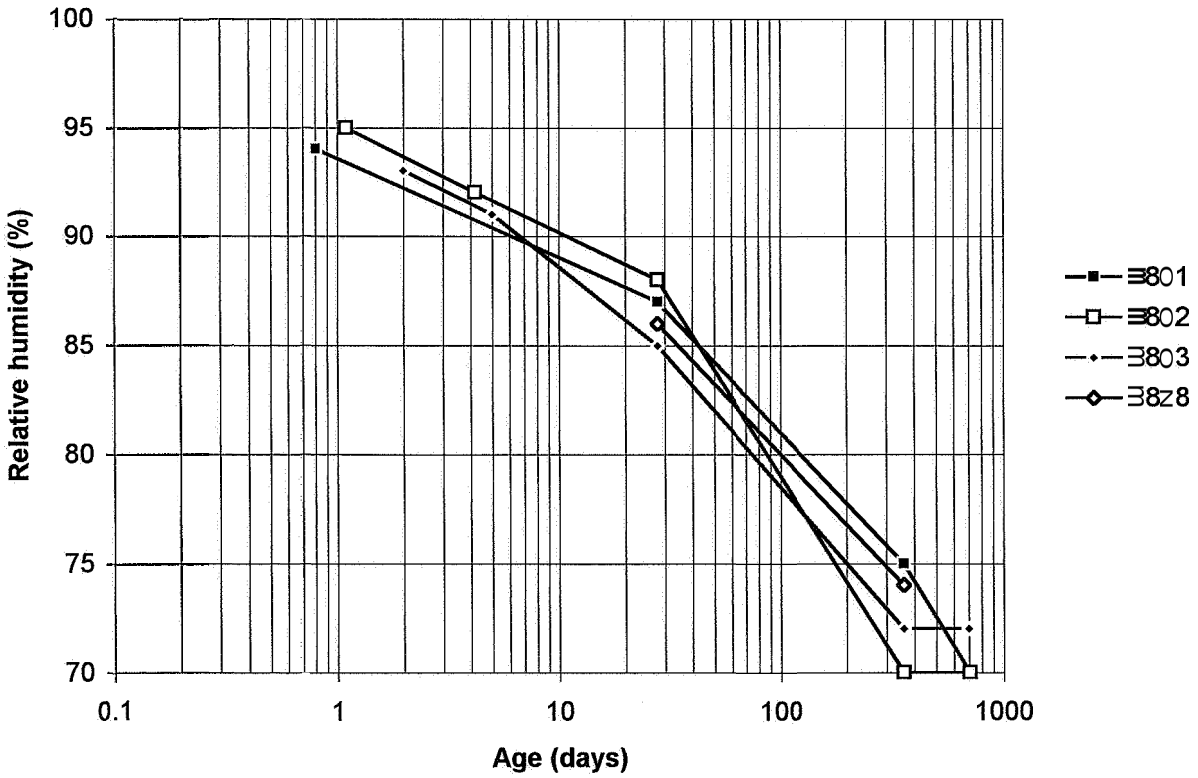

App di 5.49 - Internal elative humidity at sh t-term creep of ll mixes subiected to sealed curing

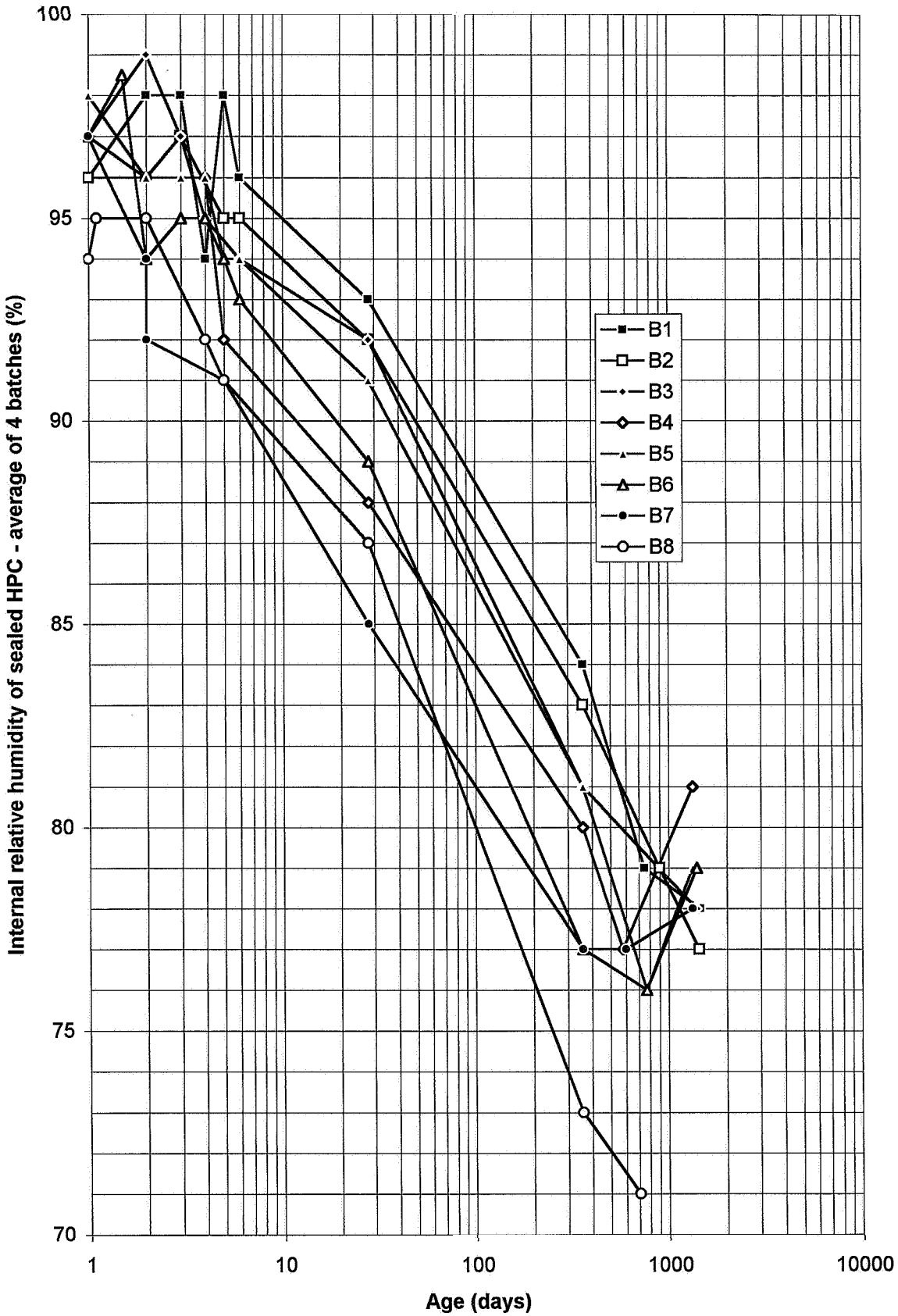

APPENDIX 6. COMPLIANCE OF CYLINDERS AFTER QUASI-INSTANTANEOUS LOADING

Symbols:

e	denotes the eccentricity of loading provided elastic conditions
B....	Basic creep (cylinder subjected to sealed curing)
D...	Drying creep (cylinder subjected to air curing)
..6..	concrete mix 6 (Table 5.1)
...01	age at loading: 1 day; stresslcylinder strength ratio: 0.84
...02	age at loading: 2 days; stresslcylinder strength ratio: 0.84
...03	age at loading: 2 days; stresslcylinder strength ratio: 0.42
...28	age at loading: 28 days; stresslcylinder strength ratio: 0.42

Appendix 6.1 - Quasi-instantaneous compliance of mix 1 subjected to air curing

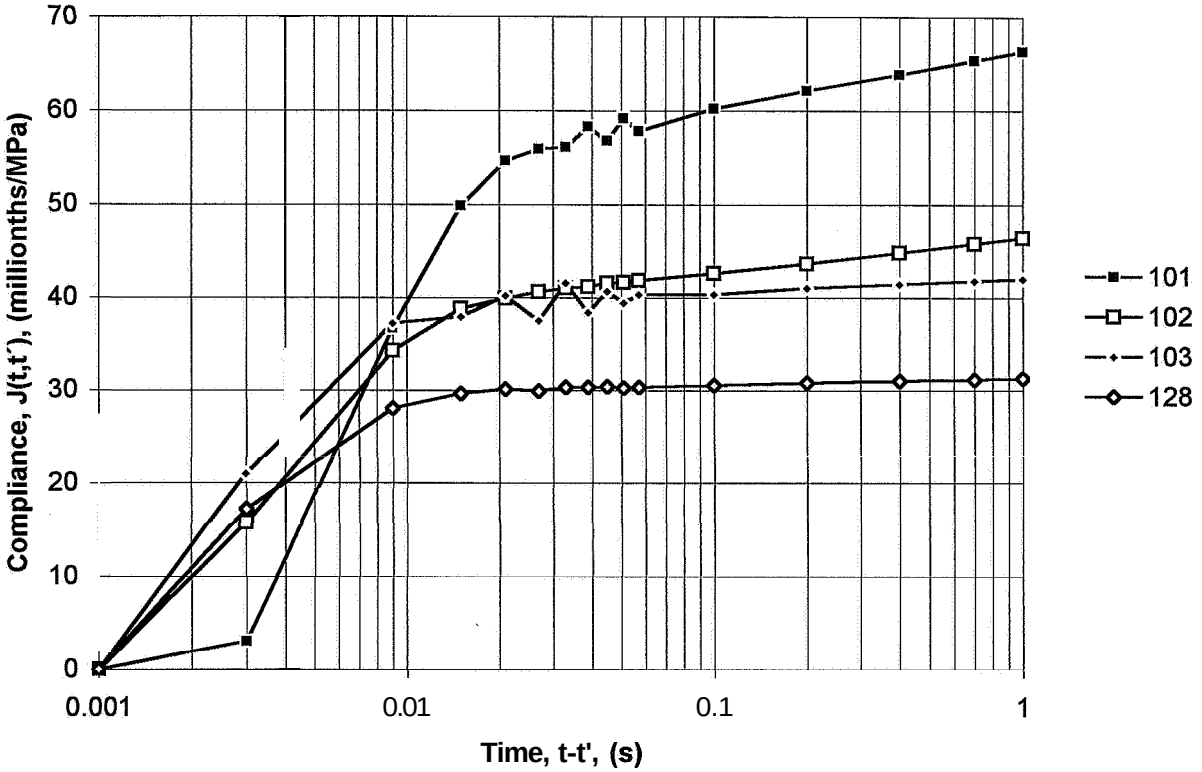

Appendix 6.2 - Quasi-instantaneous compliance of mix 2 subjected to air curing

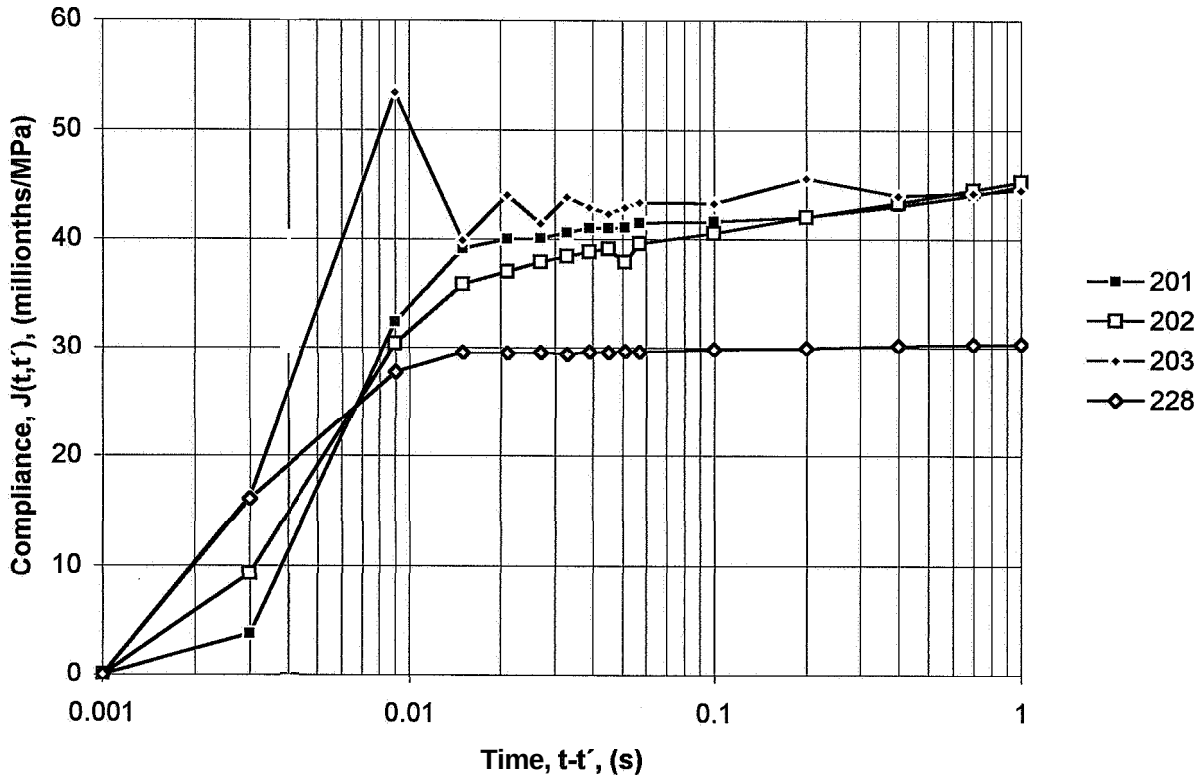

Appendix 6.3 - Quasi-instantaneous compliance of mix 3 subiected to air curing

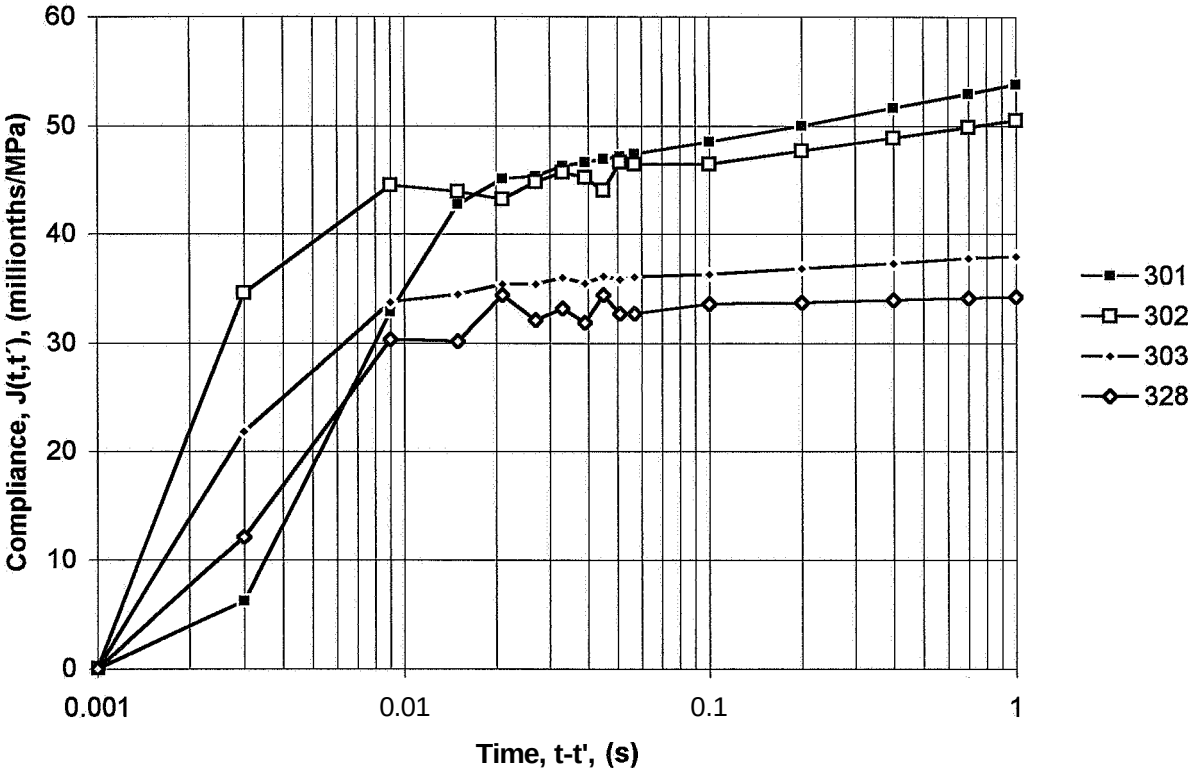

Appendix 6.4 - Quasi-instantaneous compliance of mix 4 subiected to air curing

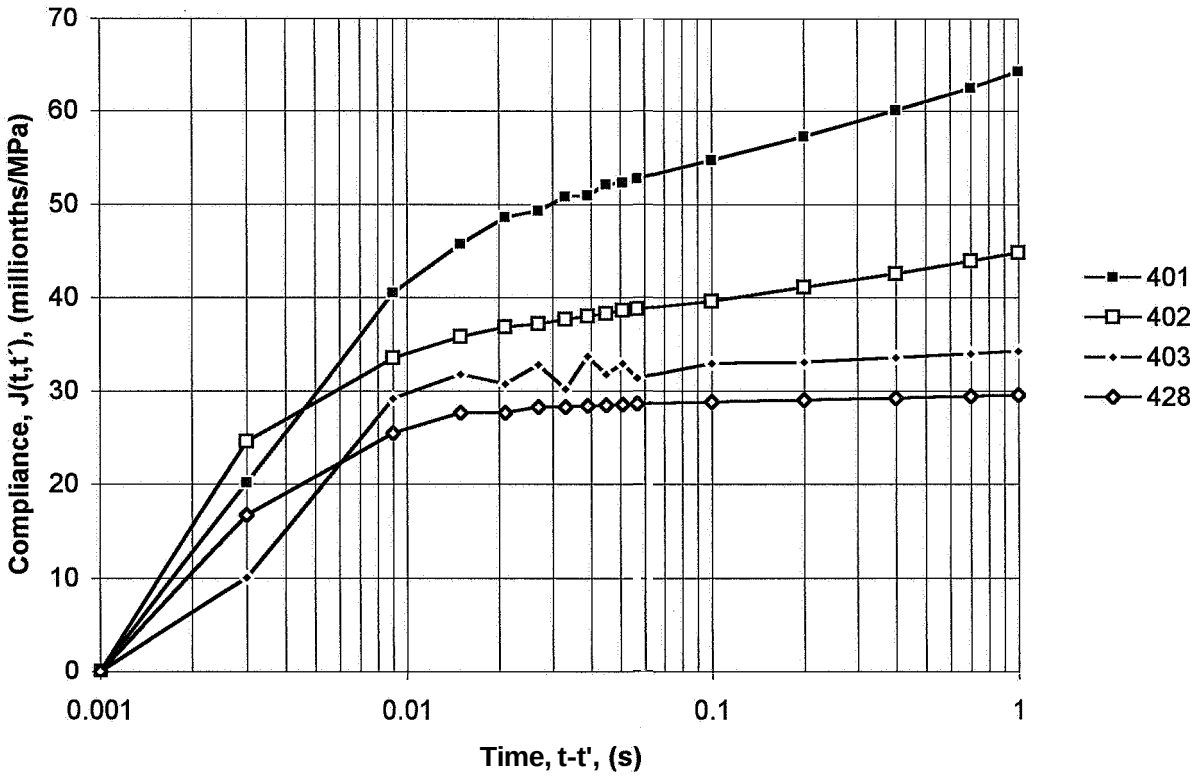

Appendix 6.5 - Quasi-instantaneous compliance of mix 5 subiected to air curing

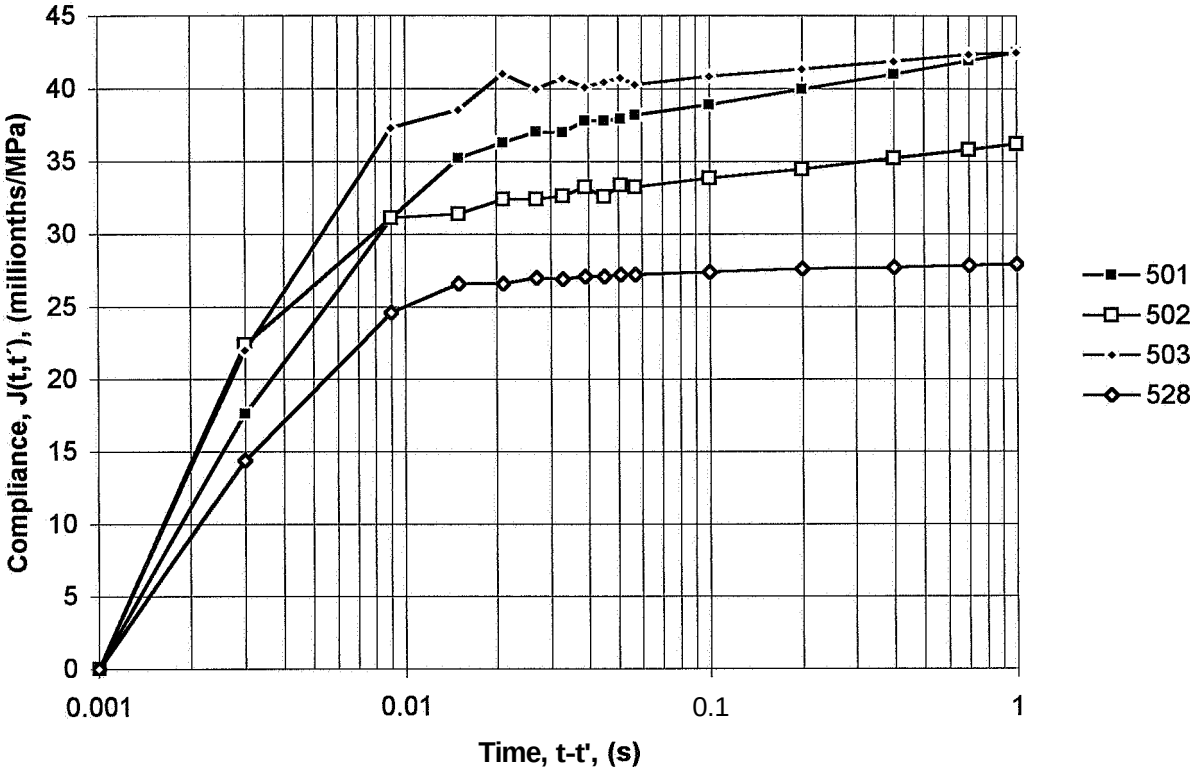

Appendix 6.6 - Quasi-instantaneous compliance of mix 6 subjected to air curing

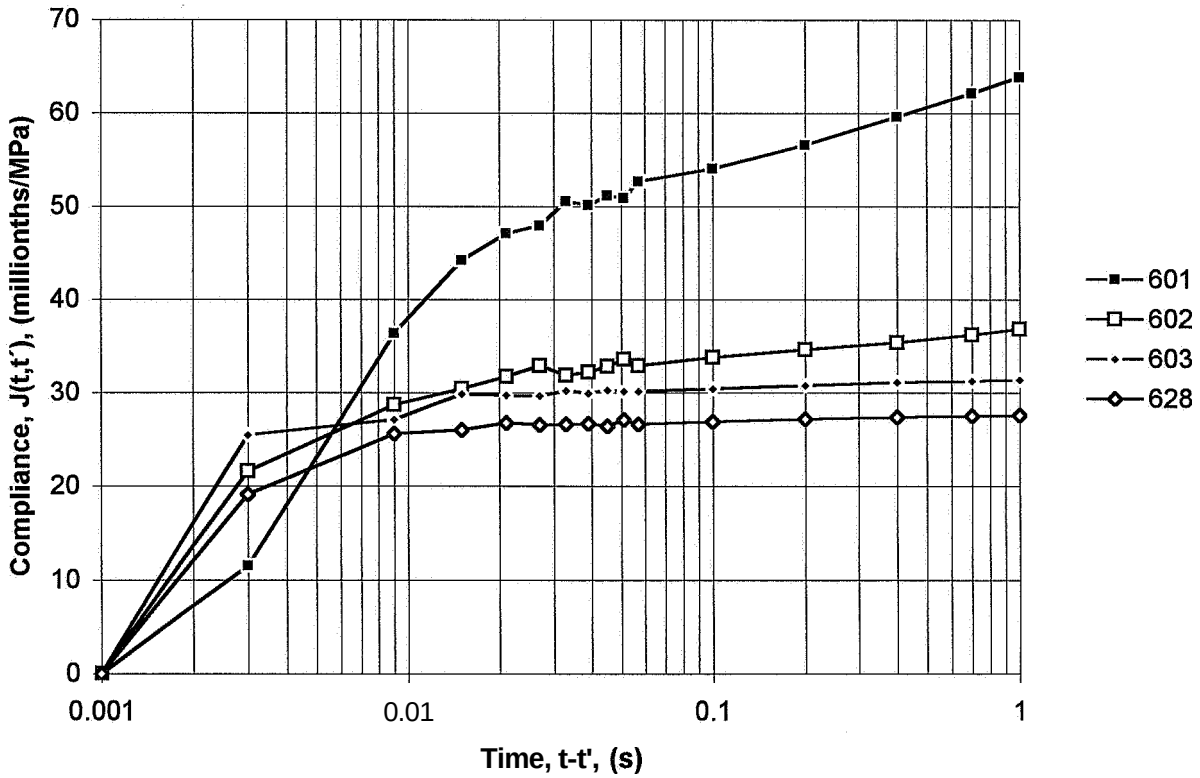

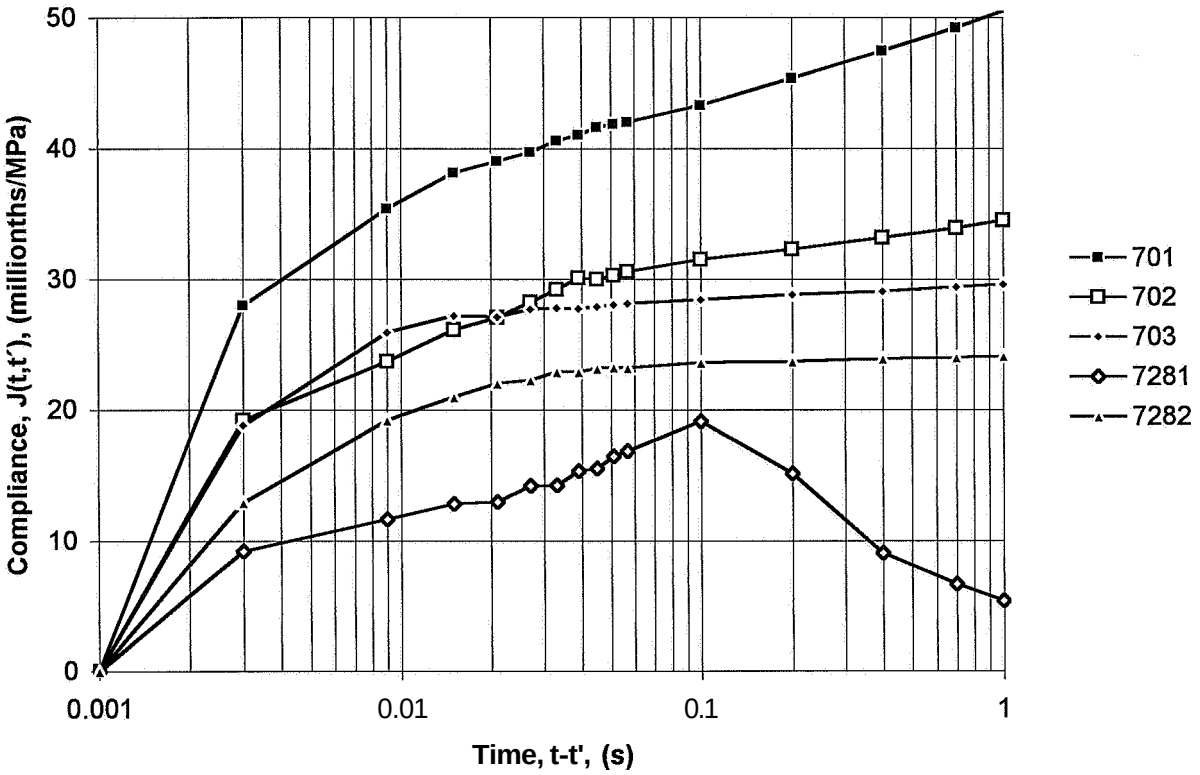

Appendix 6.8 - Quasi-instantaneous compliance of mix 8 subjected to air curing

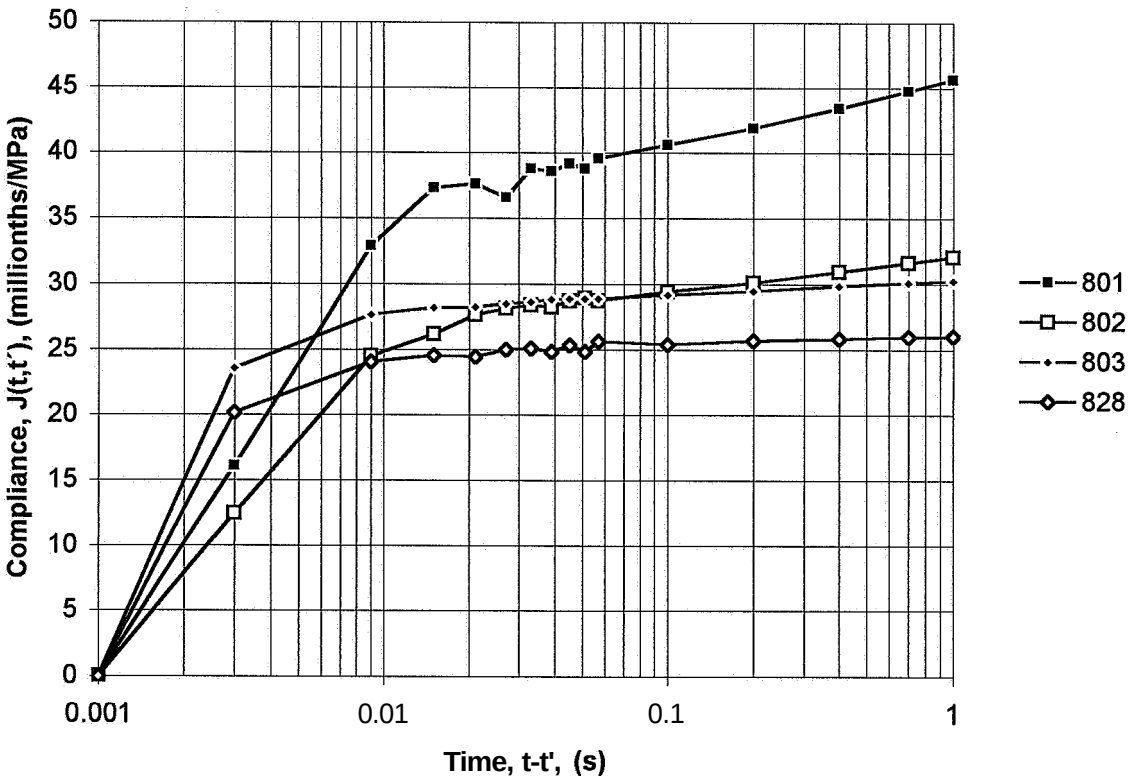

Appendix 6.9 - Quasi-instantaneous compliance of all mature mixes subjected to air curing

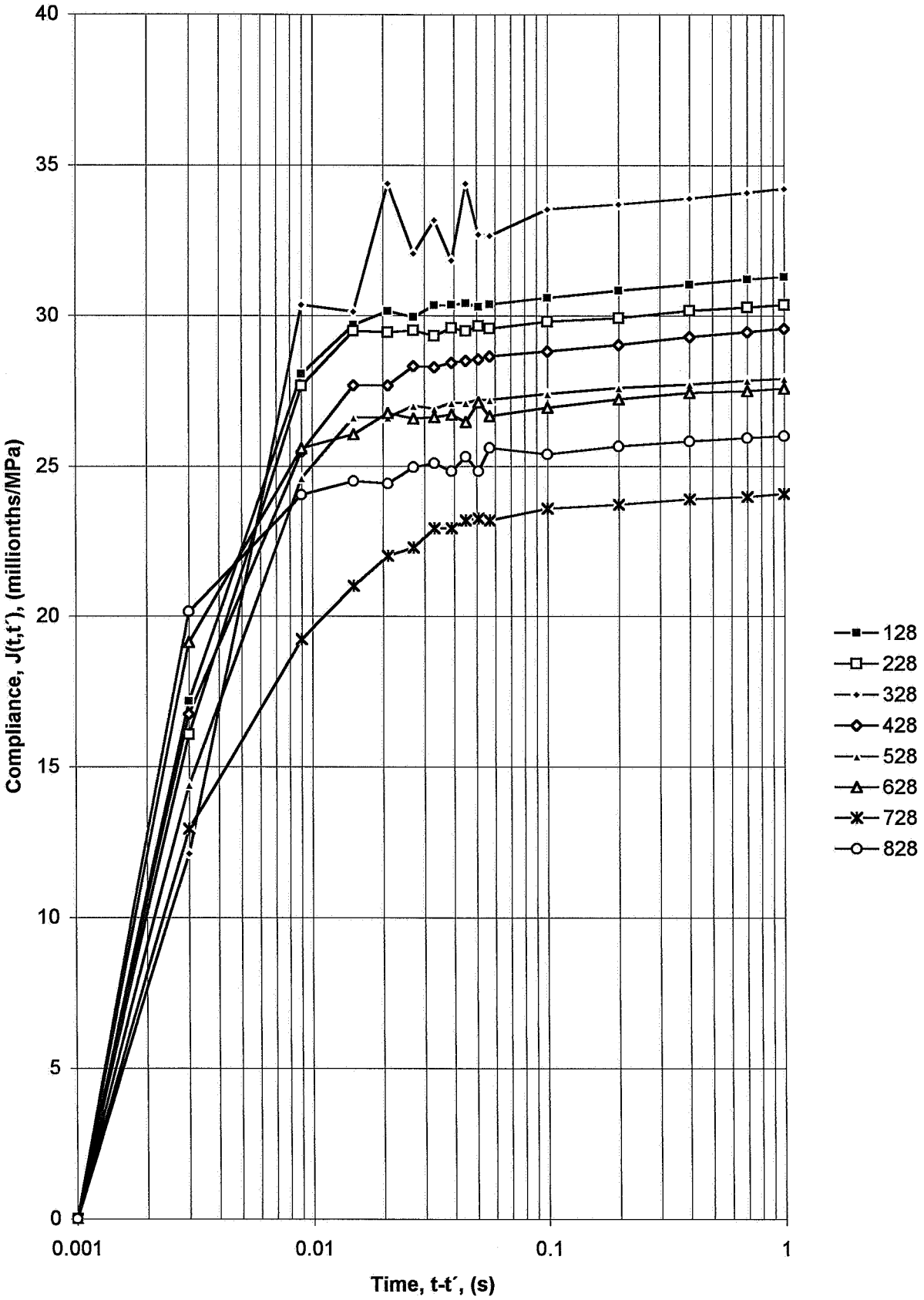

Appendix 6.10 - Q -instantaneous compliance rate f mixes subjected to air curing

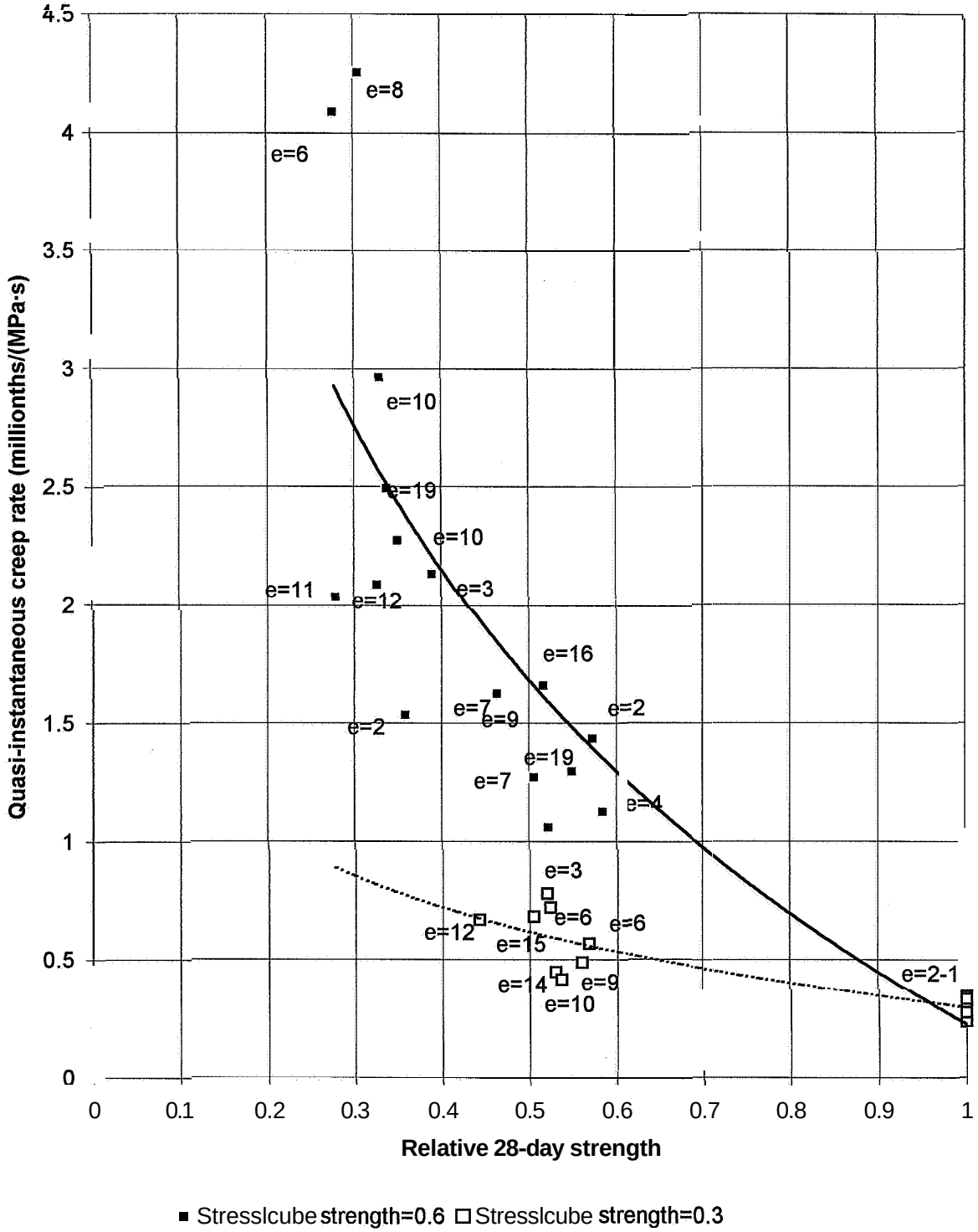

i 6.11 - Quasi-instantaneous omp an of mix 1 t to sealed curing

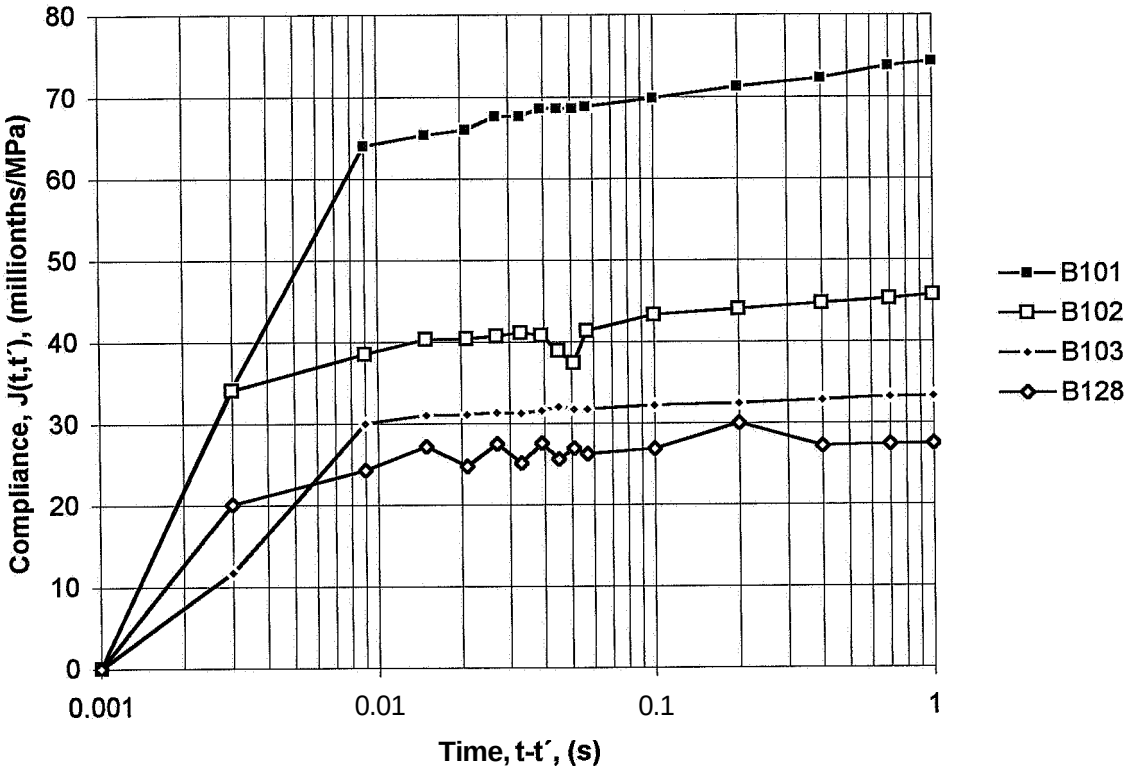

Appendix 6.12 - Quasi-instantaneous compliance of mix 2 subiected to sealed curing

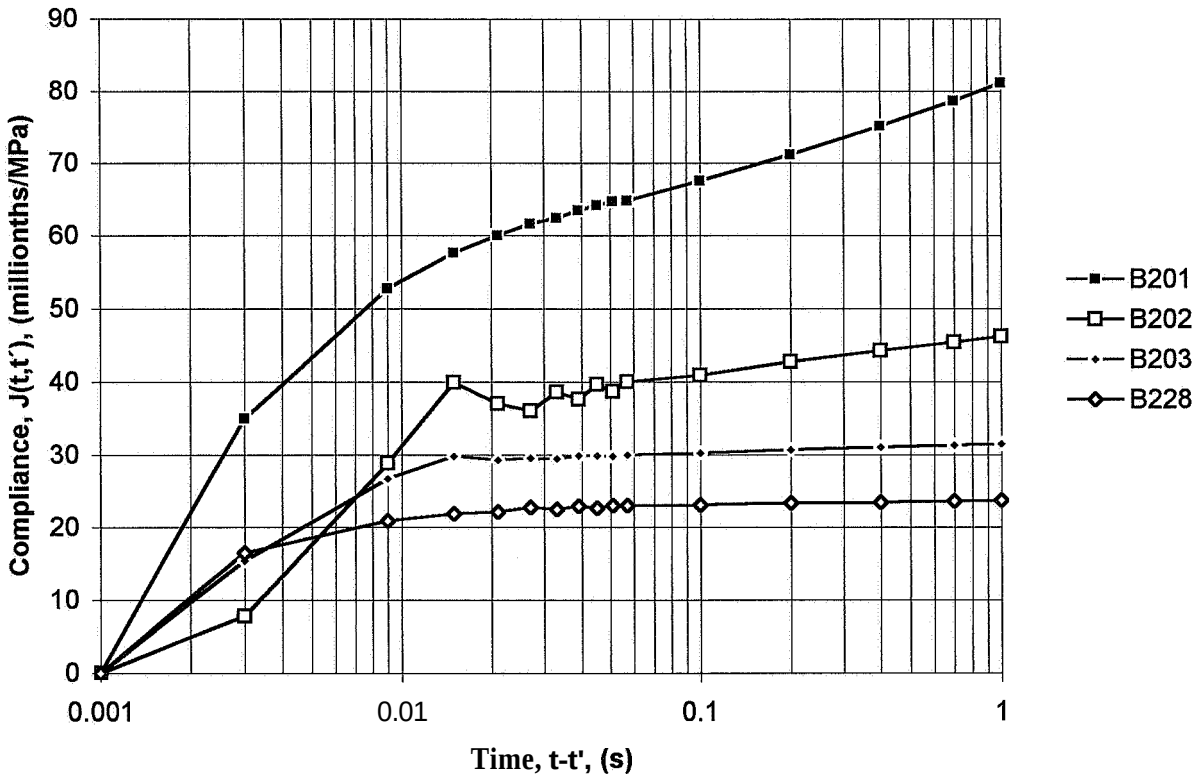

Appendix 6.13 - Quasi-instantaneous compliance of mix 3 subiected to sealed curing

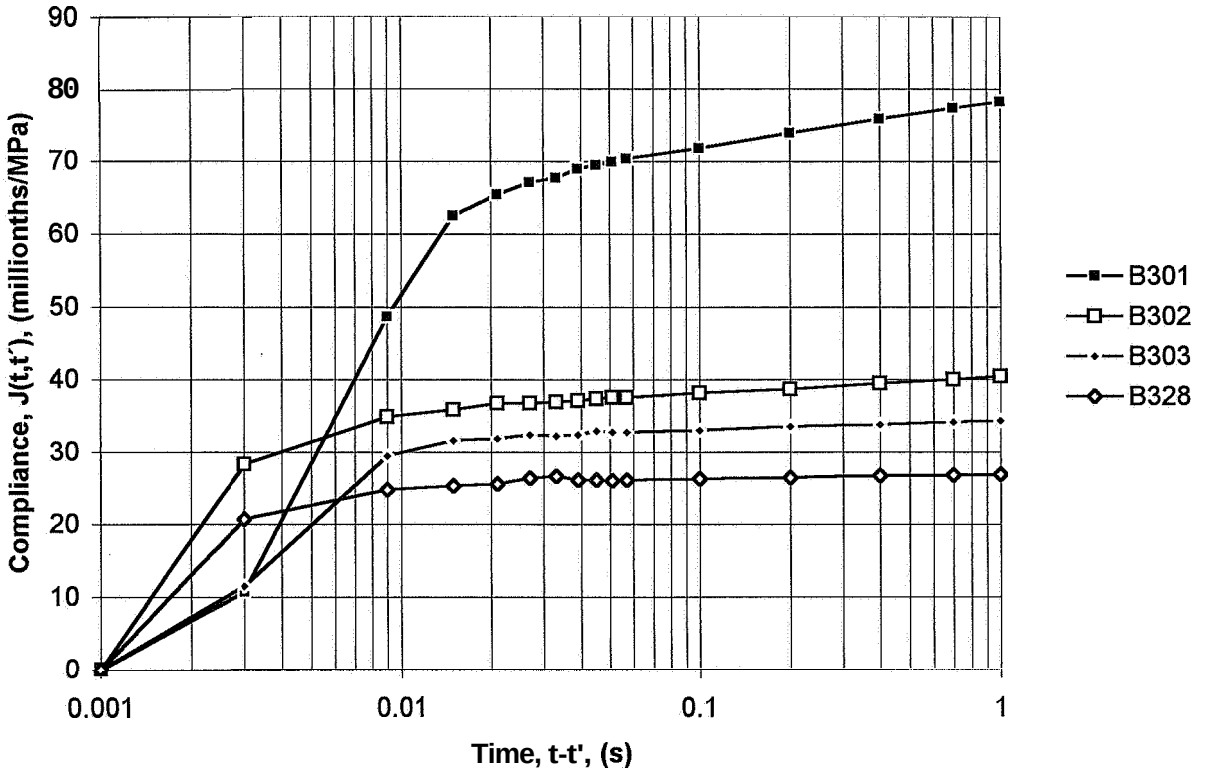

Appendi 14 - Quasi compliance of mix 4 to sealed curing;

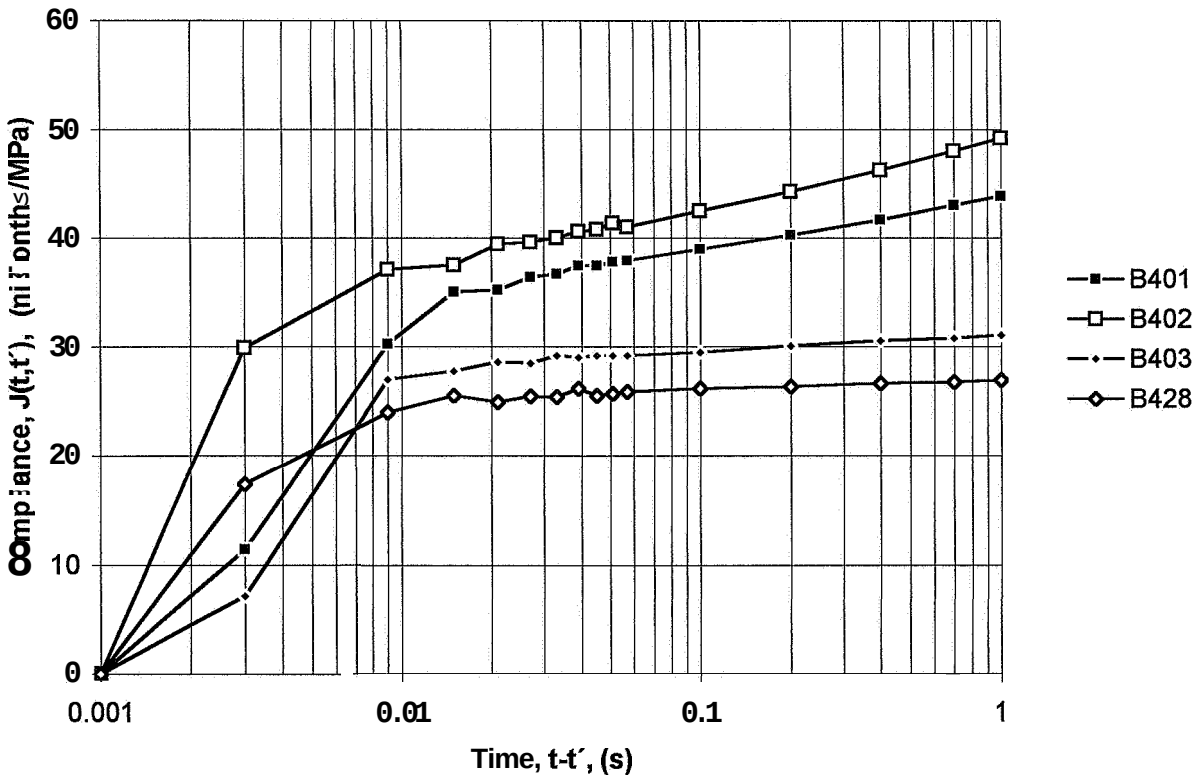

Appendix 6.15 - Quasi-instantaneous compliance of mix 5 subiected to sealed curing

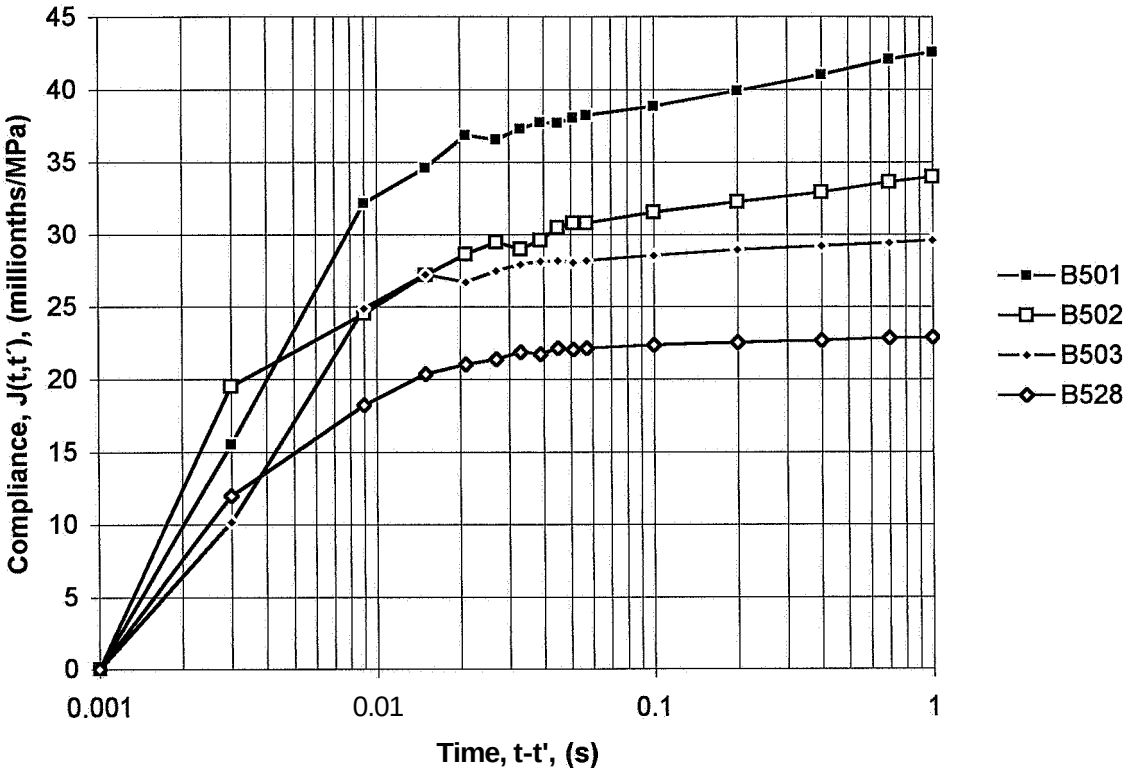

Appendix 6.16 - Quasi-instantaneous compliance of mix 6 subjected to sealed curing

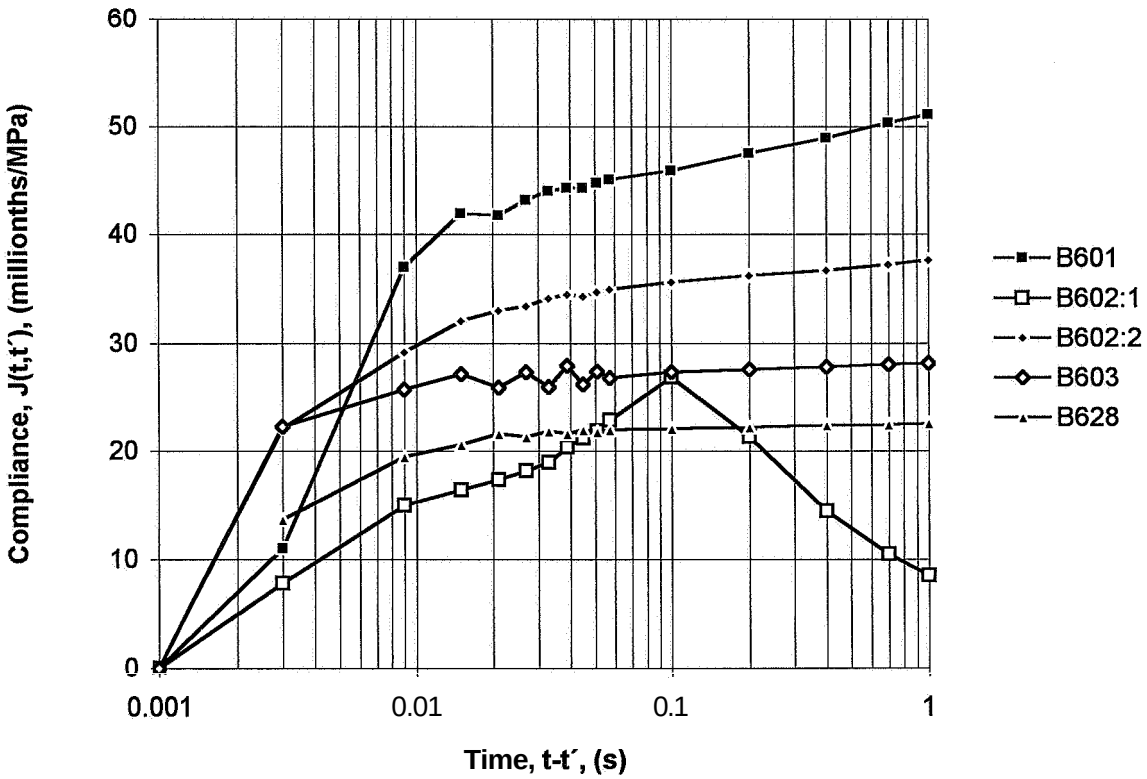

Appendix 6.17 - Quasi-instantaneous compliance of mix 7 subjected to sealed curing

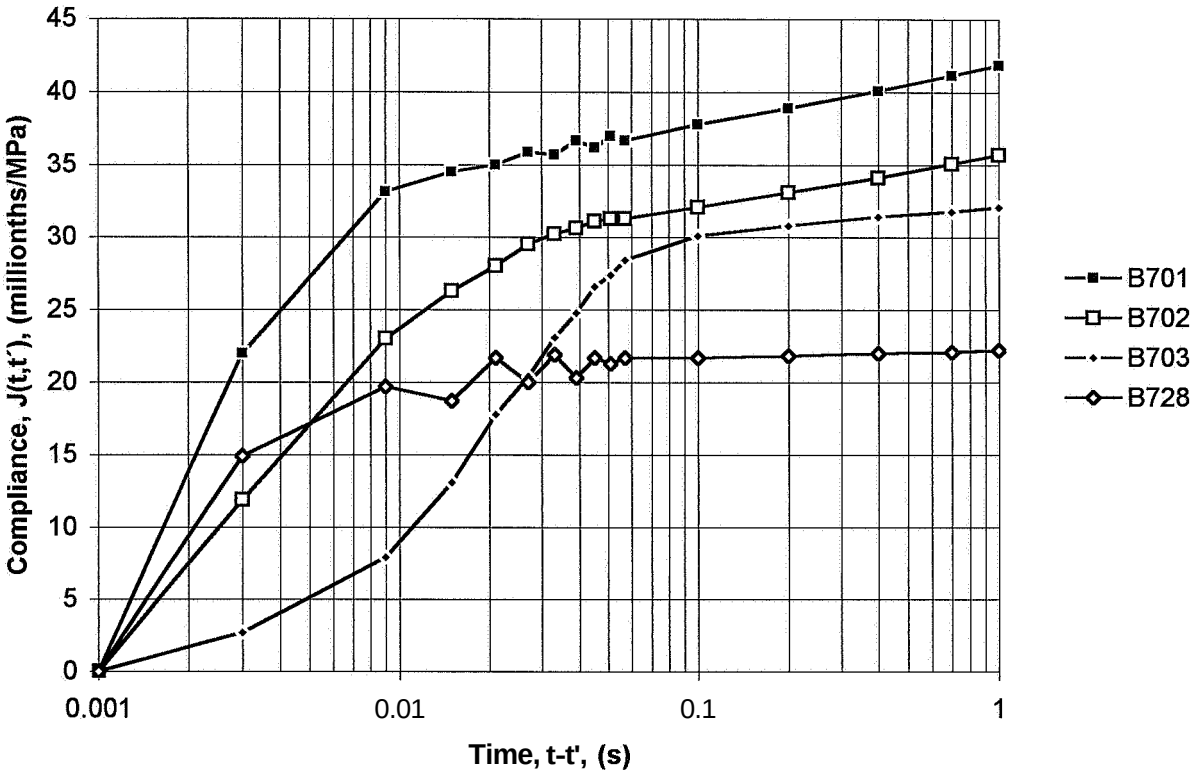

Appendix 6.18 - Quasi-instantaneous compliance of mix 8 subjected to sealed curing

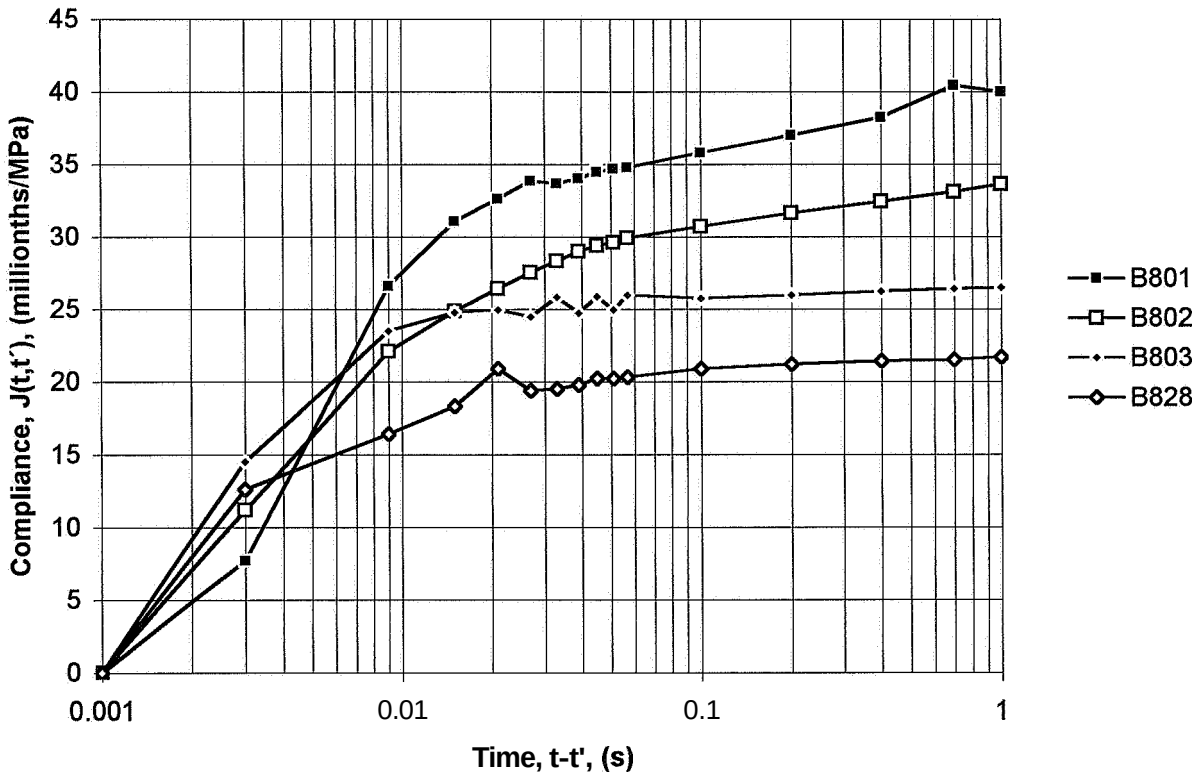

Appendix 6.19 - Quasi-instantaneous compliance creep rate of all mature mixes subjected to sealed curing

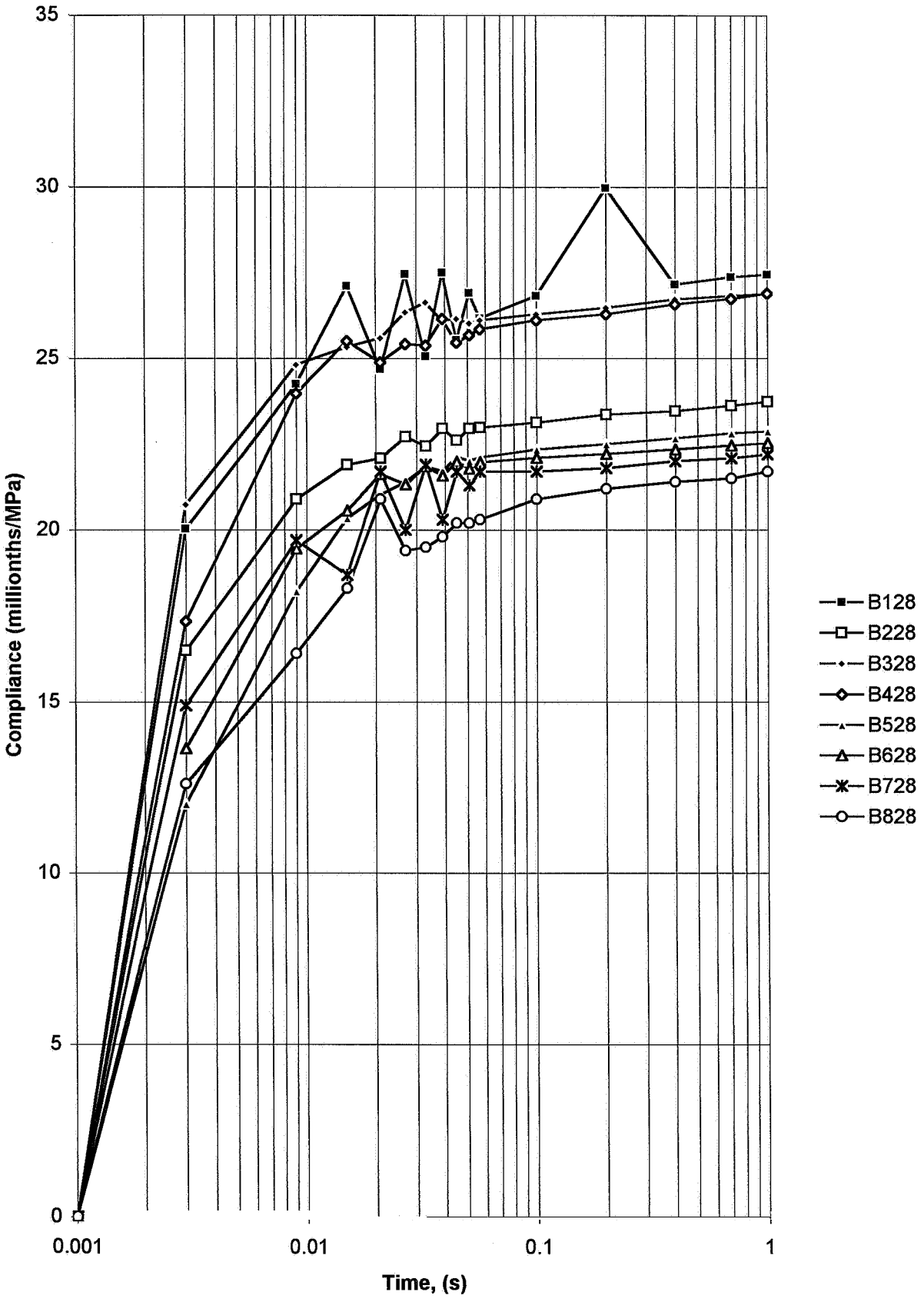

APPENDIX 7. DEFORMATION MODULUS OF CYLINDERS VERSUS COMPRESSIVE CUBE STRENGTH

Appendix 7.1 - Deformation modulus with varying eccentricity of loading.
Appendix 7.2 - Deformation modulus versus cube strength 0.01 s after loading.
Appendix 7.3 - Deformation modulus versus cube strength 0.1 s after loading.
Appendix 7.4 - Deformation modulus versus cube strength 1 s after loading.

Symbols:

e denotes the eccentricity of loading provided elastic conditions

Appendix 7.1 - Deformation modulus with varying eccentricity of loading

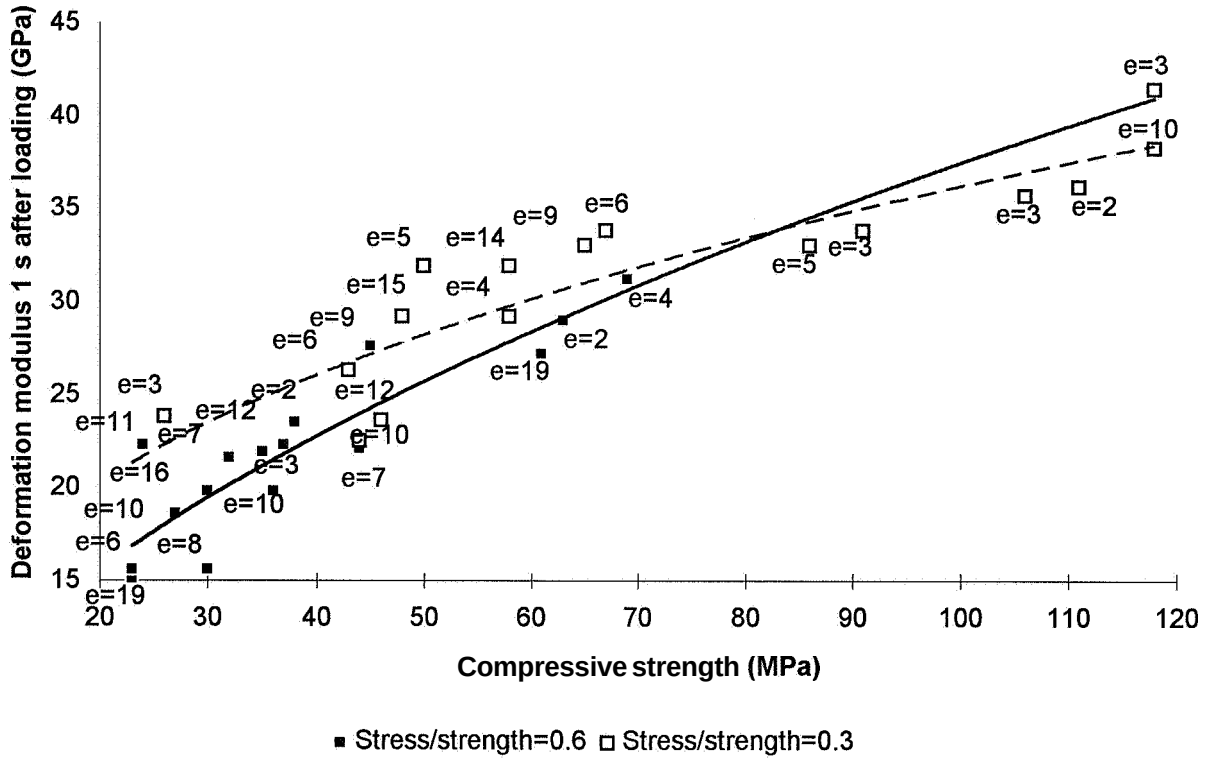

Appendix 7.2 - Deformation modulus versus cube strength 0.01 s after loading

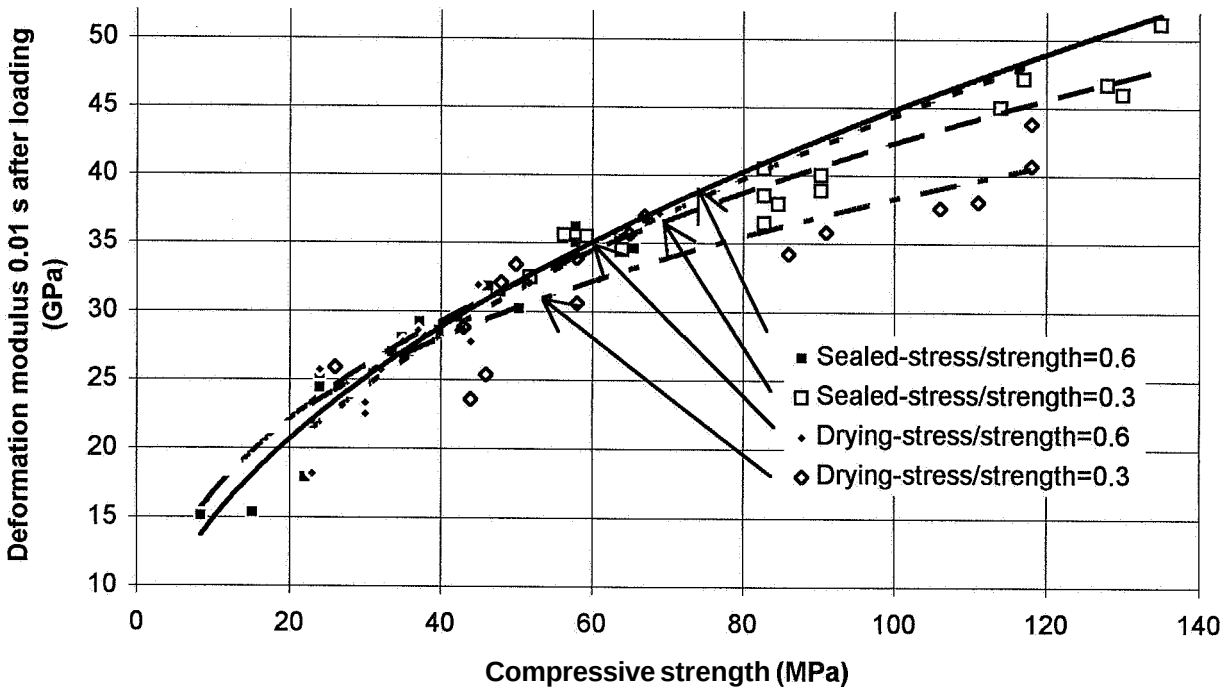

Appendix 7.3 - Deformation modulus versus cube strength 0.1 s after loading;

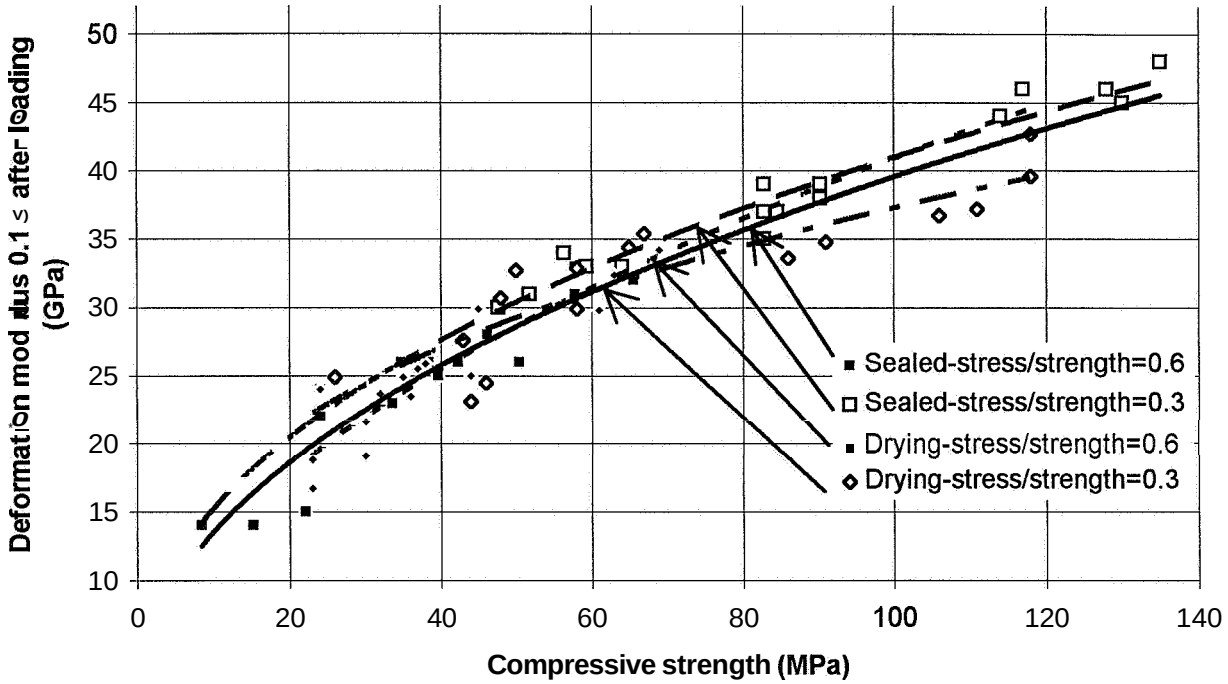

Appendix 7.4 - Deformation modulus versus cube strength 1 s after loading

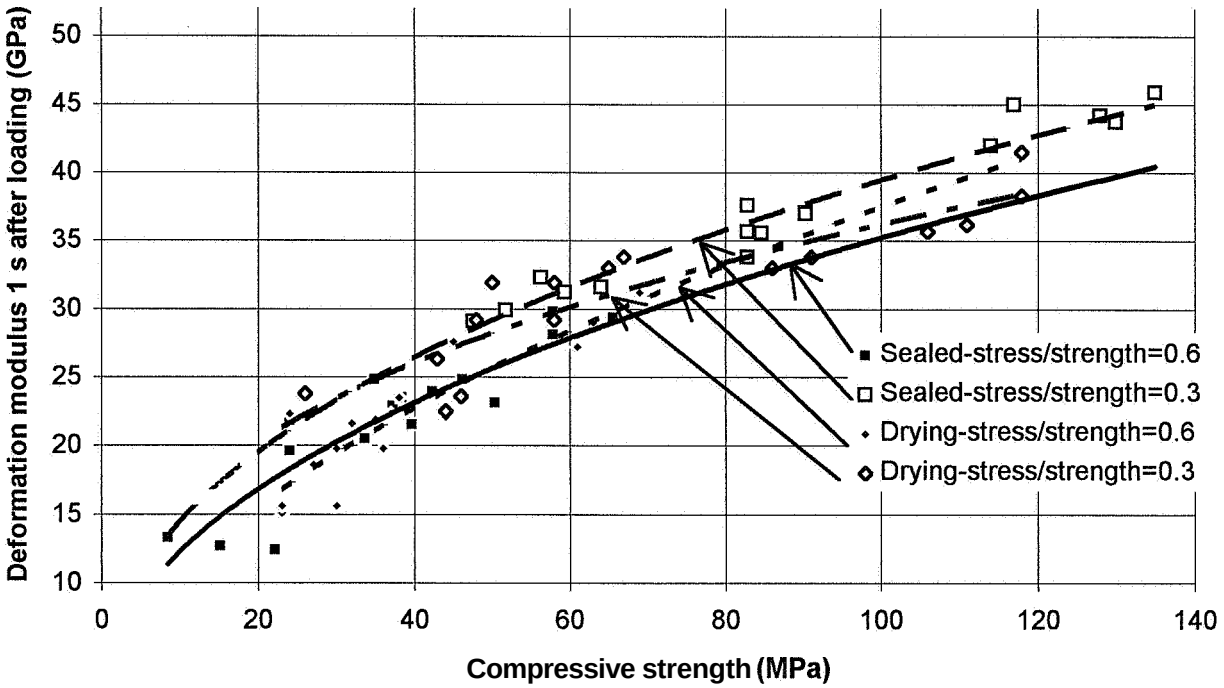

APPENDIX 8. SHRINKAGE AND LOSS OF WEIGHT OF CYLINDERS

Appendix 8.38 - Autogenous shrinkage of mix *6* versus loss of weight after short-term creep
Appendix 8.39 - Autogenous shrinkage of mix **7** versus loss of weight after short-term creep
Appendix 8.40 - Autogenous shrinkage of mix 8 versus loss of weight after short-term creep

Symbols:

w	denotes the mixing water of the concrete
w_e	denotes the evaporated water
.B..	denotes basic creep (sealed curing)
.D..	denotes drying creep (RH= 55%)
6...	denotes mix *6*
...01	age at loading: 1 day; stresslcylinder strength ratio: 0.84
...02	age at loading: 2 days; stresslcylinder strength ratio: 0.84
...03	age at loading: 2 days; stresslcylinder strength ratio: 0.42
...28	age at loading: 28 days; stresslcylinder strength ratio: 0.42

Appendix 8.1 - Shrinkage of mix 1 versus time

Appendix 8.2 - Shrinkage of mix 2 versus time

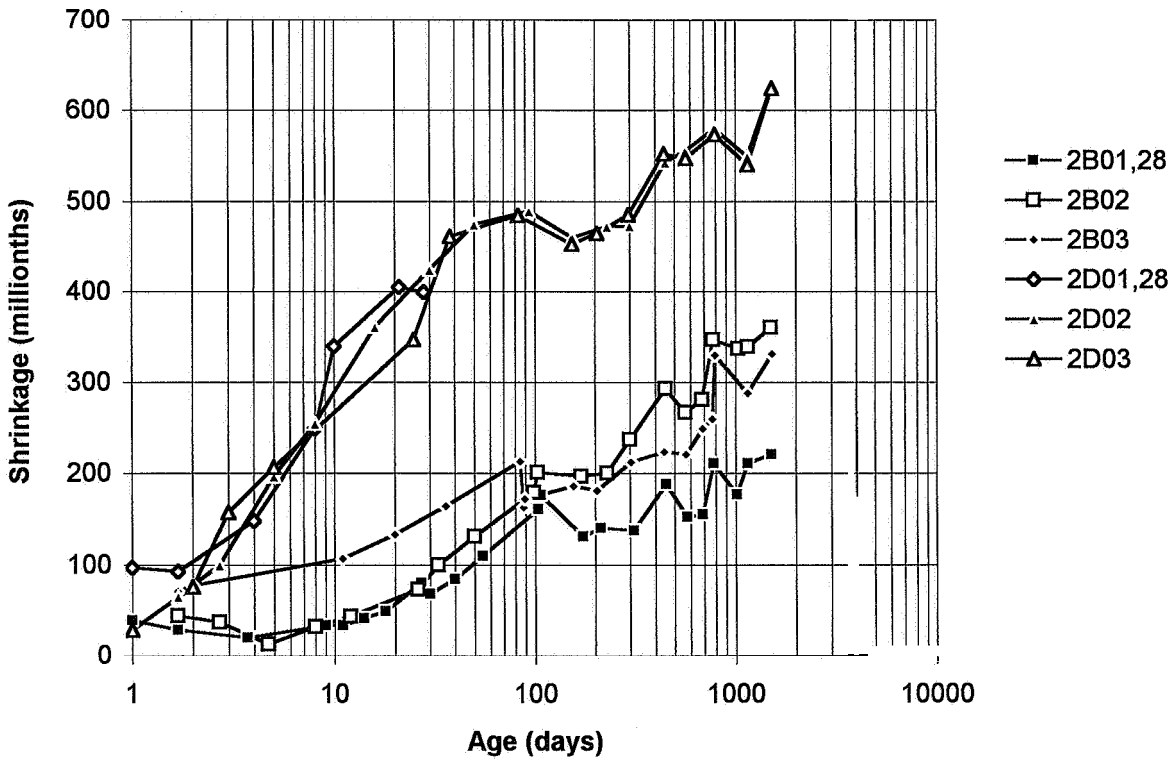

Appendix 8.3 - Shrinkage of mix 3 versus time

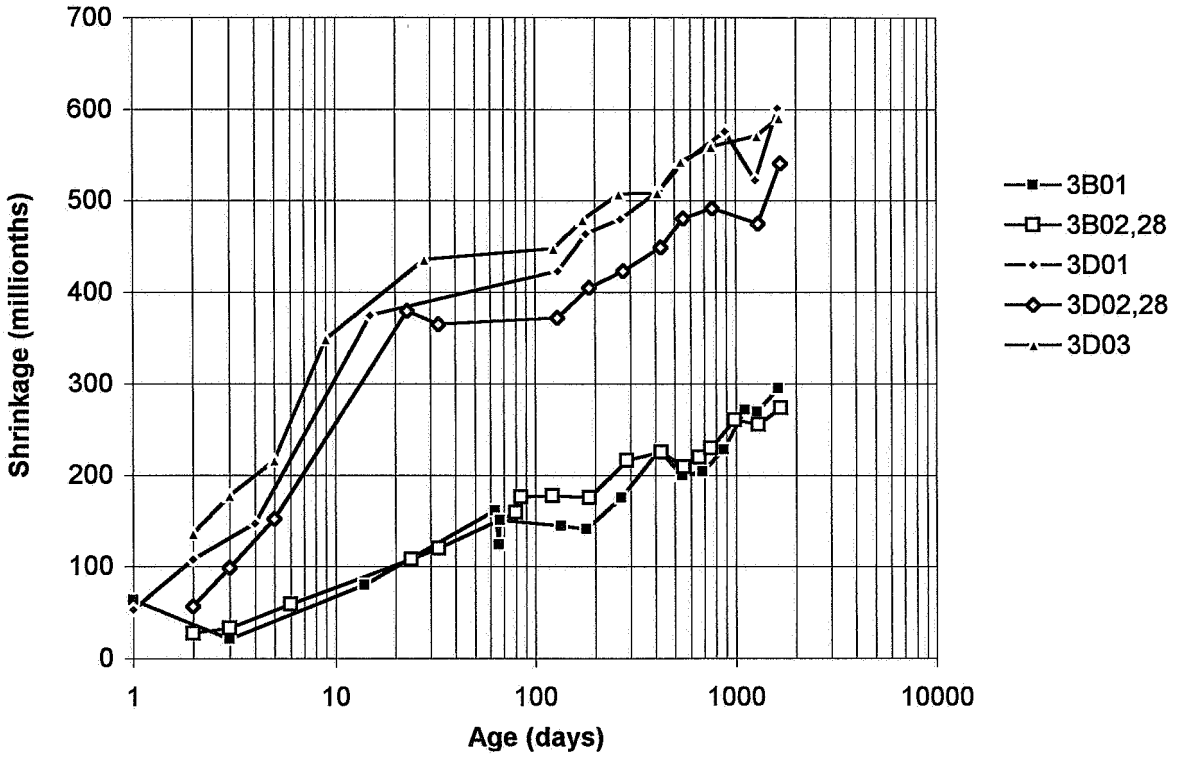

Appendix 8.4 - Shrinkage of mix 4 versus time

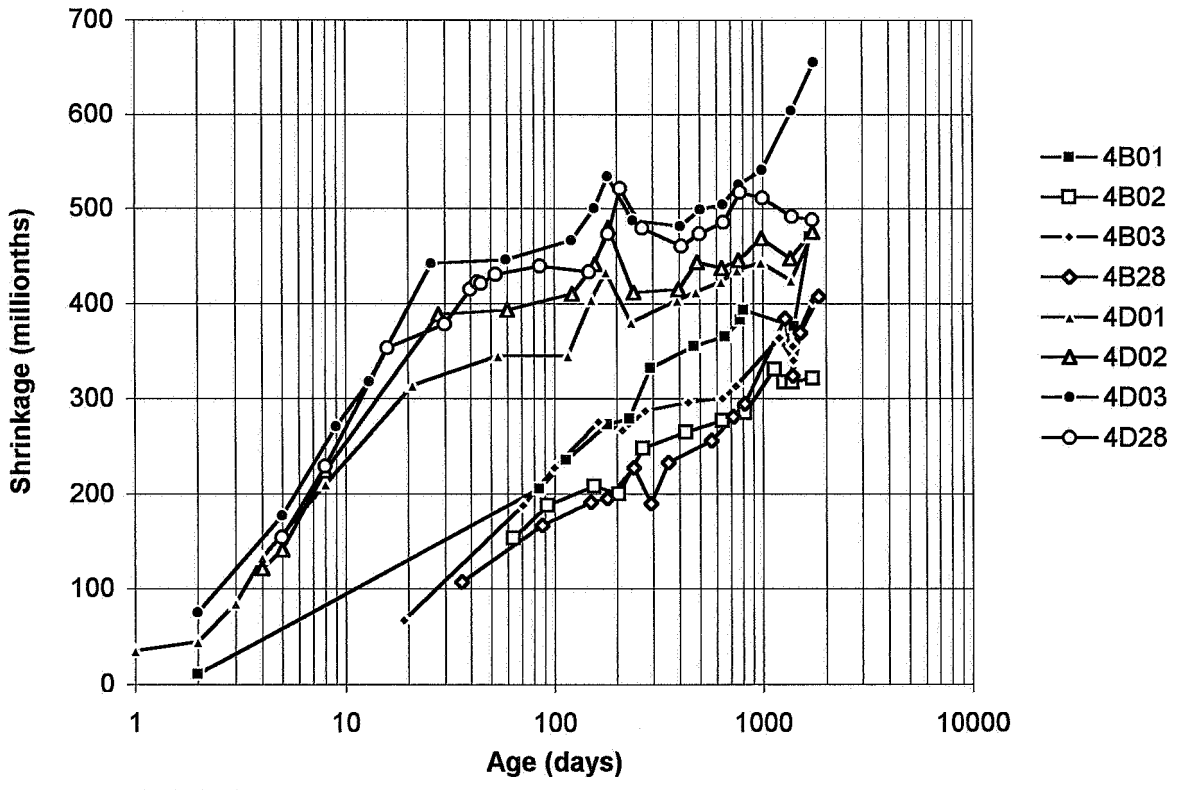

Appendix 8.5 - Shrinkage of mix 5 versus time

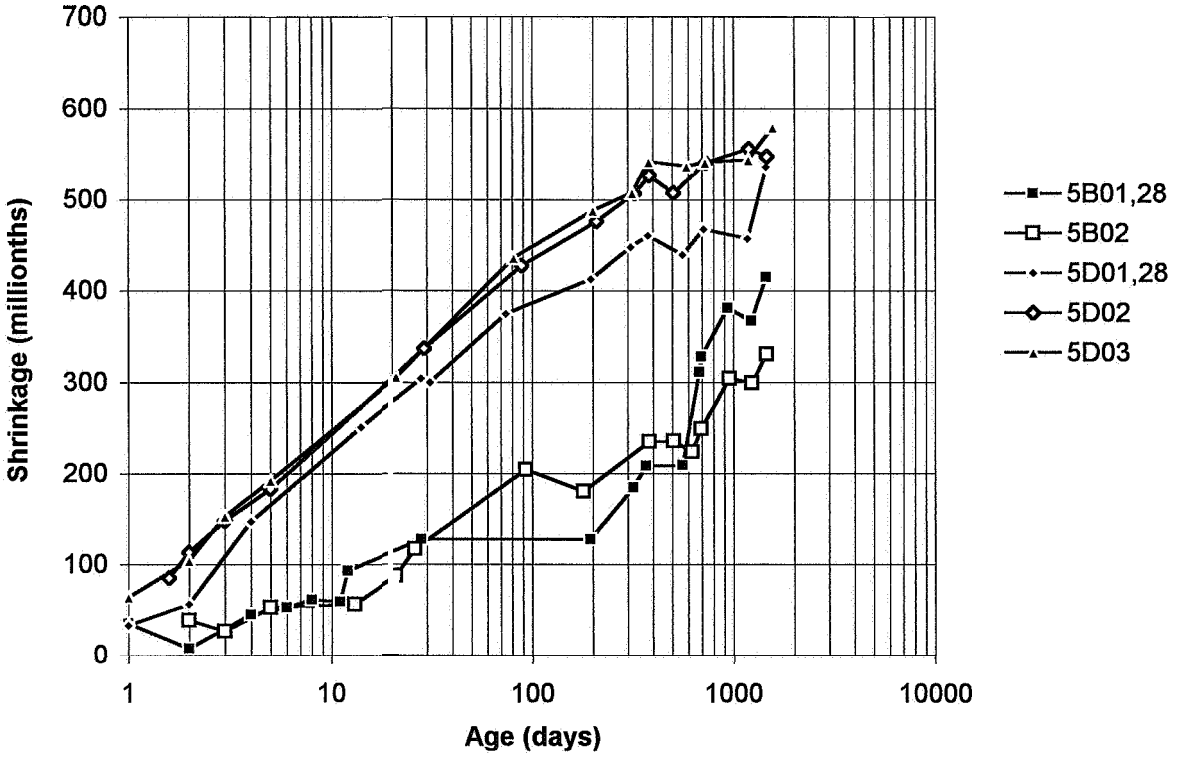

Appendix 8.6 - Shrinkage of mix 6 versus time

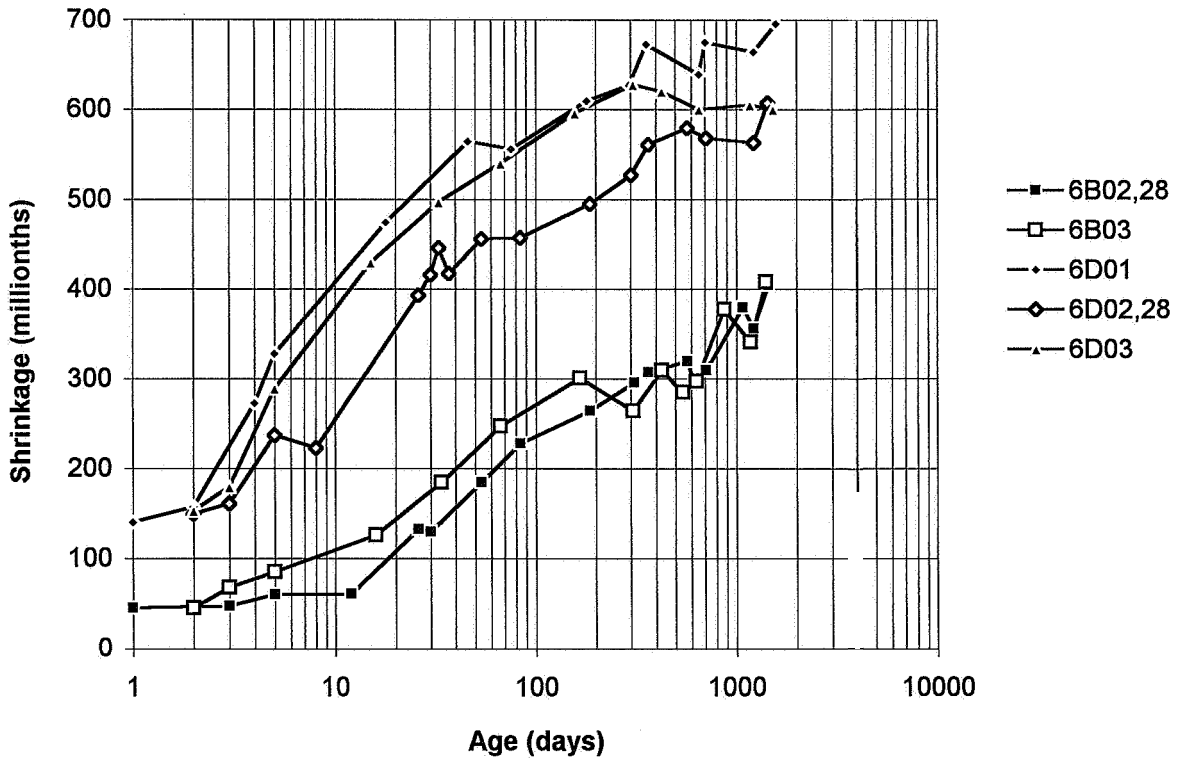

Appendix 8.7 - Shrinkage of mix 7 versus time

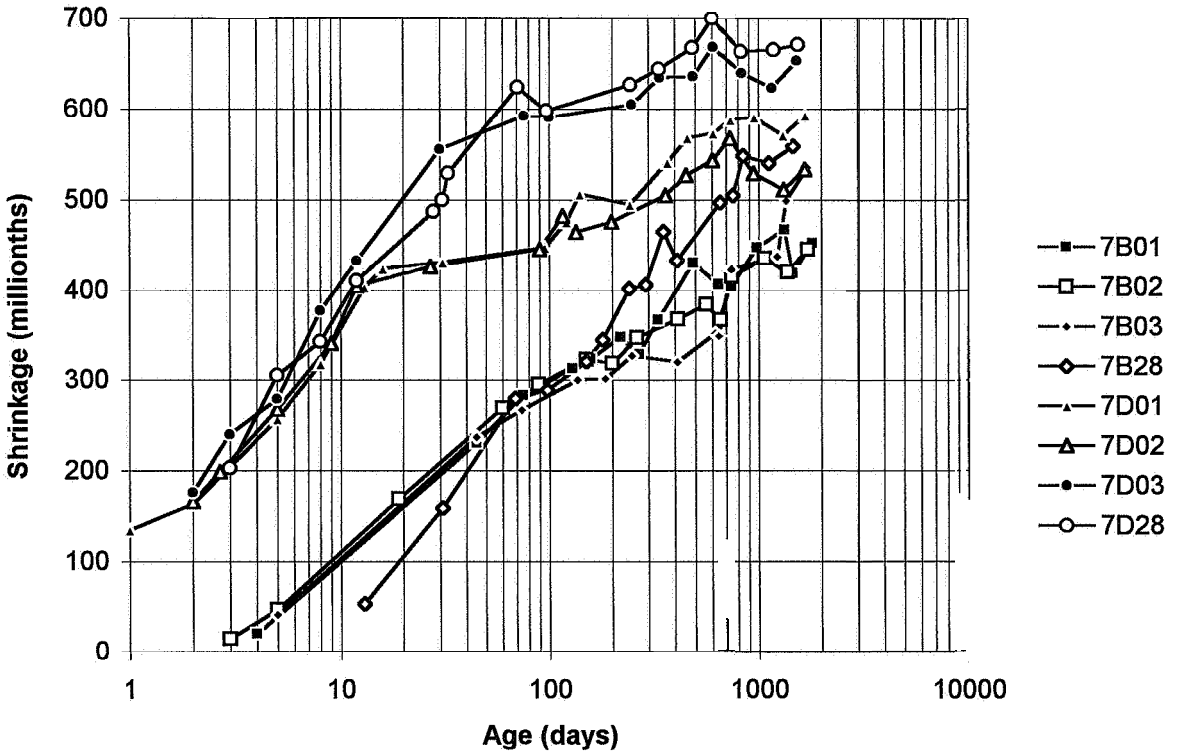

Appendix 8.8 - Shrinkage of mix 8 versus time

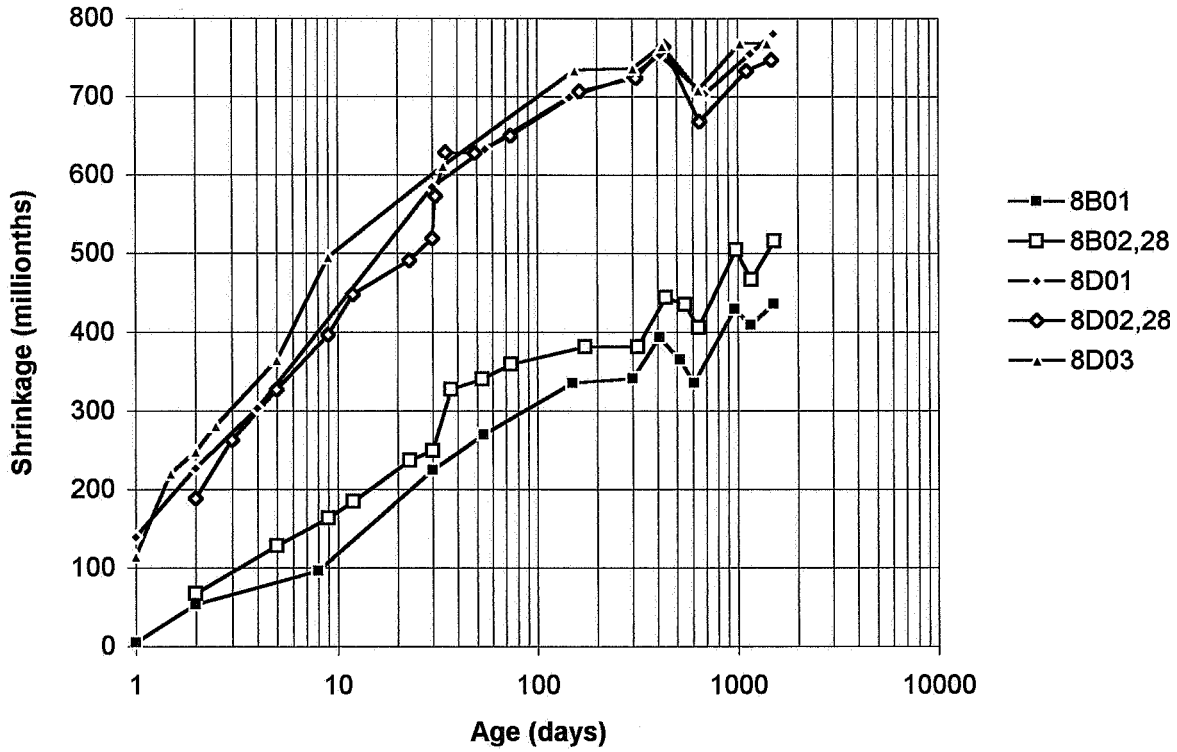

Appendix 8.9 - Loss of weight of mix 1 versus time

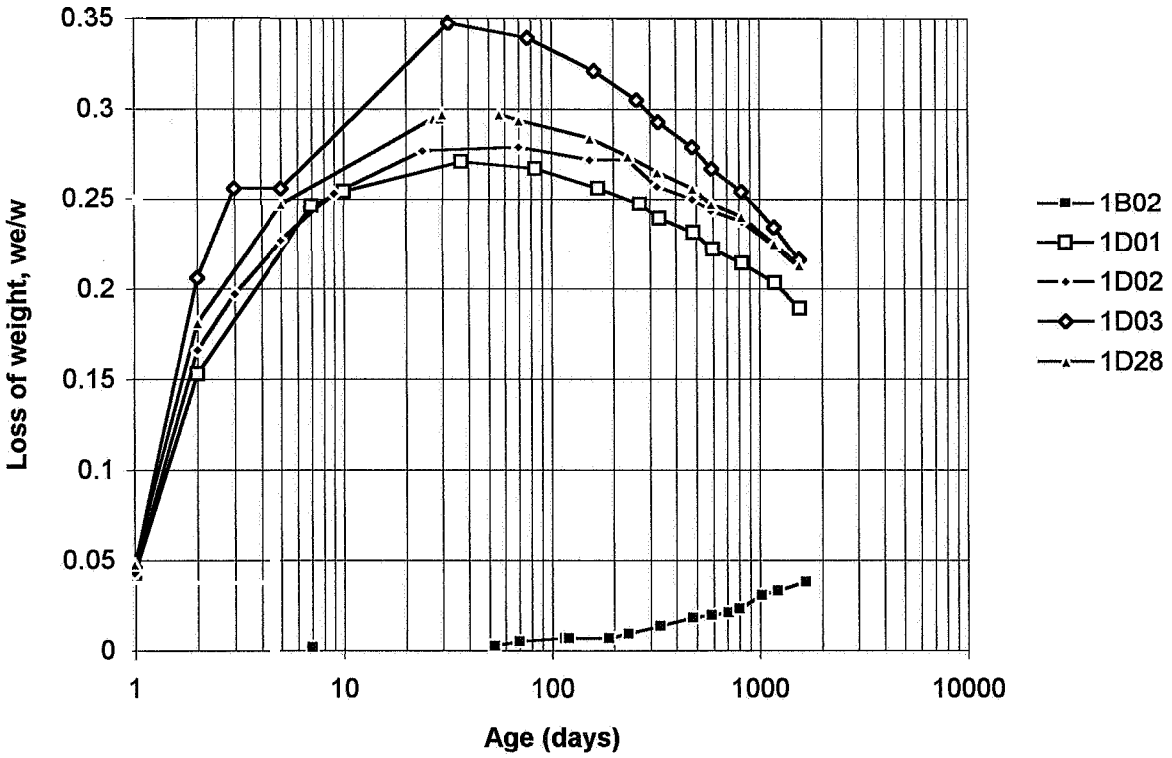

Appendix 8.10 - Loss of weight of mix 2 versus time

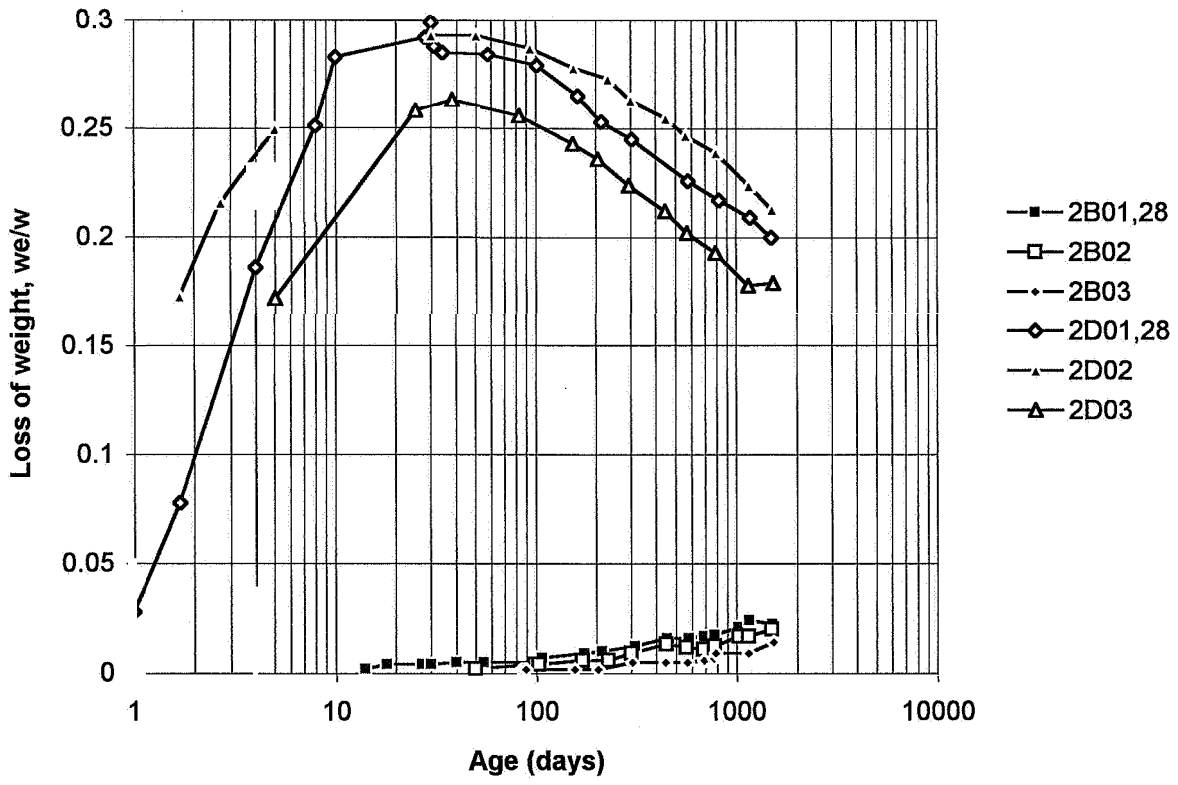

Appendix 8.11 - L of weight f i 3 versus ime

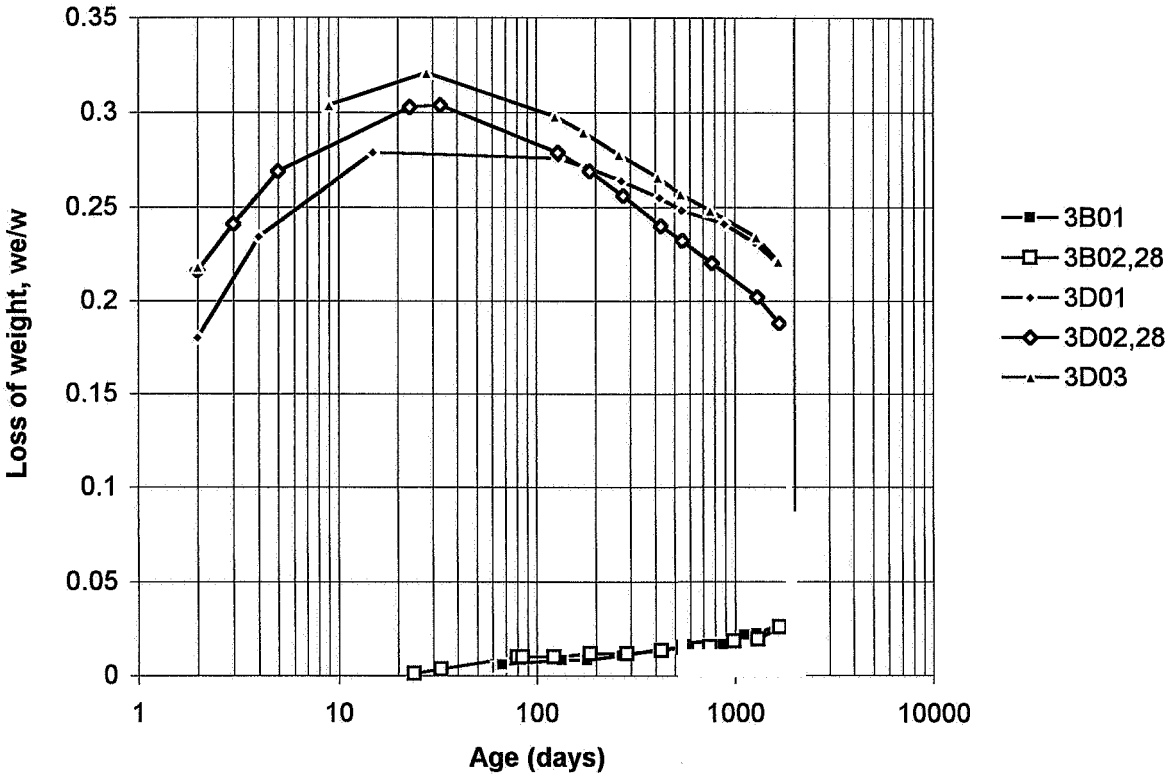

Appendix 8.12 - Loss of weight of mix 4 versus time

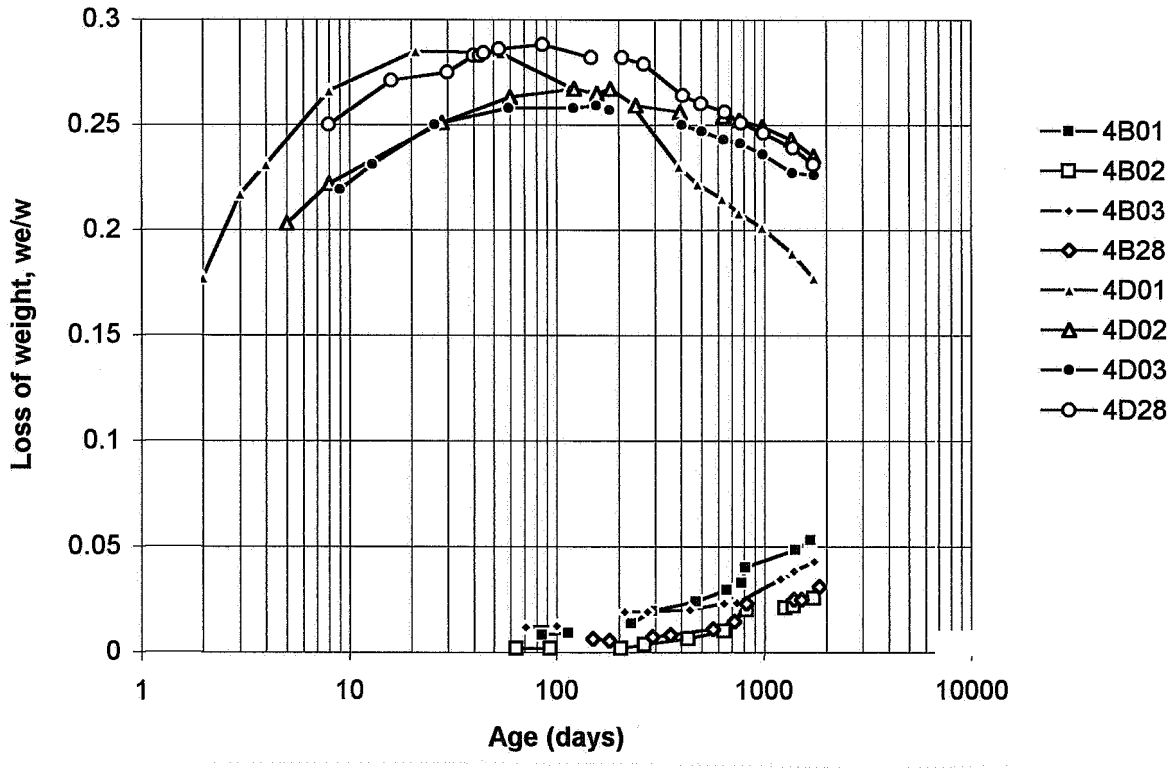

Appendix 8.13 · Loss of weight of mix 5 versus time

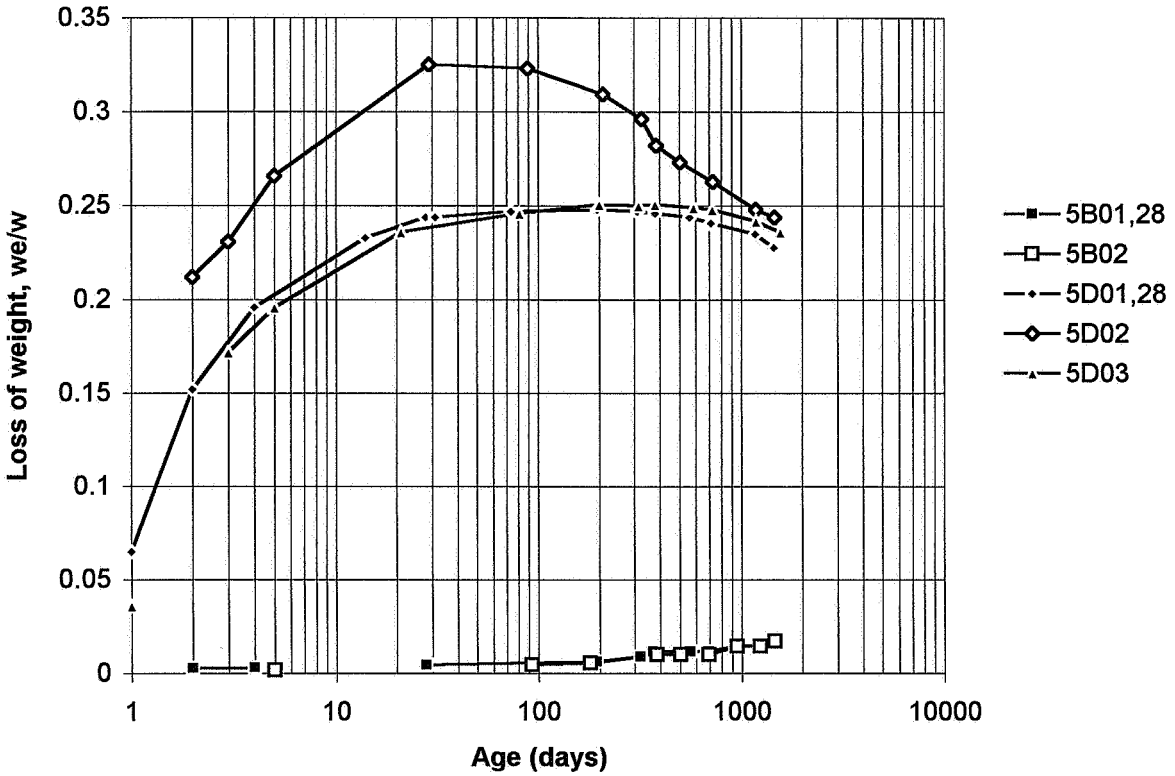

Appendix 8.14 - Loss of weight of mix 6 versus time

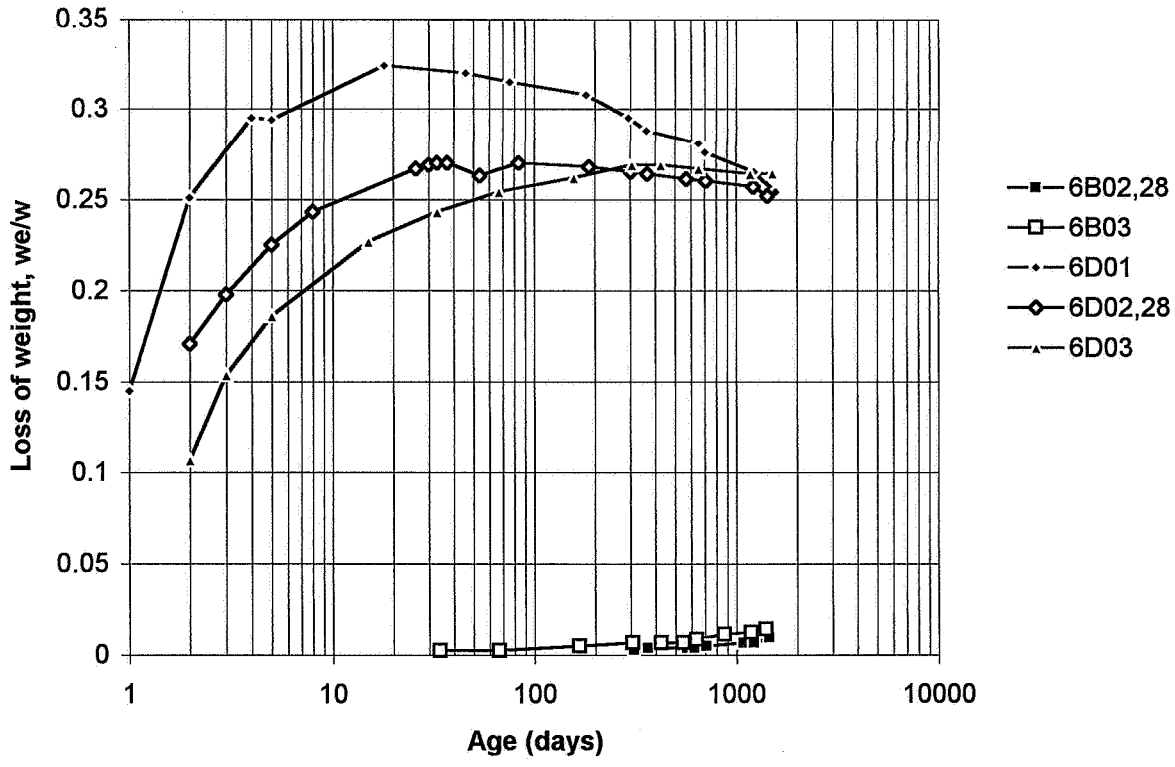

Appendix 8 - Loss of ght of mix 7 versus time

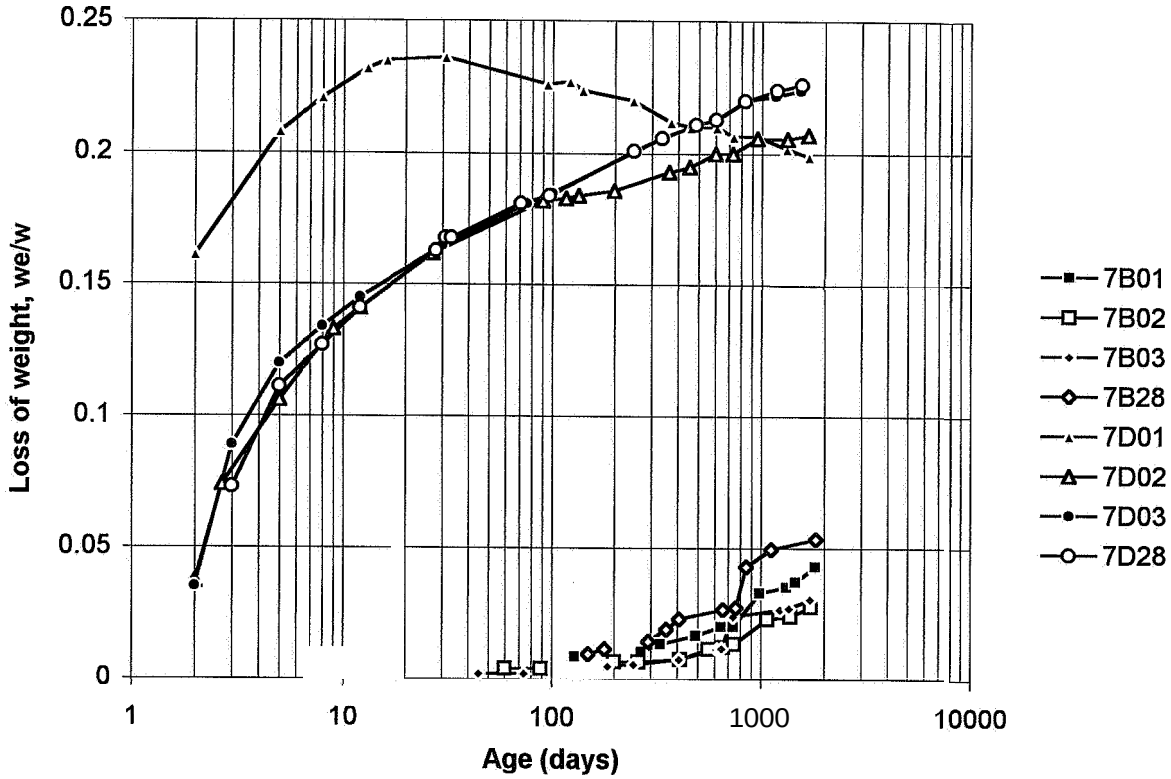

Appendix 8.16 - Loss of weight of mix 8 versus time

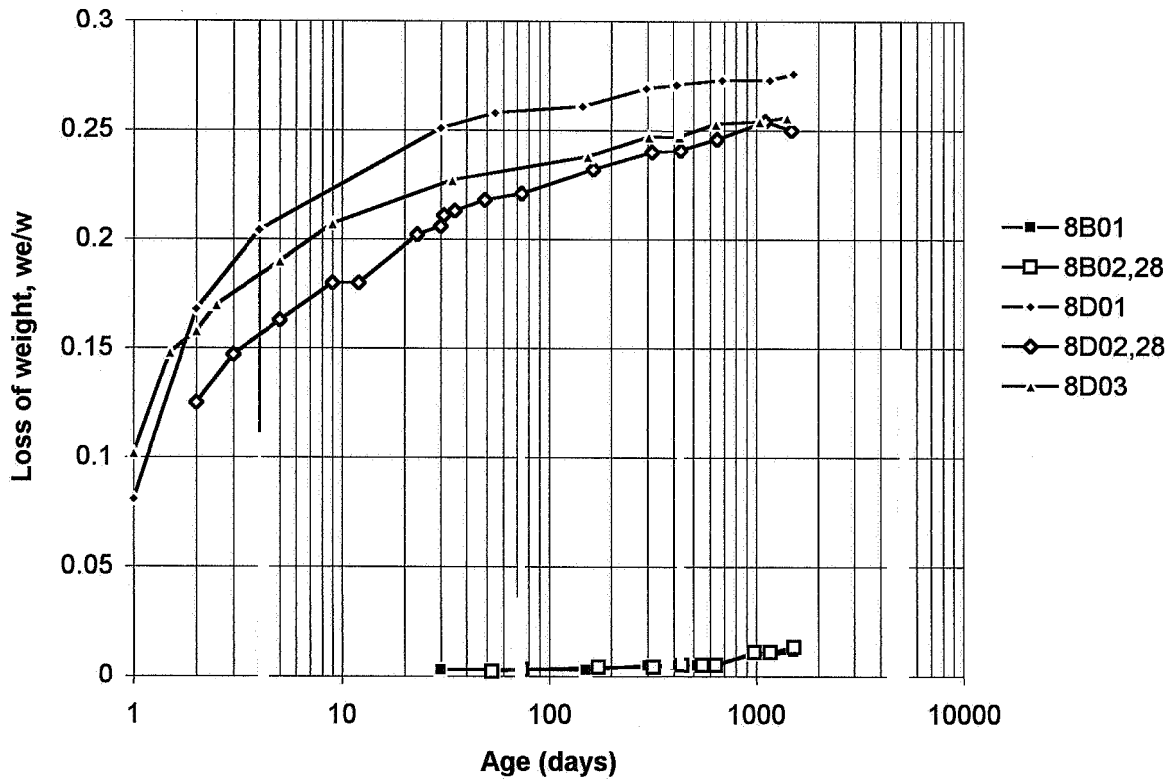

Appendix 8 - Shrinkage of mix 1 versus loss of weight

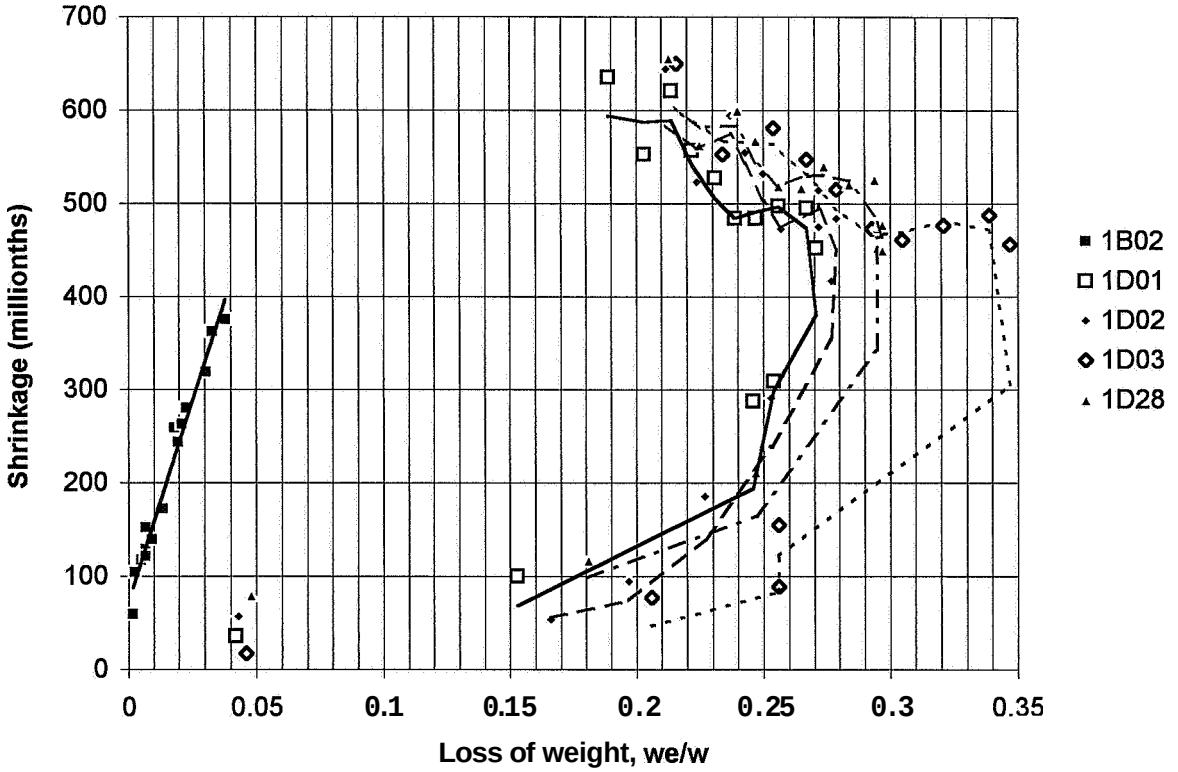

Appendix 8.18 - Shrinkage of mix 2 versus loss of weight

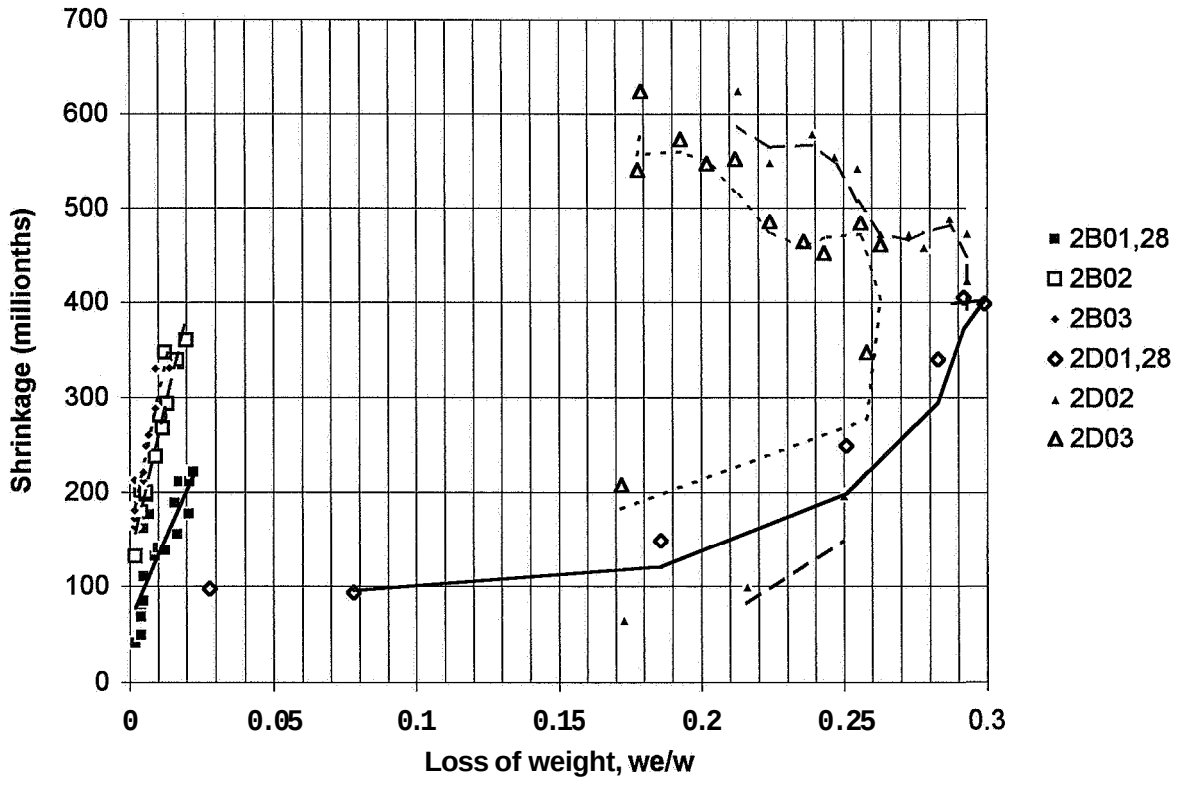

Appendix 8.19 - Shrinkage of mix 3 versus loss of weight

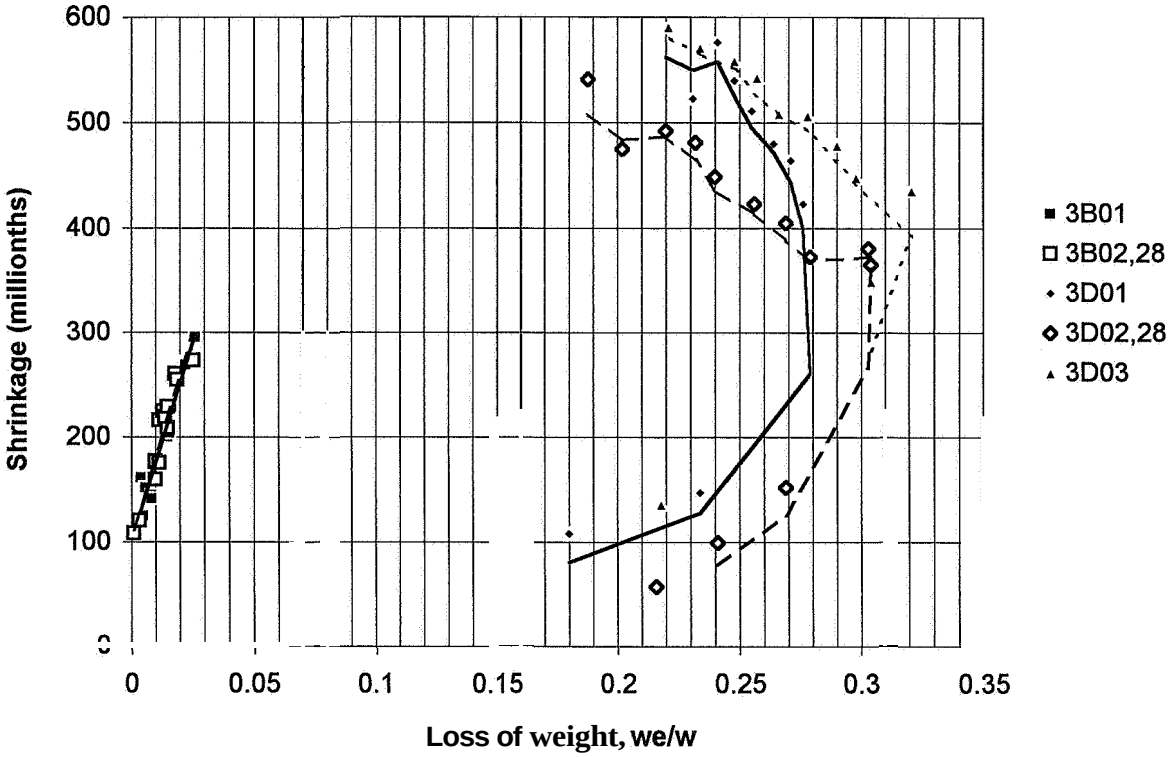

Appendix 8.20 - Shrinkage of mix 4 versus loss of weight

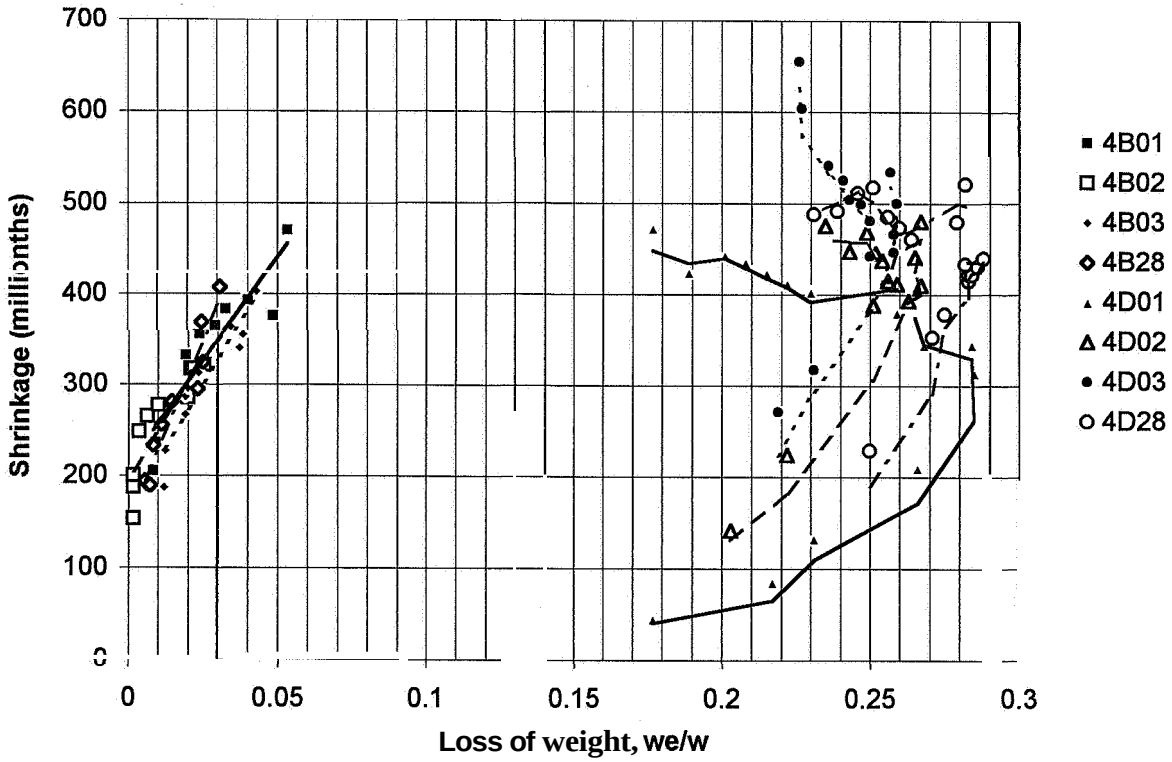

Appendix 8.21 - Shrinkage of mix 5 versus loss of weight

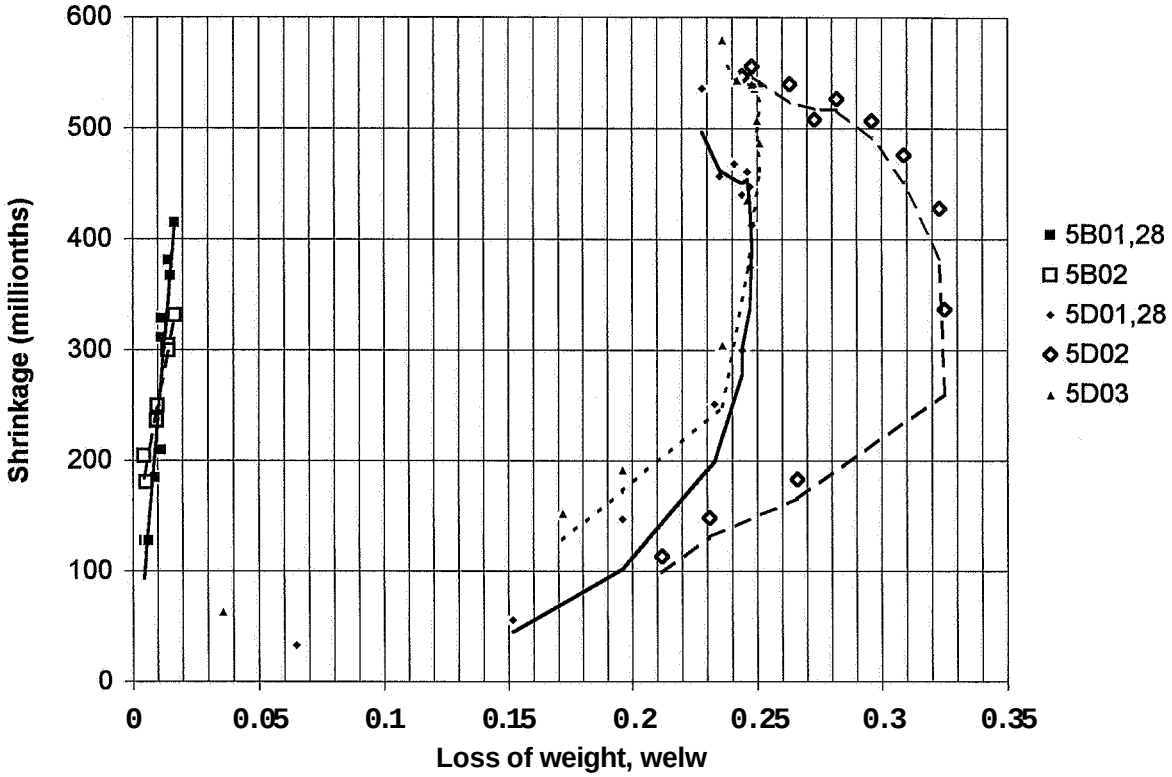

Appendix 8.22 - Shrinkage of mix 6 versus loss of weight

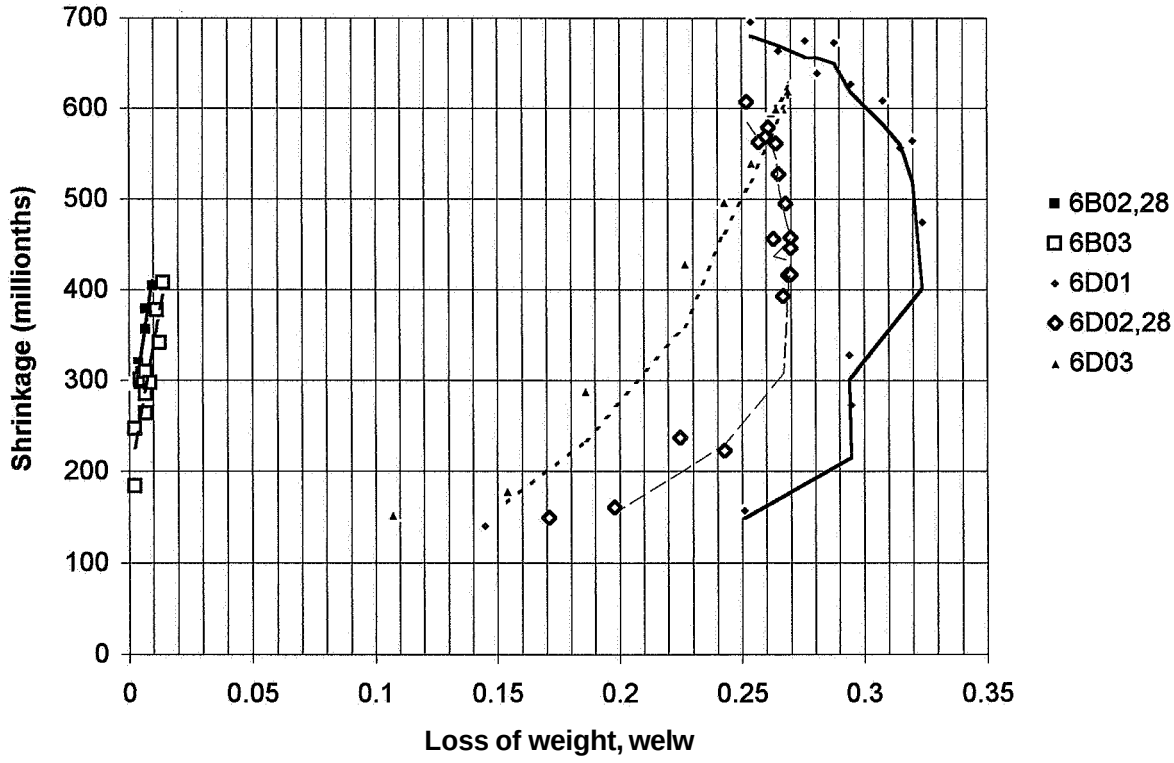

Appendix 8.23 - Shrinkage of mix 7 versus loss of weight

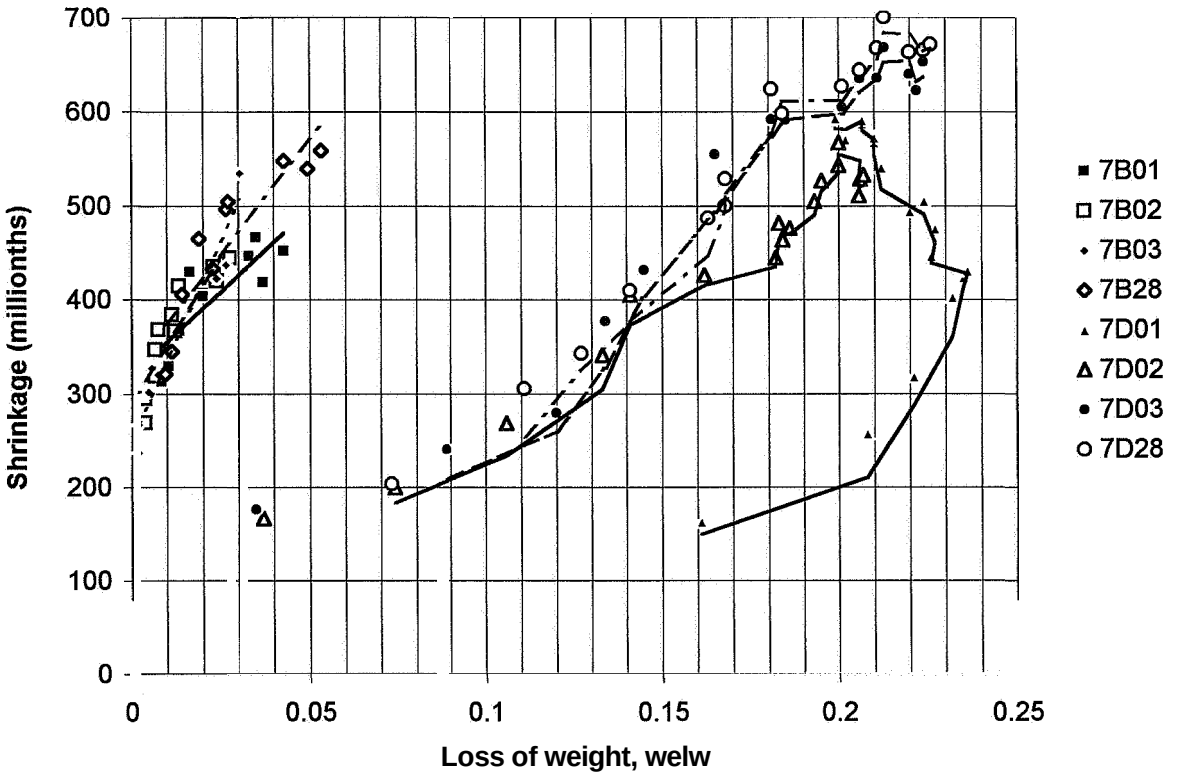

Appendix 8.24 - Shrinkage of mix 8 versus loss of weight

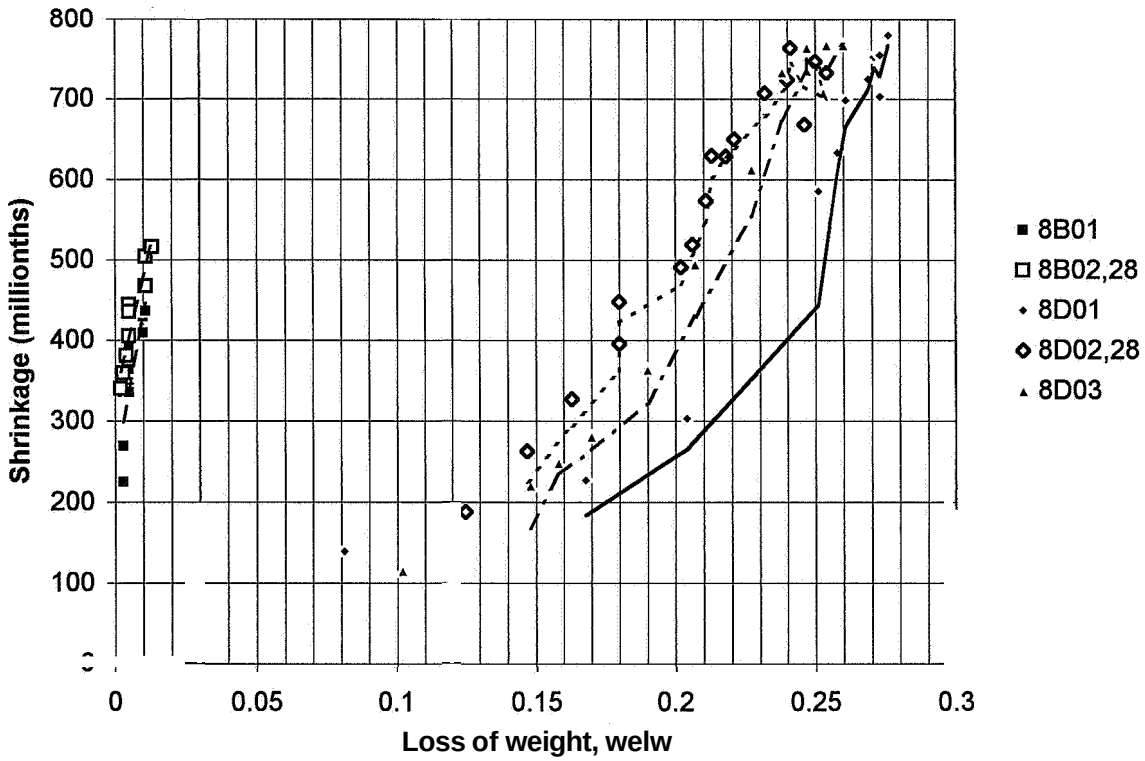

Appendix 8.25 - Autoeenous shrinkage of mix 1 versus time after short-term creep

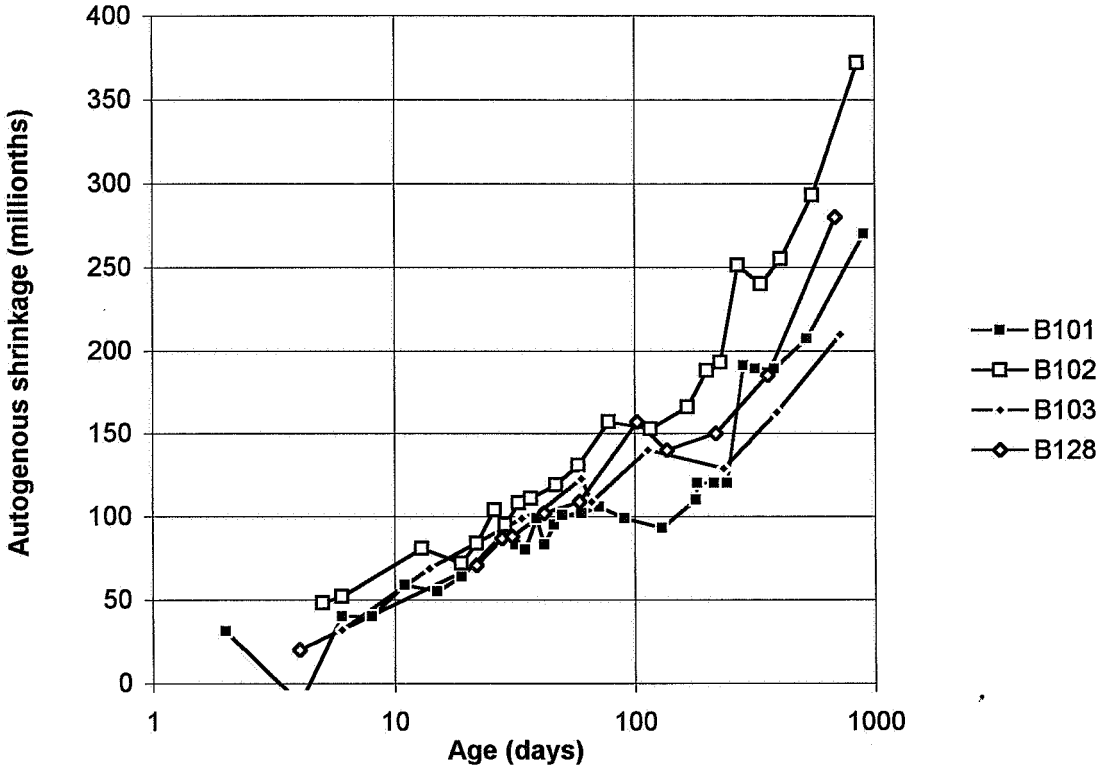

Appendix 8.26 - Autoeenous shrinkage of mix 2 versus time after short-term creep

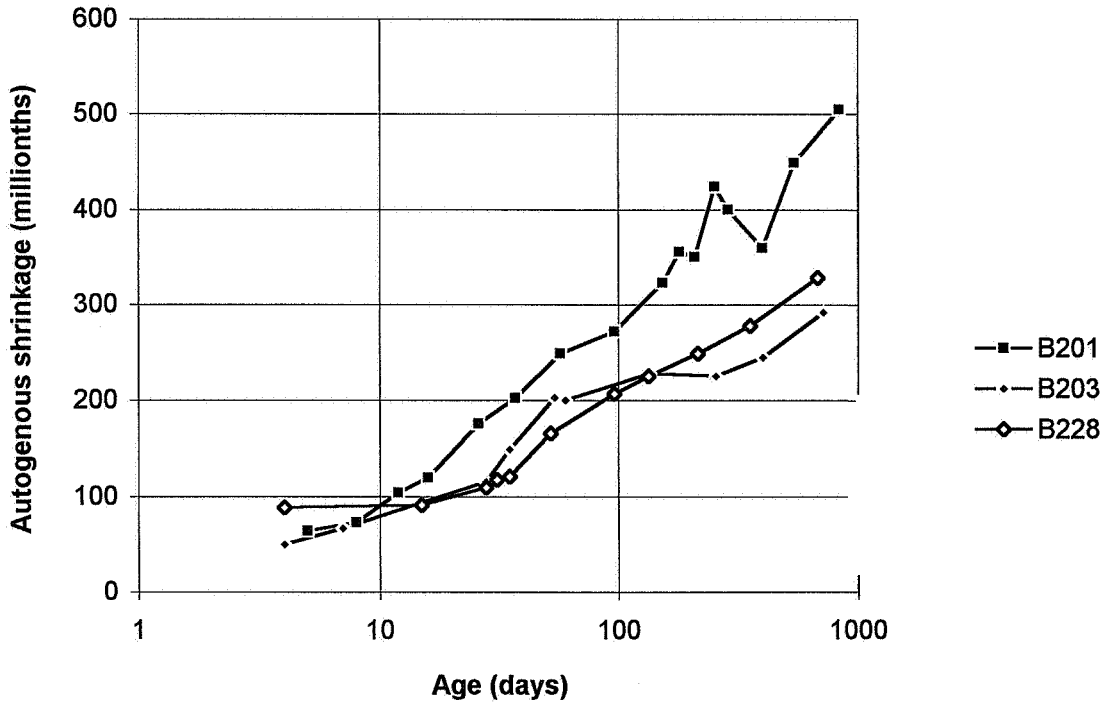

Appendix 8.27 - Autogenous shrinkage of mix 3 versus time after short-term creep

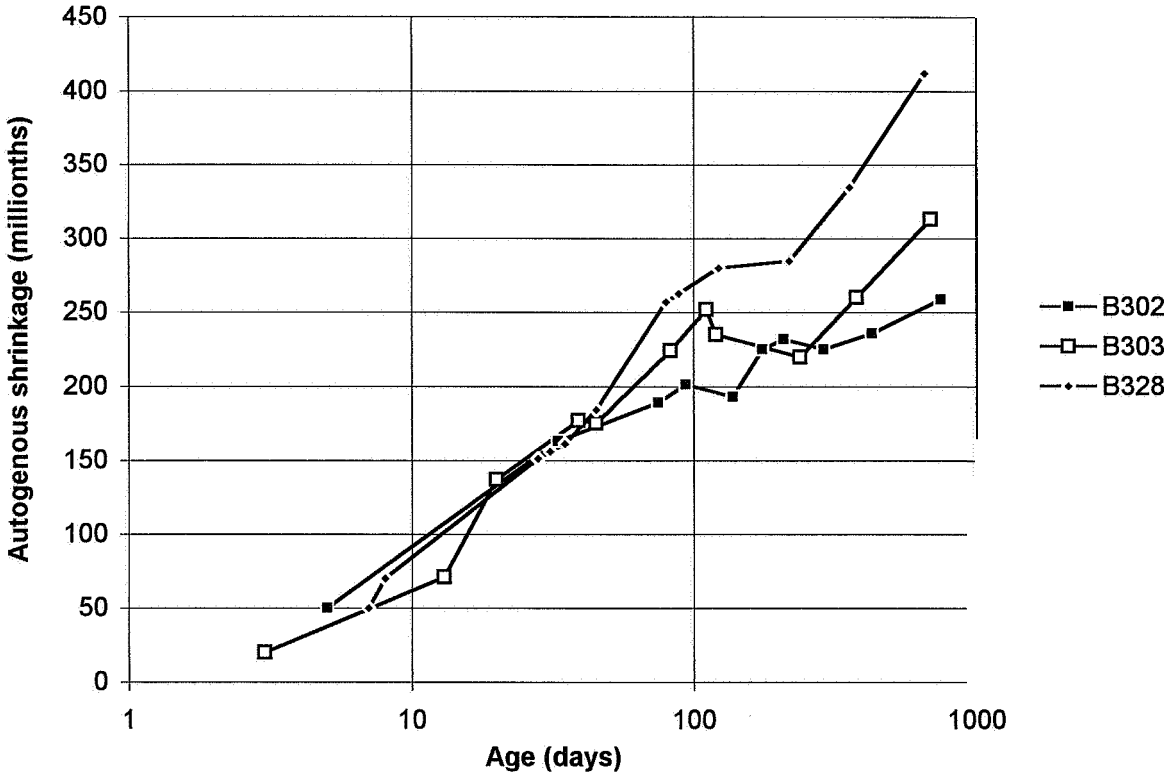

Appendix 8.28 - Autogenous shrinkage of mix 4 versus time after short-term creep

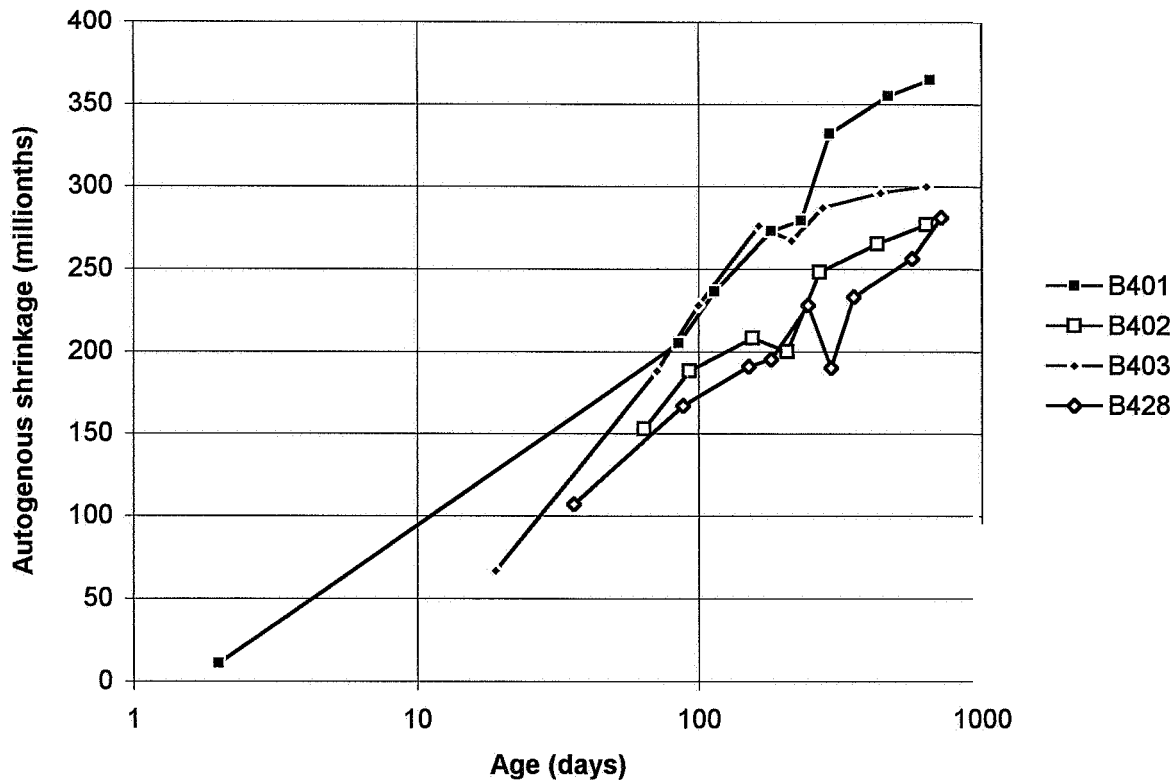

Appendix 8.29 - Autogenous shrinkage of mix 5 versus time after short-term creep

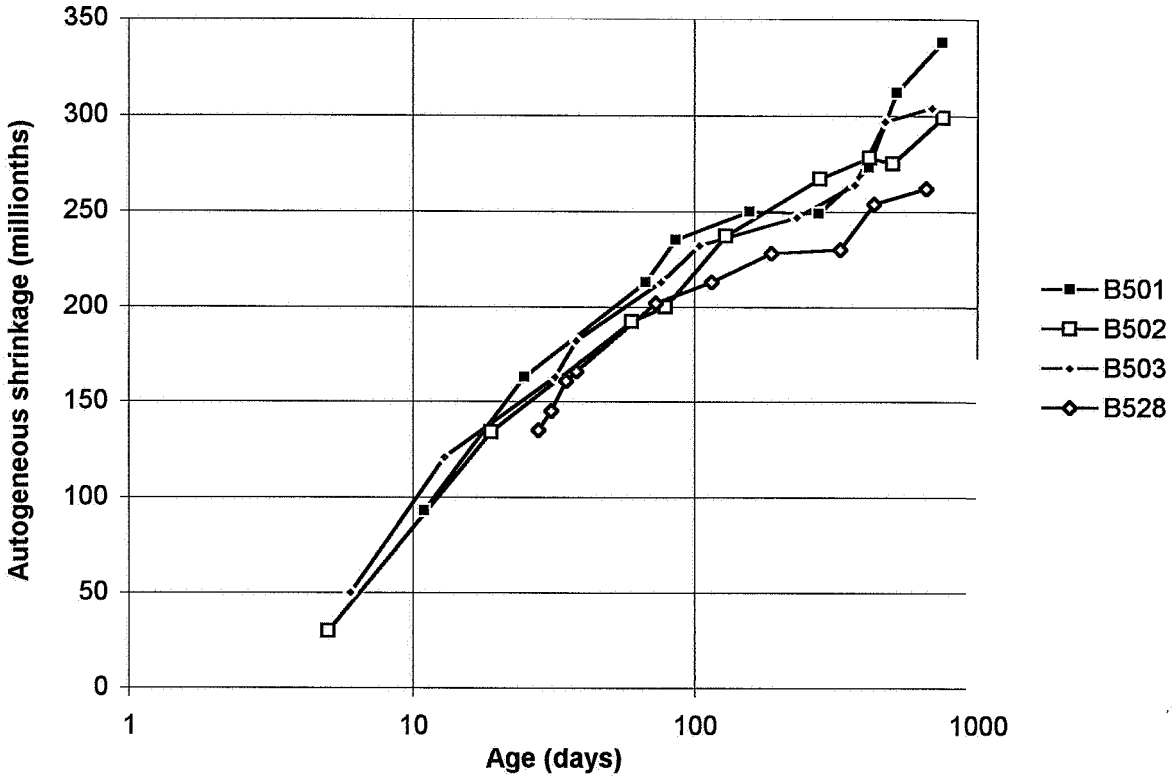

Appendix 8.30 - Autogenous shrinkage of mix 6 versus time after short-term creep

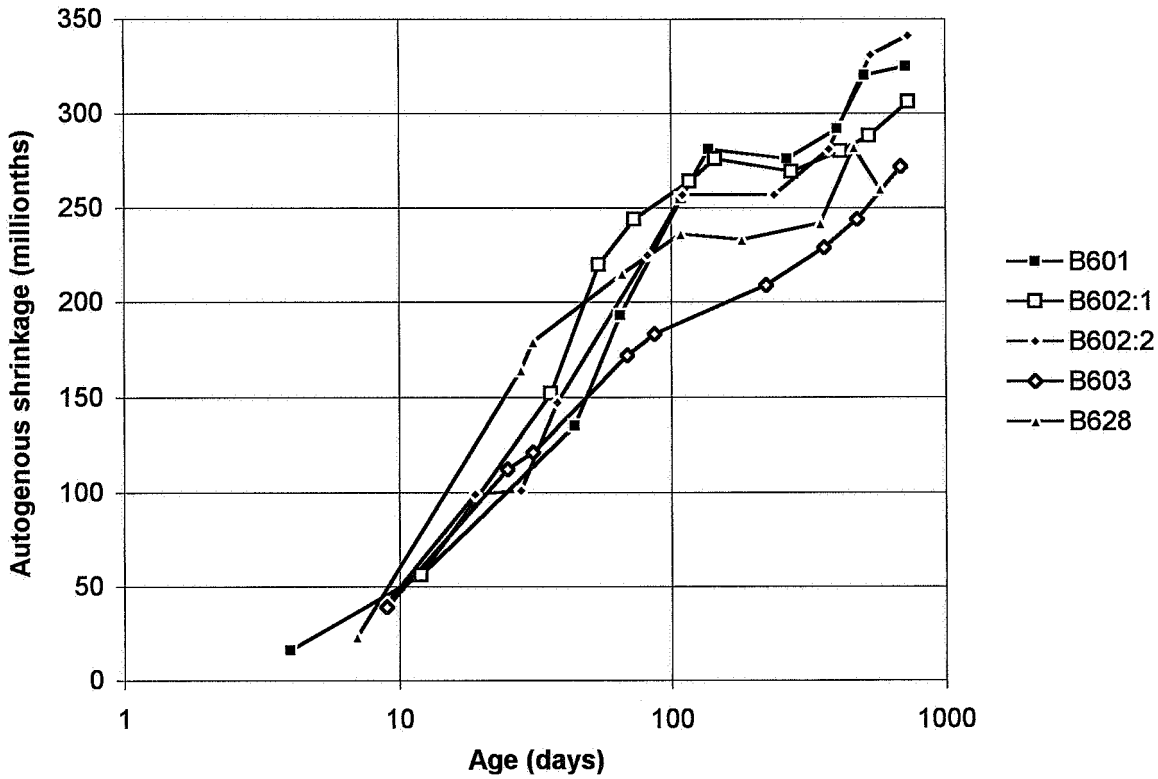

Appendix 8.31 - Autoeenous shrinkage of mix 7 versus time after short-term creep

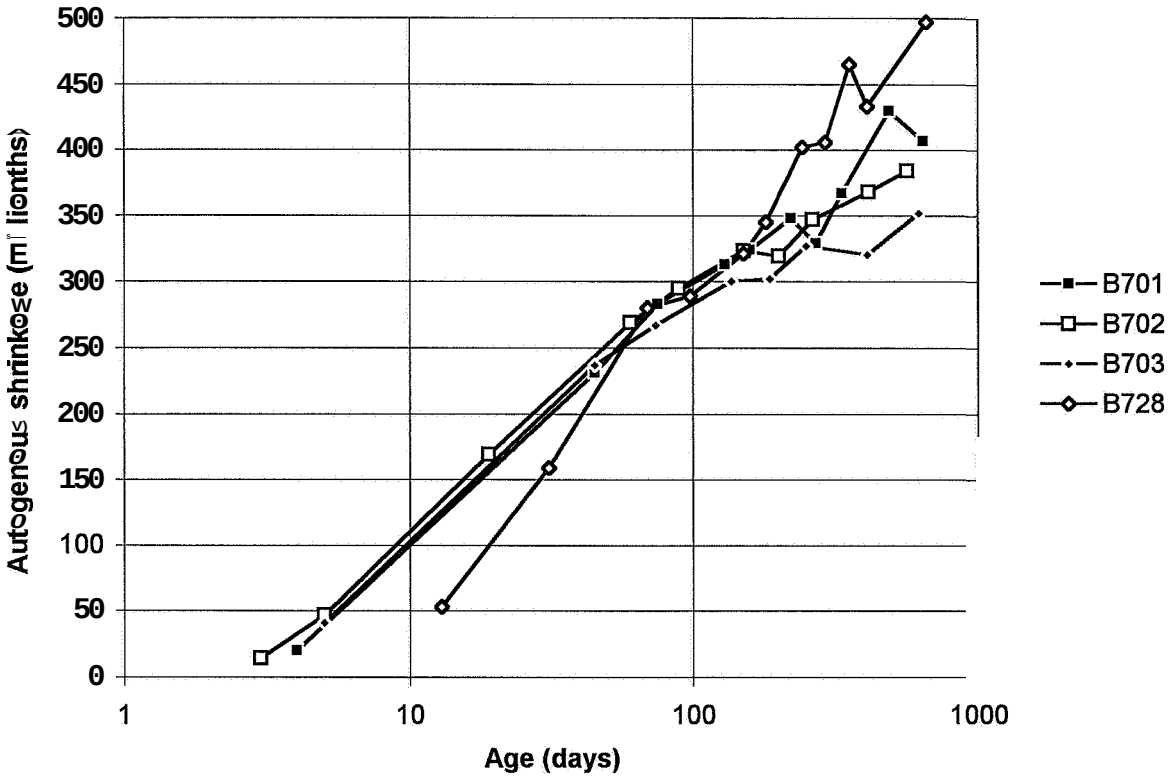

Appendix 8.32 - Autoeenous shrinkage of mix 8 versus time after short-term creep

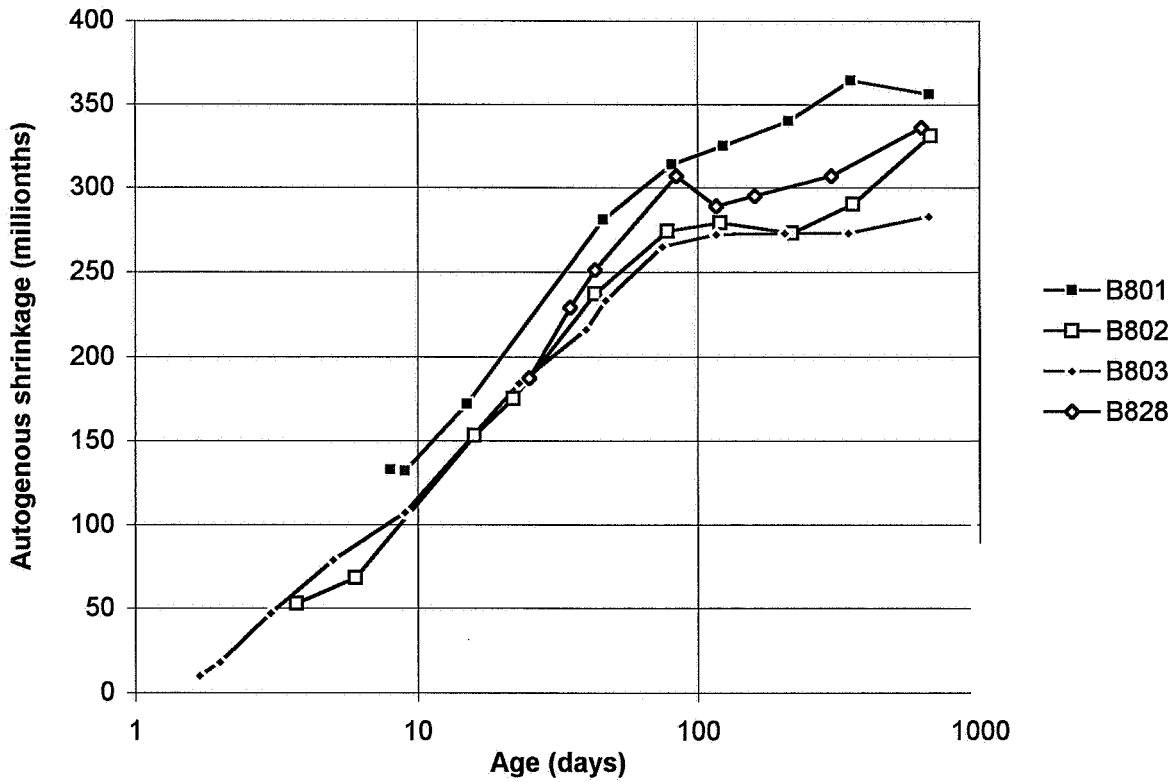

Appendix 8.33 - Autoeenous shrinkage of mix 1 versus loss of weight after short-term creep

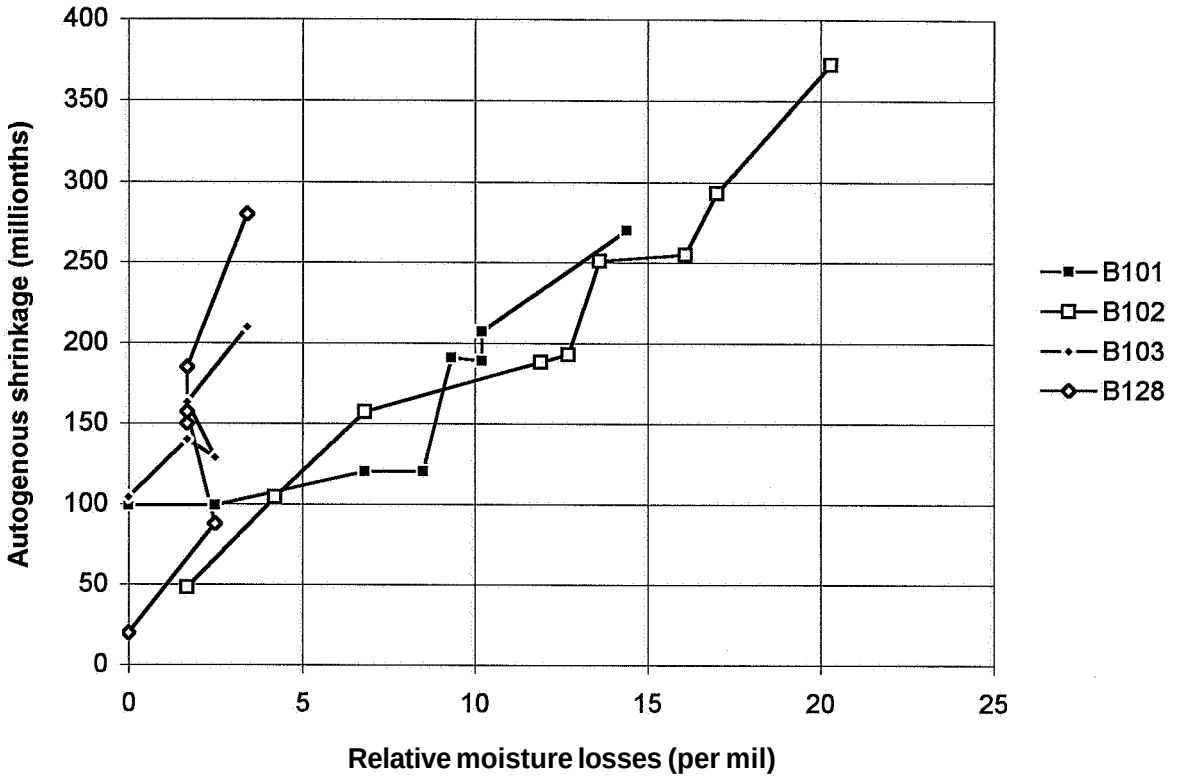

Appendix 8.34 - Autogenous shrinkage of mix 2 versus loss of weight after short-term creep

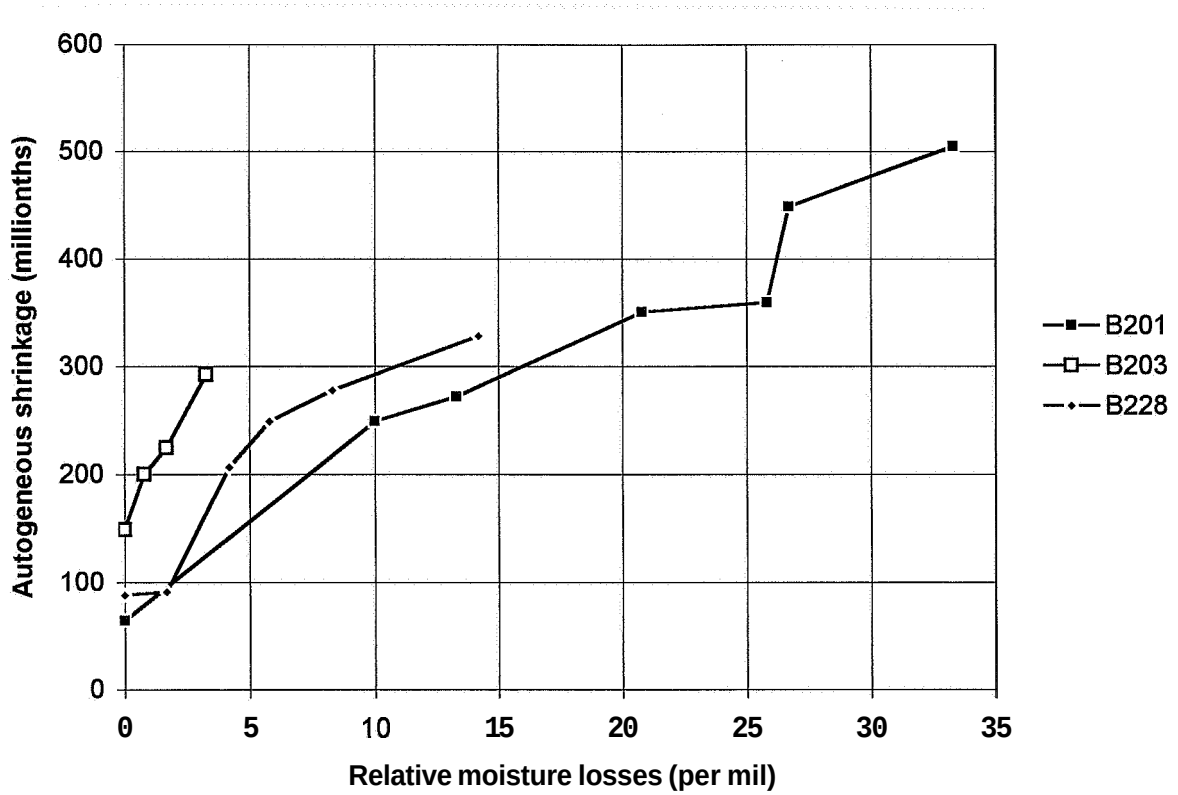

Appendix 8.35 - Autogenous shrinkage of mix 3 versus loss of weight after short-term creep

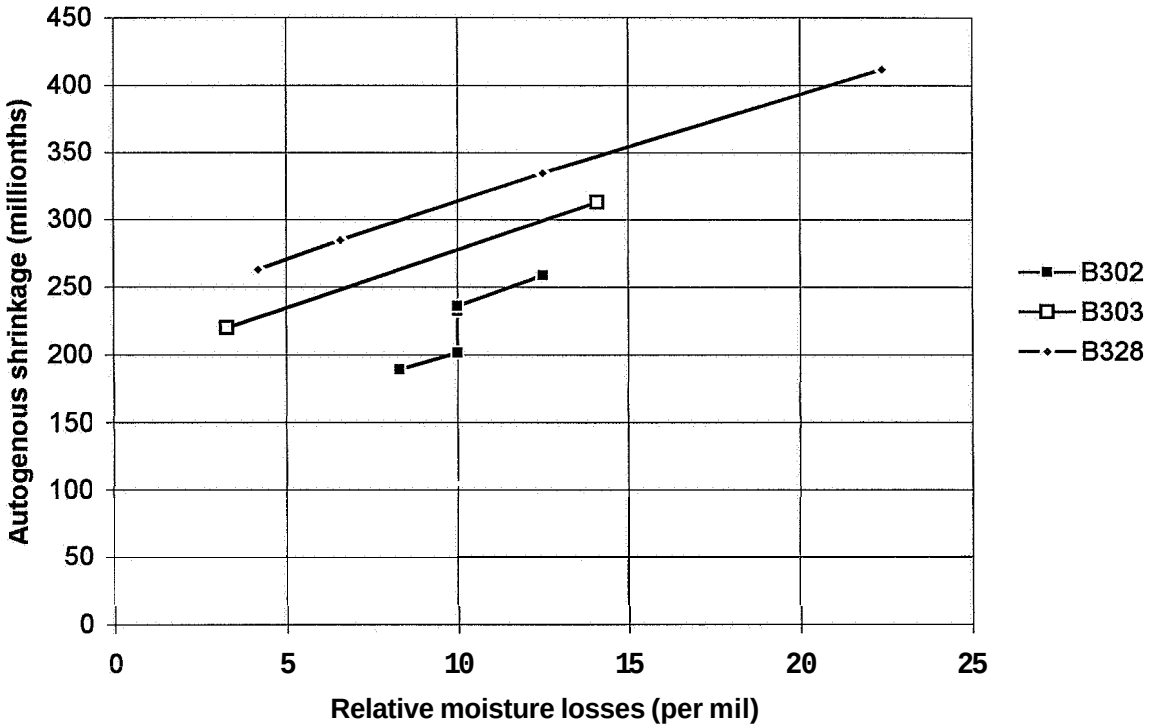

Appendix 8.36 - Autogenous shrinkage of mix 4 versus loss of weight after short-term creep

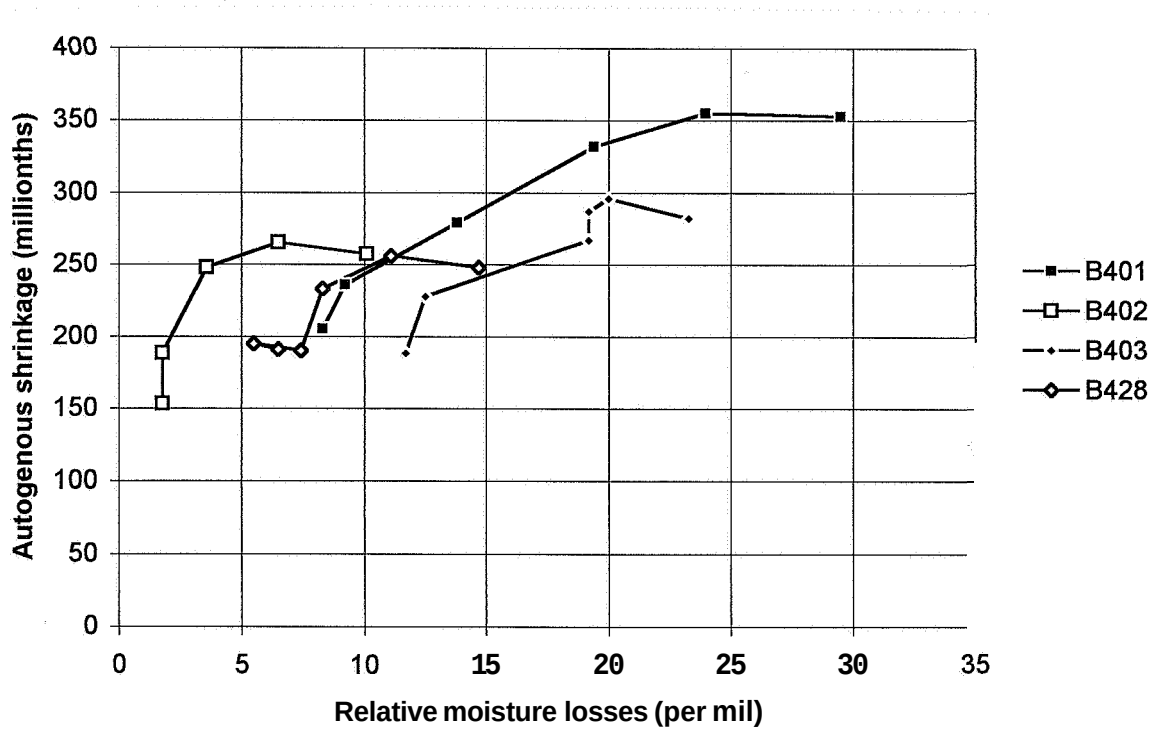

Appendix 8.37 · Autogenous shrinkage of mix 5 versus loss of weight after short-term creep

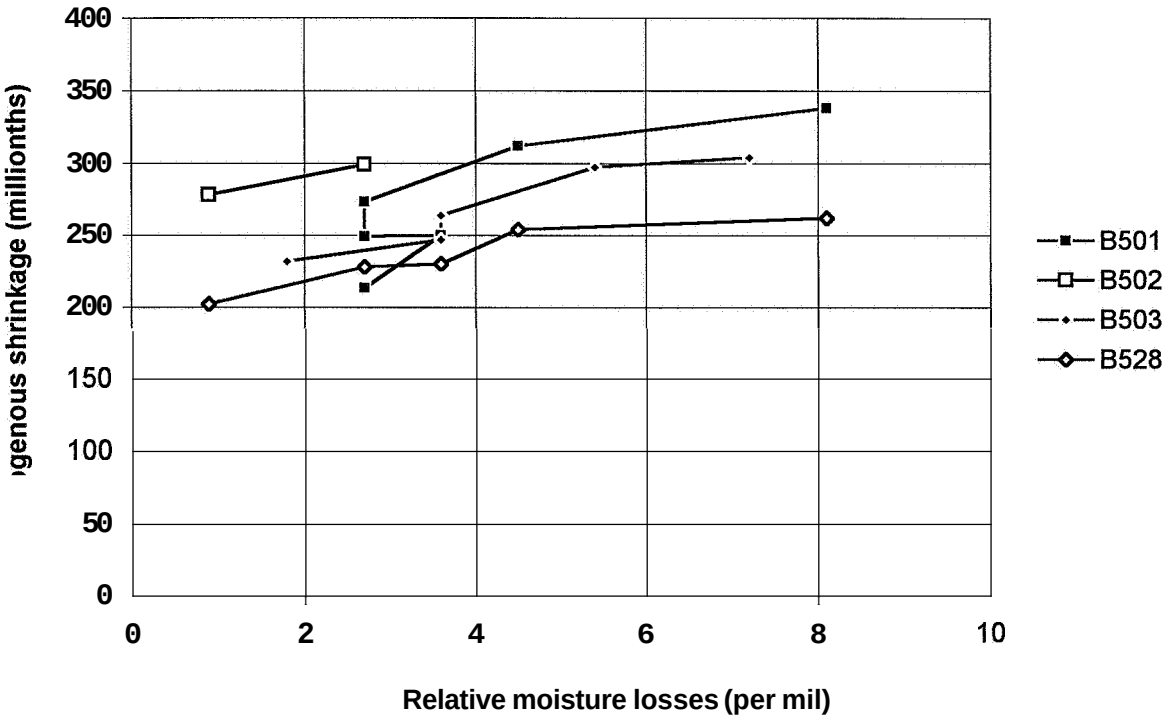

Appendix 8.38 - Autogenous shrinkage of mix 6 versus loss of weight after short-term creep

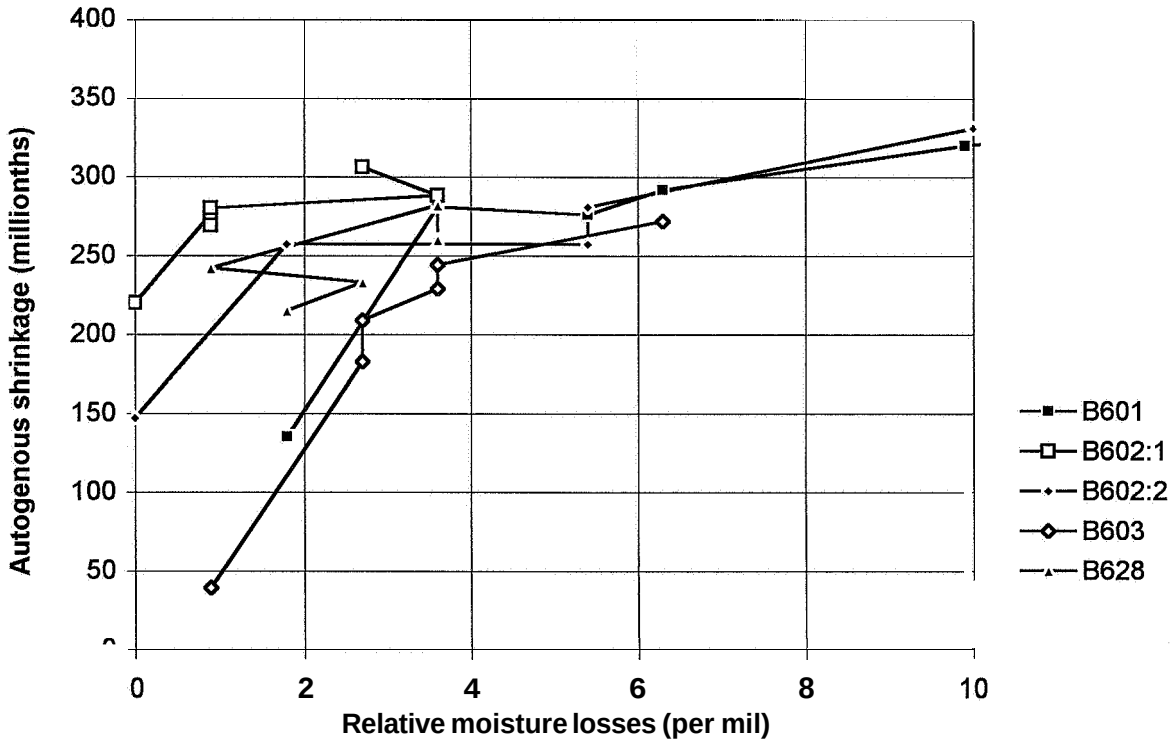

Appendix 8.39 - Autogenous shrinkage of mix 7 versus loss of weight after short-term creep

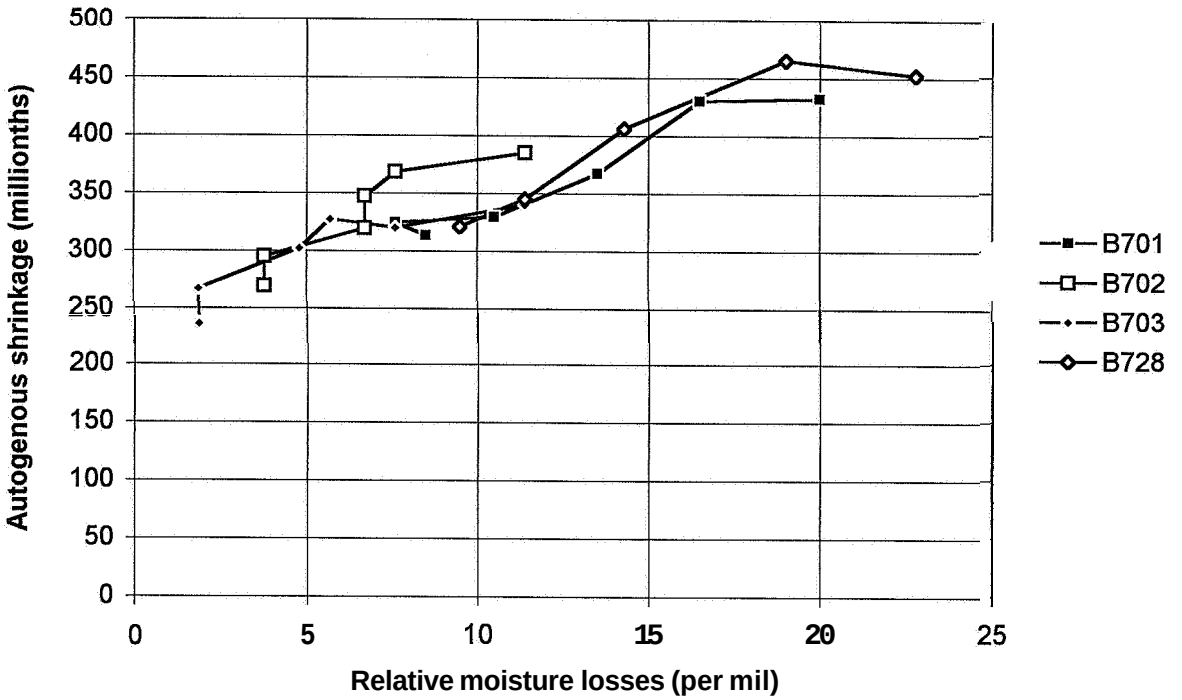

Appendix 8.40 - Autogenous shrinkage of mix 8 versus loss of weight after short-term creep

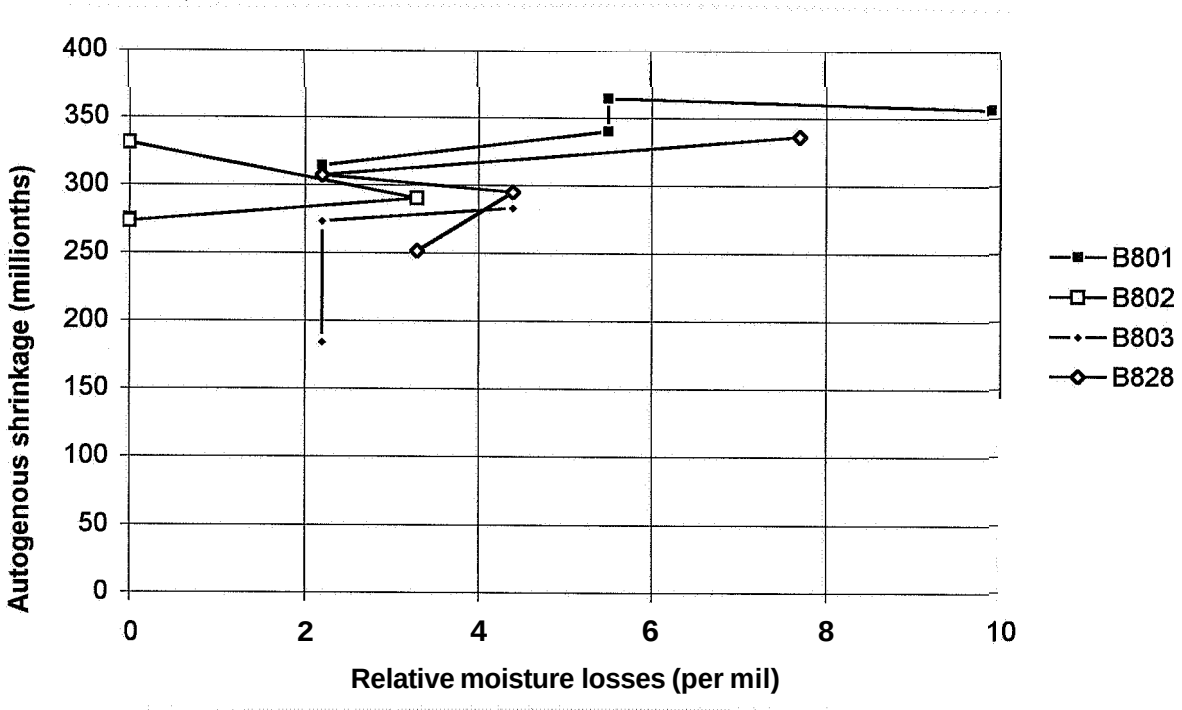

APPENDIX 9. COMPLIANCE OF CYLINDERS AT SHORT-TERM CREEP

Symbols:

B	denotes basic creep (sealed curing)
D	denotes drying creep (air curing)
6...	denotes concrete mix, **Table** 5.1
...01	age at loading: 1 day; stresslcylinder strength ratio: 0.84
...02	age at loading: 2 days; stresslcylinder strength ratio: 0.84
...03	age at loading: 2 days; stresslcylinder strength ratio: 0.42
...28	age at loading: 28 days; stresslcylinder strength ratio: 0.42

Appendix 9.1 - Short-term compliance of mix 1 subiected to air curing

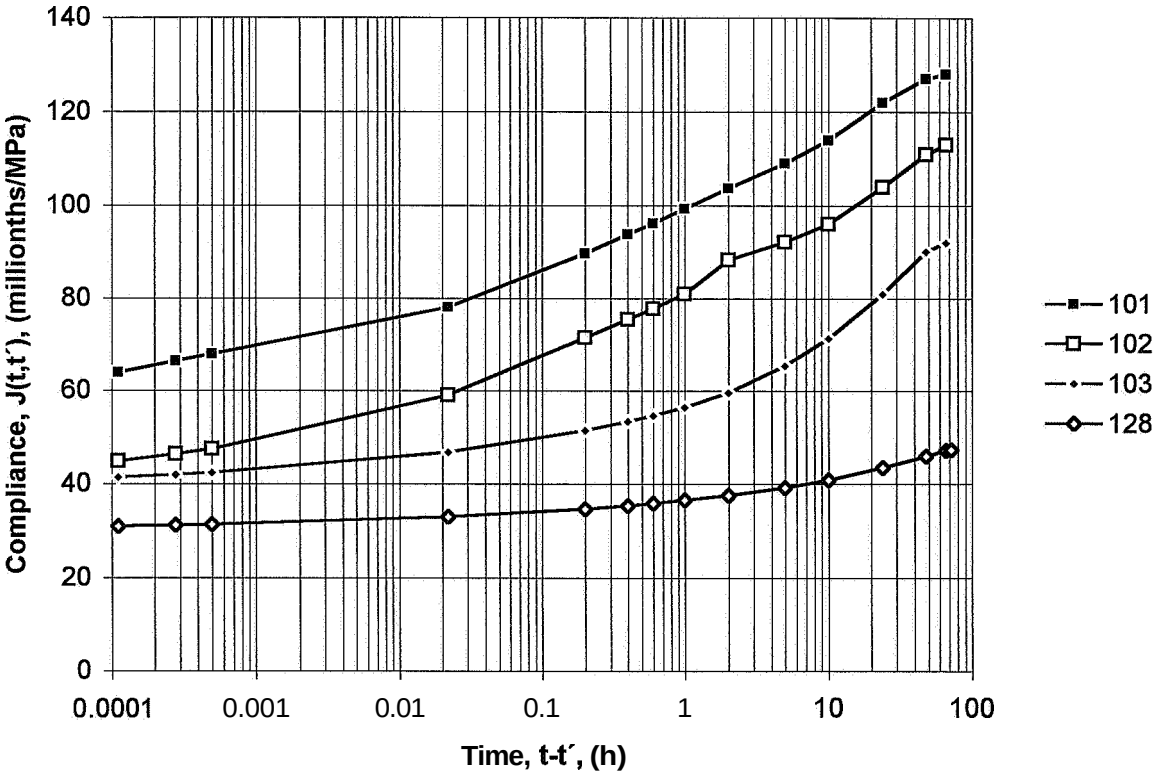

Appendix 9.2 - Short-term compliance of mix 2 subjected to air curing

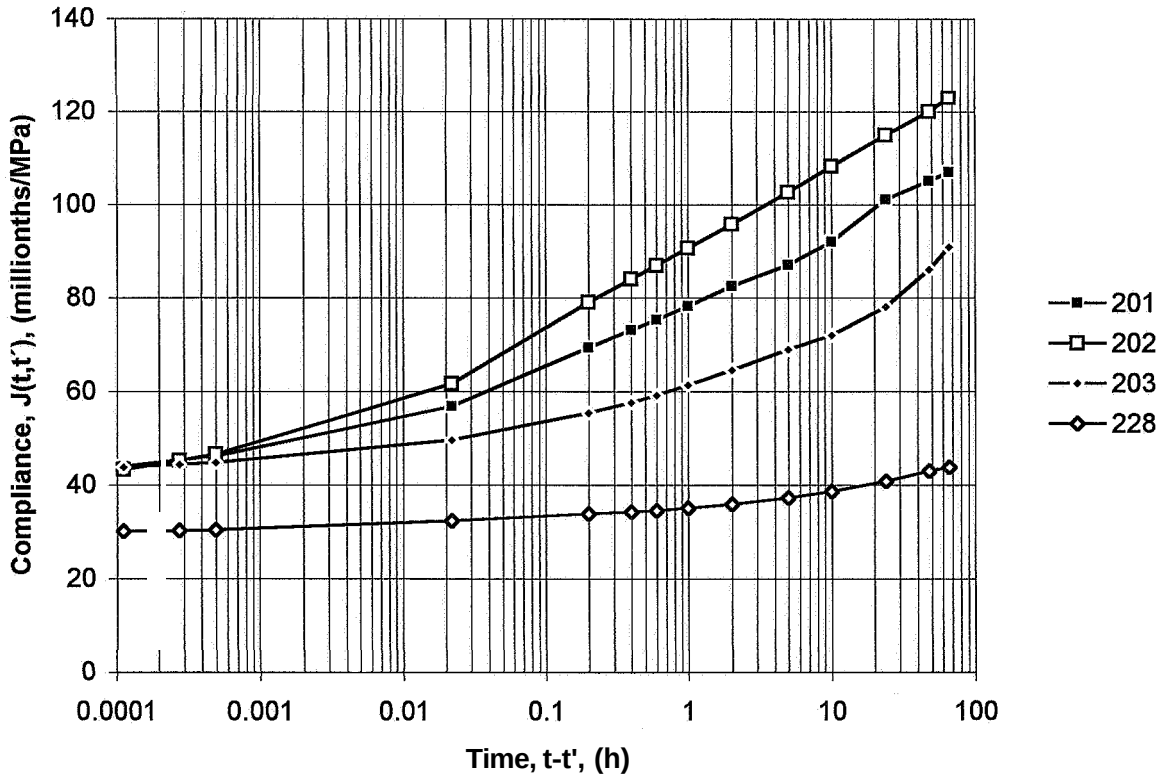

Appendix 9.3 - Short-term compliance of mix 3 subjected to air curing

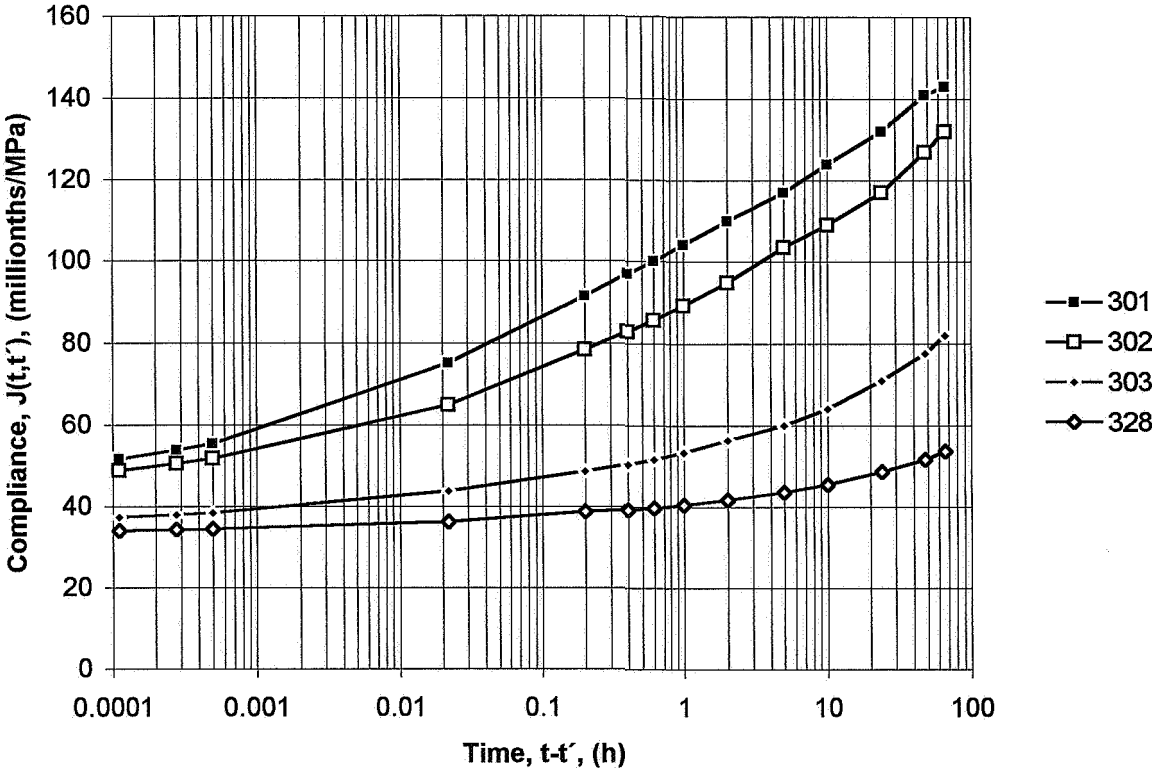

Appendix 9.4 - Short-term compliance of mix 4 subjected to air curing

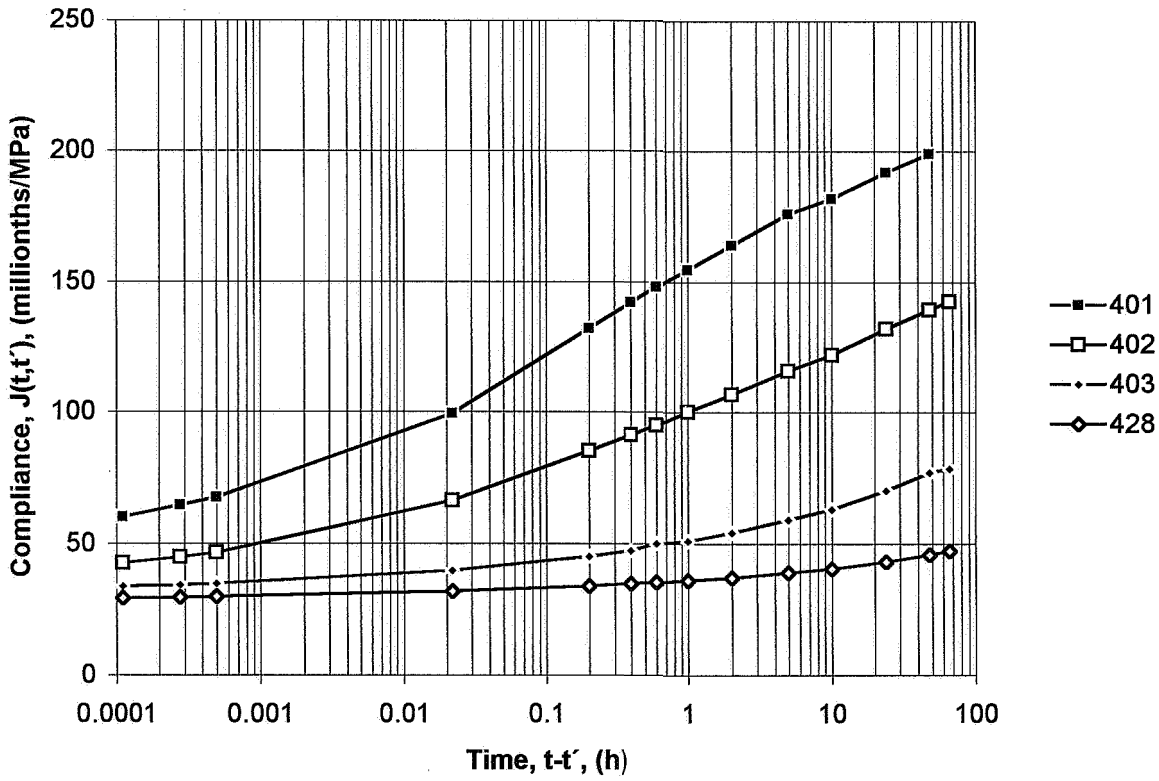

Appendix 9.5 - Short-term compliance of mix 5 subjected to air curing

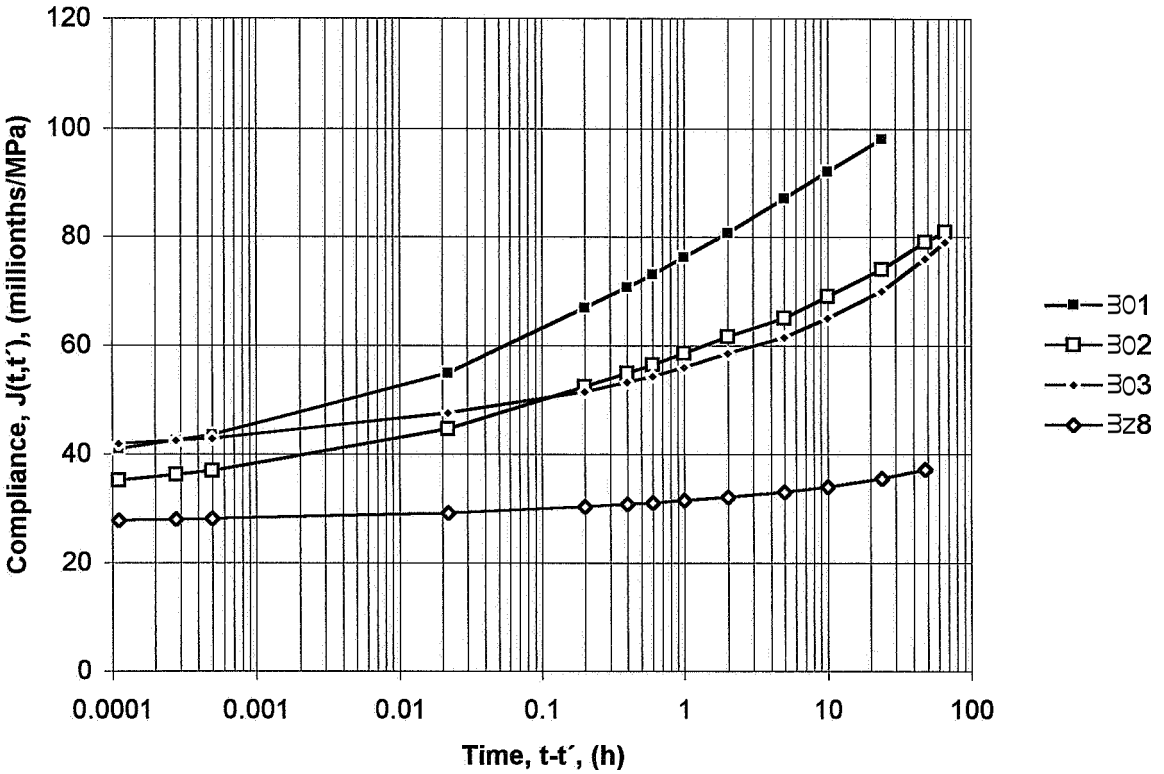

Appendix 9.6 - Short-term compliance of mix 6 subjected to air curing

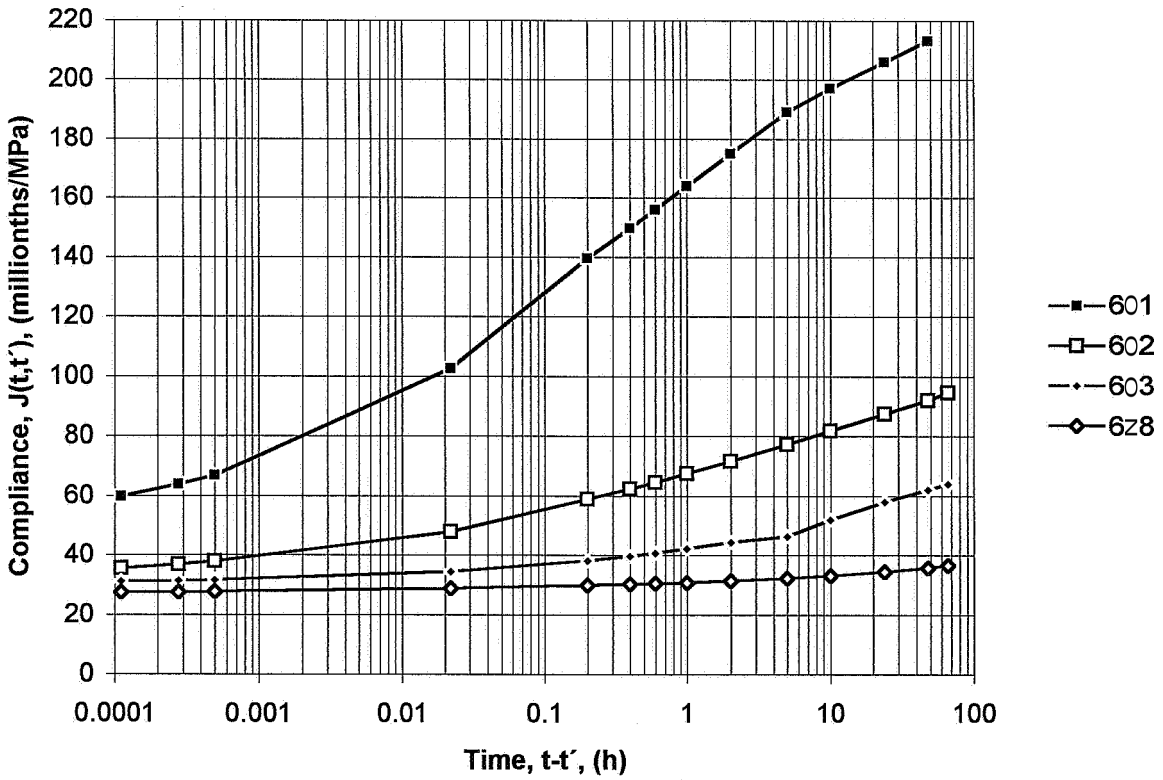

Appendix 9.7 - Short-term compliance of mix 7 subiected to air curing

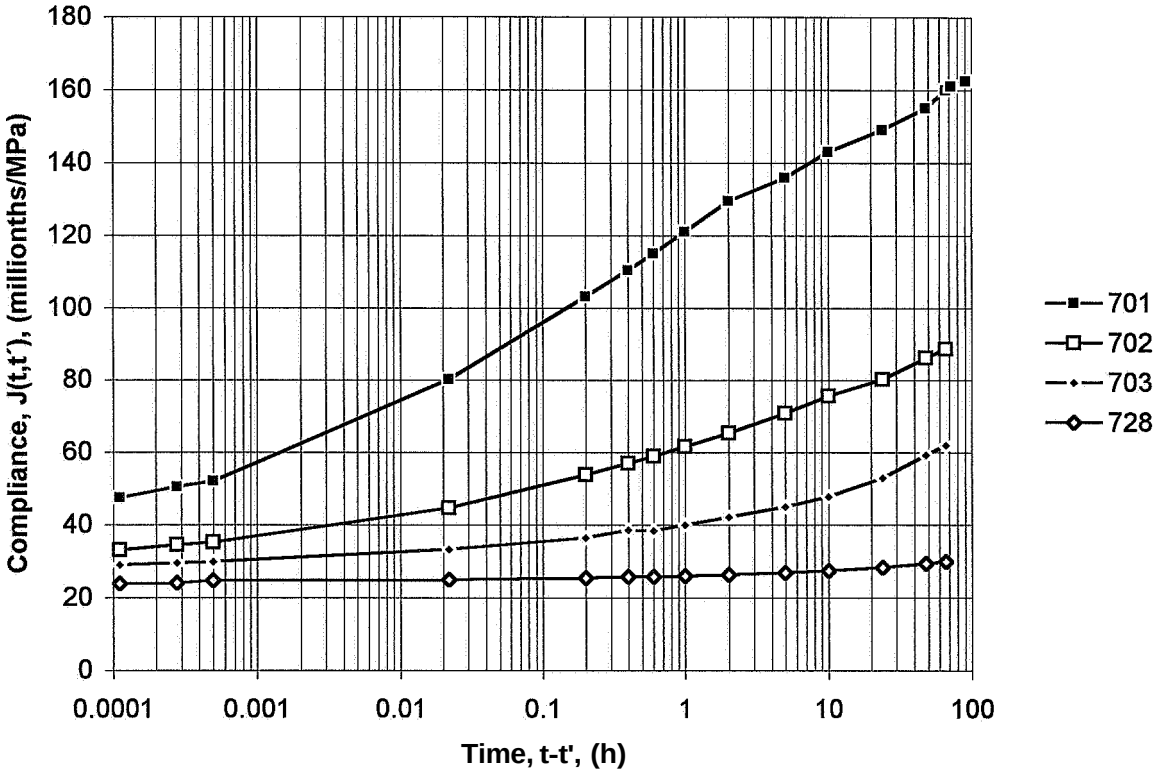

Appendix 9.8 - Short-term compliance of mix 8 subjected to air curing

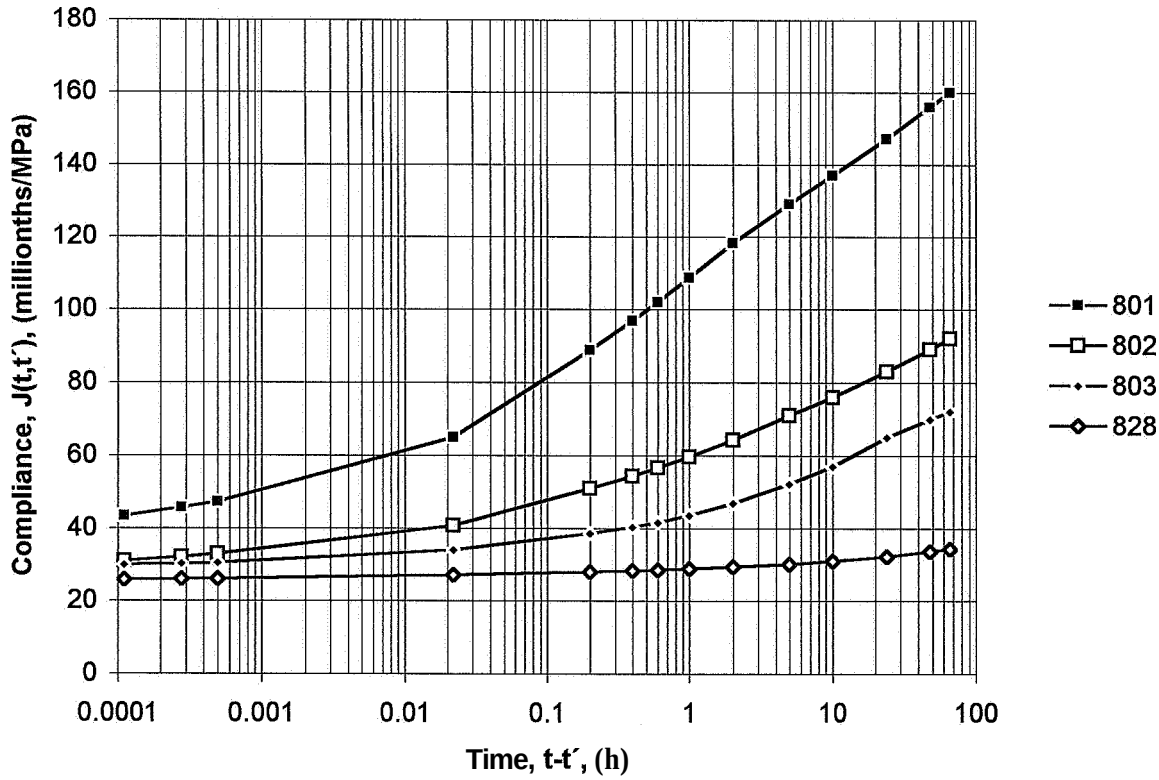

Appendix 9.9 - Short-term compliance of mix 1 subjected to sealed curing

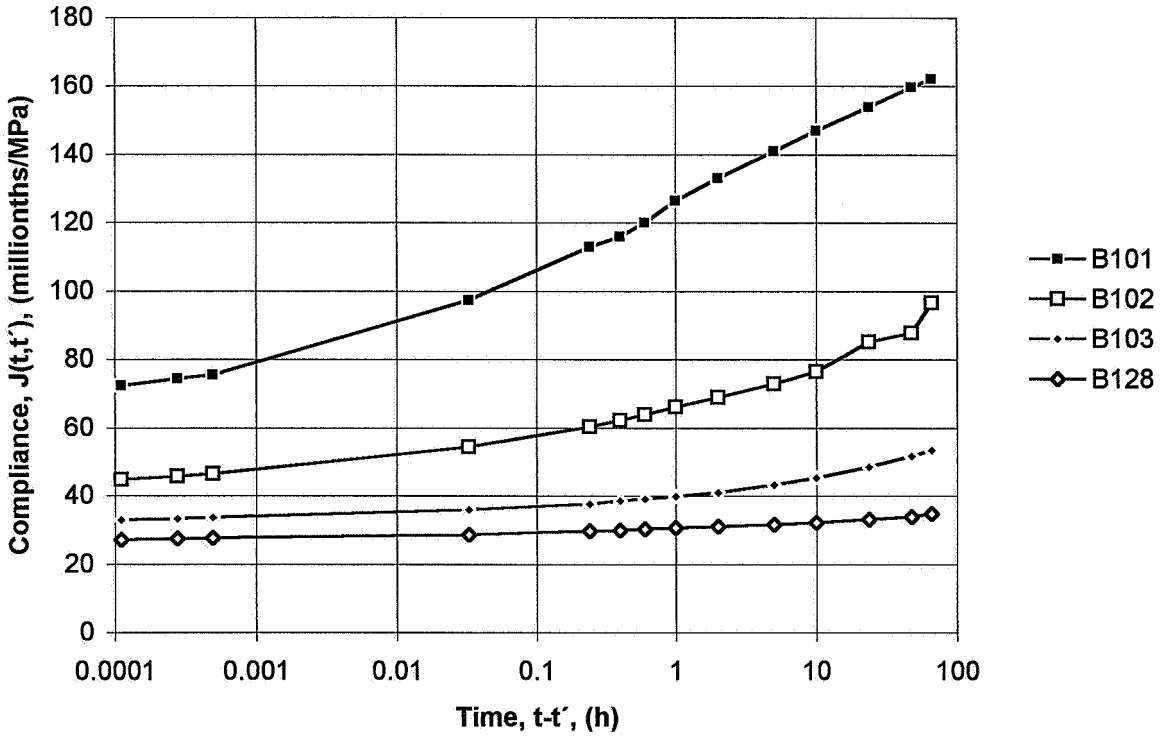

App di 9.10 - Shor compliance 1 mix 2 subjected to sealed curing

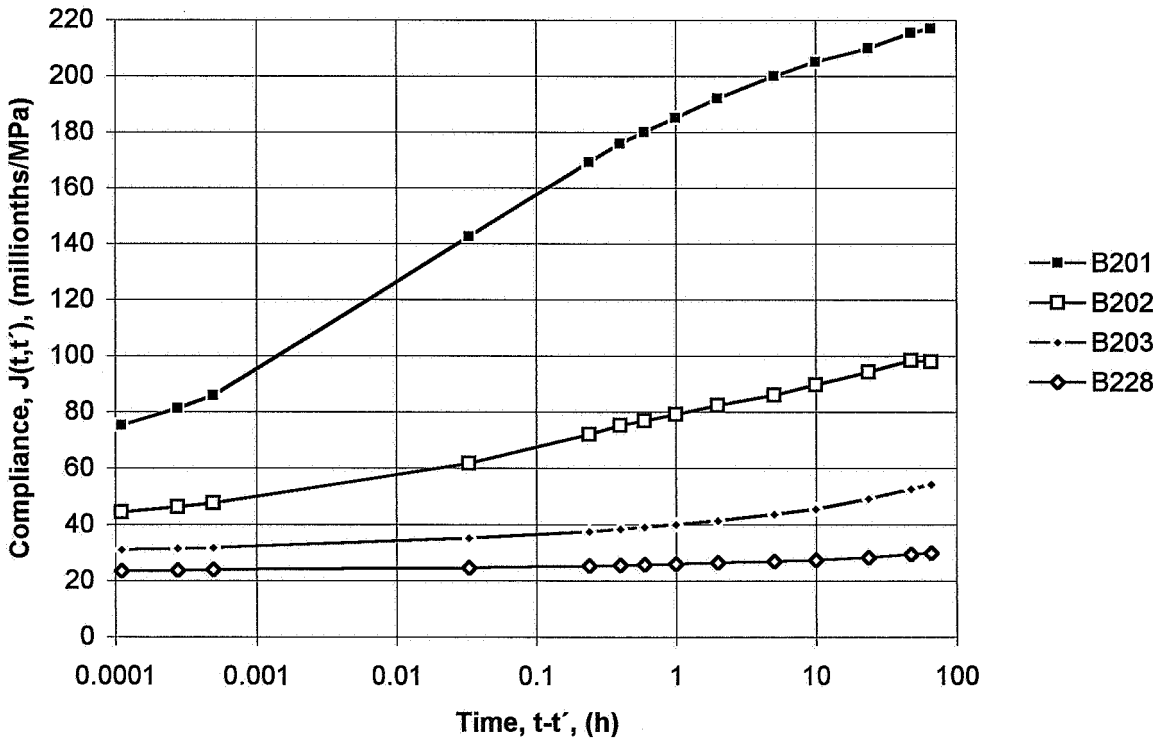

Appendix 9.11 - Short-term compliance of mix 3 subjected to sealed curing

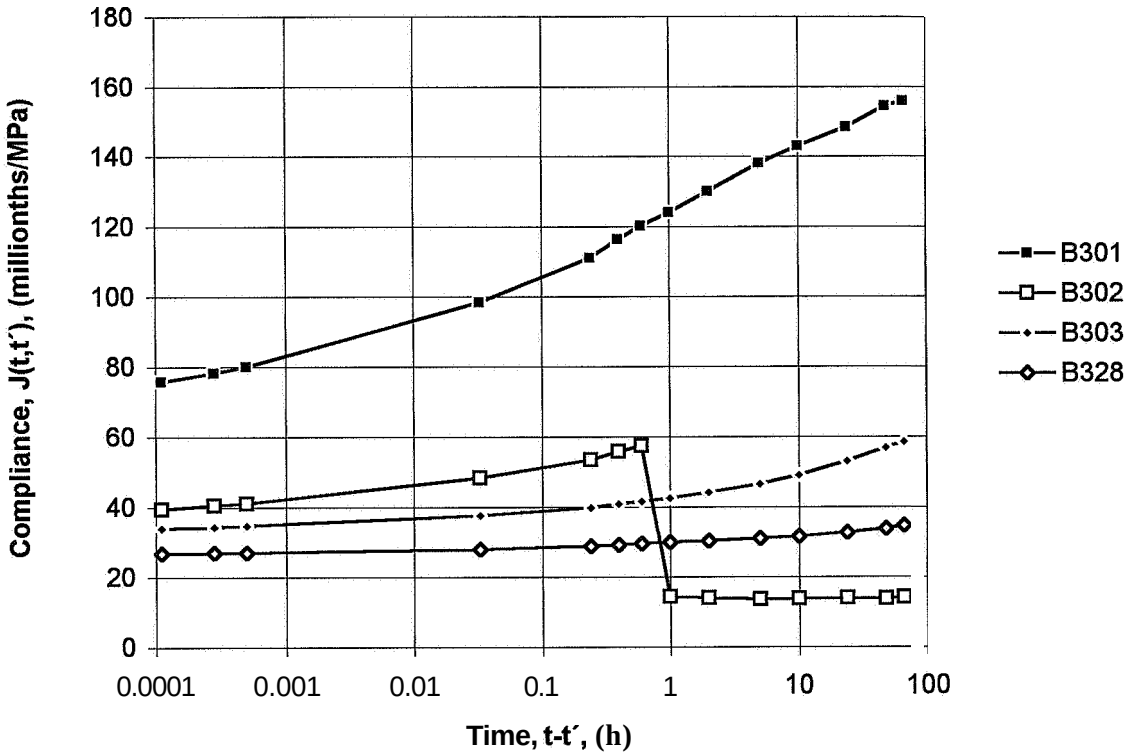

Appendix 9 Short- ompliane f mi 4 subjected to sealed cu

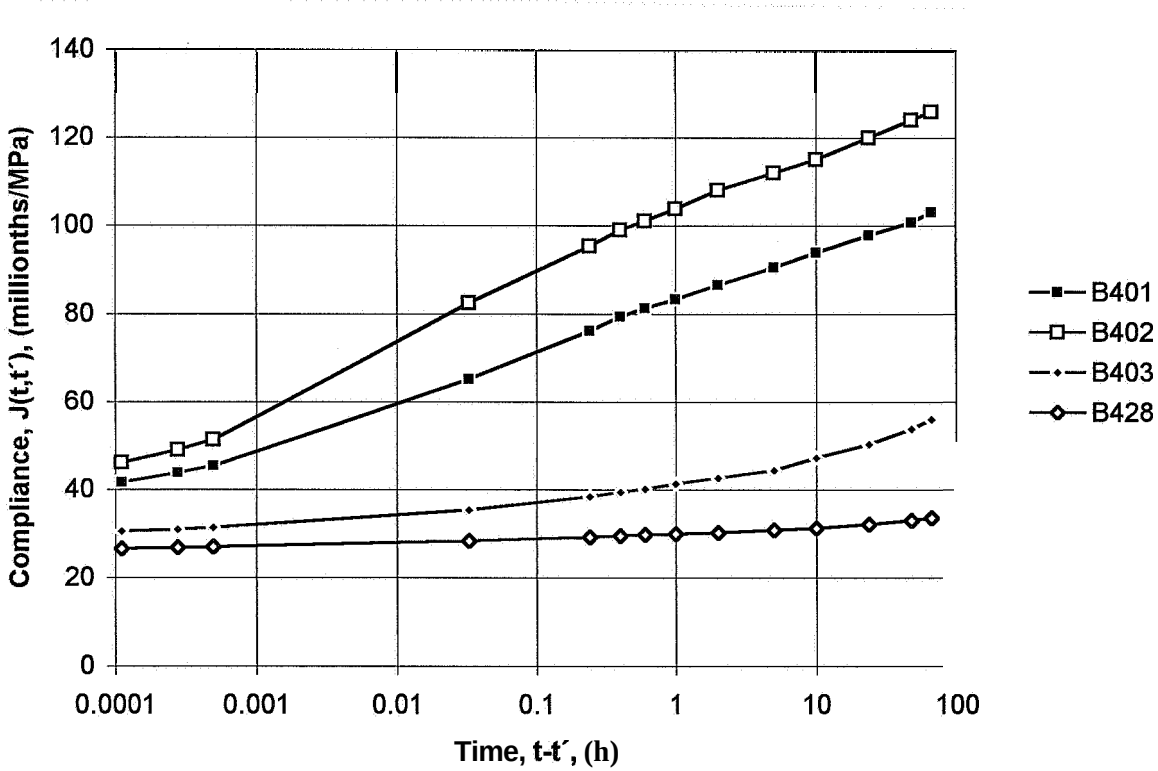

Appendix 9.13 · Short-term compliance of mix 5 subjected to sealed curing

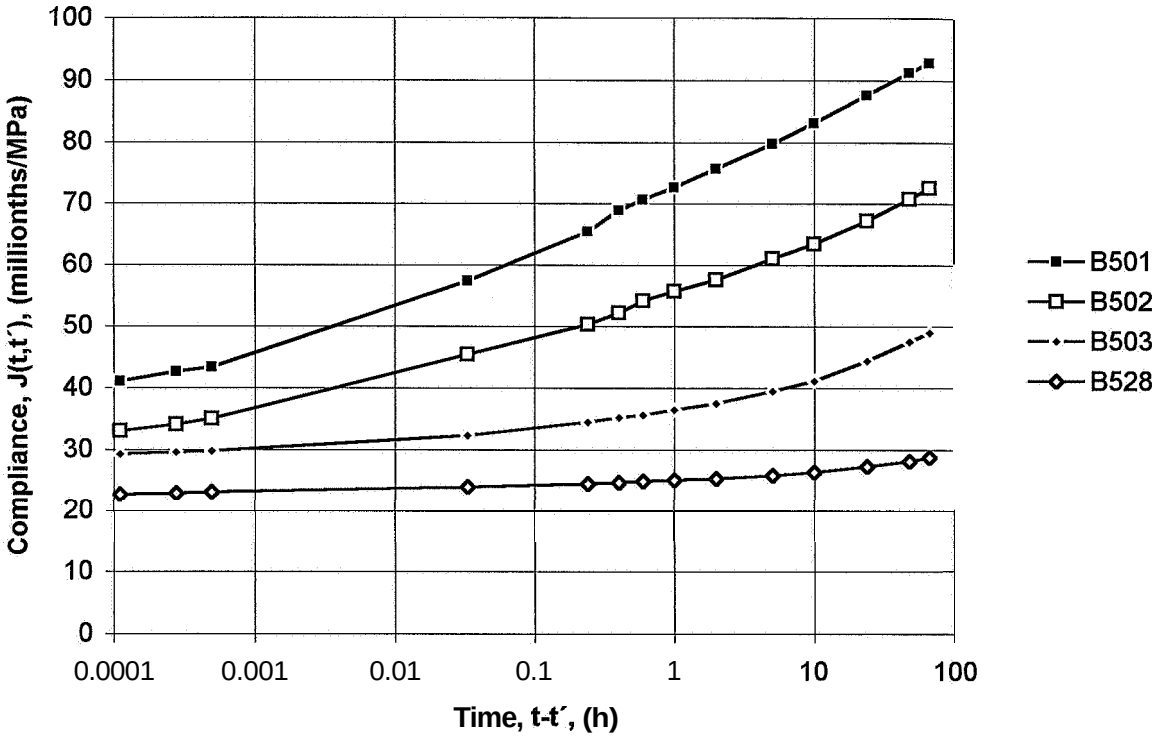

Appendix 9.14 - Short-term compliance of mix 6 subjected to sealed curing

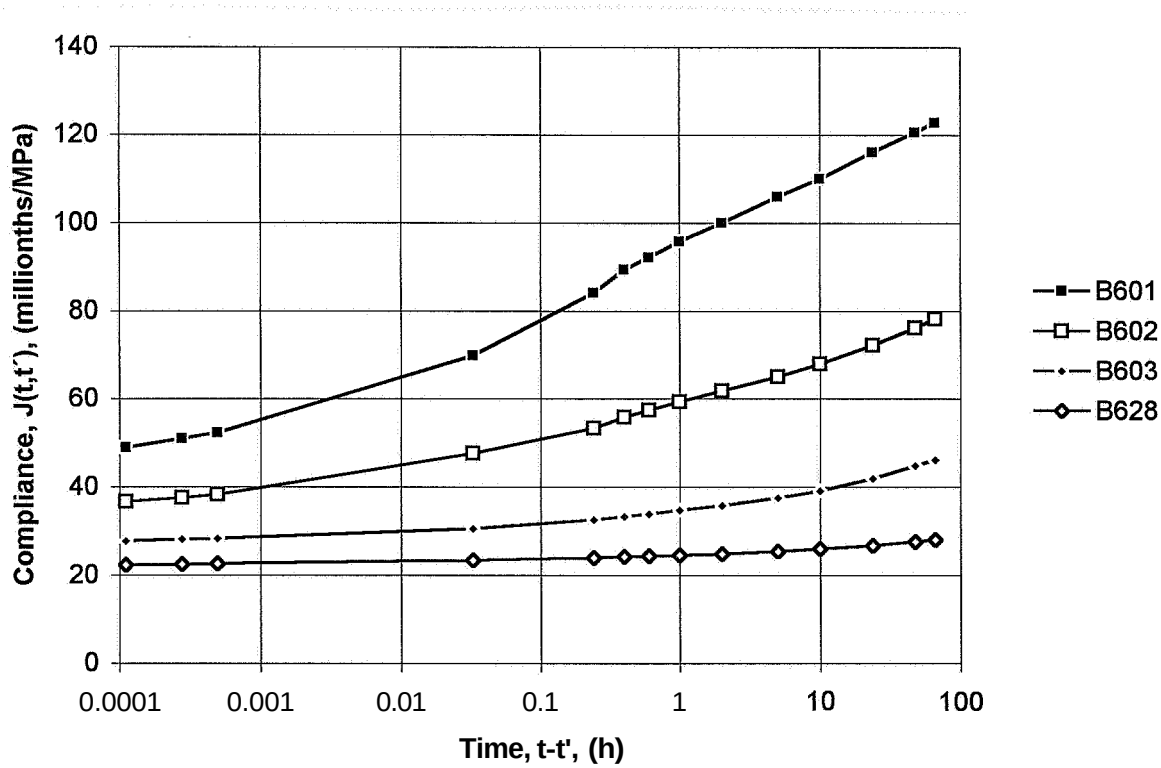

Appendix 9.15 - Short-term compliance of mix 7 subjected to sealed curing

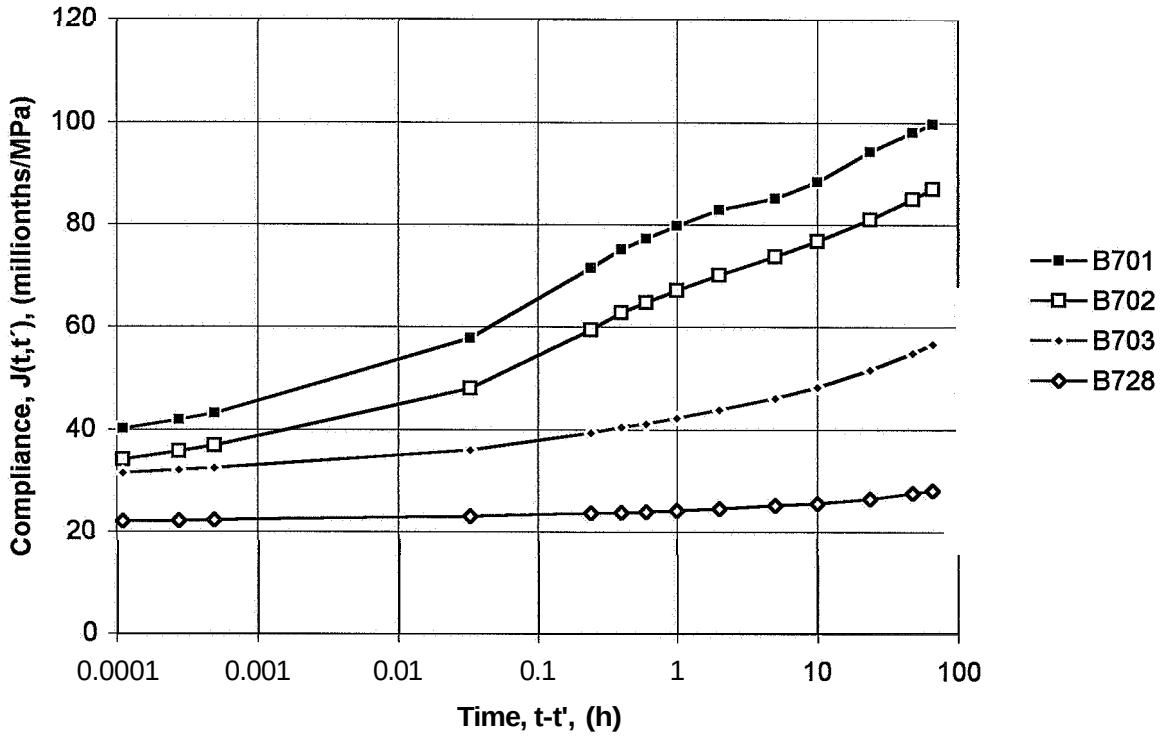

Appendix 9.16 - Short-term compliance of mix 8 subjected to sealed curing

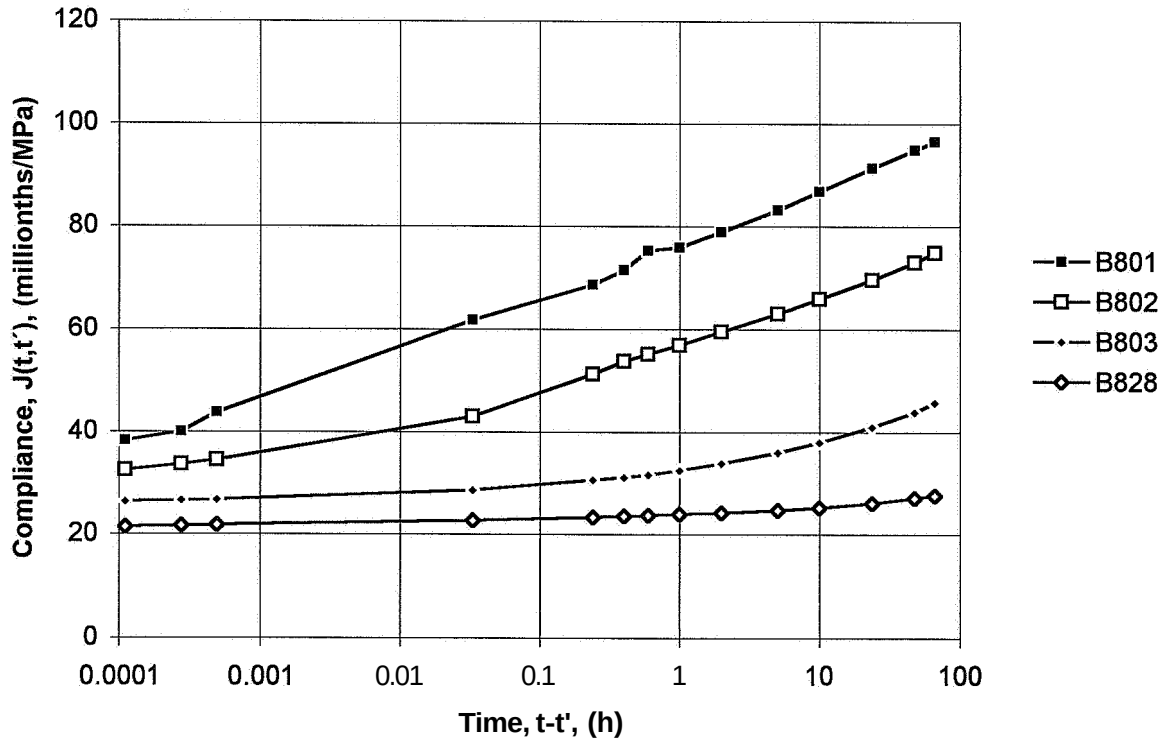

Appendix 9.17 - Short-term compliance of all mixes with sealed curing that were mature when loading

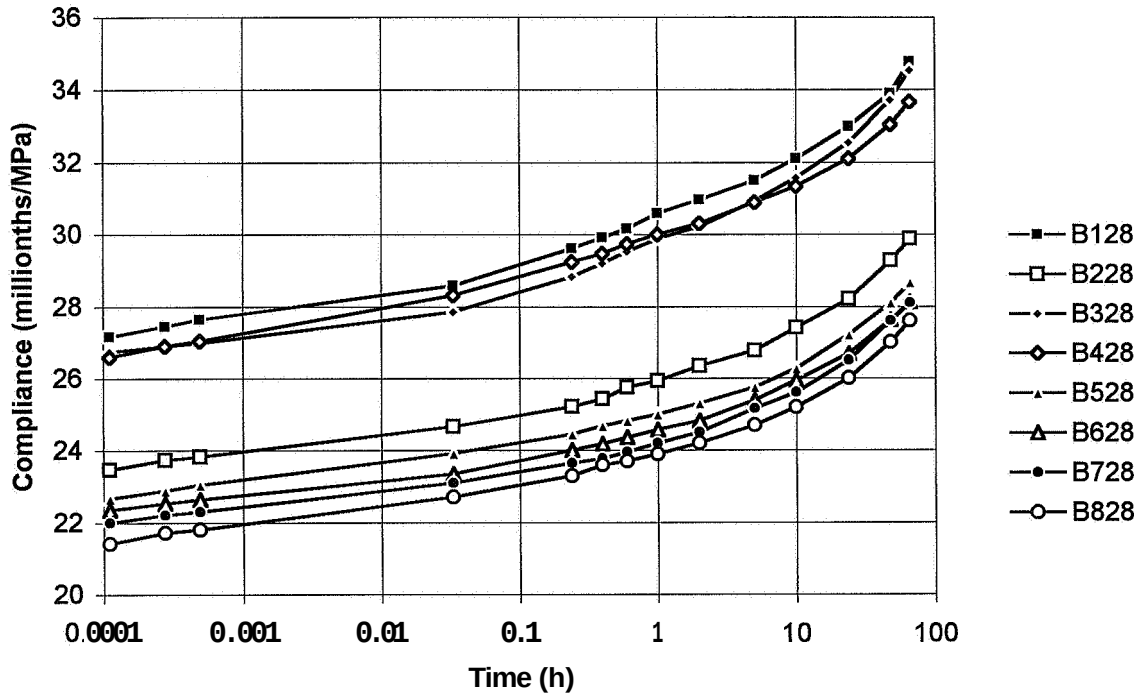

Appendix 9.18 - Short-term creep rate of mature HPCs with sealed curing versus w/c

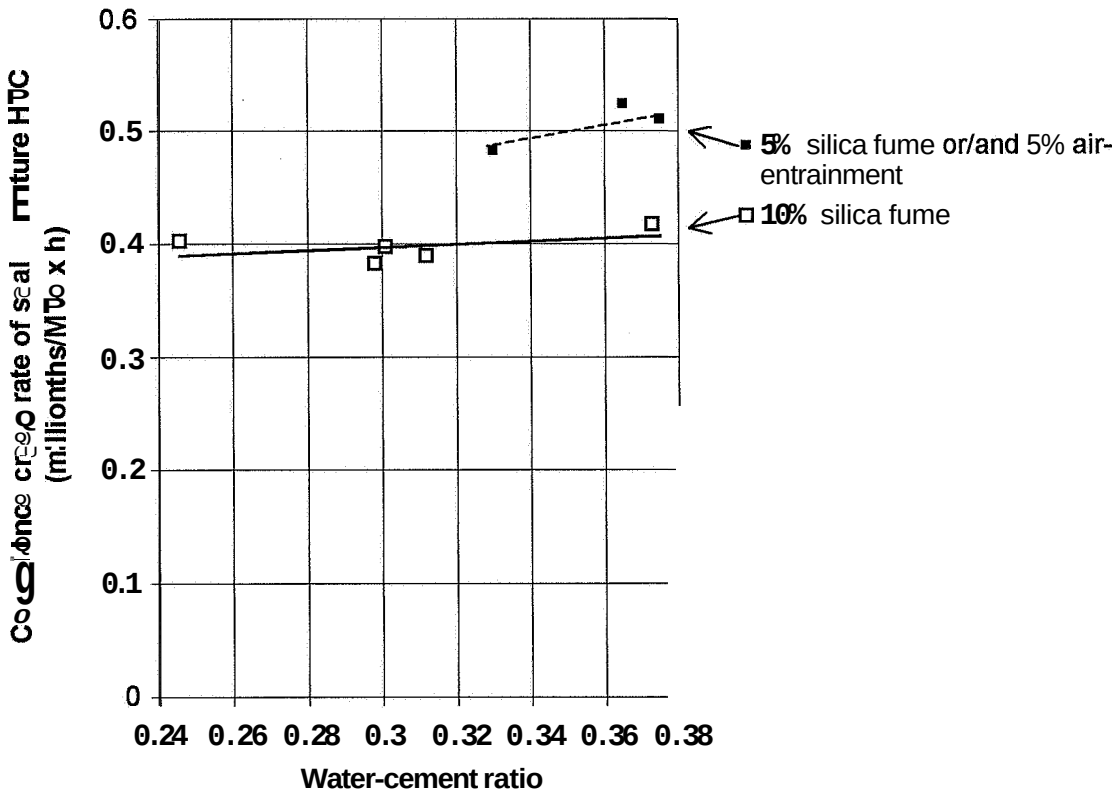

APPENDIX 10. COMPLIANCE OF CYLINDERS AT UNLOADING

Shrinkage according to Section 8 was not reduced from the measured strain.

Appendix 10.1 - Unloading compliance of mix 1 subjected to air curing
Appendix 10.2 - Unloading compliance of mix 2 subjected to air curing
Appendix 10.3 - Unloading compliance of mix 3 subjected to air curing
Appendix 10.4 - Unloading compliance of mix 4 subjected to air curing
Appendix 10.5 - Unloading compliance of mix 5 subjected to air curing
Appendix 10.6 - Unloading compliance of mix 6 subjected to air curing
Appendix 10.7 - Unloading compliance of mix 7 subjected to air curing
Appendix 10.8 - Unloading compliance of mix 8 subjected to air curing
Appendix 10.9 - Repeated loading compliance of mix 2 subjected to air curing
Appendix 10.10 - Repeated loading compliance of mix 7 subjected to air curing
Appendix 10.11 - Repeated unloading compliance of mix 2 subjected to air curing
Appendix 10.12 - Repeated unloading compliance of mix 7 subjected to air curing
Appendix 10.13 - Unloading compliance of mix 1 subjected to sealed curing
Appendix 10.14 - Unloading compliance of mix 2 subjected to sealed curing
Appendix 10.15 - Unloading compliance of mix 3 subjected to sealed curing
Appendix 10.16 - Unloading compliance of mix 4 subjected to sealed curing
Appendix 10.17 - Unloading compliance of mix 5 subjected to sealed curing
Appendix 10.18 - Unloading compliance of mix 6 subjected to sealed curing
Appendix 10.19 - Unloading compliance of mix 7 subjected to sealed curing
Appendix 10.20 - Unloading compliance of mix 8 subjected to sealed curing
Appendix 10.21 - Unloading compliance of mature HPC subjected to sealed curing
Appendix 10.22 - Repeated loading compliance of mix 5 subjected to sealed curing
Appendix 10.23 - Repeated unloading compliance of mix 5 subjected to sealed curing

B denotes basic creep (sealed curing)
D denotes drying creep (air curing)
6... denotes concrete mix, **Table 5.1**
...01 age at loading: 1 day; stresslcylinder strength ratio: 0.84
...02 age at loading: 2 days; stresslcylinder strength ratio: 0.84
...03 age at loading: 2 days; stresslcylinder strength ratio: 0.42
...28 age at loading: 28 days; stresslcylinder strength ratio: 0.42
..200 age at loading: 200 days with loading according to 28 days' age

Appendix 10.1 - Unloading compliance of mix 1 subiected to air curing

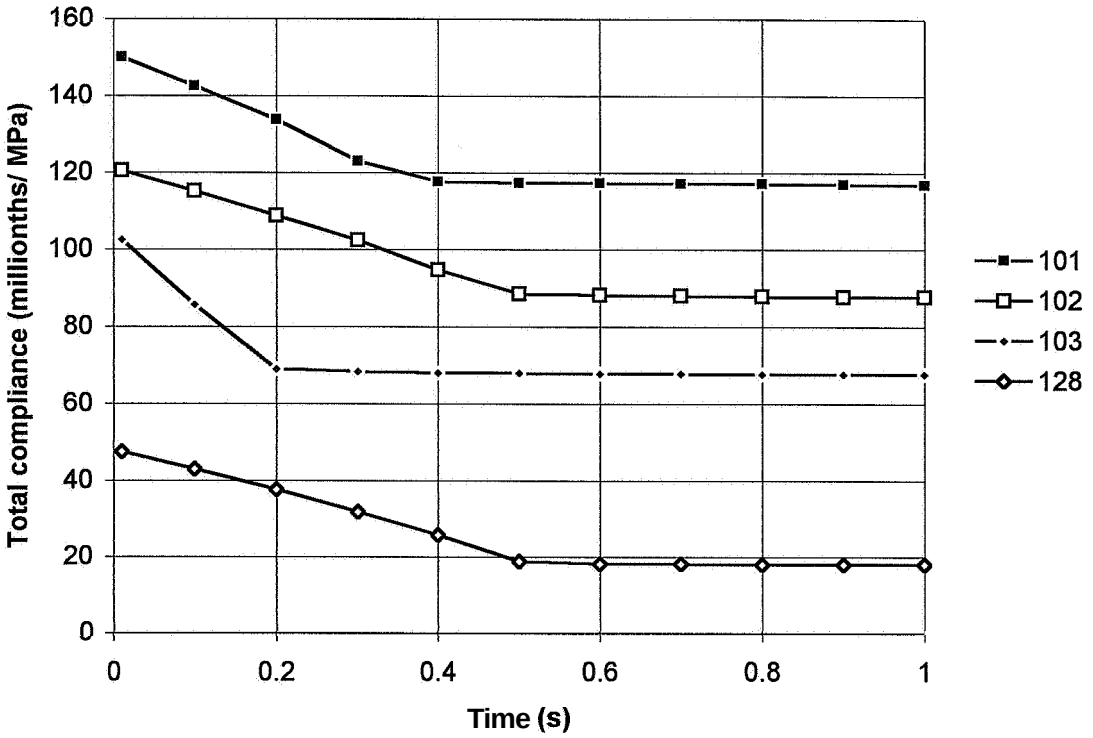

Appendix 10.2 - Unloading compliance of mix 2 subjected to air curing

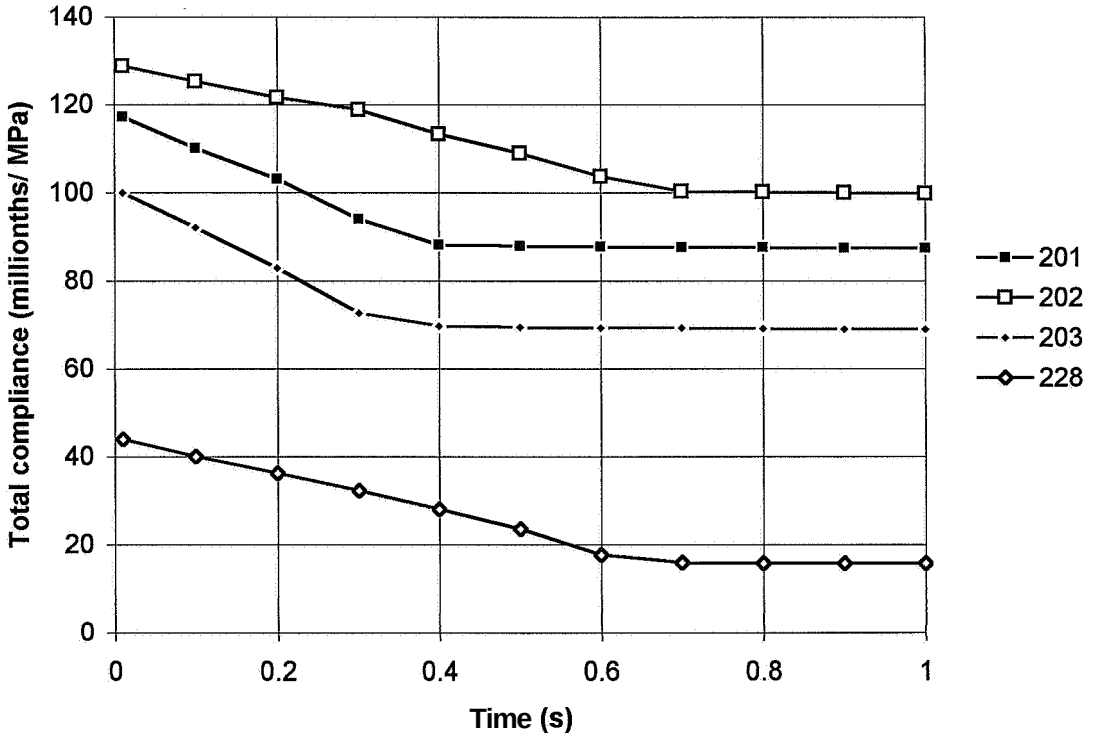

Appendix 10.3 - Unloading compliance of mix 3 subiected to air curing

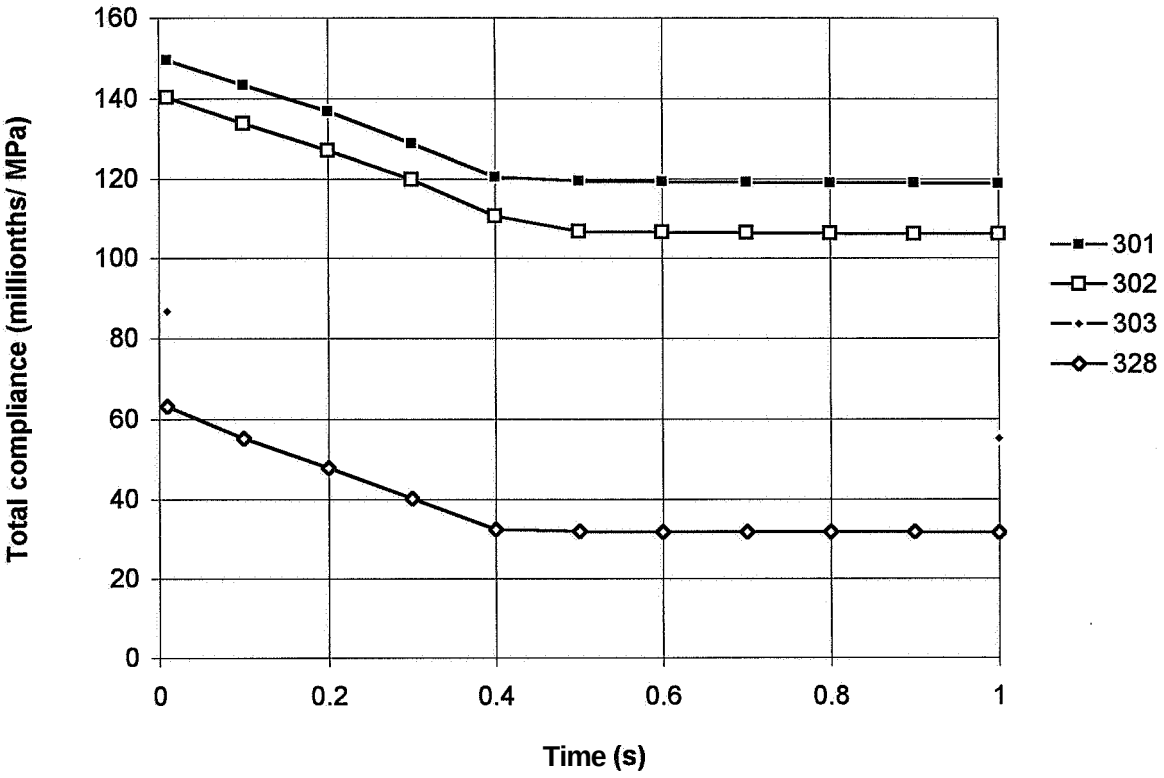

Appendix 10.4 - Unloading compliance of mix 4 subiected to air curing

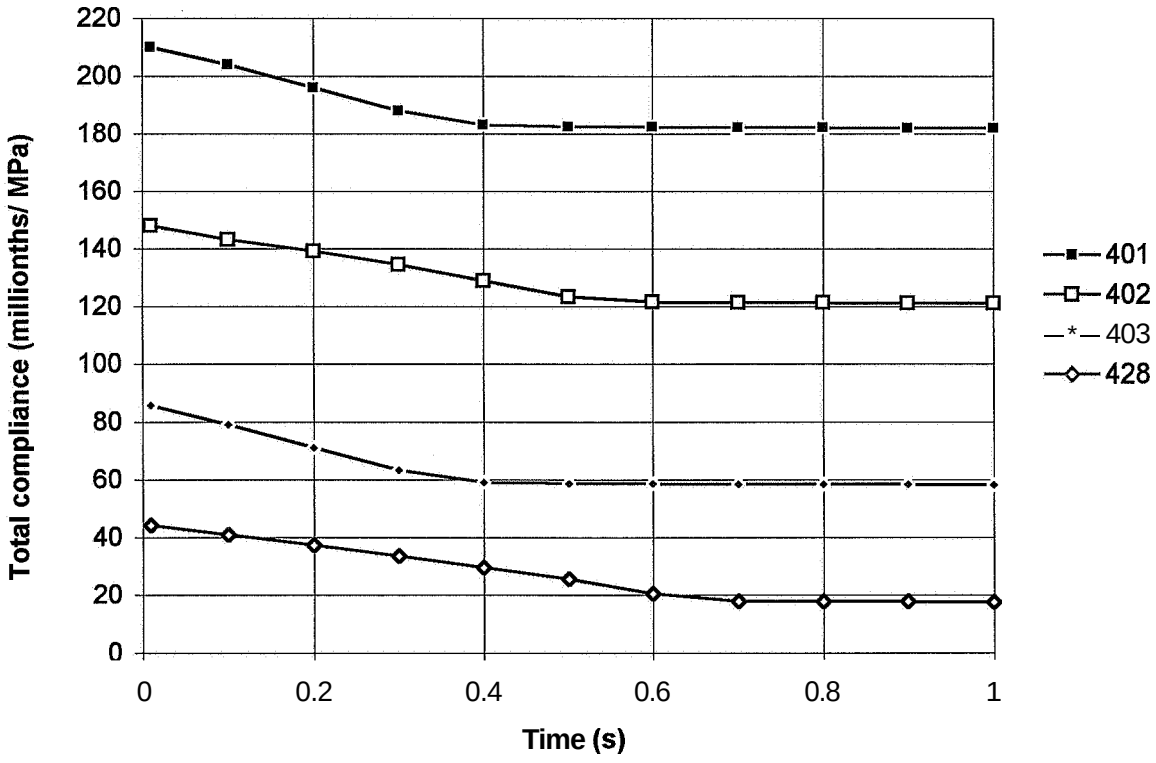

Appendix 10.5 - Unloading compliance of mix 5 subjected to air curing

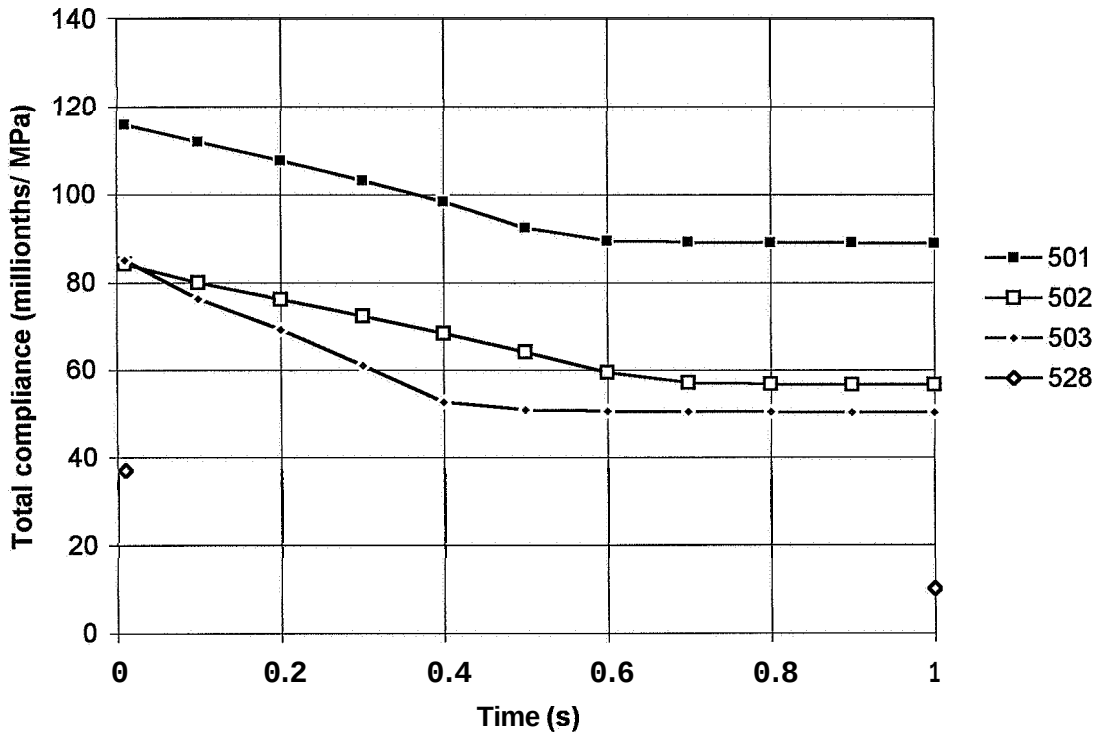

Appendix 10.6 - Unloading compliance of mix 6 subjected to air curing:

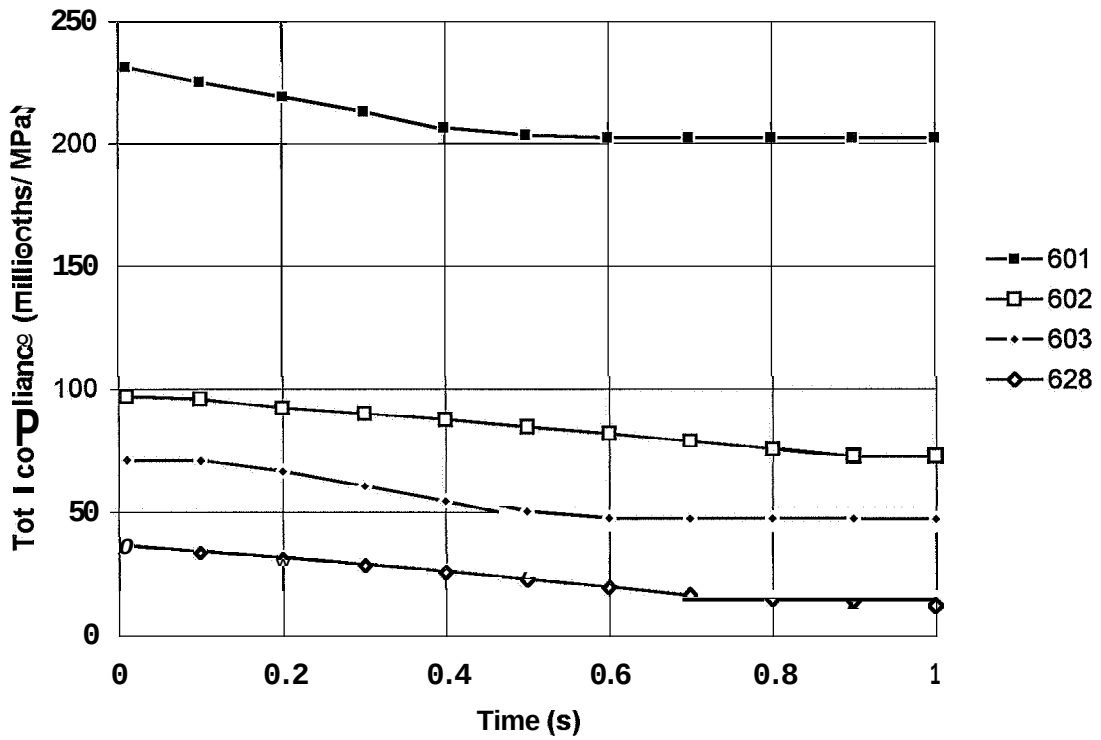

Appendix 10.7 - Unloading compliance of mix 7 subiected to air curing;

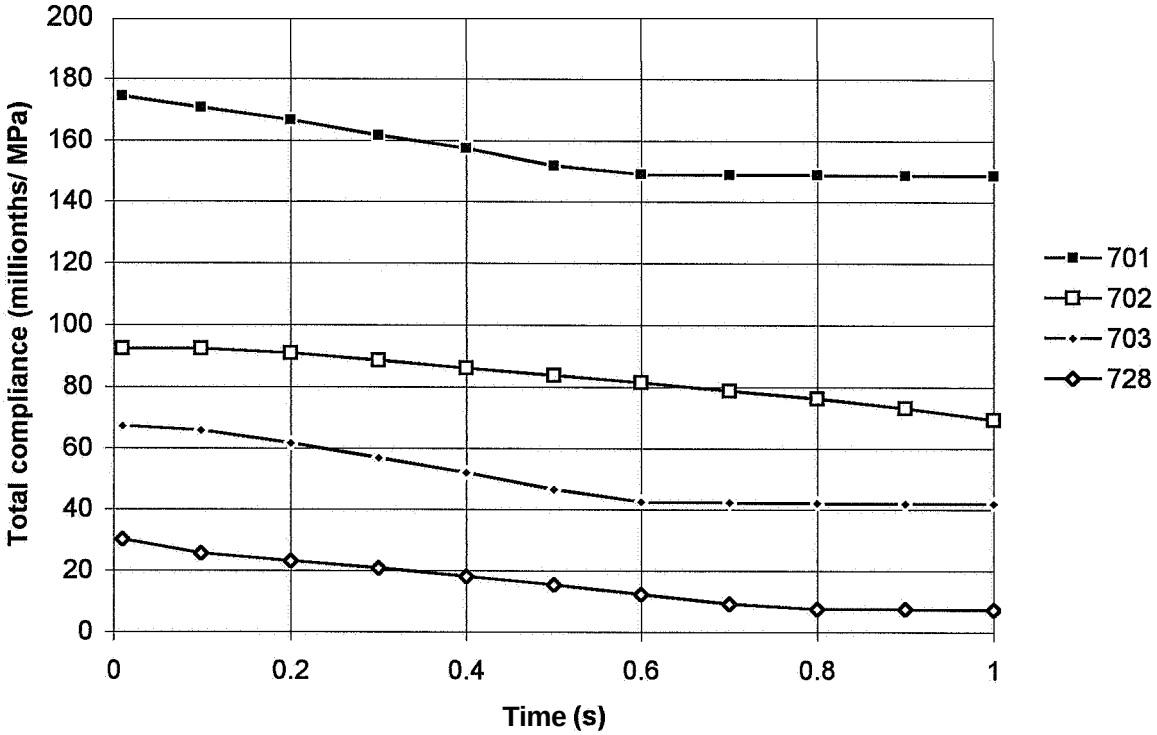

Appendix 10.8 - Unloading compliance of mix 8 subiected to air curing;

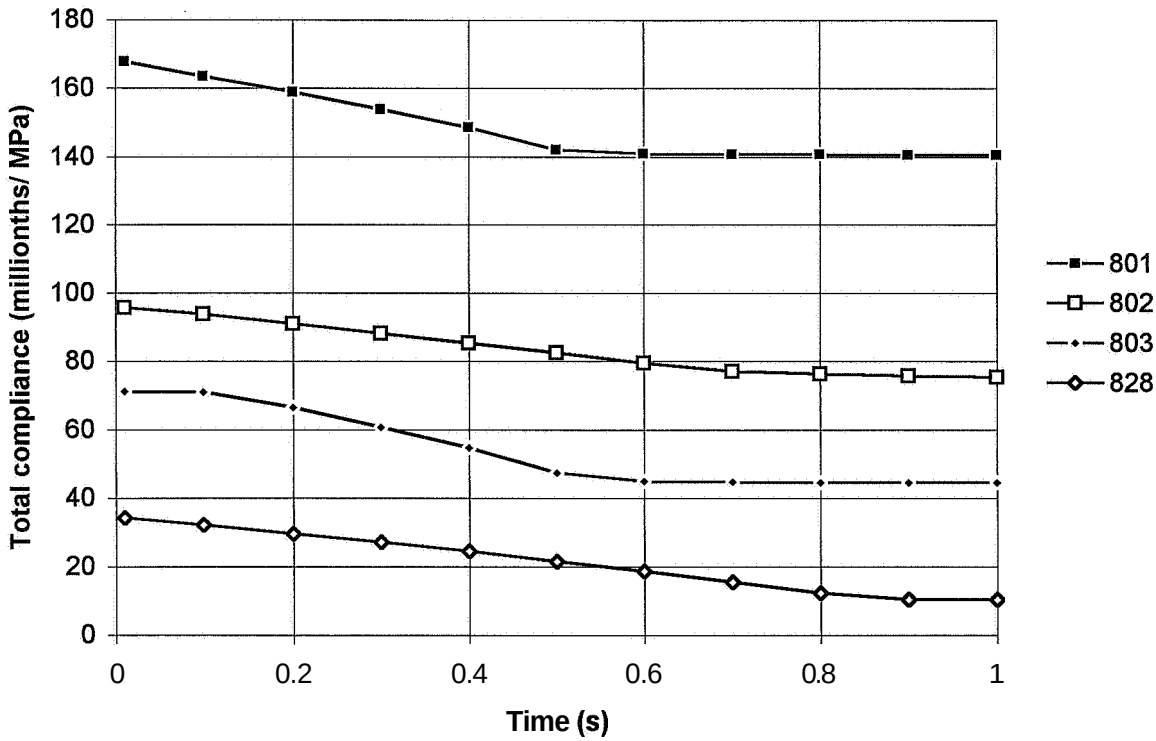

Appendix 10.9 - Repeated loading compliance of mix 2 subiected to air curing

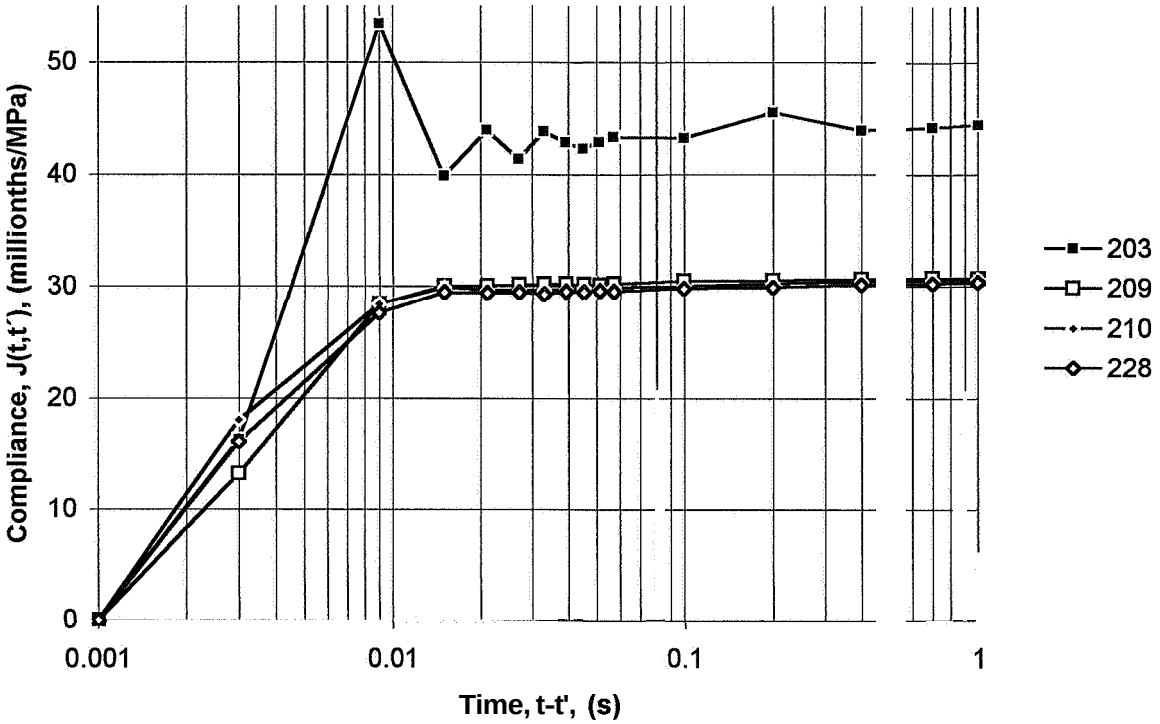

Appendix 10.10 - Repeated loading compliance of mix 7 subiected to air curing

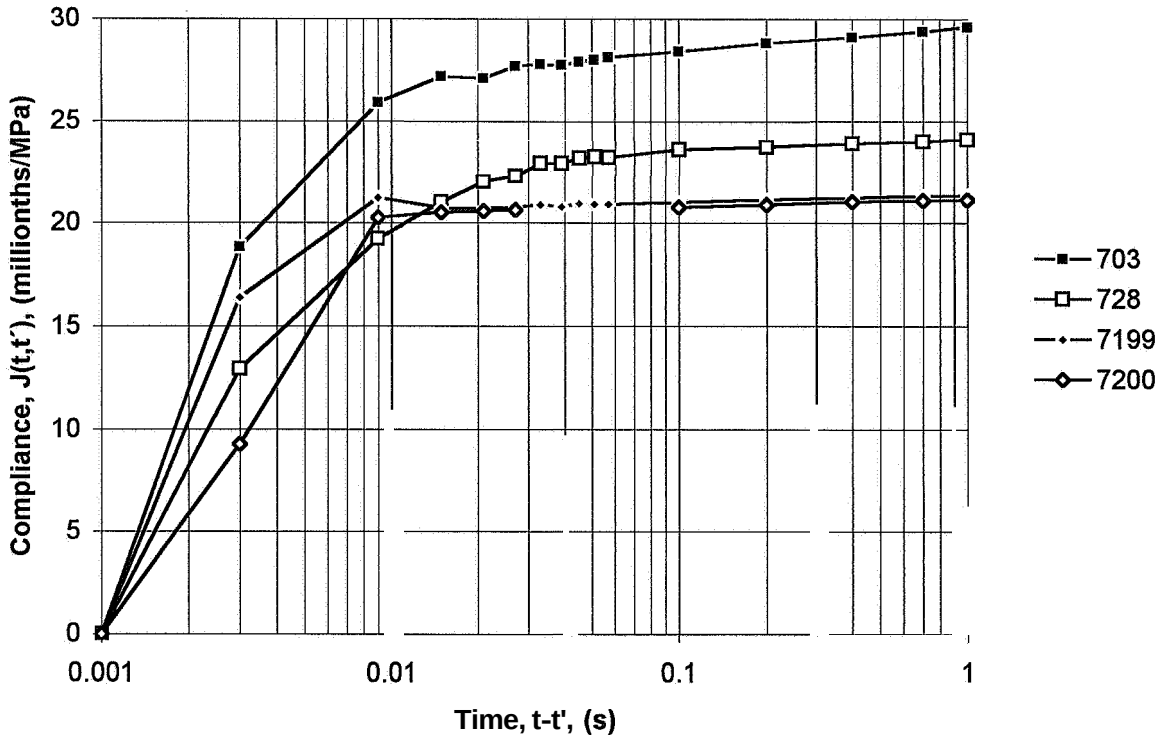

Appendix 10.11 - Repeated unloading compliance of mix 2 subjected to air curing:

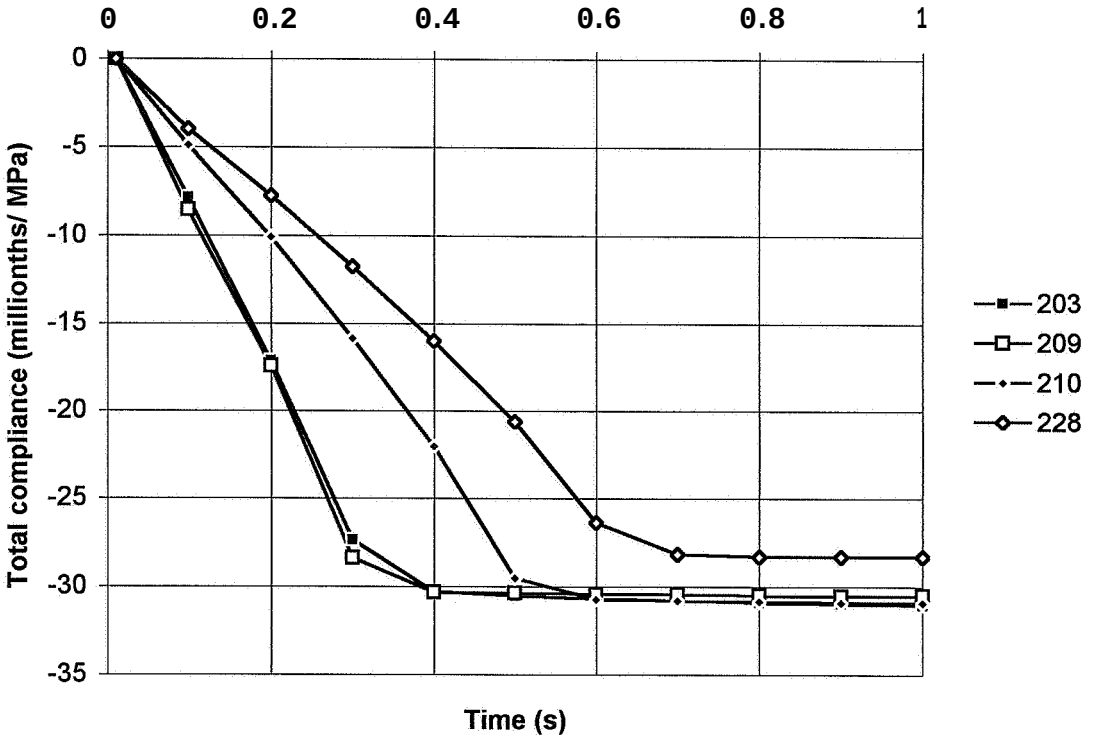

Appendix 10.12 - Repeated unloading compliance of mix 7 subjected to air curing

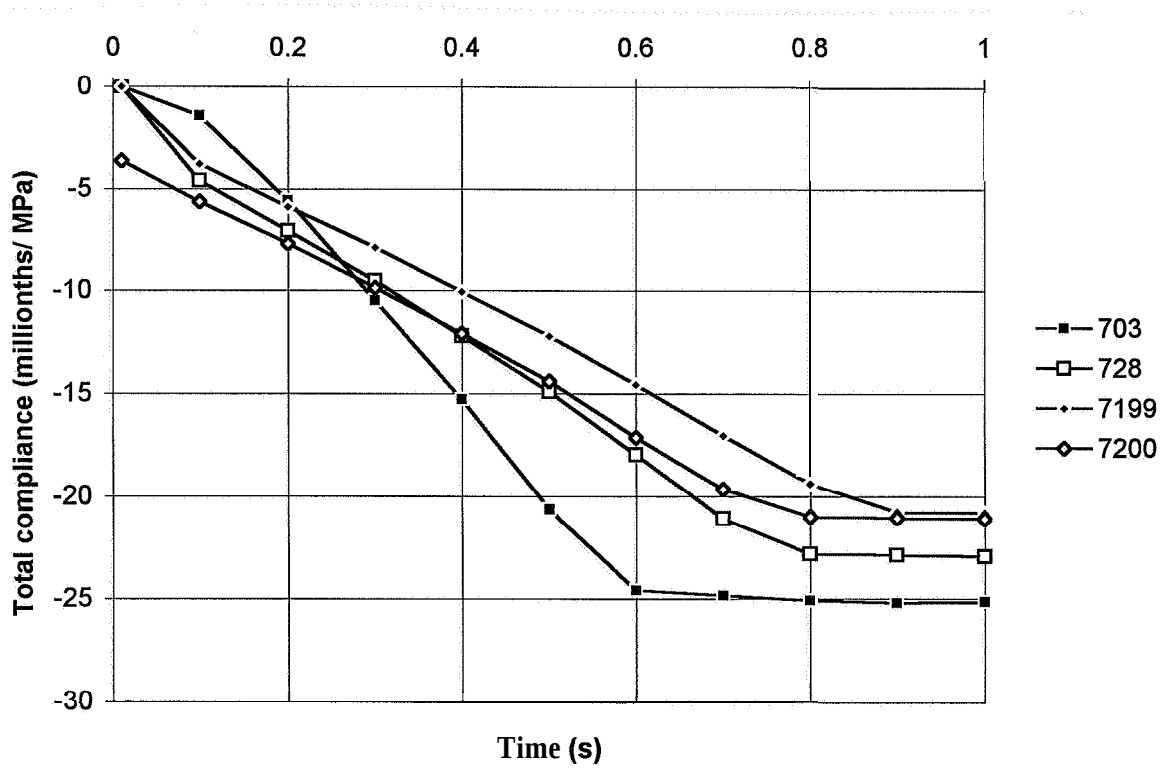

Appendix 10.13 - Unloading compliance of mix 1 subiected to sealed curing

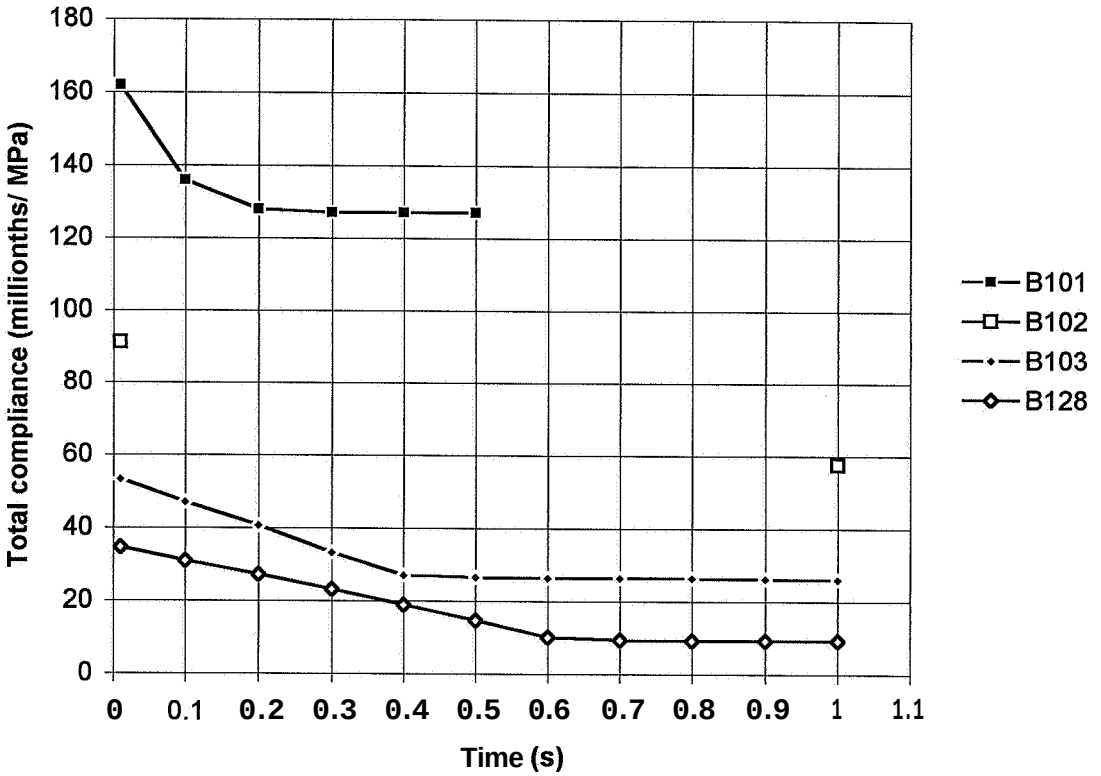

ppendix 4 - Unloading compliance of i 2 subjec to sealed curing

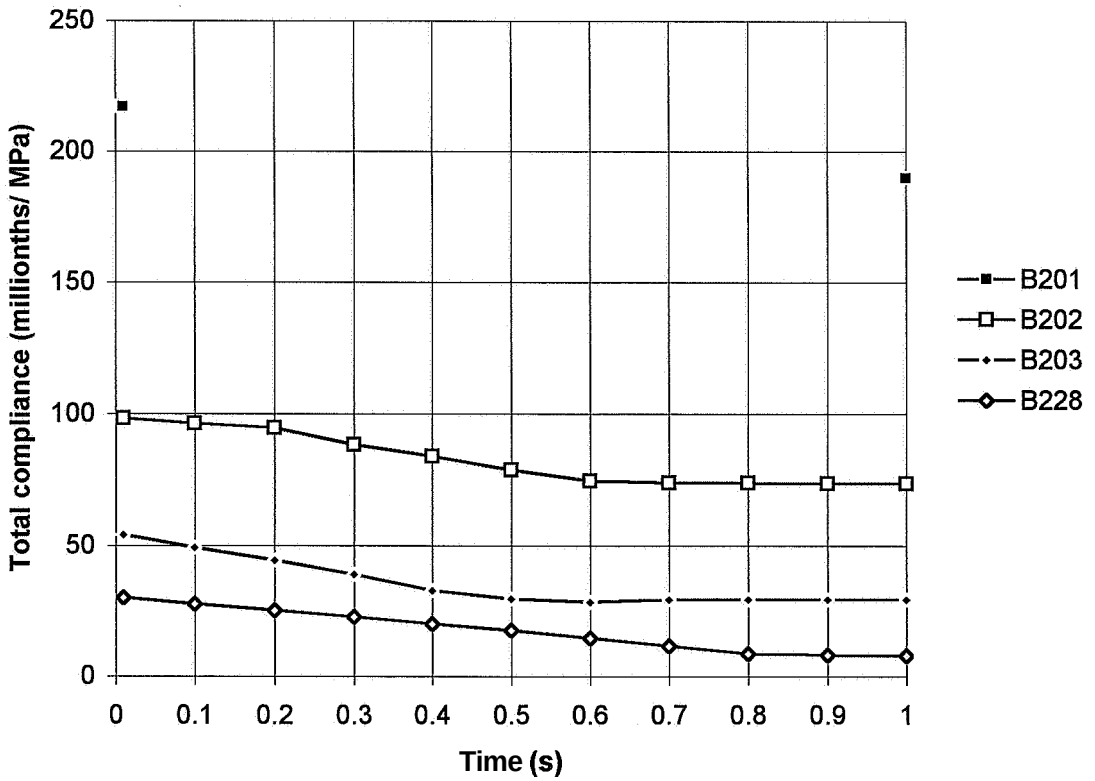

Appendix 10.15 Unloading complian of mix 3 subjected to sealed cu

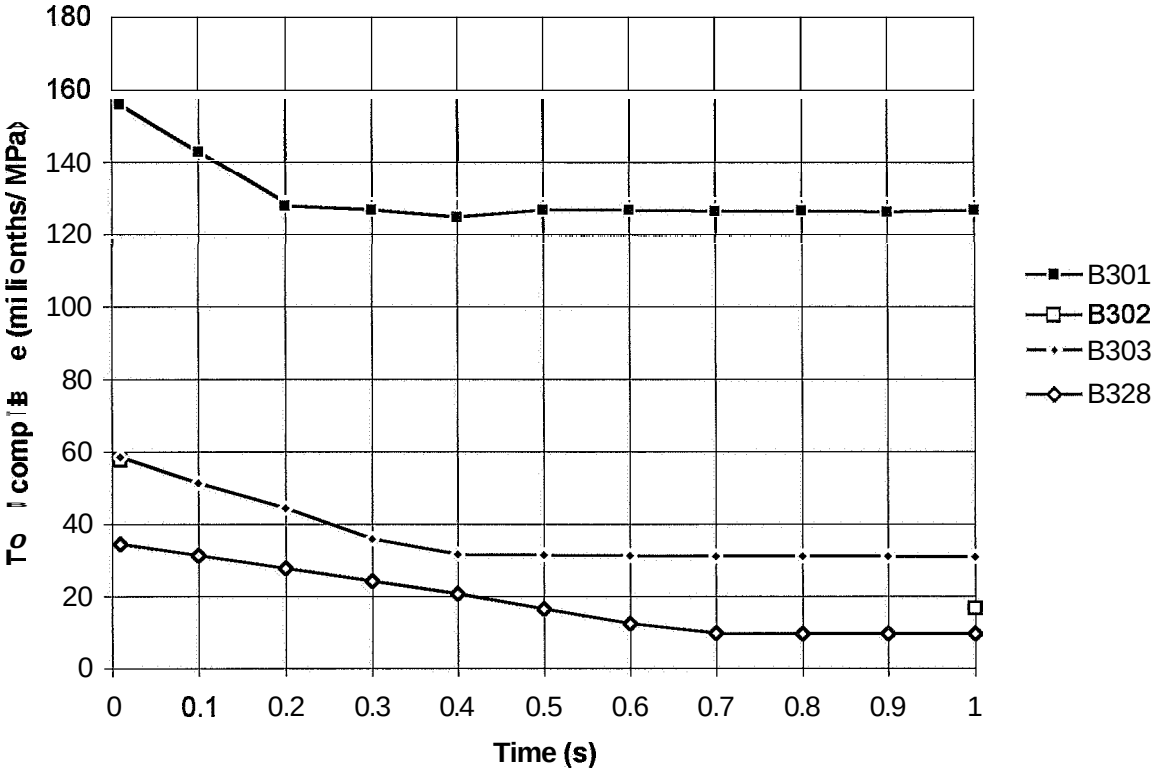

Appendix 10.16 - Unloading compliance of mix 4 subjected to sealed curing

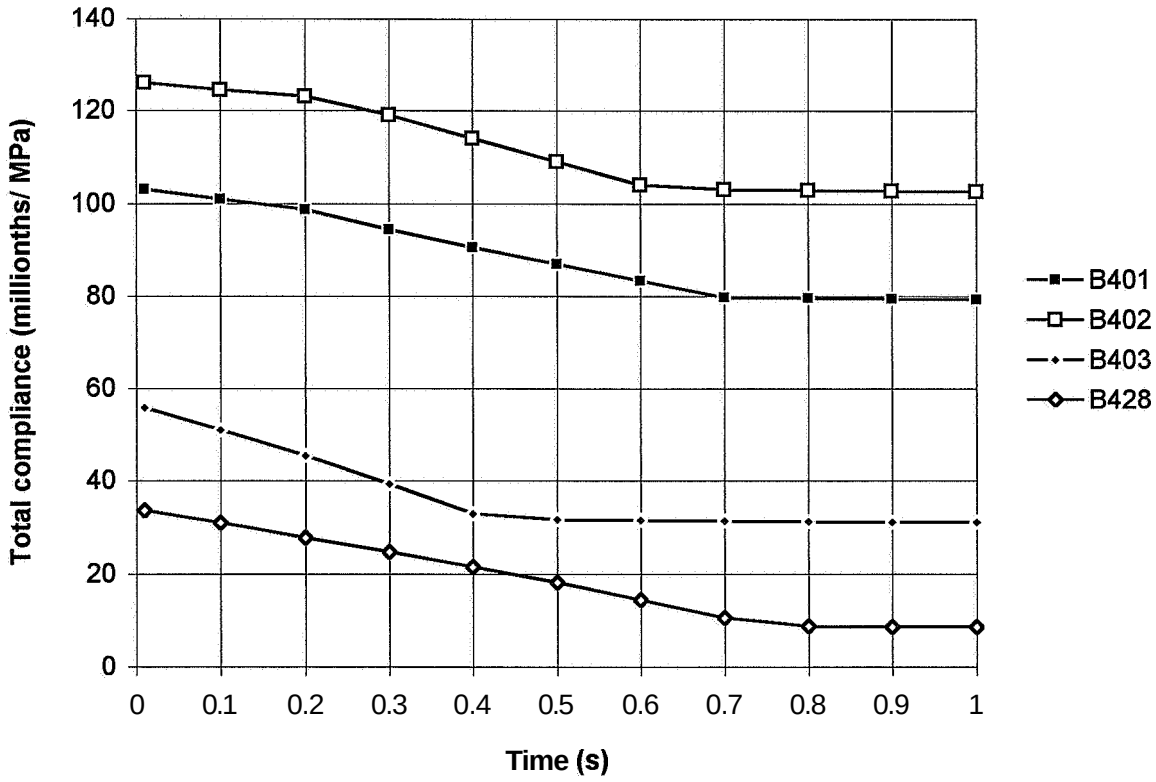

Appendix 10.17 - Unloading compliance of mix 5 subiected to sealed curing

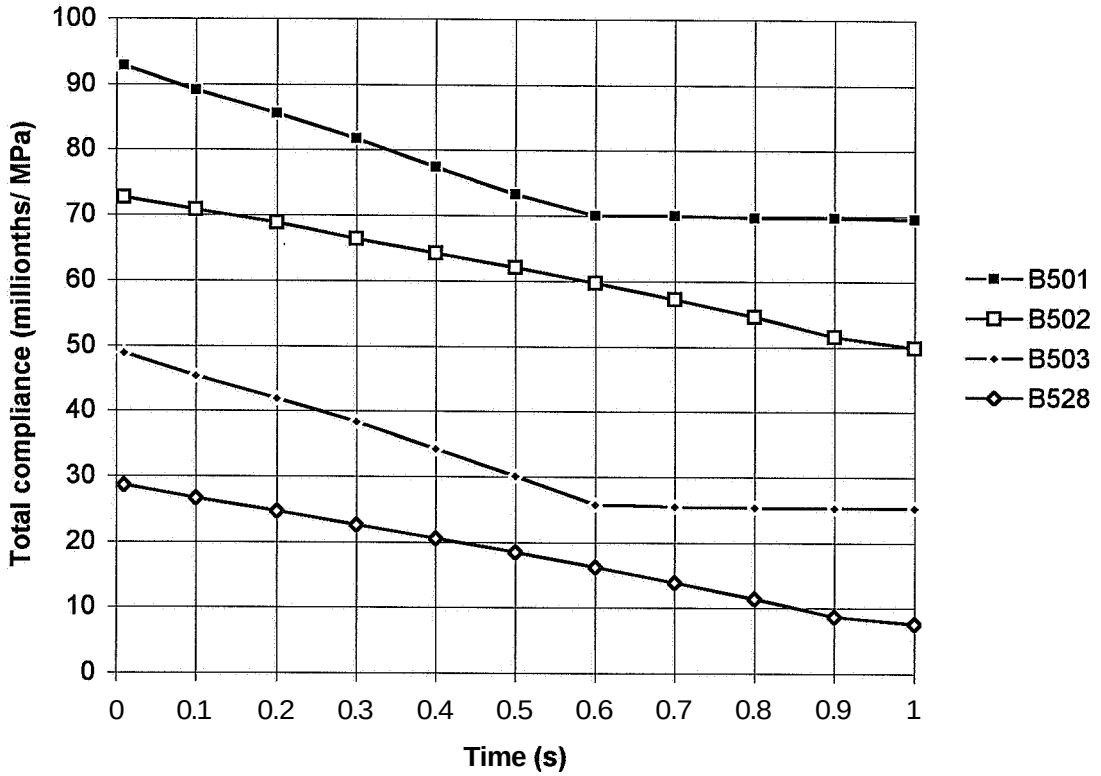

Appendix 10.18 - Unloading compliance of mix 6 subiected to sealed curing

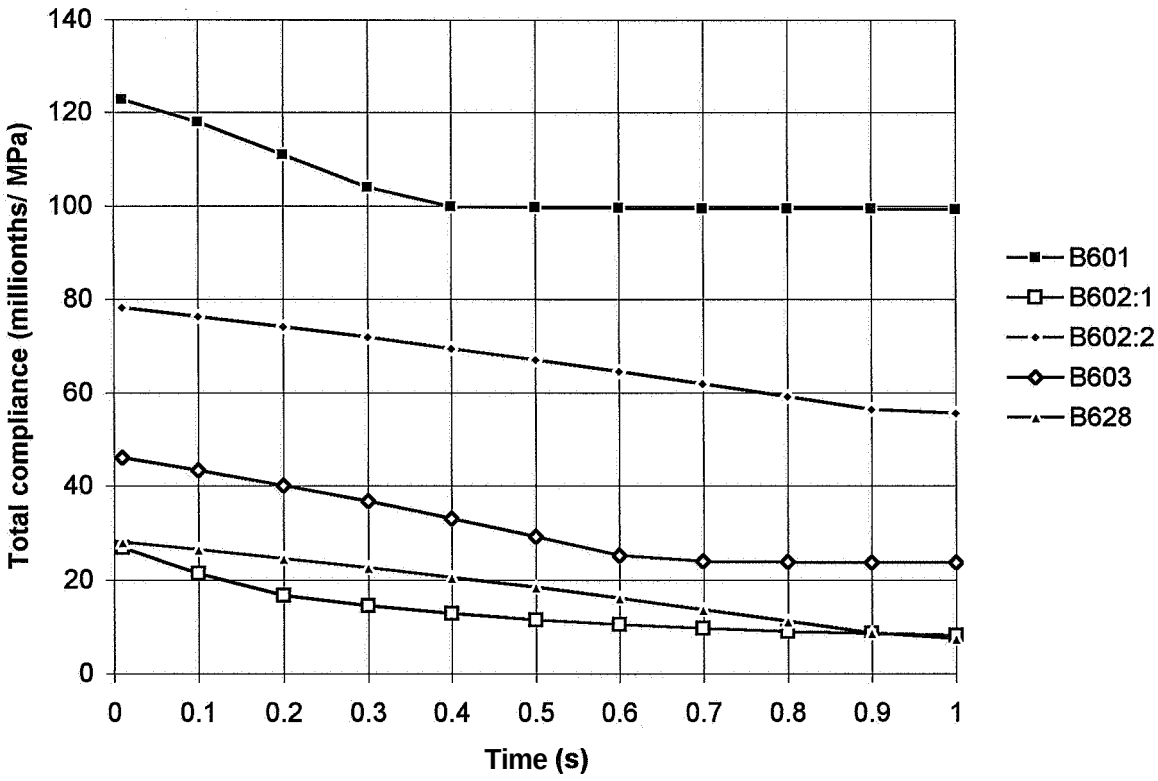

Appendix 10.19 - Unloading compliance of mix 7 subjected to sealed curing

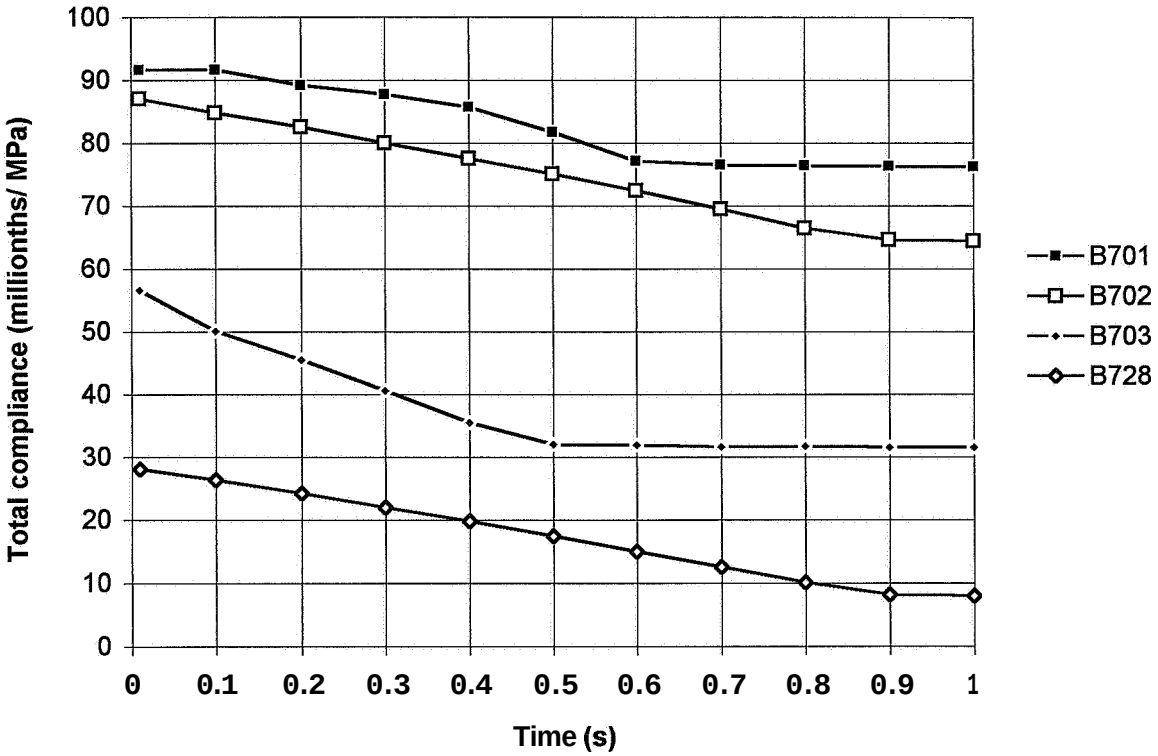

Appendix 10.20 - Unloading compliance of mix 8 subjected to sealed curing

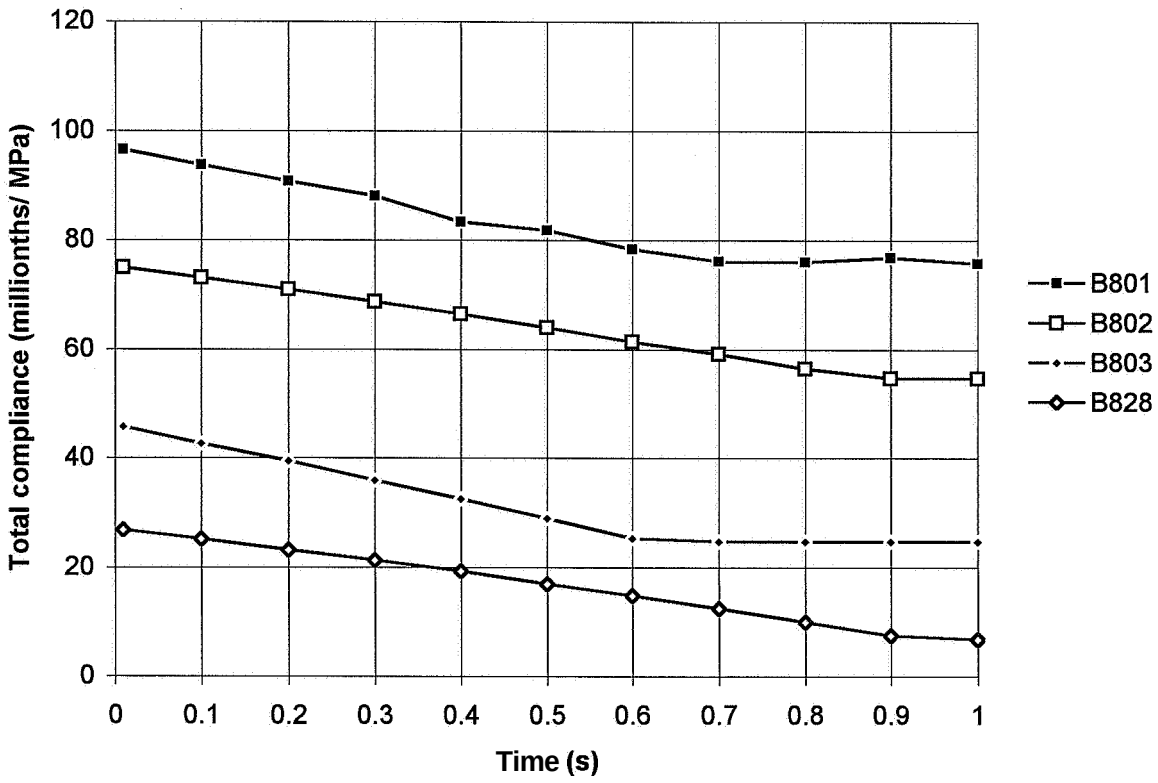

Appendix 10.21 - Unloading compliance of mature HPC subiected to sealed curing

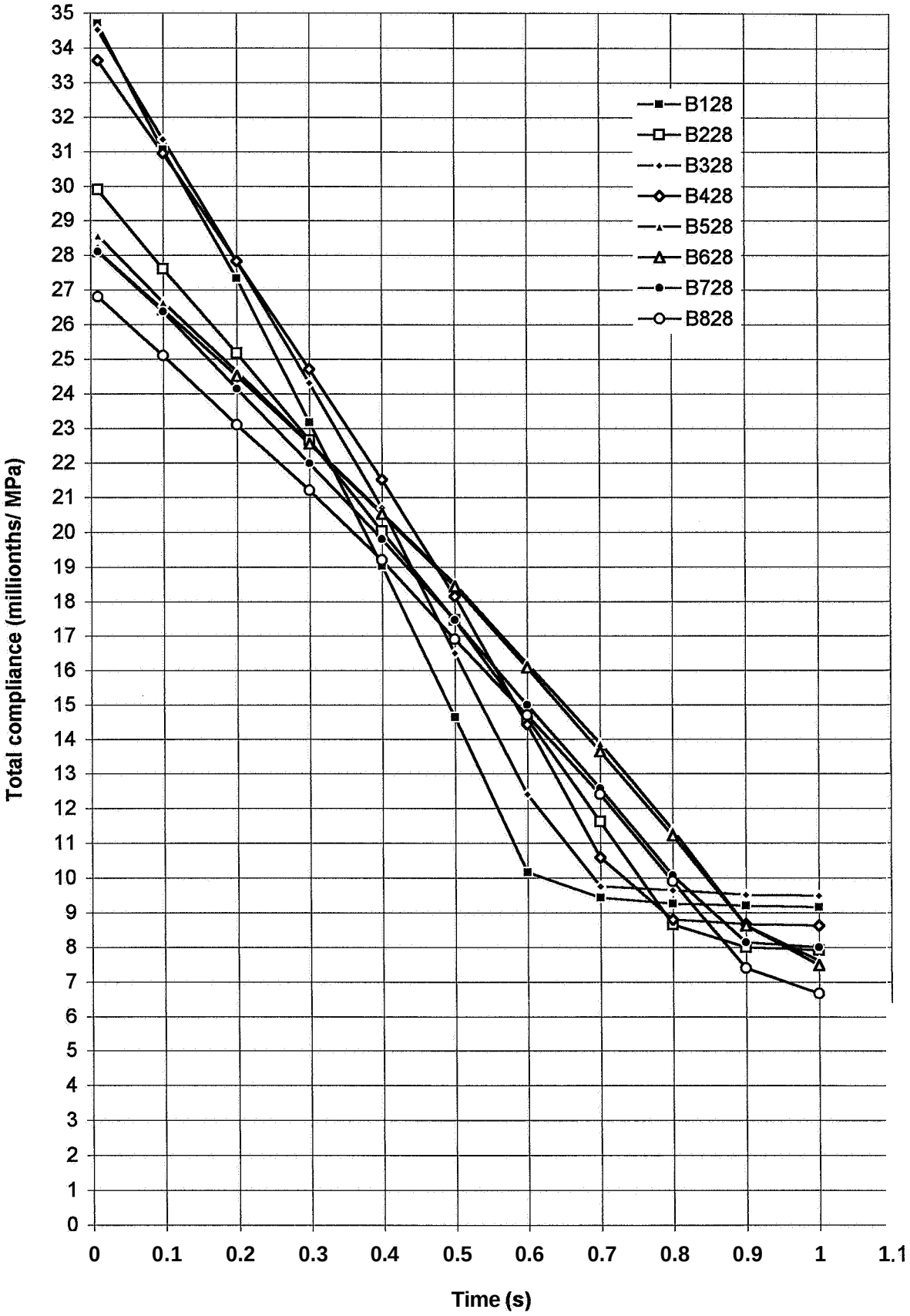

Appendix 10.22 - Repeated loading; compliance of mix 5 subiected to sealed curing

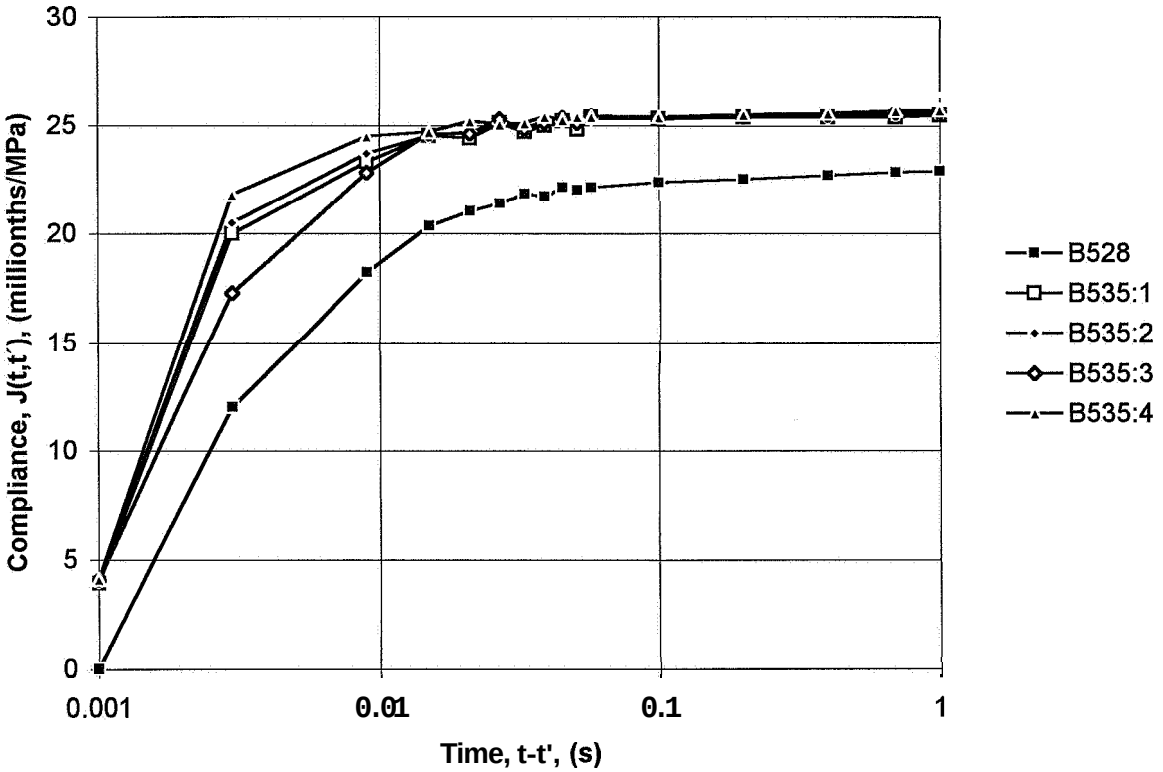

Appendix 10.23 - Repeated unloading; compliance of mix 5 subiected to sealed curing

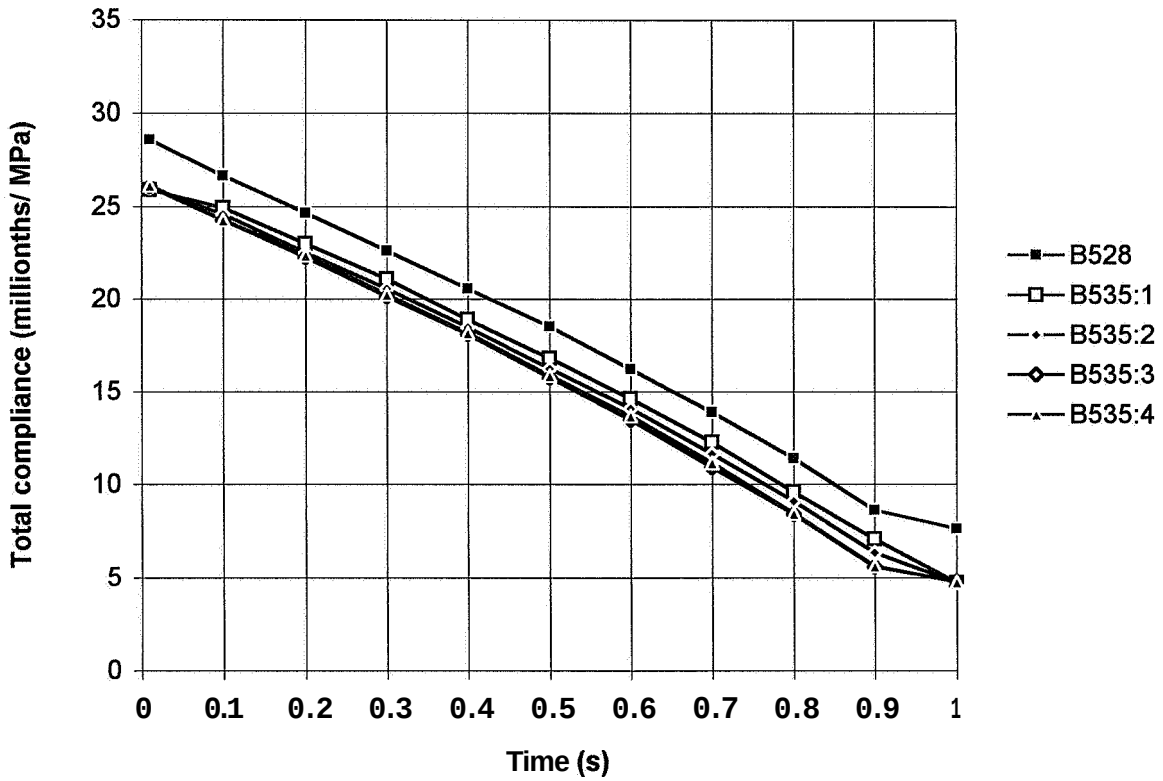

APPENDIX 11. TRANSVERSAL DEFORMATION OF CYLINDERS

Symbols:

B denotes basic creep (sealed curing)
D denotes drying creep (air curing)
∅ internal relative humidity
6... denotes concrete **mix, Table 5.1**
...01 age at loading: 1 day; stresslcylinder strength ratio: 0.84
...02 age at loading: 2 days; stresslcylinder strength ratio: 0.84
...03 age at loading: 2 days; stresslcylinder strength ratio: 0.42
...28 age at loading: 28 days; stresslcylinder strength ratio: 0.42

Appendix 11.1 - Tendency curves of transversal deformation versus maturity

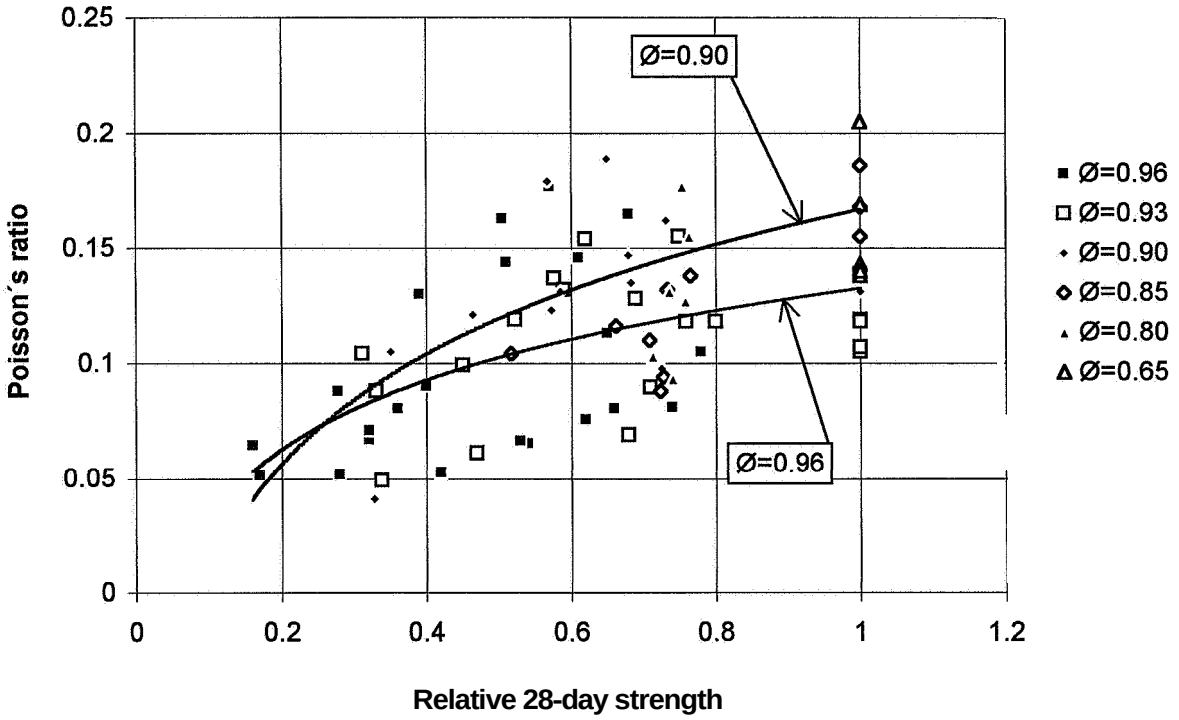

Appendix 11.2 - Transversal deformation of mature HPC versus relative humidity

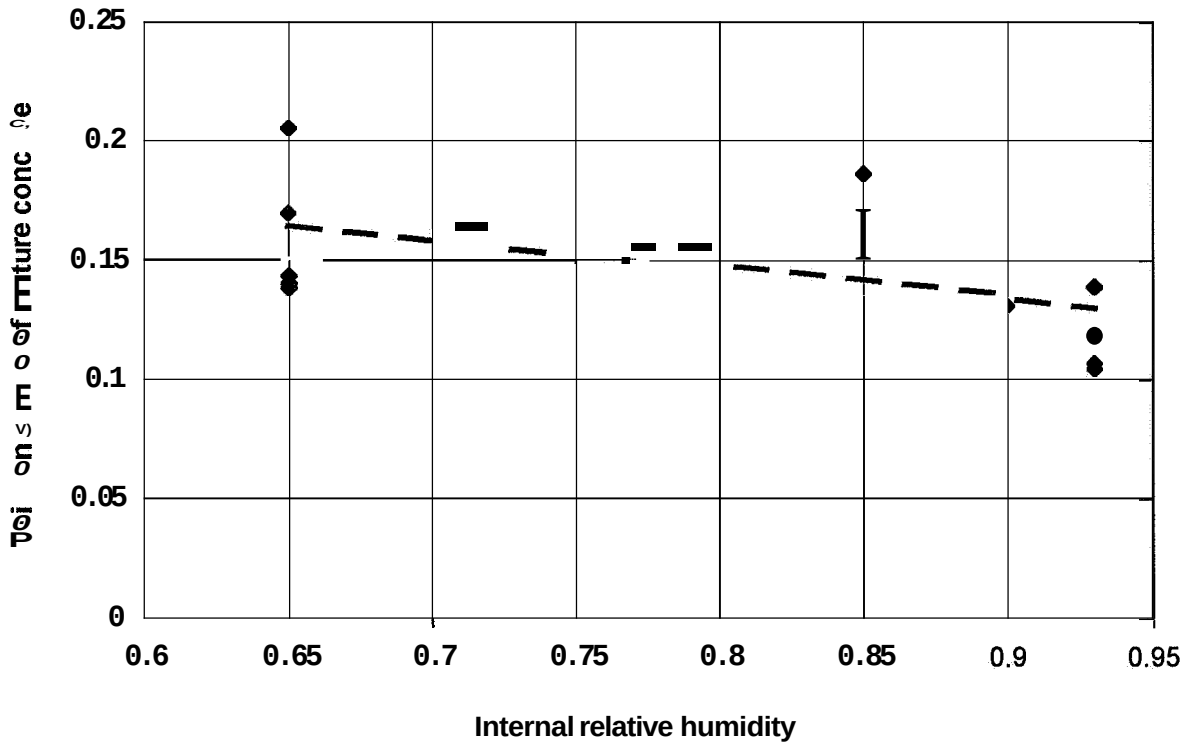

Appendix 11.3 - Transversal deformation versus current cube strength

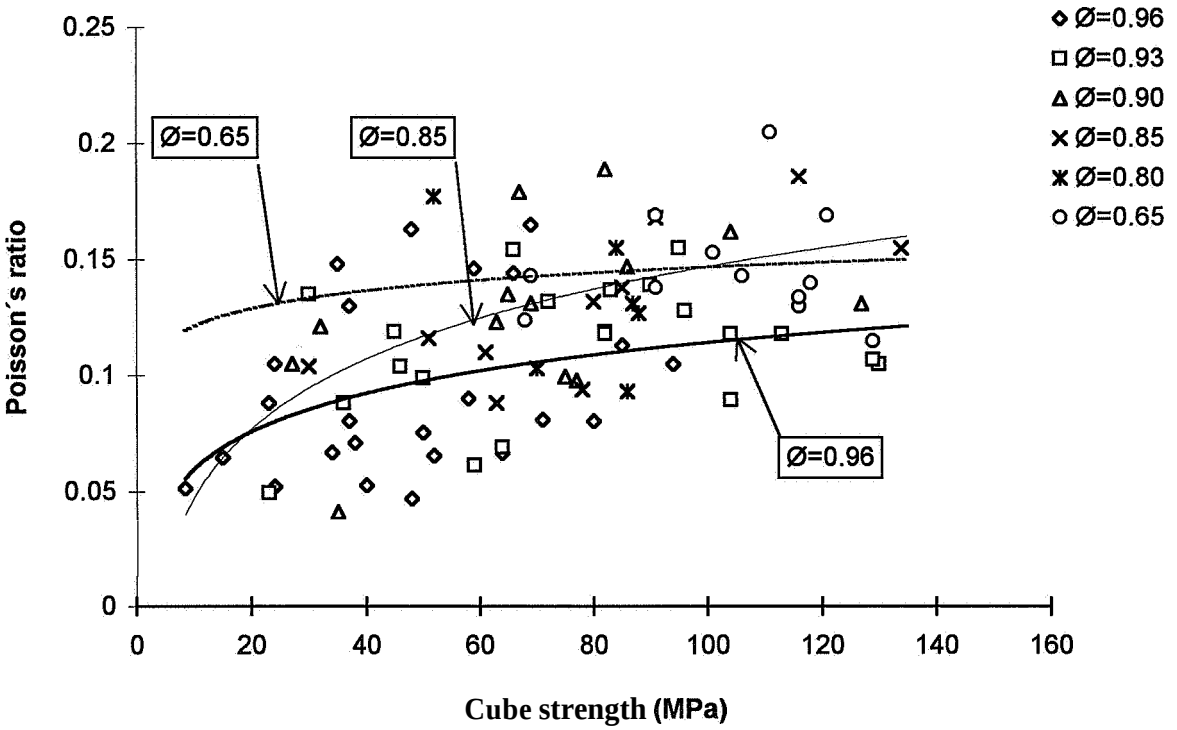

Appendix 11.4 – Transversal deformation of mix 1 subiected to sealed curing

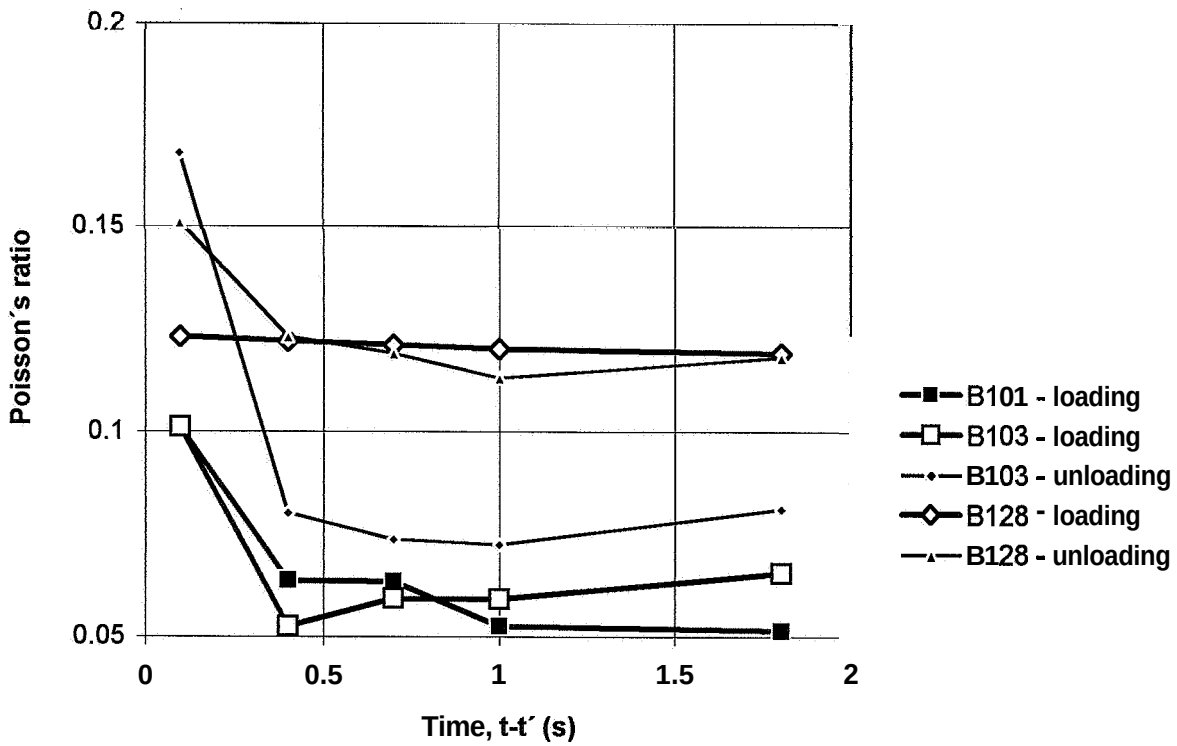

Appendix 11.5 – Transversal deformation of mix 2 subjected to sealed curing

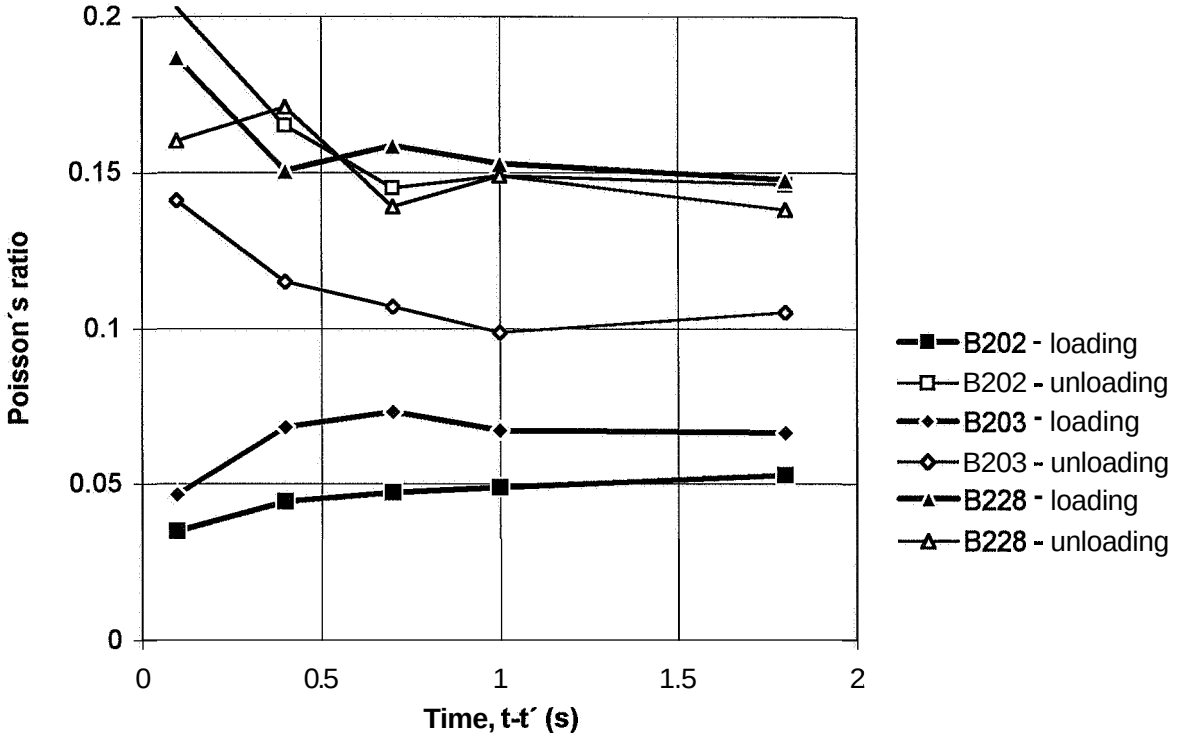

Appendix 11.6 – Transversal deformation of mix 3 subjected to sealed curing;

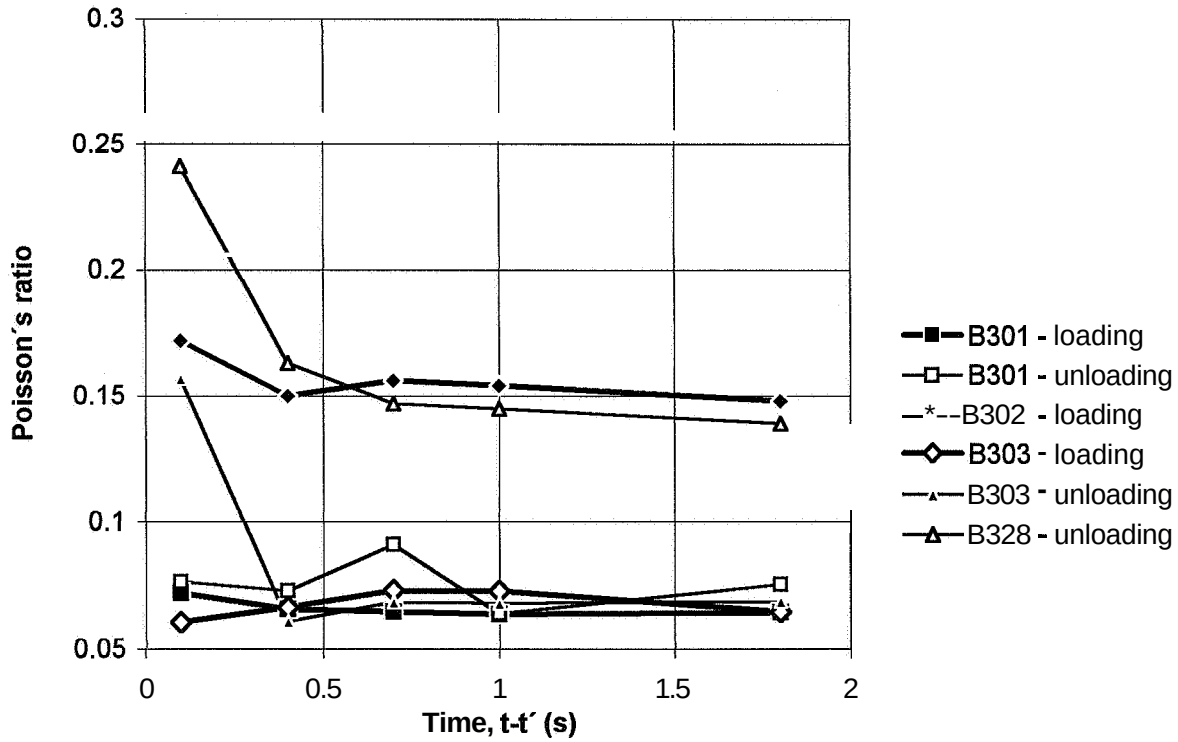

Appendix 11.7 – Transversal defo ation of mix 4 subjected to sealed cur

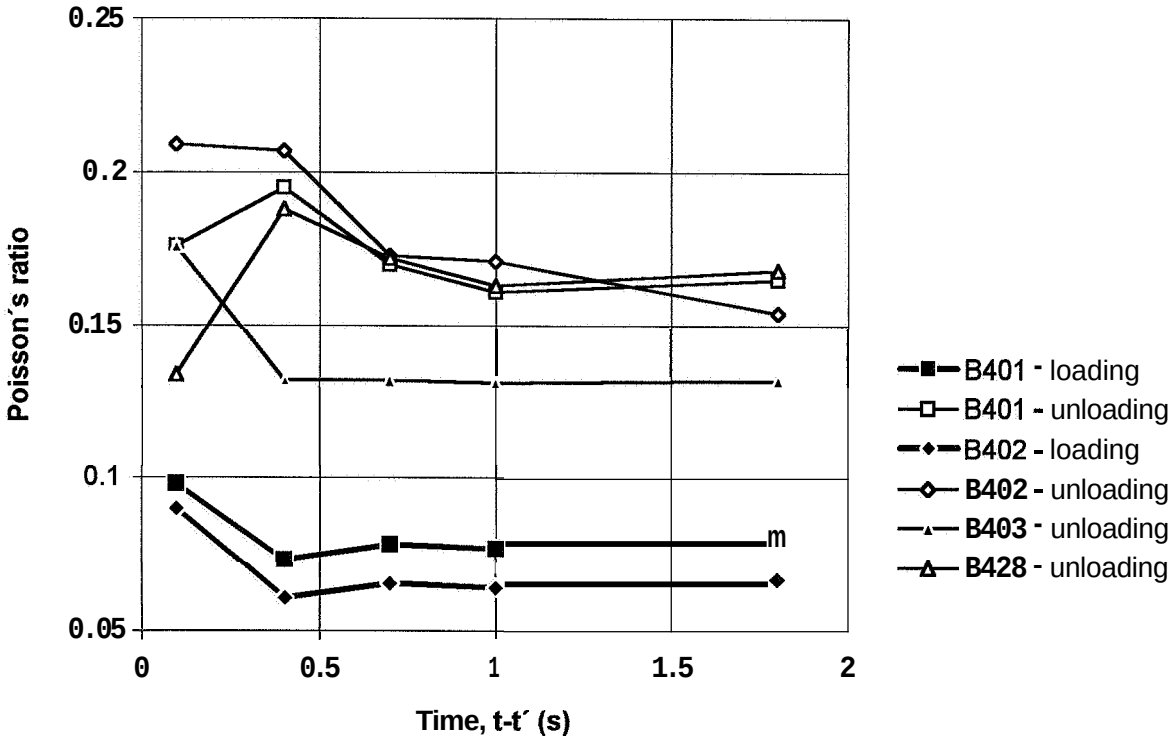

Appendix 11.8 – Transversal deformation of mix 5 subjected to sealed curing:

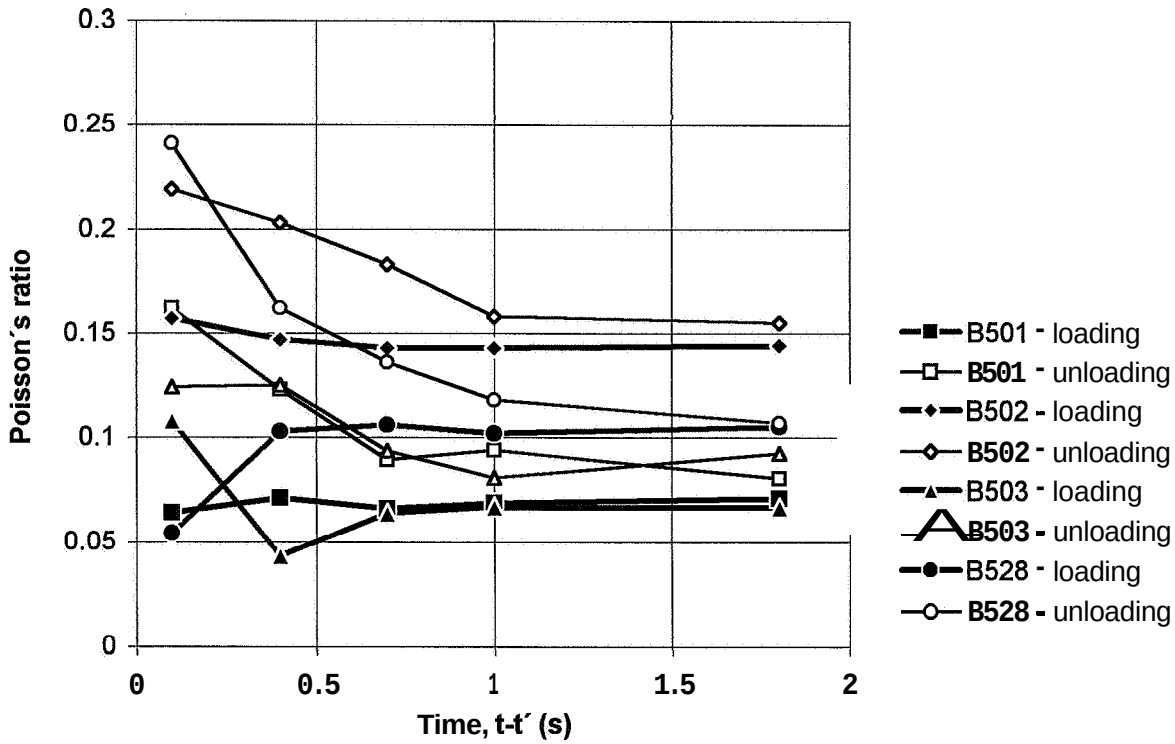

Appendix 11.9 – Transversal deformation of mix 6 subiected to sealed curing

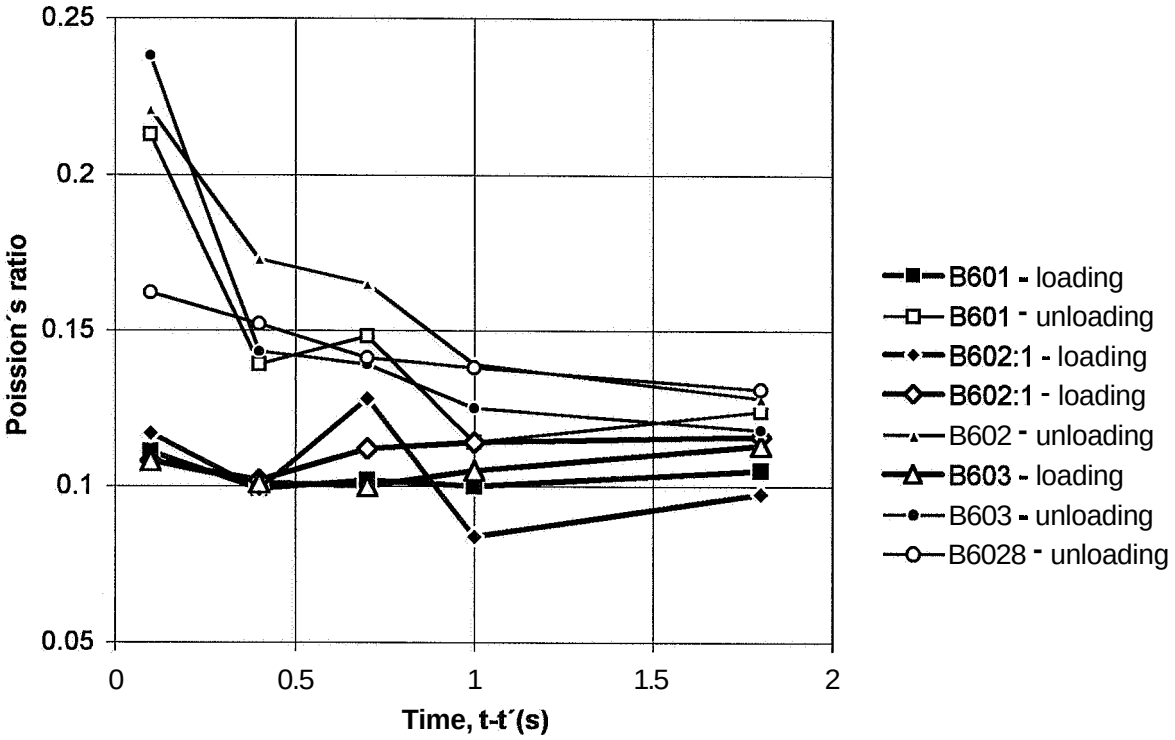

Appendix 11.10 – Transversal deformation of mix 7 subiected to sealed curing

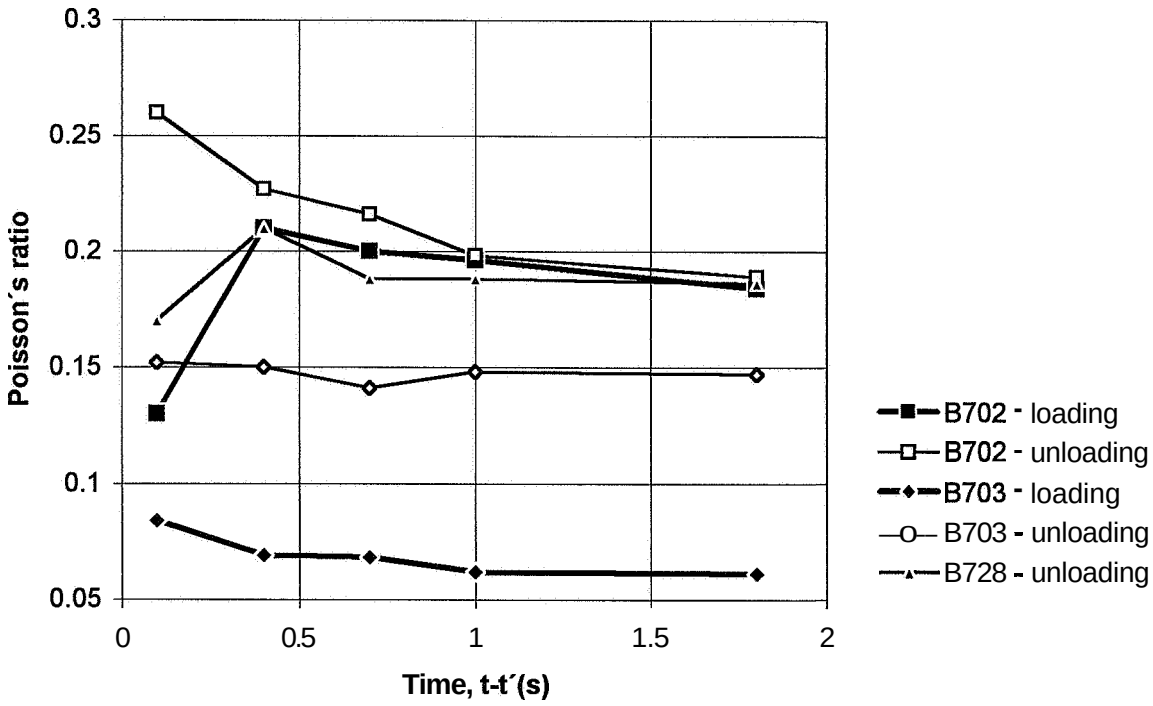

Appendix 11.11 – Transversal deformation of mix 8 subjected to sealed curing

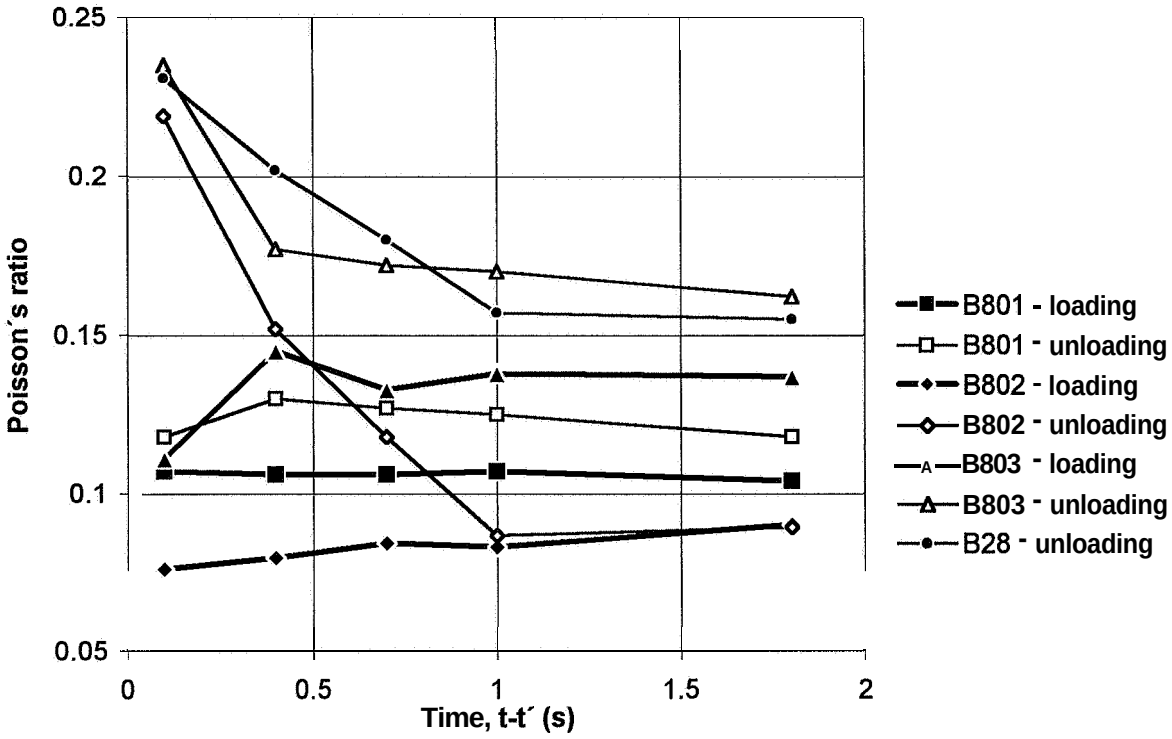

APPENDIX 12. MODULI OF ELASTICITY

1= mix 1

N.B.: The slightly inclined line before quasi-instantaneous loading is obtained directly from the computer print-out and does not reflect the true loading procedure.

Appendix 12.1 - Loading versus time of mix 1 at loading 1.

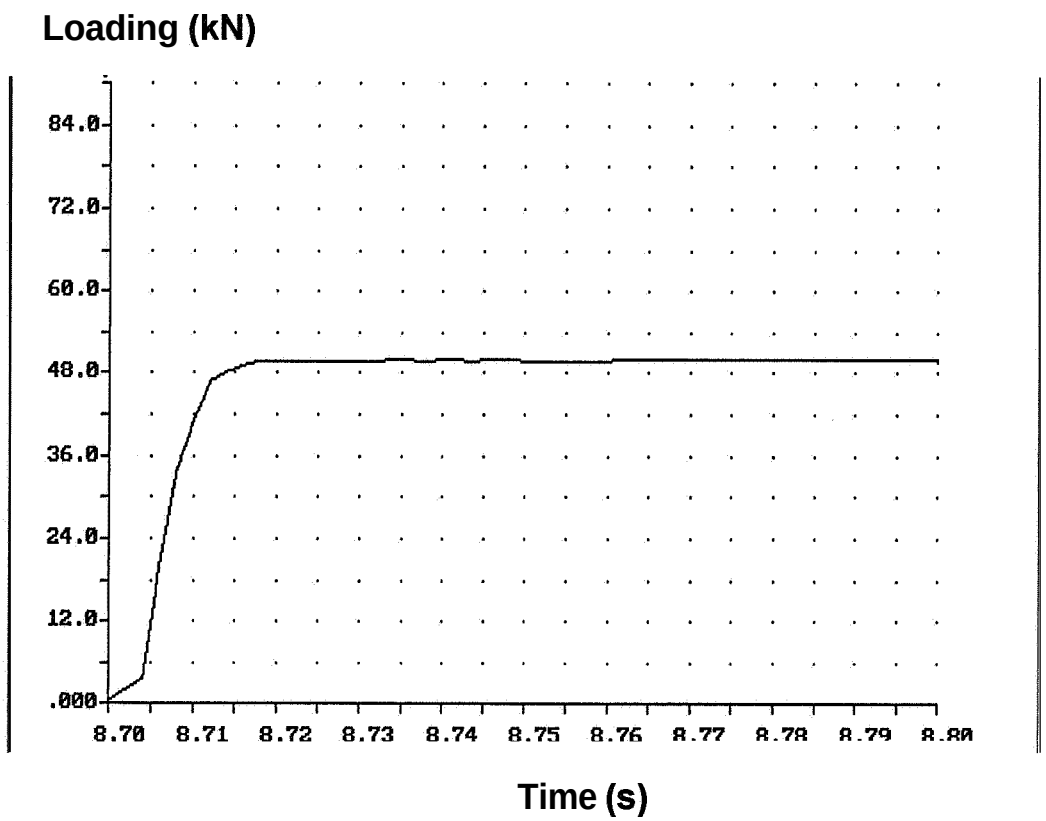

Appendix 12.2 - Loading versus time of mix 1 at loading 2.

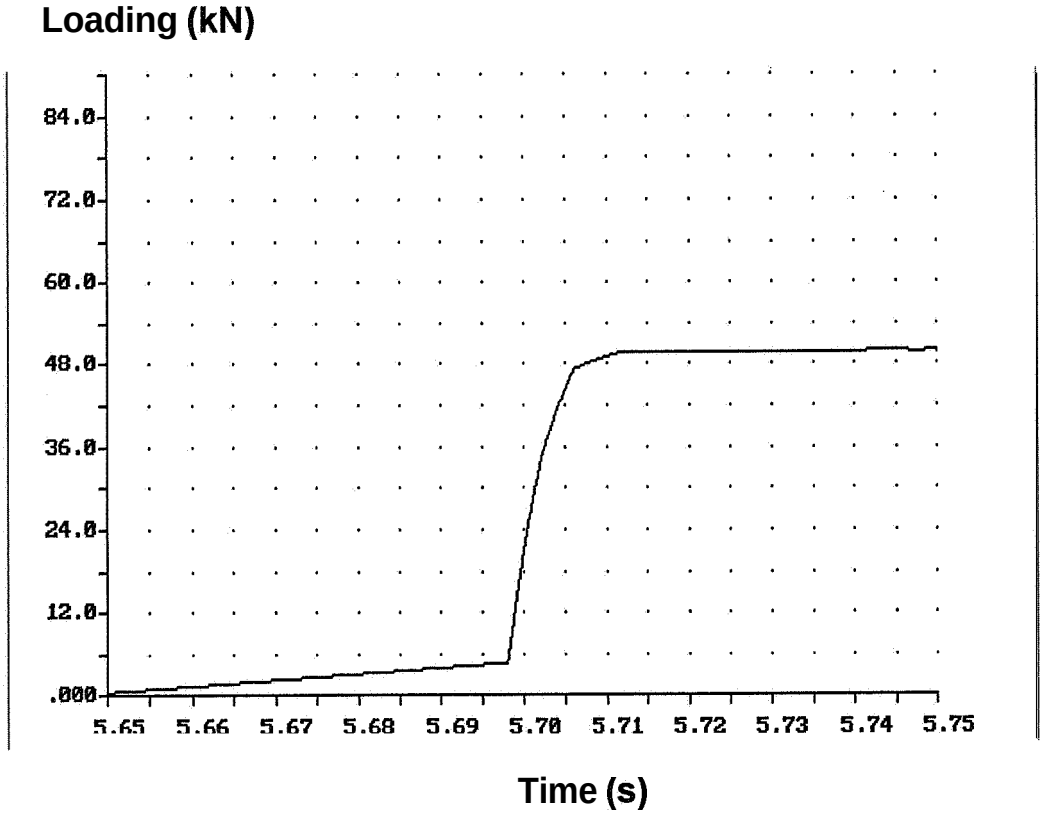

Appendix 12.3 - Loading versus time of mix 1 at loading 3.

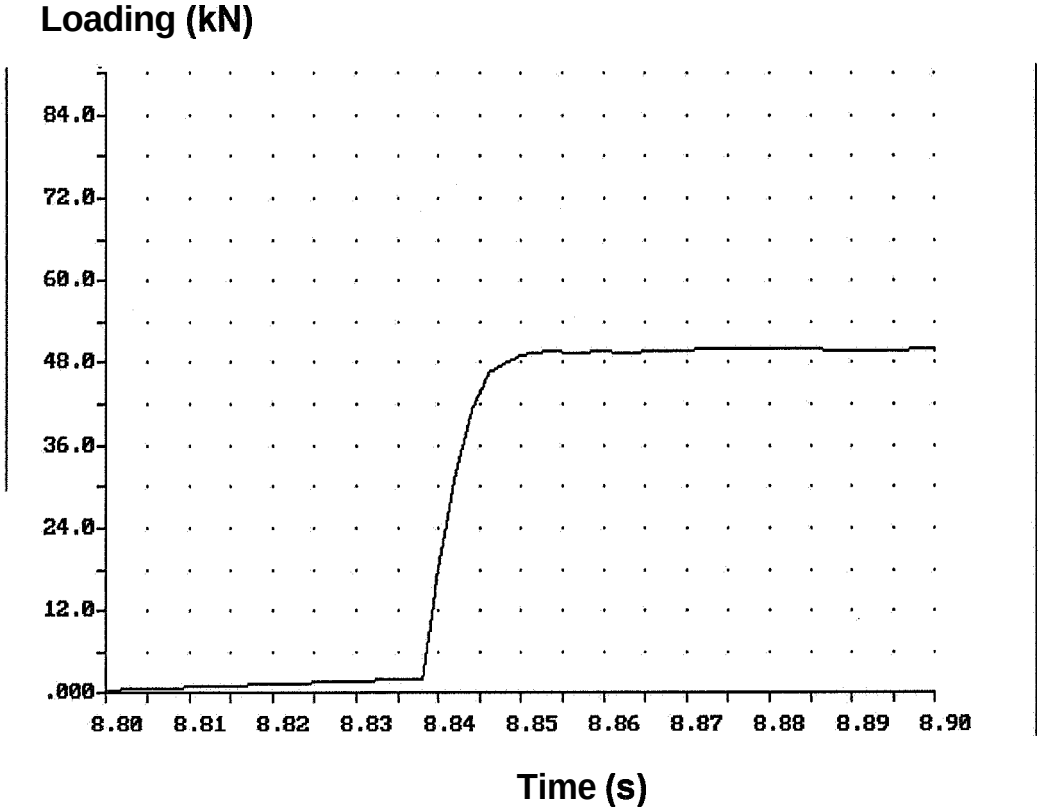

Appendix 12.4 - Loading versus time of mix 2 at loading 2.

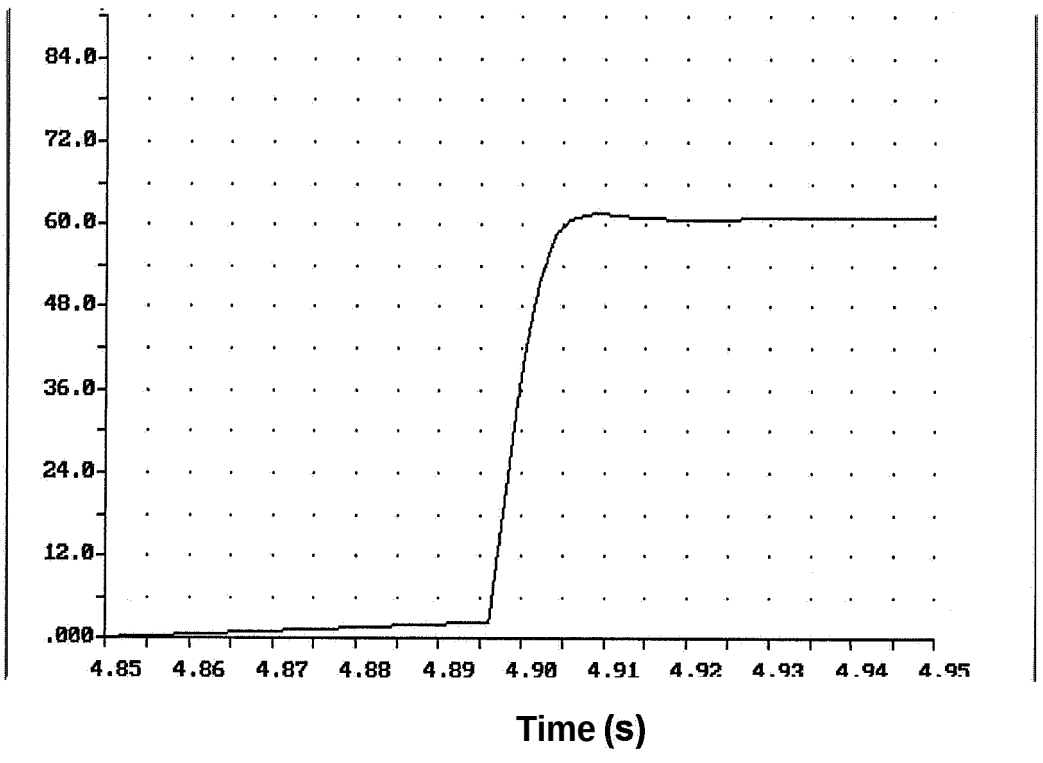

Appendix 12.5 - Loading versus time of mix 2 at loading 3.

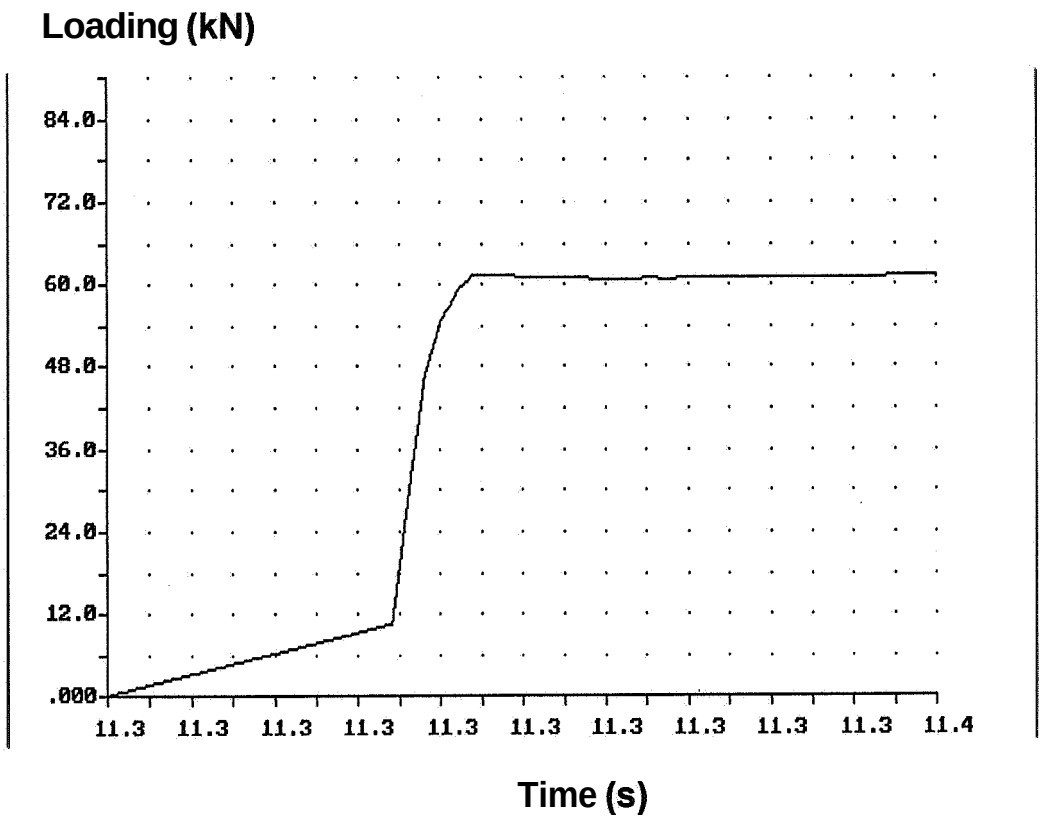

Appendix 12.6 - Loading versus time of mix 2 at loading 4.

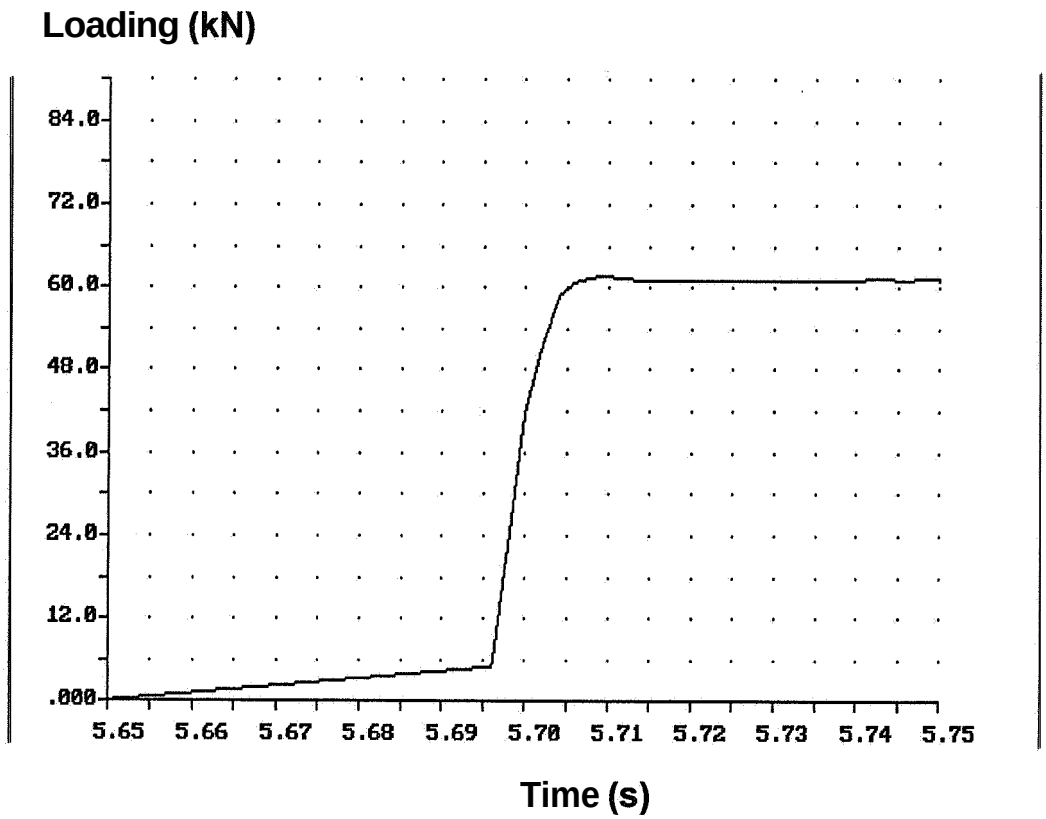

Appendix 12.7 - Loading; versus time of mix 2 at loading 5.

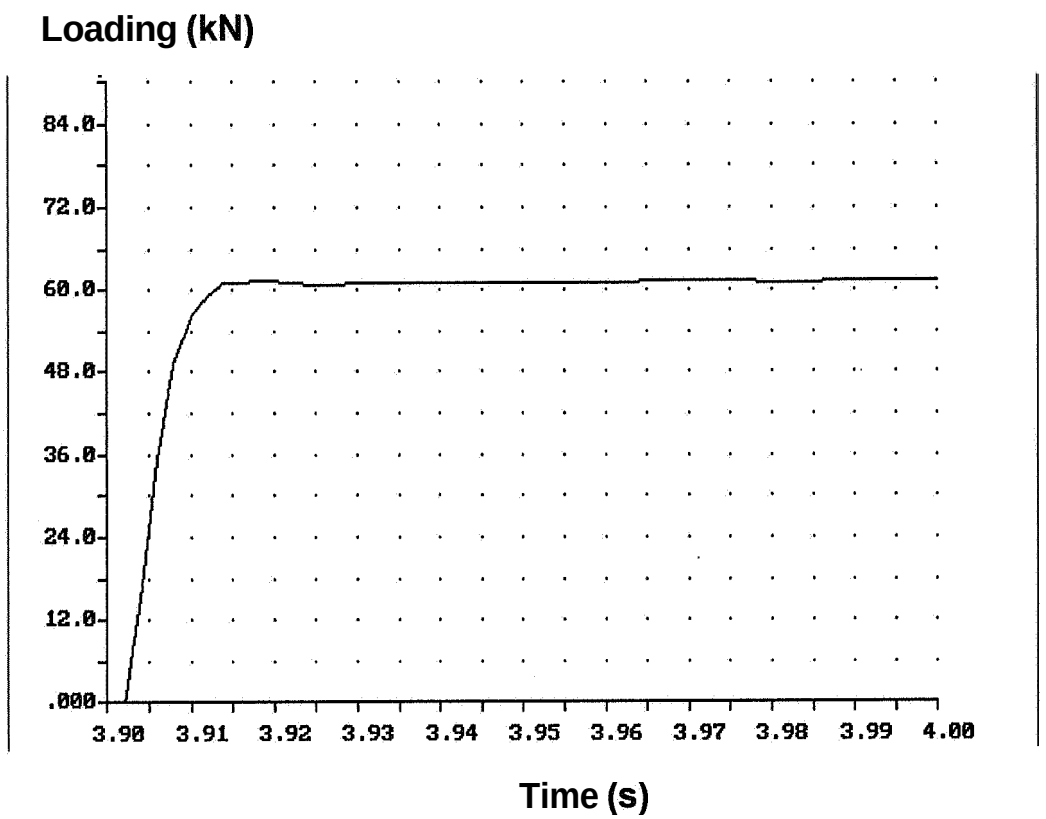

Appendix 12.8 - Loading versus time of mix 2 at loading 6.

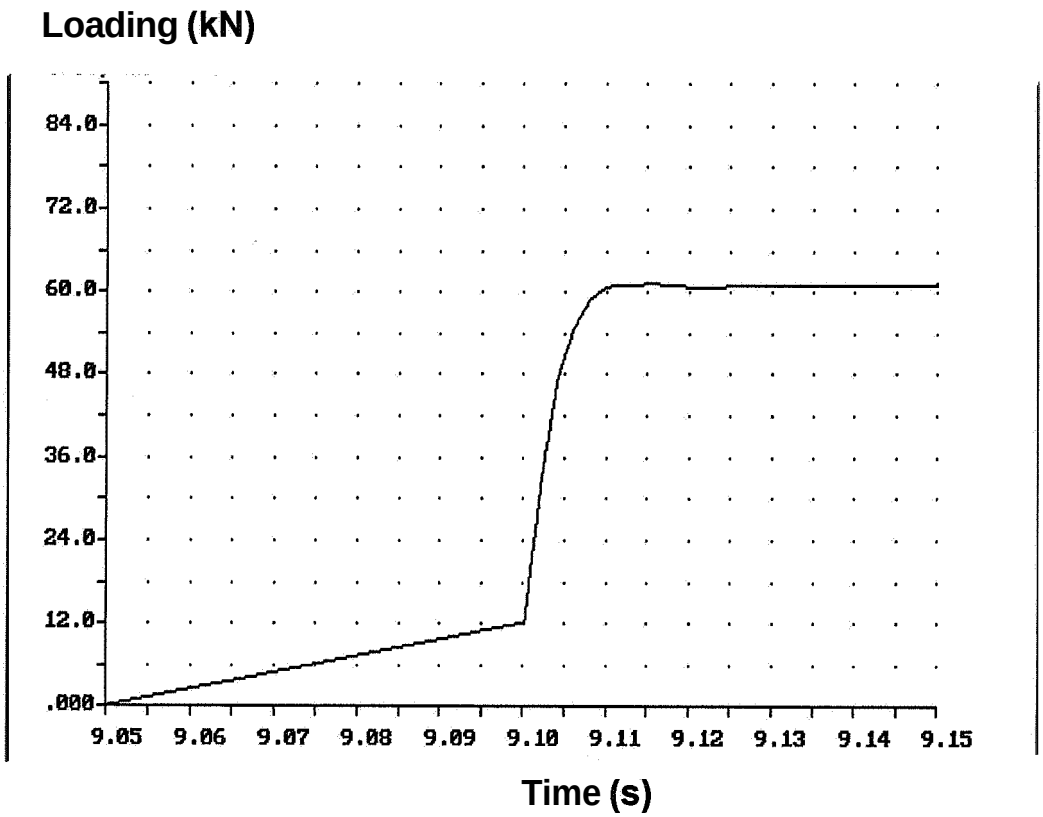

Appendix 12.9 - Loading versus time of mix 3 at loading 1.

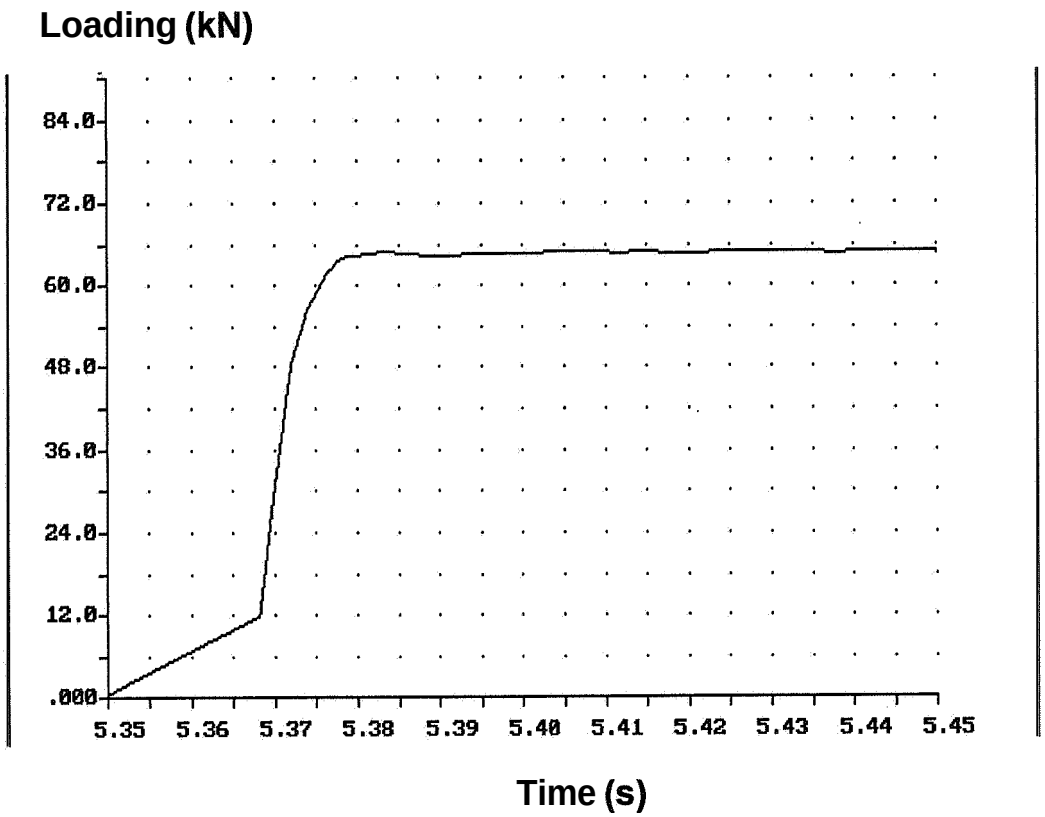

Appendix 12.10 - Loading versus time of mix 3 at loading 2.

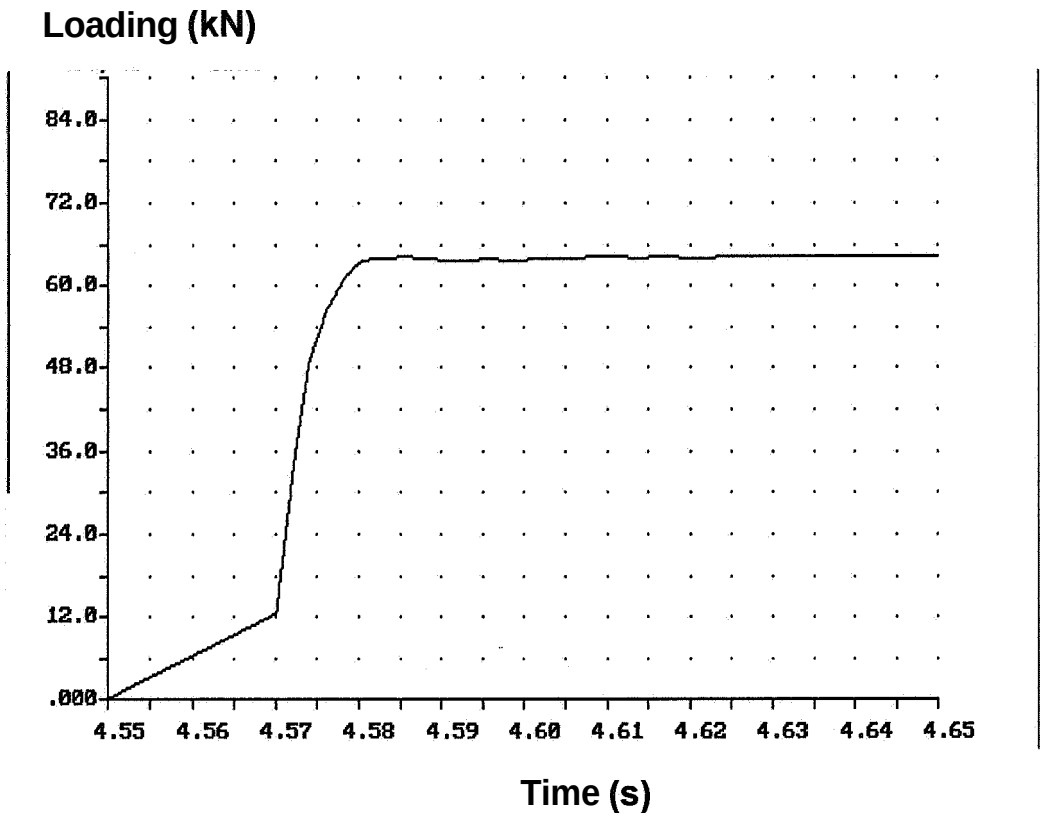

Appendix 12.11 - Loading versus time of mix 3 at loading 3.

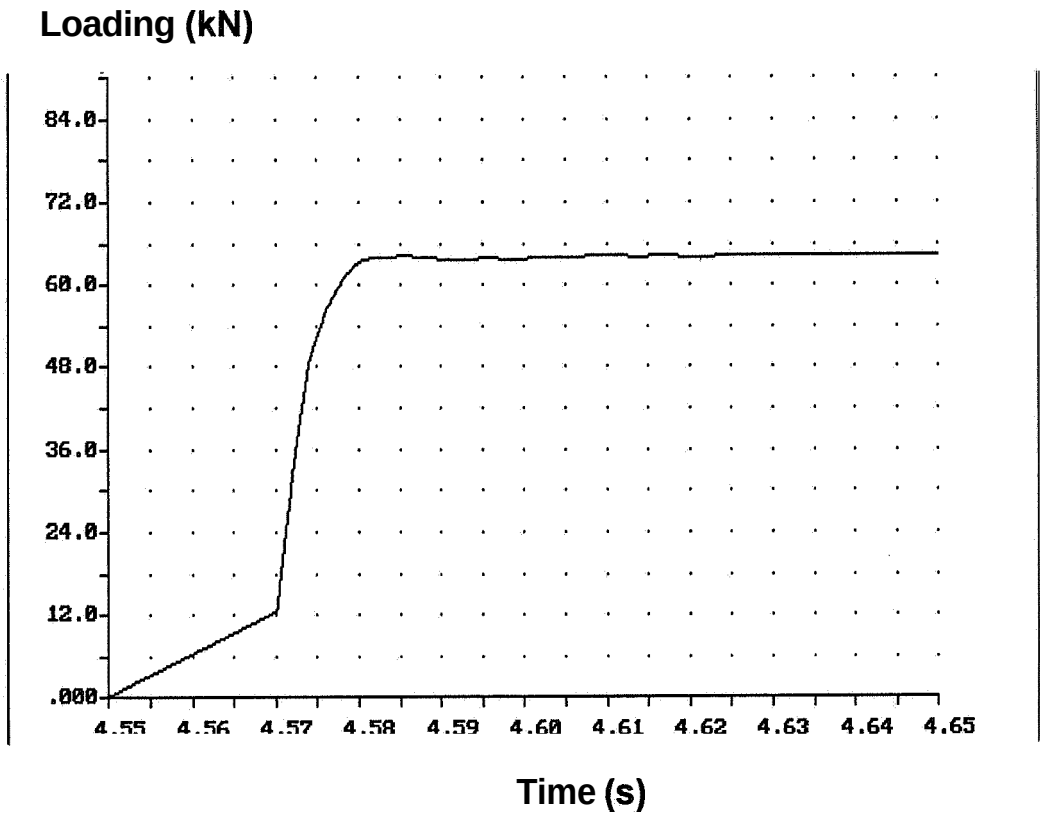

Appendix 12.12 - Loading versus time of mix 4 at loading 1.

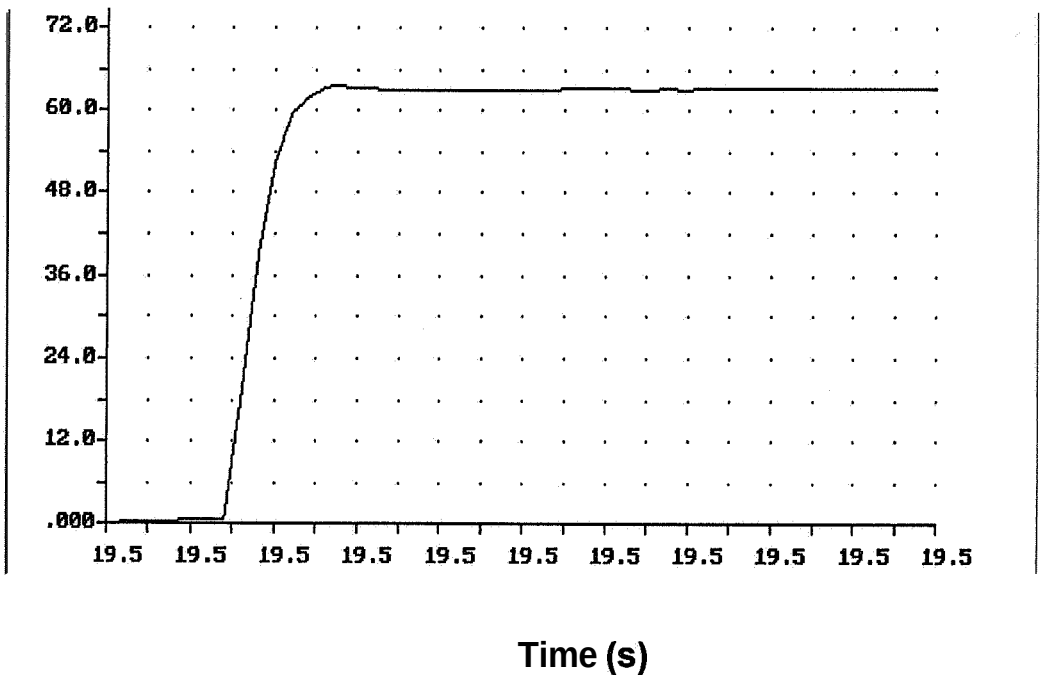

Appendix 12.13 - Loading versus time of mix 4 at loading 2.

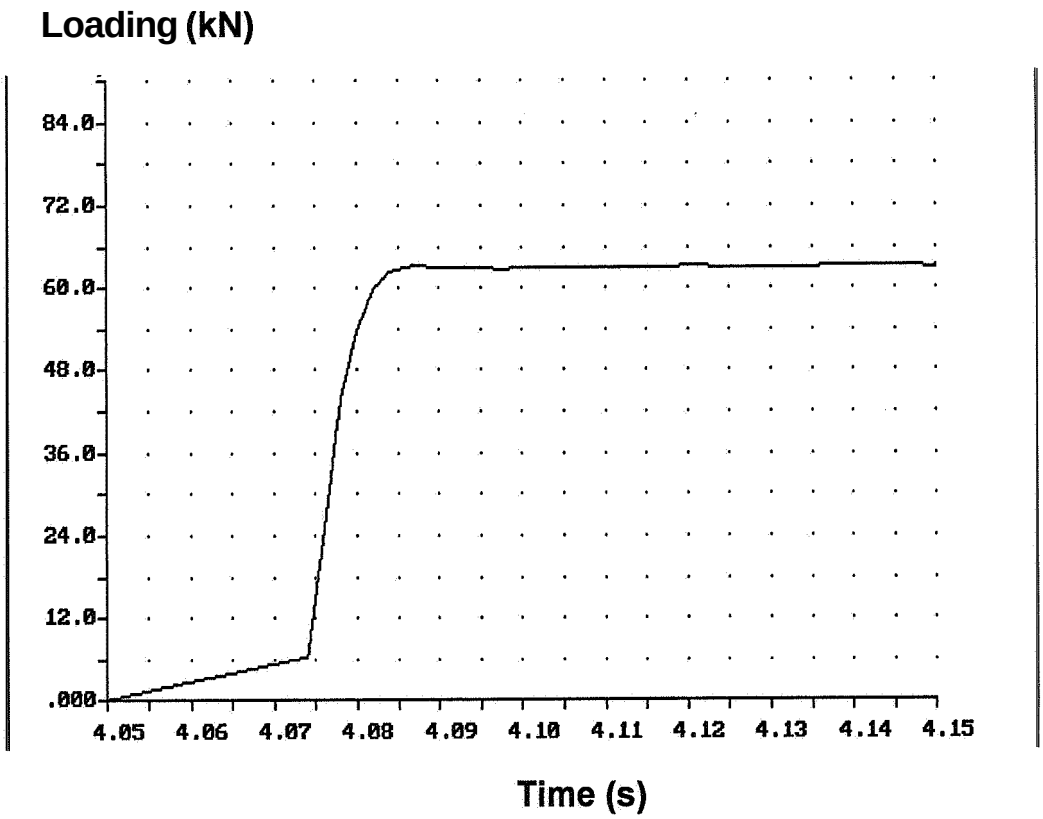

Appendix 12.14 - Loading versus time of mix 4 at loading 3.

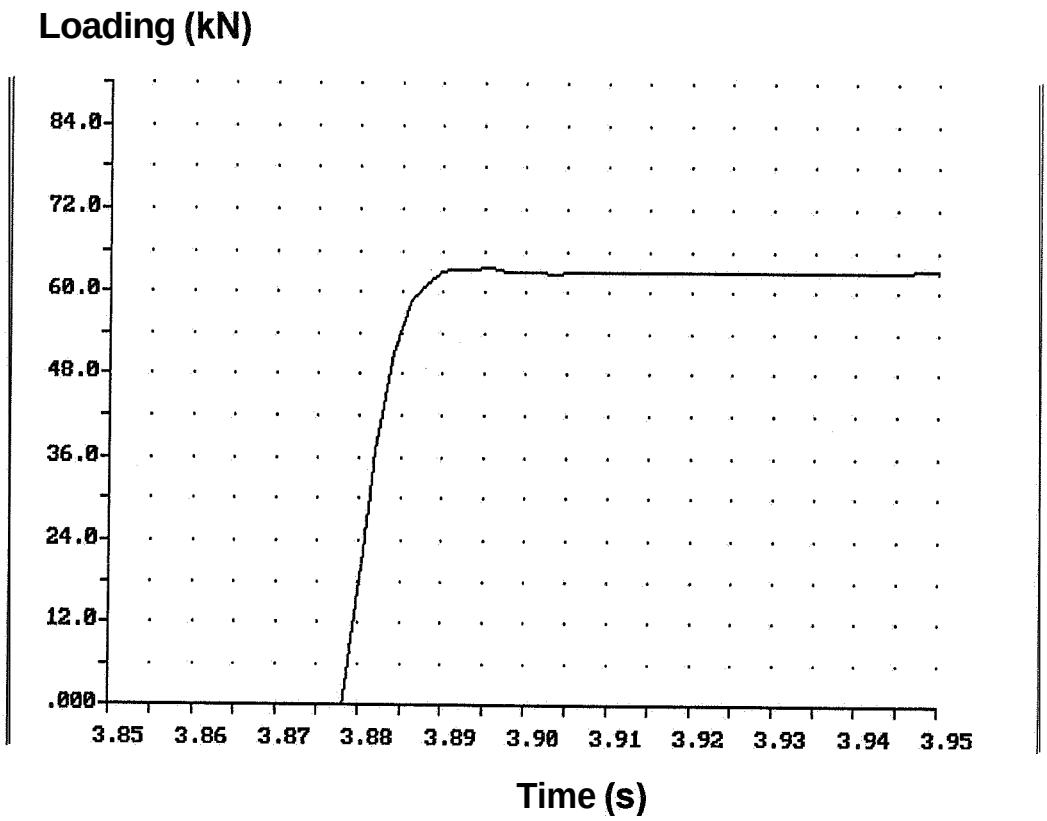

Appendix 12.15 - Loading versus time of mix 5 at loading 1.

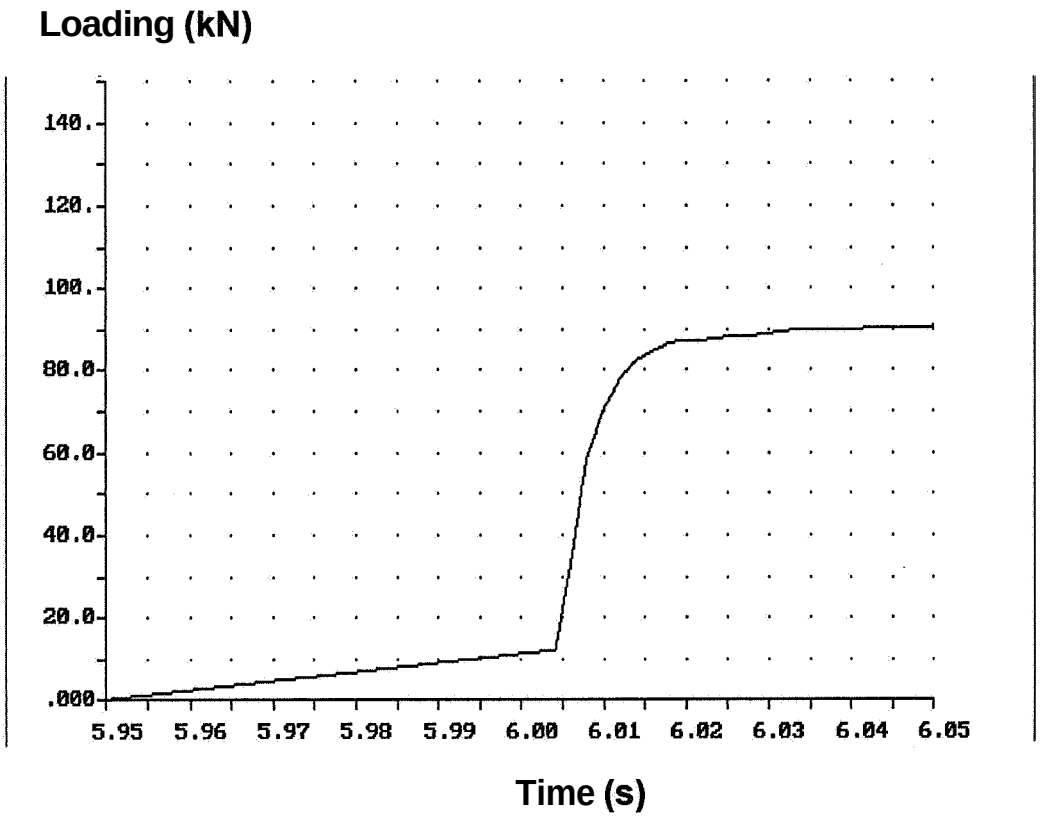

Appendix 12.16 - Loading versus time of mix 5 at loading 2.

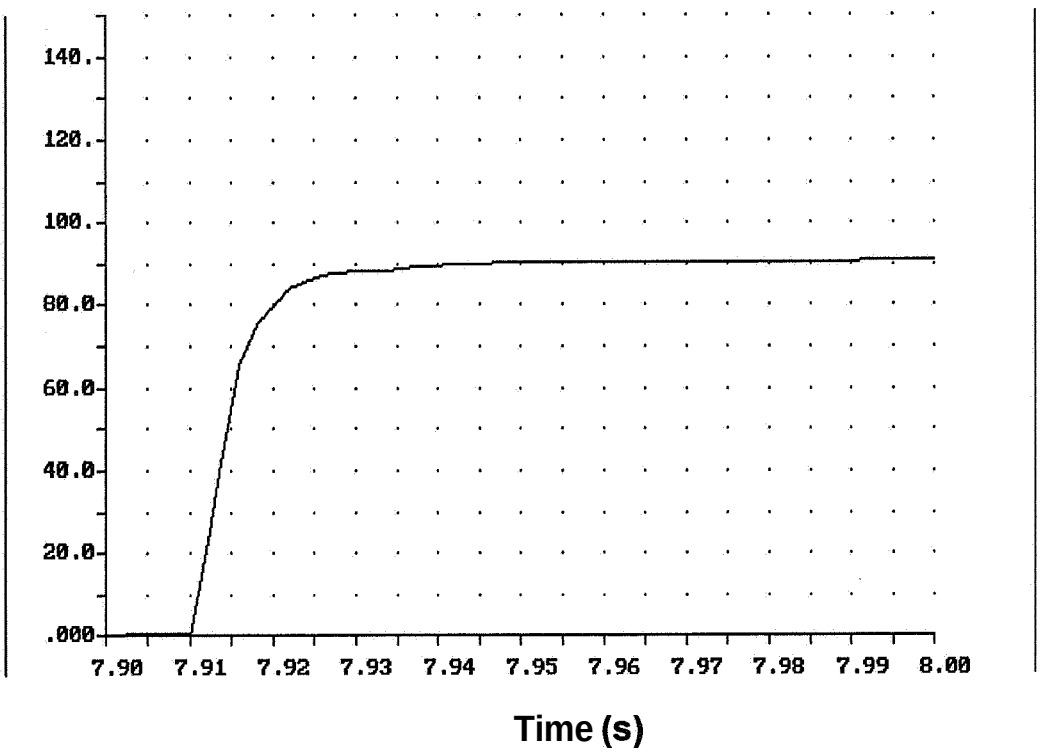

Appendix 12.17 - Loading versus time of mix 5 at loading 3.

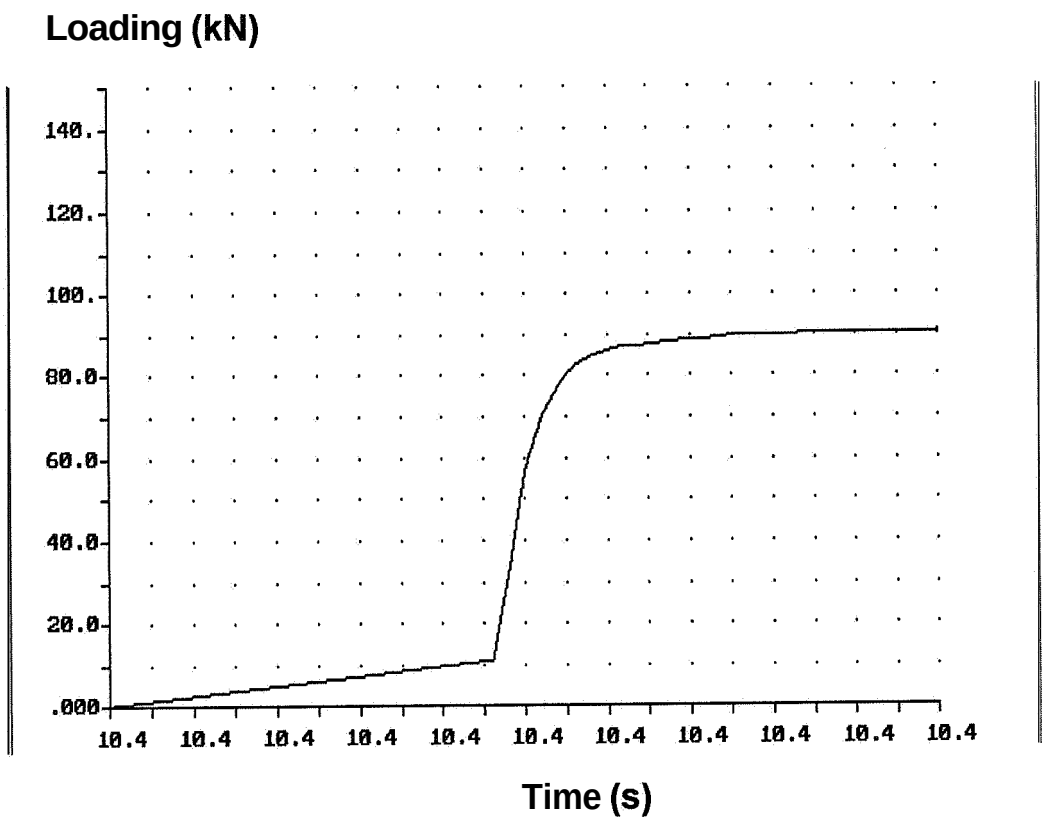

Appendix 12.18 - Loading versus time of mix 6 at loading 1.

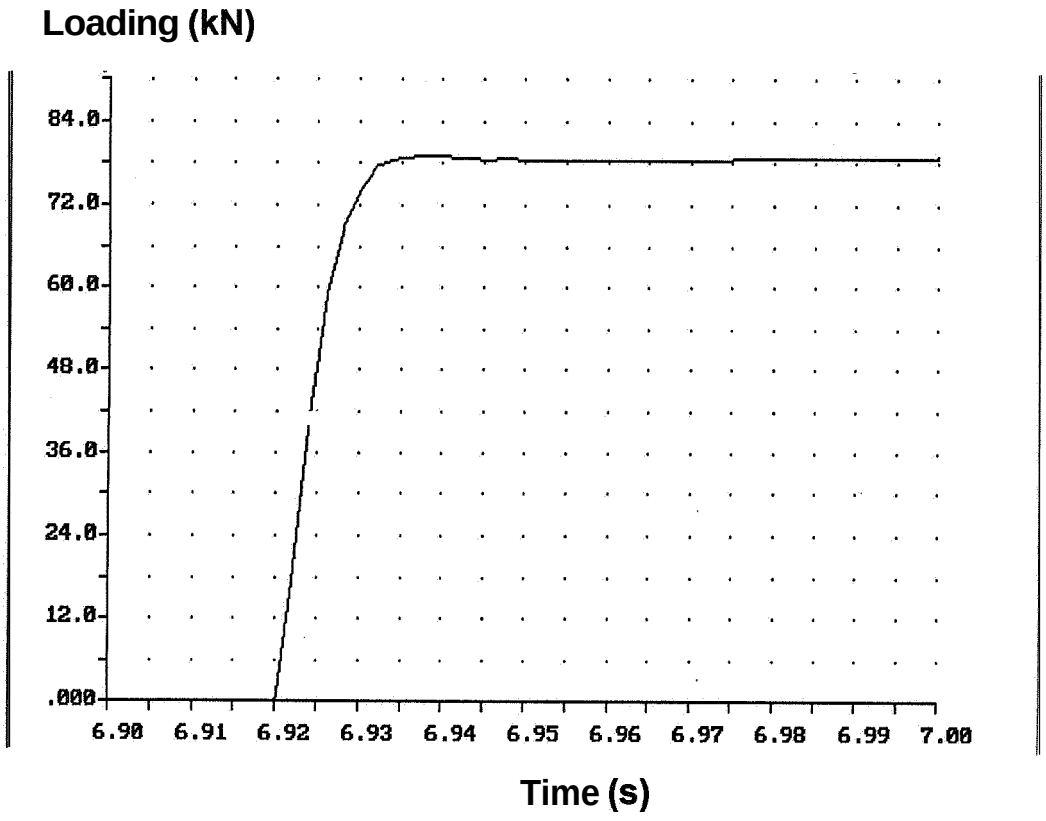

Appendix 12.19 - Loading versus time of mix 6 at loading 2.

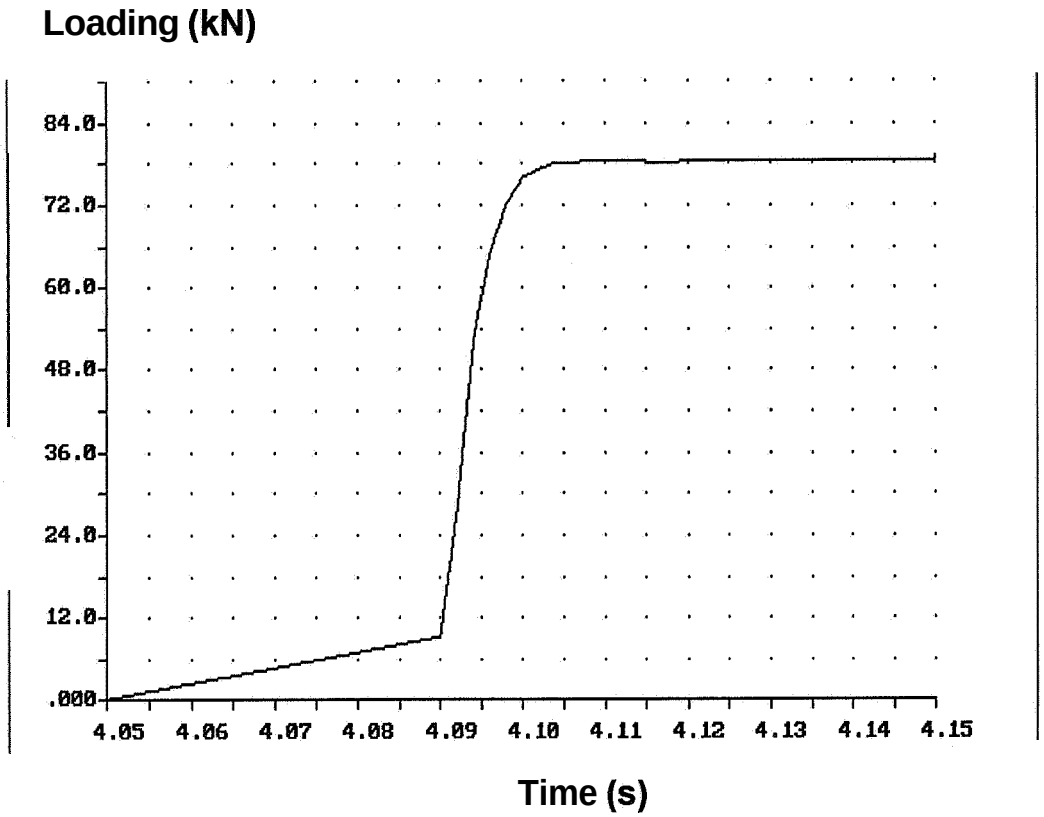

Appendix 12.20 - Loading versus time of mix 6 at loading 3.

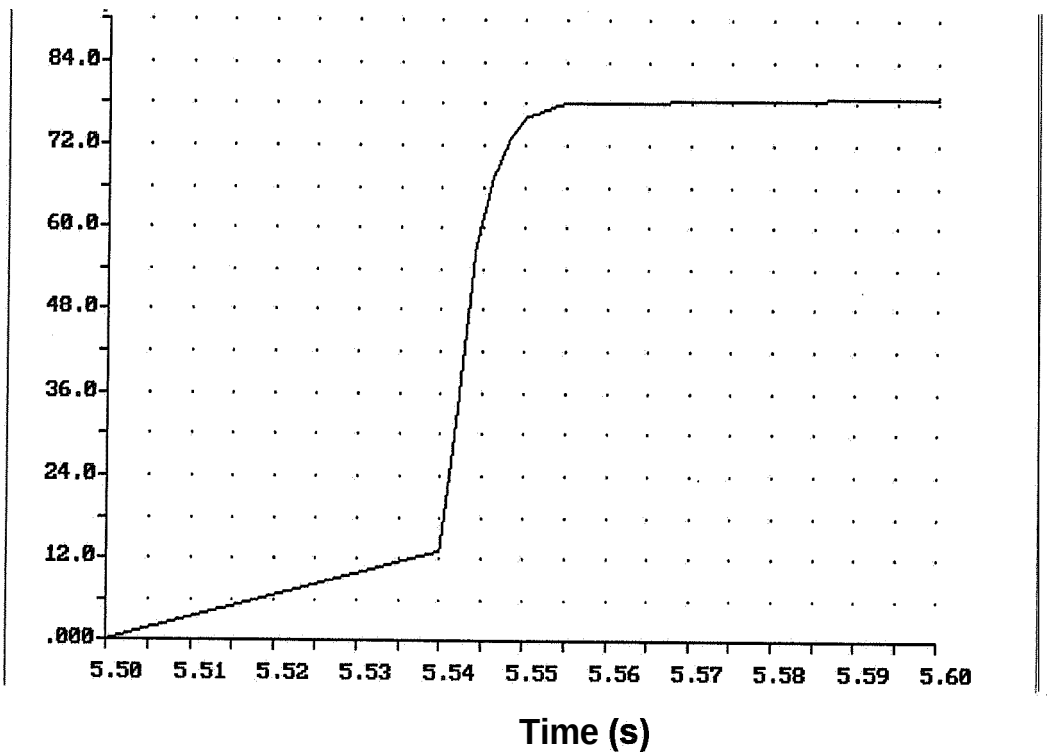

Appendix 12.21 - Loading versus time of mix 7 at loading 1.

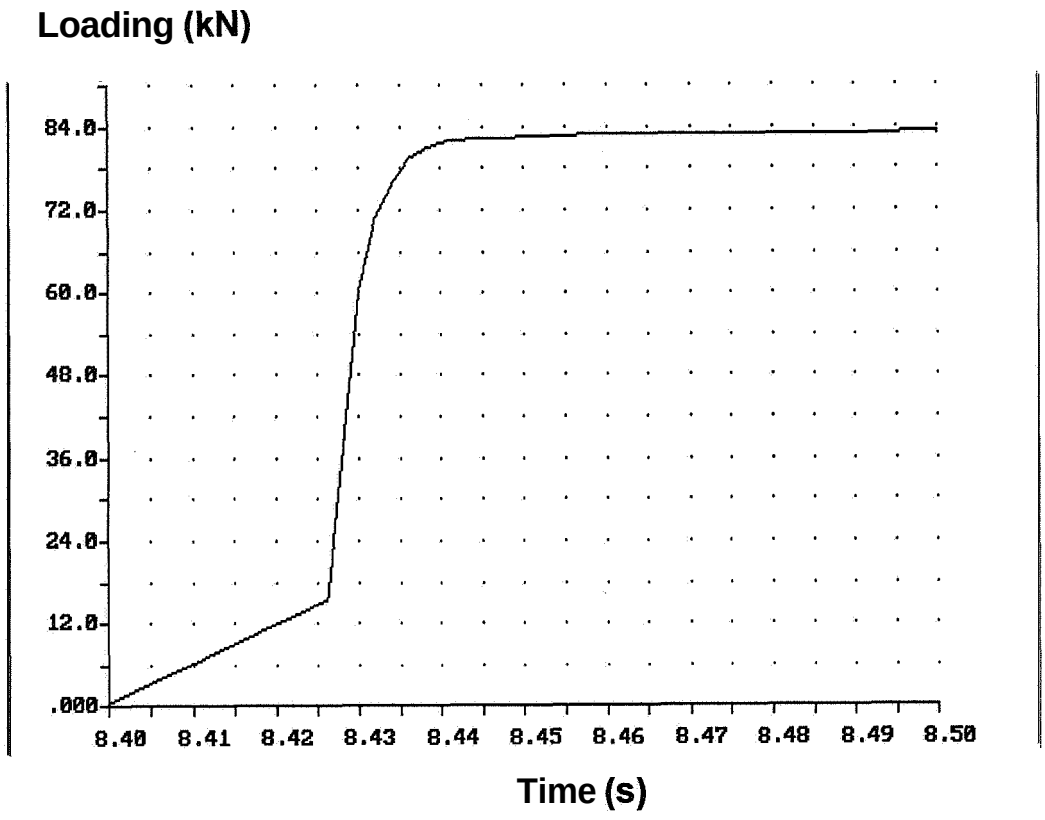

Appendix 12.22 - Loading versus time of mix 7 at loading 2.

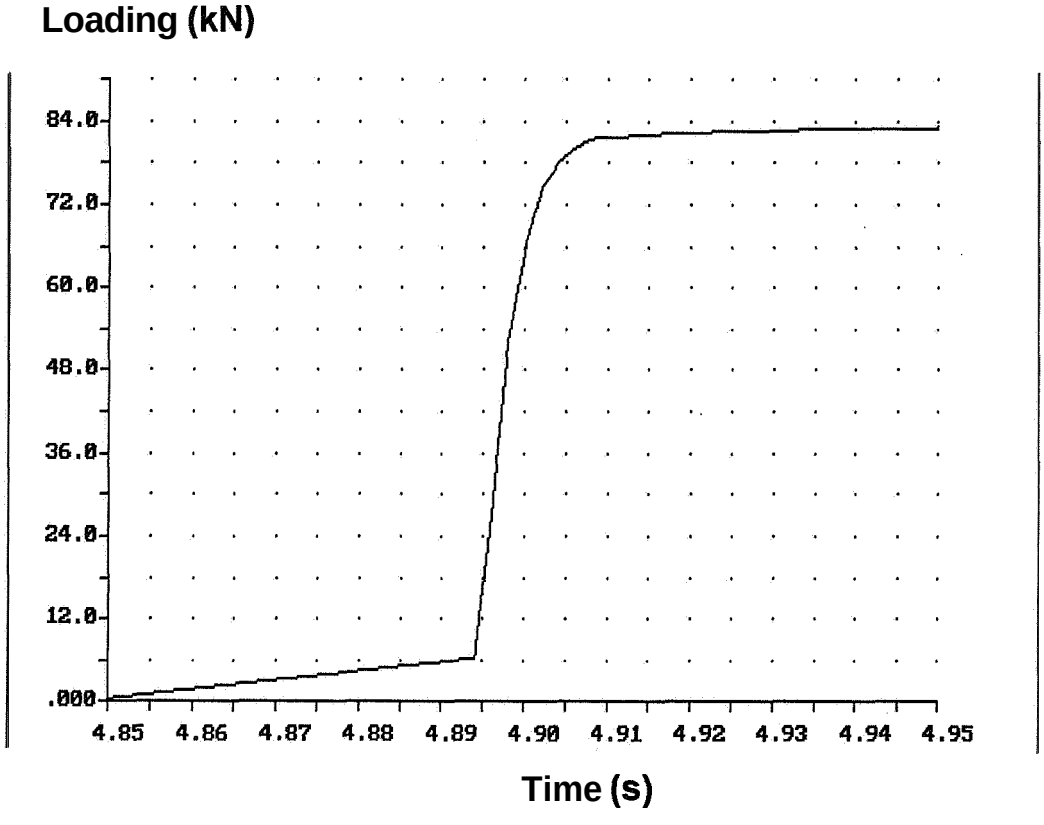

Appendix 12.23 - Loading versus time of mix 7 at loading 3.

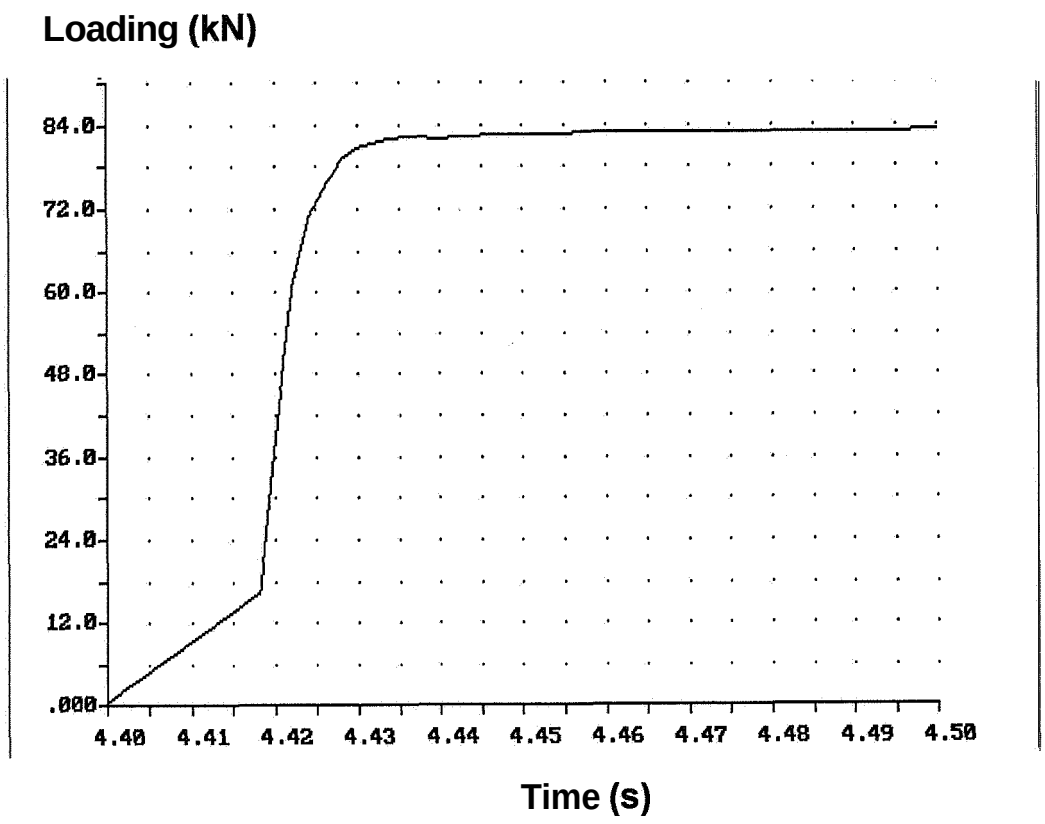

Appendix 12.24 - Loading versus time of mix 8 at loading 1.

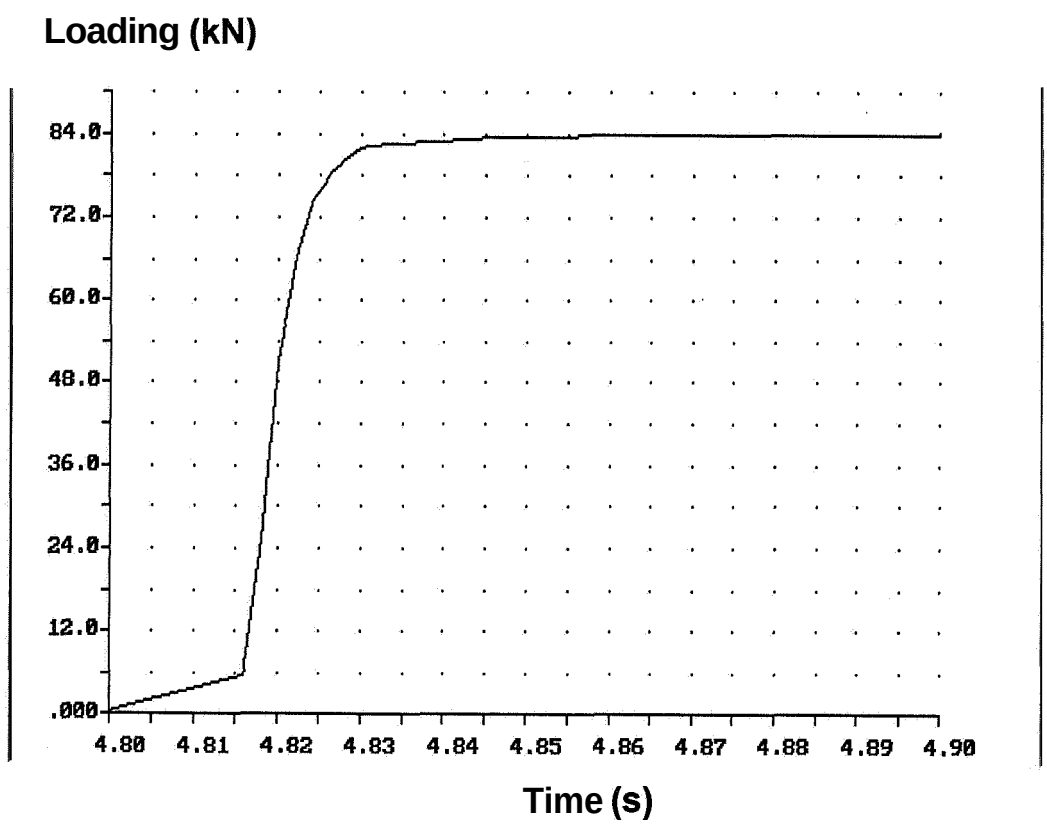

Appendix 12.25 - Loading versus time of mix 8 at loading 2.

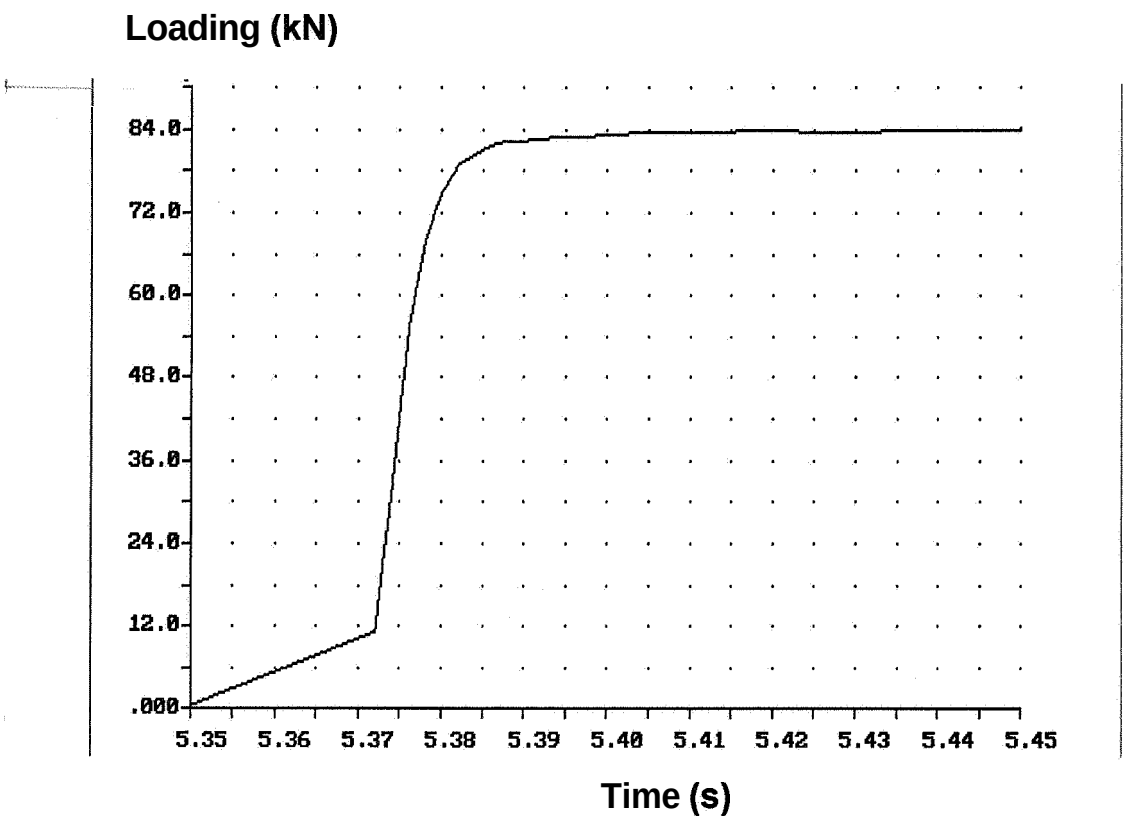

Appendix 12.26 - Loading versus time of mix 8 at loading 3.

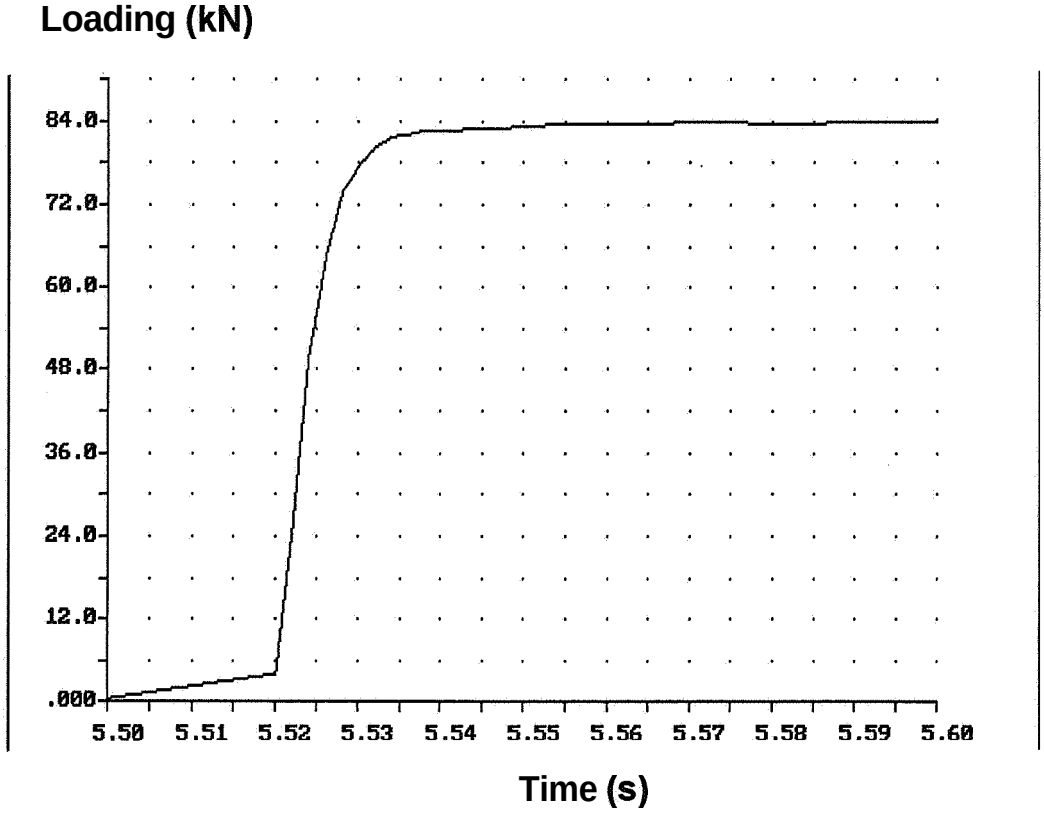

Appendix 7 - Deformations versus time of at ding 1

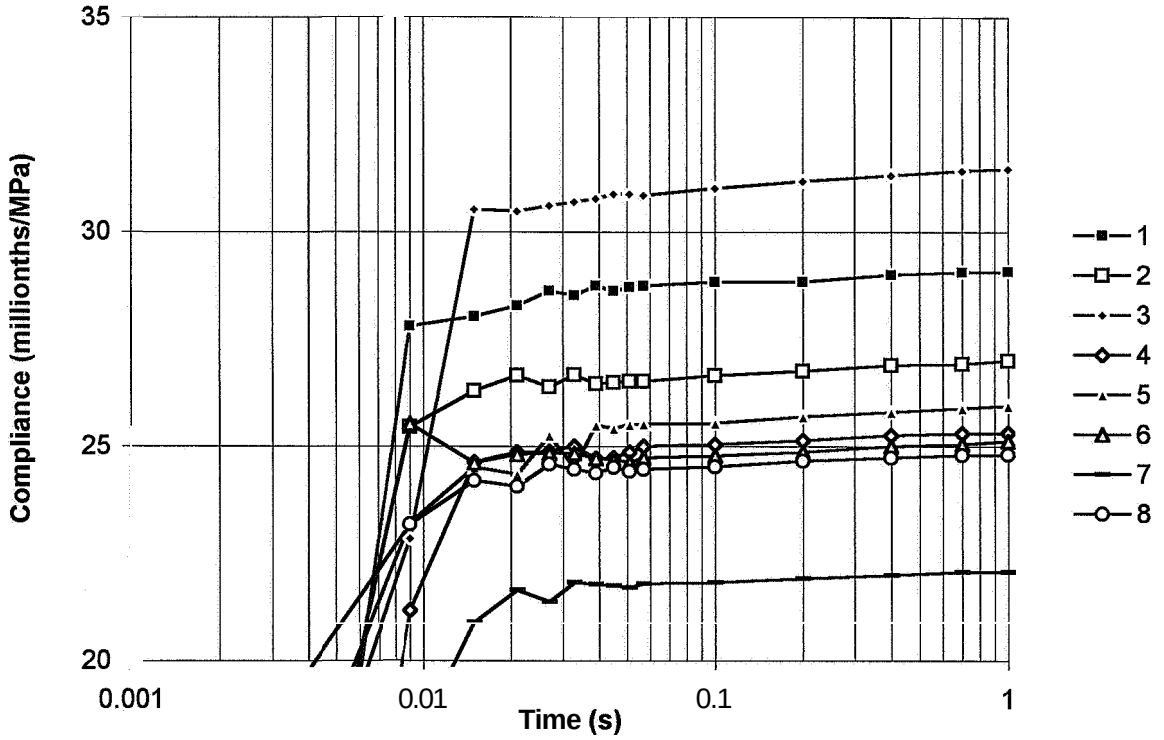

Appendix 12.28 - Deformations versus time of at loading 2

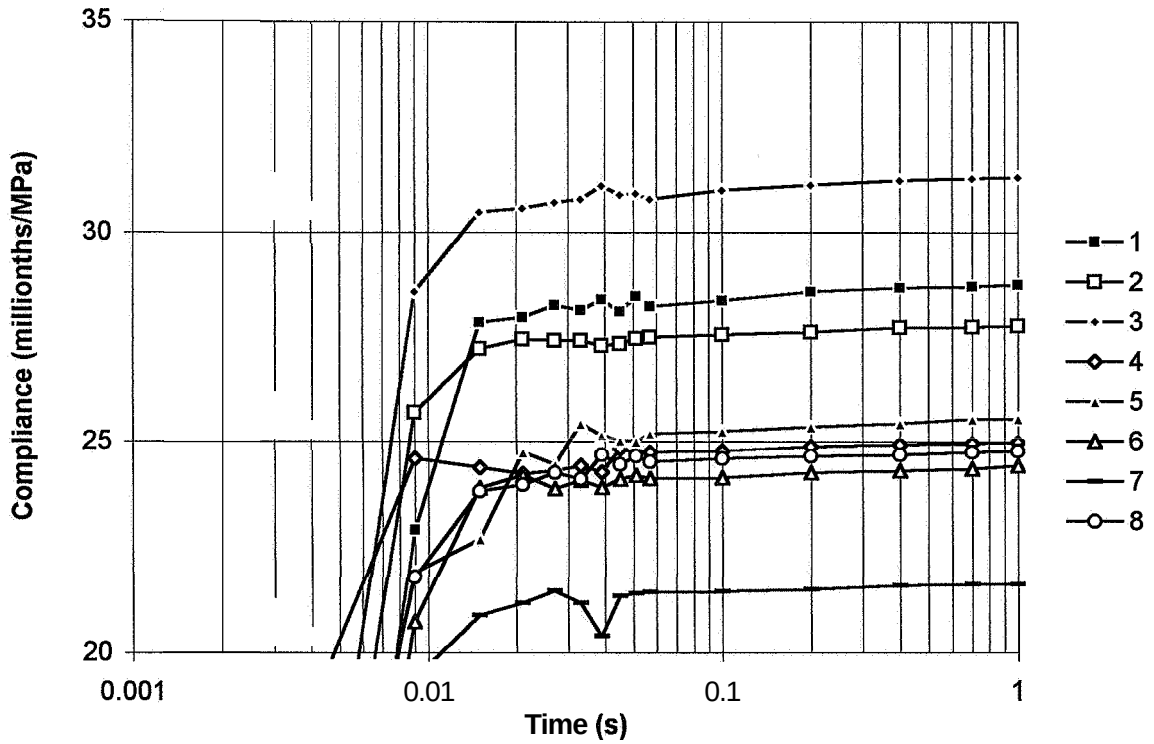

Appendix 12.29 - Deformations versus time of at loading 3

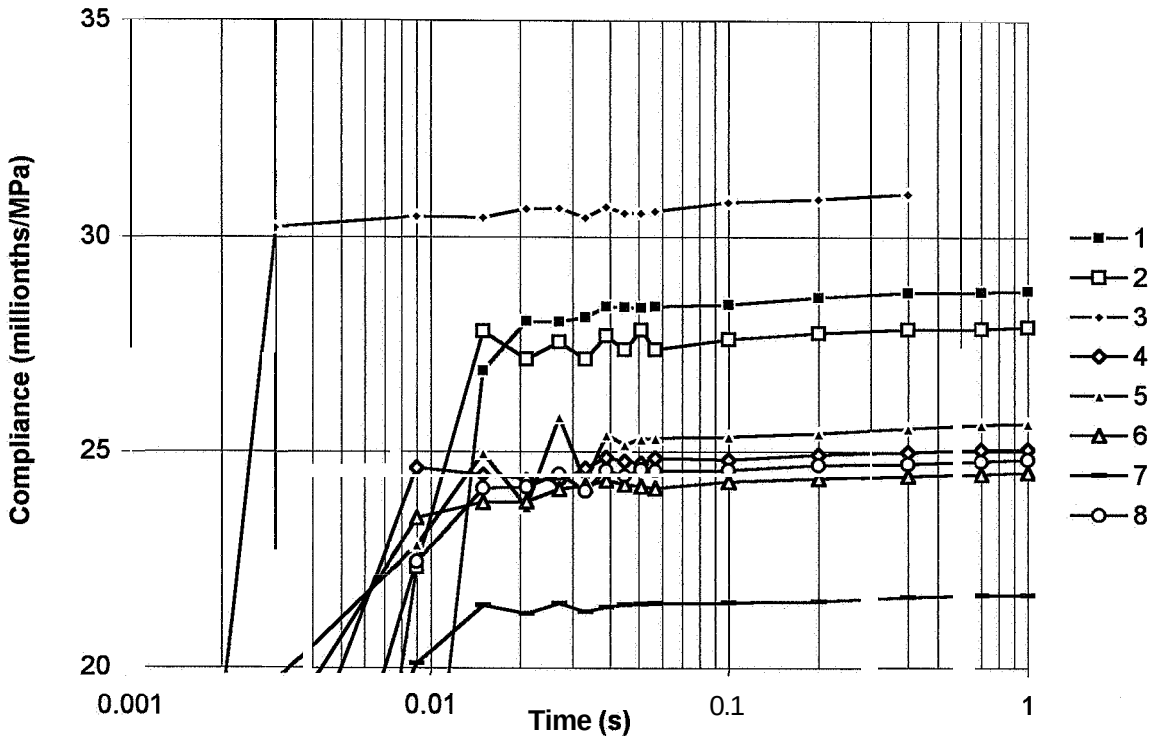

Appendix 12 30 - Deformations versus time of at loading 4

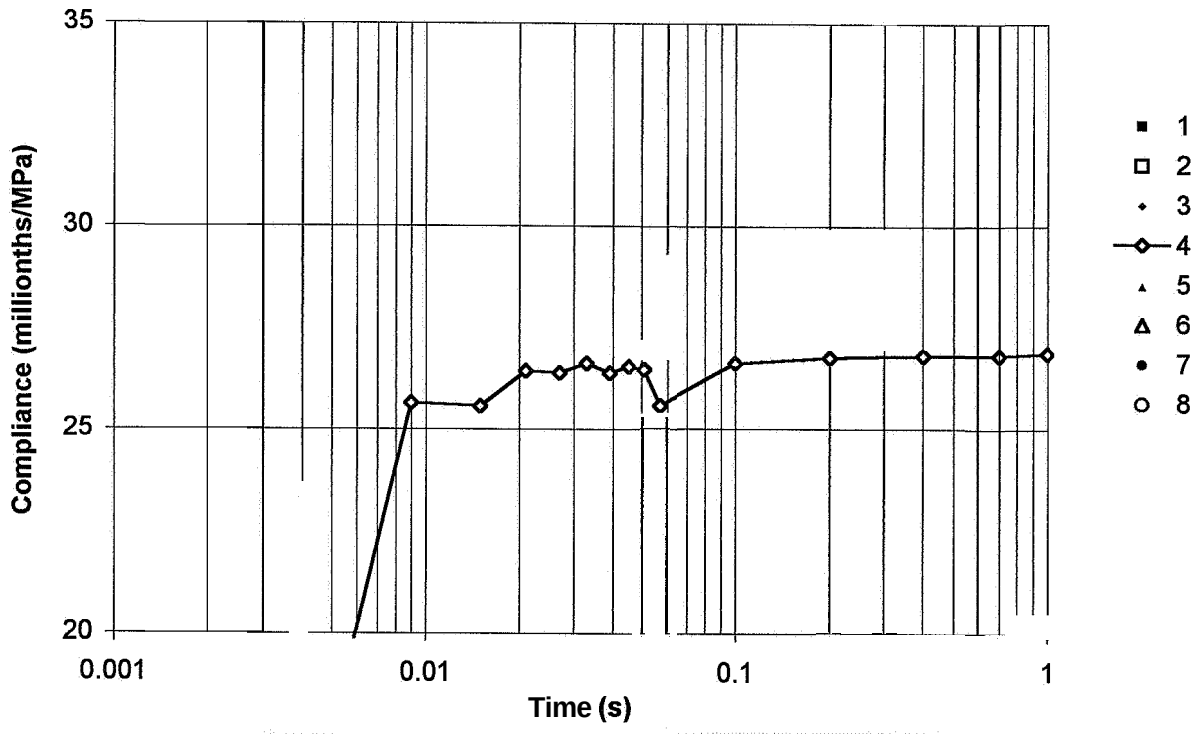

Appendix 12.31 - Deformations versus time of at loading 5

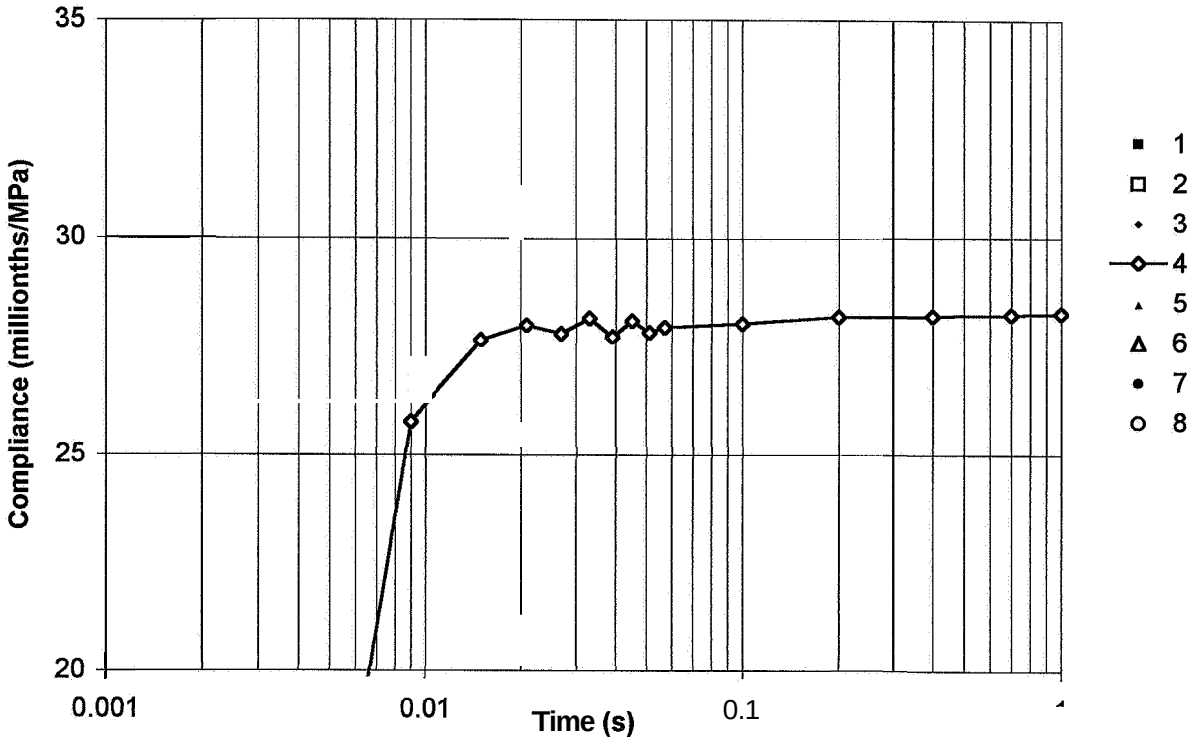

Appendix 12.32 - Deformations versus time of at loading 6

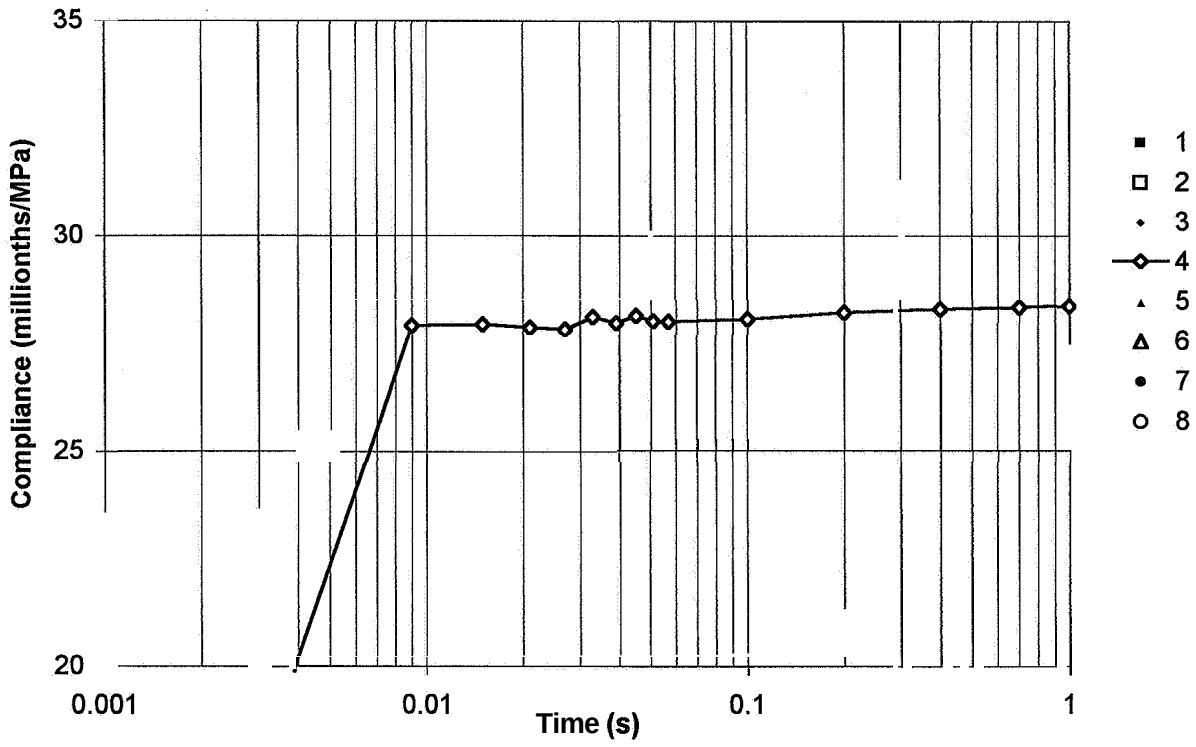

Appendix 12.33 - Deformations versus time of at unloading 1

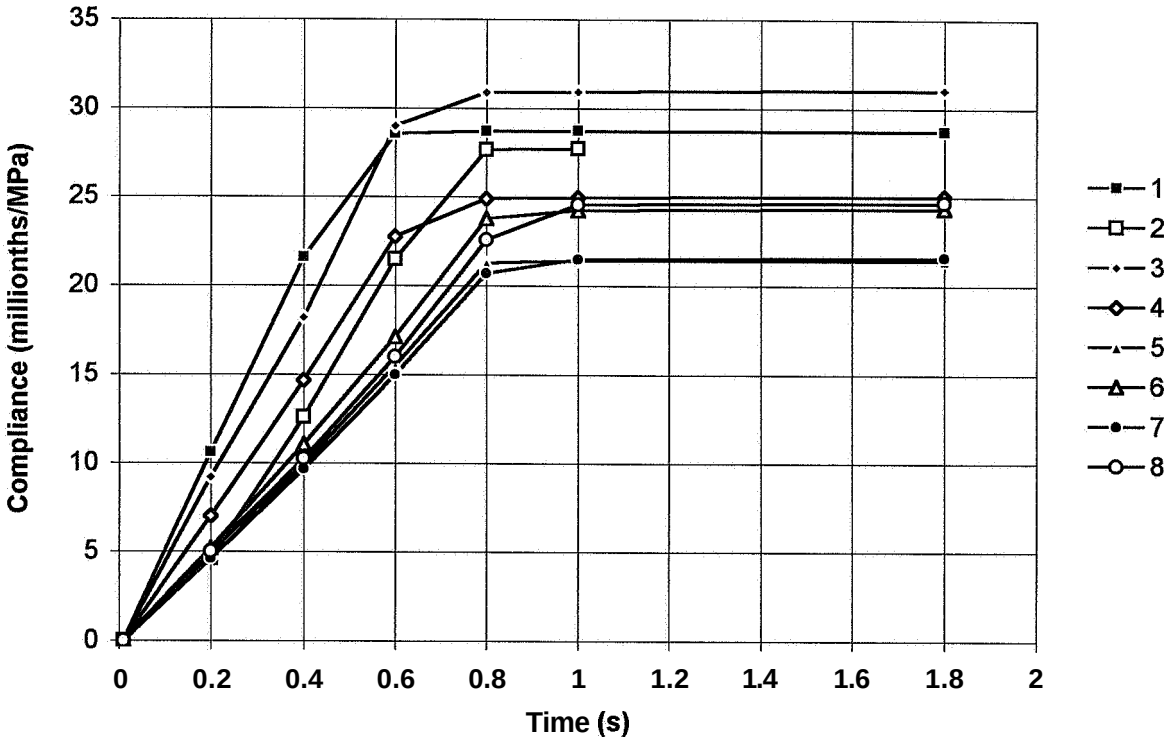

Appendix 12.34 - Deformations versus time of at unloading 2

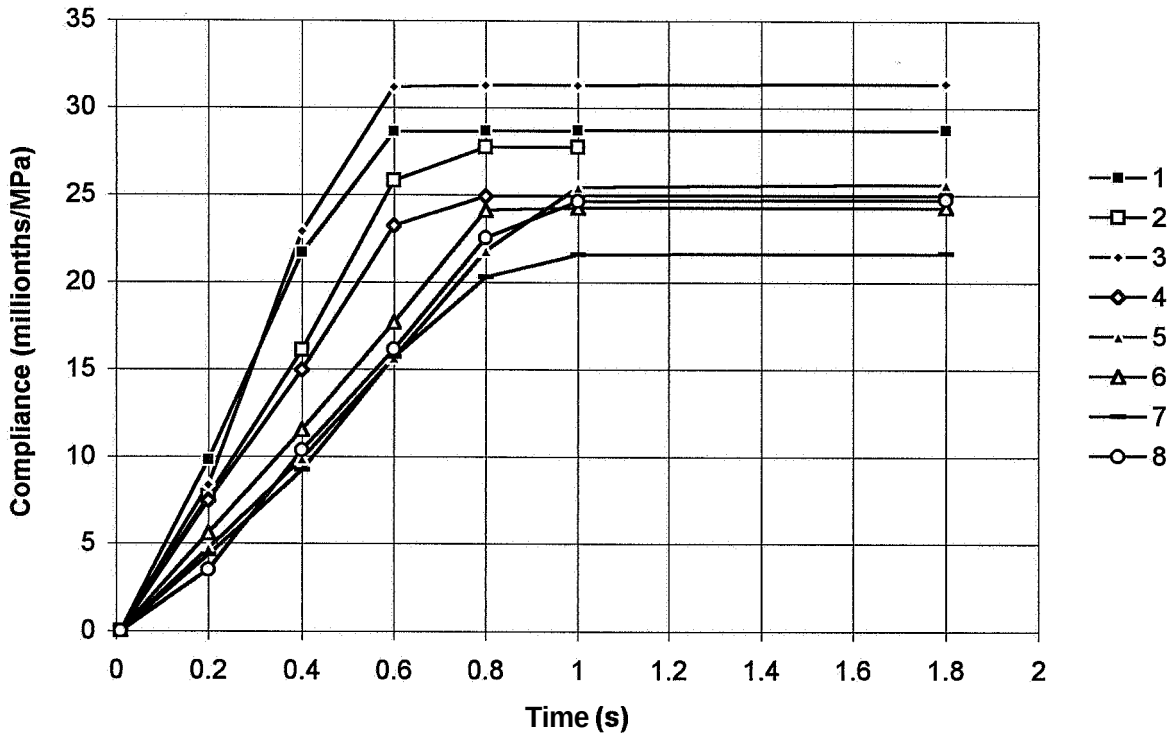

Appendix 12.35 - Deformations versus time of at unloading 3

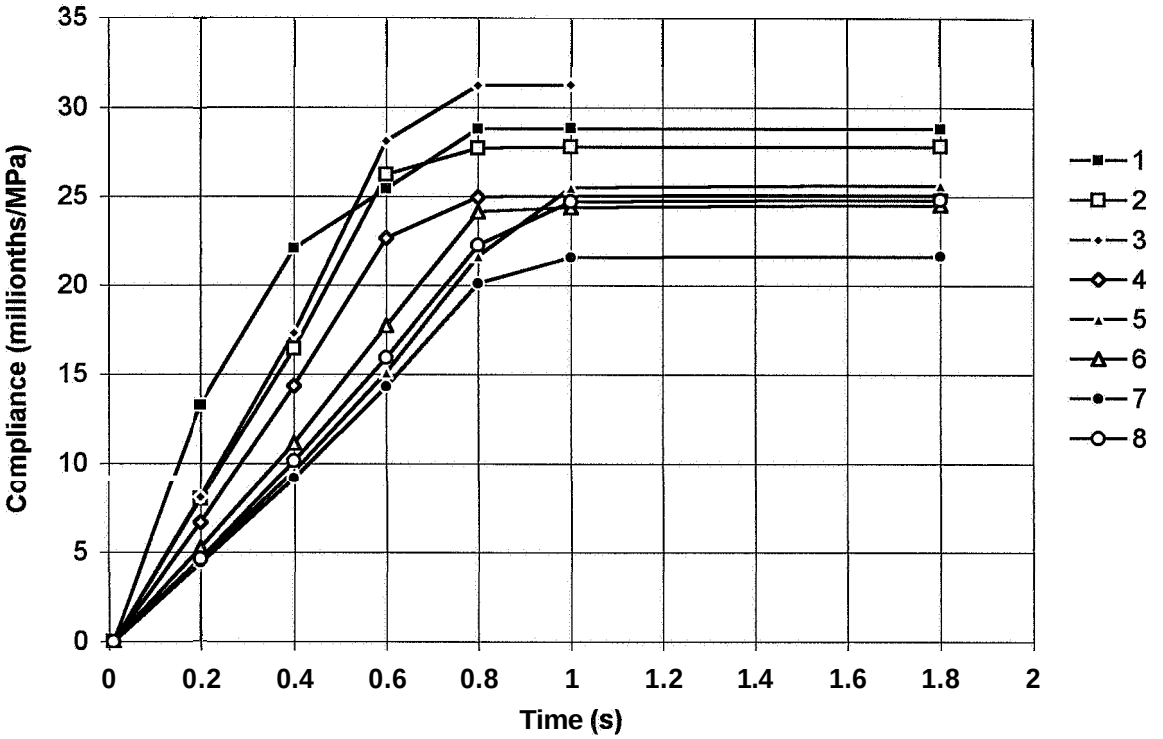

ppendix .36 - Deformations versus time of at unl di l

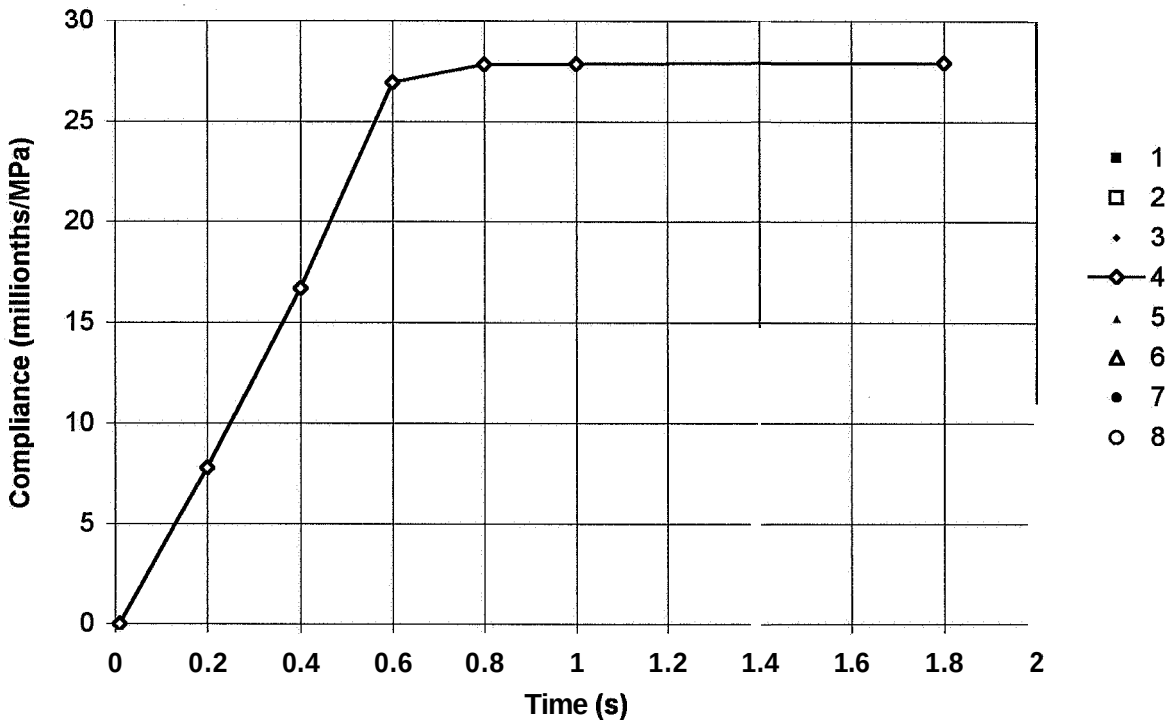

Appendix 12.37 - Deformations versus time of at unloading 5

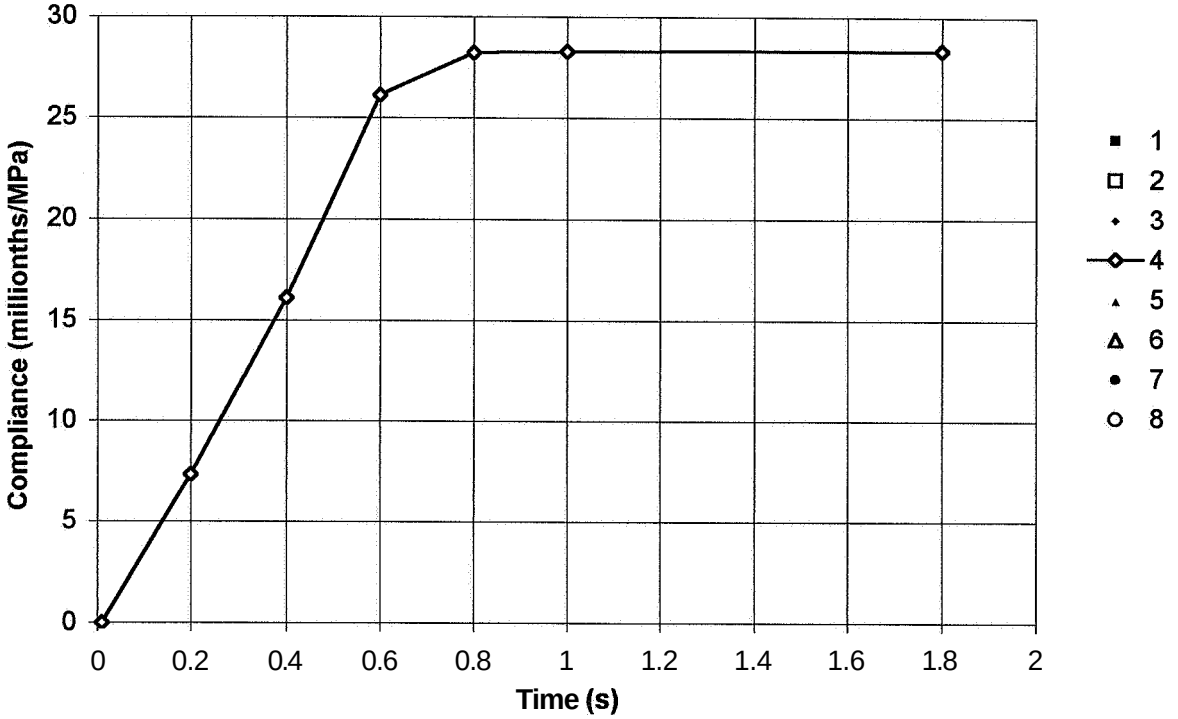

Appendix 12.38 - Deformations versus time of at unloading 6

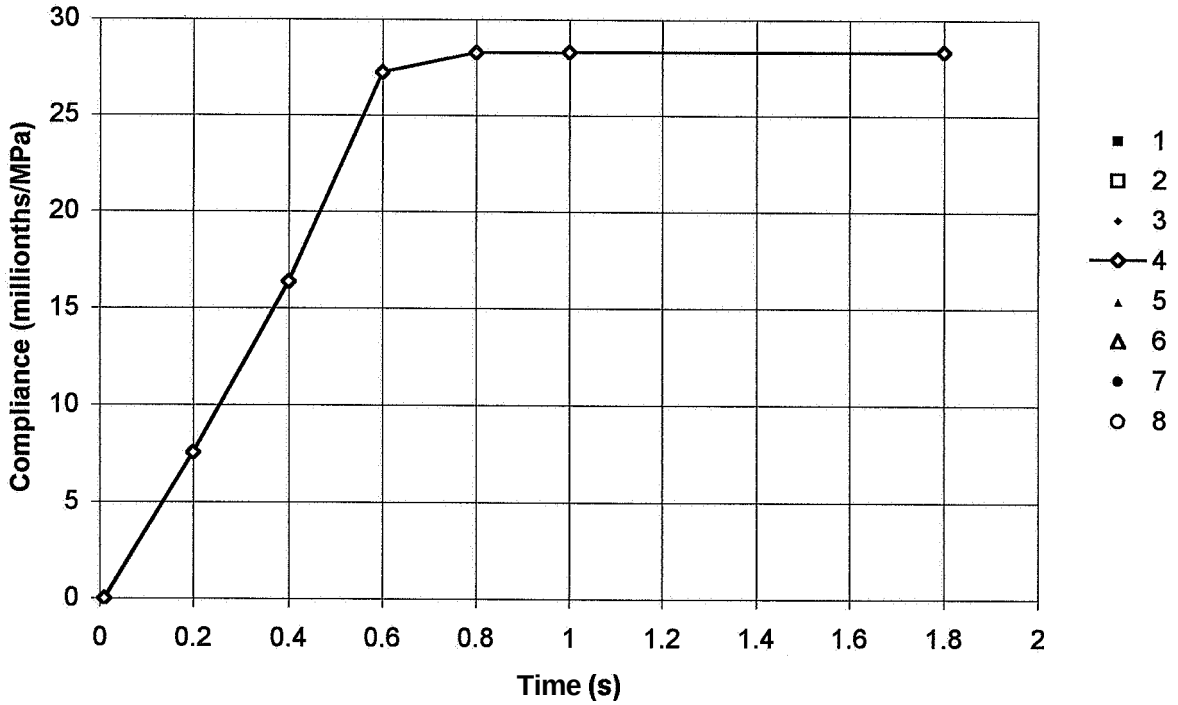

APPENDIX 13. - RECOVERY OF DEFORMATION IN HPC CYLINDERS

The shrinkage was reduced from the measured strain

Appendix 13.1 - Recovery compliance of mix 1 subjected to air curing
Appendix 13.2 - Recovery compliance of mix 2 subjected to air curing
Appendix 13.3 - Recovery compliance of mix 3 subjected to air curing
Appendix 13.4 - Recovery compliance of mix 4 subjected to air curing
Appendix 13.5 - Recovery compliance of mix 5 subjected to air curing
Appendix 13.6 - Recovery compliance of mix 6 subjected to air curing
Appendix 13.7 - Recovery compliance of mix 7 subjected to air curing
Appendix 13.8 - Recovery compliance of mix 8 subjected to air curing
Appendix 13.9 - Elastic strain of mix 1 subjected to sealed curing
Appendix 13.10 - Elastic strain of mix 2 subjected to sealed curing
Appendix 13.11 - Elastic strain of mix 3 subjected to sealed curing
Appendix 13.12 - Elastic strain of mix 4 subjected to sealed curing
Appendix 13.13 - Elastic strain of mix 5 subjected to sealed curing
Appendix 13.14 - Elastic strain of mix 6 subjected to sealed curing
Appendix 13.15 - Elastic strain of mix 7 subjected to sealed curing
Appendix 13.16 - Elastic strain of mix 8 subjected to sealed curing
Appendix 13.17 - Recovery compliance of mix 1 subjected to sealed curing
Appendix 13.18 - Recovery compliance of mix 2 subjected to sealed curing
Appendix 13.19 - Recovery compliance of mix 3 subjected to sealed curing
Appendix 13.20 - Recovery compliance of mix 4 subjected to sealed curing
Appendix 13.21 - Recovery compliance of mix 5 subjected to sealed curing
Appendix 13.22 - Recovery compliance of mix 6 subjected to sealed curing
Appendix 13.23 - Recovery compliance of mix 7 subjected to sealed curing
Appendix 13.24 - Recovery compliance of mix 8 subjected to sealed curing

6.. denotes concrete mix, **Table 5.1**
...01 age at loading: 1 day; stresslcylinder strength ratio: 0.84
...02 age at loading: 2 days; stresslcylinder strength ratio: 0.84
...03 age at loading: 2 days; stresslcylinder strength ratio: 0.42
...28 age at loading: 28 days; stresslcylinder strength ratio: 0.42

Appendix 13.1 - Recovery compliance of mix 1 subjected to air curing

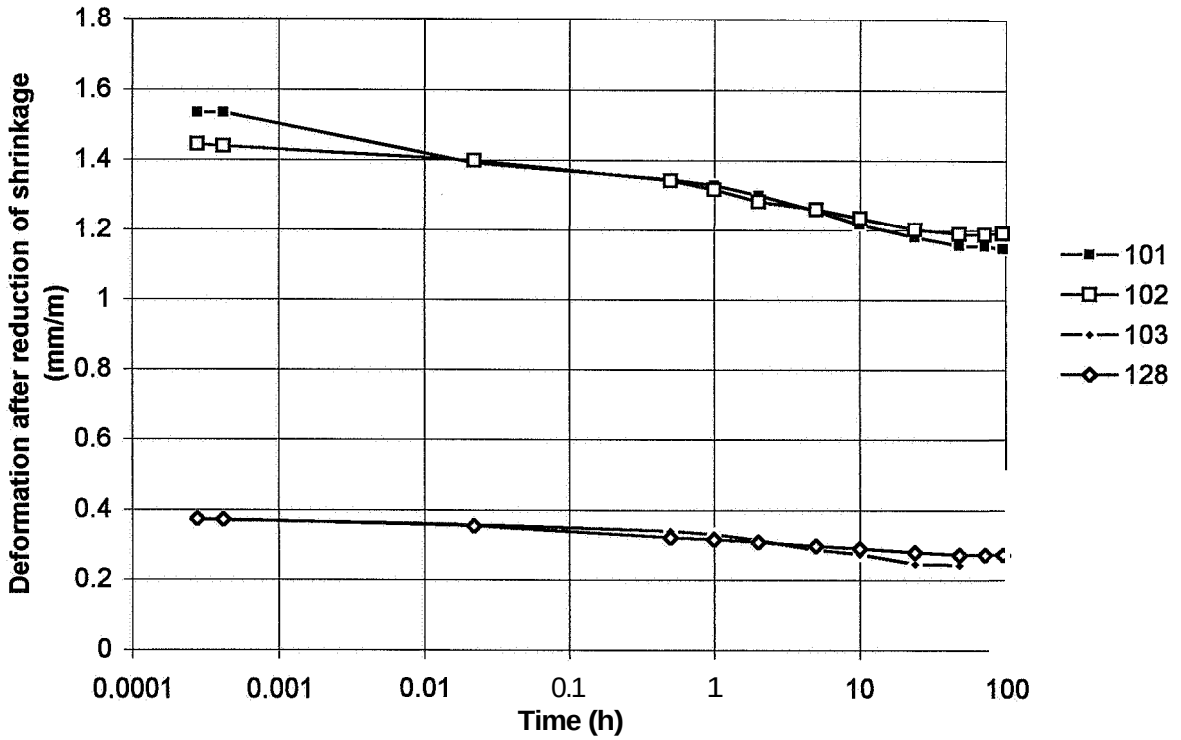

Appendix 13.2 - Recovery compliance of mix 2 subjected to air curing

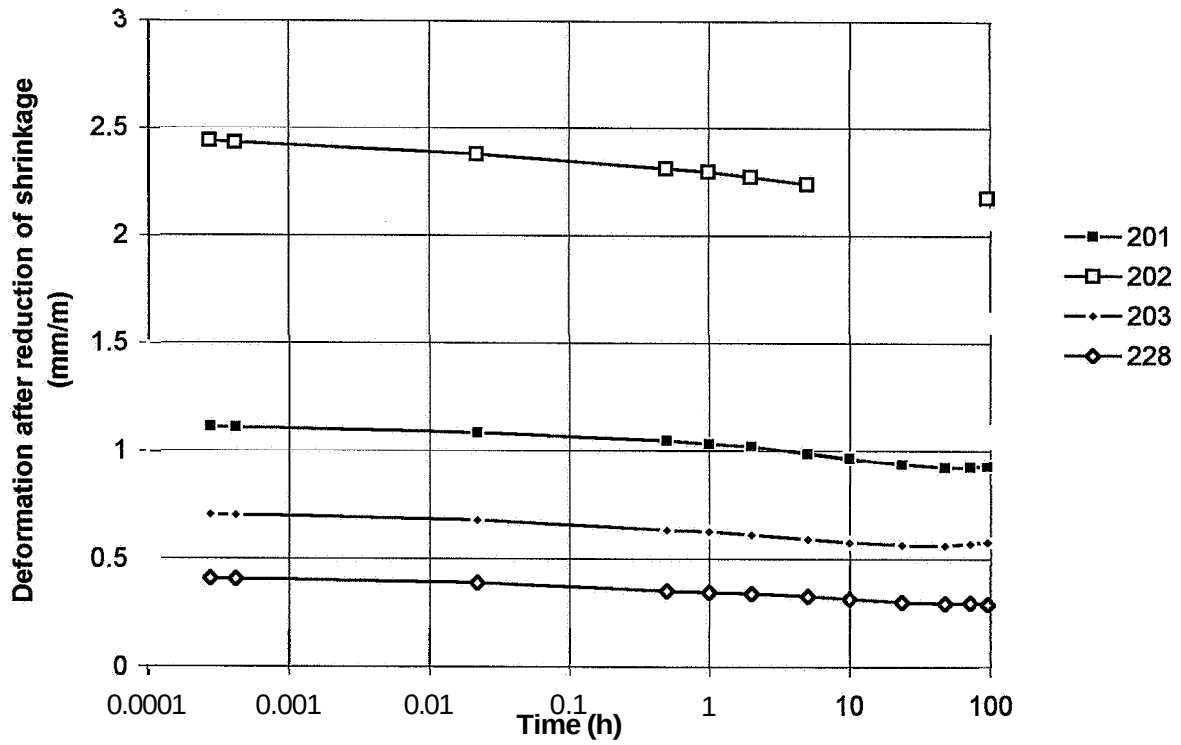

i 1′ 3 - Rec ompliance of mix 3 subjected t aii i

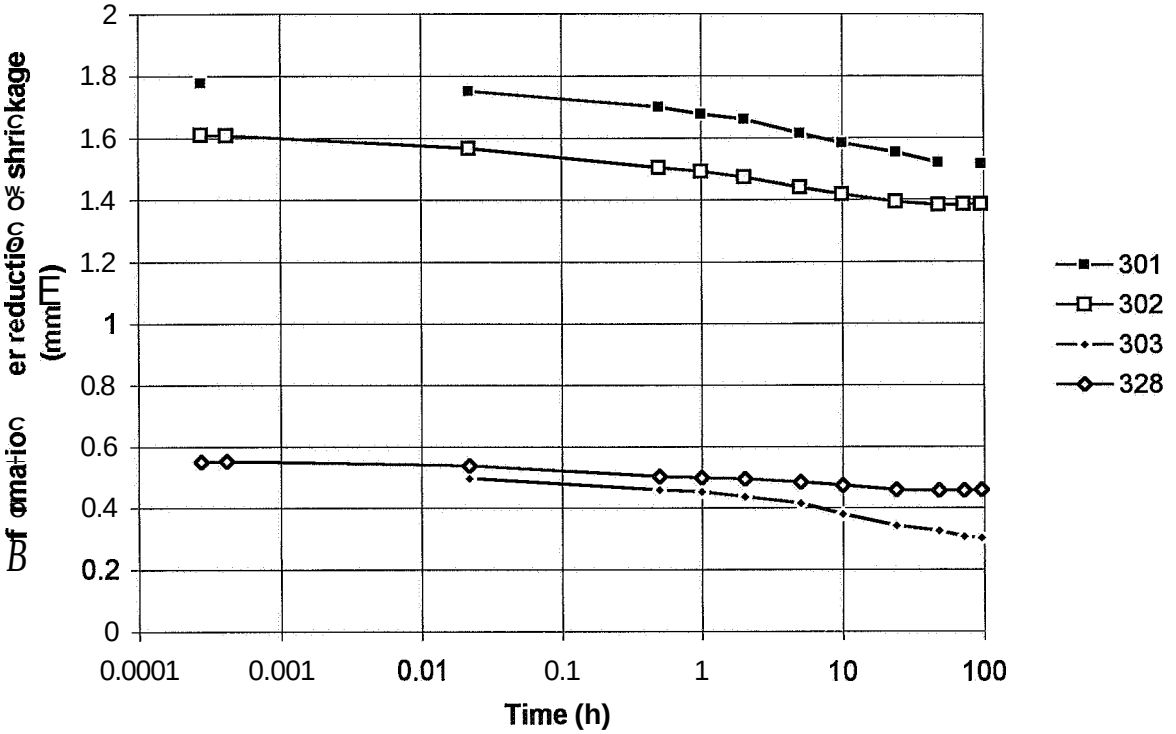

Appendix 13.4 - Recovery compliance of mix 4 subjected to air curing

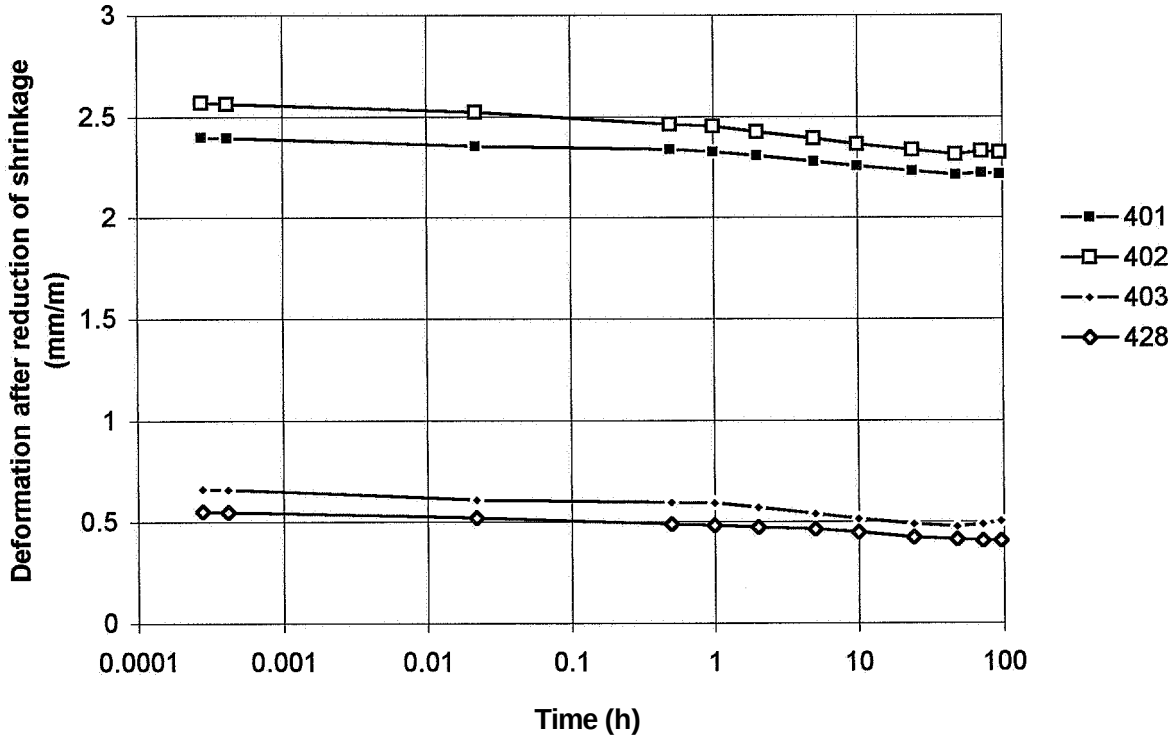

Appendix 13.5 - Recovery compliance of mix 5 subiected to air curing

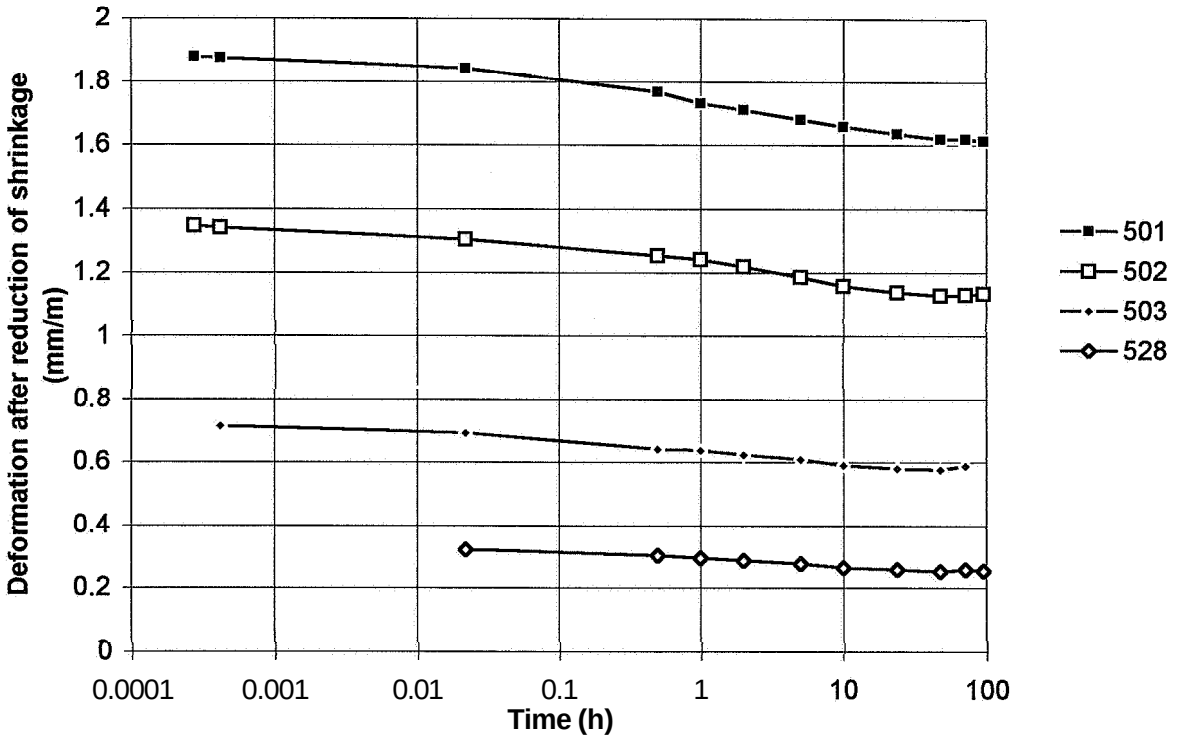

Appendix 13.6 - Recovery compliance of mix 6 subjected to air curing

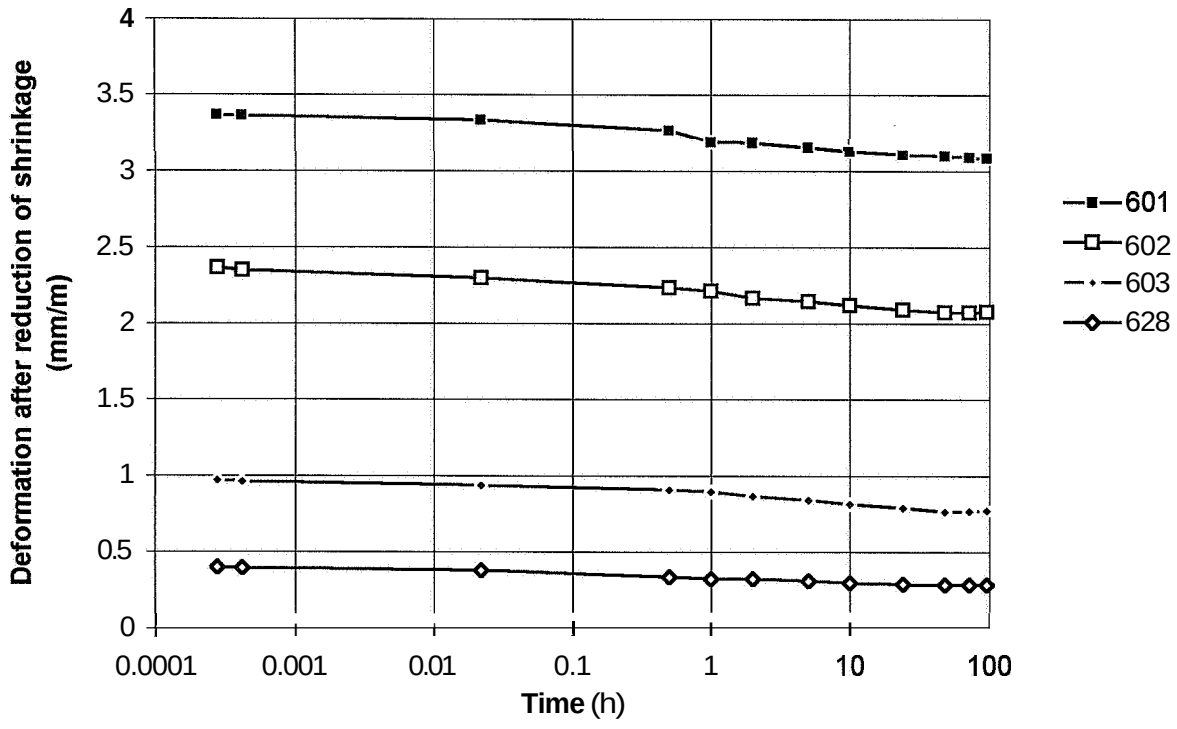

Appendix 13.7 - Recovery compliance of mix 7 subjected to air curing

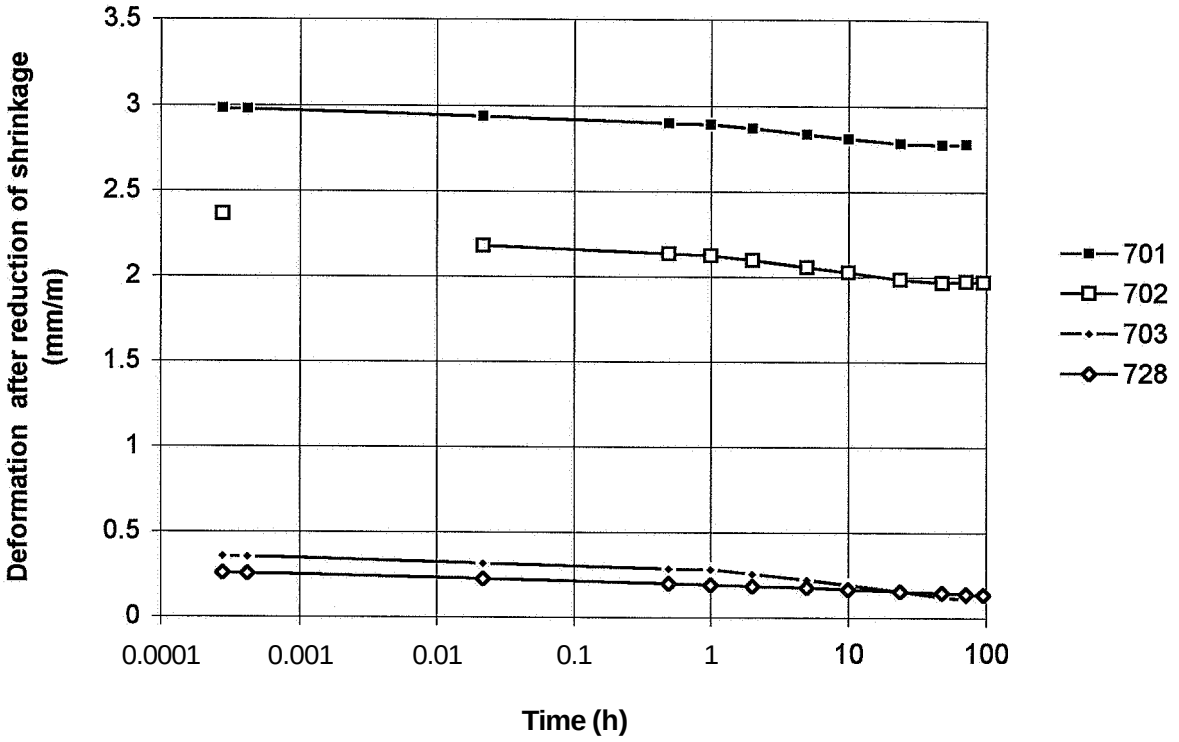

Appendix 13.8 - Recovery compliance of mix 8 subjected to air curing

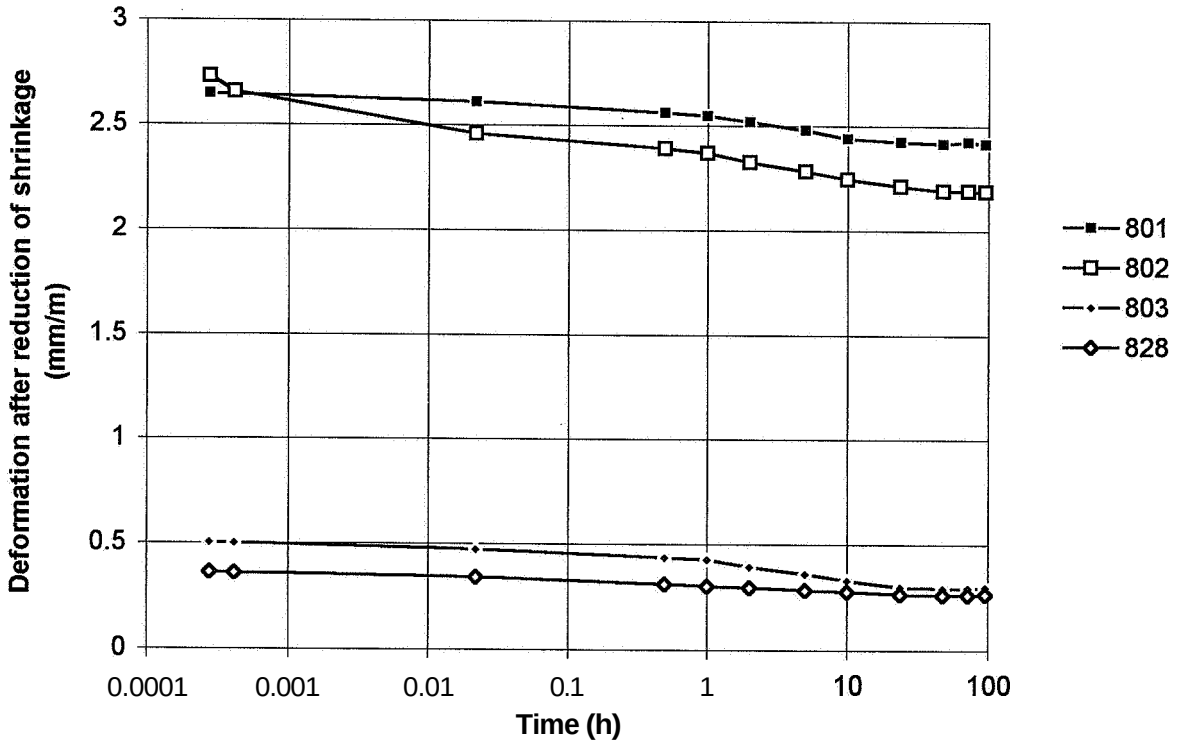

Appendix 13.9 - Elastic strain of mix 1 subjected to sealed curing

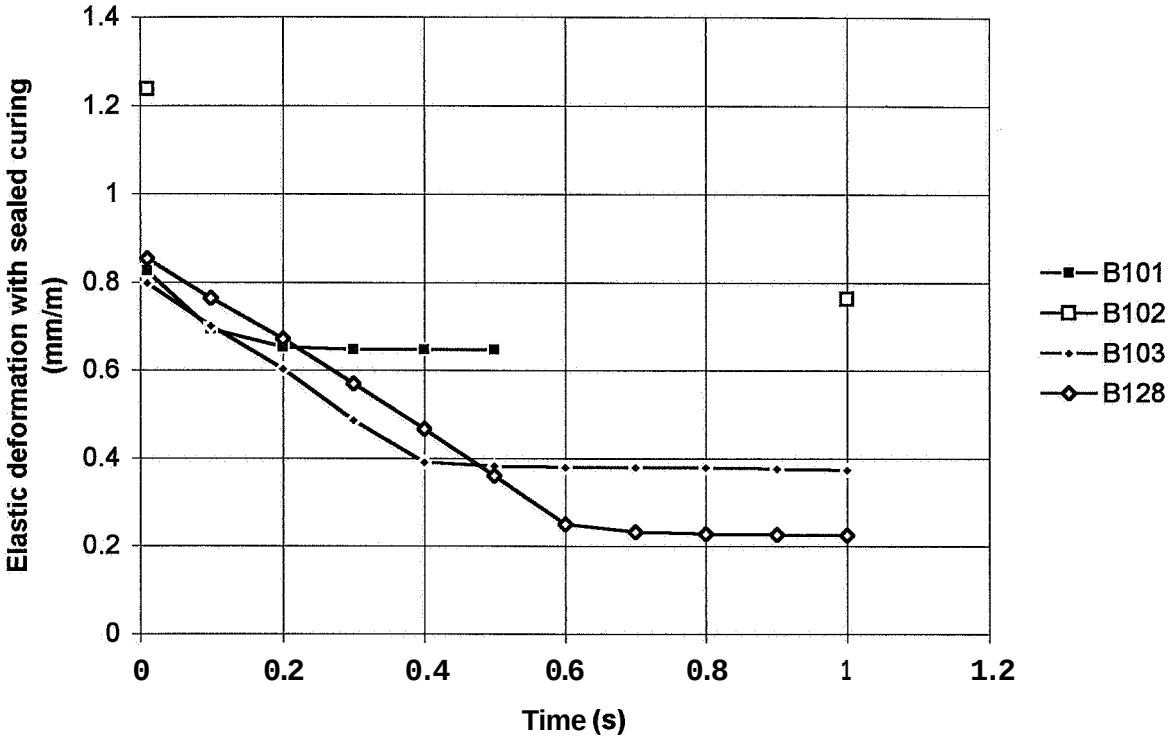

Appendix 13.10 - Elastic strain of mix 2 subjected to sealed curing

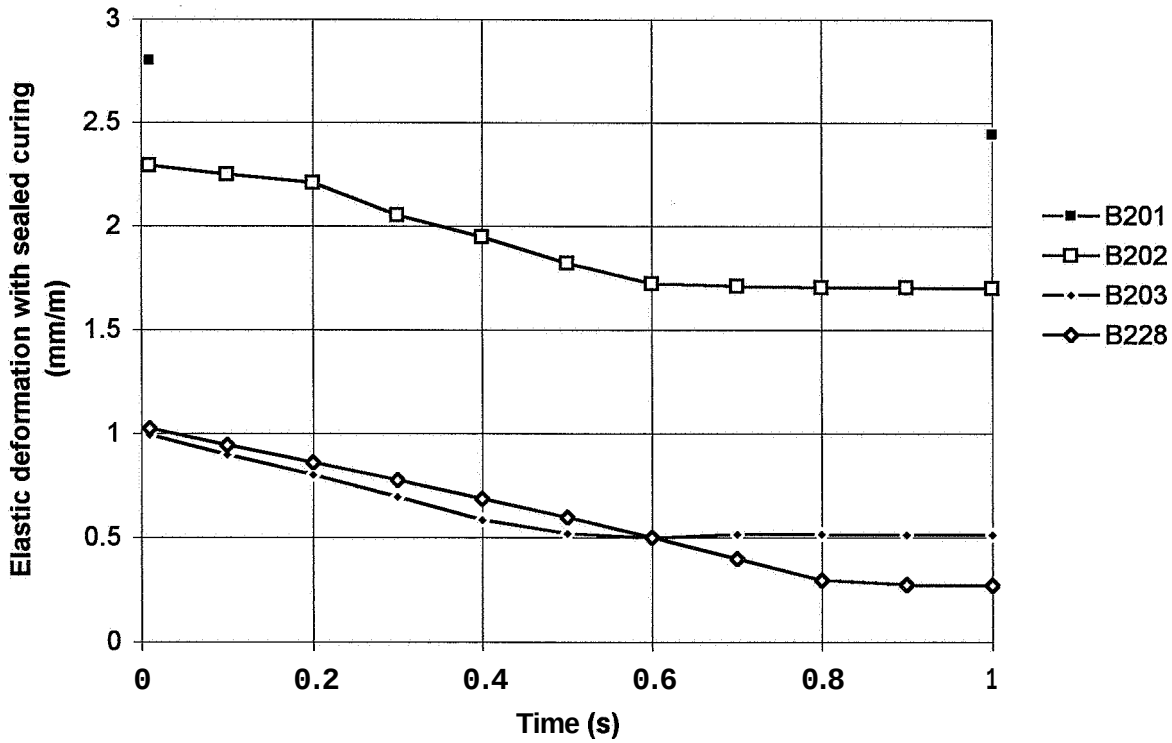

Appendix 13.11 - Elastic strain of mix 3 subiected to sealed curing

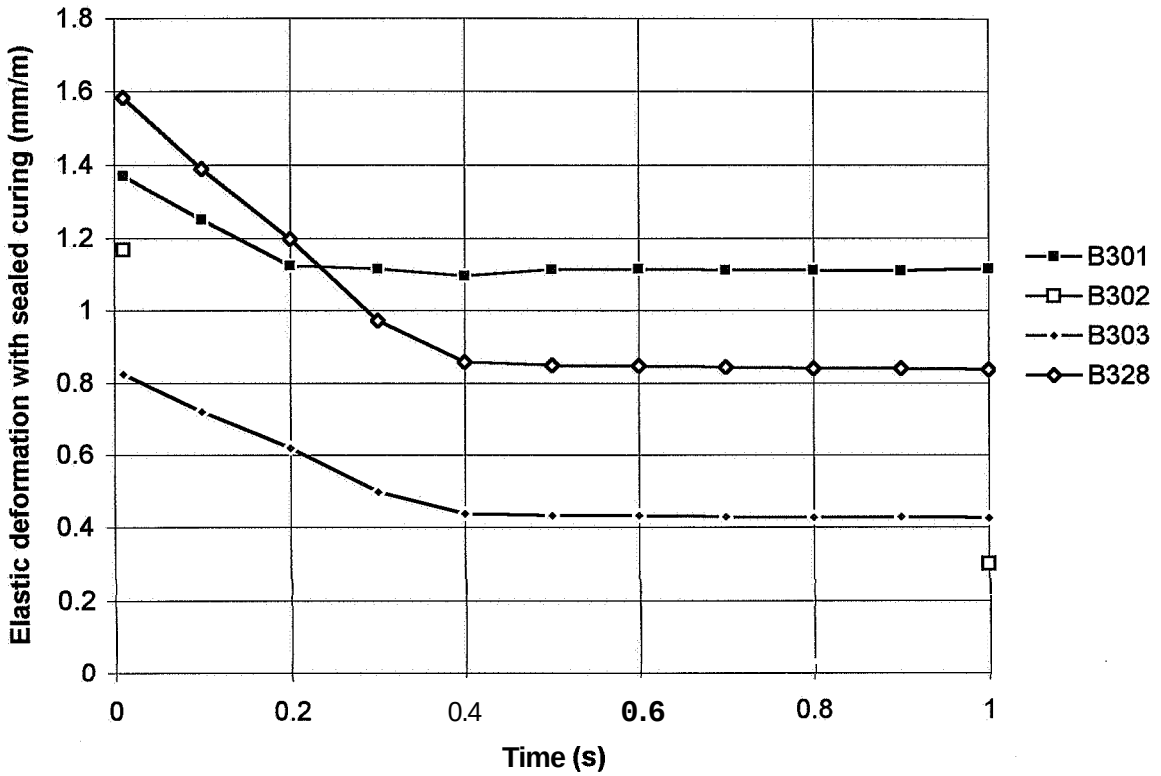

Appendix 13.12 - Elastic strain of mix 4 subiected to sealed curing

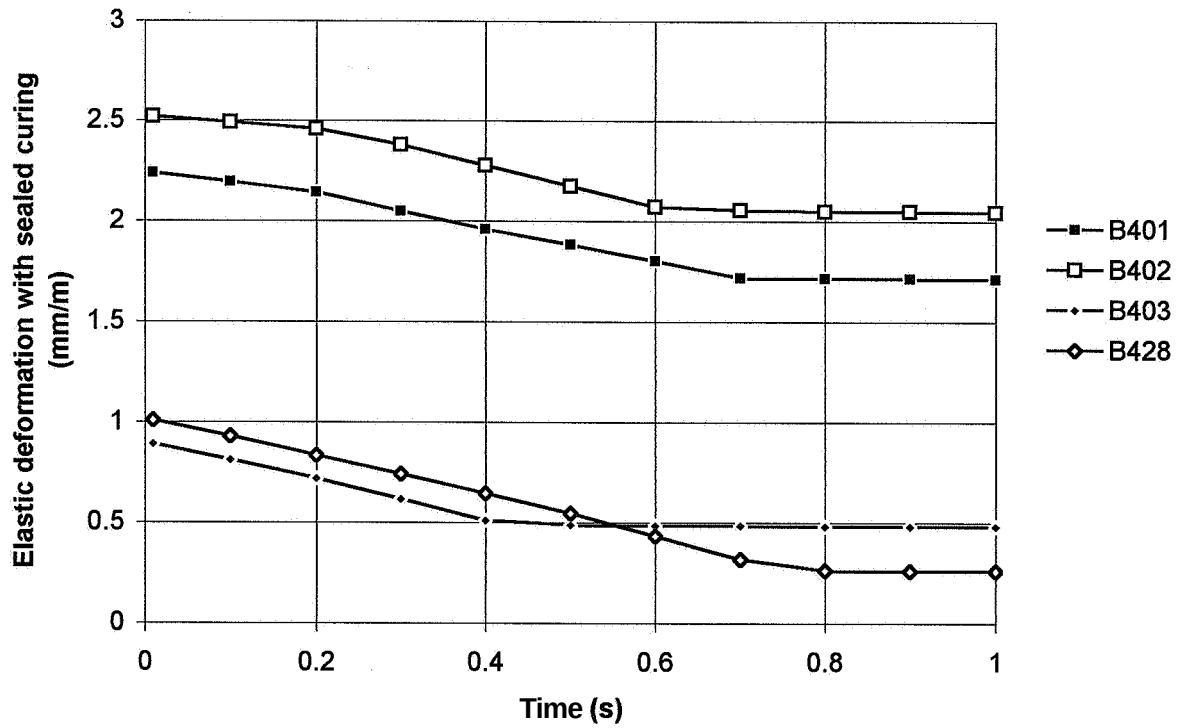

Appendix 13.13 - Elastic strain of mix 5 subjected to sealed curing

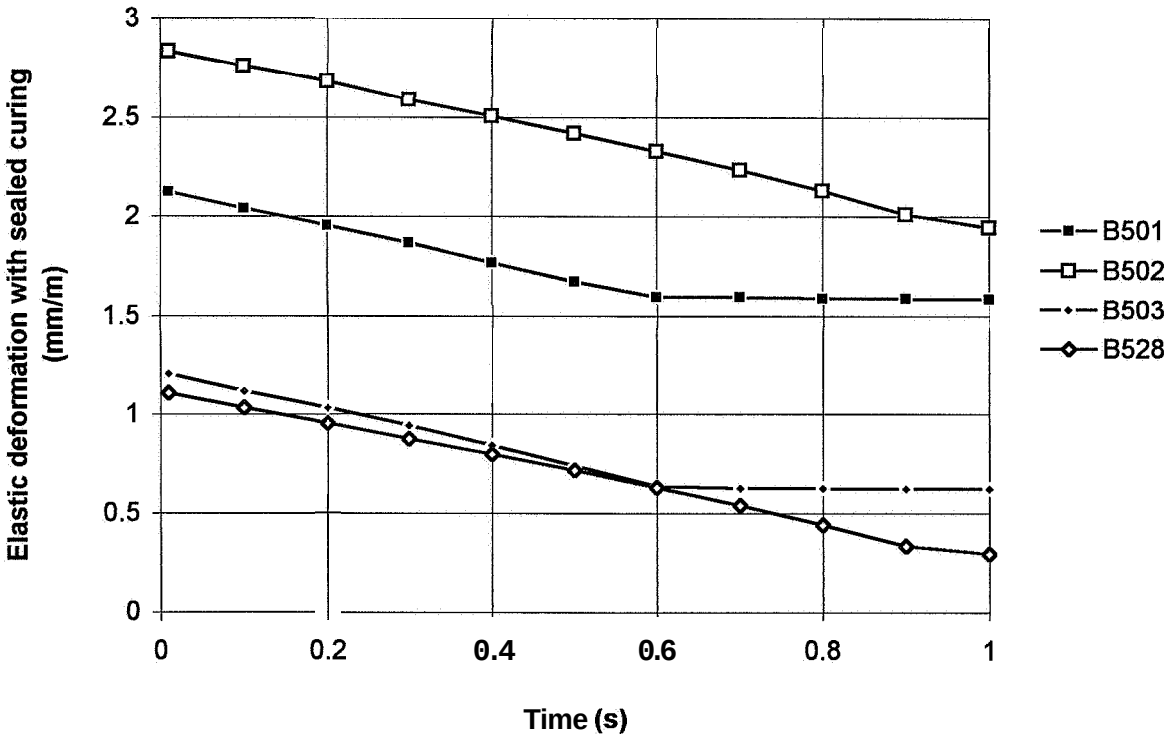

ppendi 13.1 - Elastic strain of mix 6 subjected to sea curing

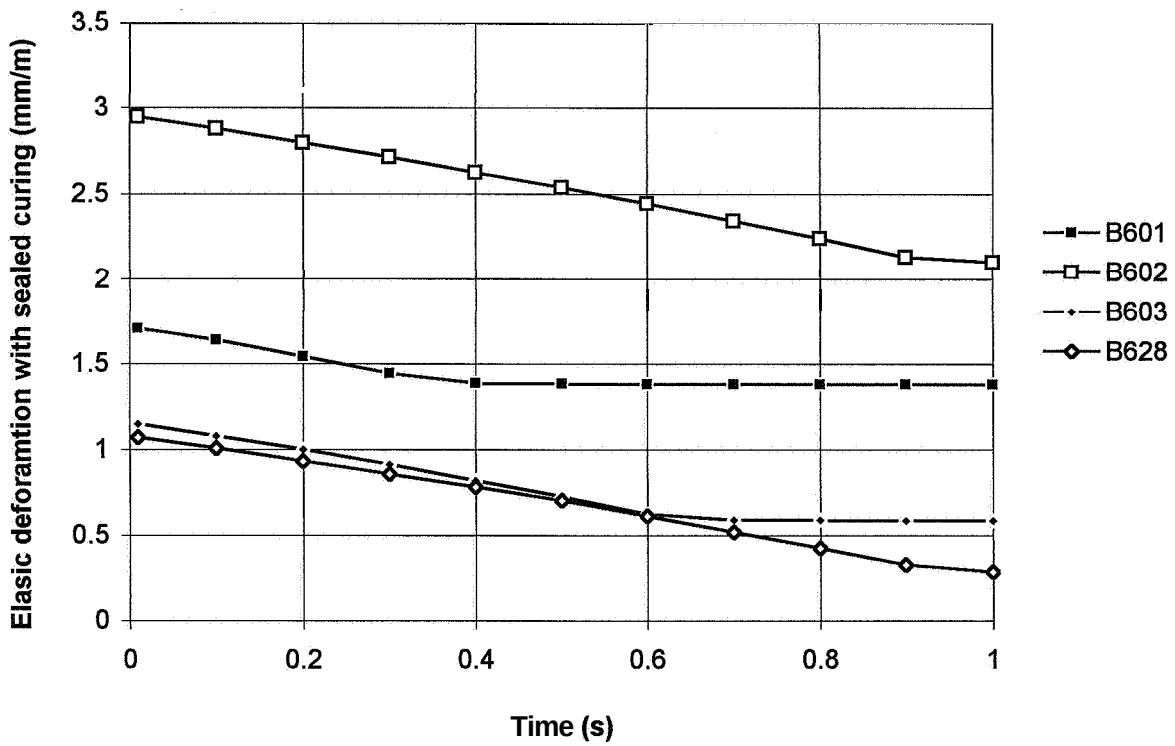

App 13.15 - Elastic strain of mix 7 subjected to sealed curing

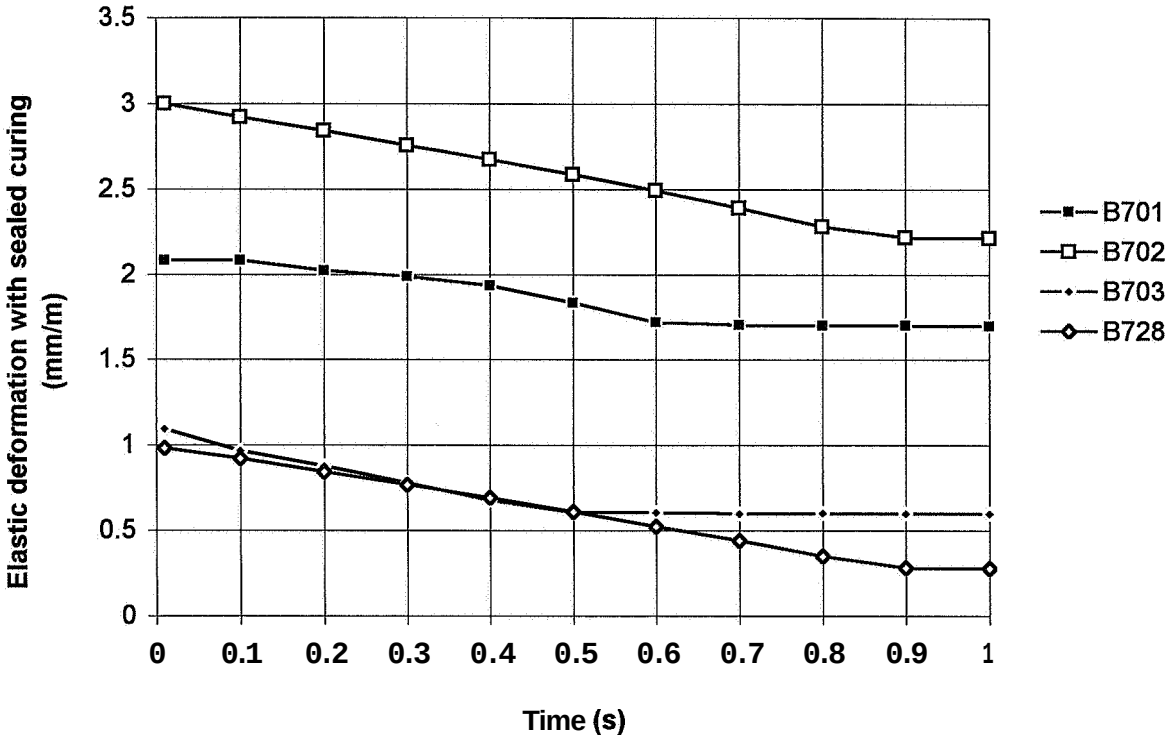

Appendi 16 - ti strain of mix 8 subjected to sealed curing

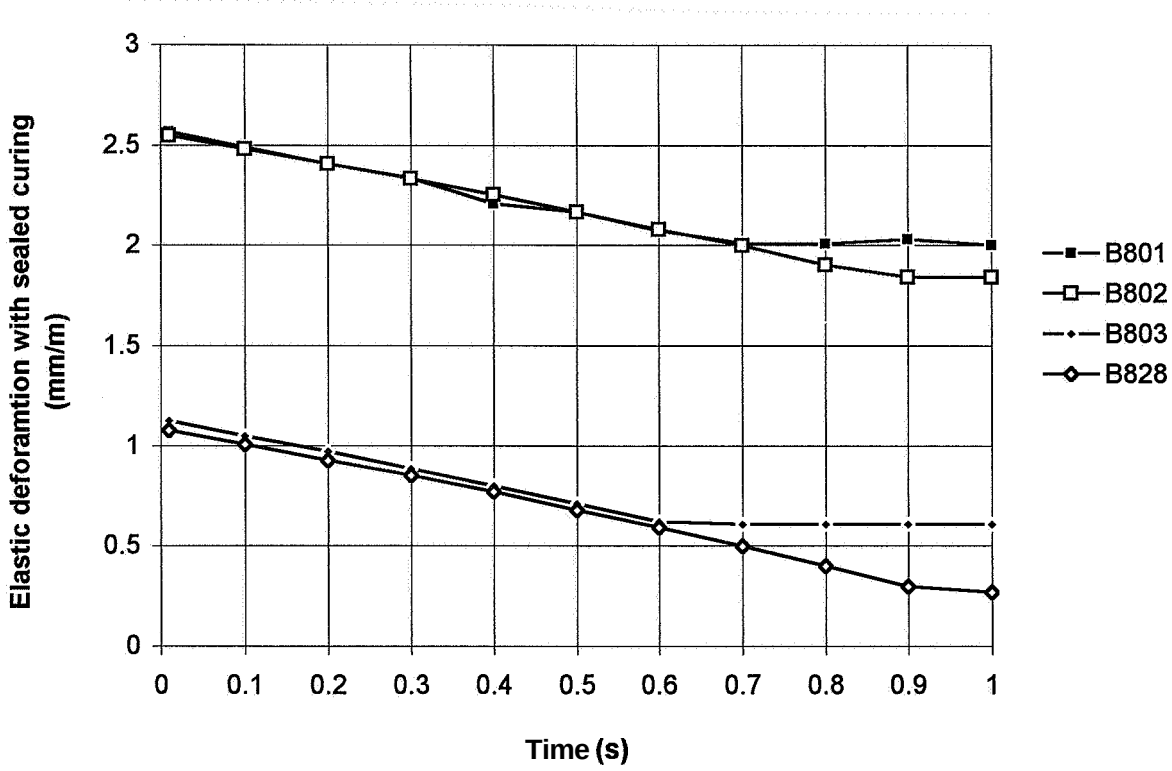

Appendix 13.17 - Recovery compliance of mix 1 subiected to sealed curing

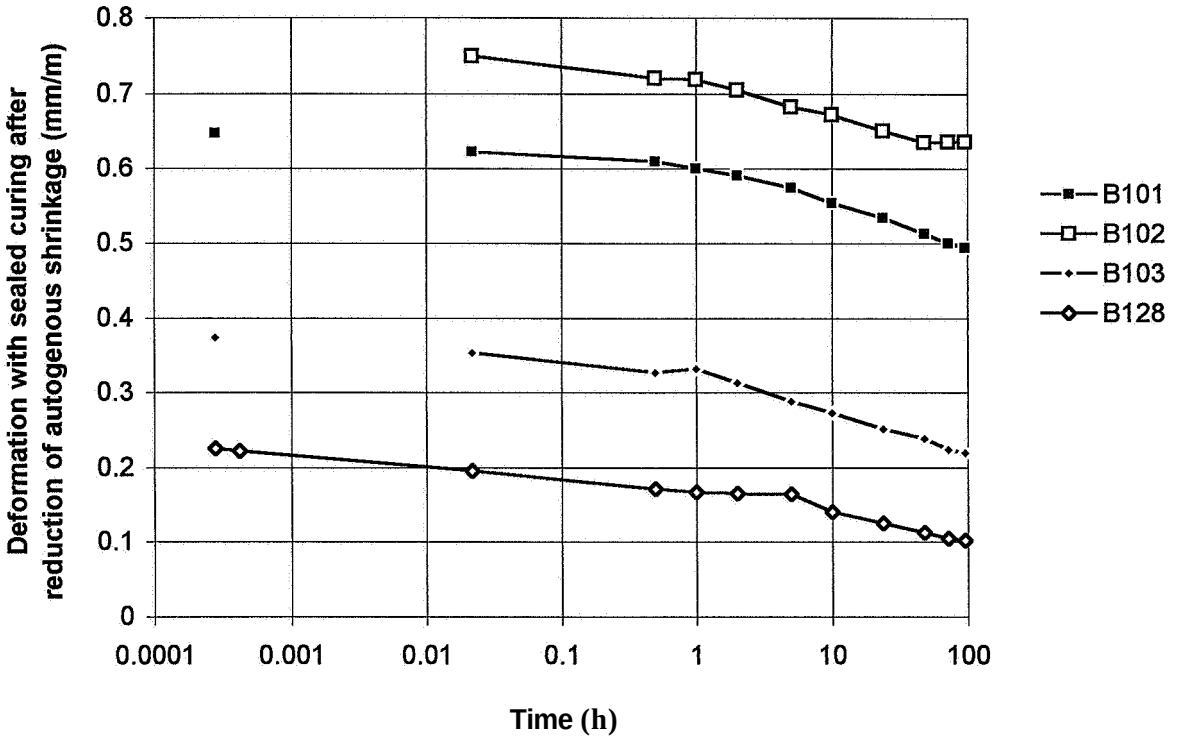

Appendix 13.18 - Recovery compliance of mix 2 subjected to sealed curing

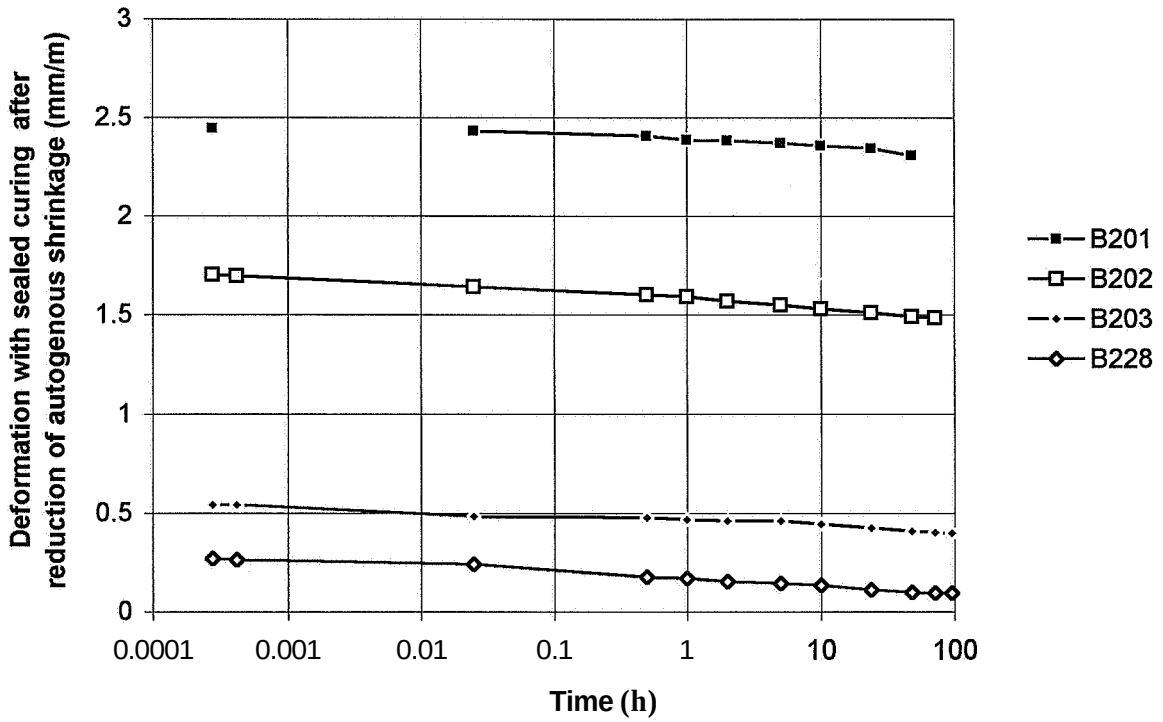

Appendix 13.19 - Recovery ompliane of mix 3 subjected to sealed curing

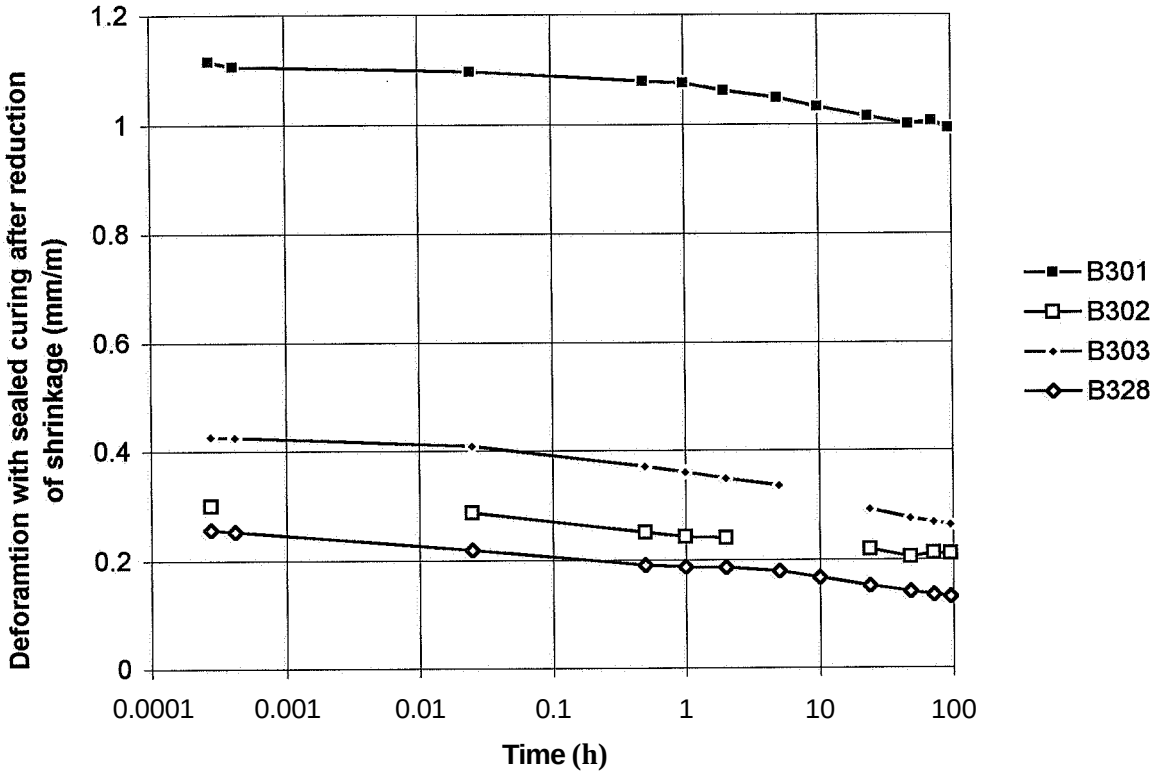

Appendix 13.20 - Recovery compliance of mix 4 subiected to sealed curing

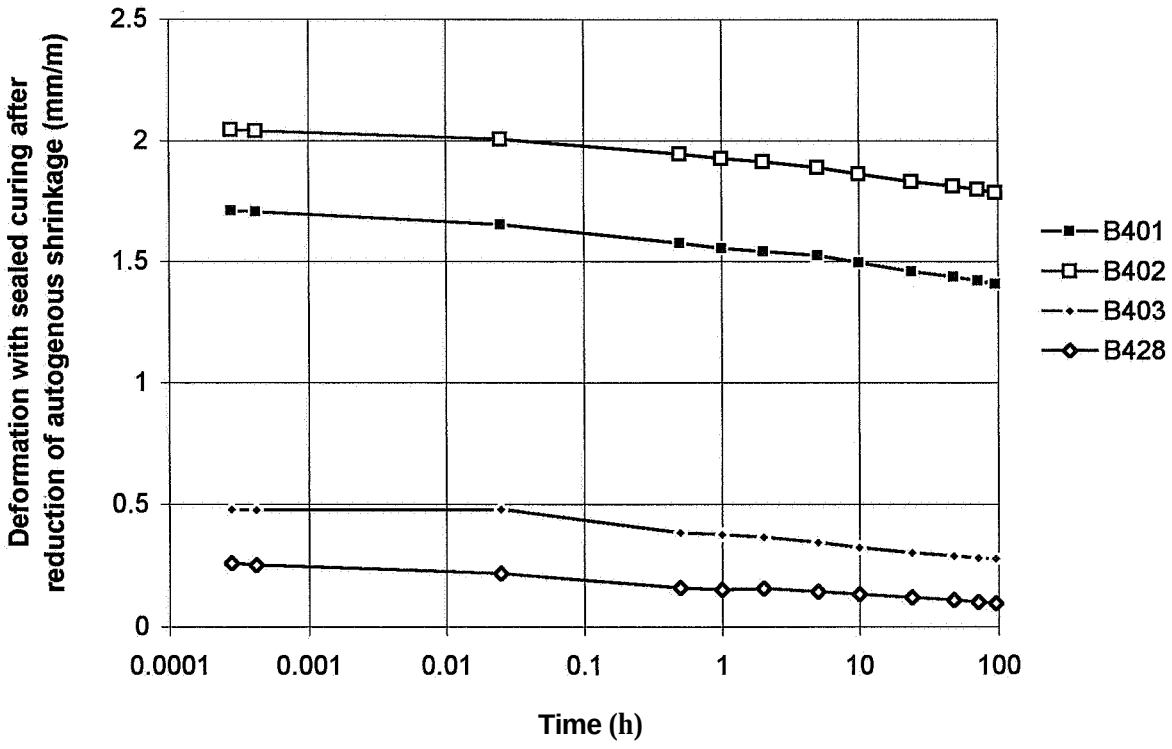

Appendix 13.21 - Recovery compliance of mix 5 subiected to sealed curing

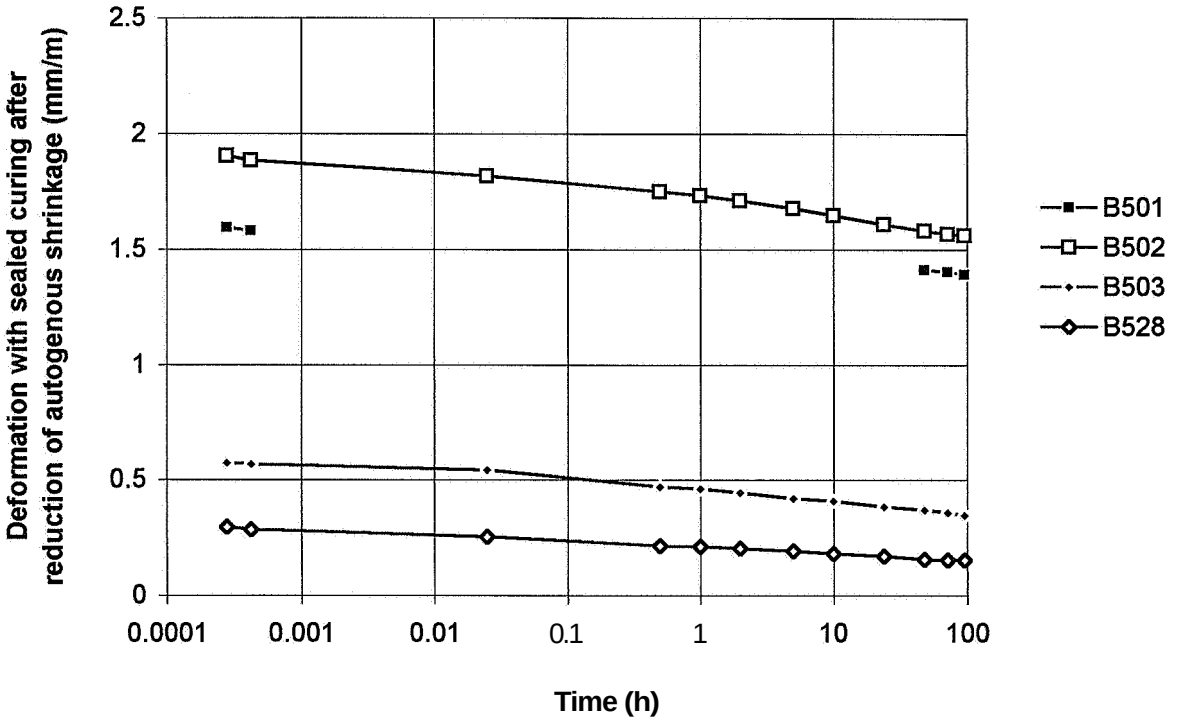

Appendix 13.22 - Recovery compliance of mix 6 subiected to sealed curing

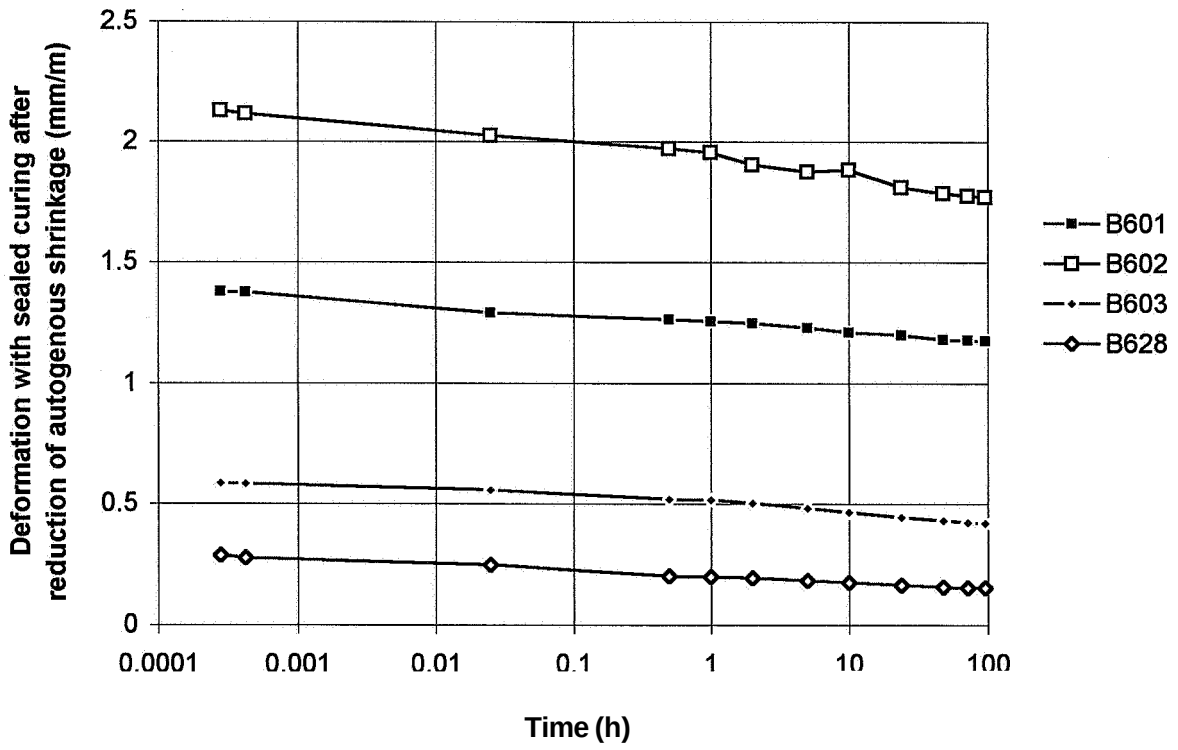

Appendix 13.23 - Recovery compliance of mix 7 subjected to sealed curing

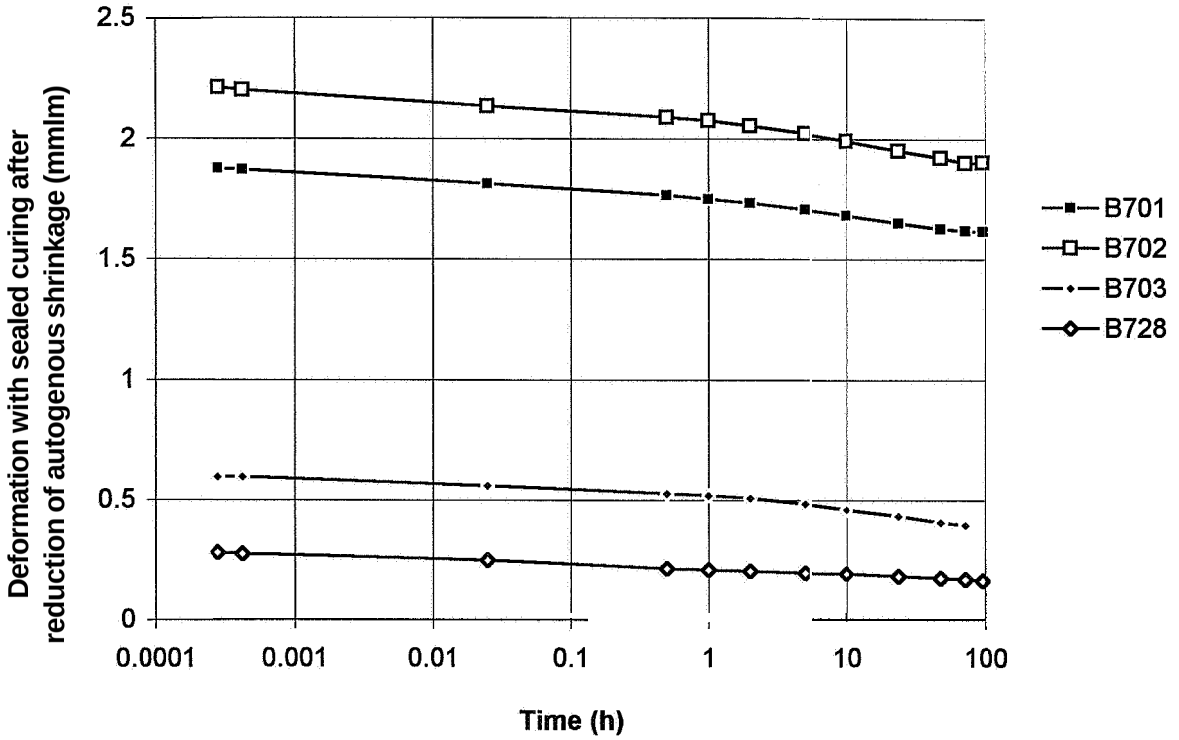

Appendix 13.24 - Recovery compliance of mix 8 subjected to sealed curing

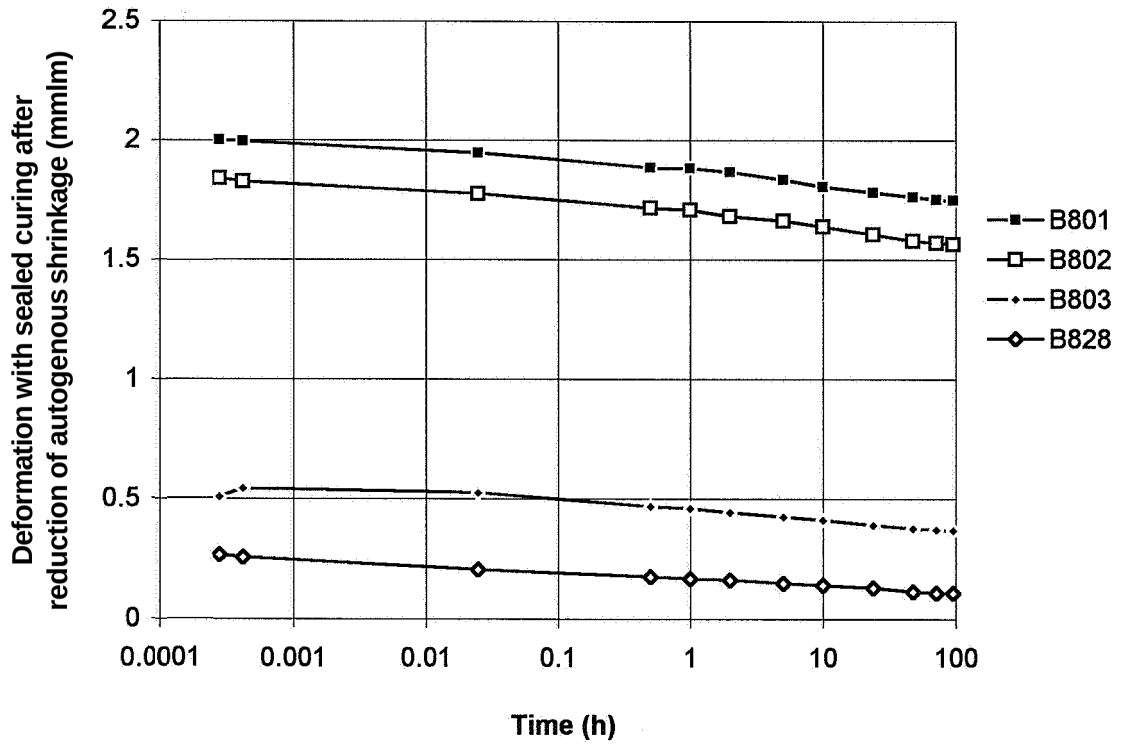

APPENDIX 14 - LONG-TERM CREEP OF CYLINDERS

Appendix 14.1 – Long-term compliance of mix 1
Appendix 14.2 – Long-term compliance of mix 2
Appendix 14.3 – Long-term compliance of mix 3
Appendix 14.4 – Long-term compliance of mix 4
Appendix 14.5 – Long-term compliance of mix 5
Appendix 14.6 – Long-term compliance of mix 6
Appendix 14.7 – Long-term compliance of mix 7
Appendix 14.8 – Long-term compliance of mix 8
Appendix 14.9 – Long-term compliance of mix 1 at unloading
Appendix 14.10 – Long-term compliance of mix 2 at unloading
Appendix 14.11 – Long-term compliance of mix 3 at unloading
Appendix 14.12 – Long-term compliance of mix 4 at unloading
Appendix 14.13 – Long-term compliance of mix 5 at unloading
Appendix 14.14 – Long-term compliance of mix 6 at unloading
Appendix 14.15 – Long-term compliance of mix 7 at unloading
Appendix 14.16 – Long-term compliance of mix 8 at unloading
Appendix 14.17 – Long-term compliance of mix 1 after short-term creep subjected to sealed curing
Appendix 14.18 – Long-term compliance of mix 2 after short-term creep subjected to sealed curing
Appendix 14.19 – Long-term compliance of mix 3 after short-term creep subjected to sealed curing
Appendix 14.20 – Long-term compliance of mix 4 after short-term creep subjected to sealed curing
Appendix 14.21 – Long-term compliance of mix 5 after short-term creep subjected to sealed curing
Appendix 14.22 – Long-term compliance of mix 6 after short-term creep subjected to sealed curing
Appendix 14.23 – Long-term compliance of mix 7 after short-term creep subjected to sealed curing
Appendix 14.24 – Long-term compliance of mix 8 after short-term creep subjected to sealed curing

B denotes basic creep (sealed curing)
D denotes drying creep (air curing)
6... denotes concrete mix, **Table 5.1**
...01 age at loading: 1 day; stresslcylinder strength ratio: 0.84
...02 age at loading: 2 days; stresslcylinder strength ratio: 0.84
...03 age at loading: 2 days; stresslcylinder strength ratio: 0.42
...28 age at loading: 28 days; stresslcylinder strength ratio: 0.42

Appendix 14.1 – Long-term compliance of mix 1

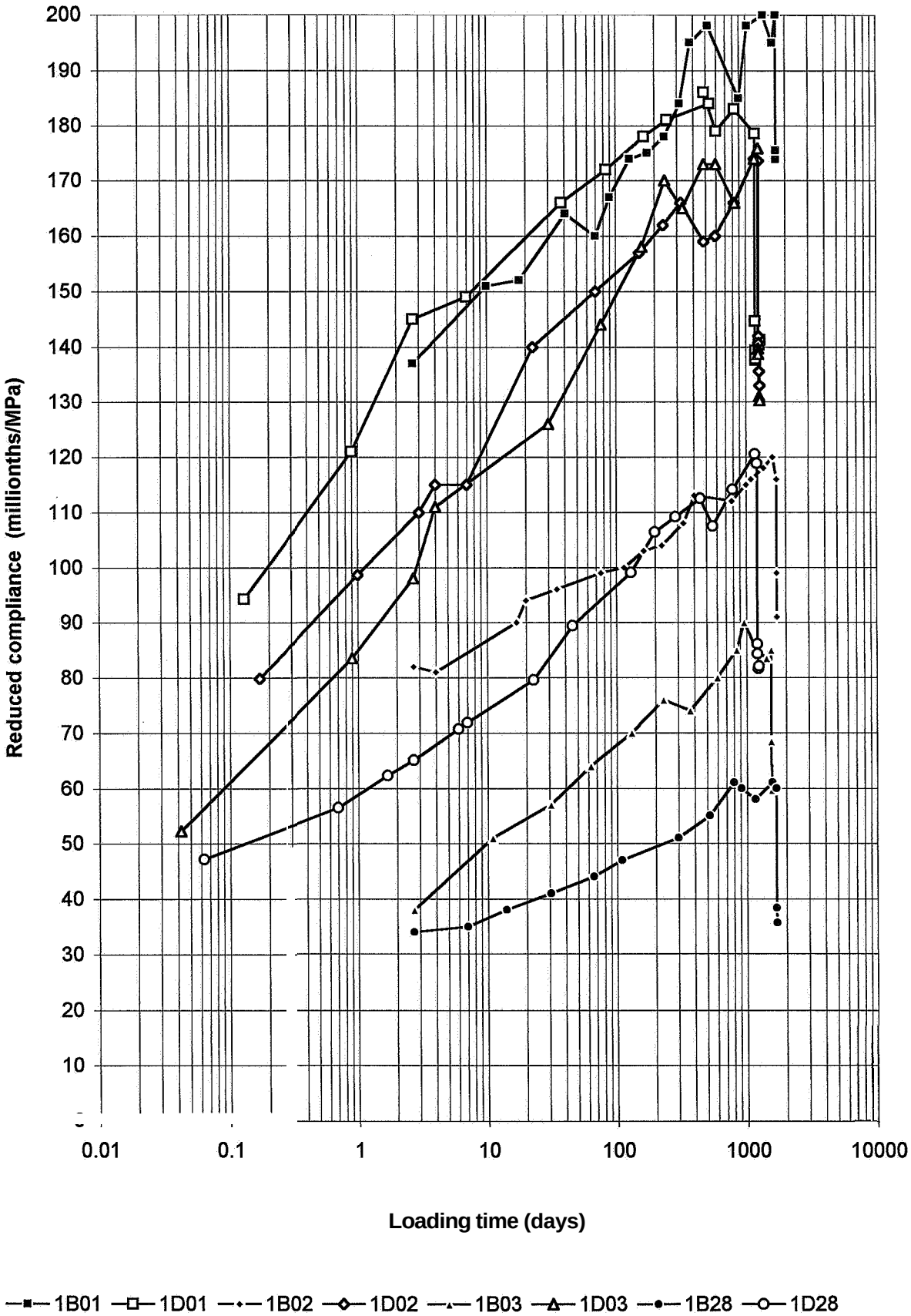

Appendix 14.2 – Long-term compliance of mix 2

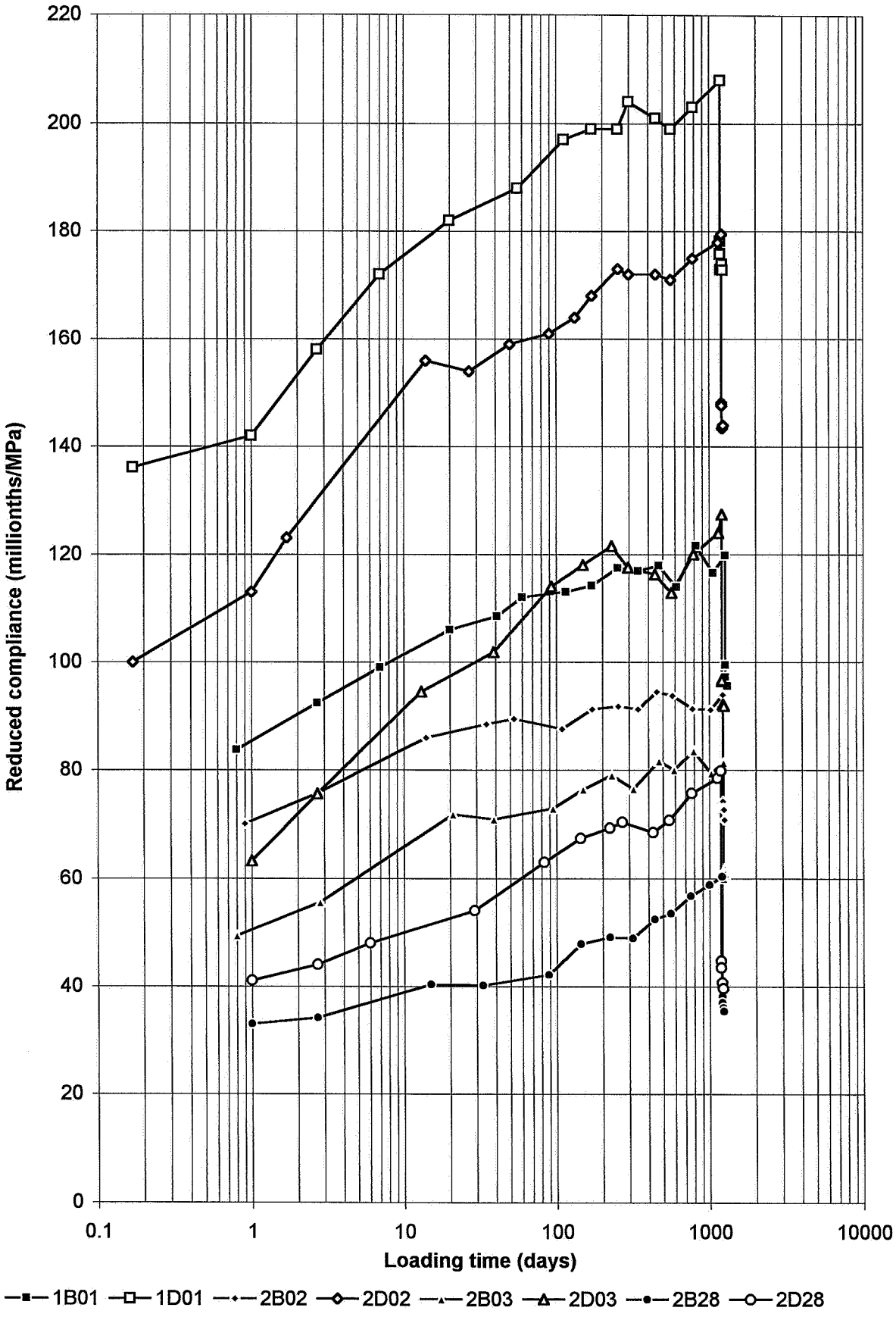

Appendix 14.3 – Long-term compliance of mix 3

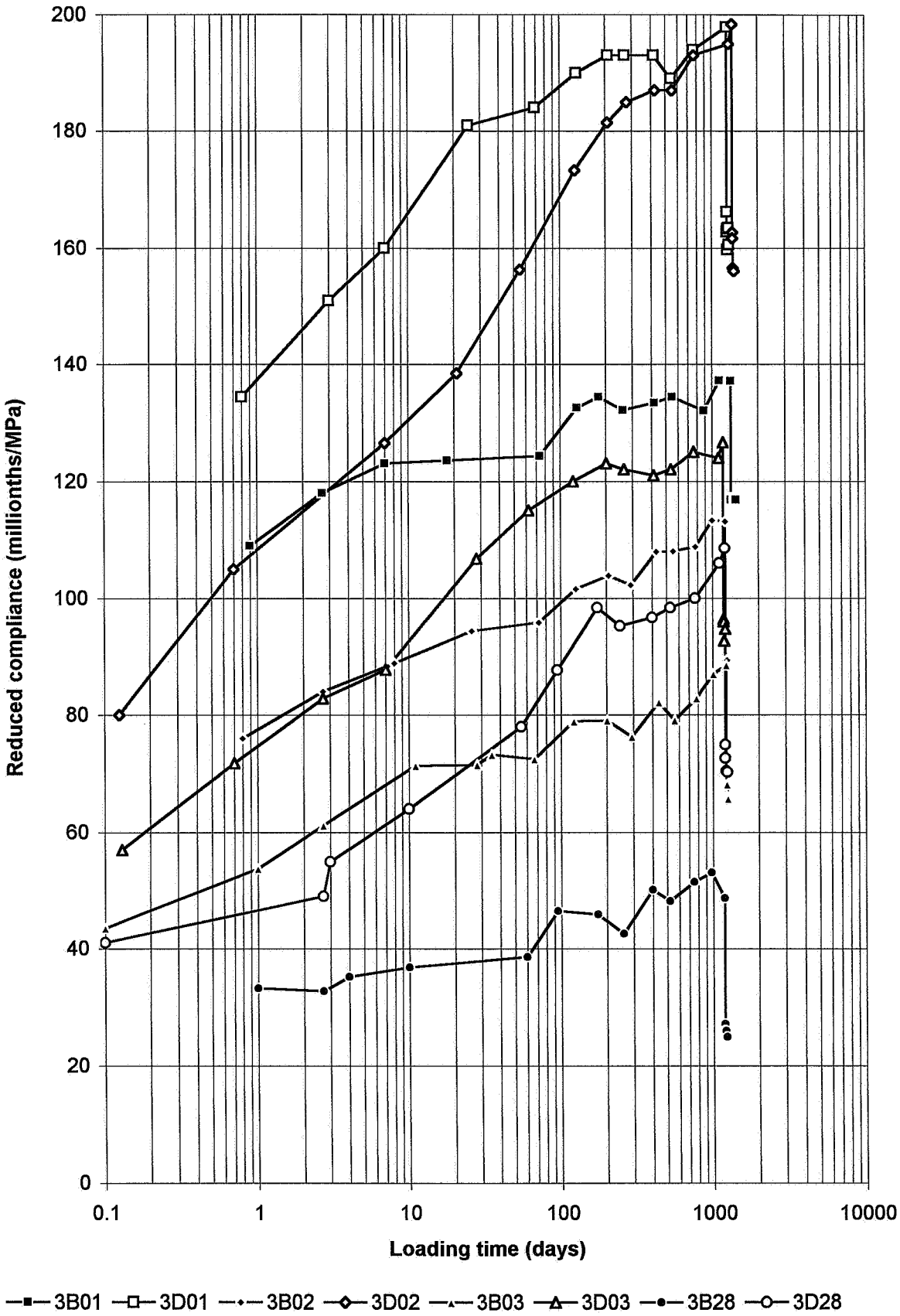

Appendix 14.4 – Long-term compliance of mix 4

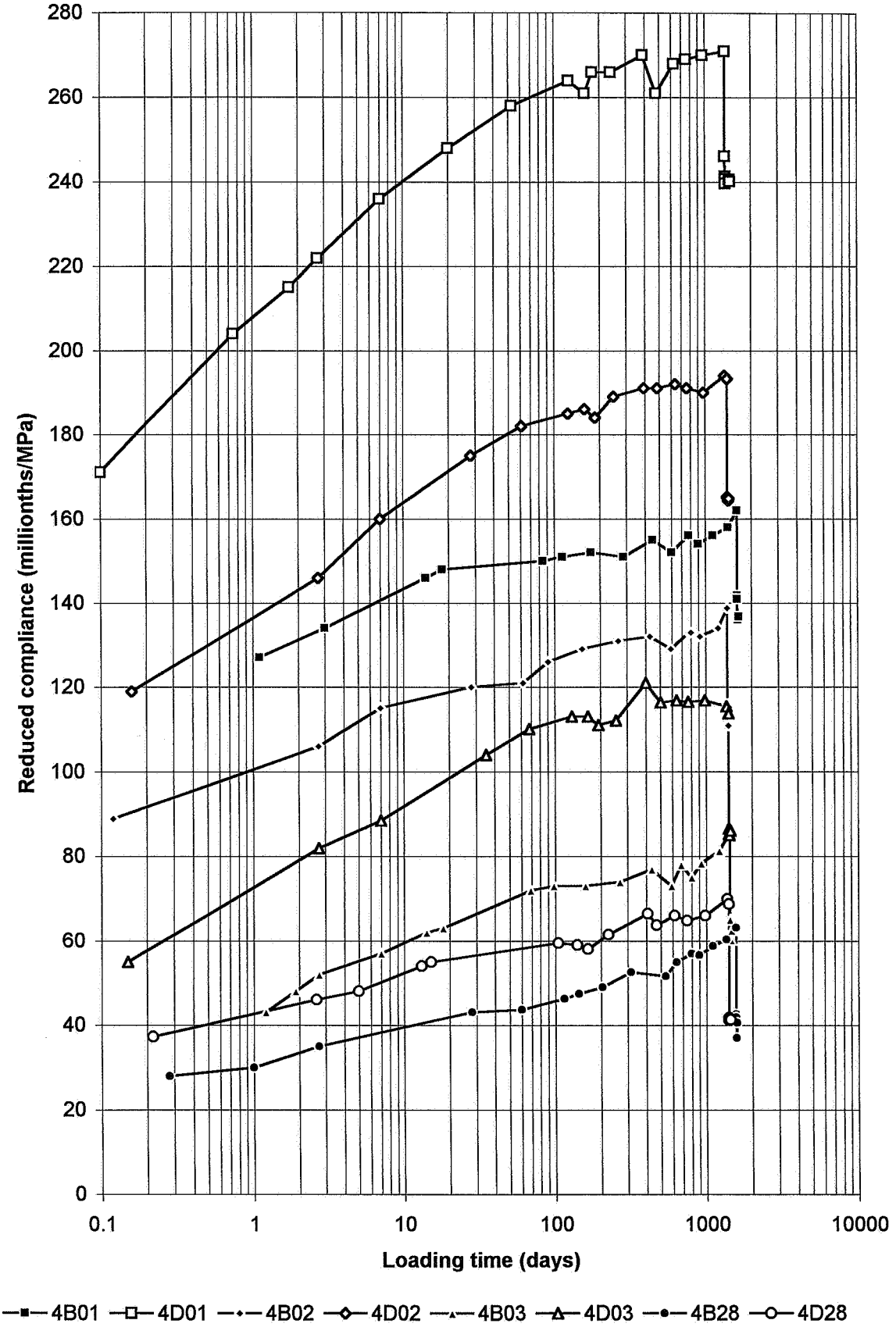

Appendix 14.5 – Long-term compliance of mix 5

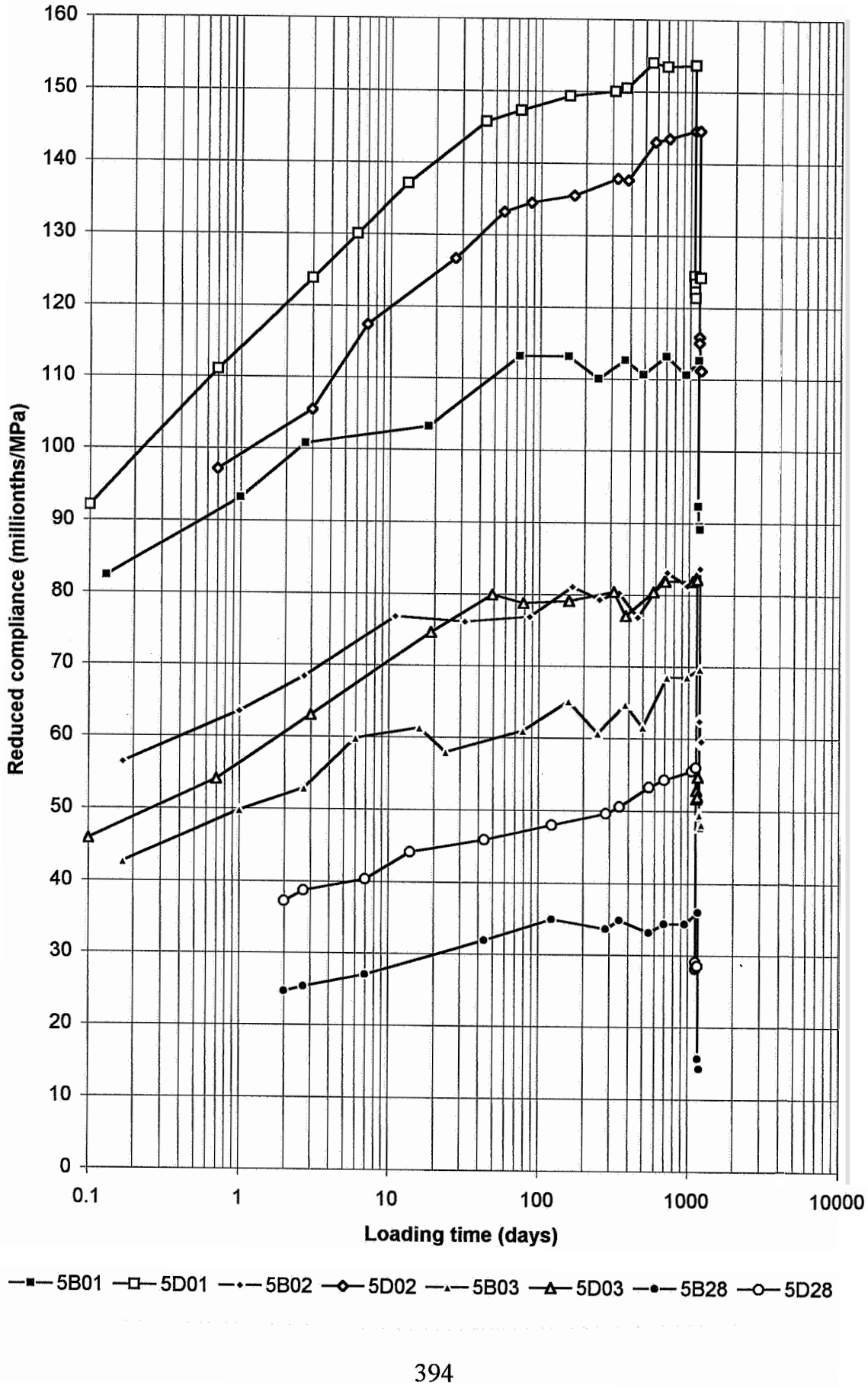

Appendix 14.6 – Lone-term compliance of mix 6

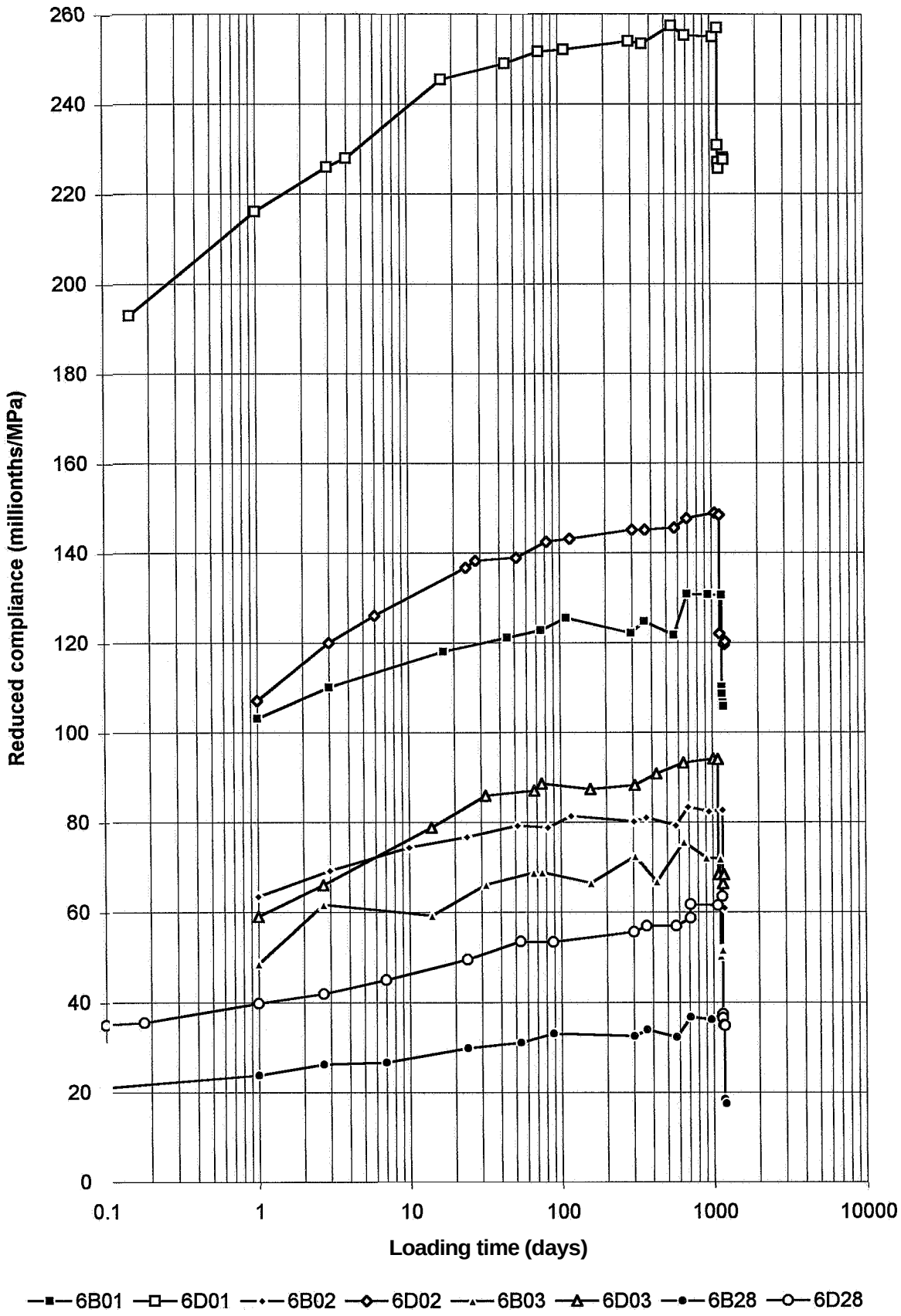

Appendix 14.7 – Long-term compliance of mix 7

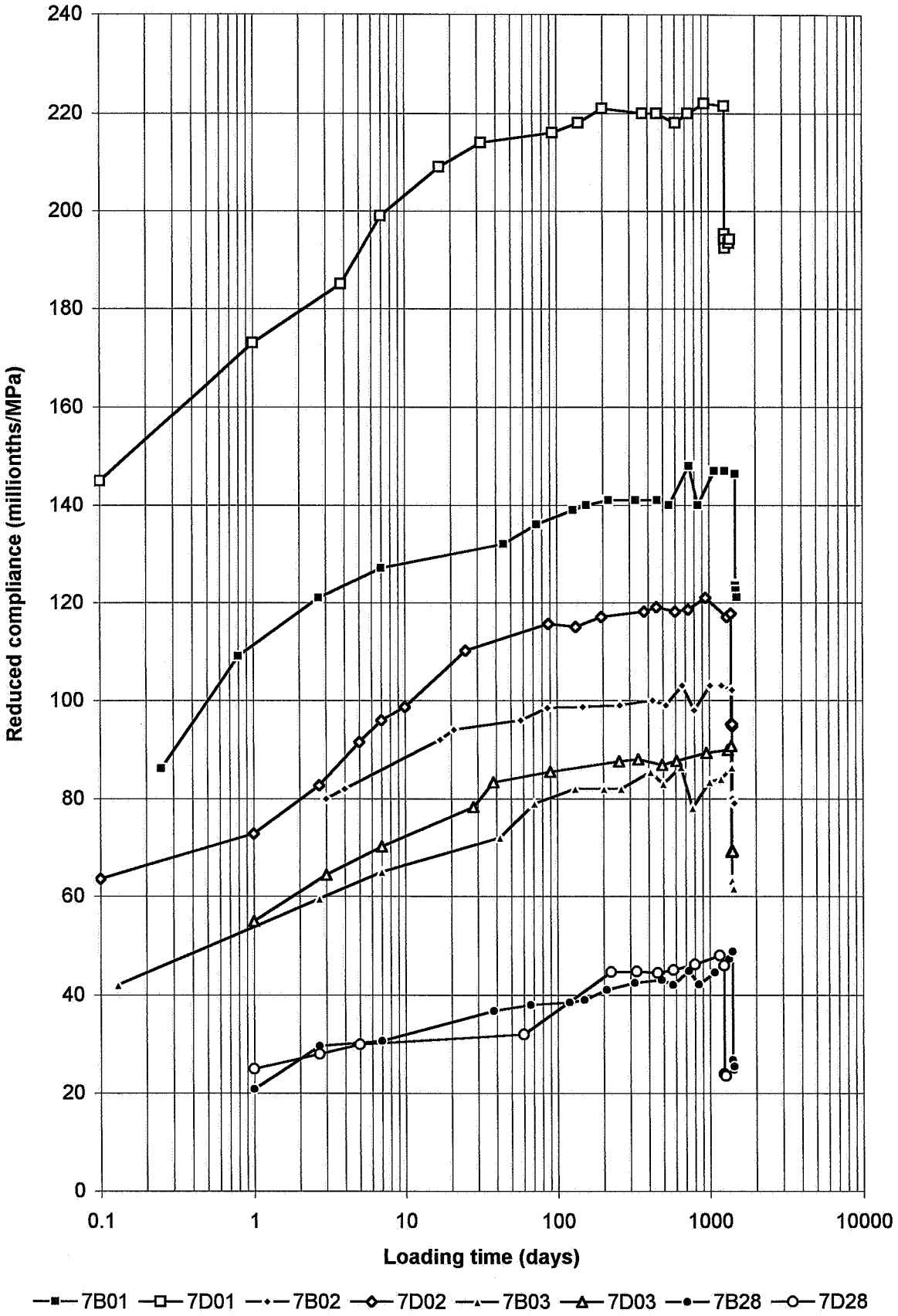

Appendix 1 .8 – Long-ter ompliance of mix 8

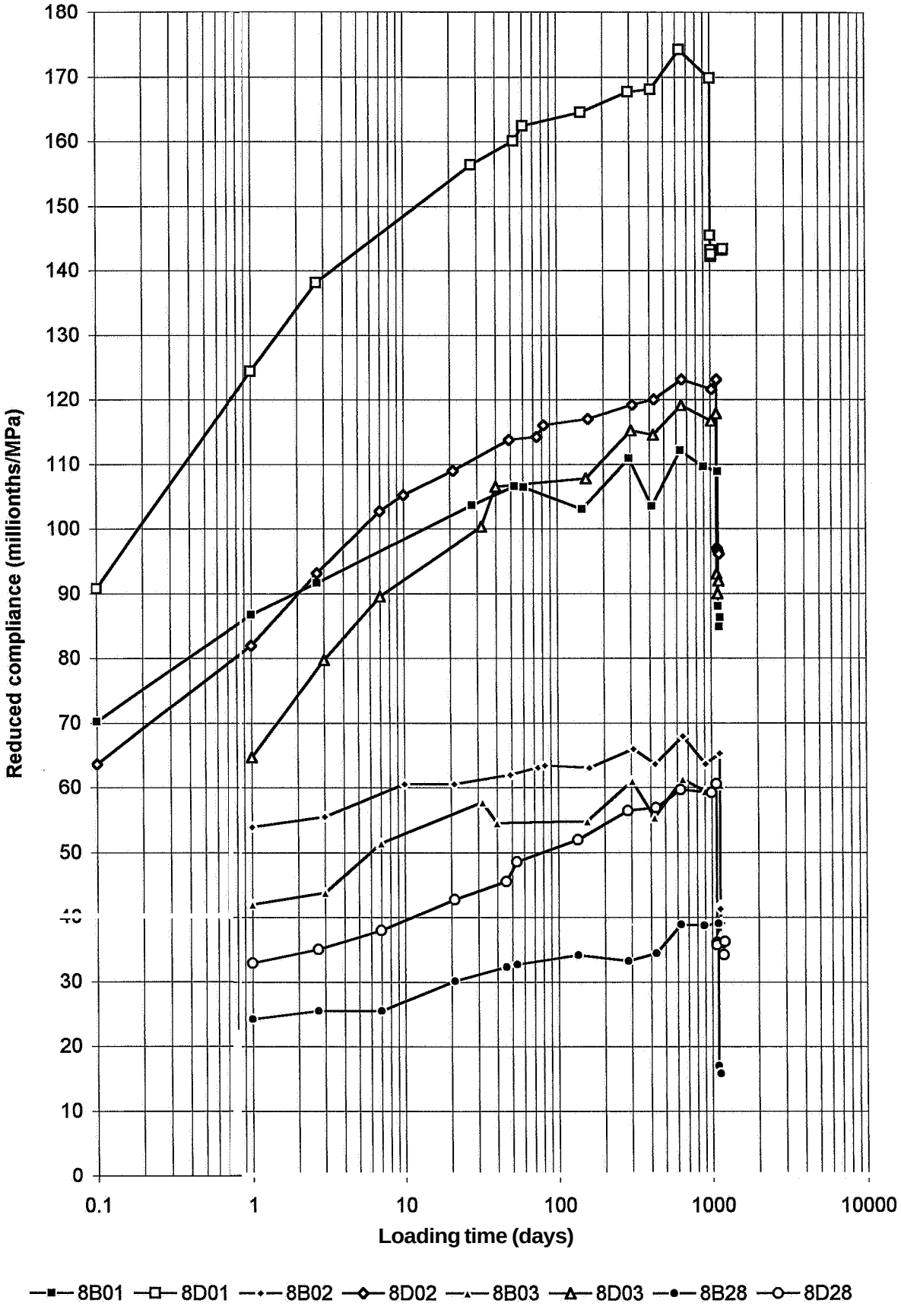

Appendix 14.9 – Long-term compliance of mix 1 at unloading

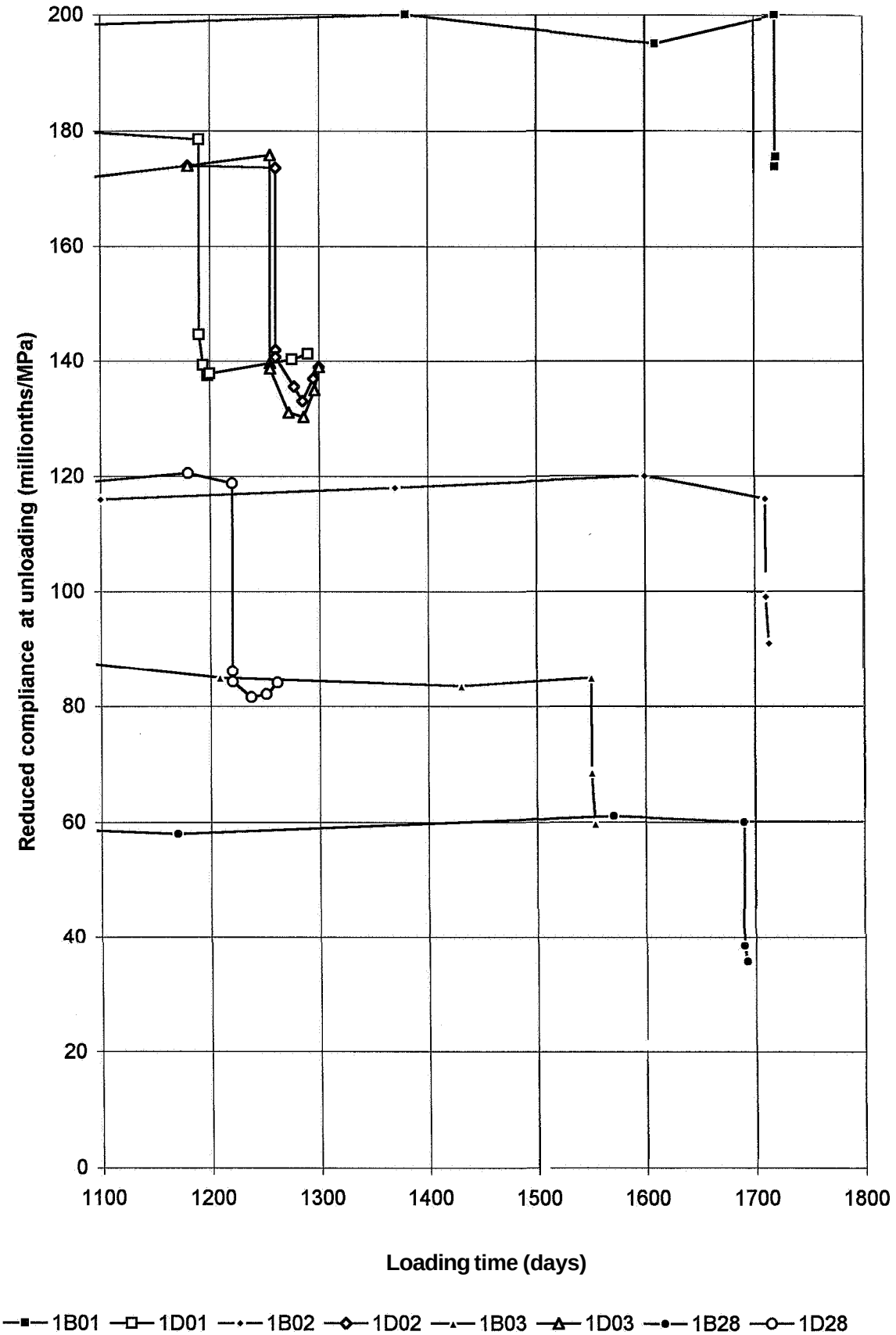

Appendix 14.10 – Long-term compliance of mix 2 at unloading

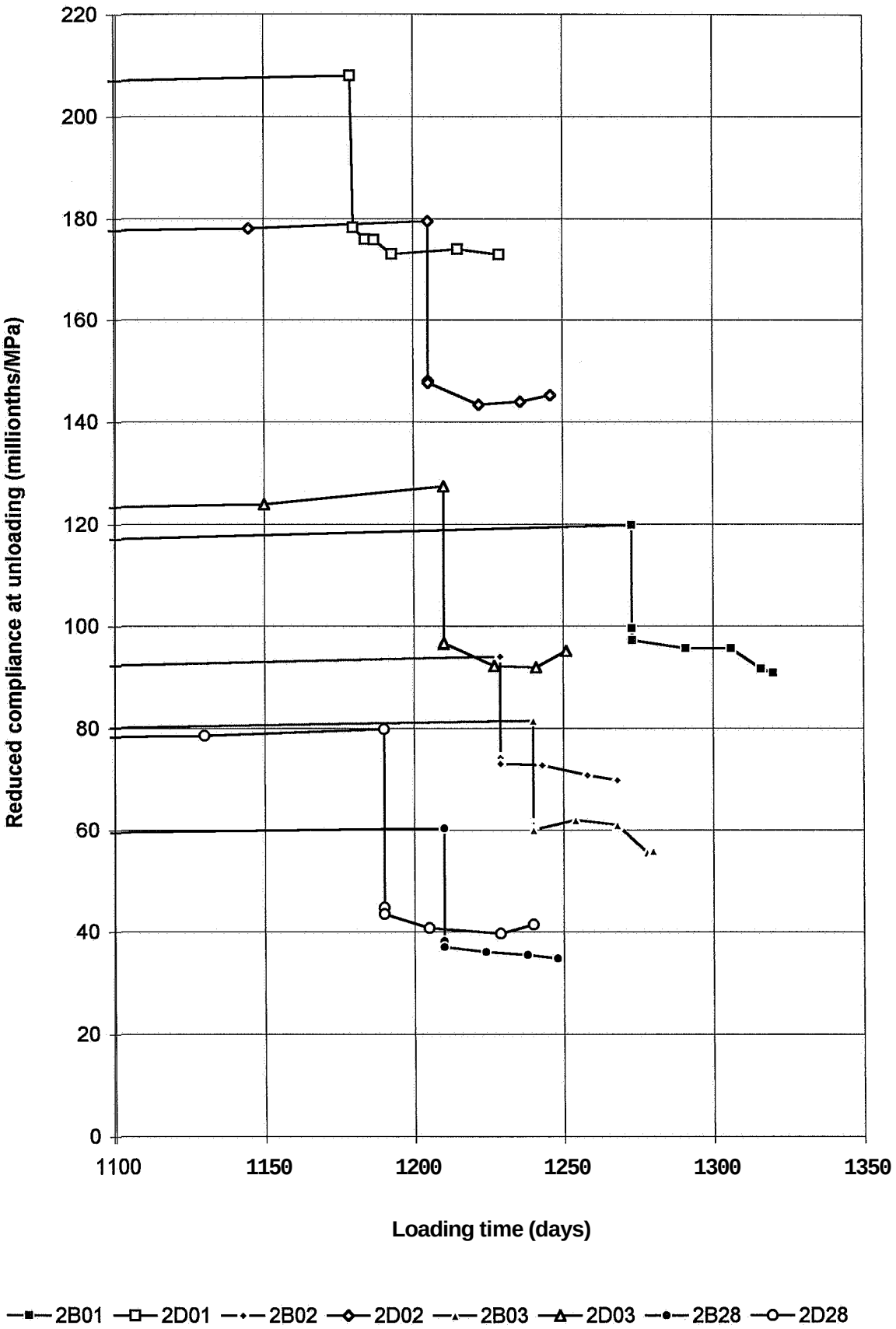

Appendix 14.11 – Long-term compliance of mix 3 at unloading

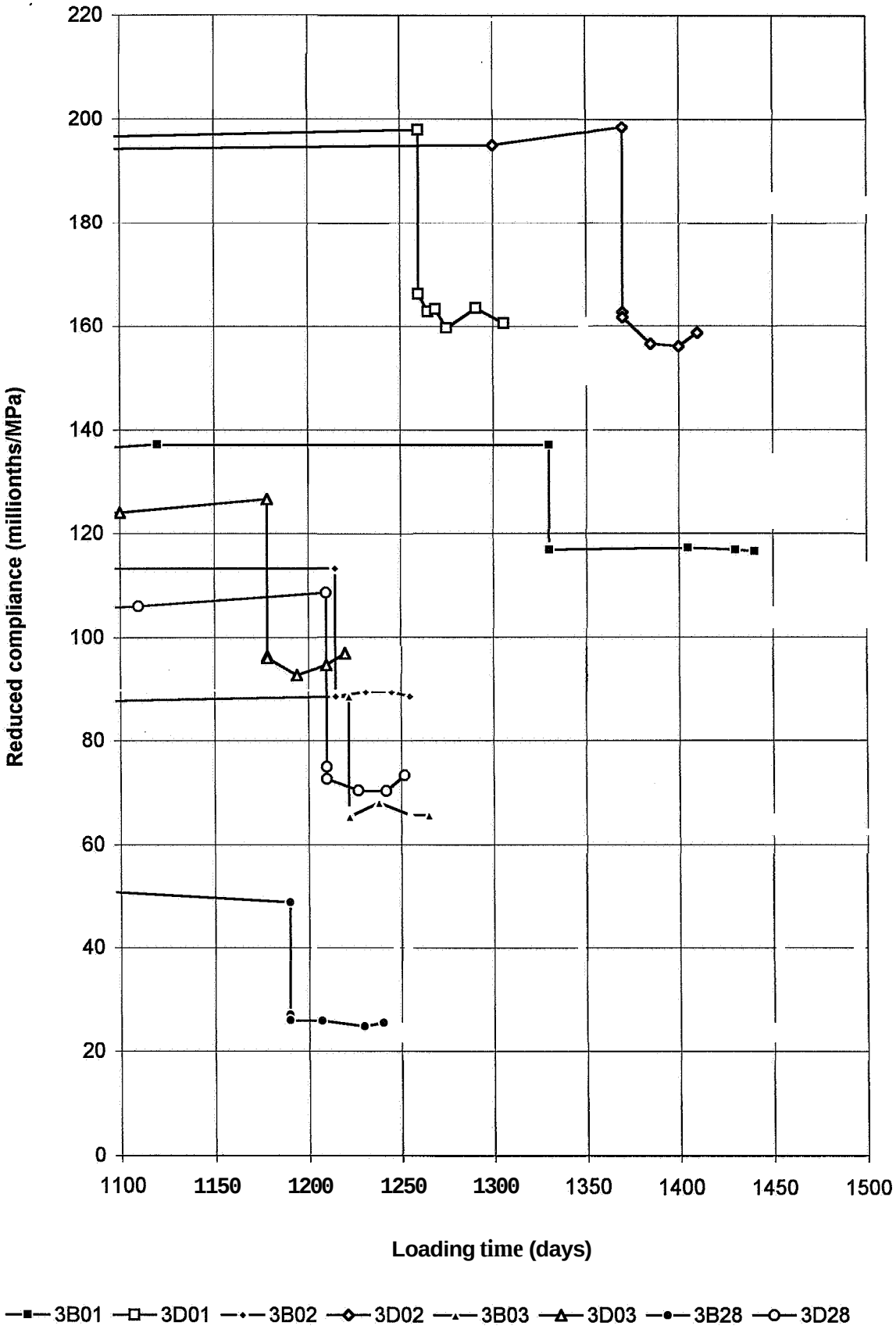

Appendix 14.12 – Long-term compliance of mix 4 at unloading

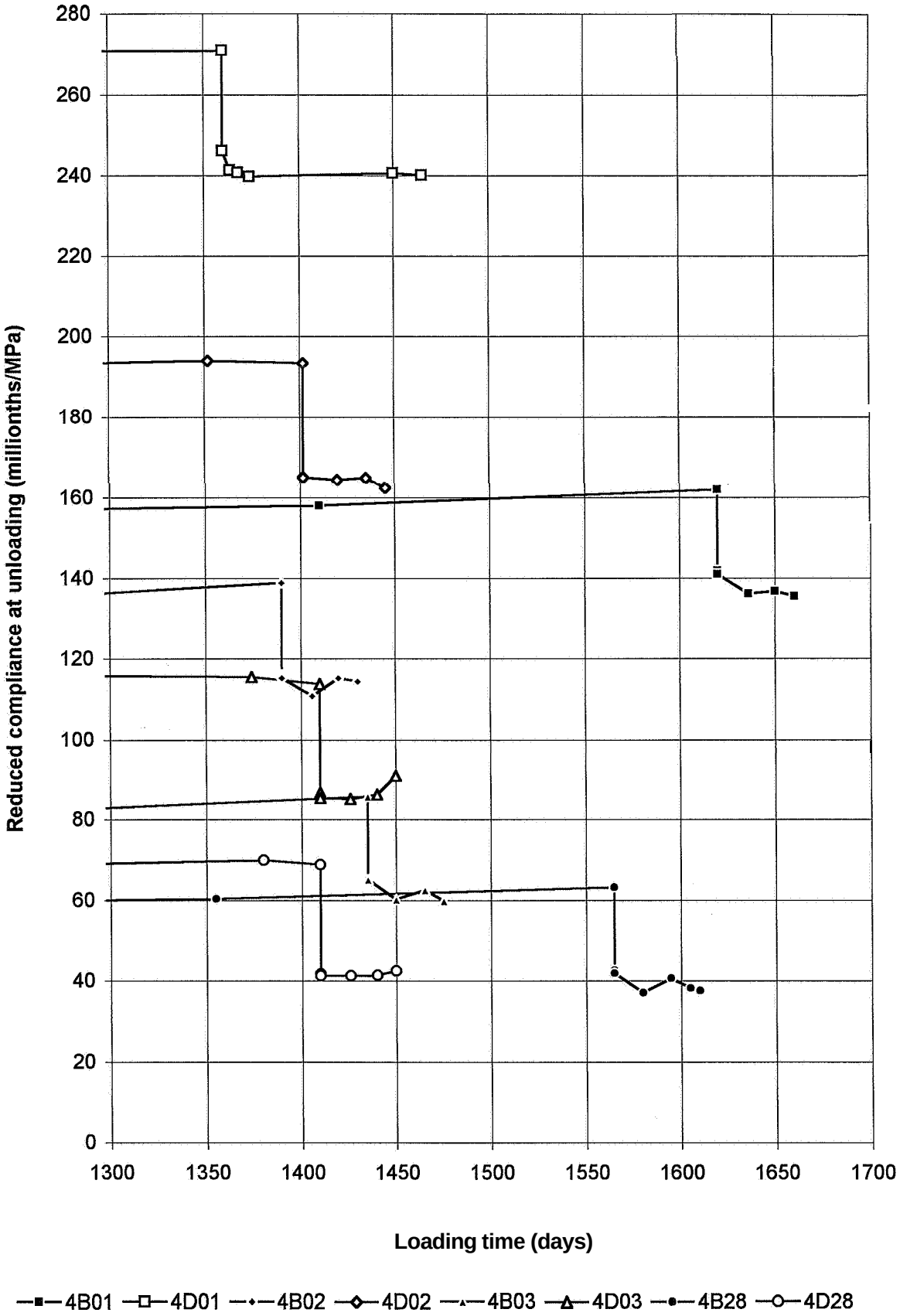

Appendix 14.13 – Long-term compliance of mix 5 at unloading

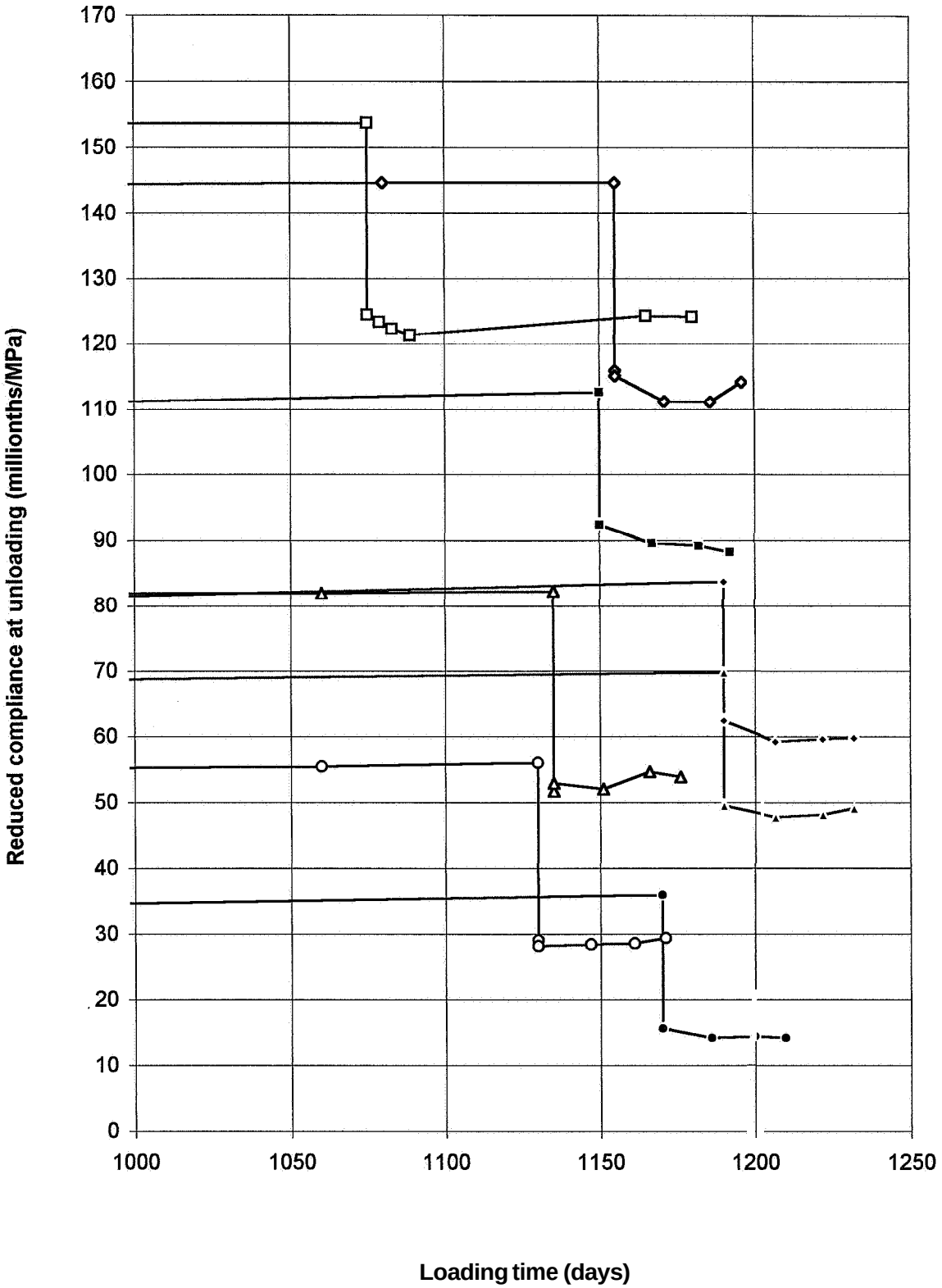

Appendix 14.14 – Long-term compliance of mix 6 at unloading

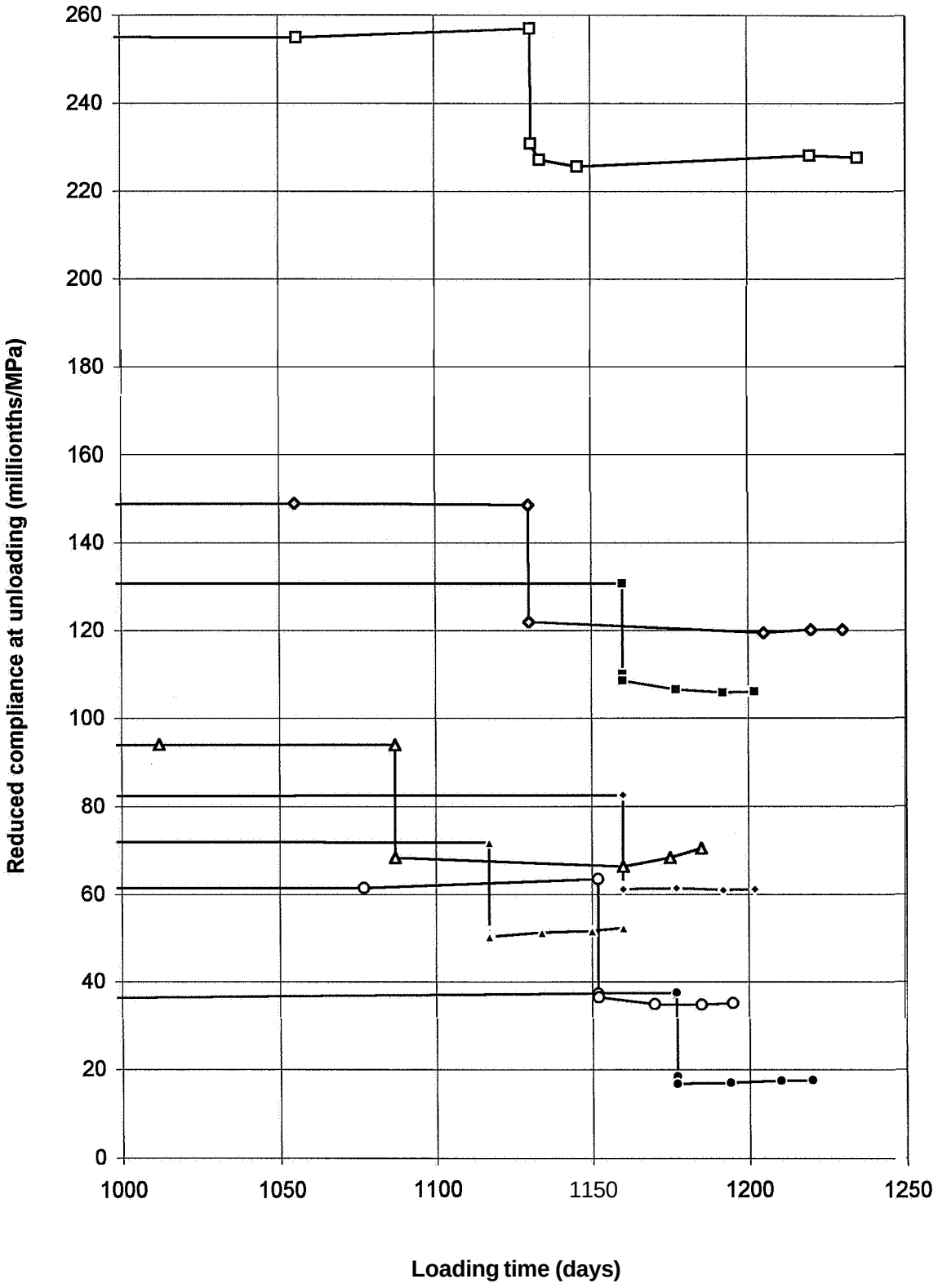

Appendix 14.15 – Long-term compliance of mix 7 at unloading

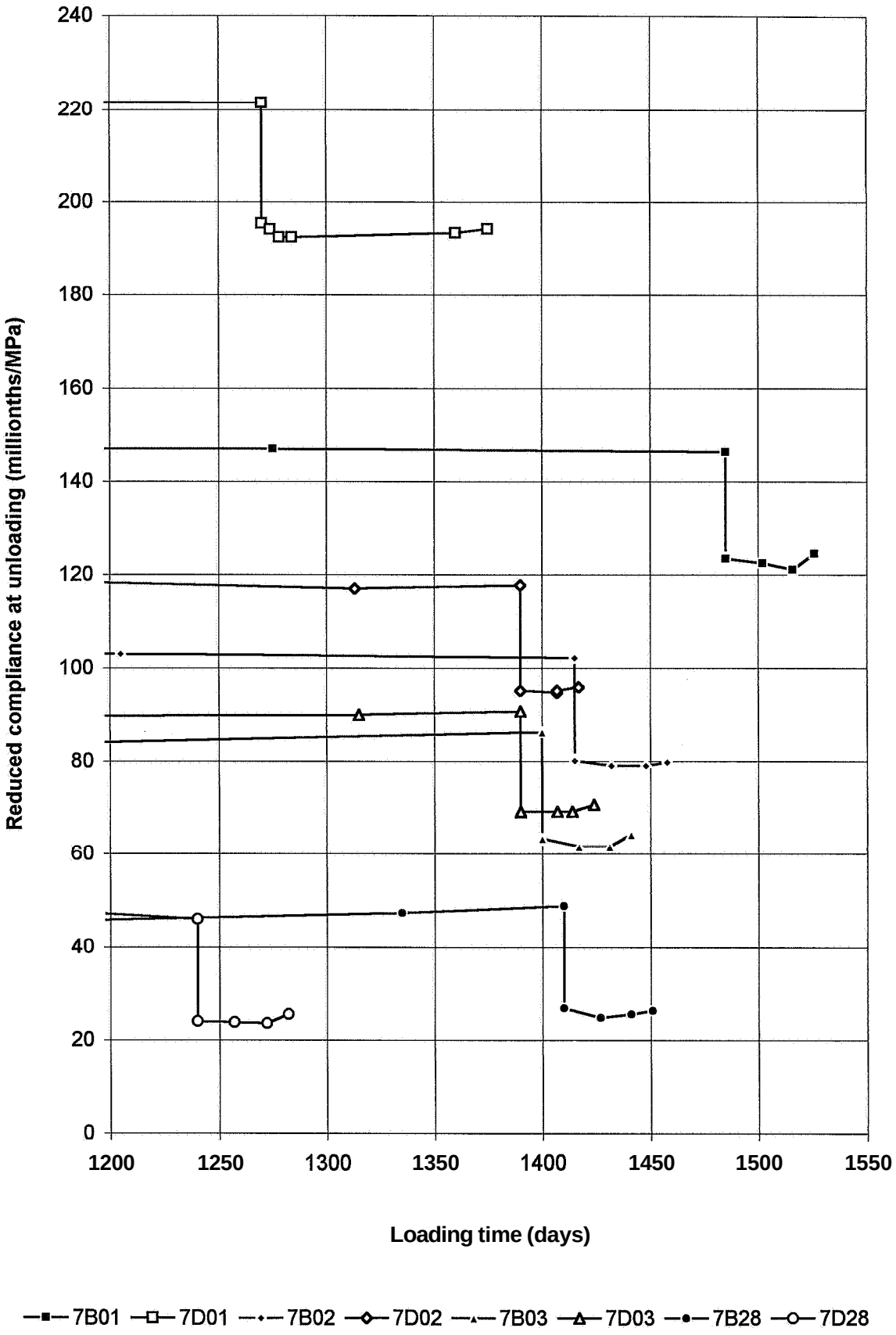

Appendix 14.16 – Long-term compliance of mix 8 at unloading

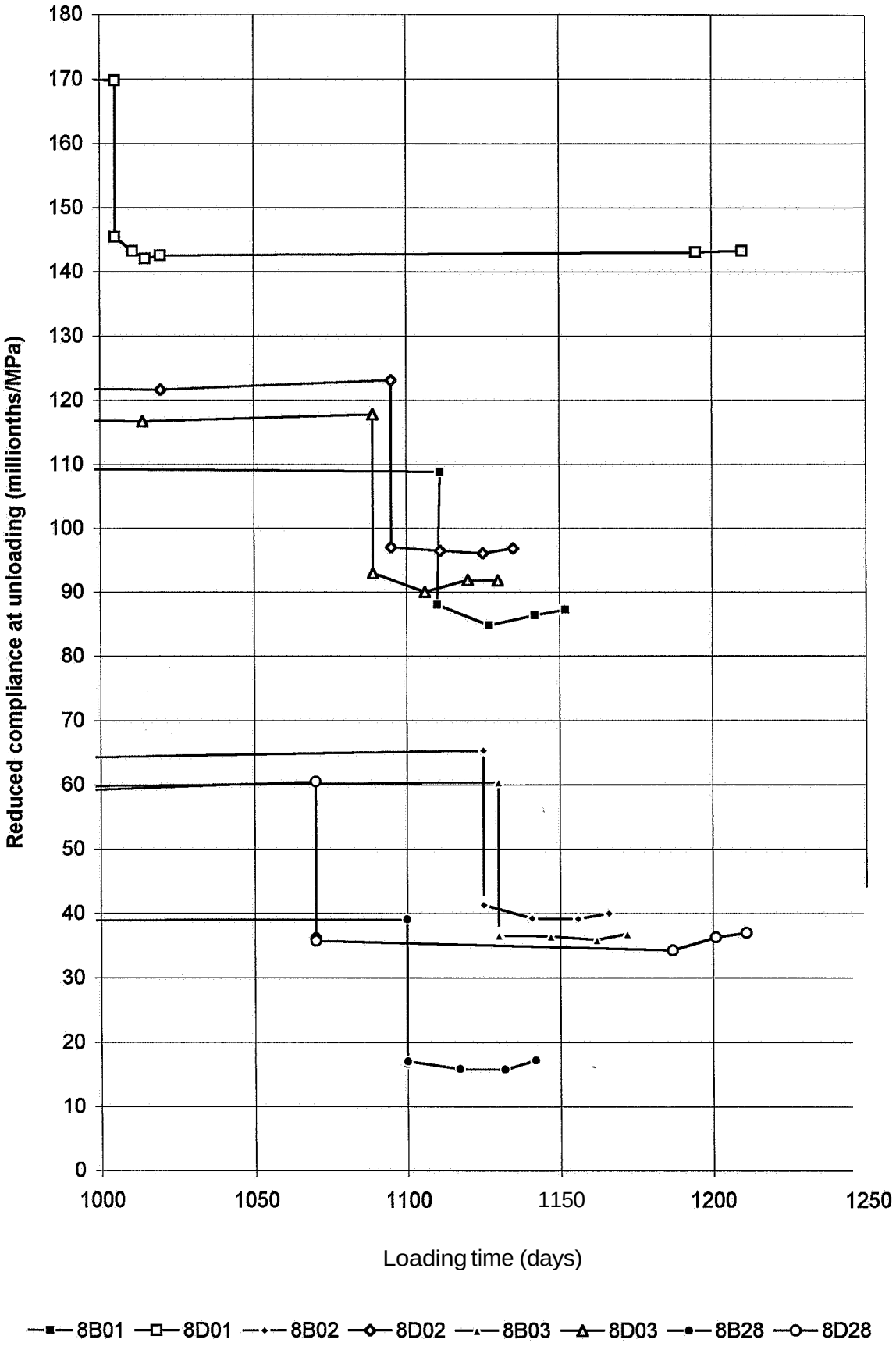

Appendix 14.17 – Long-term compliance of mix 1 after short-term creep subjected to sealed curing

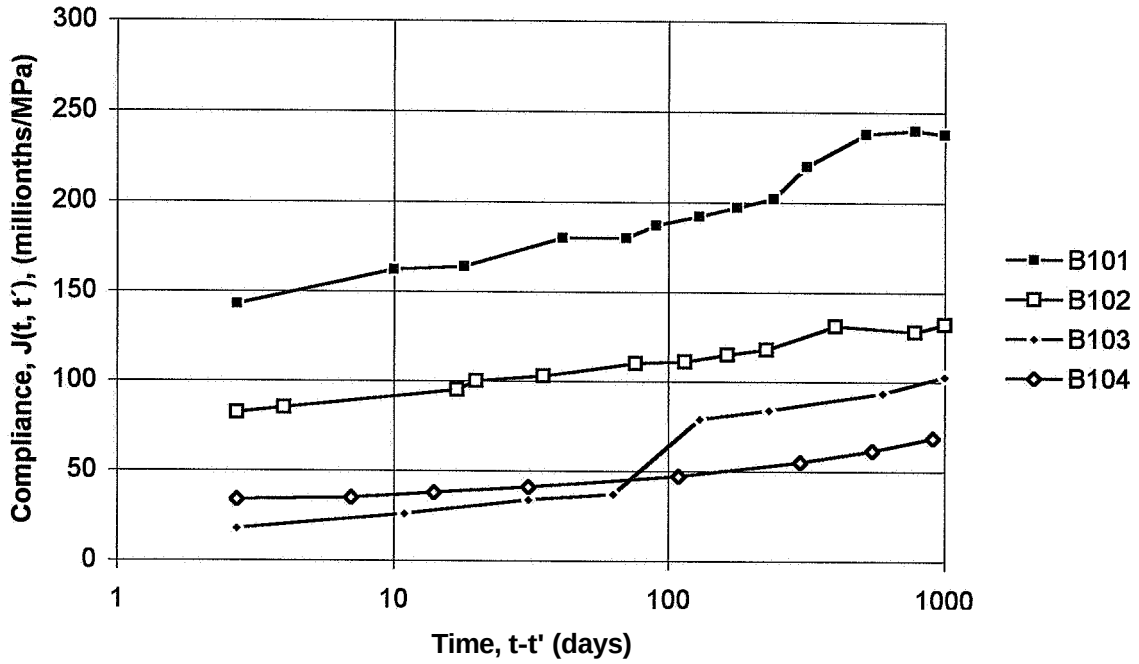

Appendix 14.18 – Long-term compliance of mix 2 after short-term creep subjected to sealed curing

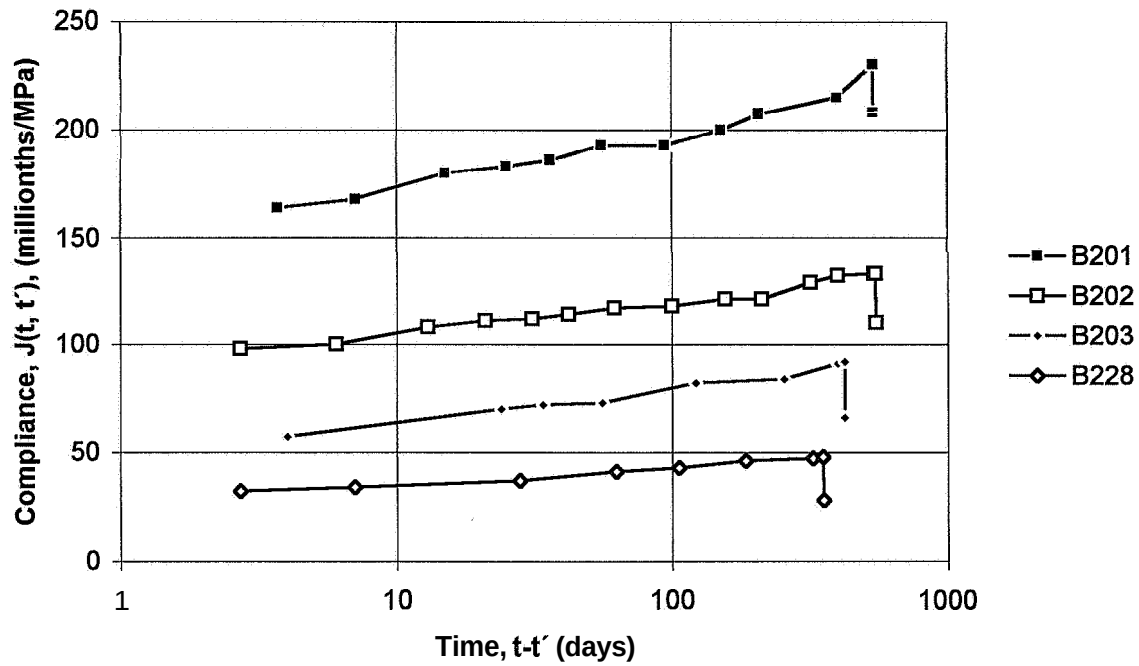

Appendix 14.19 – Long-term compliance of mix 3 after short-term creep subjected to sealed curing

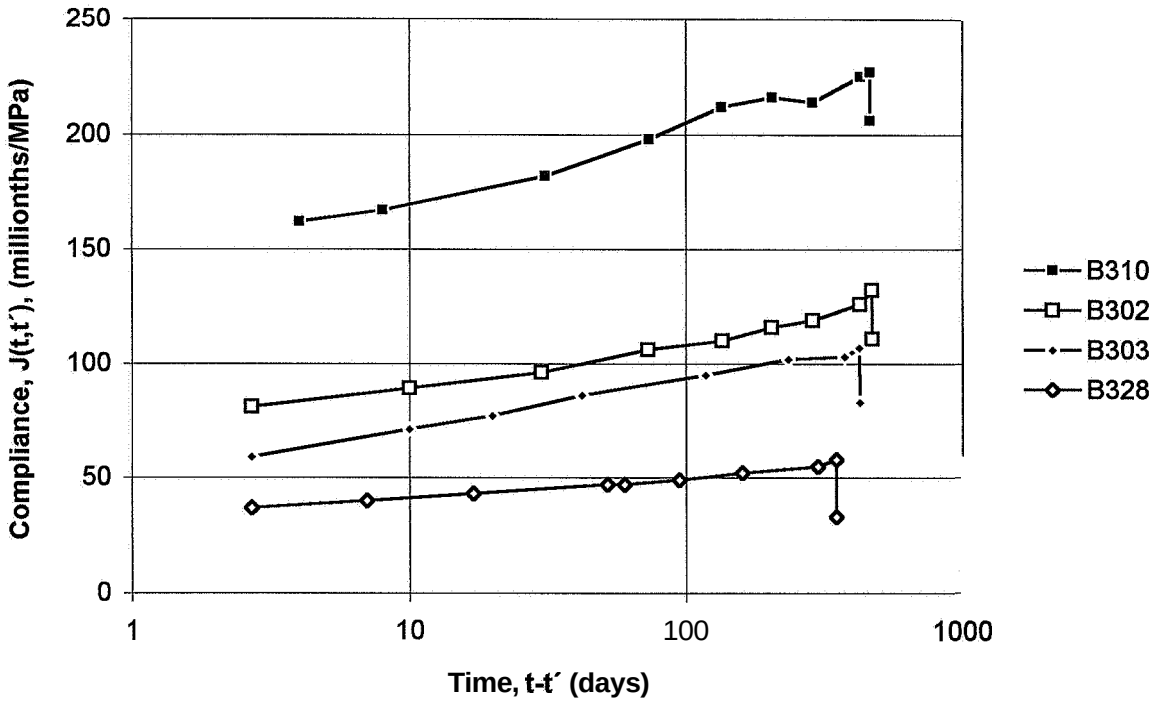

Appendix 14.20 – Long-term compliance of mix 4 after short-term creep subjected to sealed curing

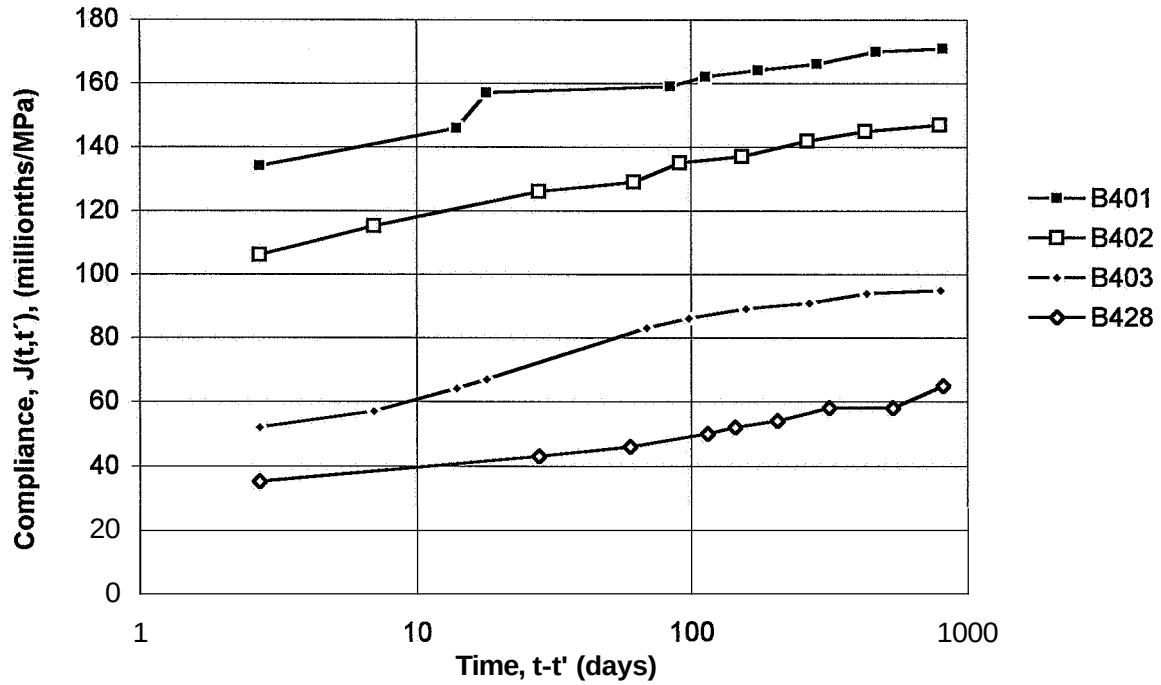

Appendix 14.21 – Long-term compliance of mix 5 after short-term creep subjected to sealed curing

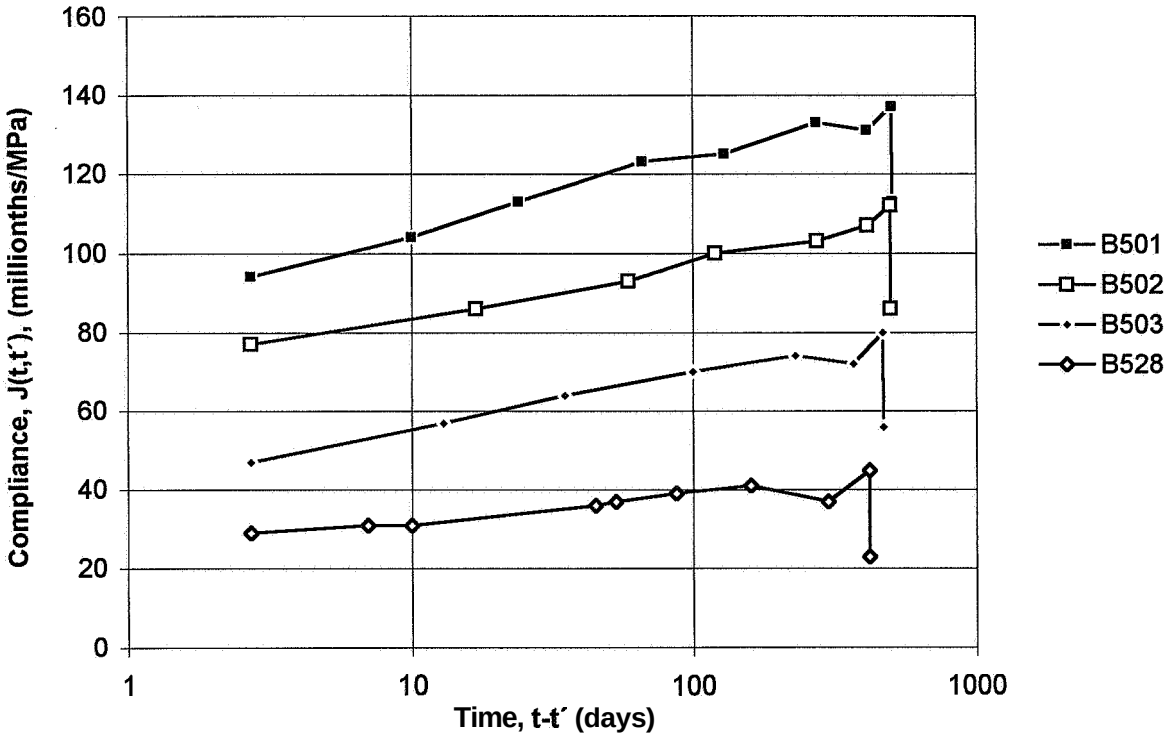

Appendix 14.22 - Long-term compliance of mix 6 after short-term creep subjected to sealed curing

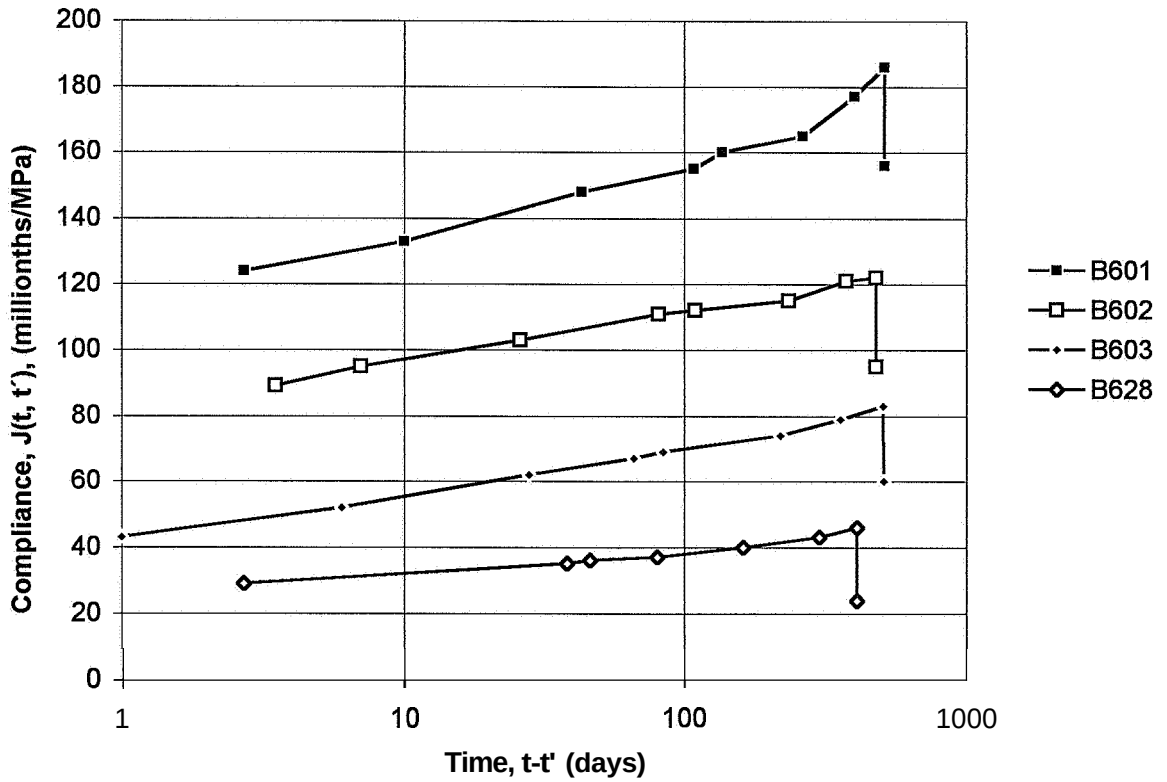

Appendix 14.23 – Long-term compliance of mix 7 after short-term creep subjected to sealed curing

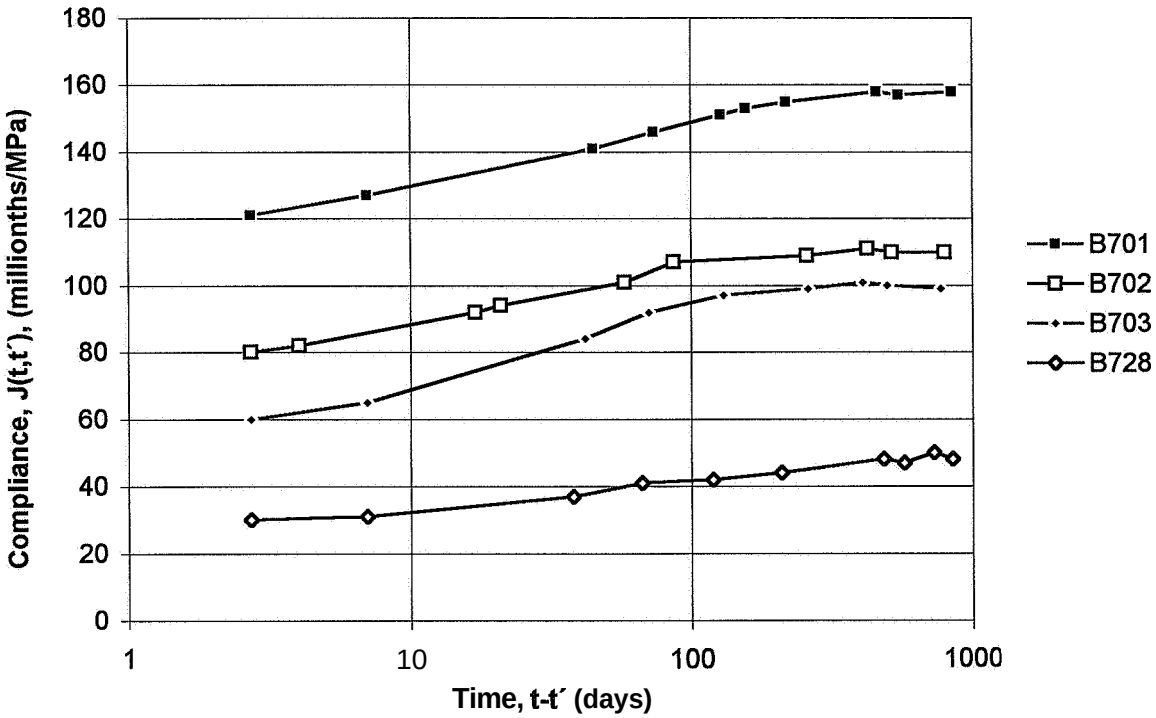

Appendix 14.24 – Long-term compliance of mix 8 after short-term creep subjected to sealed curing

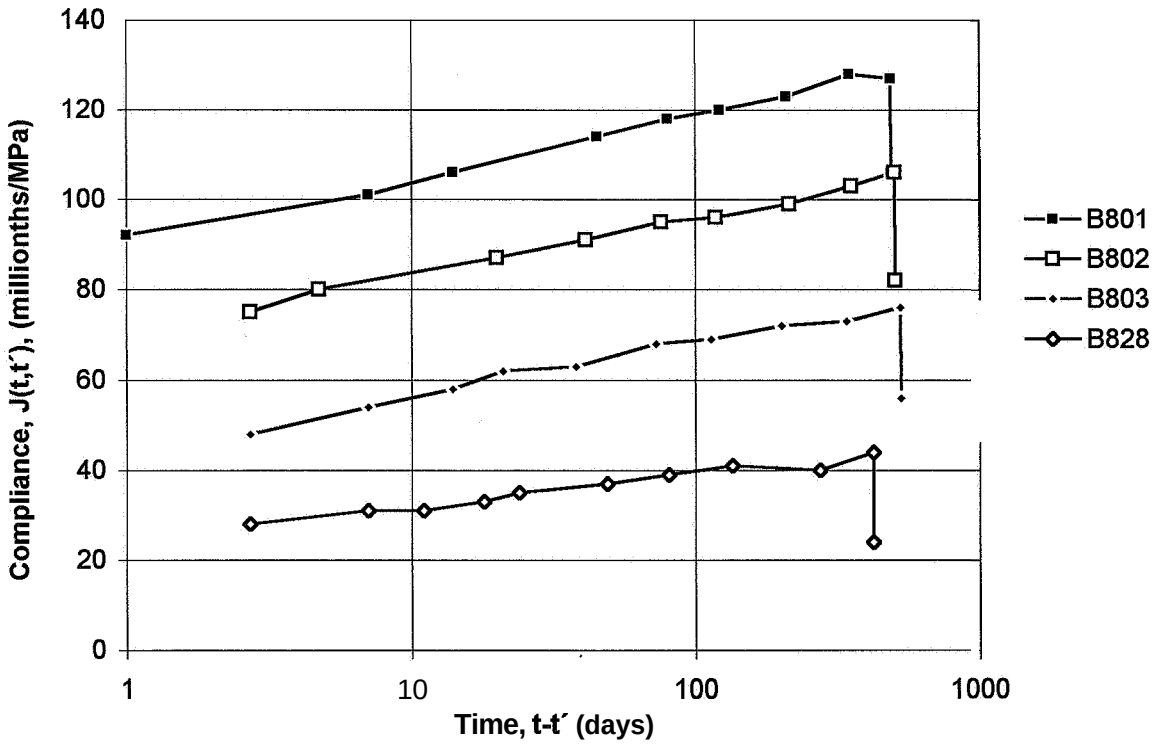

REGISTER

ERRATA

TVBM-1016. Lund Institute of Technology. Div. Building Materials. Lund. 1998:
"Quasi-instantaneous and Long-term Deformations of High-Performance Concrete with Some Related Properties"
by Bertil Persson

General: Except for Section 14.5.6 and paper III the creep rate {millionths/[MPa x (loading time)]) in the report is expressed for one unit of loading time only. In order to obtain a complete and correct expression for the creep rate, i.e. independent of the loading time, the creep rate is to be divided by the loading time (in s, h or days).

Paper	Page	Line	Instead of	Should be
Main	V	15	*(Accepted for publication, 1998.)*	Elsevier Science. New York. Vol. 8. 1998. Pp. 1-16.
		22	10 *pp. (Accepted for publication, 1998.)*	Norsk Betongforening. Oslo. Vol. 20. 1998. Pp. 120-129.
		26	*(Accepted for publication, 1998.)*	*(Submitted for publication, 1998.)*
		32	22 pp. *(Accepted for publication, 1998.)*	Elsevier Science. New York. Vol. 7. 1998. Pp. 139-155.
	VI	5	13 pp. *(Accepted for publication, 1998.)*	Elsevier Science Ltd. Pergamon Press. Vol. 28. 1998. Pp. 1023-1036.
	XII	2	a centre distance of LVDT or creep rate (mm, [millionths/(MPa·age)]}	a centre distance of LVDT or creep rate factor (mm, millionths/MPa)
		3	a_B the compliance rate with sealed curing [millionths/(MPa·age)]	a_B the compliance rate factor with sealed curing (millionths/MPa)
		4	a_D the compliance rate with air curing [millionths/(MPa·age)]	a_D the compliance rate factor with air curing (millionths/MPa)
		5	$a_{0.3}$ the creep rate with stress/strength = 0.3 [millionths/(MPa·age)]	$a_{0.3}$ the creep rate factor with stress/strength = 0.3 (millionths/MPa)
		6	$a_{0.6}$ the creep rate with stress/strength = 0.6 [millionths/(MPa·age)]	$a_{0.6}$ the creep rate factor with stress/strength = 0.6 (millionths/MPa)
	71	9	$-\mu_{ai}$	$+\mu_{ai}$
	125	19	$D_{0.01}$ was 3% smaller than	E_{stat} was 3% smaller than
	176	29	creep rate of HPC at [millionths/(MPa·h)]	creep rate factor of HPC at –1 °C (millionths/MPa)
IV	9	16	$-\mu_{ai}$	$+\mu_{ai}$

Main paper page 64:

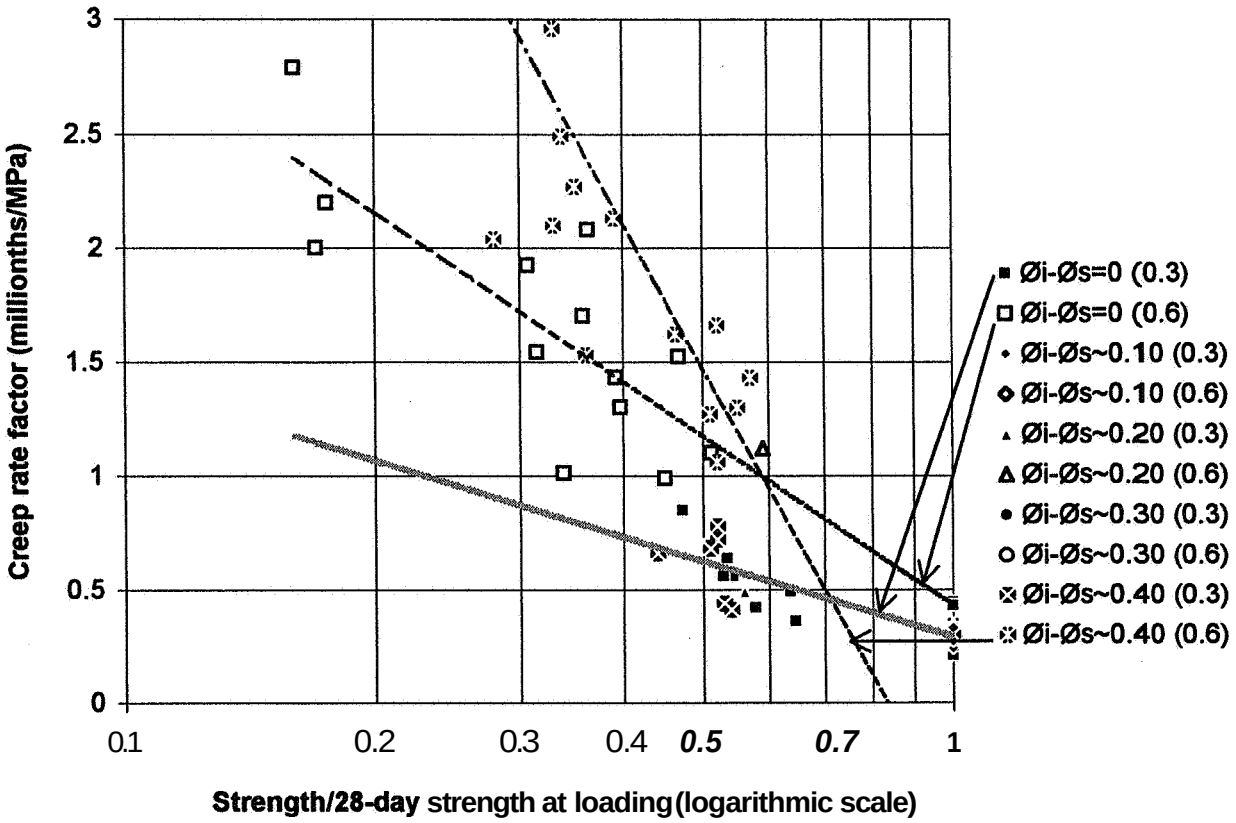

Figure 6.8 - Creep rate factor versus relative 28-day strength at loading, f_c/f_{c28}. Difference in relative humidity of cylinder surface, $Ø_s$, and inside, $Ø_i$. (0.3) = σ/f_c.